PREPARED BY

# U.S. ARMY AIR MOBILITY R & D LABORATORY

## AVIATION SYSTEMS COMMAND

AMES RESEARCH CENTER • MOFFETT FIELD • CALIFORNIA 94035







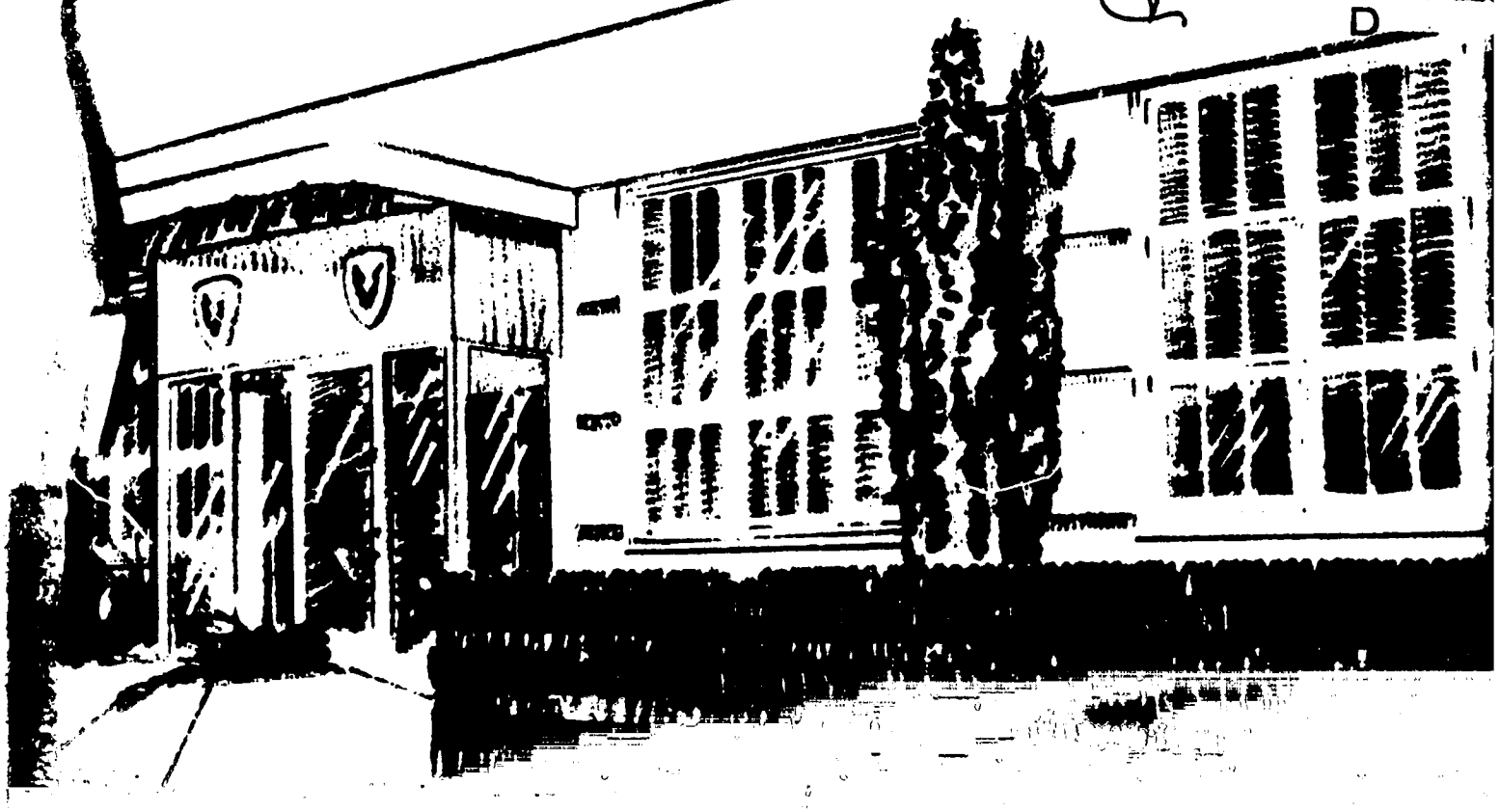

Unclassified

SECURITY CLASSIFICATION OF THIS PAGE (When Data Entered)

# REPORT DOCUMENTATION PAGE

READ INSTRUCTIONS BEFORE COMPLETING FORM

1. REPORT NUMBER

2. GOVT ACCESSION NO.

3. RECIPIENT'S CATALOG NUMBER

4. TITLE (and Subtitle)
U.S. Army Helicopter Design Datcom
Volume I, Airfoils

5. TYPE OF REPORT & PERIOD COVERED
Final rept.

6. PERFORMING ORG. REPORT NUMBER
D210-11097-1

7. AUTHOR(s)
L. U. Padone

8. CONTRACT OR GRANT NUMBER(s)
NAS2-8637

9. PERFORMING ORGANIZATION NAME AND ADDRESS
Boeing Vertol Company
P.O. Box 16858
Philadelphia, Pa. 19142

10. PROGRAM ELEMENT, PROJECT, TASK AREA & WORK UNIT NUMBERS

11. CONTROLLING OFFICE NAME AND ADDRESS
U.S. Army Aviation Systems Command
St. Louis, Missouri 63012

12. REPORT DATE
May 31, 1976

13. NUMBER OF PAGES

14. MONITORING AGENCY NAME & ADDRESS (if different from Controlling Office)
U.S. Army Air Mobility Research and Development Laboratory
Moffett Field, California 94035

15. SECURITY CLASS. (of this report)
Unclassified

15a. DECLASSIFICATION/DOWNGRADING SCHEDULE

16. DISTRIBUTION STATEMENT (of this Report)
Distribution of this document is unlimited.

17. DISTRIBUTION STATEMENT (of the abstract entered in Block 20, if different from Report)
U-HAMFLN

18. SUPPLEMENTARY NOTES

19. KEY WORDS (Continue on reverse side if necessary and identify by block number)

Airfoils
Helicopters
Rotor Blades
Lift
Drag
Pitching Moment
Sectional Characteristics

20. ABSTRACT (Continue on reverse side if necessary and identify by block number)

This report contains airfoil data of interest for rotor applications. The information was selected from sources presently available for publication. The data is presented in the form of lift, drag, and pitching moment coefficients and, in most cases, it covers the complete Mach number range from low subsonic to supercritical flow conditions. An introductory section presents airfoil data trends and information pertaining to the source and usefulness of such data.

DD FORM 1 JAN 73 1473 EDITION OF 1 NOV 65 IS OBSOLETE

Unclassified

SECURITY CLASSIFICATION OF THIS PAGE (When Data Entered)

AD-

# US ARMY
# HELICOPTER DESIGN DATCOM
# VOLUME I - AIRFOILS

USAAMRDL CR 76-2

SEPTEMBER 1976

PREPARED UNDER CONTRACT NAS 2-8637 BY

THE BOEING COMPANY

BOEING VERTOL, PO BOX 16858

PHILADELPHIA, PENNSYLVANIA 19142

FOR THE

SYSTEMS RESEARCH INTEGRATION OFFICE

US ARMY AIR MOBILITY R&D LABORATORY

US ARMY AVIATION SYSTEMS COMMAND

ST. LOUIS, MISSOURI 63102

## DISCLAIMER STATEMENT

The findings in this report are not to be construed as an official Department of the Army position.

1.0.10 **FOREWORD**

This program was conducted under the technical cognizance of M.A. Schwartzberg of the Systems Research Integration Office (SAVDL-SR),U.S. Army Air Mobility Research and Development Laboratory, U.S. Army Aviation Systems Command, St. Louis, Missouri.

The assistance and cooperation of the Aerodynamics staff and Advanced Research group is gratefully acknowledged. Particularly valuable was the assistance of J. McLaughlin in preparing the airfoil data sheets, of T. Fukushima and J. Davis for the sections on unsteady aerodynamics, compressibility, and mean line/thickness effects, W.Z. Stepniewski and E. Kisielowski for their support in the search and selection of the most useful data, and W.L. Metz and D.L. Deibler for their efforts in preparing the final document.

The assistance of Mr. R.W. Prouty (Hughes), Mr. C. Capelier (ONERA), Mr. G. Reichert (MBB) and Dr. J. Williams (RAE) is also gratefully acknowledged.

1.0.20

# TABLE OF CONTENTS

| Sheet Number | Description |
|---|---|
| 1.2.60 | Reynolds Number Effects on Airfoil Characteristics |
| 1.2.70 | Unsteady Aerodynamic Effects |
| .1 | Dynamic Stall Delay |
| .2 | Aerodynamic Damping |
| .3 | Gamma-Functions |
| 1.2.80 | Effects of Airfoil Geometry |
| .1 | Mean Line Distributions |
| .2 | Thickness Shapes |
| 1.2.90 | Effect of Airfoil Trailing Edge Modifications |
| 1.2.100 | Effect of Airfoil Leading Edge Contours |
| | **Airfoil Test Data** |
| 1.3.10 | NACA 0006 |
| 1.3.20 | NACA 0012 |
| 1.3.30 | NACA 0012 - Including Reverse Flow |
| 1.3.40 | NACA 0012 (Modified) with 0° T.E. Tab |
| 1.3.50 | NACA 0012 (Modified) with -3° T.E. Tab |
| 1.3.60 | NACA 0015 |
| 1.3.70 | NACA 23012 |
| 1.3.80 | NACA 23012 with 0.043 c T.E. Tab at 0° |
| 1.3.90 | NACA 23012 with 0.087 c T.E. Tab at 0° |
| 1.3.100 | NACA 23015 |
| 1.3.110 | NACA 63A009 |
| 1.3.120 | NACA 63A012 |
| 1.3.130 | NACA 63A012 - Including Reverse Flow |
| 1.3.140 | NACA 63A015 |

| Sheet Number | Description |
|---|---|
| 1.3.150 | NACA 63A018 |
| 1.3.160 | NACA 64A(4.5)08 |
| 1.3.170 | NACA 64A608 |
| 1.3.180 | NACA 64A312 |
| 1.3.190 | NACA 64A(4.5)12 |
| 1.3.200 | NACA 64A612 |
| 1.3.210 | NACA 64A516 |
| 1.3.220 | NACA 8-H-012 |
| 1.3.230 | V13006-0.7 |
| 1.3.240 | V(1.9)3009-1.25 |
| 1.3.250 | V23010-1.58 with 0° T.E. Tab |
| 1.3.260 | V23010-1.58 with -3° T.E. Tab |
| 1.3.270 | V23010-1.58 with 0° T.E. Tab, in Reverse Flow |
| 1.3.280 | V23010-1.58 with -3° T.E. Tab, in Reverse Flow |
| 1.3.290 | V23010-1.58 with +3° T.E. Tab, in Reverse Flow |
| 1.3.300 | V43012-1.58 with 0° T.E. Tab |
| 1.3.310 | V43012-1.58 with -6° T.E. Tab |
| 1.3.320 | SA 13109-1.58 |
| 1.3.330 | NPL 9615 |
| 1.3.340 | NPL 9626 |
| 1.3.350 | NPL 9627 |
| 1.3.360 | NPL 9660 |
| 1.3.370 | NACA-Cambre |
| 1.3.380 | VR-7 with 0° T.E. Tab |

| Sheet Number | Description |
|---|---|
| 1.3.390 | VR-7 with -3.1° T.E. Tab |
| 1.3.400 | VR-7 with -5.9° T.E. Tab |
| 1.3.410 | VR-8 with 0° T.E. Tab |
| 1.3.420 | VR-7.1 with -1° T.E. Tab |
| 1.3.430 | FX 69-H-098 |
| | **Sample Calculations** |
| 1.4.10 | Evaluation of Approximate Lift/Drag Polars |
| 1.4.20 | Lift, Drag, and Pitching Moment Coefficients at Large Angles of Attack |

## 1.0.30 INTRODUCTION

The objectives of a Data Compendium (Datcom) is to provide a source of easily accessible technical information to the engineer, designer, or scientist. Since new technical information is constantly being generated, the Datcom format has to be flexible enough to allow additional material to be included with the least amount of overall revisions.

This particular Data Compendium summarizes the key helicopter airfoil information available to date from unrestricted sources. In the future, additional airfoil data might be included which, at present, is either proprietary or classified.

At its first release, the Datcom contains forty-three (43) sheets of airfoil data, covering the basic configuration and modifications of the sections employed on most rotors, with the exception of proprietary or otherwise unavailable information on some recent rotor sections.

Besides the systematic presentation of airfoil data, the Datcom includes sections which review:

- The definition and significance of the airfoil parameters of interest in rotor applications.
- Key trends in airfoil data.
- Theoretical and experimental methods for the evaluation of section characteristics.

## 1.0.40 GUIDE TO VOLUME

The material presented in the Airfoil DATCOM is divided into four main groups:

1. Definitions

   This section explains the meaning, use, and derivation of the aerodynamic parameters of interest for rotor airfoil applications, including the classification of airfoils and the definition of basic NACA airfoil coordinates.

2. Theory and Empirical Methods

   This section covers material that will assist in the proper understanding and utilization of both theoretical methods and test data.

3. Data

   A systematic compilation of available test data presented in a standardized format. Each airfoil is shown under a separate data sheet which includes coordinates, a description of the model, and key characteristics of the method of testing.

4. Sample Calculations

   This section shows how theoretical and experimental data can be utilized to obtain information not covered by available test data.

# DATA SHEET IDENTIFICATION

The numbering system used in the present DATCOM volume identifies the broad category and the subject under which each item of information is described. This system will allow the addition of new sheets within the initial set of data sheets without having to renumber the entire volume.

The significance of the numbers identifying each data sheet is described below:

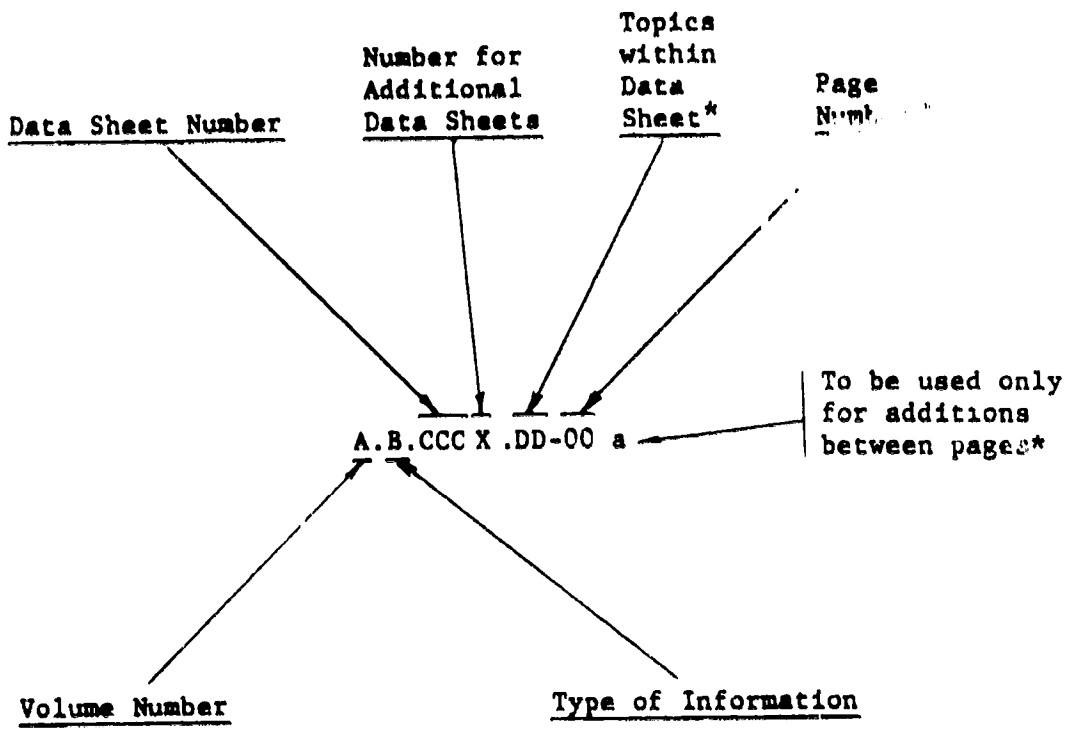


1 - Airfoil DATCOM

0 - Introduction

1 - Definitions, Standards, Sign Conventions

2 - Theoretical and Empirical Methods, Description of Physical Phenomena, and Design Methodology

3 - Theoretical and Experimental Data

4 - Sample Calculations

*Shown only when needed

## 1.1.10 LIST OF SYMBOLS

| | |
|---|---|
| $a$ | quantity used to define mean lines of NACA 6-series airfoils, where $a$ is the distance in chords from the leading edge over which the loading is uniform at the design lift coefficient |
| $a$ | speed of sound |
| $c$ | airfoil chord |
| $c_{tab}$ | chordwise length of trailing edge tab |
| $c_c$ | chordwise force coefficient |
| $c_d$ | drag coefficient |
| $c_{d_{min}}$ | minimum drag coefficient |
| $c_{d_o}$ | drag coefficient at zero lift |
| $c_f$ | skin friction drag coefficient |
| $c_l$ | lift coefficient |
| $c_{l_i}$ | design lift coefficient |
| $c_{l_{max}}$ | maximum lift coefficient |
| $c_m$ | pitching moment coefficient, resolved about the quarter-chord unless otherwise noted |
| $c_{m_o}$ | pitching moment coefficient at zero lift |
| $c_n$ | normal force coefficient |
| $c_p$ | pressure coefficient, $(p - p_\infty)/\frac{1}{2}\rho V_\infty^2$ |
| $c_{p_c}$ | pressure coefficient compensated for compressibility |
| $c_{p_i}$ | incompressible pressure coefficient |
| $f_D$ | drive frequency in oscillating airfoil test |
| $k$ | reduced frequency, $c\Omega/2V$ |
| $k_1$ | constant used in describing the mean line of NACA 5-digit series airfoils |
| $m$ | constant used in describing the mean line of NACA 5-digit series airfoils |
| $M$ | Mach number |

$M_{crit}$ critical Mach number; freestream Mach number at which the local Mach number, $M_\ell$, first equals $1.0$ at some point on an airfoil

$M_{DD}$ drag divergence Mach number, defined as the freestream Mach number at which $dC_d/dM = 0.10$

$M_\ell$ local Mach number

$n$ frequency of vortices in wake, used to define the Strouhal number

$p$ static pressure

$q$ dynamic pressure, $\frac{1}{2}\rho V^2$

$r$ leading edge radius of an airfoil section

$R$ gas constant

$Re$ Reynolds number, $\rho VL/\mu$, where for airfoils, the characteristic length $L$ is the chord. Reynolds numbers can be based on other dimensions such as maximum thickness or boundary-layer thickness

$S$ Strouhal number, $nD/V$ where $D$ is a characteristic dimension of the body

$t$ maximum thickness of airfoil

$T$ absolute temperature

$u, v$ local velocity components

$V$ velocity

$x$ abscissa

$x_u$ abscissa, upper surface of airfoil contour

$x_\ell$ abscissa, lower surface of airfoil contour

$y$ ordinate

$y_{0.0125}$ upper surface ordinate at $x/c = 0.0125$; used for correlation of lift stall characteristics

$y_c$ ordinate of the mean line of an airfoil section

$y_t$ ordinate of the thickness distribution of an airfoil section

| | |
|---|---|
| $s'$ | skewed coordinate, used in plotting suction loops |
| $\alpha$ | angle of attack, in degrees |
| $\alpha_i$ | angle of attack at the "design" condition of an airfoil section |
| $\gamma$ | ratio of specific heats of a gas |
| $\delta_{tab}$ | trailing edge tab angle measured from the chordline of an airfoil, defined as positive in the direction for which positive camber is increased |
| $\Delta$ | increment |
| $\theta$ | an angle, the tangent of which is the slope of the mean line |
| $\mu$ | absolute viscosity |
| $\mu_o$ | function used in thin airfoil theory to evaluate the pitching moment of a section |
| $\nu$ | kinematic velocity |
| $\rho$ | density |
| $\Omega$ | rotational velocity |

Subscripts

| | |
|---|---|
| *ac* | aerodynamic center |
| *c* | identification of mean line characteristics |
| *c/4* | for quantities referenced to the quarter-chord |
| *comp* | compressible |
| *cp* | center-of-pressure |
| *i* | "ideal" or design value |
| *inc* | incompressible |
| *l* | lower surface, in identification of airfoil coordinates |
| *l* | local, in reference to flow conditions |
| *L.E.* | leading edge |

| | |
|---|---|
| $max$ | maximum value |
| $o$ | zero lift condition |
| $T$ | total |
| $tab$ | trailing-edge tab |
| $u$ | upper surface, in identification of airfoil coordinates |
| $\infty$ | freestream condition |

## 1.1.20 AIRFOIL GEOMETRY - DESIGNATIONS AND CONVENTIONS

Figure 1 illustrates how mean lines and thickness forms are combined to form NACA airfoils. Although some modern airfoils are designed by taking into account the local contour curvature to optimize some specific supercritical characteristics, many airfoils for helicopter rotor applications can be approximated by the NACA classification.

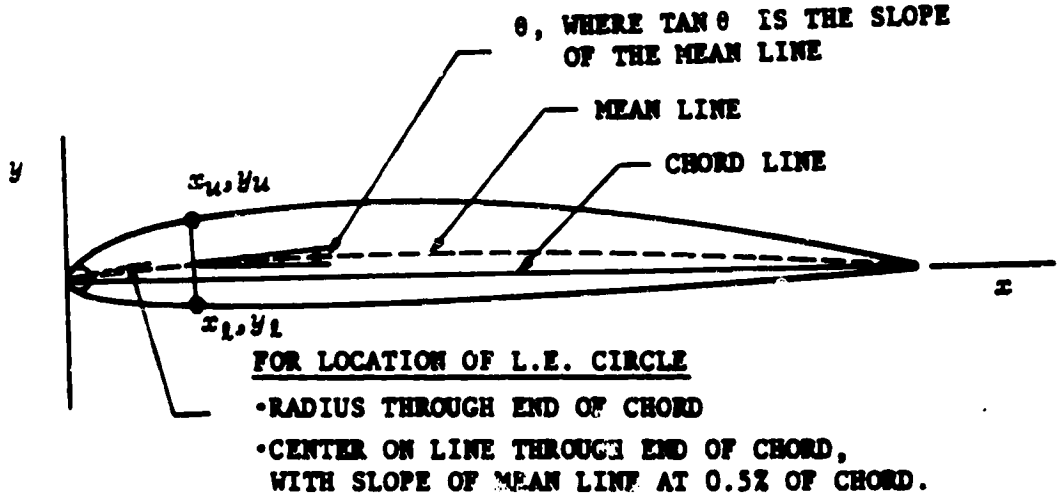


*Figure 1 Method of combining mean lines and basic-thickness forms*

In the NACA system, an airfoil shape is obtained by wrapping a symmetrical thickness form around a mean line. The airfoil thickness is applied along lines perpendicular to the mean line by the following relationships:

$$x_u = x_c - y_t \sin \theta$$

$$y_u = y_c + y_t \cos \theta$$

$$x_l = x_c + y_t \sin \theta$$

$$y_l = y_c - y_t \cos \theta$$

where

$x$ is the abscissa

$y_c$ is the ordinate of the mean line

$\theta$ is the angle whose tangent is the slope of the mean line

$y_t$ is the ordinate of the thickness distribution at $x$.

By definition,

- Leading edge and trailing edge are the forward and rearward extremities of the mean line.[1]
- The chordline is the straight line connecting the leading and trailing edges.[1]

The leading-edge circle associated with each thickness shape is applied to a cambered airfoil by

- Drawing a line passing through the leading edge with a slope corresponding to the mean-line slope at $0.005c$.
- Drawing a circle centered at one radius distance from the leading edge along such a line.
- Fairing the airfoil contour into the leading edge circle on the upper and lower surfaces.

Helicopter rotor airfoils generally fall into one of the following categories:

A. NACA Four-Digit Sections

These sections were defined from the best early airfoils. Only the symmetrical sections of this series have been used on helicopter rotors and, until recently, the majority of rotors used the NACA 0012 airfoil almost exclusively.

The thickness distributions of the NACA four-digit sections follow the relation:

$$\pm(y_t/c) = [(t/c)/0.2][0.2969\sqrt{x/c} - 0.126(x/c) - 0.3516(x/c)^2 + 0.2843(x/c)^3 - 0.1015(x/c)^4],$$

where $t$ is the maximum thickness.

The leading edge radius is

$$r/c = 1.1019(t/c)^2.$$

The significance of the numbering system is as follows:

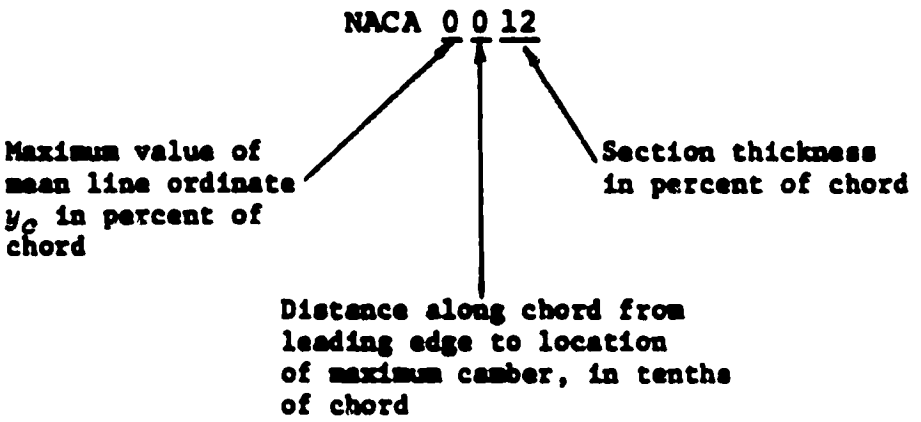


## B. NACA Five-Digit Sections

Until recently, most of the cambered sections successfully employed on helicopter rotors have been of the NACA five-digit series, or modifications thereof. In a number of instances, the closest NACA identification has been used to describe airfoils resembling NACA sections.

The thickness forms are the same as for NACA four-digit series. Mean lines are described by the following equations:

$$y_c/c = (1/6)k_1[(x/c)^3 - 3m(x/c)^2 + m^2(3 - m)(x/c)] \qquad 0 \leq x/c \leq m$$

$$y_c/c = (1/6)k_1 m^3[1 - (x/c)] \qquad m \leq x/c \leq c = 1.$$

Values for $m$ and $k_1$ are tabulated below. Equations and tables have been taken from Reference 1.

| MEAN-LINE DESIGNATION | POSITION OF MAXIMUM CAMBER, $x/c$ | $m$ | $k_1$ |
|---|---|---|---|
| 210 | 0.05 | 0.0580 | 361.400 |
| 220 | 0.10 | 0.1260 | 51.640 |
| 230 | 0.15 | 0.2025 | 15.957 |
| 240 | 0.20 | 0.2900 | 6.643 |
| 250 | 0.25 | 0.3910 | 3.230 |

The significance of the numbering system is as follows:

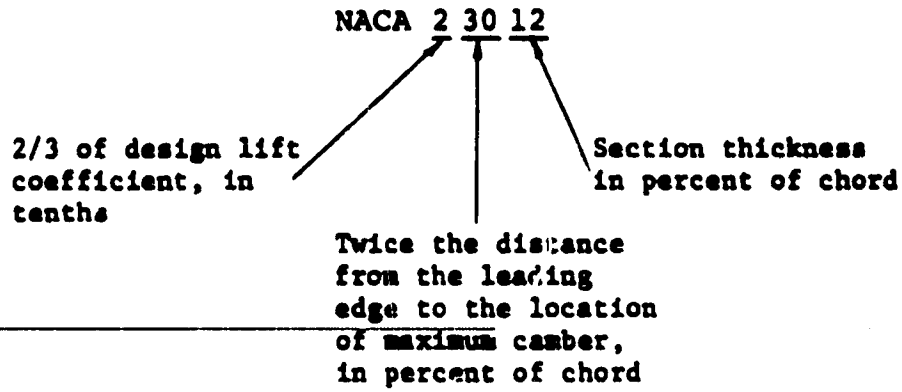


## C. NACA 6-Series Airfoils

This airfoil family includes sections with mean lines and thickness forms selected to conform to prescribed loading distributions. Such mean lines and thickness distributions cannot be summarized by simple expressions as was the case for four- and five-digit series airfoils. A tabulation of mean-line and thickness values for 6-series airfoils can be found in standard airfoil reference texts such as Reference 1.

The significance of the numbering system is summarized below:

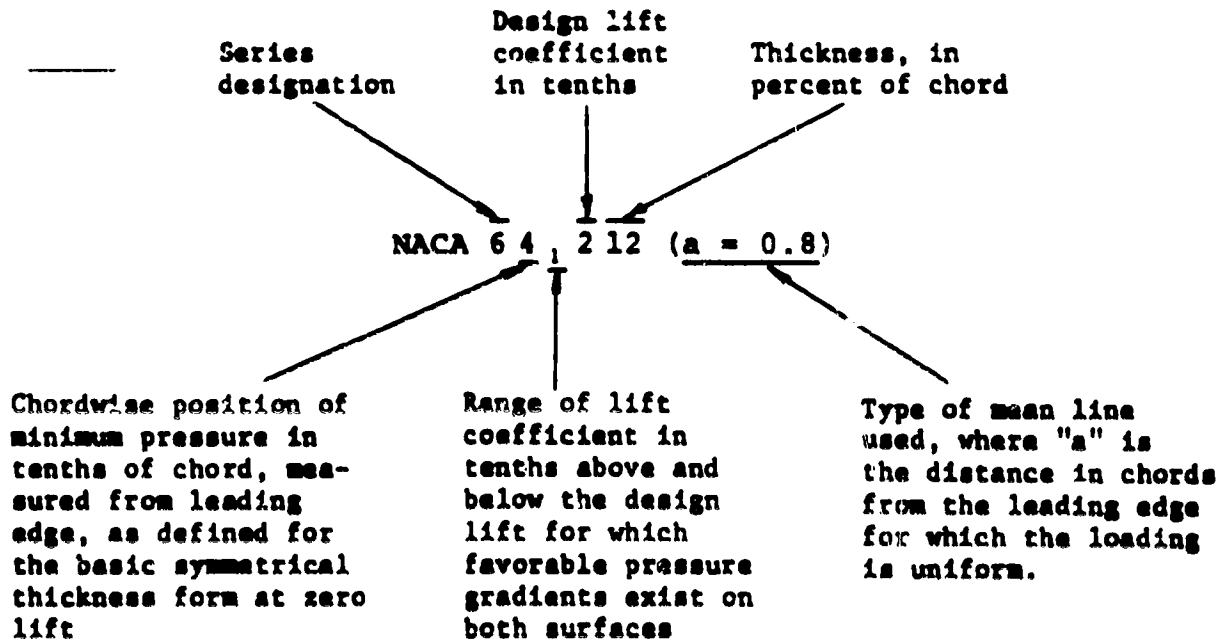

## D. NACA Helicopter Sections

During the 1940's, NACA conducted a systematic investigation of a series of cambered low drag and low pitching-moment helicopter airfoils. However, the performance of those sections was disappointing, because they rely too much on the maintenance of extensive laminar flow. The difficulty in achieving the low drag potential, and the low maximum lift characteristics, prevented their actual application to helicopters; but, in a few instances, they have been employed on gyroplanes.

NACA helicopter airfoils were identified with the following designation:[2,3]

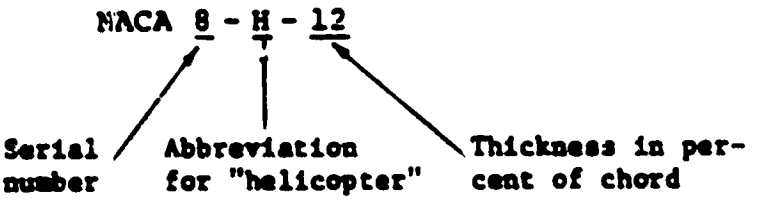


## E. Other Designations

Other designations of helicopter airfoils have been arbitrary, as they usually identify the originating organization, the serial number, and sometimes, the design lift coefficient and thickness.

## References

1. Abbott, I.H., von Doenhoff, A.E., *Theory of Wing Sections*, Dover Publications, N.Y., N.Y., 1958.

2. Tetervin, N., *Tests in the NACA Two-Dimensional Low-Turbulence Tunnel of Airfoil Sections Designed to have Small Pitching Moments and High Lift-Drag Ratios*, NACA CB No 3113, 1943.

3. Stivers, L.S., Jr., Rice, F.J., Jr., *Aerodynamic Characteristics for Four NACA Airfoil Sections Designed for Helicopter Rotor Blades*, NACA WR L-29, 1946.

## 1.1.30 DEFINITION OF AERODYNAMIC PARAMETERS

The objective of this section is to review the definition of aerodynamic parameters of interest with airfoils for helicopter rotors.

The following parameters are reviewed:

(1) Aerodynamic Center
(2) Angle-of-Attack
(3) Camber and Mean Line
(4) Center-of-Pressure
(5) Chordline
(6) Crestline
(7) Critical Mach Number
(8) Drag Divergence Mach Number
(9) Drag Rise after Drag Divergence
(10) Force and Moment Coefficients
(11) Lift-Break Boundary
(12) Lift-Curve Slope
(13) Mach Number
(14) Mach Tuck - Compressibility Effects on Pitching Moments
(15) Maximum Lift Coefficient
(16) Reynolds Number
(17) Suction Loops
(18) Stall, and Types of Stall
(19) Static Stall Hysteresis
(20) Strouhal Number

# 1. AERODYNAMIC CENTER

The aerodynamic center of an airfoil is defined as the point about which the sectional pitching moment is independent of lift, or angle of attack. The pitching moment about the aerodynamic center, identified as $C_{m_{ac}}$, is identical to the zero-lift pitching moment, $C_{m_0}$.

The zero lift pitching moment, which is a pure couple, can be easily determined from test data or by means of potential flow theory.

According to thin airfoil theory, the aerodynamic center is always located at one-quarter chord from the leading edge. Viscosity and compressibility influence the aerodynamic center so that on airfoils of finite thickness, the aerodynamic center is seldom at the quarter-chord, even at low speeds. Over the unseparated range of lift, the aerodynamic center can be determined from test data by evaluating

$$(x/c)_{ac} = dC_{m_{LE}}/dC_\ell, \text{ for } dC_\ell/d\alpha = constant.$$

or, since the pitching moment about the quarter-chord, $C_{m_{c/4}}$ is a more commonly quoted value,

$$(x/c)_{ac} = (1/4) - (dC_{m_{c/4}}/dC_\ell).$$

While not a primary design objective, the aerodynamic center location is important, and the general consensus is that at low speed, it should be as far aft as possible; typically between 27 and 28 percent of chord from the leading edge.

There is experimental evidence that by modifying a standard NACA 4- and 5-digit series trailing edge to include a cusp or undeflected trailing-edge tab, the aerodynamic center of a section will be shifted aft (p. 182 of Ref 1). This can also be seen by comparing data for the NACA 23012, with and without T.E. tab, in sheets 1.3.200, 1.3.210, and 1.3.220.

## 2. ANGLE-OF-ATTACK

On a two-dimensional basis, the angle-of-attack is defined as the angle between the remote wind and the chordline of an airfoil. The angle of attack is also defined as positive in the direction for which its increase results in increasing lift..

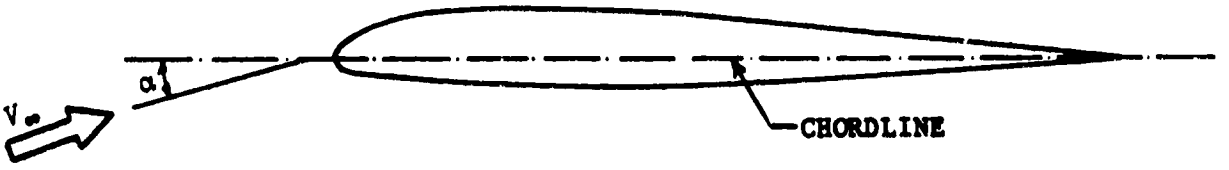


*Figure 1. Angle of Attack*

The calculation of the angle-of-attack environment in the flow field of a rotor in flight is quite complex as it involves an evaluation of the velocities induced along rotor blade elements in a flow field influenced by rotational, forward-flight, and flapping-motion components.

## 3. CAMBER AND MEAN LINE

Camber is the curvature of the airfoil section relative to its chordline. Camber distribution, magnitude, and position of maximum camber are determined by the specification of the mean line (see Figure 2; also Section 1.1.40). The shape and displacement of the mean line determine the chordwise load distribution, angle of zero lift, and pitching moment coefficient of an airfoil.

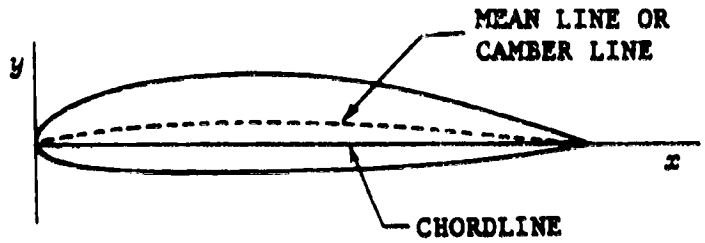


*Figure 2. Geometry of airfoil sections*

The amount and location of the maximum camber for a number of airfoils is listed in Section 1.2.40.

The mean line is the locus of points situated halfway between the upper and lower surfaces of an airfoil section—the distance between the upper and lower surfaces and the mean line being measured normal to the mean line. In the case of an uncambered airfoil, the mean and chord lines are the same.

A typical cambered airfoil section is composed of a mean line and a thickness distribution combined using the following relationships:

For the upper surface:

$$x_u = x_c - y_t \sin \theta,$$

$$y_u = y_c + y_t \cos \theta.$$

For the lower surface:

$$x_l = x_c + y_t \sin \theta,$$

$$y_l = y_c - y_t \cos \theta,$$

where $x_c$, $y_c$ and $\tan \theta$ are the abscissas, ordinates, and slopes of the mean line, and $y_t$ is the ordinate of the symmetrical thickness distribution at chordwise point $x$.

Airfoil section properties associated with the shape and magnitude of the mean line are:

(1) chordwise load distribution

(2) angle of zero lift

(3) pitching moment coefficient

(4) maximum lift coefficient.

## 4. CENTER-OF-PRESSURE

The center-of-pressure is the distance from the leading edge to a point on the chord through which the resultant pressure forces on the airfoil section can be assumed to act. The position of the center-of-pressure shifts with changes in lift coefficient, and falls outside of the chord at lift levels approaching zero lift.

The location of the center-of-pressure is:

$$x_{c.p.}/c = 0.25 - (C_{m_{c/4}}/C_l),$$

for pitching moments defined about the quarter-chord.

## 5. CHORDLINE

The chordline is defined as the straight line connecting the leading and trailing edges of an airfoil profile, where the leading and trailing edges are defined as the forward and rearward extremities, respectively, of the mean line. For some highly cambered airfoils with pronounced trailing-edge cusps, this results in the chordline passing outside of the contour (Figure 3).


*Figure 3. Chordline of an airfoil*

Some airfoils use a reference line which differs from the standard NACA chordline; e.g., the reference line on the V23010-1.58 is such that the aft 50 percent of the airfoil profile is bisected by it (Figure 4).

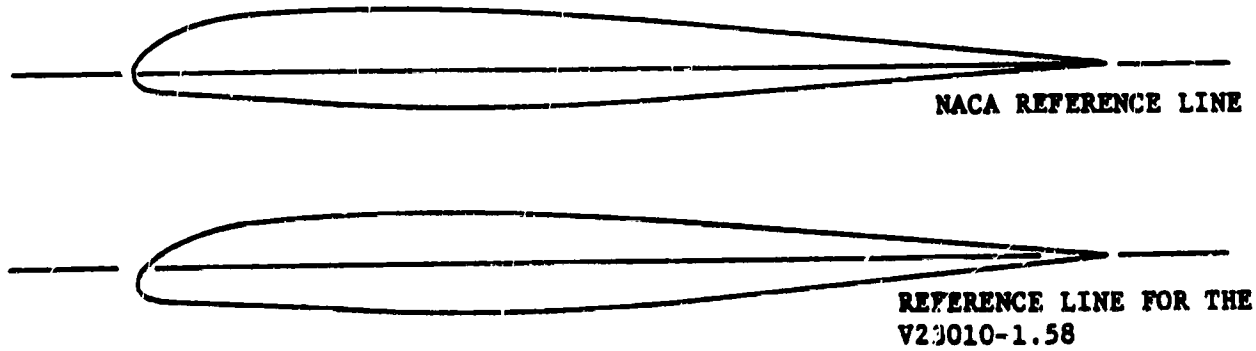


*Figure 4. Comparison between the NACA reference line and the reference line for the V23010-1.58 airfoil*

## 6. CREST LINE

The crest line is a location on the surface of a wing section which is tangent to the remote wind (Figure 5). The crest location at a given incidence is used in the methods for the theoretical determination of drag-rise conditions. At low incidence, there are two crest locations of interest, one on each surface.

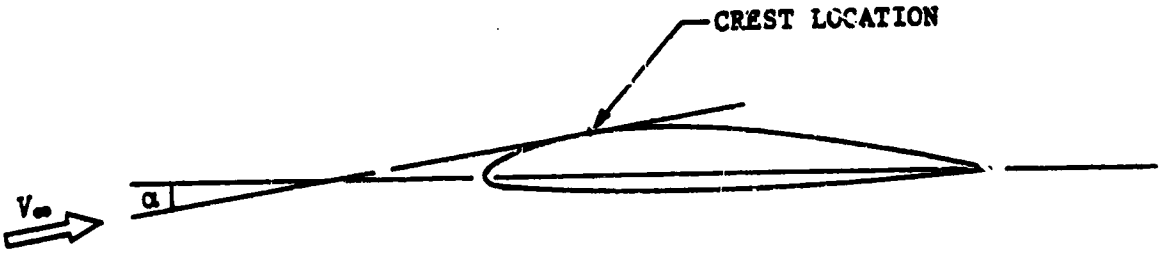


*Figure 5. Crest location over an airfoil section*

## 7. CRITICAL MACH NUMBER

By definition, the "critical" Mach number is the freestream Mach number corresponding to the first occurrence of sonic flow over the surface of a body in motion through a fluid; i.e., the condition for which $M_\ell = 1.0$ somewhere on the airfoil.

If the local Mach number first equals *1.0* in the vicinity of the leading edge of an airfoil, experience shows that no significant effects take place until $M_\ell = 1.2$ or higher, provided that the velocity peak is not so sharp as to cause boundary-layer separation.

A typical critical Mach number boundary is illustrated in Figure 6.

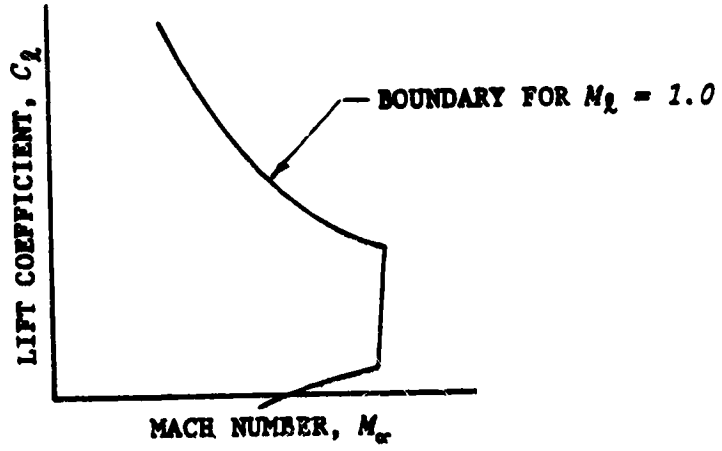


*Figure 6. Critical Mach number boundary*

The evaluation of critical Mach number boundaries from potential flow solutions for airfoils is useful for the preliminary assessment of the lift levels at which significant compressibility effects first take place.

## 8. DRAG DIVERGENCE MACH NUMBER

The drag divergence Mach number of an airfoil section is defined as the Mach number for which $dC_d/dM = 0.1$ as airspeed over the airfoil is increased at constant angle-of-attack. This is illustrated in Figure 7.

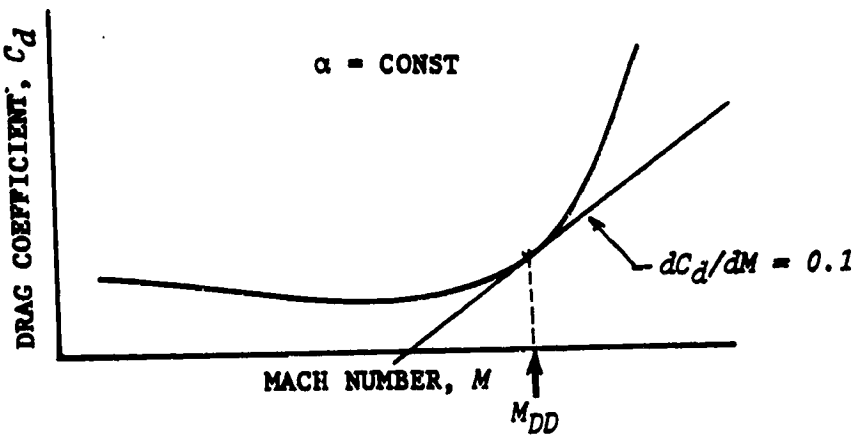


*Figure 7. Drag divergence Mach number derived from test data*

Drag divergence boundaries are generally described in terms of lift coefficient, as shown in Figure 8 for a number of sections

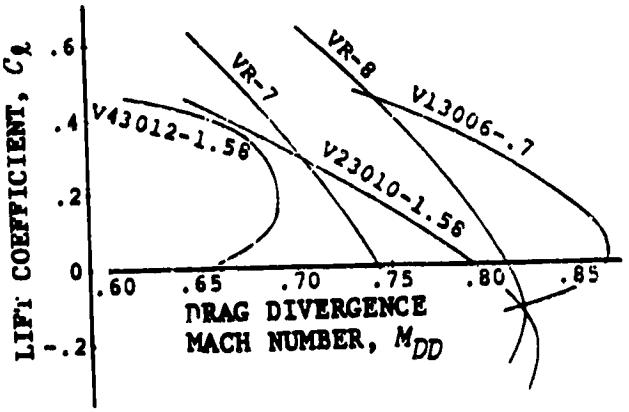


*Figure 8. Comparison of drag divergence boundaries*

This boundary can also be estimated theoretically when a potential flow solution for the velocities on the surface of an airfoil is available. The theoretical estimate of drag divergence involves identifying the conditions for which the

flow is first sonic ($M_{local} = 1.0$) at the crest of an airfoil where the crest is a location on the surface tangent to the remote wind. Although such an estimate is always somewhat conservative, theoretical $M_{DD}$ boundaries are very useful in comparing airfoil sections, as might be required during airfoil design and optimization.

Crestline theory is described in detail in Reference 2. The use of the drag divergence boundary has typically been limited to the low-lift range, but recently, it has been extended to lift levels comparable to the maximum lift boundary[3].

The drag divergence Mach number at zero lift, or at some low-lift level, can be used as an indicator of the usefulness of a section over the outboard portion of a blade on a rotor in forward flight.

## 9. DRAG RISE AFTER DRAG DIVERGENCE

This is more critical than the drag divergence Mach number because drag rise after drag divergence is the source of the power penalty and loads associated with operation at high Mach numbers on the advancing blade. One approach[4] utilizes, as a measure of the usefulness of a section, the Mach number at which the low-speed, zero-lift drag coefficient of the NACA 0012 is doubled. The drag coefficient value suggested for reference is $C_{do} = 0.018$. A further refinement could be made by using drag coefficients approximately compensated for dynamic pressure and chord, such as $C_d \times M^2$ as shown in Figure 9, or $C_d \times (chord) \times M^2$ as would be necessary to take blade taper into account.

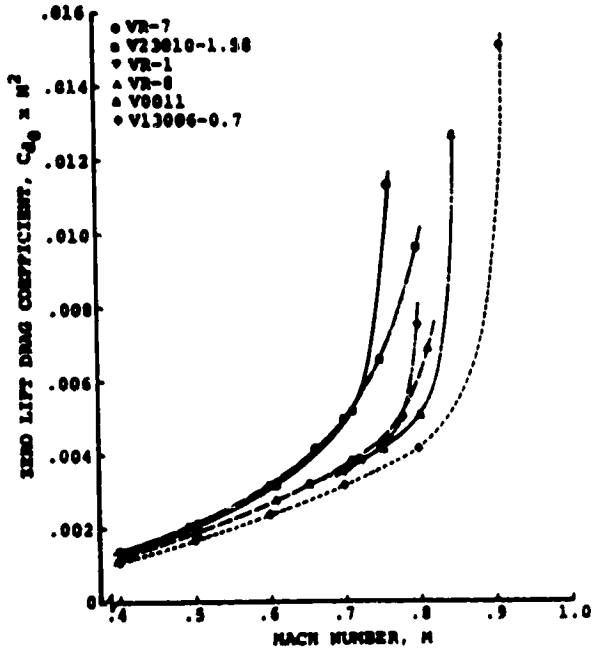


*Figure 9. Compressibility effects on airfoil drag at zero lift*

The approach used in Reference 4 is a good criterion by which to judge the usefulness of a section employed near the tip of a rotor blade; its disadvantage being that a reliable assessment of the drag rise can only be obtained through tests. However, since shock - boundary-layer interaction and flow separation are subjects of intensive research, in the near future, it might be possible to accurately estimate drag beyond drag divergence using analytical methods.

The rate of change of drag with Mach number, $dC_d/dM$, after drag divergence is not necessarily a good measure of drag performance because some sections undergo early drag "creep," followed by some leveling off of the drag with increasing Mach number until a steep drag-rise condition is reached. It is important to remember, however, that some sections display a more pronounced growth in drag after drag divergence than others; e.g., rooftop airfoils[2].

## 10. FORCE AND MOMENT COEFFICIENTS

Force and moment coefficients are nondimensionalized by the freestream dynamic pressure and a reference area. In the case of two-dimensional characteristics, the forces and moments are per unit length of span. The coefficients most commonly used in theoretical and experimental work are:

| | | | |
|---|---|---|---|
| $c_\ell$ | lift coefficient | *lift force*$/q_\infty c$ | on wind axis |
| $c_d$ | drag coefficient | *drag force*$/q_\infty c$ | on wind axis |
| $c_n$ | normal force coefficient | *normal force*$/q_\infty c$ | on body axis |
| $c_c$ | chordwise force coefficient | *chordwise force*$/q_\infty c$ | on body axis |
| $c_m$ | pitching moment coefficient | *moment*$/q_\infty c^2$ | |

where

$q_\infty = \frac{1}{2}\rho V_\infty^2$ is the freestream dynamic pressure, and $\rho$ is the density of the fluid medium.

Two-dimensional force and moment coefficients are identified by lower-case subscripts; for example, $c_\ell$, $c_d$, while three-dimensional coefficients are identified by capital subscripts; $C_L$, $C_D$. In helicopter rotor calculations, two-dimensional data is generally employed in conjunction with a strip-analysis approach.

Figure 10 illustrates the relationship and sign convention of forces and moments.

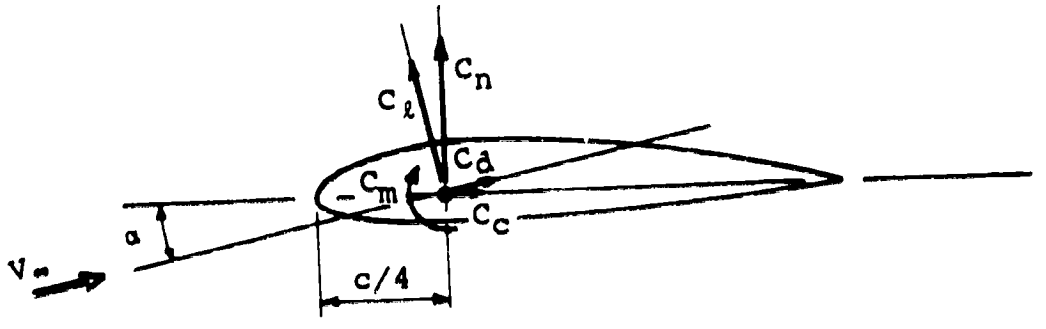


*Figure 10. Sign convention for forces and moments*

where

$$C_n = C_\ell \cos \alpha + C_d \sin \alpha$$

$$C_a = C_d \cos \alpha - C_\ell \sin \alpha.$$

The pitching moment is defined as positive in the nose-up direction (the direction of increasing angle-of-attack).

*NOTE: Unless otherwise noted, the pitching moment information contained in the DATCOM will be resolved about the quarter-chord.*

## 11. LIFT-BREAK BOUNDARY

The lift-break boundary is defined by the lift coefficient and Mach number values for which $dC_\ell/dM_\infty = 0$ when Mach number is increased at constant angle-of-attack. This boundary has been successfully related to rotor noise. Examples of lift-break boundaries are shown in Figure 11, and the derivation of a lift-break boundary is shown in Figure 12.

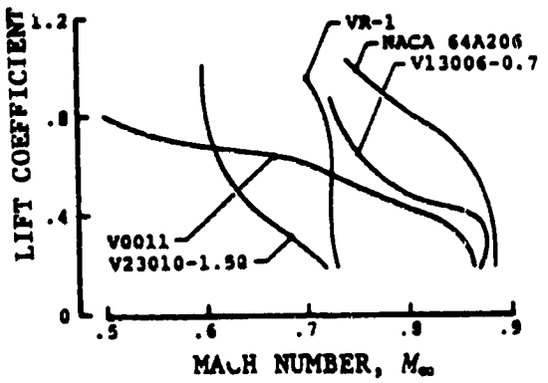


*Figure 11. Lift-divergence boundaries of several airfoils*

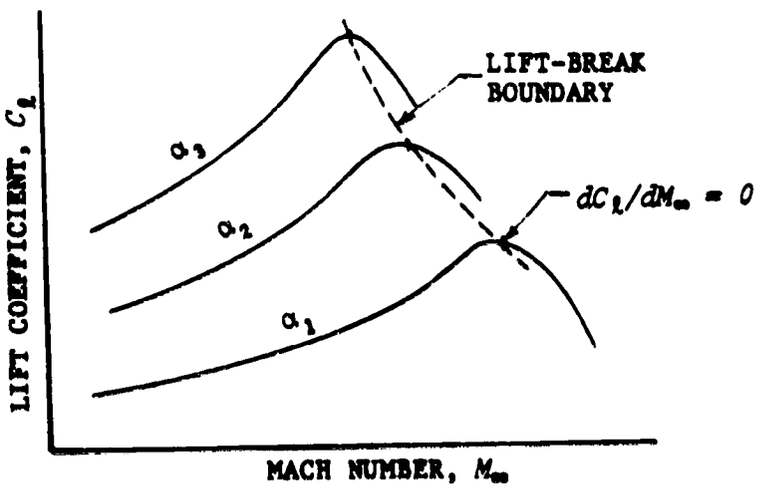


*Figure 12. Determination of lift-break boundary from lift-coefficient data*

## 12. LIFT-CURVE SLOPE

In incompressible, inviscid flow theory, the lift-curve slope $(dC_\ell/d\alpha)$ of a thin airfoil section is $2\pi/radian$ or $0.1097/deg$. Compressibility, viscous effects, and airfoil geometry influence the lift-curve slope. Compressibility effects can be accounted for by the Prandtl-Glauert rule, and the combination of thickness and compressibility by the Kaplan rule[1].

The Prandtl-Glauert relation is

$$\frac{(dC_\ell/d\alpha)_{comp}}{(dC_\ell/d\alpha)_{inc}} = \frac{1.0}{\sqrt{1.0 - M^2}} .$$

The Kaplan rule is

$$\frac{(dC_\ell/d\alpha)_{comp}}{(dC_\ell/d\alpha)_{inc}} = \mu + \frac{t/c}{1.0 + (t/c)}\left[\mu(\mu - 1.0) + \tfrac{1}{2}(\gamma + 1.0)(\mu^2 - 1.0)^2\right]$$

where

$\mu = 1.0/\sqrt{1.0 - M^2}$,

$\gamma$ *is the ratio of specific heats*, and

$t/c$ *is the thickness ratio of the airfoil.*

## 13. MACH NUMBER

Mach number is the ratio between the airspeed and the speed of sound. The Mach number is used in the correlation of phenomena in which compressibility effects cannot be considered negligible.

$$M = V/a$$

where the speed of sound: $a = \sqrt{\gamma RT}$.

In air, the specific heat ratio is $\gamma = 1.4$ for temperatures up to 1000°R, the gas constant $R = 1715\ ft\text{-}lb/slug°R$, so the speed of sound is $a_{air} = 49.1\sqrt{T}\ (ft/sec)$, for temperatures expressed in degrees Rankine.

Increasing the velocity over an airfoil section from low to high subsonic Mach numbers at constant angle-of-attack will cause flow conditions which can be described as follows:

INCREASING MACH NUMBER ↓

| | FLOW CONDITION | PHENOMENA OBSERVED |
|---|---|---|
| A. | Fully attached flow | • Drag is low<br>• Lift, pressure, and lift-curve slope vary as $1.0/\sqrt{1.0 - M^2}$<br>• $M_{local} < 1.0$ everywhere |
| B. | Incipient compressibility effects | • $M_{local} \rightarrow 1.0$ over some portion of the airfoil surface<br>• Drag is low, but no longer at minimum drag levels<br>• Loads start to deviate from the $1/\sqrt{1.0 - M^2}$ trend<br>• Early turbulent transition |
| C. | Full transition from subcritical to supercritical flow | • Drag divergence is reached, $dC_d/dM \geq 0.1$<br>• $dC_\ell/d\alpha$ reaches highest value and then decreases rapidly<br>• Lift and pitching moment start breaking (onset of lift break and "Mach tuck")<br>• $M_{local} > 1.0$ over a small portion of the airfoil surface |

D. Supercritical flow

- $M_{local} > 1.0$ over a substantial portion of the airfoil surface
- Large pitching moments
- Rapid drag rise beyond the drag divergence boundary.

## 14. COMPRESSIBILITY EFFECTS ON SECTIONAL PITCHING MOMENTS

The growth of pitching moments with Mach number became a significant parameter with the introduction of cambered airfoils and structurally softer blades. This phenomenon is referred to as "pitching moment break" or, borrowing the term from fixed-wing terminology, "Mach tuck." This growth in pitching moments coincides with the onset of transonic flow conditions, and it is associated with both a rearward shift in the aerodynamic center and an increase in pitching moments about the aerodynamic center.

The pitching moment break boundary can be defined either by some rate of change criteria; e.g., $dC_m/dM = constant$, or by an absolute pitching moment value corrected for chord and dynamic pressure, such as $C_m \times M^2$ shown in Figure 13, or $C_m \times (chord)^2 \times M^2$.

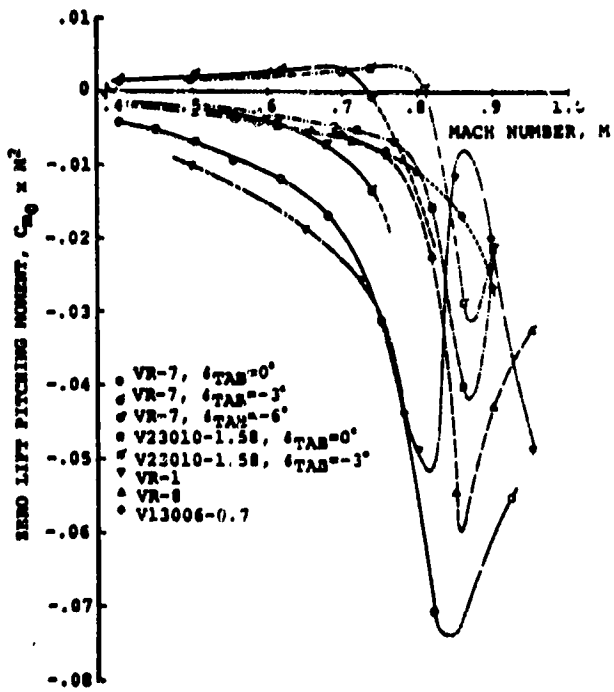


*Figure 13. Compressibility effects on airfoil pitching moment at zero lift*

## 15. MAXIMUM LIFT OR NORMAL FORCE COEFFICIENT

At low Mach numbers, the maximum lift coefficient from test data can be defined as the lift for $dC_\ell/d\alpha = 0.0$ as airfoil incidence is increased at constant Mach number. At higher Mach numbers ($M > 0.5$ for typical helicopter rotor airfoils) or, in the presence of thin airfoil stall, the maximum lift cannot always be defined as the condition at which $dC_\ell/d\alpha = 0$ because at angles-of-attack approaching stall, the lift-curve slope can decrease to low values without reaching $dC_\ell/d\alpha = 0$. This is illustrated in Figure 14. When $dC_\ell/d\alpha = 0$ is not a practical criterion, a finite value of $dC_\ell/d\alpha$ or $C_d$ can be used instead. In some airfoil work, a value of $C_d = 0.05$ has been suggested[5].

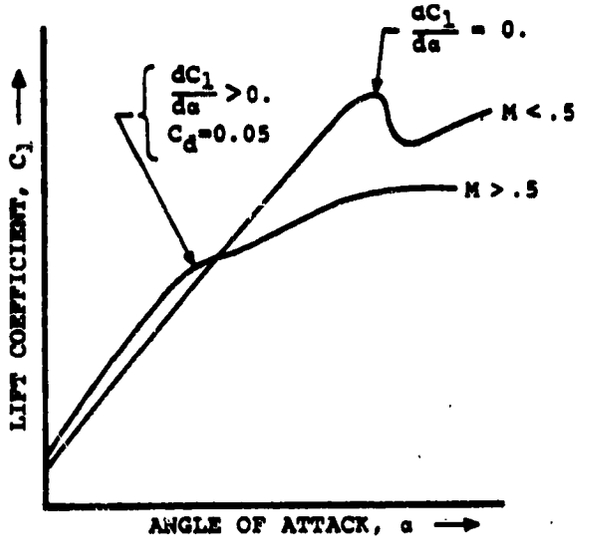


*Figure 14. Definition of maximum lift coefficient*

## 16. REYNOLDS NUMBER

The Reynolds number is a nondimensional parameter defined as the ratio of inertial to viscous forces. The Reynolds number level has to be taken into account when dealing with sectional data, since viscosity has a significant effect on key characteristics such as the drag coefficient and the maximum lift capability.

Reynolds number has the form:

$$R_e = \rho VL/\mu,$$

where

$V$ *is the velocity of the fluid*

$\rho$ *is density of the fluid*

$\mu$ *is absolute viscosity of the fluid*

$L$ *is a characteristic dimension of the body.*

In airfoil work, the characteristic dimension $L$ is taken to be the chord, although the maximum thickness could be used in correlating the drag of blunt bodies, and a Reynolds number based on boundary-layer thickness is used in boundary-layer theory.

Typical values at sea level standard conditions are:

$\rho = 0.002378$ *slugs/ft*$^3$

$\mu = 3.719 \times 10^{-7}$ *slugs/ft-sec*

*for* $M_\infty = 1.0$, $R_e = 7.1 \times 10^6$*/ft*

or $R_e = 5.93 \times 10^5$*/in.*

## 17. SUCTION LOOPS

Suction loops are used in evaluating the drag coefficient of an airfoil section from surface pressure measurements. In recent years, the suction loops obtained from incompressible, inviscid flow solutions have been used to judge the potential for good transonic performance on the basis of extensive correlation work with experimental data[2].

A suction loop is obtained by plotting theoretical or experimental pressure coefficients against a skewed coordinate, $z'/c$, measuring the distance between the surface of the airfoil and a line parallel to the remote wind, e.g. passing through the trailing edge, as illustrated in Figure 15.

As discussed in Reference 2, the transonic performance of an airfoil is related to the way in which the surface pressures, at low speeds, vary between the leading edge and the crest. A good transonic airfoil should have low-speed suction loops similar to the one shown in Figure 15, i.e. displaying a low $dC_p/d(z'/c)$ approaching the crest from the leading edge.

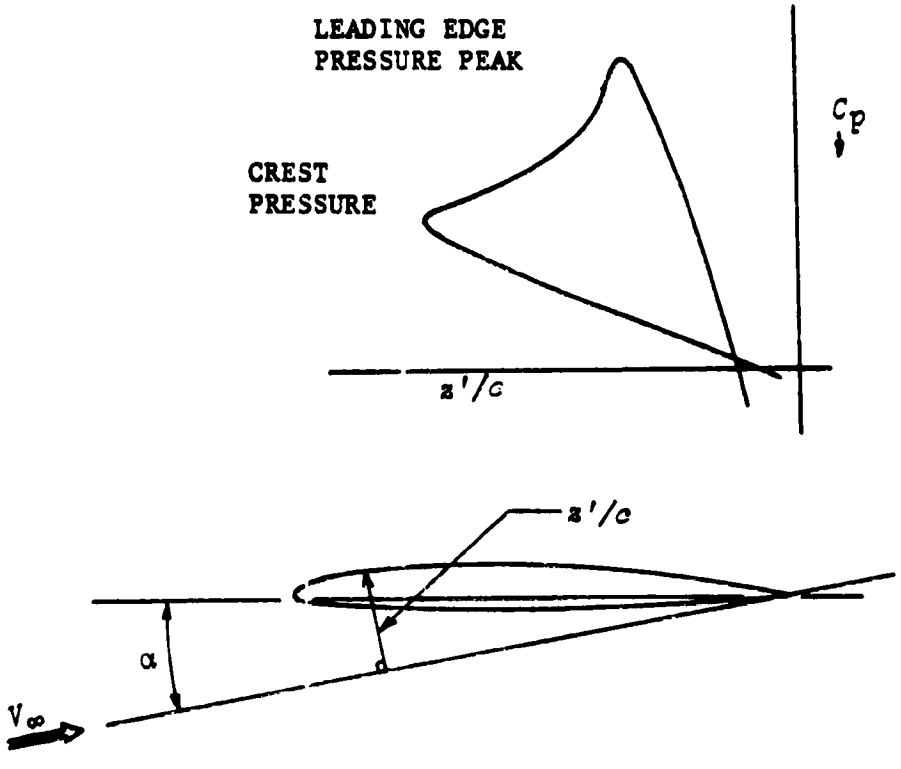


*Figure 15. Example of a suction loop*

## 18. STALL AND TYPES OF STALL

A commonly recognized definition of stall describes it as the flow condition which follows the first lift-curve peak[6]. As substantial separated regions develop with the onset of stall, sectional drag forces and pitching moments grow to very large values, while the lift, after reaching some maximum level, decreases to an after-stall level more or less rapidly, depending on the character of the stall.

The flow conditions over an airfoil as incidence is increased from zero lift through stall at constant Mach number can be summarized as follows:

INCREASED ANGLE-OF-ATTACK

| | Phenomena Observed |
|---|---|
| (1) Fully Attached Flow | • Linear $dC_\ell/d\alpha$ and $dC_m/d\alpha$<br>• Low drag coefficients |
| (2) Incipient Separation | • $dC_\ell/d\alpha$ and $dC_m/d\alpha$ become nonlinear<br>• Slow growth in drag |
| (3) Stall Events | • Attainment of maximum lift<br>• Pitching moment stall occurs within a small $\alpha$ excursion from $C_{\ell_{max}}$<br>• Reduction in lift beyond $C_{\ell_{max}}$. This change can be extremely abrupt in leading edge stall.<br>• Large increase in drag |
| (4) Separated Flow Beyond Stall | • Relatively small changes in loads with increasing angle-of-attack until angle-of-attack becomes very large ($\alpha > 20°$). |

As discussed in detail in Reference 7, there are three basic and clearly distinguishable types of stall. An airfoil can undergo one type of stall or some combination of two types, depending on its geometry, Reynolds number, and Mach number. The surface condition should be included as another variable, but there is not enough experimental information to allow any general conclusions to be drawn.

The three basic types of stall are described below, with illustrations from Reference 8.

*Trailing-Edge Stall* - Due to turbulent separation over the aft portion of an airfoil. Trailing-edge stall will start at the trailing edge and progress toward the leading edge. In some cases, the spreading of turbulent separation can be delayed by recontouring the trailing edge (e.g., eliminating the excessive cusp). Trailing-edge stall is gradual, and it is not accompanied by a sudden loss in lift. Static stall hysteresis is generally small. High-lift levels are possible.

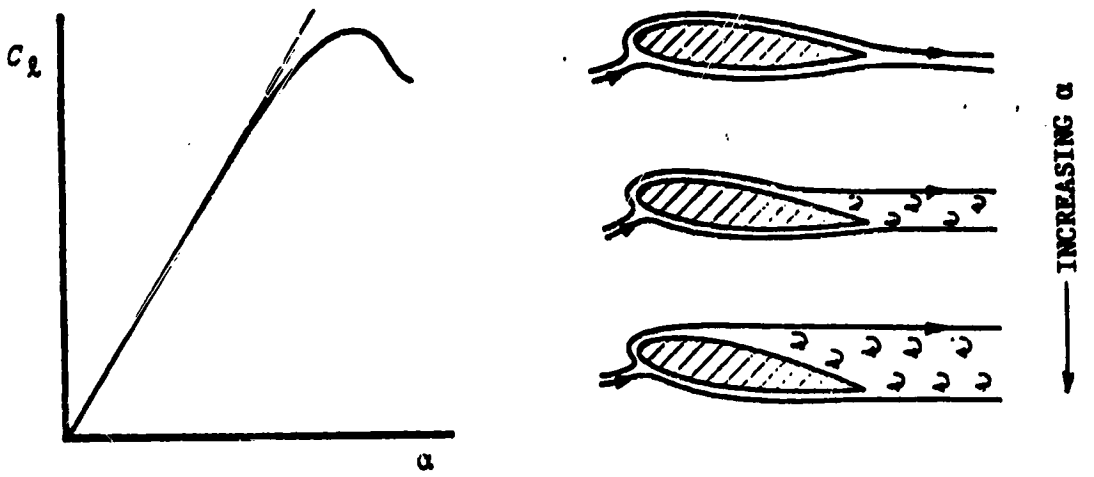


*Figure 16. Trailing-edge stall (Gradual)*

*Leading-Edge Stall* - Due to sudden separation of the boundary layer because of very high leading-edge velocities. Leading-edge stall will result in abrupt and large losses in lift. Static stall hysteresis is always large. High-lift levels are possible.

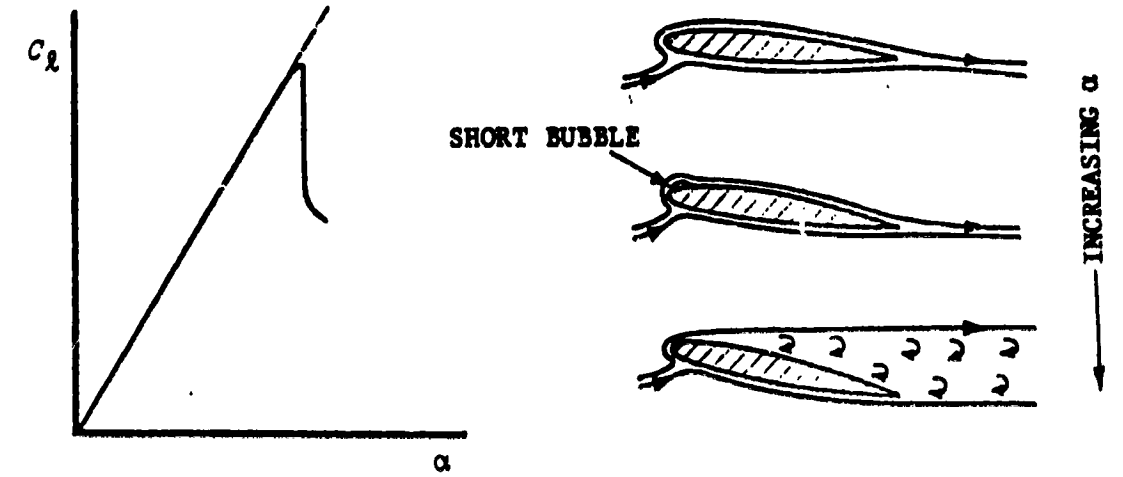


*Figure 17. Leading-edge stall (Abrupt)*

*Thin Airfoil Stall* - Associated with the growth and eventual bursting of a separated region which originates with laminar separation at the leading edge. This separated region, called a *laminar bubble*, reattaches downstream as a turbulent boundary layer. Actual stall occurs when the bubble reaches the trailing edge. Static stall hysteresis is very small, and the maximum lift-range is limited.

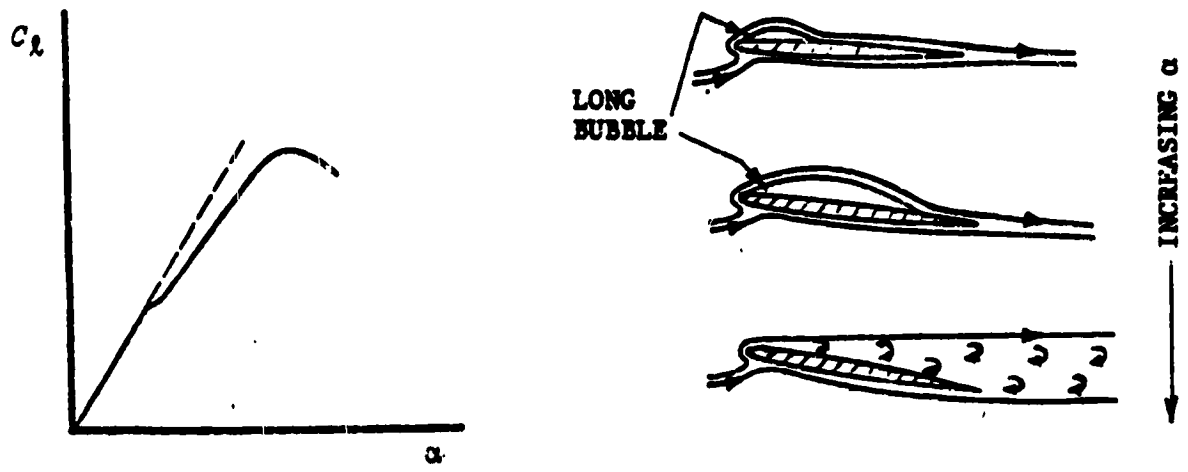


*Figure 18. Thin airfoil stall (Gradual)*

Some simple rules have been suggested to relate the leading-edge geometry of an airfoil to the type of stall[7], but such criteria do not work on all airfoils; one notable exception being airfoils of the NACA 230XX family.

## 19. STATIC STALL HYSTERESIS

Lift stall hysteresis is determined experimentally by increasing the incidence of an airfoil model until complete stall has been attained, and then by decreasing the incidence until the flow is again fully attached. Care should be taken to vary the incidence at a sufficiently slow rate to avoid any dynamic stall delay effects.

Leading edge stall airfoils display a large static stall hysteresis loop, whereas airfoils with trailing edge stall or thin airfoil stall have very little hysteresis. Oscillating airfoil experience has shown that airfoils with pronounced stall hysteresis under quasi-steady conditions will display substantial negative damping during forced pitch oscillation through stall.

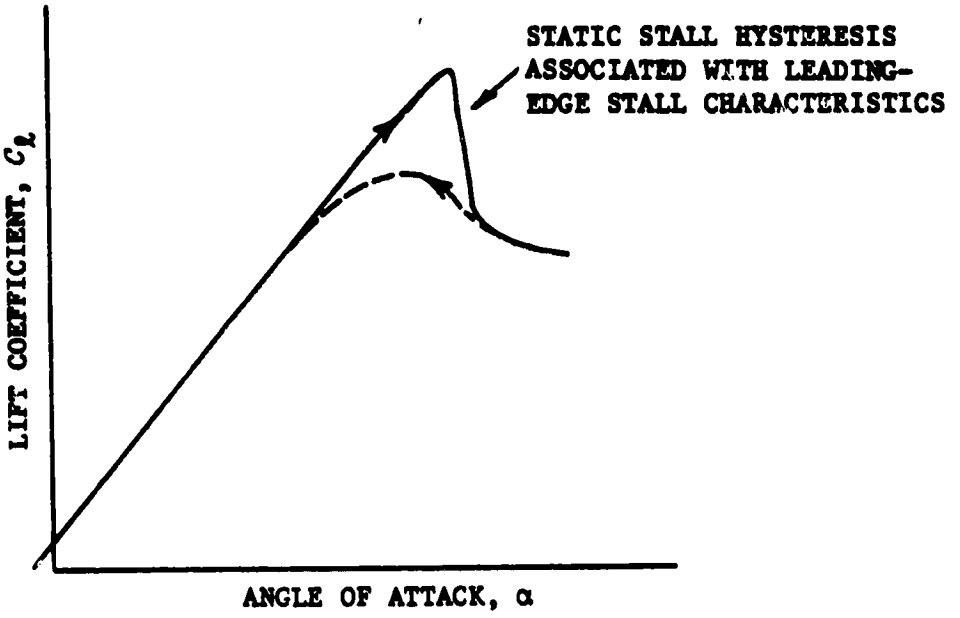


*Figure 21. Example of static stall hysteresis*

## 20. STROUHAL NUMBER

The Strouhal number relates the frequency of organized vorticity in the wake of a body to the stream velocity and some characteristic dimension of the body.

$$S = nD/V,$$

where

$n$ is the frequency of vortices in the wake

$D$ is a characteristic dimension of the body

$V$ is the stream velocity.

In the case of airfoils, the characteristic dimension is the thickness of the separated region at the trailing edge, although the trailing-edge thickness might be adequate for blunt or truncated airfoils. Trailing edge bluntness can result in vortex shedding within an audible range of frequencies.

For circular cylinders at $500 < R_e < 100{,}000$, the Strouhal number is approximately constant, with a value of $S = 0.21$ Ref. 9, p. 32).

## References


1. Abbott, I.H., von Doenhoff, A.E., *Theory of Wing Sections*. Dover Publications, Inc., N.Y., 1958.

2. Royal Aeronautical Society Transonic Aerodynamics Committee, *A Method of Estimating Drag-Rise Mach Number for Two-Dimensional Airfoil Sections*. Transonic Data Memorandum 6407, July 1964.

3. Bingham, G.J., *An Analytical Evaluation of Airfoil Sections for Helicopter Rotor Applications*. NASA TN D-7796, February 1975.

4. Davenport, F.J., Front, J.V., *Airfoil Sections for Rotor Blades - A Reconsideration*. Presented at the 22nd Annual Forum of the American Helicopter Society, May 12, 1966.

5. Dadone, L.U., McMullen, J., *HLH/ATC Rotor System Two-Dimensional Airfoil Test*. Boeing Document No. D301-10071-1.

6. McCullough, G.B., Gault, D.E., *Examples of Three Representative Types of Airfoil-Section Stall at Low Speed*. NACA TN 2502, 1951.

7. Gault, D.E., *A Correlation of Low-Speed, Airfoil-Section Stalling Characteristics with Reynolds Number and Airfoil Geometry*. NACA TN 3963, March 1957.

8. van den Berg, B., *Reynolds Number and Mach Number Effects on the Maximum Lift and the Stalling Characteristics of Wings at Low Speeds*. NLR TR 69025U, March 1969.

9. Schlichting, H., *Boundary-Layer Theory*. McGraw Hill Co. New York, N.Y., Sixth Edition, 1968.

## 1.1.40 DEFINITION OF AIRFOIL DESIGN CHARACTERISTICS

Design lift, ideal angle of attack, angle of zero lift and zero lift pitching moment are all airfoil characteristics used either to design or to catalog airfoils.

Because of the simplifying assumptions in thin airfoil theory, the best correlation with test data is obtained for airfoils with thickness not exceeding 10 to 12 percent of the chord and moderate camber slopes.

Design lift is the lift achieved at the ideal angle of attack. The ideal angle of attack is defined as the angle of attack at which the flow enters the leading edge smoothly or, more precisely, as the angle of attack at which the lift at the leading edge is zero.* The lift distribution at this particular angle is shown to be a characteristic property of the section and has been termed the "basic distribution." It is shown that the lift of a wing section may always be considered to consist of: (a) the basic distribution, and (b) the additional distribution, where the latter is independent of the mean camber line and thus, identical for all thin sections.[1]

Practically, the design lift corresponds to an operating condition close to the minimum drag level, and allows some excursion in lift above and below the design point with little penalty in drag.

Details of the determination of design characteristics can be found in any text on aerodynamics . There is one formulation by Glauert[2,3] which lends itself easily to either numerical or graphical integration. In Glauert's formulation, the angle for zero lift, the zero lift pitching moment and the design lift coefficients are, respectively:

$$\alpha_{\ell} = -\int_0^1 (y_c/c) f_1(x/c)(dx/c) \tag{1}$$

where the angle for zero lift is $\alpha_0 = -\beta_0$;

$$C_m = 2\mu_0 + (\pi/2)\alpha_{\ell} \tag{2}$$

---

* This condition of smoothness of flow at the leading edge, together with the Kutta condition at the trailing edge, are the basic assumptions of thin airfoil theory.

where

$$\mu_0 = \int_0^1 (y_c/c) f_2(x/c)(dx/c);$$

and

$$c_{\ell_i} = 2\pi(\alpha_i - \alpha_a)$$

where

$$\alpha_i = \int_0^1 (y_c/c) f_3(x/c)(dx/c). \tag{3}$$

The functions $f_1$, $f_2$, and $f_3$, respectively, are

$$f_1(x/c) = 1.0/\pi \left[1.0 - (x/c)\sqrt{(x/c)(1.0 - (x/c))}\right], \tag{4}$$

$$f_2(x/c) = \frac{1.0 - (2x/c)}{\sqrt{(x/c)[1.0 - (x/c)]}}, \tag{5}$$

$$f_3(x/c) = \frac{1.0 - (2x/c)}{2\pi\left[(x/c)[1.0 - (x/c)]\right]^{3/2}}. \tag{6}$$

The angle of zero lift, the zero lift pitching moment coefficient, and the design lift coefficient can be estimated graphically utilizing the values for $f_1$, $f_2$, and $f_3$ listed in Table I.

As the functions $f_1$, $f_2$, and $f_3$ become infinite at the leading and trailing edges, some portions of the integrals defining $\alpha_0$, $C_m$, and $\alpha_i$ must be evaluated analytically.[4] This is accomplished by assuming that near the ends, the mean line has a general form which can be expressed as

$$y/c = A + B(x/c) + C(x/c)^2. \tag{7}$$

By using Eq (7) in Eq (1), with $f_1(x/c)$ from Eq (4), and integrating from $x/c = 0.95$ to $1.0$, the contribution of the trailing edge to the angle for zero lift can be expressed as:

$$\Delta\alpha_a = -0.964 y_{0.95} + 0.0954(dy/dx)_1,$$

| $x/c$ | $f_1(x/c)$ | $f_2(x/c)$ | $f_3(x/c)$ |
|---|---|---|---|
| 0 | ∞ | ∞ | ∞ |
| 0.0125 | 2.901 | 8.774 | 113.150 |
| 0.0250 | 2.091 | 6.085 | 39.730 |
| 0.0500 | 1.537 | 4.131 | 13.840 |
| 0.0750 | 1.306 | 3.226 | 7.403 |
| 0.1000 | 1.179 | 2.667 | 4.716 |
| 0.15 | 1.049 | 1.960 | 2.447 |
| 0.20 | 0.995 | 1.502 | 1.492 |
| 0.25 | 0.980 | 1.156 | 0.980 |
| 0.30 | 0.992 | 0.873 | 0.662 |
| 0.40 | 1.083 | 0.408 | 0.271 |
| 0.50 | 1.273 | 0 | 0 |
| 0.60 | 1.624 | -0.408 | -0.271 |
| 0.70 | 2.315 | -0.873 | -0.662 |
| 0.80 | 3.979 | -1.502 | -1.492 |
| 0.90 | 10.610 | -2.667 | -4.716 |
| 0.95 | 29.210 | -4.131 | -13.840 |
| 1.00 | ∞ | ∞ | -∞ |

*TABLE I VALUES OF FUNCTIONS $f_1$, $f_2$, AND $f_3$*

where $y_{0.95}$ is the ordinate of the mean line at $x/c = 0.95$ and $(dy/dx)_1$ is the slope of the mean line at $x/c = 1.0$. At the leading edge, $f_1$ decreases so rapidly for $x/c > 0$ that a separate estimate of $\Delta\alpha_0$ for $x/c \to 0$ is unnecessary.

For the ideal angle of attack, substitute Eq (7) into Eq (3) and integrate, to obtain

$$\Delta\alpha_i = 0.467 y_{0.95} + 0.0472 (dy/dx)_0, \quad \text{from } x/c = 0 \text{ to } 0.05,$$

and

$$\Delta\alpha_i = -0.467 y_{0.95} + 0.0472 (dy/dx)_1, \quad \text{from } x/c = 0.95 \text{ to } 1.0.$$

Since $f_2(x/c)$ grows to large values only when very close to $x/c = 0$ and $x/c = 1.0$ (see Table I), a separate evaluation of the leading edge and trailing edge contributions to $\mu_0$ is not necessary.

## References

1. Theodorsen, T., *On the Theory of Wing Sections with Particular Reference to the Lift Distributions*, NACA Report No. 383, 1931.

2. Abbott, I.H., von Doenhoff, A.E., *Theory of Wing Sections*, Dover Publications, Inc., N.Y., N.Y., 1958.

3. Glauert, H., *The Elements of Aerofoil and Airscrew Theory*. Cambridge University Press, London, 1926.

4. Jacobs, E.N., Ward, K.E., and Pinkerton, R.M., *The Characteristics of 73 Related Airfoil Sections from Tests in the Variable-Density Wind Tunnel*, NACA Report No. 460, 1932.

## 1.2.10 AIRFOIL RELATED PROBLEMS AND SOLUTIONS

Knowledge of the sectional characteristics of airfoils employed on helicopter rotors, together with an understanding of the flow phenomena in the rotor environment, are essential for an evaluation of helicopter performance and optimization of a helicopter rotor for a particular mission.

The definition of airfoils resulting in an improved helicopter rotor is part of an iterative cycle. One example of such a cycle is illustrated below:

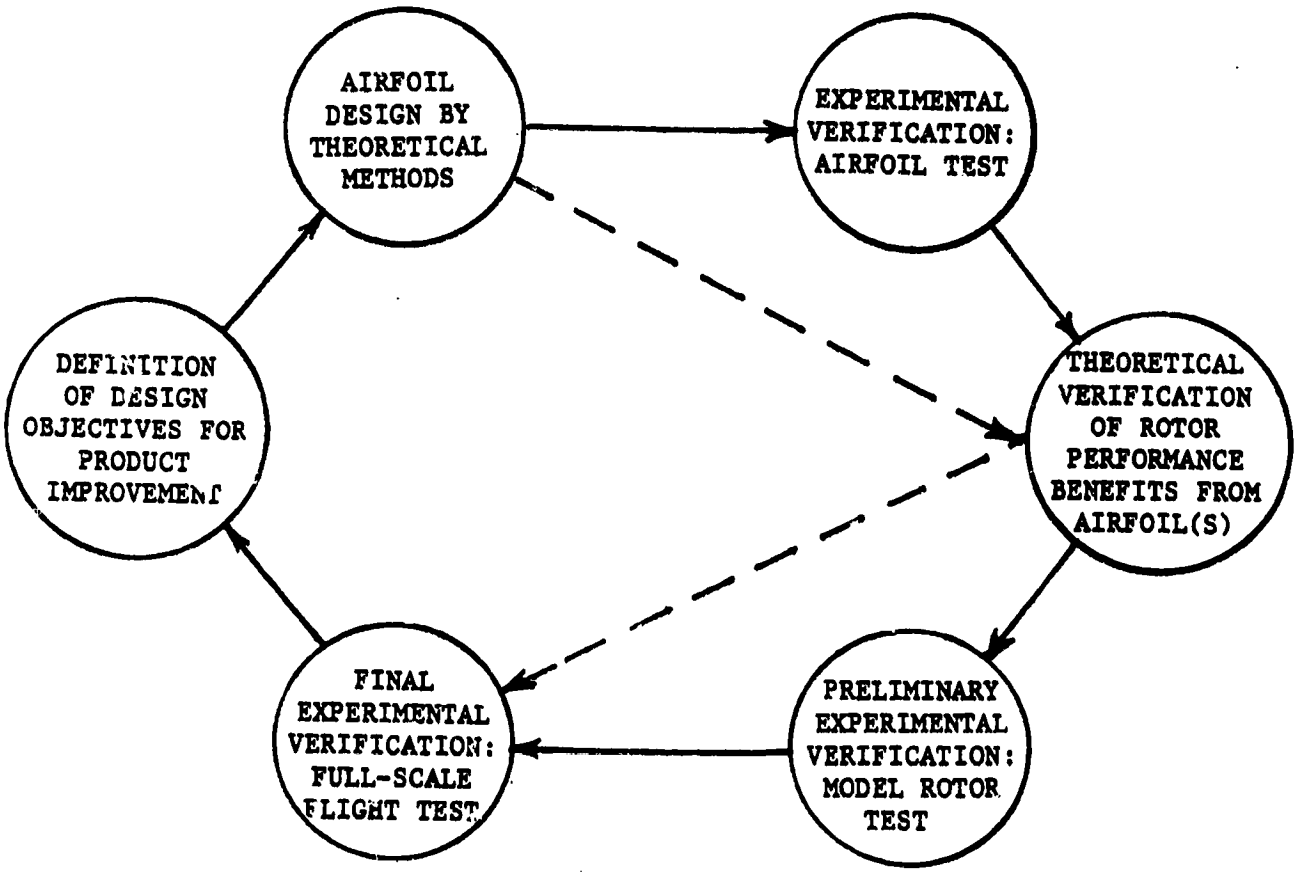


All the steps in the cycle are obviously important to the success of a rotor optimization effort, but airfoil improvement is only one of the available avenues. Concentration on airfoils alone would probably yield quite small returns.

Two of the steps in the cycle described above are particularly important and they can make the difference between a timely and successful design and a slow and costly effort. These steps are:

(1) the definition of realistic airfoil design objectives, and

(2) the ability to predict, by theoretical and empirical means, a number of key airfoil characteristics.

Of the two tasks, the definition of airfoil design objectives is the more difficult one.

As challenging as it is, rotor airfoil design is not the only reason to review and understand in detail the aerodynamics of airfoil sections. Presented below is a summary of some typical helicopter problems which could be solved through a study of rotor airfoil sections.

| PROBLEM AREA | SECTIONAL CHARACTERISTICS OF POSSIBLE INTEREST | TOOLS AVAILABLE TO SOLVE THE PROBLEM |
|---|---|---|
| Hover Performance | Drag penalty at moderate lift levels due to contour errors. | • Test data on contour errors<br>• Potential flow/boundary layer interaction methods for relatively smooth contour deviations. The effect of stimulated transition can also be verified. |
| | Sectional pitching moments not as expected, resulting in unfavorable effective twist, or pitch-link loading. | • Test data on trailing edge contour variations.<br>• Thin airfoil theory can be used to verify pitching moment levels.<br>• Test data to verify location of aerodynamic center with respect to shear center or c.g. |
| | Skin friction drag due to rough blade finish. | • Limited data on roughness effects on wings and airfoils.<br>• Theoretical determination of effect of stimulated transition. |

| PROBLEM AREA | SECTIONAL CHARACTERISTICS OF POSSIBLE INTEREST | TOOLS AVAILABLE TO SOLVE THE PROBLEM |
|---|---|---|
| Rotor Blade Tracking | Blade mismatch due to differences in local $C_m$ (and/or other blade characteristics such as mass distribution, $GJ$, and small twist differences). | • Standard solution: trim tabs over a limited portion of span.<br>• Trailing edge devices distributed along entire span for localized pitching moment correction, to be quantified by contour measurements and, if required, thin airfoil theory.<br>• Although the angle for zero lift can be shifted by changing trailing edge tab angles, this is generally undesirable because of the large changes in pitching moments associated with T.E. tab variations. Thus, T.E. tabs cannot generally be used to compensate for twist errors. |
| | Local separation due to contour error. | • Recontour locally on the basis of test data on discontinuities.<br>• Recontour locally on the basis of flow visualization observations. |
| Forward Flight Vibratory Loads Due to Inadequate Tracking | Separation effects on advancing blade at Mach number environment not covered by whirl-tower or other tracking procedures. | • Two- and three-dimensional test data on contour errors at supercritical flow conditions.<br>• Potential flow theory to determine pressure distributions. This data can be used to evaluate $M_{crit}$, $M_{dd}$, and qualitative differences between pressure distributions of actual and required contours. |
| | Inboard contour mismatch not determined on whirl tower because of low dynamic pressures. | • Thin airfoil theory for overall camber errors.<br>• Thin airfoil theory and test data on effect of T.E. contour variations. |

| PROBLEM AREA | SECTIONAL CHARACTERISTICS OF POSSIBLE INTEREST | TOOLS AVAILABLE TO SOLVE THE PROBLEM |
|---|---|---|
| Forward Flight Vibratory Loads Due to Premature Retreating Blade Stall | Maximum lift capability on retreating blade ($0.3 \leq M \leq 0.5$) due to:<br>• unexpected requirement exceeding sectional capability<br>• contour error resulting in loss in maximum lift capability. | • Loads prediction methodology utilizing quasi-steady sectional data and unsteady aerodynamic corrections for dynamic stall delay.<br>• Potential flow/boundary layer interaction methods for airfoils with separation criteria calibrated against test data.<br>• Experimental data on quasi-steady maximum lift capability and empirical understanding of contour variations. |
| Forward Flight Vibratory Loads on Advancing Blade | Pitching moment break on advancing blade resulting in torsional deflections and pitch link loads of unexpected magnitude. Such condition is due to operation beyond the critical Mach number boundary over the outboard portion of the blade because of:<br>• unexpected requirement exceeding sectional capability<br>• contour errors. | • Two- and three-dimensional test data on some contours and contour errors at supercritical flow conditions.<br>• Test data on the effect of trailing edge variation on supercritical pitching moments.<br>• Two-dimensional transonic flow analysis programs are available, but Mach tuck correlation is not yet complete.<br>• Contour inspection and review of surface waviness tolerances over portions of surface over which local flow is supersonic.<br>• Review of three-dimensional relief corrections used in performance and load-prediction methodology. |

| PROBLEM AREA | SECTIONAL CHARACTERISTICS OF POSSIBLE INTEREST | TOOLS AVAILABLE TO SOLVE THE PROBLEM |
|---|---|---|
| Forward Flight Vibratory Loads on Advancing Blade (Cont'd) | On "soft blades, drag can result in an additional torsional load due to outboard flap bending. | • Contour inspection and review of surface discontinuities in areas over which local flow is supersonic.<br>• If contours are correct, some drag reduction beyond drag divergence might be possible by local recontouring guided by some transonic flow analysis. |
| Speed Stability | Tilt of tip-path plane due to pitching moment break on advancing blade. | • Test data on the effect of trailing edge variations on pitching moments at supercritical conditions.<br>• Same overall approach as for Forward Flight Vibratory Loads. |
| Premature Power Limit in Forward Flight | If fuselage drag and other sources of power loss have been excluded:<br>• Overall drag level is too high due to surface finish or paint. | • If nonreflecting paint is used, an alternative might be to decrease grain size.<br>• In absence of test data, potential flow/boundary layer interaction methods can be used to evaluate effect of stimulated transition. |
| | • Due to manufacturing contour error consistent from blade to blade, and as such, not detectable in tracking. | • Review blade contours through systematic geometry measurements.<br>• Verify camber effects through thin airfoil theory or a thick airfoil potential flow method.<br>• Verify drag divergence boundaries. |

Cont....

| PROBLEM AREA | SECTIONAL CHARACTERISTICS OF POSSIBLE INTEREST | TOOLS AVAILABLE TO SOLVE THE PROBLEM |
|---|---|---|
| Premature Power Limit in Forward Flight (Cont'd) | | • Verify effect of curvature changes by potential flow/ boundary-layer interaction techniques.<br>• Two- and three-dimensional test data on some contours and contour errors at supercritical flow conditions. |
| Rotor Noise | Due to operation beyond the drag divergence boundary and the lift-break boundary. | • Determination of theoretical or experimental drag divergence boundaries.<br>• Experimental determination of lift-break boundaries.<br>• Rotor performance evaluation methods to establish flow environment and correlate noise with local flow conditions. |
| | Due to trailing edge bluntness. | • Noise frequency correlation with Strouhal number and thickness of separated region.<br>• Trailing edge modifications to decrease thickness without changing the effective mean line. |
| Tail Rotor Vibration at High Thrust Levels | Blade mismatch due to contour errors. | • Review of blade contours through systematic geometry measurements.<br>• Verification of camber effects through thin airfoil theory.<br>• Verify premature separation by means of potential flow/boundary layer interaction techniques. |

| PROBLEM AREA | SECTIONAL CHARACTERISTICS OF POSSIBLE INTEREST | TOOLS AVAILABLE TO SOLVE THE PROBLEM |
|---|---|---|
| Tail Rotor Vibration at High Thrust Levels | Camber or leading edge contour deviations affecting maximum lift capability of sections. | • Review of blade contours through systematic geometry measurements.<br>• Correlation of camber and leading edge contour data with information on maximum lift and stall characteristics.<br>• Potential flow/boundary layer interaction methods with separation criteria calibrated against test data.<br>Note:<br>The same airfoil section used on both main and tail rotors can have radically different maximum lift and stall characteristics because of differences in chord (Reynolds number). |

## 1.2.20 THEORETICAL METHODS OF AIRFOIL ANALYSIS

The determination of the theoretical characteristics of airfoils generally involves lengthy and complex calculations, but such calculations have become practical since the advent of high-speed computers. However, while such calculations are now possible and practical, a considerable amount of experience is often necessary to prepare the input to such methods and to correctly interpret the results.

This portion of the airfoil DATCOM summarizes the key features of various methods for the solution of the flow about an airfoil. Computer programs to carry out calculations by these methods are available to qualified users through various government agencies.

| METHOD | DESCRIPTION | APPLICATION | SOURCE |
|---|---|---|---|
| Thin Airfoil Theory | A potential flow method in which an airfoil is replaced by its mean line. The mean line is simulated by a vortex sheet of co tinuously varying vortex strength. The chordwise load distribution is a function of the vortex distribution. A condition for solution is that the mean line must coincide with a streamline; i.e., there is no flow through it. The most commonly used approach is the one by Glauert (see Sheet 1.1.40). | Although the thin airfoil theory can be used to design mean lines, modern airfoils are designed by studying the entire airfoil surface with thick airfoil methods. However, the thin airfoil theory can be used quite successfully in evaluating pitching moment levels and camber effects on airfoil incidence in conjunction with rotor blade tracking problems. | 1,2,7 |
| Thick Airfoils: Closed Form Solutions | As the potential flow field about a cylinder with circulation can easily be estimated, the flow field of an airfoil can be mapped into a circle by some conformal transformation. Joukowski airfoils can be mapped into a circle by the transformation $\zeta = z + a^2/z$ where $a$ is a real constant. | Joukowski airfoils are of little practical interest because they are limited to one type of thickness distribution (with a very thin and cusped trailing edge) and one type of mean line. However, they are sometimes used in theoretical work because of the ease with which camber and thickness effects can be evaluated. | 1,3 |
| Thick Airfoils: Modified Joukowski Transformation for Arbitrary Airfoil Shapes | This method, suggested by T. Theodorsen, is based on the fact that all airfoils are similar at the leading edge, with some small, but finite, curvature; all have sharp trailing edges, and continuously varying surfaces between leading and trailing edges. Because of this, the Joukowski transformation will map most airfoils into a nearly circular shape. Theodorsen showed that the "near-circle" can be mapped into a circle by a rapidly converging iterative method. | This method is seldom used because singularity methods are easier to use on high-speed computers. | 1,4,5,6 |

| METHOD | DESCRIPTION | APPLICATIONS | SOURCE |
|---|---|---|---|
| Thick Airfoils: Singularities Method (Vortex Polygon) | In the vortex polygon method, the airfoil surface is replaced by straight vortex sheet segments, and the strength of the corner vortices is computed on the basis of satisfying a flow direction constraint in the middle of each segment joining the corner points. | • Preliminary airfoil design<br>• Contour error verification<br>• Subcritical pressure distributions (inviscid with compressibility corrections)<br>• Estimate of $M_{crit}$<br>• Estimate of the drag divergence Mach number. | 8 |
| Potential Flow Boundary Layer Interaction Methods | These methods involve an iterative process through which an incompressible and inviscid airfoil solution is successively applied to an airfoil contour modified by the boundary layer thickness evaluated on the basis of velocity distributions from the previous iteration. Compressibility corrections are applied by means of the Karman-Tsien rule, or similar methods. Boundary layer calculations are based on airfoil Reynolds number. The methods available to date do not apply to the following conditions:<br>• shock/boundary layer interaction<br>• laminar bubbles (Ref. 1.1.30)<br>• separated regions<br>• surface roughness, except for that simulated by fixing the transition from laminar to turbulent boundary layer. | These methods are the main tool for airfoil design. The only precaution to be taken is that each method and set of conditions should be carefully calibrated against some set of test data.<br>Applications include:<br>• airfoil design<br>• evaluation of contour deviation effects<br>• drag optimization<br>• evaluation of maximum lift potential (conditional to absence of shock/boundary layer interaction effects). | 8,9,10, 11,12 |

| METHOD | DESCRIPTION | APPLICATIONS | SOURCE |
|---|---|---|---|
| Thin Airfoil Transonic Potential Method | Steady transonic flow past thin airfoils formulated using small disturbance theory. The governing transonic potential equation is a non-linear mixed (elliptic-hyperbolic) differential equation. Boundary value problem is resolved by analytical far-field solution. Near field is evaluated by a mixed finite difference system. Thickness effects are applied as transonic scaling parameters. This method offers rapid convergence and good correlation for lifting airfoils at transonic speeds as long as the substantial supersonic region is confined to one surface. As the method utilizes surface slopes and not actual airfoil contours, it cannot be extended to solutions including viscous (boundary-layer) effects. | Useful for preliminary design of transonic sections. Used in the evaluation of chordwise load distributions at transonic speeds. | 13,14 |
| Thick Airfoil Transonic Flow Solutions | Reference 16 describes an inverse method based on the hodograph transformation, utilizing finite differences to solve a characteristic initial value problem in complex space. | Used in the design of advanced airfoils for fixed-wing applications. Some advanced helicopter sections have also been studied (e.g., Ref. 17). | 16 |
| Thick Airfoil Transonic Flow Analysis with Viscous Effects | The Garabedian-Korn analysis (Ref. 16) has recently been extended to include boundary-layer effects. | When available, this method could be used for the design of airfoil sections to be employed near the tip of helicopter rotor blades. Pending verification of shock/boundary layer interaction criteria, this new method could also be used in studying Reynolds number effects at the transonic speeds necessary for model/full-scale rotor performance correlation. | 18 |

| METHOD | DESCRIPTION | APPLICATIONS | SOURCE |
|---|---|---|---|
| Unsteady Flow Modeling | A potential flow method for thick airfoils, which includes empirical models of:<br>• laminar bubble<br>• separated regions<br>• unsteady wake | The method was defined for helicopter rotor applications; however, the program is difficult to use because of the limitations imposed by the empirical models incorporated in it. | 15 |
| Superposition Methods | The velocity distribution about an airfoil can be shown to be a function of the separable effects of:<br>• thickness shape<br>• mean line<br>• angle of attack<br>where the velocities due to the mean line can be evaluated by thin airfoil theory, and the effect of thickness distribution and angle of attack by a thick airfoil solution.<br>Note:<br>This method has recently been extended to include the effect of $d\alpha/dt$, making use of appropriately modified Theodorsen functions. | Useful for the evaluation of approximate pressure distributions in absence of separation when mean line and thickness contributions are known. | 1<br>19,20 |

## References


1. Abbott, I.H., and von Doenhoff, A.E., *Theory of Wing Sections*. Dover Publications, Inc., New York, N.Y., 1959.

2. Glauert, H., *The Elements of Aerofoils and Airscrew Theory*. Cambridge University Press, London, 1926.

3. Milne-Thomson, L.M., *Theoretical Hydrodynamics*. MacMillan Co., New York, 1960.

4. Theodorsen, T., *Theory of Wing Sections of Arbitrary Shape*. NACA Report No. 411, 1931.

5. Theodorsen, T., Garrick, I.E., *General Potential Theory of Arbitrary Wing Sections*. NACA Report No. 452, 1933.

6. Rauscher, M., *Introduction to Aeronautical Dynamics*. New York, N.Y., 1953.

7. Bisplinghoff, R.L., Ashley, H., and Halfman, R.L., *Aeroelasticity*. Cambridge, Mass., 1955.

8. Dvorak, F.A., Brune, G., Knutsen, R.W., and Mahal, A.S., *Viscous/Potential Flow Interaction Program*. USAAMRDL, 1972.

9. Stevens, W.A. Goradia, S.H., and Braden, J.A., *Mathematical Model for Two-Dimensional Multi-Component Airfoils in Viscous Flow*. NASA CR-1843, July 1971.

10. Nitzberg, G.E., *A Concise Theoretical Method for Profile-Drag Calculation*, NACA ACR No. 4B05, 1944.

11. Squire, H.B., and Young, A.D., *The Calculation of the Profile Drag of Aerofoils*, R&M No. 1838, British ARC, 1938.

12. Schlichting, H., *Boundary-Layer Theory*. McGraw-Hill, New York, N.Y., 6th Edition, 1968.

13. Murman, E.M., Cole, J.D., *Calculation of Plane Steady Transonic Flows*. BSRL Doc. No. D1-82-0943, Jan. 1970.

14. Krupp, J.A., *The Numerical Calculation of Plane Steady Transonic Flows Past Thin Lifting Airfoils*, BSRL Doc. No. D180-12958-1. (Also published as a Ph.D. Thesis, Dept. of Aeronautics and Astronautics, Univ. of Washington, June 1971).

15. Crimi, P., and Reeves, B.L., *A Method for Analysing Dynamic Stall of Helicopter Rotor Blades*. NASA CR-2009, May 1972.

16. Bauer, F., Garabedian, P., Korn, D., *A Theory of Supercritical Wing Sections, with Computer Programs and Examples.* Springer-Verlog, Berlin, Heidelberg, N.Y., 1972.

17. Kemp, L.D., *An Analytical Study for the Design of Advanced Rotor Airfoils.* NASA CR-112297, March 1973.

18. Bauer, F., Garabedian, P., Korn, F., and Jameson, A., *Supercritical Wing Sections II.* Springer-Verlog, Berlin, Heidelberg, N.Y., 1975.

19. McCroskey, W. J., *The Inviscid Flowfield of an Unsteady Airfoil.* AIAA Paper No. 72-681, 1972.

20. McCroskey, W.J., Philippe, J.J., *Unsteady Viscous Flow on Oscillating Airfoils.* AIAA Paper No. 74-182, 1974.

## 1.2.30 EXPERIMENTAL TECHNIQUES FOR THE DETERMINATION OF AIRFOIL CHARACTERISTICS

An ideal test setup allows quantitative measurements of a phenomenon within the actual environment in which the phenomenon takes place. The tools employed to carry out such measurements should have as little effect as possible on the environment.

To the extent that an *ideal* test setup cannot be achieved, the comparison of data from different tests measuring the same phenomenon can easily be misleading. This is quite true of the flow environment around airfoil sections.

The objective of this portion of the DATCOM is to review the overall significance of airfoil data acquired in two- and three-dimensional testing.

### Two-Dimensional Models

An airfoil model can be defined as two-dimensional when provisions have been made to eliminate flow variations along the entire span of the model, thus simulating an infinite aspect ratio.

However, while two-dimensionality is possible when the flow over a model is fully attached, this definition becomes arbitrary when any degree of flow separation is present because of the intrinsic three-dimensional character of separated flows. Three-dimensional effects within regions of separated flow are significantly influenced by the actual length of a two-dimensional model. For this reason, while data at lift levels below the maximum lift are affected to a relatively small degree by model characteristics and testing techniques; at lift levels approching the maximum lift, the flow ceases to be truly two-dimensional over an ever increasing portion of the airfoil surface, and the test setup conditions have a significant impact on maximum lift, stall, and after-stall behavior.

### Test Setup

The finer details concerning the equipment in each test are rarely described in the test documentation. Therefore, it is assumed that no problems were encountered when such details are not covered in the reports. Some examples of this assumption would be:

- The balance system, when employed, always operated correctly.
- Balance tares and interactions were checked out and applied to the data.

- The measuring equipment was always correctly sized to the magnitude of the loads to be measured.
- Model motions and deflections were negligible.
- An adequate seal was provided between model and tunnel walls.
- Wake probe data was obtained by surveying with an adequate sampling rate over a sufficiently large wake area.

Since differences among test setups cannot be defined either quantitatively or qualitatively with any accuracy, the value of comparative test data on different airfoils can be judged only on the basis of consistency. If the data is to be comparable from the point of view of Mach and Reynolds number conditions, such consistency can be achieved in two ways:

(1) By testing different airfoils in the same wind-tunnel facility with the same kind of models.

(2) By assessing the compatibility of different sources through the comparison of test data for at least one reference airfoil.

A substantial portion of the data sheets have been devoted to Boeing-Vertol airfoil sections because they were tested at the same wind tunnel, with the same test section configuration, and with models similar to each other in chord and span. Although the absolute level of the data might be questionable, the results are still valuable because they provide the basis for assessing the effect of a number of geometry variations on aerodynamic performance.

It would be impossible to discuss all wind-tunnel test variables and test corrections; in most cases, a detailed description of the test variables is not available. The following tables (I through IV) describe some of the equipment and techniques used in wind-tunnel testing, and will provide the user of the DATCOM with guidance as to the value of a comparison of airfoil data from different sources.

| DESCRIPTION | LIMITATIONS AND MAIN EFFECTS ON DATA |
|---|---|
| Closed Circuit Atmospheric | Reynolds number and Mach number combinations limited to values set by model chord. Since the tunnel can run continuously, the amount of data is limited only by the capabilities of the data acquisition system. |
| Closed Circuit Pressurized | Reynolds number and Mach number combinations can be varied as a function of both model chord and tunnel pressure . Tunnel pressures can be selected to match full-scale conditions, while employing reduced-scale models, within the pressure capability of the system. |
| Open Circuit Tunnels - Blowdown | Typically, in blowdown tunnels, the pressure in the test section can be varied. Therefore, the Reynolds number and Mach number capability is the same as for pressurized tunnels. However, the amount of data is limited by the relatively short duration of each run. |
| Water Tunnels | Small chords can be used to explore large Reynolds number conditions, with the limitation that the flow is incompressible and locally subject to cavitation. |

*TABLE I - TYPE OF WIND TUNNEL*

| DESCRIPTION | LIMITATIONS AND MAIN EFFECTS ON DATA |
|---|---|
| Wall Porosity | To simulate, in a wind tunnel, the streamline pattern occurring around an object in flight through free air, the walls in the test section have to be porous to allow some flow through them. If the model size is negligible compared to the size of the test section, this precaution is not necessary.<br><br>In two-dimensional testing, the sidewalls establishing the two-dimensional character of the flow must be solid (possibly with provisions to control the wall boundary layer); but some porosity is necessary above and below the airfoil to minimize wall influence on the streamlines. Through its effect on the streamlines, wall porosity influences the effective angle-of-attack of a wing or airfoil model, and it will influence the lift-curve slope, $dC_\ell/d\alpha$, and the pitching moment slope, $dC_m/d\alpha$.<br><br>Typically, a solid floor and ceiling will cause a low value in the lift-curve slope. With increasing porosity, such value will increase to about the theoretical value; to decrease again if the flow through the boundaries is excessive. Note, however, that since wind-tunnel wall corrections are available to account for wall effects, it is not always necessary, though desirable, to employ wall porosity. |
| Wall Boundary-Layer Control | Wall boundary-layer control (BLC) is often necessary to minimize separation at the intersection between the airfoil model and the walls of the test section. This is particularly important at high-lift levels.<br><br>The main disadvantage in employing BLC is that it might suppress some separation which is not due to wall interference and thus cause misleading maximum lift and stall patterns. Wall suction is probably better than wall blowing from this standpoint, but suction is difficult to achieve and it is seldom used. |
| Turbulence Level | The flow in the test section of every wind tunnel is turbulent to some degree. Some tunnels have a very low turbulence level because of the use of turbulence reduction devices, such as honeycomb or screens ahead of the test section inlet. Typically, turbulence levels are obtained from drag measurements on a sphere. Turbulence, as a velocity fluctuation referenced to the freestream velocity, can be measured with hot wire or hot film anemometers. Cont'd... |

*TABLE II - TEST-SECTION CHARACTERISTICS*

| DESCRIPTION | LIMITATIONS AND MAIN EFFECTS ON DATA |
|---|---|
| Turbulence Level (Cont'd) | A very turbulent flow environment will cause premature transition on airfoils which have a potential for extensive laminar boundary layers, thus reducing the characteristic low drag "bucket" that such sections display over some lift range above and below design lift, and under some circumstances, a turbulent flow environment might also affect the maximum lift capability of a section.<br><br>The combination of surface roughness on airfoil models and turbulence level in the test section makes determination of minimum drag levels a very difficult task. |
| Velocity Gradients | At some conditions, an uneven velocity distribution across the test section is possible even in the absence of a model. Of course, such a condition is accentuated by the presence of a model, particularly at high-lift levels or at high subsonic Mach numbers. Some testing techniques provide a flow environment in which substantial velocity gradients are always present. An example of this is the transonic "bump" technique. Pre-existing velocity gradients can have a severe impact on data, particularly when the data involves velocity surveys, as in the case of momentum loss (drag) measurements. |
| Model Size vs Test-Section Size | In two-dimensional testing, the presence of a floor and ceiling prevents the normal curvature of the streamlines, and it causes an apparent increase in camber. Although wall effects can be accounted for, it is desirable to test airfoil models with a chord as small as possible compared to tunnel height. In most tests, a tunnel height-to-chord ratio, $h/c$, of at least 4, has been commonly employed. Wall effects can be further reduced by wall porosity. |

*TABLE II - TEST-SECTION CHARACTERISTICS (CONT'D)*

| DESCRIPTION | LIMITATIONS AND MAIN EFFECTS ON DATA |
|---|---|
| Two-Dimensional Models | • Low span-to-chord ratio will result in excessive sensitivity to sidewall separation effects.<br>• High span-to-chord ratio can limit the test range because of model deflections.<br>• For good two-dimensional characteristics, the model must be adequately sealed at the tunnel walls.<br>• If the model is equipped with end-plates to minimize detrimental effects, such plates must be:<br>a) Flush with the walls of the test section<br>b) Properly sealed to avoid leakage<br>c) Free to move (small excursions) along a plane parallel to the walls of the test section when an external balance system is the source of data<br>d) Properly calibrated to determine force and pitching moment tares. |
| Three-Dimensional Models | For fixed-wing applications, models of actual wing configurations are tested either in conjunction with a complete aircraft model or as half-span wing models mounted on the floor, or a sidewall, of the test section. For helicopter applications, wings of rectangular planform have been tested, although such data is hard to relate to two-dimensional characteristics and tests of this nature have value mostly on a comparative basis. |
| End Plates | End plates will cause problems if they<br>1) Leak around their perimeter<br>2) Cause wall boundary-layer separation<br>3) Cause balance interference.<br>When both airfoil model and end-plates are mounted on a balance, an end-plate contribution to the drag and the pitching moment must be accounted for. |
| End Seals | Wings and airfoil models cannot be firmly attached to the walls of the test section for a number of reasons, including the fact that some means has to be available to change the angle of incidence. Cont'd... |

*TABLE III - MODEL CONFIGURATION*

| DESCRIPTION | LIMITATIONS AND MAIN EFFECTS ON DATA |
|---|---|
| End Seals (Cont'd) | Air leakage in the proximity of tunnel sidewalls can occur in many places, often with significant impact on the overall flow environment. Whenever leakage can be foreseen, some method of restricting it has to be provided without interfering with the mechanical functions of the model and instrumentation.<br><br>It is impossible to generalize on the sources of possible air leaks. The following areas have shown the greatest potential for problems:<br>• Edge of end-plates, resulting in flow through the sidewalls<br>• Model mounting assembly, resulting in flow through the sidewalls<br>• Edges of airfoil model - flow from pressure to suction side of airfoil.<br><br>The effect of leakage can be determined from force and moment measurements and flow visualization techniques. Only flow visualization, however, will help in isolating the trouble areas. |
| Surface Roughness and Stimulated Boundary-Layer Transition | During the 1940's, NACA established a criterion for "standard" roughness. In accordance with that criterion, a level of roughness was applied systematically to many airfoils tested during that period. The standard leading-edge roughness selected by NACA for 24-inch models consisted of 0.011-inch carborundum grains applied to the surface of the model at the leading edge over a surface length of $0.08c$, measured from the leading edge on both surfaces. The grains were thinly applied to cover 5 to 10 percent of the area.<br><br>Such roughness is representative only of wing surfaces under the most extreme conditions. At standard operating conditions, the resulting conditions would be considerably less severe. "Standard" roughness is seldom used today.<br><br>Current practice calls for the application of narrow "trip" strips over wing and airfoil surfaces. This is done to verify the sensitivity of the drag to various extents of laminar flow, and to stimulate larger "effective" Reynolds numbers by precipitating earlier transition. When employing this technique, care should be exercised to apply only the minimum<br>Cont'd... |

*TABLE III - MODEL CONFIGURATION (CONT'D)*

| DESCRIPTION | LIMITATIONS AND MAIN EFFECTS ON DATA |
|---|---|
| Surface Roughness and Stimulated Boundary-Layer Transition (Cont'd) | grit size necessary to stimulate boundary-layer transition. Excessive grit size would cause an increase in drag beyond the amount due to a reduction in the extent of laminar boundary layer. |

*TABLE III - MODEL CONFIGURATION (CONT'D)*

| DESCRIPTION | LIMITATIONS AND MAIN EFFECTS ON DATA |
|---|---|
| Force and Moment Measurements by Balance | Body axis measurements have to be resolved along the wind axis. This can result in large errors in drag (see Sheet 1.1.30-15).<br>Wall interference will cause drag increments and penalties in maximum lift which are proportional to the amount of wall-induced separation.<br>Accurate balance tares and interactions are necessary. |
| Pressure Measurements and Integration of Pressures | Pressure orifices have to be located at sufficient distance from the tunnel walls to avoid the effects of wall boundary-layer or wall-induced separation.<br>Differential pressures; i.e., the measurement of the pressure difference between top and bottom surface at the same chordwise position, will allow the determination of normal forces and pitching moments only. Since the determination of absolute pressures would require twice as many pressure measurements as differential pressures, absolute pressure data is required only when differential data would not provide meaningful information.<br>Insufficient instrumentation near the trailing edge of an airfoil will result in erroneous pitching moments.<br>The determination of detailed load distributions at transonic flow conditions requires a large number of pressure orifices distributed along the entire chord. This is necessary to determine the chordwise location of the recompression boundary, since that boundary shifts considerably as a function of incidence and Mach number.<br>When time-varying pressure measurements are made, the resonant frequency as well as the time-lag effects introduced by the ducts have to be taken into account. When it is anticipated that these effects would be significant, the data must be acquired by means of pressure transducers located very close to each pressure port. |
| Wake Momentum Loss Measurements | The most accurate method for the determination of drag involves the measurement of the momentum loss in the wake of a wing or airfoil.<br>Three methods are commonly used:<br>1) Wake traversing probes<br>Cont'd... |

*TABLE IV. MEASUREMENT SYSTEM*

| DESCRIPTION | LIMITATIONS AND MAIN EFFECTS ON DATA |
|---|---|
| Wake Momentum Loss Measurements (Cont'd) | 2) Wake rakes<br>3) Direct integration wake probes.<br><br>Wake traversing probes consist of a total pressure probe and a static pressure probe supported by a mechanism which moves them through the wake of an object. Records are made of probe position and pressure values. The area traversed in a momentum survey must include positions above and below the airfoil for which the momentum loss is no longer measureable.<br><br>A wake rake performs the same function as a traversing wake probe, but instead of moving across the wake, it is fixed in space and samples the entire momentum loss region with a large number of individual pressure probes. While wake rakes allow rapid acquisition of data, the resolution capability of a rake can be severely impaired at low drag levels by the size of the momentum loss region compared to the distance between pressure measurement locations.<br><br>Direct integration probes determine, with one measurement, the total momentum loss in the wake. Typically, direct integration techniques are used on wake rakes modified to channel the ducts from each individual tube to a common plenum chamber. The pressure in the plenum is then measured and referenced to the freestream total pressure.<br><br>The usefulness of momentum loss measurements is limited to conditions resulting in relatively small momentum loss regions. Stall or flow conditions causing extensive shock systems will create wakes which cannot be easily surveyed. |

*TABLE IV. MEASUREMENT SYSTEM (CONT'D)*

## 1.2.40 TABULATION OF KEY THEORETICAL AND EXPERIMENTAL CHARACTERISTICS

This data sheet summarizes the sectional characteristics most often used in comparing helicopter rotor airfoils. The data in the following table is for the airfoils presented in data sheets 1.3.10 through 1.3.43.

The information for each airfoil includes:

1. Maximum lift coefficient values at Mach numbers of interest in assessing the potential for delaying retreating blade stall $(0.3 \leq M \leq 0.5)$.

2. Zero lift drag divergence Mach number as a measure of advancing blade performance.

3. Drag coefficient at $M = 0.6$ and $C_\ell = 0.6$ as a measure of hover performance potential.

4. Zero lift angle-of-attack and pitching moment coefficient at low speeds $(M < 0.4)$.

5. Reynolds number levels. For reference, the table shows the test Reynolds number at $M = 0.4$.

6. Geometric characteristics: thickness, camber, and leading-edge radius.

7. Trailing-edge configuration, when different from the standard NACA configuration (e.g., trailing-edge tab).

| AIRFOIL | DATA SHEET NUMBER | t/c | L.E.R. r/c | MAXIMUM CAMBER | | T.E. TAB | | MODEL CHORD (in) |
|---|---|---|---|---|---|---|---|---|
| | | | | x/c | y/c | $\frac{c_{tab}}{c}$ | $\delta_{tab}$ (deg) | |
| NACA 0006 | 1.3.10 | 0.06 | 0.004 | — | — | — | — | 7.0 |
| NACA 0012 | 1.3.20 | 0.12 | 0.0158 | — | — | — | — | 10.0 |
| NACA 0012 Reverse flow data | 1.3.30 | 0.12 | 0.0158 | — | — | — | — | 6.0 |
| NACA 0012 with 0° T.E. Tab | 1.3.40 | 0.117 | 0.0154 | — | — | 0.04 | 0.0 | 16.4 |
| NACA 0012 with -3° T.E. Tab | 1.3.50 | 0.117 | 0.0154 | — | — | 0.04 | -3.0 | 16.4 |
| NACA 0015 | 1.3.60 | 0.15 | 0.0248 | — | — | — | — | 6.0 |
| NACA 23012 | 1.3.70 | 0.12 | 0.0158 | 0.15 | 0.01838 | — | — | 5.0 |
| NACA 23012 with .043c T.E. Tab | 1.3.80 | 0.12 | 0.0158 | 0.15 | 0.01838 | 0.043 | 0.0 | 5.0 |
| NACA 23012 with .087c T.E. Tab | 1.3.90 | 0.12 | 0.0158 | 0.15 | 0.01838 | 0.087 | 0.0 | 5.0 |
| NACA 23015 | 1.3.100 | 0.15 | 0.0248 | 0.15 | 0.01838 | — | — | 6.0 |
| NACA 63A009 | 1.3.110 | 0.09 | 0.00607 | — | — | — | — | 8.0 |
| NACA 63A012 | 1.3.120 | 0.12 | 0.01075 | — | — | — | — | 8.0 |
| NACA 63A012 Reverse flow data | 1.3.130 | 0.12 | 0.0107 | — | — | — | — | 8.0 |

| $C_{l_{MAX}}$ at | | | $M_{DD}$ @ ZERO LIFT | $C_d$ at M=0.6 $C_l$=0.6 | LOW SPEED (M<0.4) | | $Re \times 10^{-6}$ at M=0.4 | REMARKS | REF. |
|---|---|---|---|---|---|---|---|---|---|
| M=0.3 | M=0.4 | M=0.5 | | | $C_{m_o}$ | $\alpha_o$ (deg) | | | |
| 1.037 | 1.017 | | 0.875 | 0.015 | 0.0 | 0.0 | 5.2 | | 7<br>8 |
| 1.144 | 1.080 | 0.967 | 0.765 | 0.0122 | 0.0 | 0.0 | 2.2 | Test 1 with leading edge roughness | 2 |
| — | — | — | — | — | 0.0 | 0.0 | 1.8 at low speed | Tested for angles of attack from 0° to 180° | 16 |
| 1.27 | 1.14 | 1.01 | insuff. data | 0.0077 | 0.0 | 0.0 | 2.6 | H-34 main rotor airfoil | 3 |
| 1.205 | 1.08 | 0.96 | no drag data | | 0.015 | 0.8 | 2.6 | H-34 main rotor airfoil | 3 |
| 1.07 | 0.99 | 0.92 | 0.74 | 0.0132 | 0.0 | 0.0 | 1.3 | | 20 |
| — | 1.38 | 1.22 | 0.795 | 0.029 | -0.010 | -1.2 | 2.5 | | 12 |
| — | 1.42 | 1.28 | 0.78 | 0.029 | -0.0075 | -1.0 | 2.5 | | 12 |
| — | 1.42 | 1.28 | 0.78 | 0.029 | -0.005 | -0.95 | 2.5 | | 12 |
| 1.24 | 1.30 | 1.08 | 0.72 | 0.0138 | -0.01 | -1.2 | 1.3 | | 20 |
| — | 0.87 | 0.7 | 0.805 | 0.0137 | 0.0 | 0.0 | 4.0 | | 17 |
| 0.98 | 0.85 | 0.78 | 0.770 | 0.011 | 0.0 | 0.0 | 4.0 | | 17 |
| — | — | — | — | — | 0.0 | 0.0 | 3.5 at M = 0.3 | Tested for angles of attack from 0° to 180° | 17 |

| AIRFOIL | DATA SHEET NUMBER | t/c | L.E.R. r/c | MAXIMUM CAMBER | | T.E. TAB | | MODEL CHORD (in) |
|---|---|---|---|---|---|---|---|---|
| | | | | x/c | y/c | $\frac{c_{tab}}{c}$ | $\delta_{tab}$ (deg) | |
| NACA 63A015 | 1.3.140 | 0.15 | 0.0163 | — | — | — | — | 8.0 |
| NACA 63A018 | 1.3.150 | 0.18 | 0.0228 | — | — | — | — | 8.0 |
| NACA 64A(4.5)08 | 1.3.160 | 0.08 | 0.00456 | 0.5 | 0.02993 | — | — | 6.38 |
| NACA 64A608 | 1.3.170 | 0.08 | 0.00456 | 0.5 | 0.03991 | — | — | 6.38 |
| NACA 64A312 | 1.3.180 | 0.12 | 0.01044 | 0.5 | 0.01995 | — | — | 6.38 |
| NACA 64A(4.5)12 | 1.3.190 | 0.12 | 0.01044 | 0.5 | 0.02993 | — | — | 6.38 |
| NACA 64A612 | 1. 200 | 0.12 | 0.01044 | 0.5 | 0.03991 | — | — | 6.38 |
| NACA 64A516 | 1.3.210 | 0.16 | 0.01807 | 0.5 | 0.03326 | — | — | 6.38 |
| NACA 8-H-012 | 1.3.220 | 0.117 | 0.01325 | | | — | — | 24.0 |
| V13006-0.7 | 1.3.230 | 0.06 | 0.007 | | | — | — | 7.0 |
| V(1.9)3009 -1.25 | 1.3.240 | 0.09 | 0.0125 | | | — | — | 6.0 |
| V23010-1.58 0° T.E. Tab | 1.3.250 | 0.102 | 0.0158 | 0.16 | 0.0175 | 0.04 | 0.0 | 6.38 |
| V23010-1.58 3° T.E. Tab | 1.3.260 | 0.102 | 0.0158 | 0.16 | 0.0175 | 0.04 | -3.0 | 6.38 |

| $C_{\ell_{MAX}}$ at | | | $M_{DD}$ @ ZERO LIFT | $C_d$ at M=0.6 $C_\ell$=0.6 | LOW SPEED (M<0.4) | | $Rex10^{-6}$ at M=0.4 | REMARKS | REF. |
|---|---|---|---|---|---|---|---|---|---|
| M=0.3 | M=0.4 | M=0.5 | | | $C_{m_o}$ | $\alpha_o$ (deg) | | | |
| 1.22 | 1.01 | 0.9 | 0.74 | 0.011 | 0.0 | 0.0 | 4.0 | | 17 |
| 1.11 | 1.0 | 0.87 | approx. 0.725 | 0.015 | 0.0 | 0.0 | 4.0 | | 17 |
| — | 1.23 | 1.15 | 0.752 | 0.007 | -0.095 | -3.2 | 7.5 | | 18 |
| — | 1.40 | 1.37 | 0.755 | 0.006 | -0.13 | -4.6 | 7.5 | | 18 |
| — | 1.29 | 1.21 | 0.758 | 0.0074 | -0.065 | -2.4 | 7.5 | | 18 |
| — | 1.43 | 1.38 | 0.735 | 0.0085 | -0.095 | -3.35 | 7.5 | | 18 |
| — | 1.45 | 1.5 | 0 69 | 0.008 | -0.125 | -4.5 | 7.5 | | 18 |
| — | 1.47 | 1.41 | 0.685 | 0.0089 | -0.102 | -3.9 | 7.5 | | 18 |
| 1.26 (Low Mach No.) | — | — | — | — | 0.005 | -1.6 | 2.6 at low speed | | 15 |
| 1.13 (0.98) | 1.04 (0.97) | 1.03 (0.97) | 0.865 | 0.0075 | -0.012 | 0.0 | 5.3 | non-standard reference line | 7 8 |
| 1.315 (est.) | 1.225 | 1.12 (est.) | 0.815 | 0.0084 | -0.012 | 0.2 | 5.3 | non-standard reference line | 7 |
| 1.66 | 1.46 | 1.22 | 0.794 | 0.0108 | -0.009 | 0.35 | 7.1 | non-standard reference line | 9 10 |
| 1.62 | 1.42 | 1.18 | 0.798 (est.) | 0.011 (est.) | 0.006 | 0.9 | 7.1 | non-standard reference line | 9 10 |

| AIRFOIL | DATA SHEET NUMBER | t/c | L.E.R. r/c | MAXIMUM CAMBER | | T.E. TAB | | MODEL CHORD (in) |
|---|---|---|---|---|---|---|---|---|
| | | | | x/c | y/c | $\frac{c_{tab}}{c}$ | $\delta_{tab}$ (deg) | |
| V23010-1.58 Reverse flow data | 1.3.270 | 0.102 | 0.0158 | 0.16 | 0.0175 | 0.04 | 0.0 | 6.38 |
| V23010-1.58 Reverse flow data | 1.3.280 | 0.102 | 0.0158 | 0.16 | 0.0175 | 0.04 | -3.0 | 6.38 |
| V23010-1.58 Reverse flow data | 1.3.290 | 0.102 | 0.0158 | 0.16 | 0.0175 | 0.04 | 3.0 | 6.38 |
| V43012-1.58 | 1.3.300 | 0.12 | 0.0158 | 0.16 | 0.035 | 0.1 | 0.0 | 7.018 |
| V43012-1.58 | 1.3.310 | 0.15 | 0.0158 | 0.16 | 0.035 | 0.1 (C.05 deflec-ted) | -6.0 | 7.018 |
| SA 13109-1.58 | 1.3.320 | 0.118 | 0.0158 | | | — | — | 8.27 |
| NPL 9615 | 1.3.330 | 0.113 | 0.01883 | | | — | — | 10.0 |
| NPL 9626 | 1.3.340 | | | | | — | — | 10.0 |
| NPL 9627 | 1.3.350 | | | | | — | — | 10.0 |
| NPL 9660 | 1.3.360 | 0.113 | 0.0198 | | | 0.035 | 0.0 | 10.0 |
| NACA Cambré | 1.3.370 | 0.118 | | | | — | — | 8.46 |
| VR-7 0° T.E. Tab | 1.3.380 | 0.12 | 0.0113 | 0.3 | 0.03138 | 0.05 | 0.0 | 6.38 |
| VR-7 3° T.E. Tab | 1.3.390 | 0.12 | 0.0113 | 0.3 | 0.03138 | 0.05 | -3.1 | 6.38 |

| $C_{l_{MAX}}$ at | | | $M_{DD}$ @ ZERO LIFT | $C_d$ at M=0.6 $C_l$=0.6 | LOW SPEED (M<0.4) | | $Re \times 10^{-6}$ at M=0.4 | REMARKS | REF. |
|---|---|---|---|---|---|---|---|---|---|
| M=0.3 | M=0.4 | M=0.5 | | | $C_{m_o}$ | $\alpha_o$ (deg) | | | |
| 0.82<br>-0.76 | 0.90<br>-0.75 | — | — | — | — | approx.<br>181 | 5.0 | non-standard reference line | 11 |
| 0.80<br>-0.71 | 0.86<br>-0.72 | — | — | — | — | approx.<br>181 | 5.0 | non-standard reference line | 11 |
| 0.80<br>-0.80 | 0.88<br>-0.80 | — | — | — | — | approx.<br>181 | 5.0 | non-standard reference line | 11 |
| 1.89 | 1.665 | 1.21 | 0.65 | — | 0.001 | -1.8 | 8.0 | T.E. Tab extends beyond basic chord. Nondim. by total chord | 10 |
| 1.81 | 1.55 | 1.145 | 0.65<br>(estim.) | — | 0.022 | -0.05 | 8.0 | T.E. Tab exten. Loads nondim'd by total chord | 10 |
| 1.2 | 1.05 | 0.96 | 0.825 | 0.0102 | approx.<br>0.0 | -0.7 | 2.2 | | 22 |
| 1.23 | 1.17 | 1.10 | 0.785 | 0.0116 | -0.009 | 0.3 | 2.2 | non-standard reference line | 2 |
| 1.2 | 1.1 | 0.97 | insuff.<br>data | 0.0115 | -0.007 | 0.1 | 2.2 | non-standard reference line | 19 |
| 1.24 | 1.16 | 1.03 | insuff.<br>data | 0.011 | -0.011 | 0.1 | 2.2 | non-standard reference line | 19 |
| 1.3 | 1.18 | 1.15 | 0.792 | 0.0114 | -0.006 | 0.1 | 2.2 | non-standard reference line<br>Used on the Lynx Helicopter | 13 |
| 1.28 | 1.26 | 1.14 | approx.<br>0.79 | approx.<br>0.011 | -0.012 | 0.2 | 2 0 | non-standard reference line | 21 |
| 1.63 | 1.50 | 1.65 | 0.742 | 0.0081 | -0.025 | -1.9 | 7.3 | | 10 |
| 1.57 | 1.46 | 1.57 | 0.75<br>(est.) | 0.0084<br>(est.) | -0.007 | -1.1 | 7.3 | | 10 |

| AIRFOIL | DATA SHEET NUMBER | t/c | L.E.R. r/c | MAXIMUM CAMBER | | T.E. TAB | | MODEL CHORD (in) |
|---|---|---|---|---|---|---|---|---|
| | | | | x/c | y/c | $\frac{c_{tab}}{c}$ | $\delta_{tab}$ (deg) | |
| VR-7<br>6° T.E. Tab | 1.3.400 | 0.12 | 0.0113 | 0.3 | 0.03138 | 0.05 | -5.9 | 6.38 |
| VR-8<br>0° T.E. Tab | 1.3.410 | 0.08 | 0.00585 | 0.3 | 0.0125 | 0.05 | 0.0 | 6.38 |
| VR-7.1 | 1.3.420 | 0.12 | 0.0113 | 0.3 | 0.03138 | 0.05 | -1.0 | 6.38 |
| FX-69-H-098 | 1.3.430 | 0.098 | 0.0062 | | | — | — | not available |
| | | | | | | | | |
| | | | | | | | | |
| | | | | | | | | |
| | | | | | | | | |
| | | | | | | | | |
| | | | | | | | | |
| | | | | | | | | |
| | | | | | | | | |
| | | | | | | | | |

| $C_{\ell_{MAX}}$ at | | | $M_{DD}$ @ ZERO LIFT | $C_d$ at M=0.6 $C_\ell$=0.6 | LOW SPEED (M<0.4) | | Rex10$^{-6}$ at M=0.4 | REMARKS | REF. |
|---|---|---|---|---|---|---|---|---|---|
| M=0.3 | M=0.4 | M = 0.5 | | | $C_{m_o}$ | $\alpha_o$ (deg) | | | |
| 1.53 | 1.41 | 1.51 | 0.757 (est.) | 0.009 (est.) | 0.009 | -0.5 | 7.3 | | 10 |
| 1.06 | 1.04 | 1.235 | 0.811 | 0.007 | -0.011 | -0.8 | 7.3 | | 10 |
| 1.63 | 1.5 | 1.53 | — | — | -0.020 | -1.7 | 7.3 | | 10 |
| 1.4 | — | 1.33 | 0.79 | 0.0064 | -0.01 | -0.8 | 4.0 to 5.0 | | 14 |
| | | | | | | | | | |
| | | | | | | | | | |
| | | | | | | | | | |
| | | | | | | | | | |
| | | | | | | | | | |
| | | | | | | | | | |
| | | | | | | | | | |
| | | | | | | | | | |
| | | | | | | | | | |

## References


1. Ladson, C.L., *Description and Calibration of the Langley 6 by 19-inch Transonic Tunnel.* NASA TN D-7182.

2. Gregory, N., Wilby, P.G., *NPL 9615 and NACA 0012-A Comparison of Aerodynamic Data.* ARC C.P. No. 1261, 1973.

3. Lizak, A.A., *Two-Dimensional Wind-Tunnel Tests of an H-34 Main Rotor Airfoil Section.* TREC TR 60-53, September 1960.

4. Chaddock, D.R., *A Tunnel Spanning Airfoil Testing Technique.* AHS Meeting in Hartford, Conn., March 6, 1975.

5. Liiva, J., Davenport, F.J., Gray, L., Walton, I.C., *Two-Dimensional Tests of Airfoils Oscillating Near Stall.* USAAVLABS

6. LaPrete, R. Storwick, E.M., Peterson, L.D., *Boeing Wind-Tunnel Test 527 - High-Speed Force Tests to Determine Section Characteristics of VR-910M-1, Full-Scale Airfoil Sections, for Product Improvement of Vertol Division CH-47.* Boeing Document D2-24066-1, 1966.

7. Gabriel, E., *Analysis of Two-Dimensional Wind-Tunnel Tests of Rotor Blade Airfoils of Varying Camber and Leading-Edge Radius.* Boeing Aero Inv. III-288, 11 November 1965.

8. Gray, L., Liiva. J., Davenport, F.J., *Wind-Tunnel Tests of Thin Airfoils Oscillating Near Stall.* USAAVLABS TR 68-89A, 1969.

9. Eierman, R.L., Nyholm, J.R., Schreiber, R.E., Russell, J.H., *Data Report BSWT 412, A Force Test on VR-890E-1, A 0.25-Scale Vertol 23010-1.58 Two-Dimensional Airfoil Model in the BSWT Two-Dimensional Subsonic Insert.* Boeing Document No. D6-20518, December 1967.

10. Dadone, L.U., McMullen, J.. *HLH/ATC Rotor System Two-Dimensional Airfoil Test.* Boeing Document No. D301-10071-1, December 1971.

11. Gray, L. Dadone, L.U., Gross, D.W., Child, R.F., *Wind-Tunnel Investigation of Airfoils Oscillating in Reverse Flow.* USAAVLABS TR

12. Uhle, H., *Windkanalmessungen am Profil NACA 23012 mit Original-und modifizierter Hinterkante.* MBB TN D127-2/71, November 1971.

13. Wilby, P.G., *Effect of Production Modifications to Rear of Westland Lynx Rotor Blade on Sectional Aerodynamic Characteristics.* RAE TR 73043, February 1973.

14. Kemp, L.D., *An Analytical Study for the Design of Advanced Rotor Airfoils.* NASA CR-112297, March 1973.

15. Stivers, L.S., Jr., Rice, F.J., Jr., *Aerodynamic Characteristics of Four NACA Airfoil Sections Designed for Helicopter Rotor Blades.* NACA WR L-29, 1946.

16. Critzos, Heyson, Boswinkle, *Aerodynamic Characteristics of NACA 0012 Airfoil Section at Angles of Attack from 0° to 180°.* NACA TN 3361, January 1955.

17. Sipe, O.E., Jr., and Gorenberg, N.B., *Effect of Mach number, Reynolds Number, and Thickness Ratio on the Aerodynamic Characteristics of NACA 63A-Series Airfoil Sections.* AML TR 65-28, June 1965.

18. Dadone, L.U., *Experimental Investigation of the Properties of a Family of NACA 64AXXX Airfoils.* Boeing Document D170-10021-1, November 1969.

19. Wilby, Gregory, and Quincey, *Aerodynamic Characteristics of NPL 9626 and NPL 9627, Further Airfoils Designed for Helicopter Rotor Use.* ARC CP 1262, 1973.

20. Graham, D.J., Nitzberg, G.E., and Olson, R.N., *A Systematic Investigation of Pressure Distributions at High Speed Over Five Representative NACA Low-Drag and Conventional Airfoil Sections.*

21. ONERA Note Technique D'Information No. 3 - 0805 GY fascicule 1/2, *Essais en courant plan a' S3MA du profil NACA 0012 a' extension cambree de bord d'attaque (resultats couriges des effets de parois).*

22. PV d'Essais ONERA No. 1 - 604 GY fasicule 1/4, *Essais en courant de Profils de Pale d'Helicoptere pour Sud-Aviation-Profil SA 13109-1.58.*

## 1.2.50 COMPRESSIBILITY EFFECTS ON AIRFOIL CHARACTERISTICS

As freestream velocity increases, the local velocities around an airfoil section increase until sonic velocity is reached at some point on the profile. With further increases in freestream velocity, local regions of supersonic flow are established along portions of an airfoil surface. The recompression occurring downstream of such supersonic regions gives rise to the formation of shock waves which continue to grow in size and intensity as the speed of the flow increases. The major effect of recompression waves, besides establishing the transition from supersonic back to subsonic flow, is the disruption of the boundary layer. Initially, this results in slight increases in the profile drag of the airfoil as the flow begins to separate; but ultimately, this leads to large increases in profile drag and loss of lift as the boundary layer flow completely separates from the airfoil. Clearly, it is very important to understand the effect of compressibility on airfoil characteristics in order to estimate the airfoil performance limits associated with Mach number, and to apply whatever compressibility corrections are possible to extend the value of available data. In this section, the most important flow corrections are listed and explained, Mach number limits are discussed, and a brief illustration of typical compressibility effects on lift, drag, pitching moment, aerodynamic center, and center-of-pressure is provided.

In order to estimate the effects of compressibility on the flow around airfoils, various corrections have been derived. They are:

(1) The Prandtl-Glauert Rule
(2) The Karman-Tsien Rule
(3) The Kaplan Rule
(4) Laitone's Modification to the P-G Rule.

A brief summary of these corrections and their ranges of applicability is given in Table I, Data Sheet 1.2.50.1. It is important to realize that all of these corrections were developed on the assumption of linearized flow with small perturbation velocities. Thus, strictly speaking, they are most valid for situations involving thin airfoils operating at low lift coefficients. It should also be noted that the various rules are applicable over different ranges of Mach number. For example, the Prandtl-Glauert Rule is good for low freestream Mach numbers, but it decreases in accuracy at the higher Mach numbers, while the Karman Tsien Rule can be applied with very good results to higher Mach numbers. In fact, it is still possible to utilize the Karman-Tsien Rule with fairly good results if the local flow exceeds the speed of sound without the formation of a strong shock

wave. Besides their obvious application in making compressibility corrections to incompressible flow data, these rules can also be applied to the approximate determination of various Mach number related airfoil limits. These limits are discussed in Section 1.2.50.1.

Subsonic flow tables (sheet 1.2.50-3) are presented to assist in the determination of local flow conditions when the speed of the flow and the fluid stagnation conditions are known. Note that these tabulated functions can be used only to compensate for compressible flow conditions, and cannot be used directly with airfoil pressure and force coefficients. Also note that the range of validity of the subsonic flow tables encompasses only isentropic flow at velocities up to $M = 1$.

Finally, Sections 1.2.50.4 - .8 illustrate typical compressibility effects on airfoil lift, drag, pitching moment, aerodynamic center, and center-of-pressure.

| RULE | APPLICATION | REMARKS - RANGE OF APPLICATION |
|---|---|---|
| Prandtl-Glauert | Correction of incompressible values of $C_p$, $dC_\ell/d\alpha$, $C_\ell$, $C_m$ | Predicts effects of $M_\infty$ with good accuracy for very thin profiles at Mach numbers below drag rise. For thick profiles and high Mach numbers, provides a guide to orders of magnitude, but is not accurate enough for design purposes. |
| Prandtl-Glauert (Laitone's Modification) | Correction of incompressible values of $C_p$ | Predicts variation of $C_p$ with $M_\infty$ somewhat better than does Prandtl-Glauert rule. If airfoil section incompressible pressure distribution is known, compressible flow pressure may be obtained using this rule, and by integration, compressible flow force coefficients ($C_\ell$ and $C_m$) are determined. |
| Kaplan's Rule | Correction of incompressible values of $C_p$, $dC_\ell/d\alpha$, $C_\ell$, $C_m$ | Remarks concerning range of applicability of Prandtl-Glauert rule also apply to this rule. However, this rule has an advantage over the P-G rule in that it predicts the variation in compressibility effects due to the finite thickness of an airfoil section. (The Prandtl-Glauert rule assumes zero thickness/chord.) |
| Karman-Tsien | Correction of incompressible values of $C_p$ | Predicts effects of $M_\infty$ with good accuracy for very thin profiles. Not limited to low Mach numbers, as is the P-G rule. If airfoil section incompressible pressure distribution is known; compressible flow pressure distribution may be obtained using this rule, and by integration, compressible flow force coefficients ($C_\ell$ and $C_m$) are determined. |

*TABLE I - COMPRESSIBLE FLOW CORRECTIONS - SUMMARY*

## Prandtl-Glauert Correction

The Prandtl-Glauert correction is expressed as:

$$C_{p_{comp}} = C_{p_{inc}} / \sqrt{1 - M_\infty^2}$$

where

$C_{p_{comp}}$ = the pressure coefficient at a given point for compressible flow past a profile

$C_{p_{inc}}$ = the pressure coefficient at the same point for incompressible flow past the same profile

$M_\infty$ = freestream Mach number.

The Prandtl-Glauert correction is derived for the case of small perturbation velocities and low freestream Mach numbers. These assumptions limit the applicability of the rule to thin airfoil sections with small amounts of camber at low $C_\ell$ and Mach numbers. The further assumption that these perturbation velocities are applied uniformly over the entire profile allows application of this rule to force and moment coefficients; namely, $C_\ell/d\alpha$, $C_\ell$, and $C_m$. For example,

$$C_{\ell_{comp}} = C_{\ell_{inc}} / \sqrt{1 - M_\infty^2}$$

at constant angle-of-attack.

Prandtl-Glauert Correction (Laitone's Modification)

The Prandtl-Glauert rule, as originally derived, is based on the assumption that the linearized flow equations (and the small perturbation velocity) can be applied uniformly to the entire field of flow of the profile. Laitone's modification to the Prandtl-Glauert rule consists of assuming that the compressibility correction to the incompressible pressure coefficient at a given point on a profile can be performed using the local Mach number at that point rather than the freestream Mach number; i.e.,

$$C_{p_{comp}} = C_{p_{inc}} / \sqrt{1 - M_\ell^2}$$

where $M_\ell$ is the local Mach number.

Combining the pressure coefficient and isentropic relations,

$$C_p = \frac{(p_\ell / p_\infty) - 1}{(1/2)\gamma M_\infty^2}, \qquad \frac{p_\ell}{p_\infty} = \left[\frac{1 + [(\gamma - 1)/2]M_\infty^2}{1 + [(\gamma - 1)/2]M_\ell^2}\right]^{\gamma/(\gamma-1)}.$$

Solving for $M_\ell^2$ and substituting the solution with the equations for $C_{p_{comp}}$ results in

$$C_{p_{comp}} = \frac{C_{p_{inc}}}{\sqrt{1 - M_\infty^2} + \dfrac{M_\infty^2\{1 + [(\gamma - 1)/2]M_\infty^2\}}{2\sqrt{1 - M_\infty^2}} C_{p_{inc}}}$$

where

$\gamma$ = the ratio of specific heats ($\gamma = 1.4$ for air).

Since this correction is based on local flow conditions, the effect on $C_p$ is different at each point on the profile. Thus, this correction cannot be applied to forces and moments directly. However, if the complete incompressible pressure distribution for an airfoil is known, this correction can be applied to obtain the compressible pressure distribution, which may then be integrated to give the total lift force and moment.

## Kaplan's Rule

The Prandtl-Glauert rule was derived for the case of a very thin profile (in fact, a profile of zero thickness). In an attempt to account for the effects of compressibility on the lift of airfoil profiles of finite thickness, Kaplan derived a relationship based on his study of the compressible flow past elliptic cylinders at various angles of attack. The equation is as follows:

$$\frac{C_{\ell_{comp}}}{C_{\ell_{inc}}} = \mu + \frac{t/c}{1.0 + (t/c)}\left[\mu(\mu - 1.0) + \tfrac{1}{2}(\gamma + 1.0)(\mu^2 - 1.0)^2\right]$$

where

$t/c$ = section thickness/chord ratio

$\gamma$ = ratio of specific heats ($\gamma = 1.4$ for air).

$\mu = 1.0/\sqrt{1 - M_\infty^2}$.

Note that for the case of zero thickness/chord ratio, the above equation reduces to the Prandtl-Glauert rule.

Fig 2 illustrates the comparison between lift coefficients calculated using this relation and the Prandtl-Glauert rule. These curves are in fairly good agreement with experimental results for airfoil profiles having the same thickness/chord ratios as the elliptical profiles.

The Kaplan rule can be used to estimate compressibility corrections for the same coefficients as the Prandtl-Glauert rule; namely, $C_p$, $dC_\ell/d\alpha$, $C_\ell$, and $C_m$.

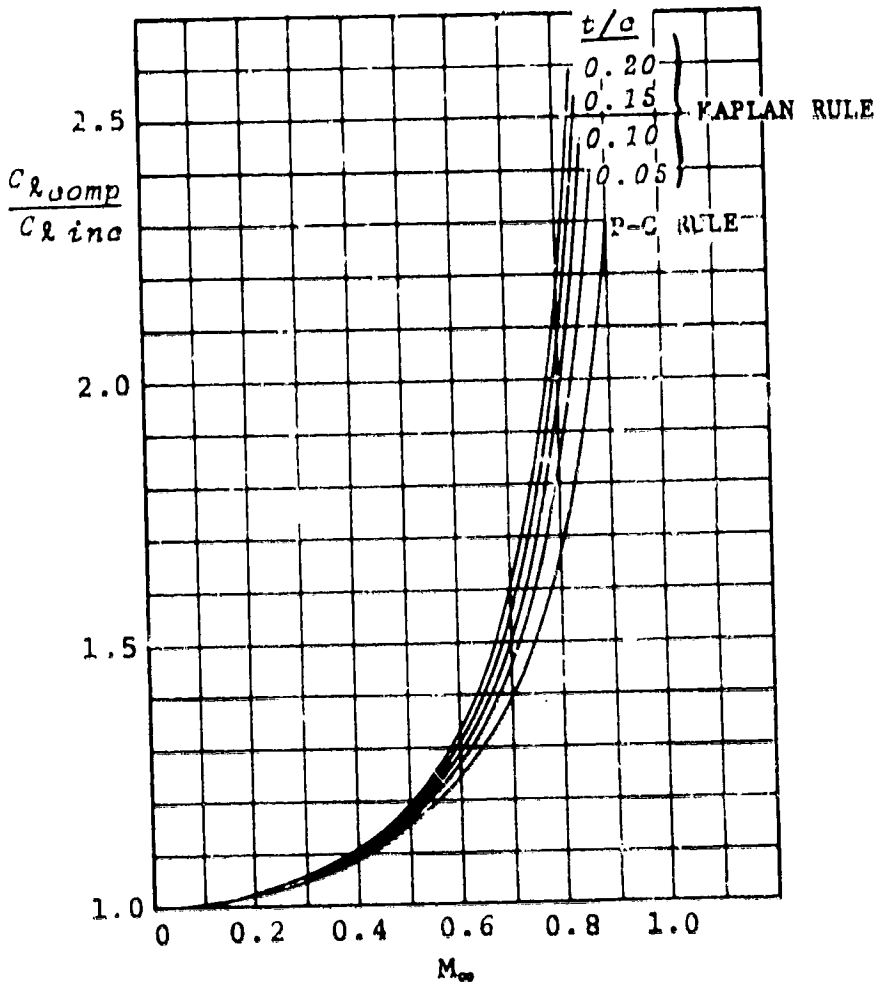


*Figure 2. Ratio of lift for compressible and incompressible fluids as a function of stream Mach number*

Karman-Tsien Rule

The relationship for the Karman-Tsien rule is expressed as:

$$C_{p_{comp}} = \frac{C_{p_{inc}}}{\sqrt{1 - M_\infty^2} + \frac{M_\infty^2}{1 + \sqrt{1 - M_\infty^2}} \frac{C_{p_{inc}}}{2}}.$$

As in the case of the Prandtl-Glauert rule, the Karman-Tsien rule derivation is based on the assumption of small perturbation velocities and, therefore, can be expected to be reasonably accurate only for thin profiles at small angles of attack. Unlike the Prandtl-Glauert rule, however, the Karman-Tsien rule is related to local velocity perturbations. This results in better accuracy than the Prandtl-Glauert rule (see Fig 1), but also limits the direct application of the rule to pressure coefficients.

However, if the complete incompressible pressure distribution for a profile is known, the Karman-Tsien rule can be applied to obtain the compressible pressure distribution which may then be integrated to give the total lift force and moment.

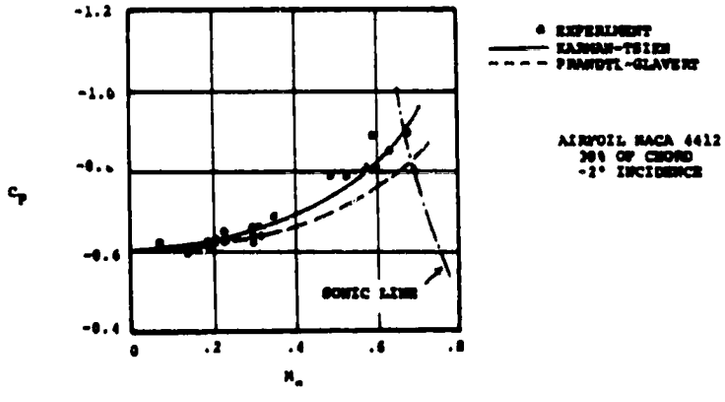


*Figure 1. Comparison of Karman-Tsien rule with experiment*

## 1.2.50.2 LOCAL MACH NUMBER LIMITS

The freestream Mach number ($M_\infty$) at which the local velocity becomes sonic ($M_\ell = 1$) at some point on the airfoil profile is known as the *lower critical Mach number*. As freestream Mach number continues to increase, shock waves appear and grow stronger, causing an increase in profile drag and ultimately, a shock-induced separation of the boundary layer. This results in a sudden increase in profile drag and a sudden loss of lift. The Mach numbers at which these latter effects occur are known as the *drag divergence and lift divergence Mach numbers*, and are defined as the values of $M_\infty$ where $dC_d/dM_\infty = 0.1$, and $dC_\ell/dM_\infty = 0$, and $d^2C_\ell/dM_\infty^2 < 0$, respectively. Generally, drag divergence Mach number occurs before lift divergence Mach number, and both can occur at considerably higher values of Mach number than the lower critical Mach number. Fig 1 is a typical plot of these Mach number limits as a function of $C_\ell$.

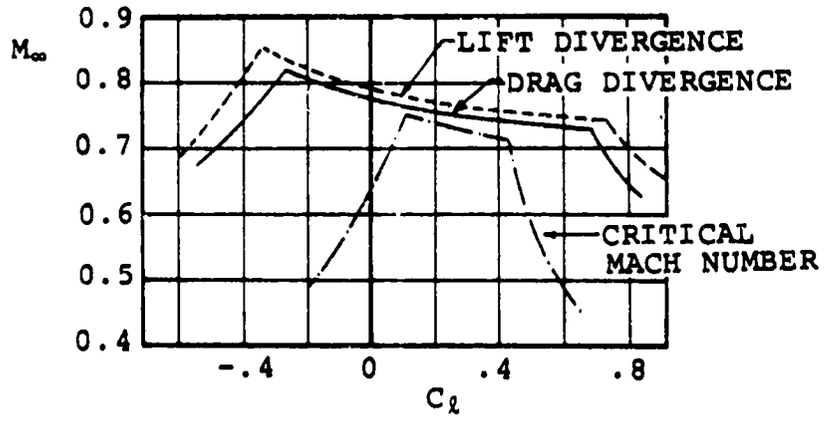


*Figure 1. Force-divergence Mach numbers for NACA 66-210 profile*

As noted previously, the value of the lower critical Mach number can be considerably below that of either the lift or drag divergence Mach numbers. However, it is useful as an indicator of the lower bounds of major compressibility effects on lift and drag. Thus, it is of interest to note that the lower critical Mach number can be approximately estimated by use of a simple analytical technique.

The isentropic relation between Mach number and pressure ratio is:

$$C_p = \frac{2}{\gamma M_\infty^2}\left[\left(\frac{1 + [(\gamma - 1)/2]M_\infty^2}{1 + [(\gamma - 1)/2]M^2}\right)^{\gamma/(\gamma-1)} - 1\right]$$

where $M$ is the local Mach number at the crest line and it is assumed to be $M = 1$.

By the iterative process of assuming successive values of $M_\infty$, a value of the pressure coefficient can be obtained which equals the value of $C_p$ known, through experiment, to exist at the crest line. The $M_\infty$ at which this occurs corresponds to the lower critical Mach number. This type of approximation has been used widely in the past, and a plot of critical Mach number $C_p$ is shown in Figure 2.

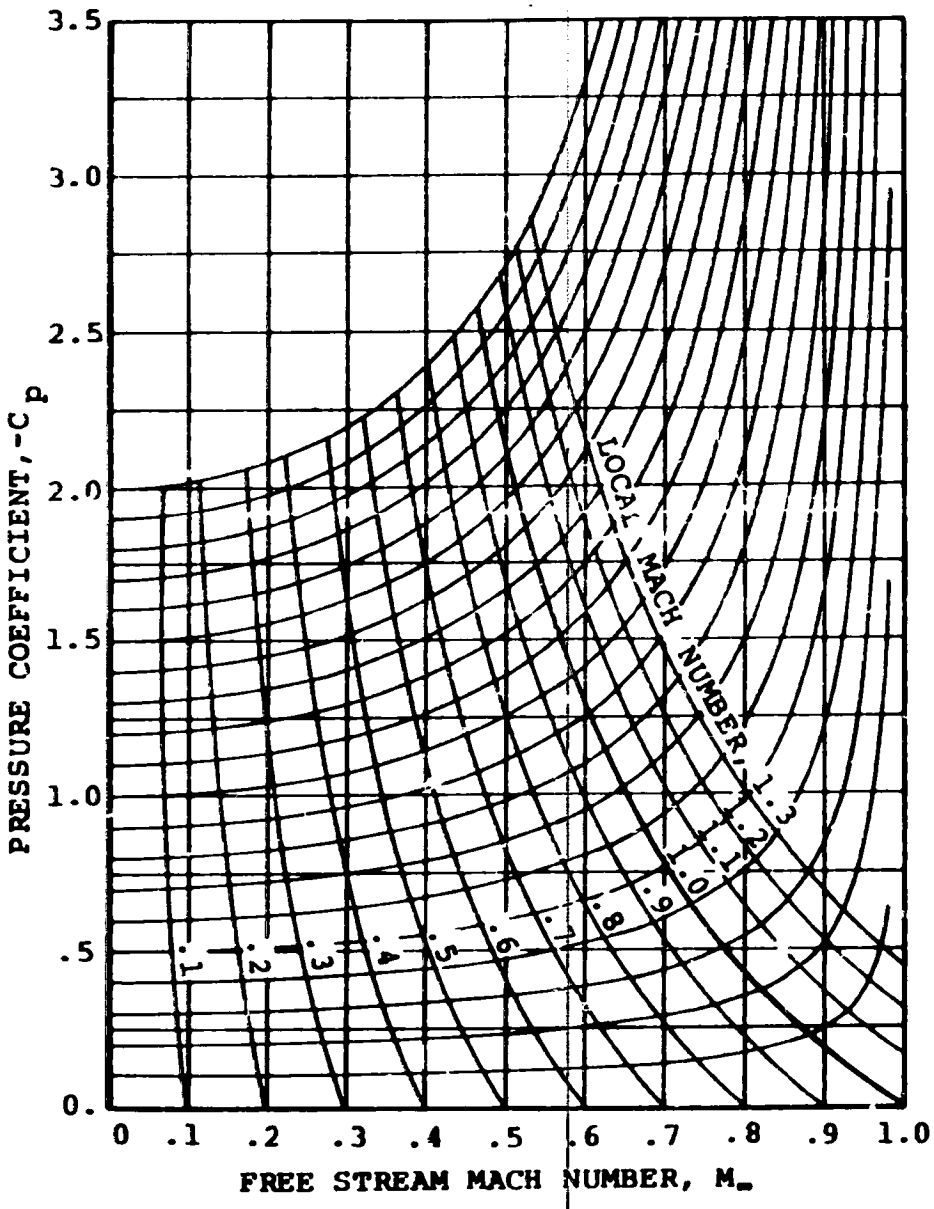


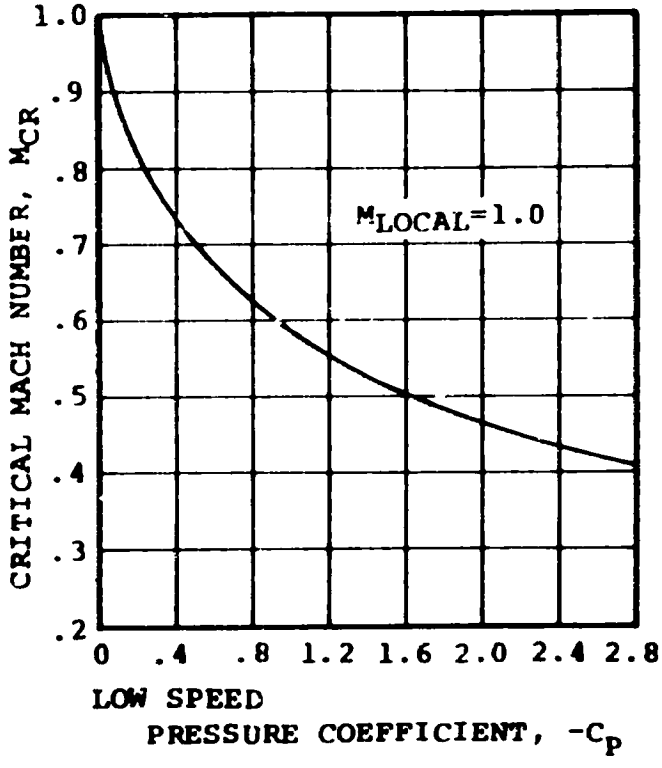


*Figure 2. (a) Variation of $C_p$ with $M_\infty$ according to Karman-Tsien rule, and (b) corresponding curve of lower critical Mach number vs maximum negative pressure coefficient for incompressible flow*

## 1.2.50.3 SUBSONIC FLOW TABLES

Table I lists the equations relating local and stagnation values of pressure, temperature, and density for the isentropic flow of a perfect gas. Table II lists values of these parameters as a function of Mach number. Given the reference stagnation conditions ($V = 0$) of a gas, this table is utilized for determining local flow conditions at a given Mach number.

## ISENTROPIC SUBSONIC FLOW

### EQUATIONS

$$\frac{T}{T_t} = \left(1 + \frac{\gamma - 1}{2} M^2\right)^{-1}$$

$$\frac{p}{p_t} = \left(1 + \frac{\gamma - 1}{2} M^2\right)^{-\gamma/(\gamma-1)}$$

$$\frac{\rho}{\rho_t} = \left(1 + \frac{\gamma - 1}{2} M^2\right)^{-1/(\gamma-1)}$$

$$\frac{q}{p_t} = \frac{\gamma}{2} M^2 \left(1 + \frac{\gamma - 1}{2} M^2\right)^{-\gamma/(\gamma-1)}$$

$$\left(\frac{V}{a^*}\right)^2 = \frac{\gamma + 1}{2} M^2 \left(1 + \frac{\gamma - 1}{2} M^2\right)^{-1}$$

$$\frac{A_*}{A} = \left(\frac{\gamma + 1}{2}\right)^{(\gamma+1)/2(\gamma-1)} M \left(1 + \frac{\gamma - 1}{2} M^2\right)^{-(\gamma+1)/2(\gamma-1)}$$

NOTE: Subscript $t$, when applied to a given parameter, designates the isentropic stagnation state ($V = 0$)

### NOTATION

$T/T_t$ = ratio of local static temperature to total (stagnation) temperature

$p/p_t$ = ratio of local static pressure to total (stagnation) pressure

$\rho/\rho_t$ = ratio of local static density to total (stagnation) density

$q/p_t$ = ratio of local dynamic pressure to total (stagnation) pressure

$V/a^*$ = ratio of local speed to speed of sound at the point where $M = 1$

$A/A_*$ = ratio of local cross-sectional area of an isentropic streamtube to cross-sectional area at the point where $M = 1$

$M$ = local Mach number

$\beta = \sqrt{1 - M^2}$

$\gamma$ = ratio of specific heats (air = 1.4)

TABLE I

$\gamma = 7/5$

| $M$ | $\frac{p}{p_t}$ | $\frac{\rho}{\rho_t}$ | $\frac{T}{T_t}$ | $\theta$ | $\frac{q}{p_t}$ | $\frac{A}{A_*}$ | $\frac{V}{a_*}$ | $M$ | $\frac{p}{p_t}$ | $\frac{\rho}{\rho_t}$ | $\frac{T}{T_t}$ | $\theta$ | $\frac{q}{p_t}$ | $\frac{A}{A_*}$ | $\frac{V}{a_*}$ |
|---|---|---|---|---|---|---|---|---|---|---|---|---|---|---|---|
| 0 | 1.0000 | 1.0000 | 1.0000 | 1.0000 | 0 | $\infty$ | 0 | 0.50 | 0.8430 | 0.9037 | 0.9524 | 0.0000 | 0.1473 | 1.3398 | 0.55430 |
| .01 | .9999 | 1.0000 | 1.0000 | 1.0000 | .7000 $\rightarrow^2$ | 57.8738 | .01686 | .51 | .8374 | .8978 | .9505 | .0047 | .1526 | 1.3263 | .54660 |
| .02 | .9997 | .9998 | .9999 | .9999 | .2798 $\rightarrow^2$ | 28.9121 | .02191 | .52 | .8317 | .8708 | .9487 | .0142 | .1578 | 1.3134 | .53903 |
| .03 | .9991 | .9996 | .9994 | .9995 | .6290 $\rightarrow^2$ | 19.3086 | .02694 | .53 | .8259 | .8723 | .9468 | .0140 | .1630 | 1.3008 | .53160 |
| .04 | .9980 | .9992 | .9987 | .9982 | .1119 $\rightarrow^2$ | 14.4815 | .04381 | .54 | .8201 | .8679 | .9449 | .0417 | .1674 | 1.2888 | .52431 |
| .05 | .9963 | .9986 | .9976 | .9957 | .1747 $\rightarrow^2$ | 11.5914 | .05478 | .55 | .8142 | .8634 | .9430 | .0332 | .1734 | 1.2768 | .51715 |
| .06 | .9975 | .9982 | .9991 | .9932 | .2514 $\rightarrow^2$ | 9.6650 | .06570 | .56 | .8082 | .8589 | .9410 | .0285 | .1776 | 1.2653 | .51007 |
| .07 | .9948 | .9976 | .9980 | .9975 | .3418 $\rightarrow^2$ | 8.2915 | .07664 | .57 | .8022 | .8544 | .9389 | .0238 | .1825 | 1.2543 | .50314 |
| .08 | .9933 | .9968 | .9967 | .9962 | .4460 $\rightarrow^2$ | 7.2616 | .08758 | .58 | .7962 | .8498 | .9370 | .0146 | .1873 | 1.2438 | .49630 |
| .09 | .9944 | .9960 | .9984 | .9950 | .5636 $\rightarrow^2$ | 6.4613 | .09851 | .59 | .7901 | .8451 | .9349 | .0094 | .1923 | 1.2338 | .48959 |
| .10 | .9930 | .9950 | .9960 | .9950 | .6951 $\rightarrow^2$ | 5.8218 | .10944 | .60 | .7840 | .8404 | .9328 | .0000 | .1974 | 1.2242 | .48301 |
| .11 | .9916 | .9940 | .9976 | .9939 | .8360 $\rightarrow^2$ | 5.2982 | .12035 | .61 | .7778 | .8357 | .9307 | .7924 | .2028 | 1.2151 | .47656 |
| .12 | .9900 | .9928 | .9971 | .9929 | .9879 $\rightarrow^2$ | 4.8643 | .13126 | .62 | .7716 | .8310 | .9286 | .7846 | .2078 | 1.2064 | .47025 |
| .13 | .9883 | .9916 | .9966 | .9915 | .1100 $\rightarrow^1$ | 4.4980 | .14217 | .63 | .7654 | .8263 | .9264 | .7768 | .2127 | 1.1980 | .46407 |
| .14 | .9864 | .9902 | .9961 | .9902 | .1353 $\rightarrow^1$ | 4.1824 | .15306 | .64 | .7591 | .8213 | .9243 | .7684 | .2177 | 1.1900 | .45802 |
| .15 | .9844 | .9888 | .9955 | .9887 | .1550 $\rightarrow^1$ | 3.9103 | .16393 | .65 | .7528 | .8164 | .9221 | .7599 | .2227 | 1.1824 | .45209 |
| .16 | .9823 | .9873 | .9949 | .9871 | .1760 $\rightarrow^1$ | 3.6727 | .17482 | .66 | .7465 | .8115 | .9199 | .7513 | .2278 | 1.1751 | .44630 |
| .17 | .9800 | .9857 | .9943 | .9854 | .1983 $\rightarrow^1$ | 3.4635 | .18568 | .67 | .7401 | .8066 | .9176 | .7424 | .2328 | 1.1679 | .44062 |
| .18 | .9778 | .9840 | .9936 | .9837 | .2217 $\rightarrow^1$ | 3.2778 | .19654 | .68 | .7338 | .8016 | .9153 | .7332 | .2375 | 1.1609 | .43507 |
| .19 | .9751 | .9822 | .9928 | .9818 | .2464 $\rightarrow^1$ | 3.1123 | .20739 | .69 | .7274 | .7966 | .9131 | .7238 | .2424 | 1.1540 | .42965 |
| .20 | .9725 | .9803 | .9921 | .9799 | .2723 $\rightarrow^1$ | 2.9635 | .21822 | .70 | .7209 | .7916 | .9107 | .7141 | .2473 | 1.1474 | .42435 |
| .21 | .9697 | .9784 | .9913 | .9777 | .2994 $\rightarrow^1$ | 2.8288 | .22904 | .71 | .7145 | .7866 | .9084 | .7042 | .2521 | 1.1410 | .41917 |
| .22 | .9668 | .9762 | .9901 | .9755 | .3276 $\rightarrow^1$ | 2.7078 | .23984 | .72 | .7080 | .7814 | .9061 | .6938 | .2568 | 1.1348 | .41410 |
| .23 | .9638 | .9740 | .9896 | .9732 | .3568 $\rightarrow^1$ | 2.5984 | .25063 | .73 | .7016 | .7763 | .9037 | .6831 | .2617 | 1.1287 | .40915 |
| .24 | .9607 | .9718 | .9886 | .9708 | .3874 $\rightarrow^1$ | 2.4986 | .26141 | .74 | .6951 | .7712 | .9013 | .6720 | .2664 | 1.1228 | .40430 |
| .25 | .9575 | .9694 | .9877 | .9682 | .4188 $\rightarrow^1$ | 2.4077 | .27217 | .75 | .6888 | .7660 | .8989 | .6604 | .2711 | 1.1171 | .39957 |
| .26 | .9541 | .9670 | .9867 | .9656 | .4515 $\rightarrow^1$ | 2.3173 | .28291 | .76 | .6823 | .7608 | .8964 | .6484 | .2758 | 1.1115 | .39495 |
| .27 | .9508 | .9645 | .9856 | .9629 | .4851 $\rightarrow^1$ | 2.2355 | .29364 | .77 | .6758 | .7557 | .8940 | .6360 | .2804 | 1.1060 | .39043 |
| .28 | .9470 | .9619 | .9846 | .9600 | .5197 $\rightarrow^1$ | 2.1606 | .30435 | .78 | .6691 | .7505 | .8915 | .6234 | .2849 | 1.1007 | .38602 |
| .29 | .9433 | .9592 | .9835 | .9570 | .5553 $\rightarrow^1$ | 2.0919 | .31504 | .79 | .6625 | .7453 | .8889 | .6103 | .2894 | 1.0956 | .38171 |
| .30 | .9395 | .9564 | .9823 | .9539 | .5919 $\rightarrow^1$ | 2.0351 | .32572 | .80 | .6560 | .7400 | .8865 | .5970 | .2939 | 1.0905 | .37751 |
| .31 | .9355 | .9535 | .9811 | .9507 | .6293 $\rightarrow^1$ | 1.9785 | .33637 | .81 | .6495 | .7347 | .8840 | .5861 | .2983 | 1.0855 | .37339 |
| .32 | .9315 | .9504 | .9799 | .9474 | .6677 $\rightarrow^1$ | 1.9219 | .34701 | .82 | .6430 | .7295 | .8815 | .5721 | .3027 | 1.0806 | .36935 |
| .33 | .9274 | .9474 | .9787 | .9440 | .7069 $\rightarrow^1$ | 1.8707 | .35762 | .83 | .6365 | .7242 | .8790 | .5578 | .3070 | 1.0758 | .36540 |
| .34 | .9231 | .9443 | .9774 | .9404 | .7470 $\rightarrow^1$ | 1.8229 | .36822 | .84 | .6300 | .7189 | .8765 | .5430 | .3112 | 1.0711 | .36154 |
| .35 | .9188 | .9411 | .9761 | .9367 | .7879 $\rightarrow^1$ | 1.7780 | .37879 | .85 | .6235 | .7136 | .8737 | .5280 | .3153 | 1.0667 | .35777 |
| .36 | .9143 | .9378 | .9747 | .9330 | .8295 $\rightarrow^1$ | 1.7358 | .38935 | .86 | .6170 | .7083 | .8711 | .5103 | .3195 | 1.0623 | .35409 |
| .37 | .9095 | .9347 | .9733 | .9290 | .8719 $\rightarrow^1$ | 1.6961 | .39988 | .87 | .6106 | .7030 | .8685 | .4911 | .3235 | 1.0581 | .35048 |
| .38 | .9052 | .9313 | .9719 | .9250 | .9149 $\rightarrow^1$ | 1.6587 | .41039 | .88 | .6041 | .6977 | .8658 | .4750 | .3273 | 1.0539 | .34695 |
| .39 | .9004 | .9278 | .9705 | .9208 | .9587 $\rightarrow^1$ | 1.6234 | .42087 | .89 | .5977 | .6924 | .8632 | .4566 | .3314 | 1.0498 | .34349 |
| .40 | .8956 | .9243 | .9689 | .9165 | .1008 | 1.5901 | .43133 | .90 | .5913 | .6870 | .8606 | .4330 | .3353 | 1.0460 | .34010 |
| .41 | .8907 | .9207 | .9675 | .9121 | .1059 | 1.5587 | .44177 | .91 | .5849 | .6817 | .8579 | .4146 | .3390 | 1.0421 | .33679 |
| .42 | .8857 | .9170 | .9658 | .9075 | .1094 | 1.5288 | .45218 | .92 | .5785 | .6764 | .8552 | .3919 | .3427 | 1.0384 | .33354 |
| .43 | .8807 | .9132 | .9643 | .9028 | .1140 | 1.5007 | .46257 | .93 | .5721 | .6711 | .8525 | .3678 | .3464 | 1.0348 | .33036 |
| .44 | .8755 | .9094 | .9627 | .8980 | .1187 | 1.4740 | .47293 | .94 | .5658 | .6658 | .8498 | .3412 | .3500 | 1.0313 | .32725 |
| .45 | .8703 | .9055 | .9611 | .8930 | .1234 | 1.4489 | .48326 | .95 | .5595 | .6604 | .8471 | .3122 | .3534 | 1.0280 | .32421 |
| .46 | .8650 | .9016 | .9594 | .8879 | .1281 | 1.4248 | .49357 | .96 | .5532 | .6551 | .8444 | .2800 | .3569 | 1.0246 | .32123 |
| .47 | .8598 | .8976 | .9577 | .8827 | .1329 | 1.4018 | .50386 | .97 | .5469 | .6498 | .8416 | .2431 | .3602 | 1.0215 | .31831 |
| .48 | .8543 | .8935 | .9560 | .8773 | .1378 | 1.3801 | .51410 | .98 | .5407 | .6445 | .8389 | .1980 | .3635 | 1.0185 | .31545 |
| .49 | .8488 | .8894 | .9542 | .8717 | .1426 | 1.3595 | .52433 | .99 | .5345 | .6392 | .8361 | .1411 | .3667 | 1.0156 | .31265 |
| | | | | | | | | 1.00 | .5283 | .6339 | .8333 | .0000 | .3698 | 1.0128 | 1.00000 |

TABLE II SUBSONIC FLOW (NACA Report 1135)

## 1.2 .4 COMPRESSIBILITY EFFECTS ON THE LIFT COEFFICIENT

Three flow conditions are possible over an airfoil as a function of the viscous effects present at a particular lift and Mach number level. Such conditions are:

(1) Fully attached flow (at least, to the extent that regions of separated flow are negligible).

(2) Flow separation over significant portions of the airfoil surface, induced by velocity gradients and not primarily connected with compressibility effects.

(3) Shock-induced separation due to recompression downstream of significant supersonic regions.

The effect of compressibility on the maximum lift boundary of an airfoil is of primary interest in the selection of airfoils for helicopter rotor applications. The maximum lift coefficients at $M = 0.4$ and $M = 0.5$ are particularly significant, as they have been correlated with the occurrence of retreating blade stall on rotors in forward flight. The prediction of the maximum lift at these Mach numbers presents unusual difficulties because of the possibility of favorable shock-boundary layer interaction effects.

To illustrate the variety of maximum lift boundaries encountered in helicopter rotor airfoils, a number of such boundaries for several airfoil sections is presented in Figure 1. It is evident from inspection of the trends that the airfoils can be divided into two groups:

(1) Airfoils which do not benefit from any favorable shock/boundary layer interaction. Sections such as the V0012 (NACA 0012), V43012-1.58, and V23010-1.58 have maximum lift boundaries which degenerate with increasing Mach number without any leveling off or secondary peaks in the maximum lift trend.

(2) Airfoils displaying an increase in maximum lift capability at higher Mach numbers, after having shown a normal trend in maximum lift reduction at low Mach numbers. The VR-1, VR-7, and VR-8 in Figure 1 display such secondary peaks. It should be noted that the VR-1 is a "peaky" transonic section, while the VR-7 and VR-8 are "rooftop" airfoils. All of these sections deviate from the NACA four- and five-digit geometries of the sections in the first group above.

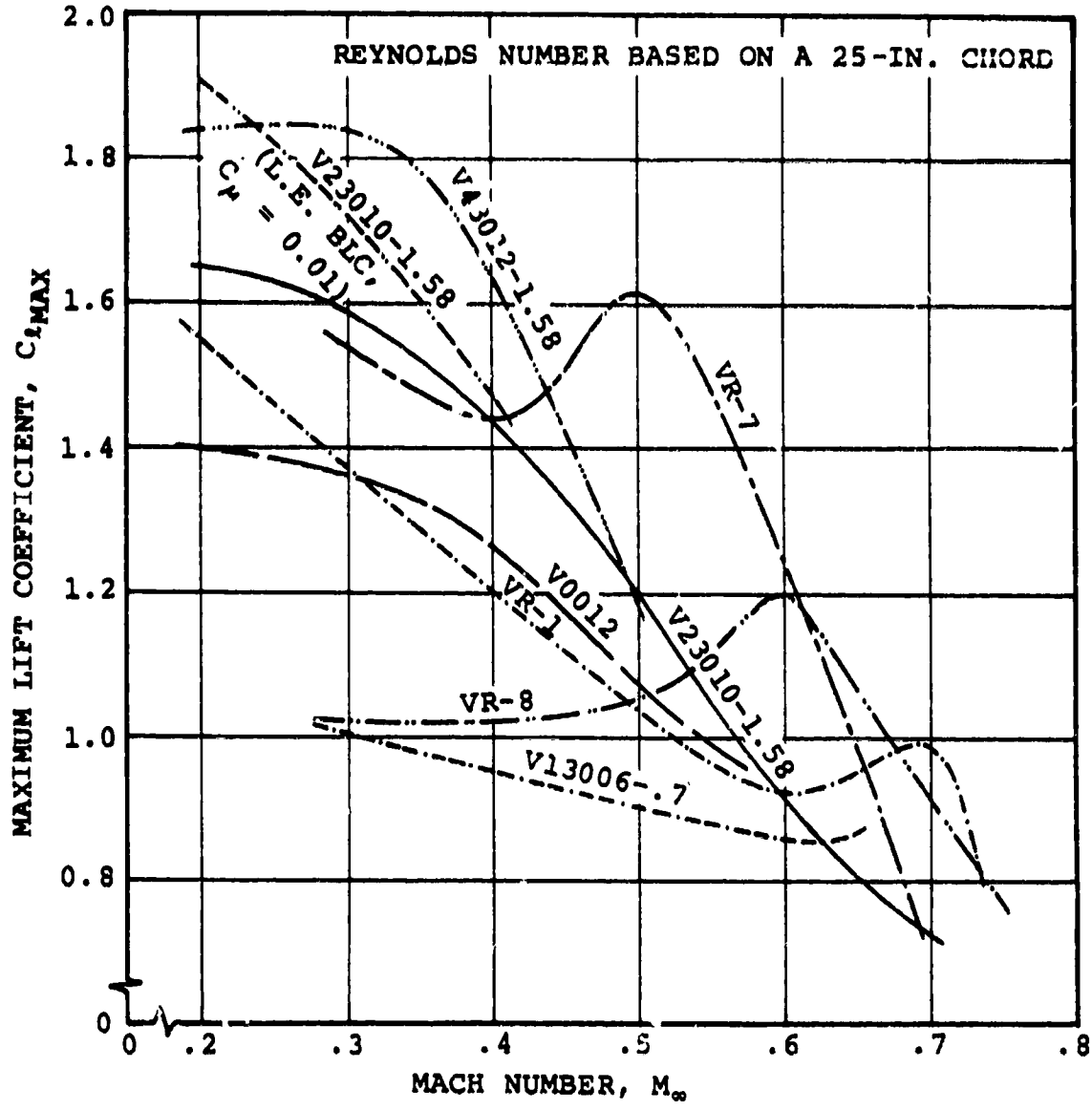


*Figure 1. An Example of Compressibility Effects on Typical Maximum Lift Boundaries*

## 1.2.50.5 COMPRESSIBILITY EFFECTS ON DRAG

Airfoils employed on helicopter rotors have to operate over a range of Mach numbers and lift levels which encompasses almost the entire spectrum of subsonic flow conditions. Under such circumstances, the selection of airfoil sections is not as straightforward, relatively speaking, as it is for fixed-wing aircraft. A detailed performance evaluation of the benefits derived by replacing one rotor section with another must be based on a complete set of airfoil data.

The effects of compressibility on drag are hard to summarize in a manner that would meaningfully assist the DATCOM user. However, the drag at some typical flow conditions has often been used for preliminary performance evaluation. Such "typical" conditions are representative of hover and forward-flight requirements.

For hover, the key drag requirement is at Mach numbers $0.5 \leq M \leq 0.6$, at lift levels of approximately $C_\ell = 0.6$. Drag values for $C_\ell = 0.6$ and $M = 0.6$ are tabulated in Section 1.2.40.

In forward flight, two sources of high profile drag are possible. The first is associated with retreating blade stall and, as such, is primarily a function of maximum lift capability. The second source of drag is the tip of the blade as it flies through the region of supercritical flow on the advancing side. The best airfoil for this situation would be the one having the most productive supercritical performance at very low lift levels—a thin symmetrical section. Thin symmetrical sections, however, cause premature retreating blade stall because of their low maximum lift capability. If thicker and cambered sections are used, a penalty in advancing blade drag must be paid. Figure 1 illustrates how lift capability and advancing blade drag can be approximately evaluated. The Mach number, at which $C_{d_o} = 0.018$, can be used as a measure of the growth in drag after drag divergence. The airfoil with the slowest rate of growth in drag; i.e., the highest Mach number for $C_{d_o} = 0.018$, and the highest maximum lift capability would be the best choice for a high performance rotor blade.

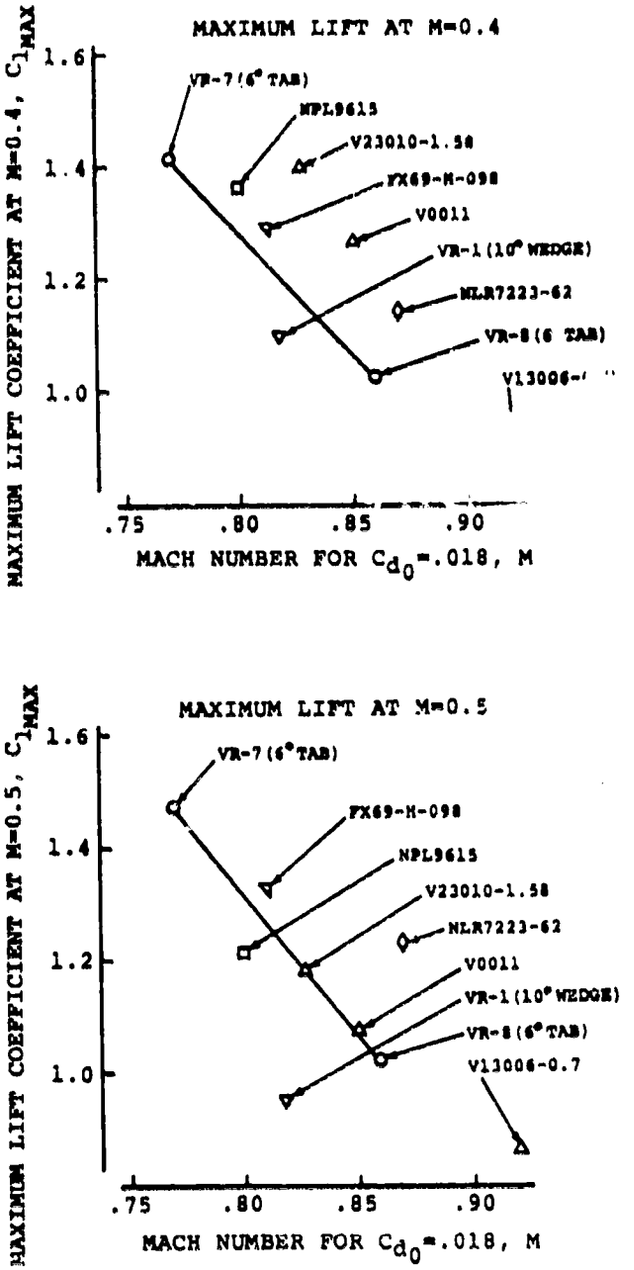


*Figure 1. Comparison of Maximum Lift Capability and Drag Rise Characteristics of Several Helicopter Rotor Airfoil Sections*

## 1.2.50.6 COMPRESSIBILITY EFFECTS ON PITCHING MOMENTS

The flow about an airfoil operating beyond the critical Mach number boundary is characterized by a supersonic region over some portion of the airfoil surface. The extent of this supersonic region depends on how far the airfoil is operating from the critical Mach number. Downstream of the supersonic flow region, a shock wave system marks the deceleration of the flow to subsonic conditions. The velocity distributions over airfoils in supercritical flow are characterized by the rapid changes in local velocity occurring across the shock-wave boundary; and such distributions differ very significantly from their subcritical counterparts. The qualitative changes in velocity and therefore, pressure distributions, are illustrated in Figure 1.

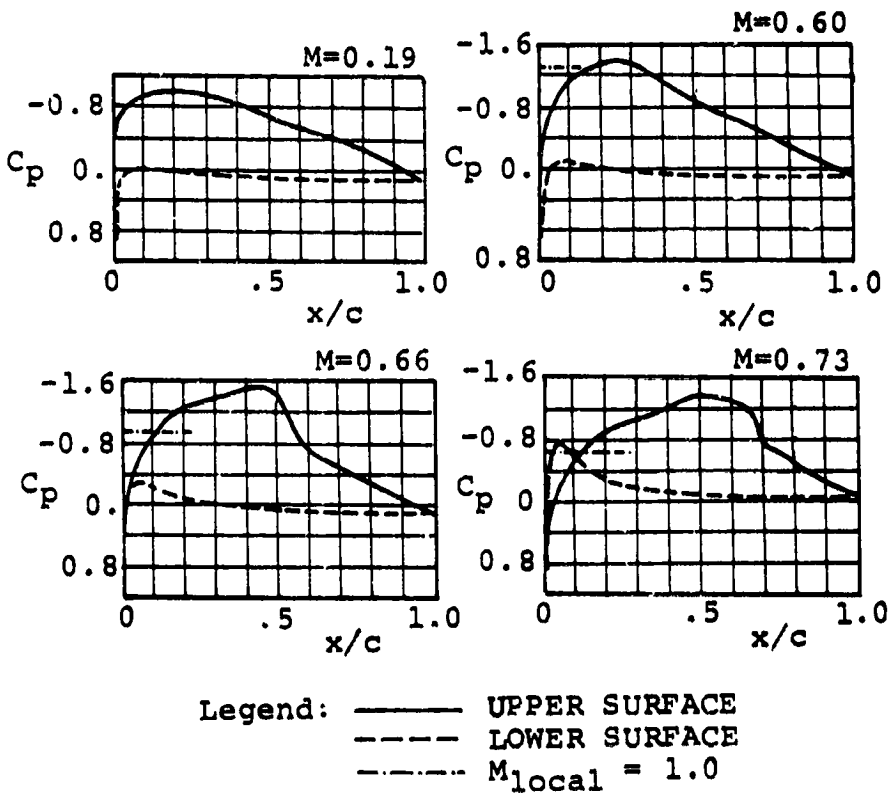


*Figure 1. Compressibility Effects on the Pressure Distributions Over the NACA 4412 Profile at α = 1.87°*

Note that as the Mach number is increased, the recompression boundary moves toward the trailing edge. This shifts the center-of pressure aft, thus increasing pitching moments.

The growth in pitching moments with increasing Mach number beyond the critical Mach number is often referred to as "Mach tuck" from the nose-down, "tucking" under, motion induced on airplane wings at high speeds. Two-dimen ional pitching moments at the zero lift level for a number of sections are illustrated in Figure 2.

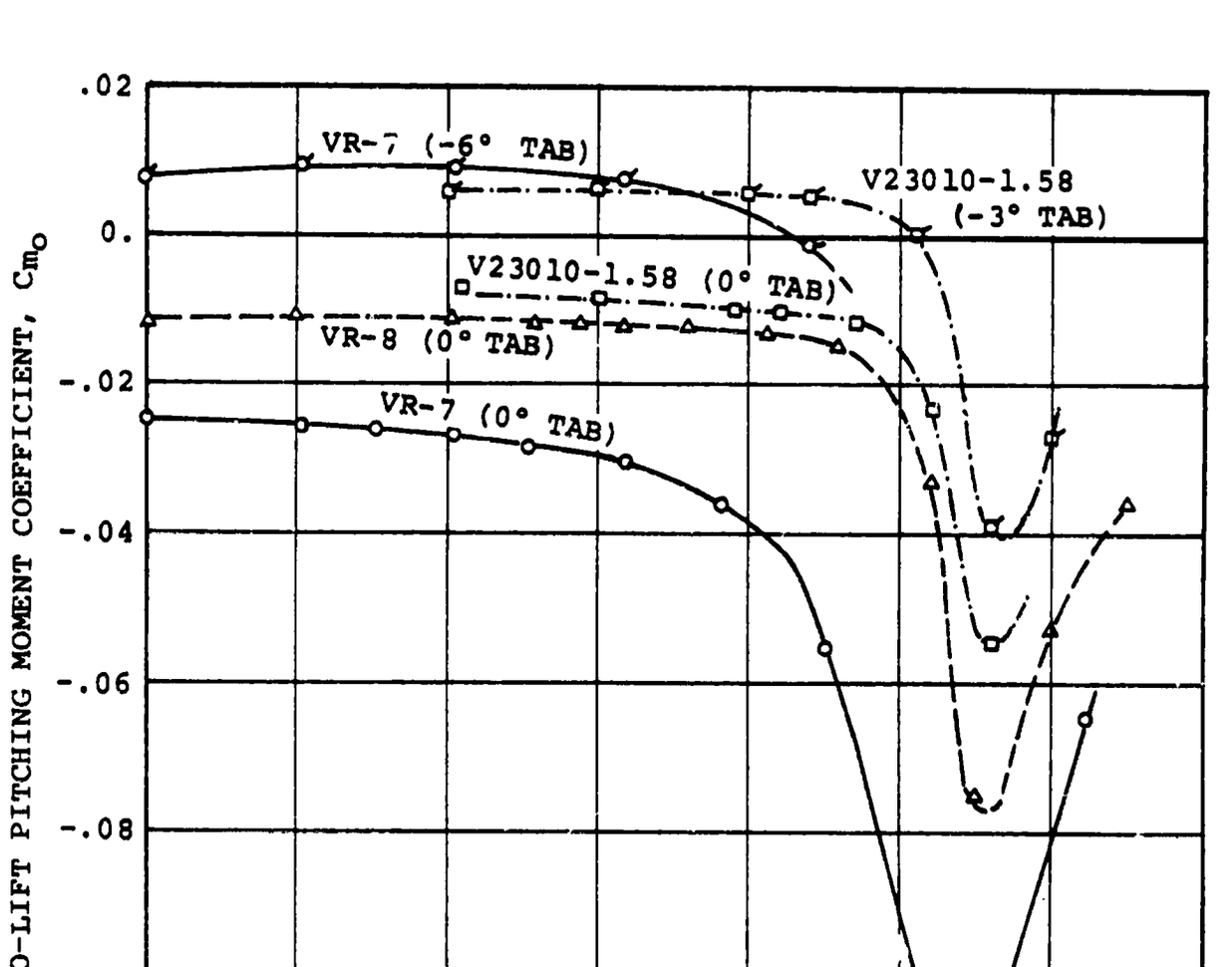


*Figure 2. An Example of Compressibility Effects on the Zero-Lift Pitching Moment Coefficient*

## 1.2.50.7 COMPRESSIBILITY EFFECTS ON THE LOCATION OF THE AERODYNAMIC CENTER

As defined in Section 1.1.30.1, the aerodynamic center is the point about which the section pitching moment is independent of lift, or angle-of-attack. By potential flow theory, this point should always occur one-quarter-chord aft of the leading edge. However, due to viscosity and compressibility effects, the aerodynamic center seldom occurs at the quarter-chord.

Figure 1 shows the variation in aerodynamic center with Mach number for several airfoil sections. The excursion of the aerodynamic center from the quarter-chord toward the mid-chord above the critical Mach number is due to the change in pressure distributions over an airfoil in the presence of local supersonic flow, as discussed in Section 1.2.50.6.

Generally, values of the aerodynamic center for a section, as quoted in the literature, are for low speeds only.

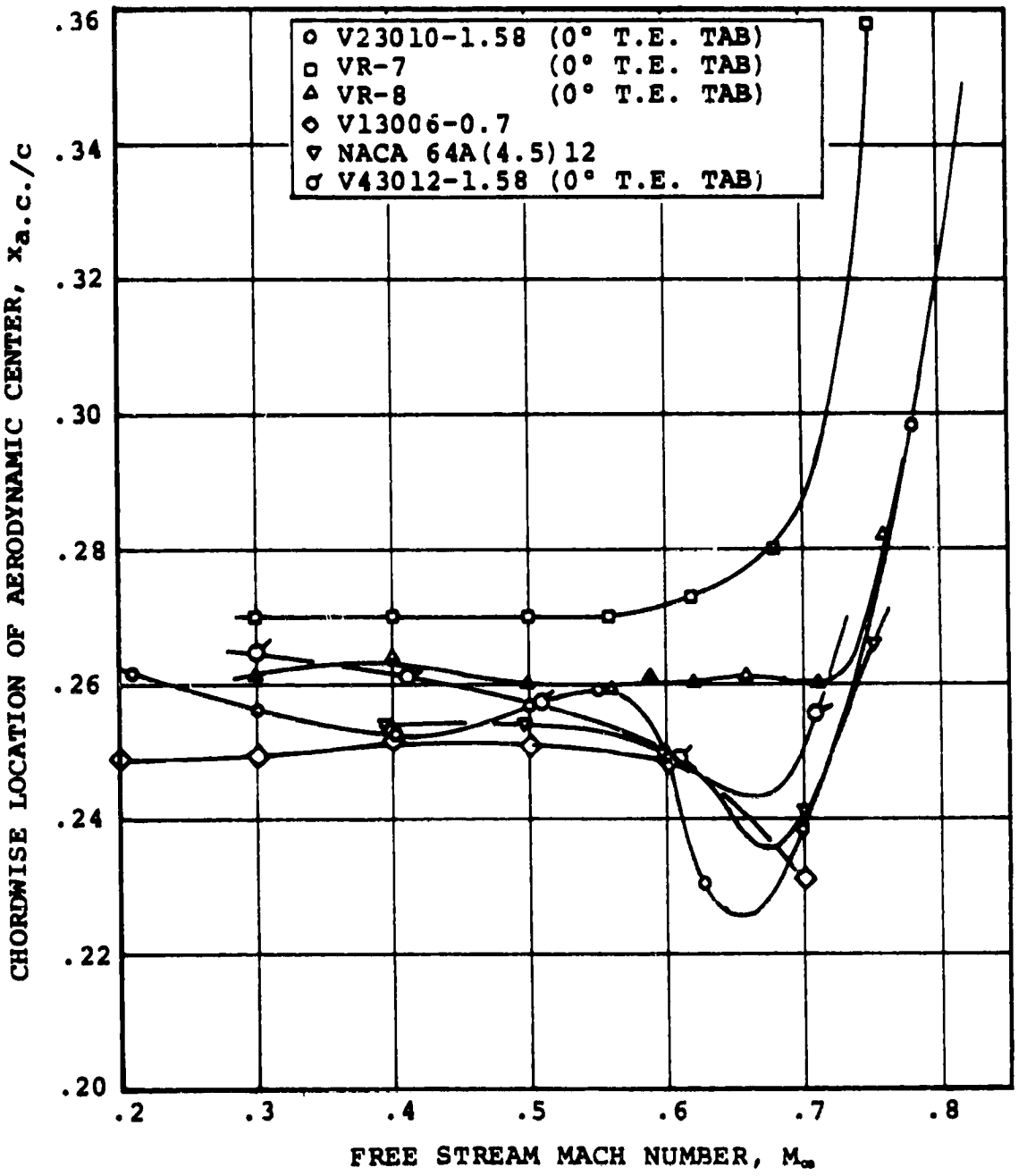


*Figure 1. Effect of Compressibility on the Location of the Aerodynamic Center*

## 1.2.50.8 COMPRESSIBILITY EFFECTS ON THE CENTER-OF-PRESSURE

The effect of compressibility on the center-of-pressure location of a typical airfoil (VR-7) with a trailing edge tab deflected 3° above the reference line is shown in Figure 1.

The center-of-pressure, like the aerodynamic center, moves aft when the Mach number is increased beyond the critical value.

The effect of trailing edge tab deflection is discussed in Section 1.2.90.

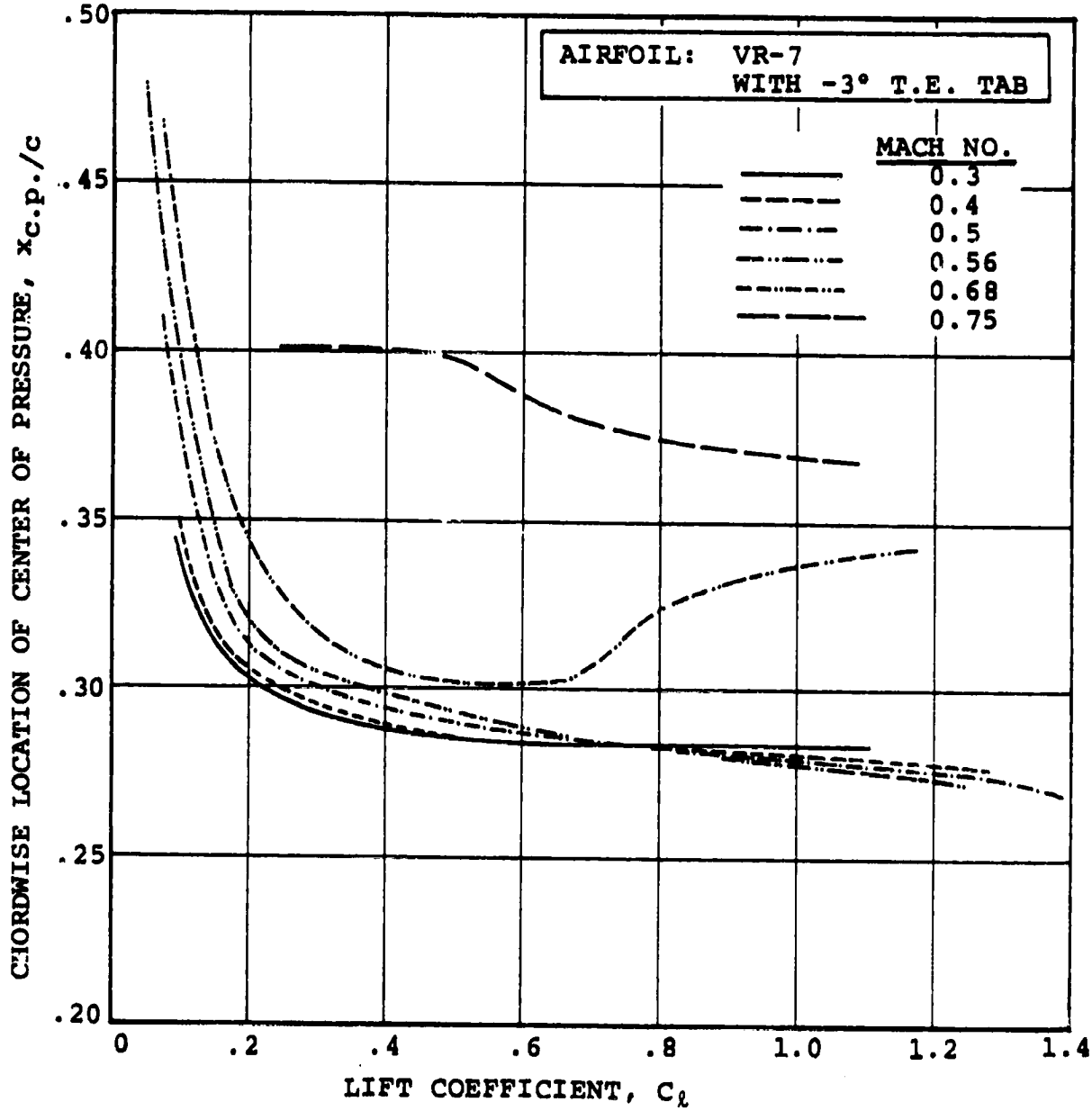


*Figure 1. Effect of Compressibility on the Location of the Center of Pressure of the VR-7 Airfoil*

## 1.2.60 REYNOLDS NUMBER EFFECTS ON AIRFOIL CHARACTERISTICS

A reduction in chord and therefore, in Reynolds number, is generally associated with undesirable changes in section characteristics. The phenomena associated with substantial reductions in chord are particularly significant in conjunction with model rotor tests. There is practically no data corresponding to model-scale rotor airfoil sections at Reynolds and Mach numbers; however, some approximate values can be obtained by correcting the full scale data with the methods described in the numerical examples (1.4.10).

The majority of the data shown in the figures in this section was obtained in NACA wind-tunnel tests and published in NACA reports. However, the figures have been taken from Reference 1, except for Figure 5, from Reference 2.

Figures 1 and 2 illustrate the various types of stall possible and the Reynolds number regimes over which different stall patterns are likely to occur. The correlation of Figure 1 is not valid for NACA 230-series sections and related airfoils such as the V23010-1.58, because, by this correlation, all moderately thick profiles of the 230 family should display trailing-edge stall (i.e., gradual stall) and not leading-edge stall (abrupt), as the test data demonstrate.

Figures 3 and 4 summarize the effect of Reynolds number variation on the maximum lift capability at low speeds for a number of airfoils of interest, if not directly applicable, to helicopter rotors.

Figure 5 summarizes data trends for drag used to estimate hover power corrections between full-scale and model-scale rotors in Reference 2.

Figure 6, again from Reference 1, shows the combined effect of Mach and Reynolds number variations on three airfoils.

References:


1. van den Berg, B., *Reynolds Number and Mach Number Effects on the Maximum Lift and Stalling Characteristics of Wings at Low Speeds.* NLR TR 69025U, March 1969.

2. Gormont, R.E., *A Mathematical Model of Unsteady Aerodynamics and Radial Flow for Application to Helicopter Rotors.* USAAMRDL TR 72-67, May 1973.

3. Gault, D.E., *A Correlation of Low-Speed, Airfoil -Section Stalling Characteristics with Reynolds Number and Airfoil Geometry.* NACA TN 3963, March 1957.

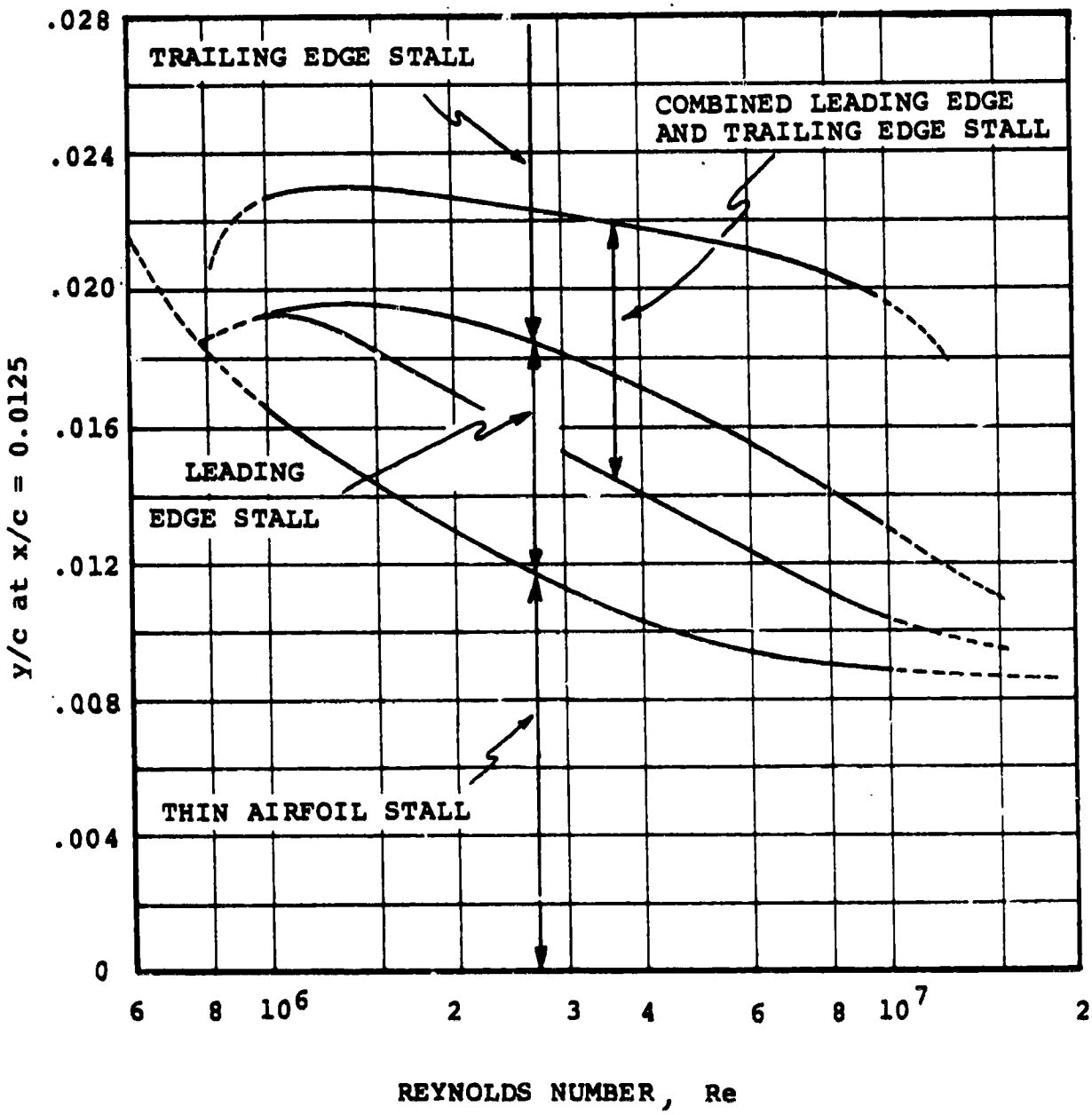


*Figure 1* *Dependence of the Airfoil Section Stalling Characteristics on the Nose Shape Parameter $y_{1.25}/c$ and the Reynolds Number According to Gault (Reference 3)*

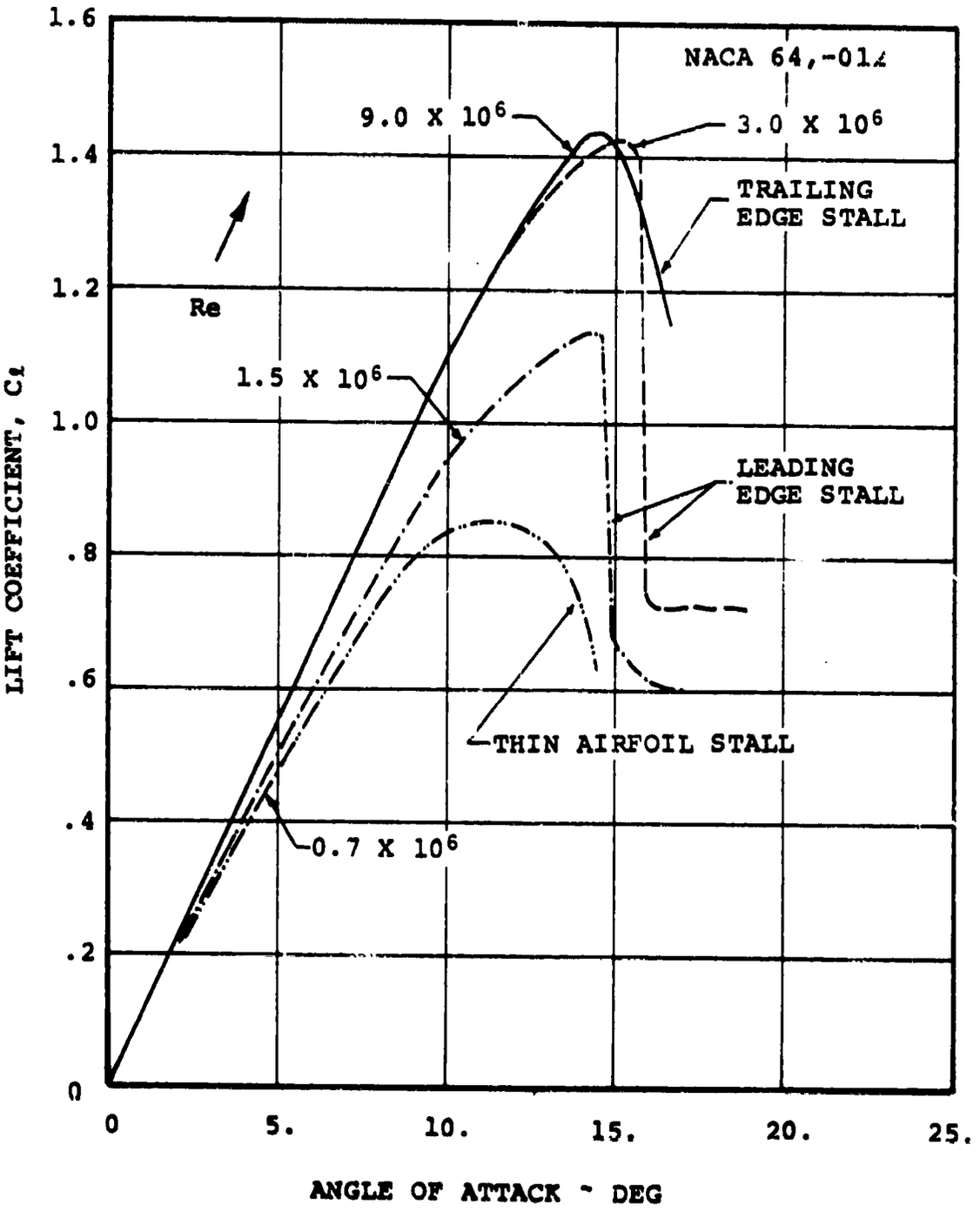


*Figure 2* *Typical Lift Curves at Various Reynolds Numbers for a Moderately Thick Airfoil*

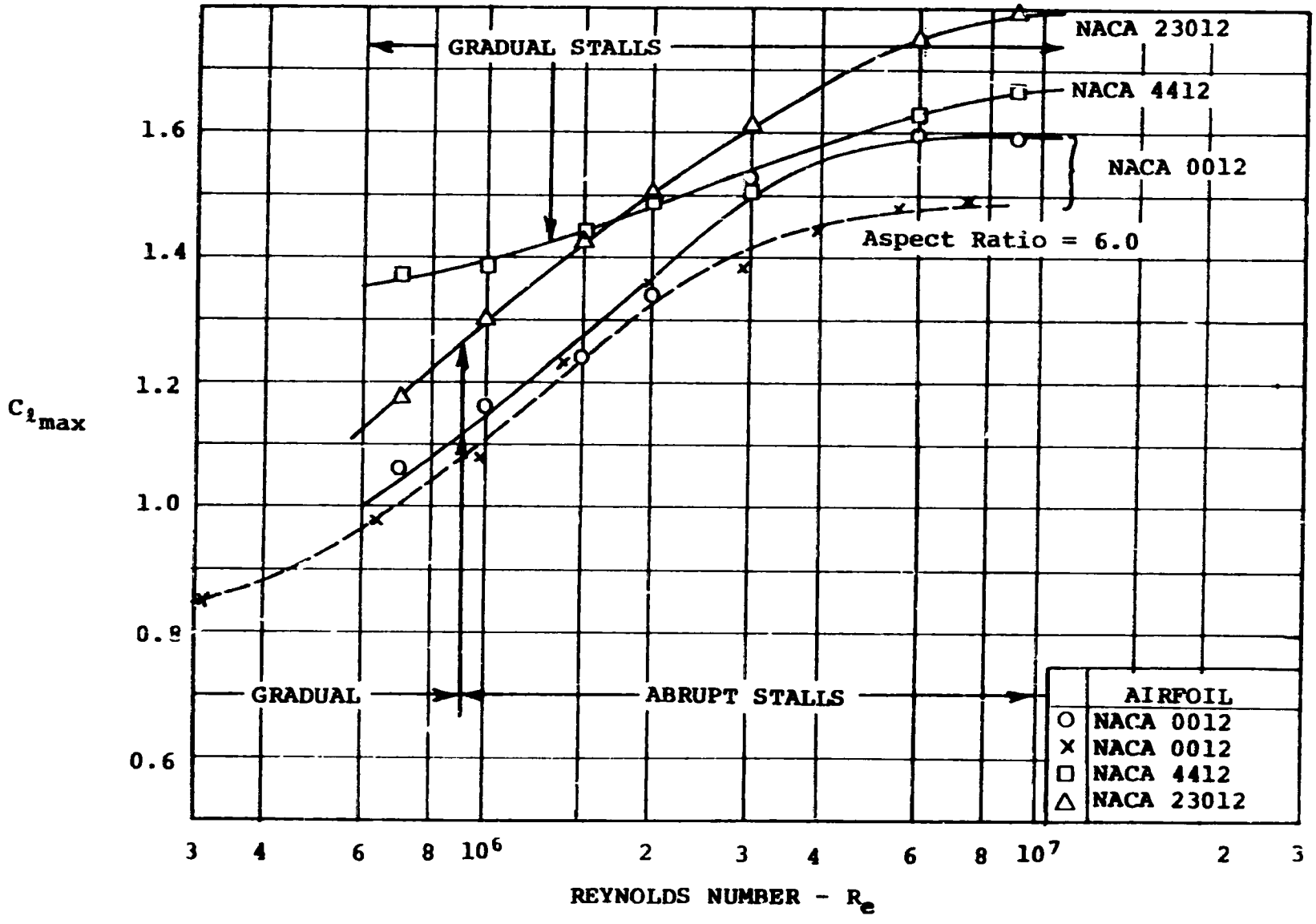


*Figure 3 Effect of Reynolds Number on the Maximum Lift of Several 12% Thick Airfoils*

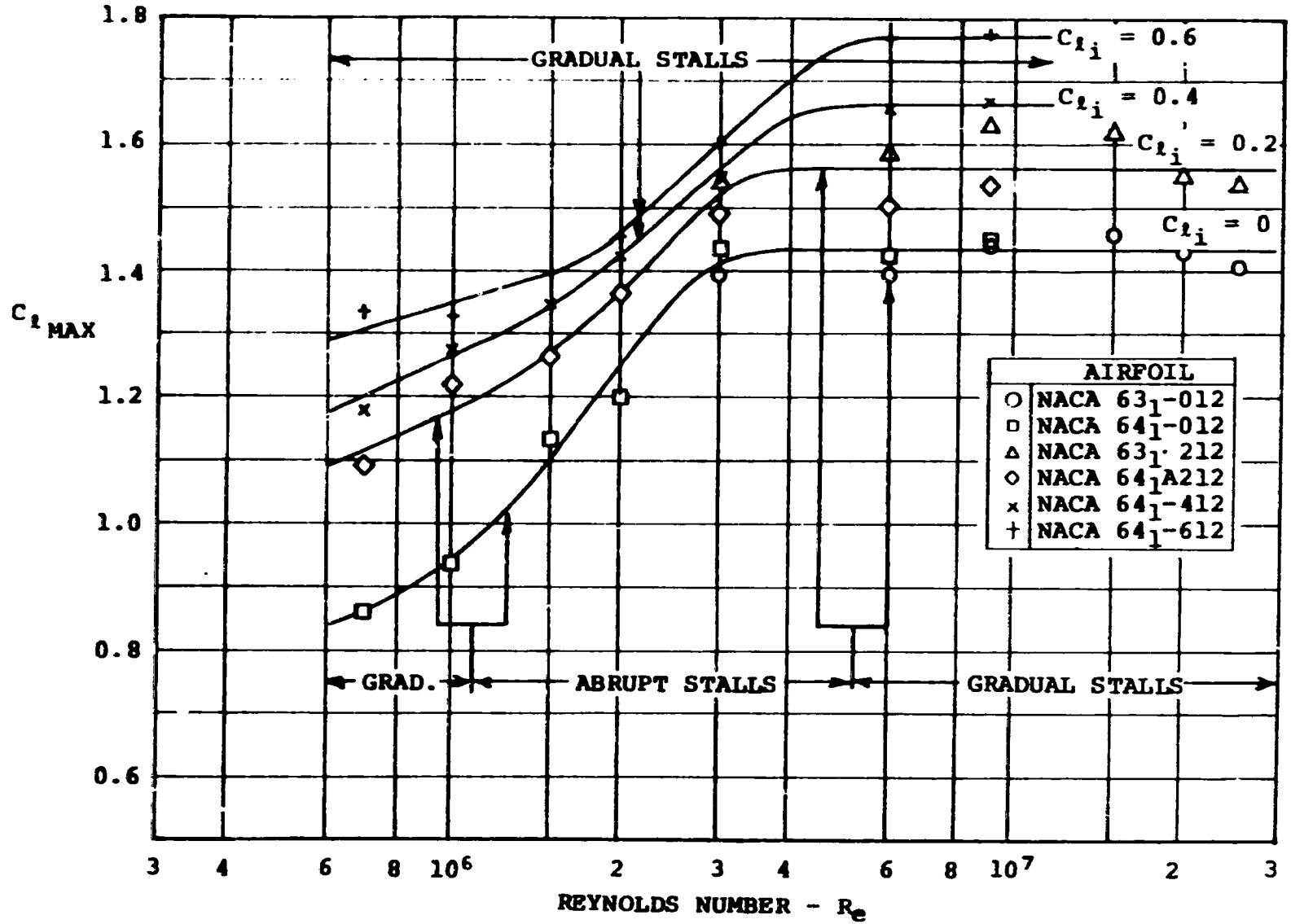


*Figure 4 Effect of Reynolds Number on the Maximum Lift of NACA 6-Series Airfoils*

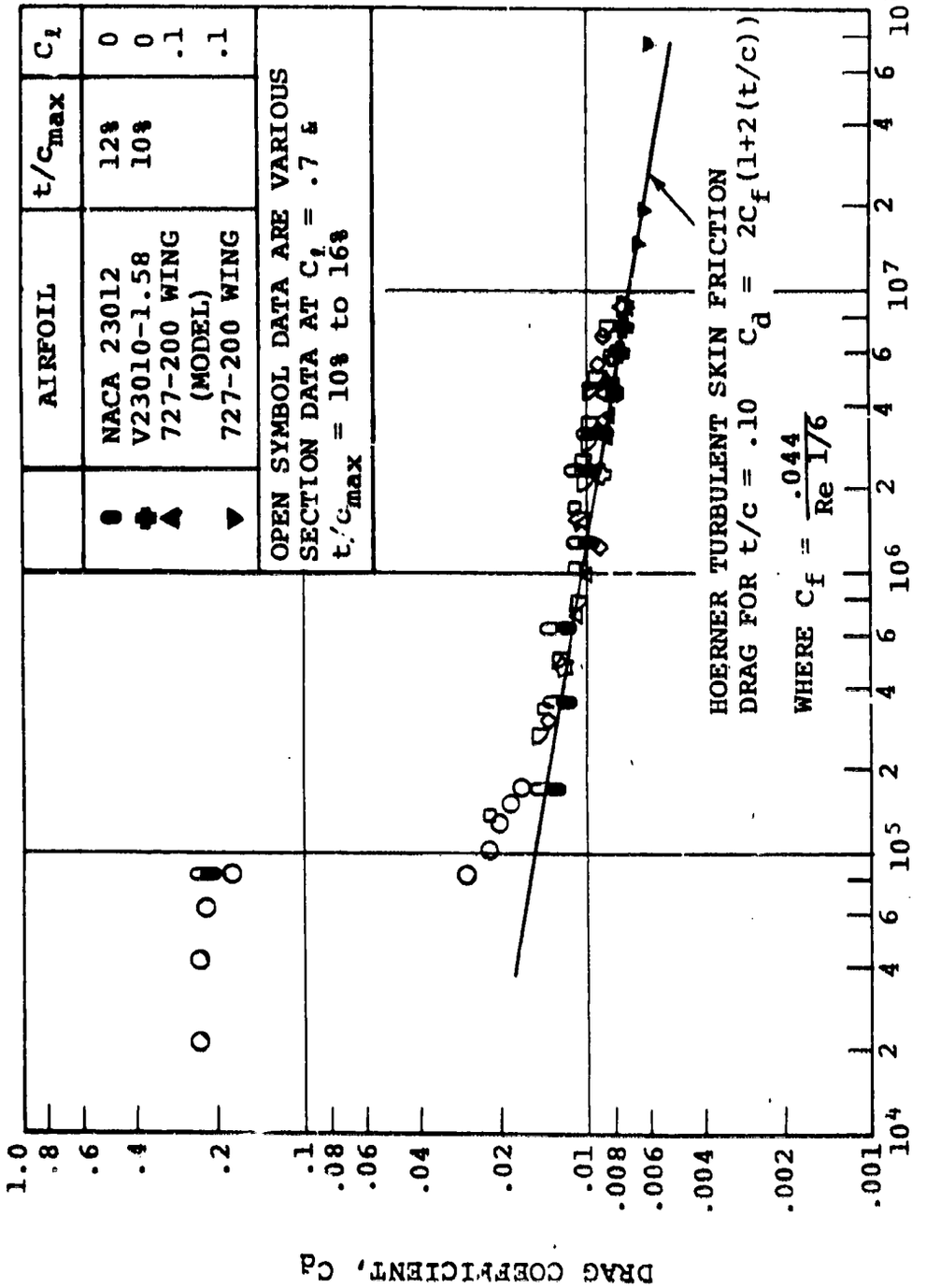


*Figure 5 Effect of Reynolds Number on Drag*

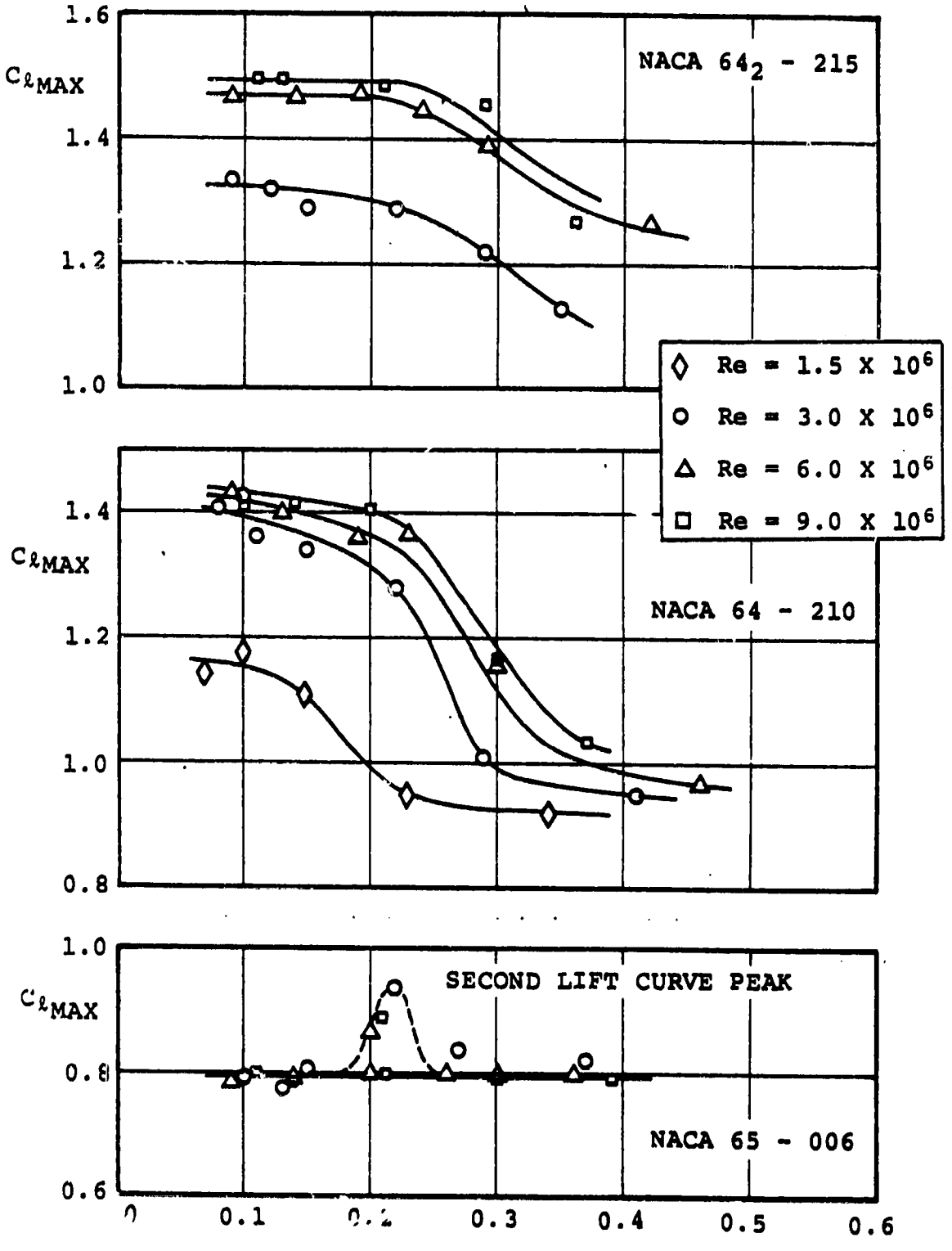


*Figure 6* *Effect of Mach Number at Constant Reynolds Number on the Maximum Lift of Various Airfoils*

## 1.2.70 REVIEW OF UNSTEADY AERODYNAMIC EFFECTS

The blade motions associated with forward flight in conjunction with the non-uniform downwash field in which the helicopter rotor operates give rise to unsteady flow phenomena which significantly alter the aerodynamic characteristics obtained for airfoils at quasi-steady conditions.

The unsteady aerodynamic effects over airfoils in the absence of flow separation were analyzed by T. Theodorsen[1] with a mathematical model in which the shed wake elements which give rise to the unsteady effects are trailed downstream from the airfoil. For rotor (with helical wakes) the shed wake is embedded under the rotor. Loewy[2] has shown that for this case a modified Theodorsen function can be used. In either instance, the unsteady effects have been applied to helicopter rotor performance methodology as shown by Harris, et al[3].

Apart from these effects, rotor tests have shown that rotor stall does not follow the trends which would be indicated by quasi-steady airfoil data. Oscillating airfoil tests conducted by Carta[4] and by Liiva, et al[5] demonstrated that dynamic stall is considerably different from static or quasi-steady stall, and that in the presence of airfoil motions the stall could be delayed to higher angles of attack resulting in considerably extended maximum lift capability.

Recovery from stall was found to be dependent on the nature of the stall, i.e. leading edge or trailing edge, etc. This was found to influence the aerodynamic damping coefficient, where negative damping values can lead to self-sustained oscillations.

## 1.2.70.1 DYNAMIC STALL DELAY

By far, the most important effect evident from oscillating airfoil tests is the delay in the onset of stall. A typical set of $C_N$ and $C_M$ response curves is compared with the steady data in Figure 1 for oscillations with a constant value of excursions in angle of attack, $\Delta\alpha$. When the mean angle ($\alpha_o$ = 7.33°) is such that the total excursion is below stall, the elliptical loops predicted by unsteady airfoil theory, i.e., Theodorsen, follow the steady data. When the mean angle is increased to 14.92° and the excursion extends beyond the static stall angle, the maximum normal force is found to exceed the steady state value. The angle for pitching moment stall also exceeds the steady data in this regime. When the mean angle is increased so that the flow is fully separated, the loops again follow the steady data, as shown in Figure 1.

The dynamic effects are significantly altered with changes in the pitch frequency and Mach number

- "The airfoil is partially stalled during the decreasing portion of the cycle for the higher frequency case, even though the $C_N$ trace shows a superficial resemblance to the elliptical shape characteristic of unstalled flow." (Ref. 6)
- The sudden stalling apparent at the low frequency does not occur at the high frequency. (Ref. 7)
- The available test data show that at M = 0.6 the dynamic $C_N$ and $C_M$ loops follow closely the static lines. The cycle damping is always positive and there are no sharp breaks in the $C_N$ and $C_M$ curves for either steady or oscillatory data. (Ref. 7)

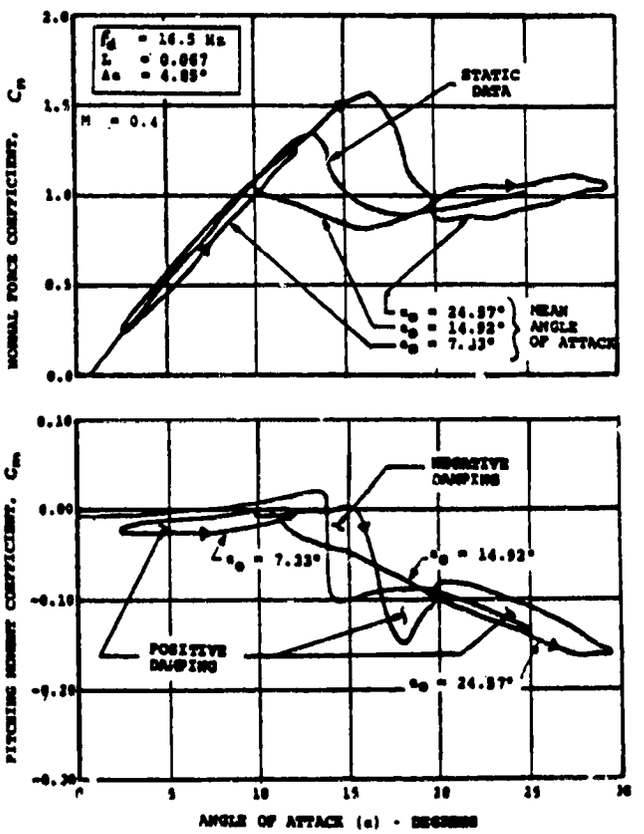


AVERAGE CYCLE DAMPING IS DEFINED AS

$-\oint C_m \, d\alpha$ FOR PITCHING OSCILLATION

$-\oint C_n \, d\alpha$ FOR PLUNGE OSCILLATION

*Figure 1 Typical Pitch Oscillation Data*

Dynamic stall data are used in rotor performance calculations either directly in a table lookup format, or indirectly by empirical

methods which synthesize dynamic data from the available static data. The key parameters to the latter method are deduced from test data. One of the current empirical methods developed by Gross and Harris[8], and also presented by Gormont[9], uses a so-called "gamma" function, as described in Section 1.2.0070.03.

The "gamma" function used to calculate the increment in stall angle between quasi-steady and dynamic data is defined as:

$$\Delta\alpha_{Dynamic} = K\gamma_{C_\ell, C_m} \left|\frac{c\dot{\alpha}}{2V}\right|$$

where $K = +1.0$ for positive $d\alpha/dt$,
$K = -0.5$ for negative $d\alpha/dt$,

and the $\gamma$ corresponding to lift or pitching moment is obtained from oscillating airfoil test data. (See Section 1.2.70.3) The delayed stall angle due to dynamic stall can be evaluated as,

$$\alpha_{\substack{dynamic \\ stall}} = \alpha_{\substack{static \\ stall}} + \Delta\alpha_{dynamic}$$

To synthesize from quasi-steady data the dynamic force coefficients acting on a blade element at angle of attack $\alpha_{BE}$, angle of attack rate $\dot{\alpha}_{BE}$ and Mach number, M, a reference angle of attack $\alpha_{REF}$ is calculated as $\alpha_{REF} = \alpha_{BE} - \Delta\alpha_{dynamic}$.

The lift coefficient values corrected for dynamic effects are based on a linear lift curve determined by the angle for zero lift and the lift at $\alpha_{REF}$, Figure 2. The lift coefficient is given by:

$$C_\ell = \frac{C_{\ell_{REF}}}{\alpha_{REF} - \alpha_o} \alpha_{BE}$$

When $\alpha_{REF}$ is below the static stall angle, the dynamic lift coefficient is estimated along an extended linear lift curve as shown in Figure 2a. When $\alpha_{BE}$ is greater than the angle of attack for static stall, lift coefficients considerably greater than the static $C_{\ell_{max}}$ can be attained, Figure 2b. When $\alpha_{REF}$ is greater than the angle for static stall the linear lift curve constructed from $\alpha_o$ and $\alpha_{REF}$ is greatly reduced in size and the dynamic lift extension is decreased proportionally, as illustrated in Figure 2c.

The inclusion of the unsteady effects due to pitching and heaving motions of the rotor blade accounting for the non-circulatory contribution to the lift, and including the Theodorsen functions for attenuation and phase shift, are discussed by Gormont[9].

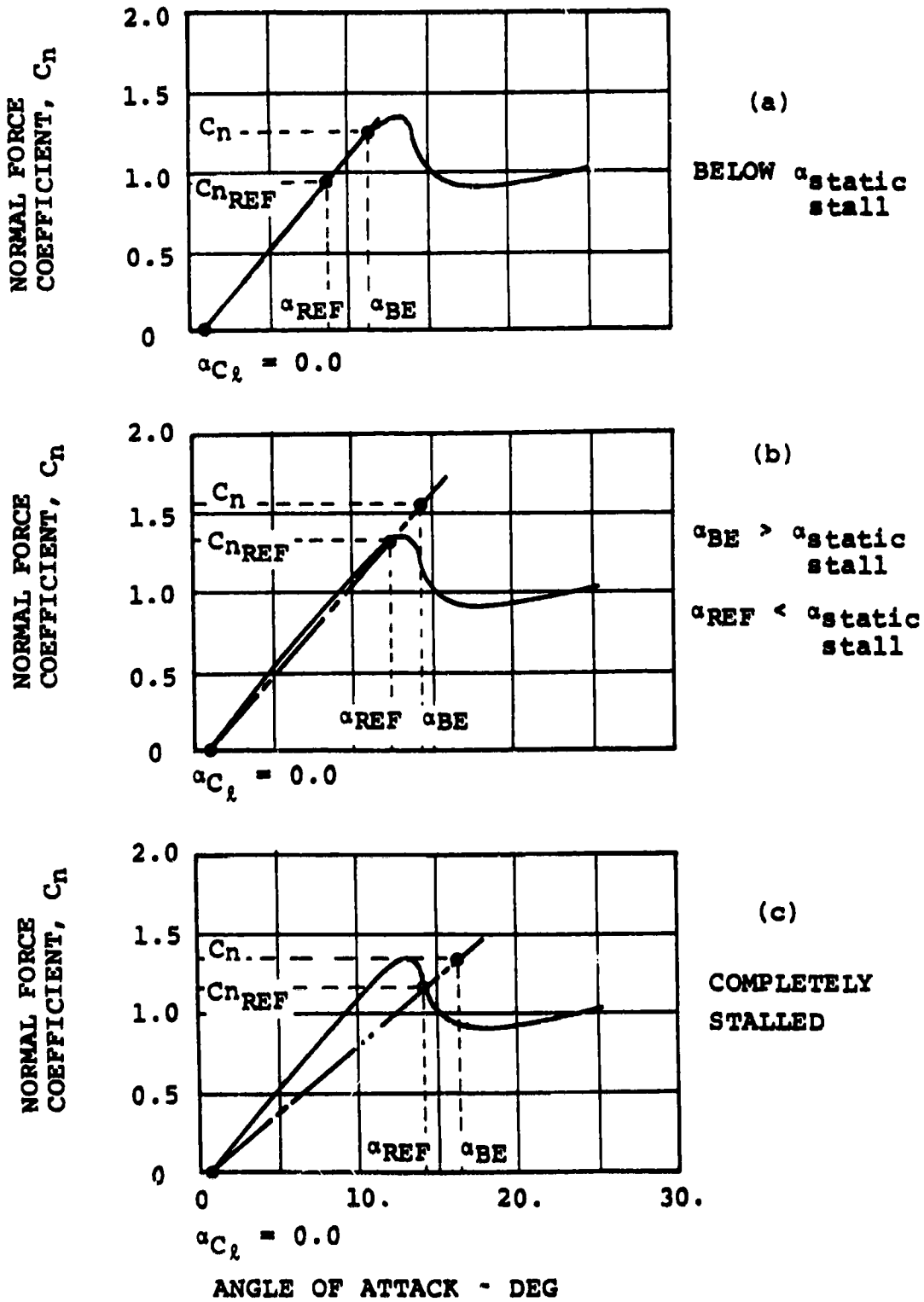


*Figure 2 Approximation of Dynamic Stall Conditions from Quasi-Steady Data*

### 1.2.70.2 DYNAMIC PITCHING MOMENT COEFFICIENT, DRAG COEFFICIENT AND AERODYNAMIC DAMPING

The synthesis of the dynamic pitching moment and drag coefficients given in Reference 9 requires the computation of $\alpha_{REF}$ using the $\gamma$ function derived from the moment stall data. However, the dynamic coefficient is obtained from a simple table look-up at $\alpha_{REF}$ and at the Mach number of the blade element. This technique limits the maximum values of $C_M$ and $C_d$ to the values obtained during static tests while a significant overshoot in the nose-down (negative) pitching moments have been observed in the dynamic data.

The area enclosed by the $C_m$ loop indicates the work per cycle. When the circuit is counter-clockwise, the airfoil is transferring energy to the airstream. When the circuit is clockwise, the airfoil extracts energy from the airstream. This implies that the aerodynamic damping is negative and can lead to self-excited oscillation, i.e., flutter.

## 1.2.70.3 GAMMA FUNCTION

The ability to evaluate dynamic airfoil data from the static data with a good degree of accuracy simplifies rotor performance calculations. One of the empirical methods available for such evaluation is the so-called "gamma" function technique originated by Gross and Harris[8]. A description of the methodology is also given by Gormont[9].

The "gamma" functions for the lift and pitching moment coefficients are constructed from dynamic test data by making records of the angle of attack $\alpha$ and the rate $\dot{\alpha}$ (for 270° only) at which lift stall and moment stall occur at each Mach number. The variation of $\alpha$ with $\sqrt{c\dot{\alpha}/2V}$ is plotted as illustrated in Figure 3.

From a linear curve fit, the slope of $\alpha$ vs. $\sqrt{c\dot{\alpha}/2V}$ is defined as the "gamma" function.

The $\gamma$ function has to be estimated over a range of Mach numbers to at least M = 0.6 because it is very sensitive to compressibility effects. With increasing Mach number the effect of dynamic stall delay is reduced, and $\gamma$ functions are generally very small or identically zero at M > 0.6.

V23010-1.58 AIRFOIL
MACH NO. = 0.4

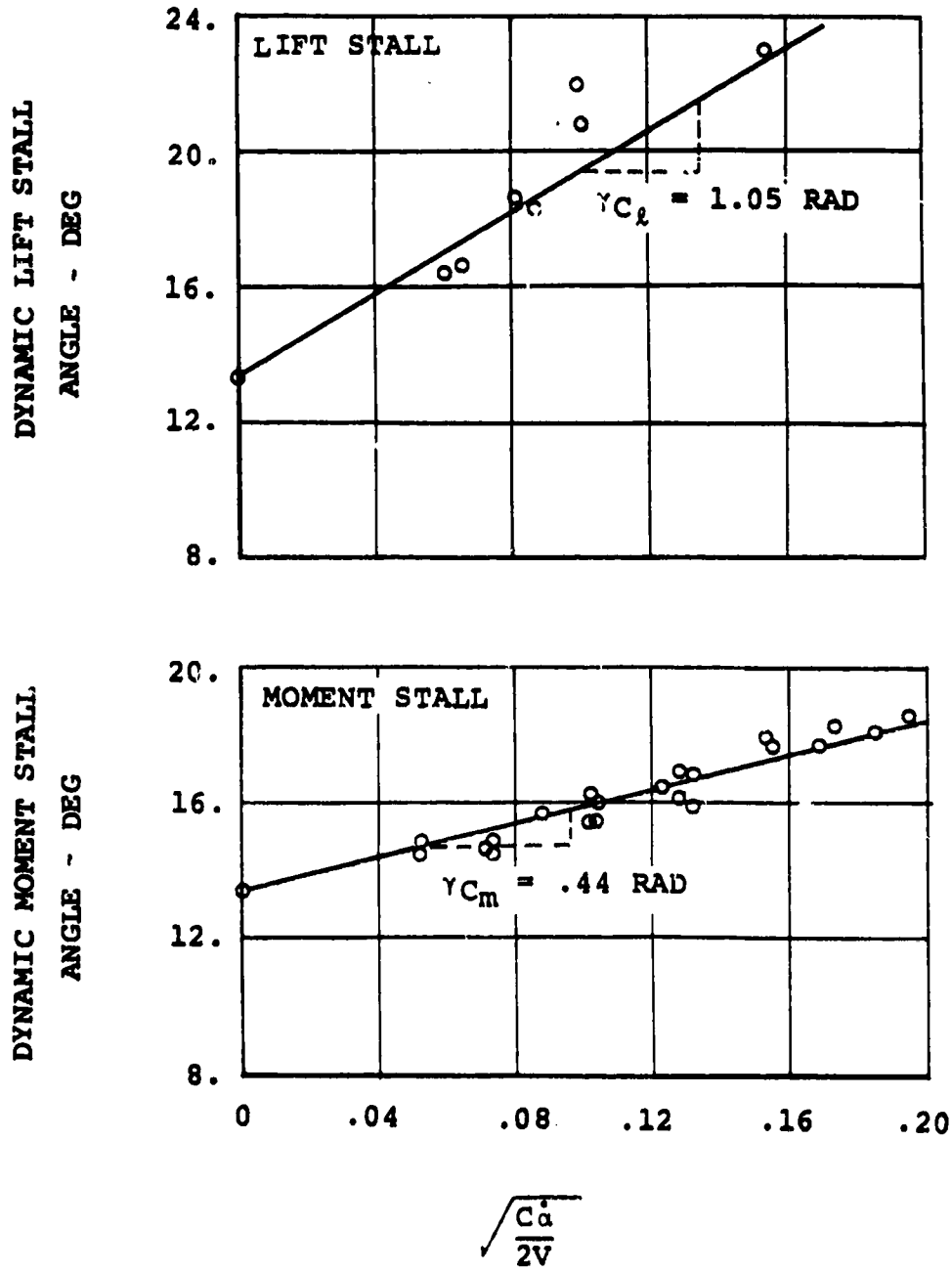


*Figure 3 Definition of Stall Delay Function ("Gamma" Functions)*

## REFERENCES


1. Theodorsen, T. "General Theory of Aerodynamic Instability and the Mechanism of Flutter", NACA Report 496, 1935.

2. Loewy, R.G., "A Two Dimensional Approach to the Unsteady Aerodynamics of Rotary Wings", JAS, February 1957, Vol 24, No. 2.

3. Harris, F.D., Tarzanin, F., and Fisher, R.K., "Rotor High Speed Performance, Test Vs. Theory", Journal AHS, July 1970.

4. Carta, F.O., "Unsteady Normal Force on an Airfoil in a Periodically Stalled Inlet Flow", Journal of Aircraft, Vol. 4, No. 5, Sept-Oct 1967.

5. Liiva, J., Davenport, F.J., Gray, L., and Walton, I.C., "Two Dimensional Tests of Airfoils Oscillating Near Stall", U.S. Army AVLABS TR 68-13.

6. Liiva, J., and Davenport, F.J., "Dynamic Stall of Airfoil Sections for High Speed Rotors", 24th Annual National Forum of the American Helicopter Society, May 1968.

7. Liiva, J., "Unsteady Aerodynamic and Stall Effects on Helicopter Rotor Blade Airfoil Sections", 6th Aerospace Sciences Meeting, American Institute of Aeronautics and Astronautics, January 1968.

8. Gross, D.W., and Harris, F.D., "Prediction of Inflight Stalled Airloads From Oscillating Airfoil Data", 25th Annual National Forum of the American Helicopter Society, May 1969.

9. Gormont, R.E., "A Mathematical Model of Unsteady Aerodynamics and Radial Flow for Application to Helicopter Rotors", USAAMRDL Technical Report 72-67, May 1973.

## 1.2.80 EFFECT OF GEOMETRY - MEAN LINE AND THICKNESS EFFECTS

An airfoil section consists of a mean (or camber) line combined with a thickness distribution. Airfoil theory states that the mean line can be replaced by a distribution of vortices and the airfoil contour (thickness) by a distribution of sources. The mean line determines the overall chordwise distribution of pressures and therefore the airfoil characteristics associated with it. The thickness shape affects the chordwise loading less significantly than the mean line, but it has a strong influence on the local velocity gradients, particularly in the vicinity of the leading edge, and therefore it influences the development of the boundary layer and other parameters, as summarized in Table I.

TABLE I

| AIRFOIL GEOMETRY COMPONENT | SECTION AERODYNAMIC CHARACTERISTIC AFFECTED |
|---|---|
| Mean Line Distribution | Chordwise Load Distribution<br>$\alpha_{\ell_0}$ , Angle of Zero Lift<br>$C_m$<br>$C_{d_{min}}$, $C_{\ell_{max}}$ } weakly |
| Thickness Distribution | $C_{d_{min}}$<br>Critical Mach Number<br>$dC_\ell/d\alpha$<br>$C_{\ell_{max}}$ |

Sections 1.2.80.1 and 1.2.80.2 discuss the effects of mean line distributions and thickness shapes on airfoil characteristics.

## 1.2.80.1 MEAN LINE DISTRIBUTION

A mean line can be designed to give a desired chordwise load distribution. Typical are the mean lines used with the NACA 6-series airfoil sections. They were designed for a design lift coefficient $C_{\ell_i}$ of 1.0 and have uniform loading up to some specified chordwise location from the leading edge, beyond that location the loading decreases linearly to zero at the trailing edge. Figure 1 shows the mean line and the associated chordwise loading for the case with the uniform loading extending to x/c = 0.4, i.e., a = 0.4. For any other desired value of the design lift coefficient, e.g. $C_{\ell_i}$ = 0.5 and the same load distribution, the mean line ordinates for $C_{\ell_i}$ = 1.0 are multiplied by the desired value of $C_{\ell_i}$ as illustrated.

As the point of maximum camber is moved rearward and the load distribution is moved aft, the pitching moment about the quarter chord ($C_{mc/4}$, nose down) is increased. Increasing the camber (or $C_{\ell_i}$) at a given maximum camber position will also increase the negative pitching moment coefficient.

When the camber is increased, i.e. as $C_{\ell_i}$ is increased, the result is an increase in the angle for zero lift, $\alpha_0$, this means that the camber line (the airfoil) will have to be pitched further nose-down to achieve zero lift.

Because the camber is relatively small, pressure drag changes with camber changes are small. Boundary layer effects which determine frictional effects and stall are weak functions of the mean line distribution.

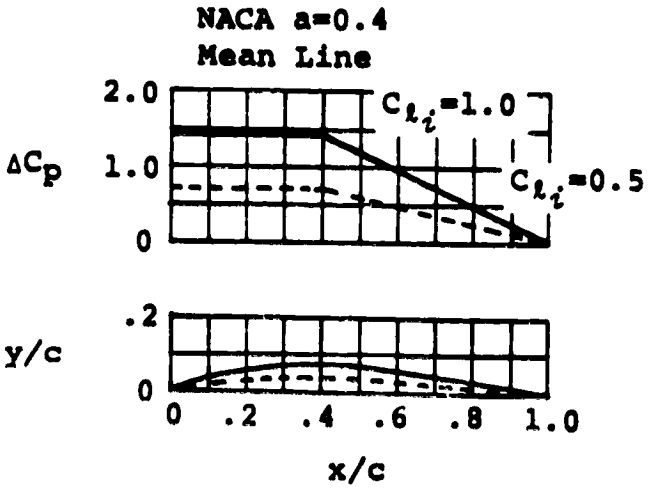


*Figure 1. Typical mean lines and chordwise pressures.*

## 1.2.80.2 THICKNESS EFFECTS

The type of thickness distribution added to the mean line (camber) determines the overall pressure distribution. The geometry of the leading edge determines the magnitude of leading edge velocities and the location of the stagnation point. Euler's equation in natural coordinates states that the pressure gradient normal to curved streamlines is inversely proportional to the radius of curvature and that it decreases approaching the center of curvature. Thus, the thickness distribution determines the location of the minimum pressure (i.e., maximum velocity) and the pressure recovery (deceleration of the flow) approaching the trailing edge, which has a destabilizing effect on the boundary layer.

Typical examples of pressure coefficients, $C_p$, for the NACA 0012 and NACA 63A012 thickness forms are presented in Figure 1. The NACA 0012 airfoil achieves its minimum pressure near the leading edge. The NACA 63A012 airfoil is typical of airfoils developed for low-drag and high Mach number operation. For the same lift level the minimum pressure of the NACA 63A012 is lower and it is attained further back on the chord than for the NACA 0012, so that a favorable pressure gradient is maintained further aft on the chord.

The decreased suction pressure on the 63A012 airfoil also aids in delaying of the onset of compressibility effects. By moving the minimum pressure position away from the leading edge, the drag coefficient is reduced as a result of the lowered velocities over the leading edge, the extended favorable velocity gradients, and the delay in transition from laminar to turbulent boundary layer.

Thick airfoil theory states that $dC_\ell/d\alpha$ should increase (in the absence of viscous effects) with airfoil thickness. Airfoils having relatively poor boundary layer characteristics, such as the 0012, do not exhibit this trend. However, airfoils such as the 63A012 , designed to sustain extensive laminar flow, do follow the expected trends.

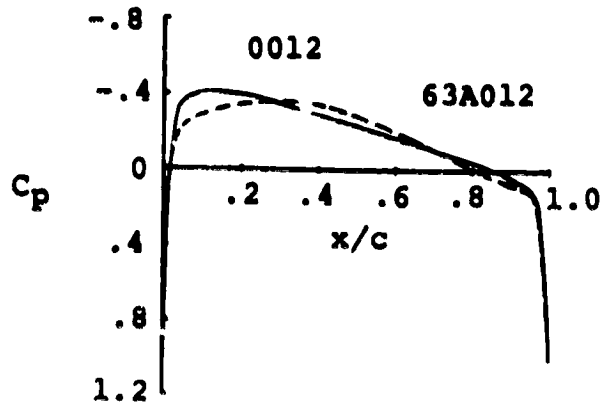


*Figure 1. Variation of chordwise pressure distribution with thickness forms.*

## 1.2.90 EFFECT OF AIRFOIL TRAILING EDGE MODIFICATIONS

The following paragraphs illustrate the most common airfoil trailing edge modifications.

### 1. Trailing Edge Angle

The angle between the upper and lower surfaces at the trailing edge of an airfoil affects both the location of the aerodynamic center and the lift curve slope. Increasing the trailing edge angle will:

- Decrease the lift curve slope (as illustrated in Figure 1)
- Move the aerodynamic center forward, i.e., closer to the leading edge (Reference 1, p. 182).

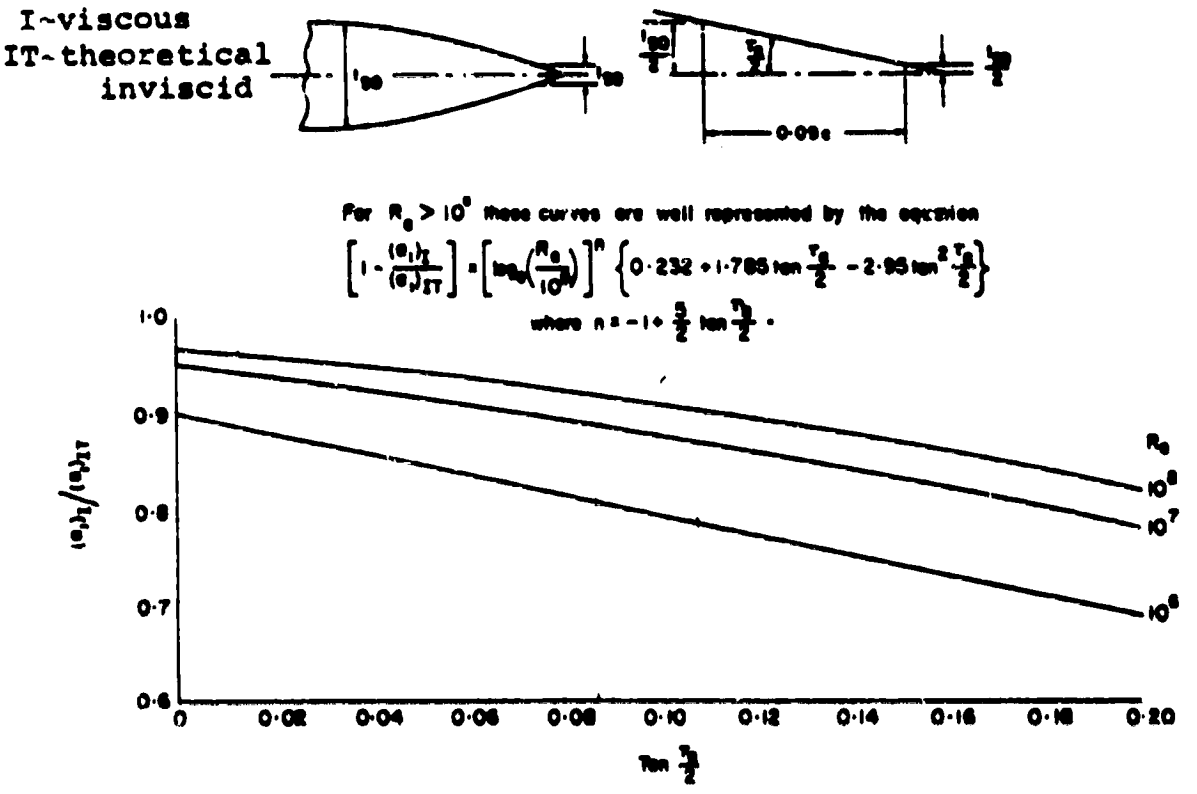


FIG. 1 LIFT-CURVE SLOPE FOR TWO-DIMENSIONAL FLOW WITH TRANSITION AT THE LEADING EDGE

[REPRODUCED FROM ROYAL AERONAUTICAL SOCIETY AERODYNAMICS DATA SHEET WINGS 01.01.05 - ISSUED JANUARY 1958]

## 2. Trailing Edge Tabs

Helicopter airfoils are often modified so that the aft 5% to 10% of the chord has parallel surfaces with sufficient thickness to satisfy rotor blade structural requirements. The portion of trailing edge with parallel surfaces is referred to as a trailing edge tab, and it is often deflected ("reflexed") to change the section pitching moment characteristics. Two kinds of T.E. tabs are common in rotor applications:

a) Trailing edge tabs applied along the entire span of a rotor blade.

b) Trim tabs, i.e., bendable tabs applied over a short portion of the blade span and used to "track" or match one blade to other blades on the same rotor.

Data sheets 1.3.250 and 1.3.260 for the V23010-1.58; 1.3.380, 1.3.390, 1.3.40 for the VR-7 airfoil and 1.3.30, 1.3.31 for the V43012-1.58 show the following trends:

- Deflecting the trailing edge tab will shift pitching moments at the zero lift level at the rates -

  $dC_m/d\delta_{tab} = -0.0062$/Deg for a 0.05c Tab

  $dC_m/d\delta_{tab} = -0.005$/Deg for a 0.05c Tab

  The sensitivity of this effect to Mach number is illustrated in Figure 2.

- Since the pitching moment corrections required of a trailing edge tab (not a trim tab) are generally in the nose up direction, such corrections decrease the net camber of the airfoil and cause some penalty in its maximum lift capability. This trend is illustrated in Figure 3.

- The angle for zero lift is affected by the trailing edge tab angle. A 0.05c tab will shift the angle for zero lift by 0.23 degrees per degree of tab deflection.

- Deflecting a trailing edge tab in the direction to generate nose-up pitching moments will cause the aerodynamic center to move aft. On the VR-7 airfoil this shift amounts to 0.005c for a tab angle change from 0° to -3° at M=0.4, with no further shift when the tab angle is increased to -6°.

- Tab deflection will also cause a radical change in the location of the center of pressure, as shown in Figure 4.

- For small tab deflections ($\Delta\delta_{TAB} < 3°$) drag changes are negligible.

3. Trailing Edge Wedges

In some instances it is desirable to make small pitching moment adjustments without changing the trailing edge tab angle. Trailing edge wedges such as shown in Figure 5 have proven to be quite effective, although not as effective as changes in trailing edge tab angle.

4. Trailing Edge Bluntness

Generally, trailing edge bluntness is associated with an increase in drag level. Approximate values for such an increase can be evaluated by the expression (Reference 2) -

$$\Delta C_d = k(A)^{-1/3} (h/c)^{4/3}$$

where A is the drag coefficient of the unmodified airfoil, i.e., with a sharp trailing edge, h/c is the thickness of the thickened trailing edge in fraction of chord. k is a constant which takes into account the character of the shed wake; namely,

k = 0.1 for a wake without a vortex street

k = 0.14 for wake with organized vorticity (vortex street)

Hoerner, Reference 2, suggests that a regular vortex street (requiring k=0.14) will not occur if:

- h has a small value, roughly thinner than half of the boundary layer thickness at the T.E., as is often the case at transonic flow conditions because of early transition.

- The overall flow is unsymmetrical, i.e., $|C_\ell| > 0.1$ for a symmetrical section

For example, if an airfoil with a sharp trailing edge has a drag coefficient (Cd) of 0.01 and the trailing edge thickness is increased to 3%.

$\Delta C_d = 0.00433$ without vortex street ($k = 0.1$)

$\Delta C_d = 0.00605$ with vortex street ($k = 0.14$)

## REFERENCES

1. Abbott, I.H., and Von Doenhoff, A.E., Theory of Wing Sections. Dover Publications, Inc., New York, N.Y. 1953

2. Hoerner, S.F., Fluid Dynamic Drag, Published by the Author, 1965.

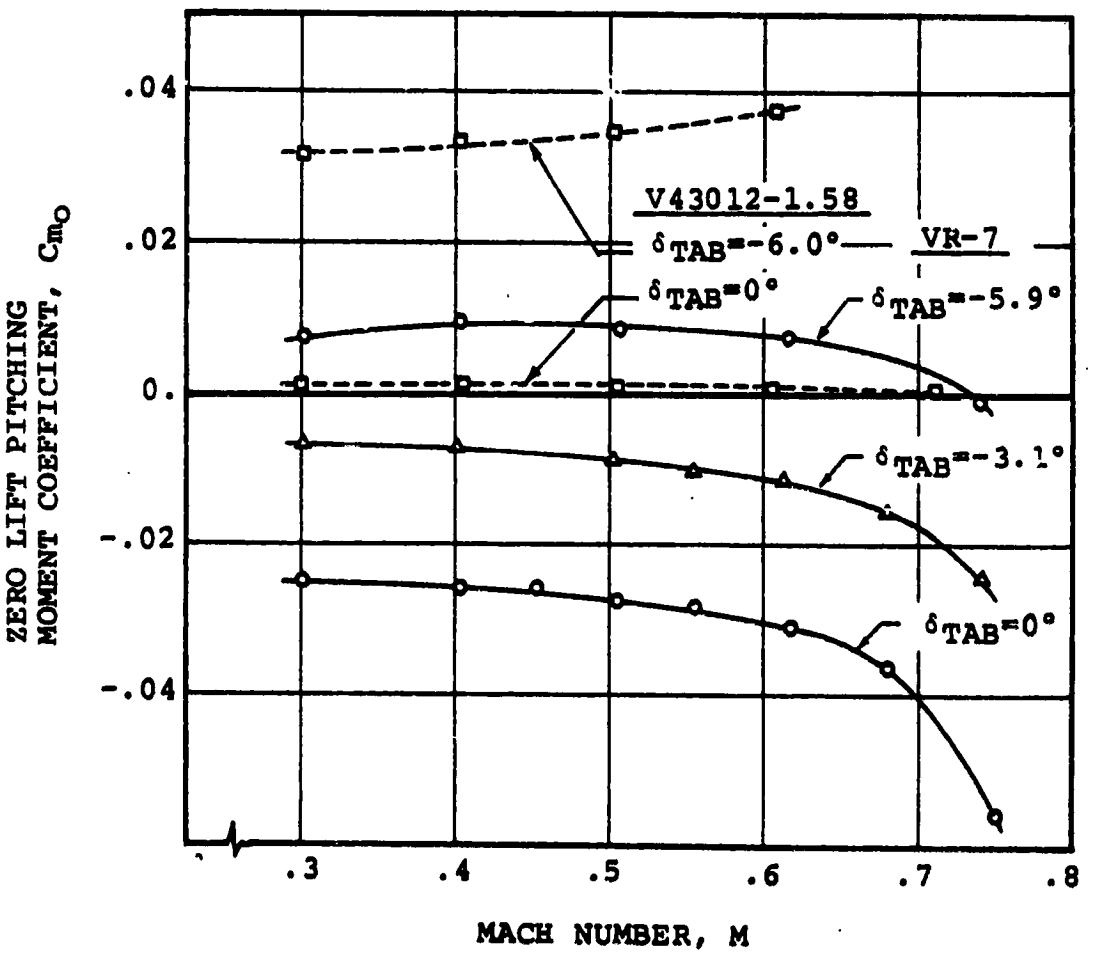


*Figure 2. Effect of Tab Deflection Angle on the Zero-Lift Pitching Moments of the VR-7 and V43012-1.58 Airfoils*

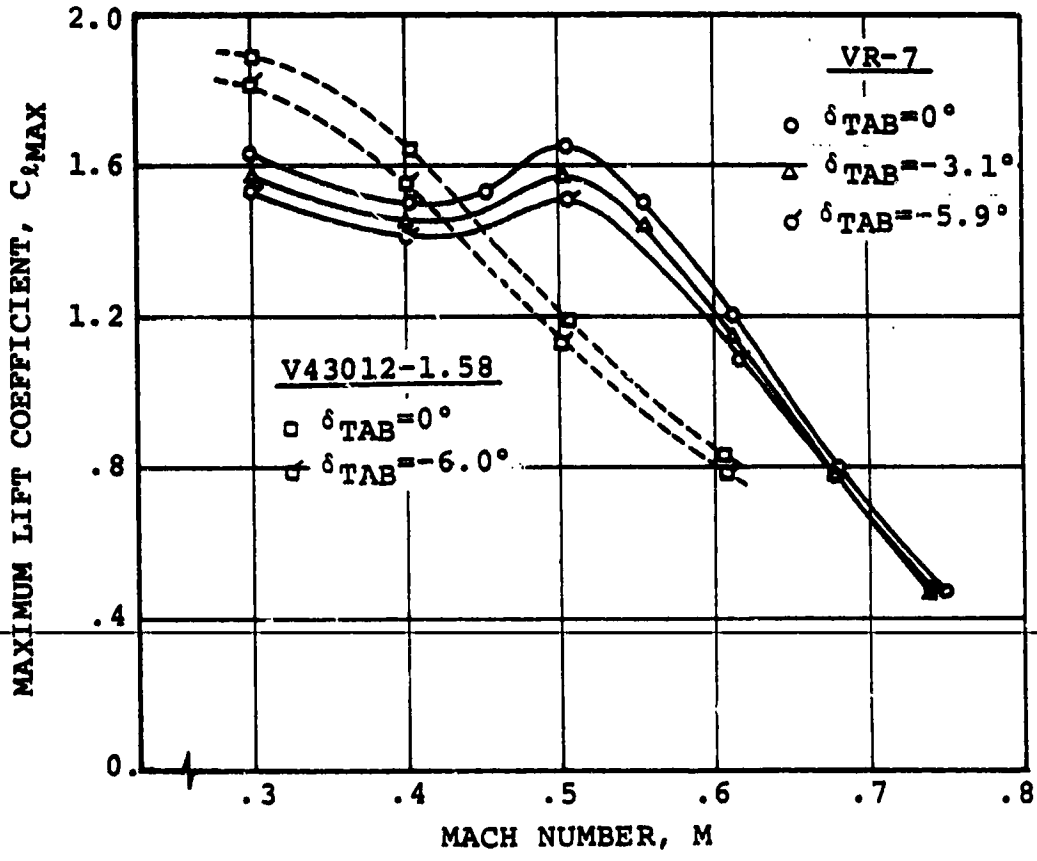


*Figure 3. Effect of Tab Deflection Angle on the Maximum Lift of the VR-7 and V43012-1.58 Airfoils*

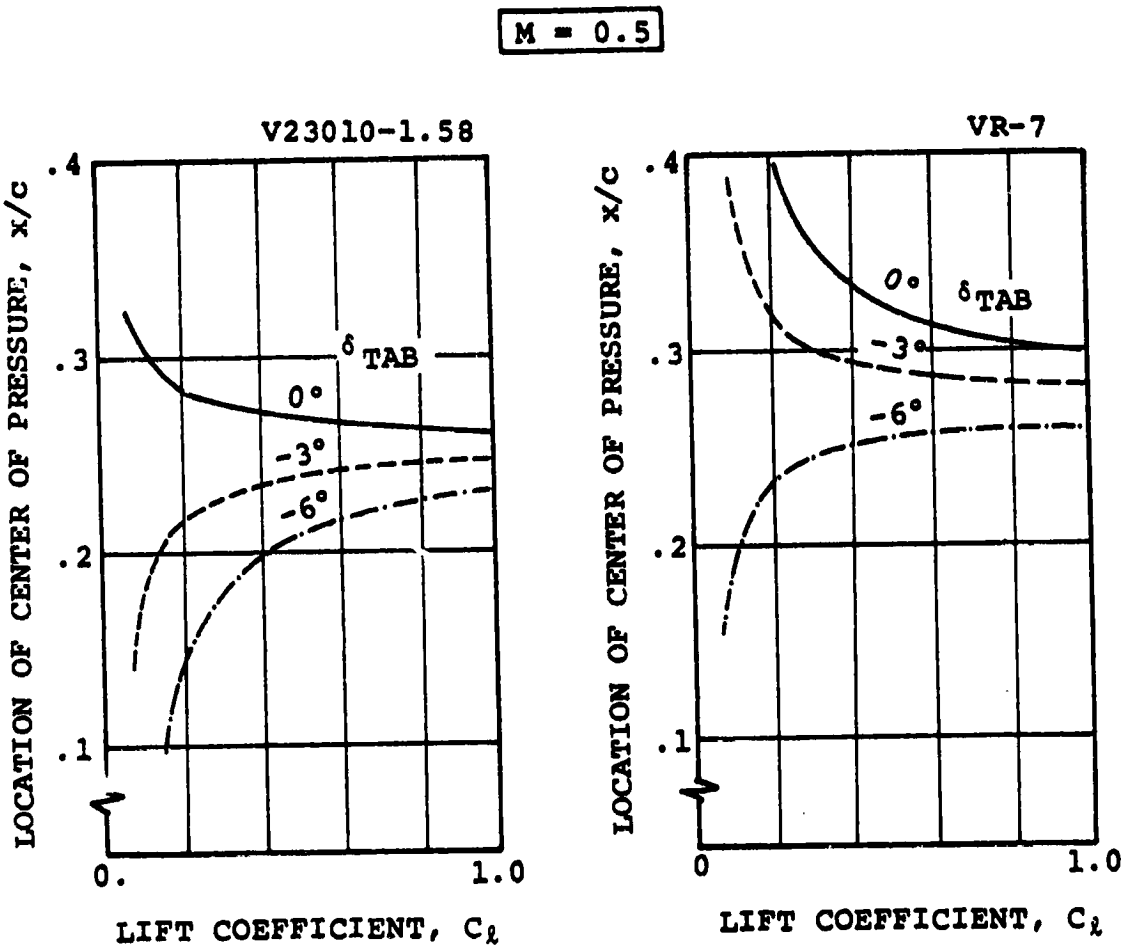


*Figure 4. Effect of Trailing Edge Tab Angle on the Location of the Center of Pressure*

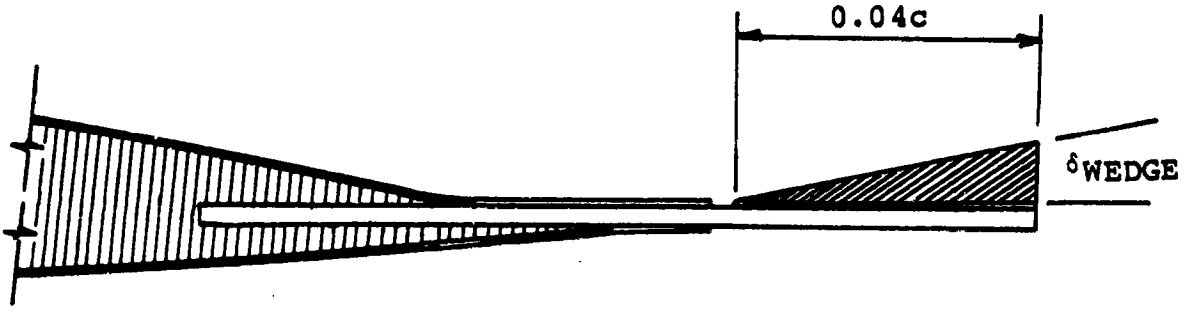


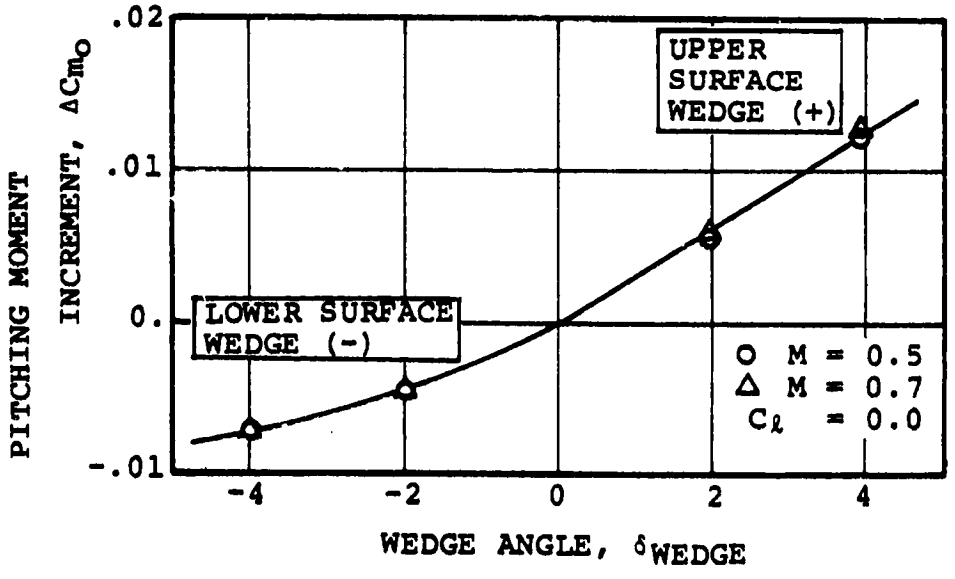


*Figure 5. Effect of the Trailing Edge Wedge Applied to the V23010-1.58 Airfoil*

## 1.2.100 EFFECT OF AIRFOIL LEADING EDGE CONTOURS

The flow about the leading edge plays a dominant role in the performance of airfoil sections because it influences the early growth and, therefore, the favorable or unfavorable development of the boundary layer.

Premature boundary layer transition and/or separation can be precipitated by:

- Surface roughness
- Surface discontinuities
- An excessive rate of deceleration in the flow
- Recompression shocks

Leaving aside surface roughness and discontinuities, the objective of this data sheet is to illustrate some of the effects of leading edge geometry on airfoil performance.

### 1. Leading Edge Curvature

The shape of the leading edge is generally closely related to the overall shape of airfoils. In the case of NACA profiles, the shape of an airfoil, including the shape of its leading edge, is uniquely defined by prescribing the symmetrical thickness form and the mean line (1.1.20). The leading edge radius of NACA airfoils is not strictly a function of the thickness form, but the values recommended represent the result of an extensive optimization effort.

The leading edge curvature of some airfoils has been modified to optimize the lift and drag characteristics at specific transonic flow conditions. Such airfoils have blunt leading edges which deviate from the standard NACA definitions. References 1 and 2 discuss criteria for high speed airfoil design.

### 2. Effect on Airfoil Characteristics

Excluding roughness effects, leading edge contours generally have:

<u>a strong effect on</u>

- type of stall
- maximum lift
- drag level at $M < M_{DD}$
- onset of significant compressibility effects
- appearance of laminar separation "bubbles"

<u>a weak effect on</u>

- pitching moments
- angle for zero lift
- lift curve slope
- center of pressure
- aerodynamic center

where "leading edge contour" refers to the portion of airfoil surface extending from the leading edge to approximately 15% of chord on both upper and lower surfaces.

It is important to keep in mind that good leading edge characteristics are a necessary but not sufficient condition for good airfoil performance.

A typical illustration of leading edge contour effects is the correlation between the thickness of airfoils at 1.25% of chord and the character of stall, suggested by Gault (1.2.60).

Figure 1, from Reference 3, relates the maximum lift capability of several families of symmetrical NACA profiles to the leading edge radius and to the location of the maximum thickness.

Figure 2, also from Reference 3, shows the effect of variations in leading edge radius on the maximum lift coefficient.

Figure 3 illustrates the effect of an upper surface leading edge modification of the VR-7 airfoil. For reference see data sheets 1.3.380 and 1.3.420. At a Mach number of 0.5, the contour modification caused a loss in maximum lift $C_{\ell_{max}} = -0.15$. The only beneficial effect was a change in the character of the stall from leading edge stall for the VR-7 (1.3.380) to a less abrupt form of stall for the VR-7.1 (1.3.420).

Figure 4 shows the rationale for the selection of the V13006-0.7 airfoil over other versions of the same section with 0.4% and 1.0% leading edge radii. The V13006-0.7, with an 0.7% radius, offers the best compromise in maximum lift capability and low drag rise at high Mach numbers.

REFERENCES

1. Pearcey, H.H., The Aerodynamic Design of Section Shapes for Swept Wings, Advances in Aeronautical Sciences, Volume 3, Proceedings of 2nd International Congress in the Aeronautical Sciences, 1960.

2. Wortmann, F.X., Drees, J.M., Design of Airfoils for Rotors, Paper presented at CAL/AVLABS 1969 Symposium on Aerodynamics of Rotary Wing and VTOL Aircraft.

3. Schwartzberg, M.A., Burch, J.L., Lifting Capabilities of Wings with and without High-Lift Devices," G. L. Martin Company Engineering Report No. 8055, April 1956.

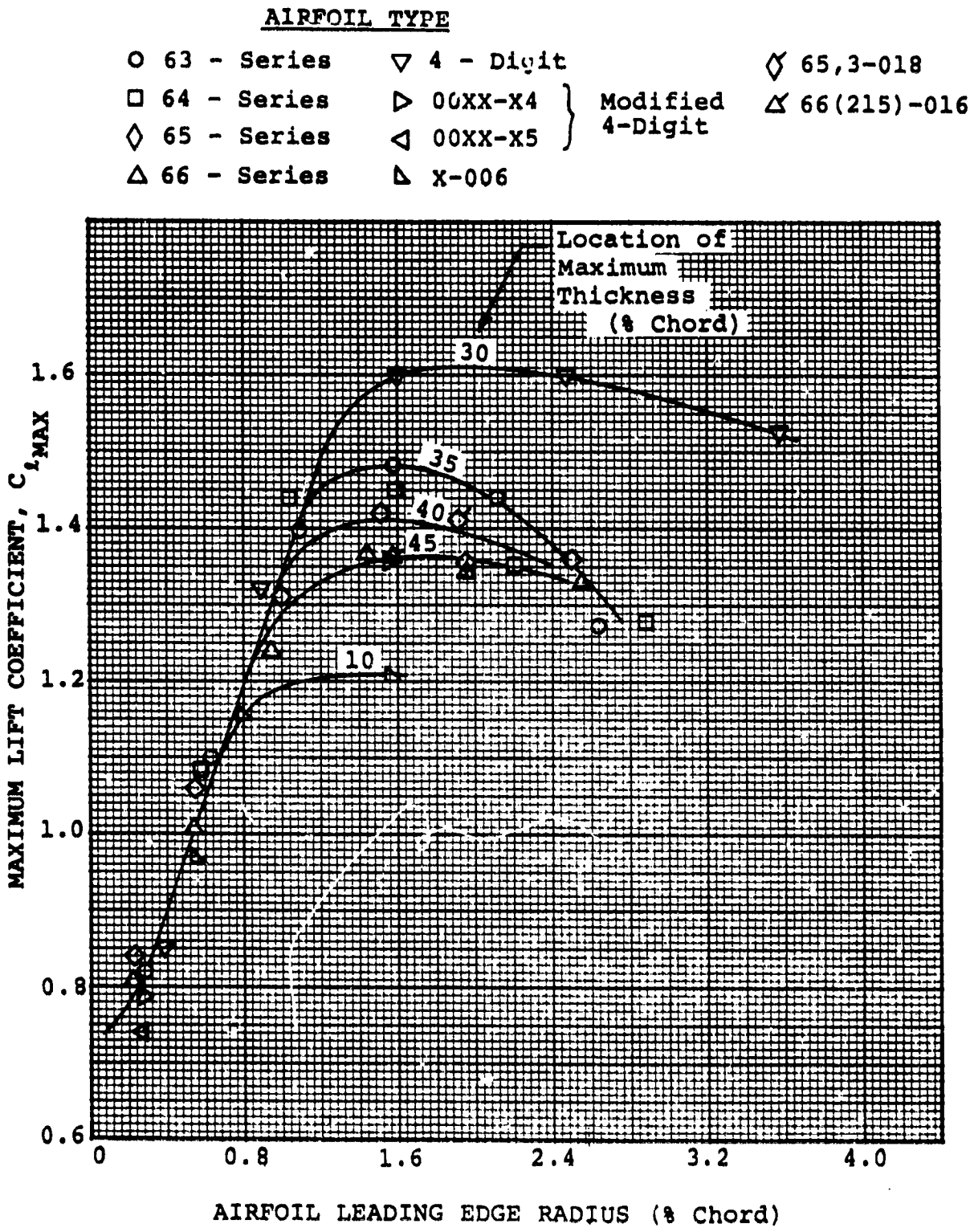


*Figure 1 Variation of Airfoil Maximum Lift Coefficient with Leading Edge Radius for Several Families of Uncambered Airfoils at a Reynolds Number of $6 \times 10^6$*

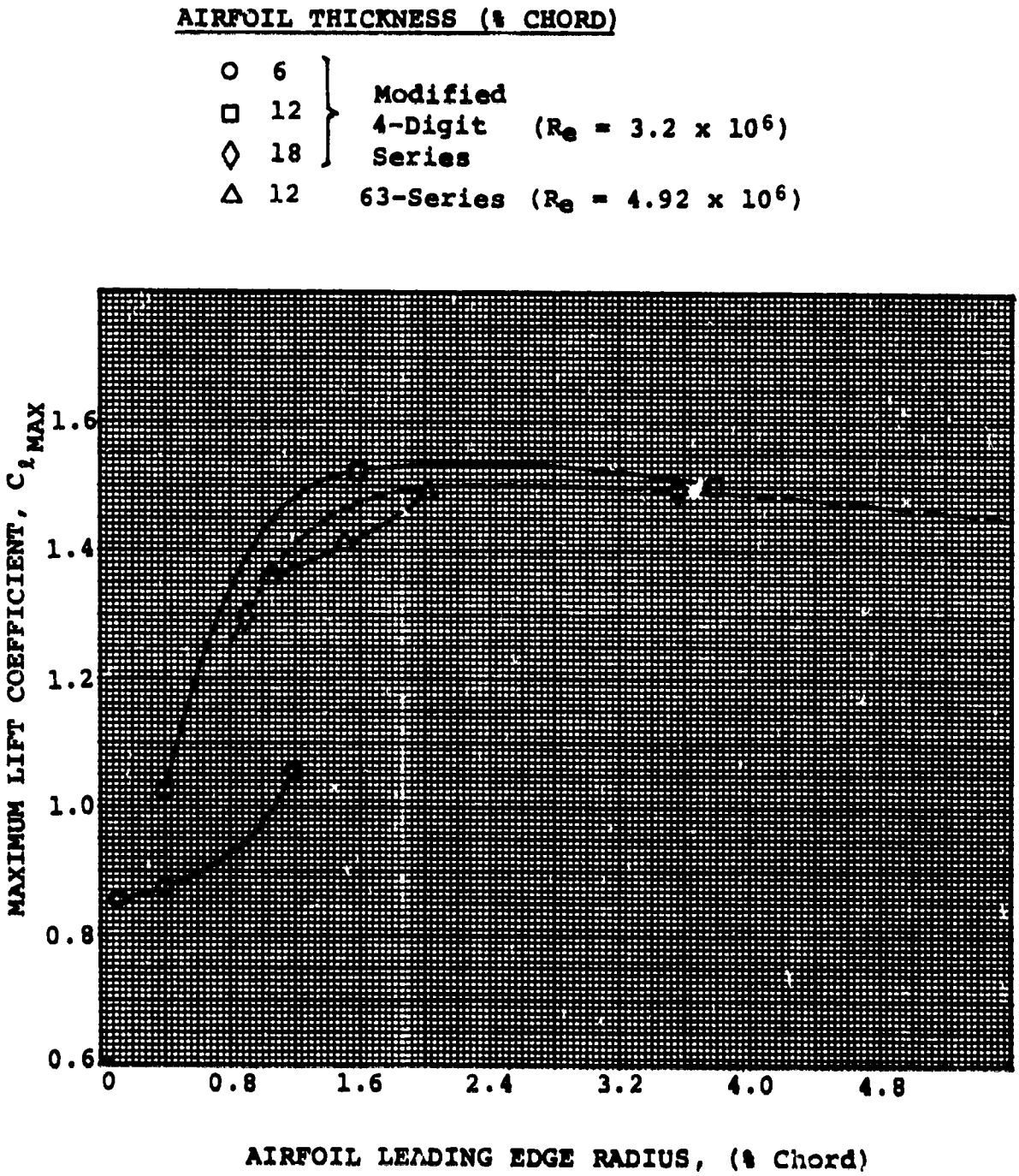


*Figure 2 Effect of Leading Edge Radius on Airfoil Maximum Lift Coefficient*

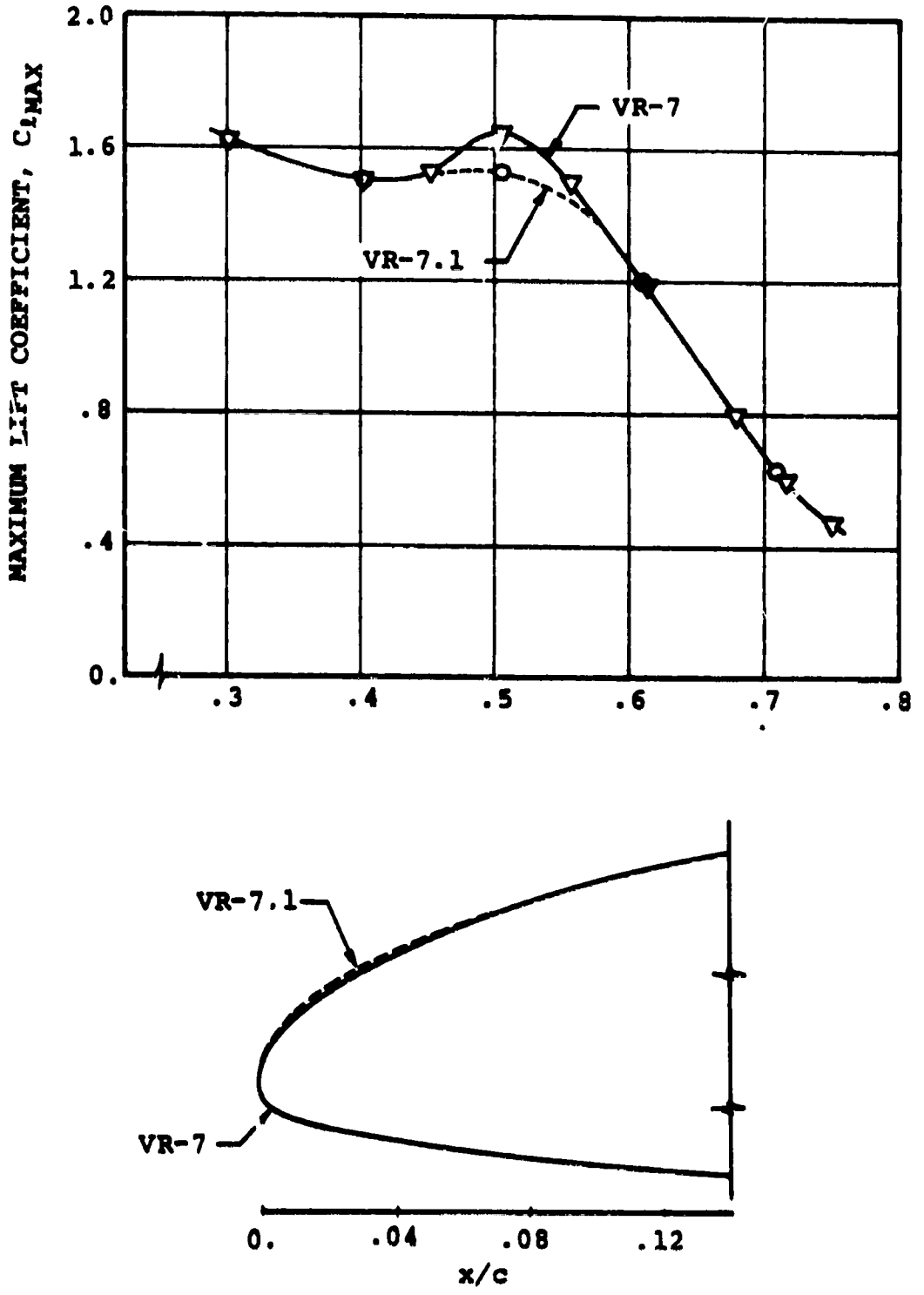


*Figure 3* *Effect of Leading Edge Modification on the Maximum Lift of the VR-7 Airfoil*

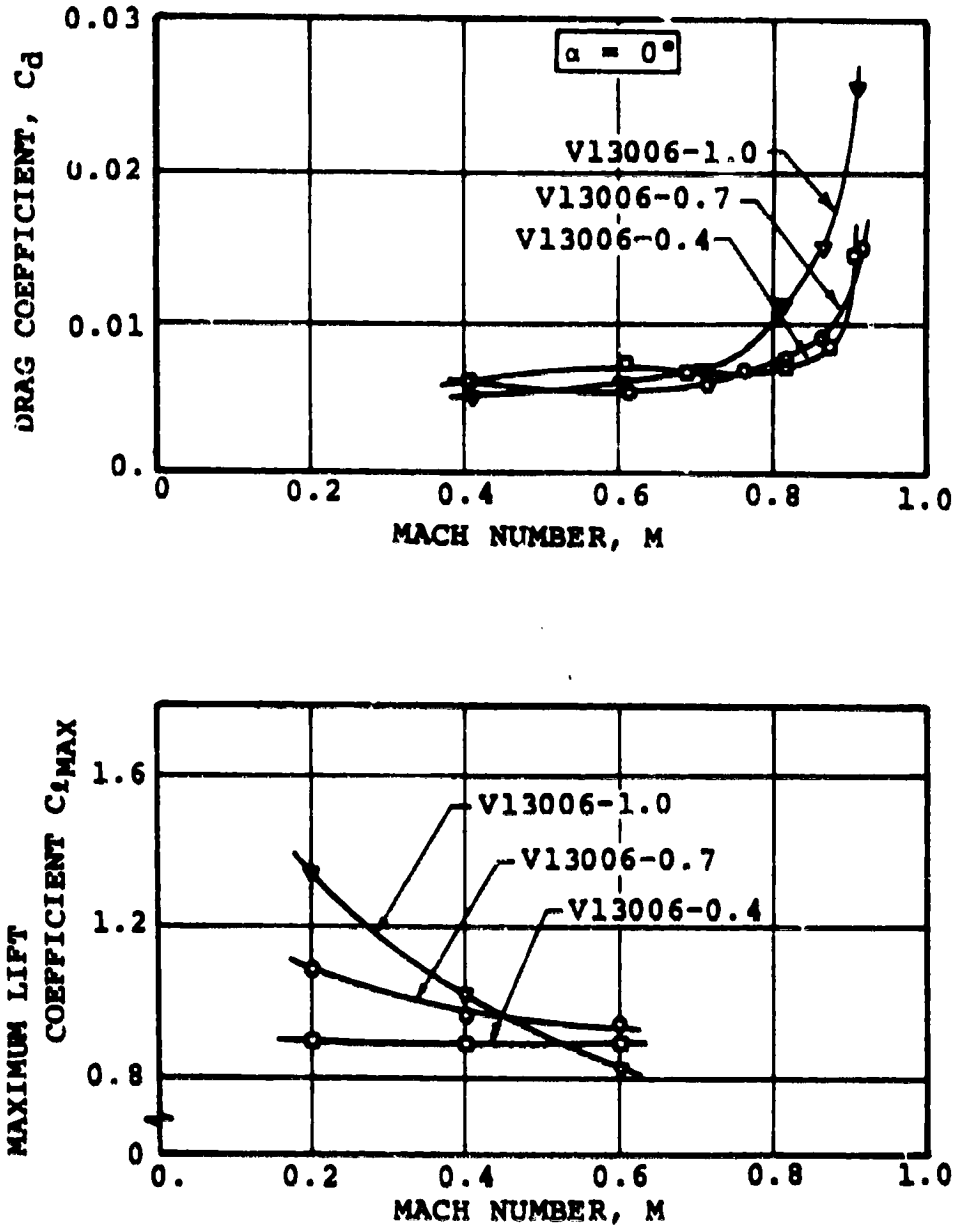


*Figure 4 Effect of Leading Edge Radius Variation on Drag and Maximum Lift*

AIRFOIL: NACA 0006



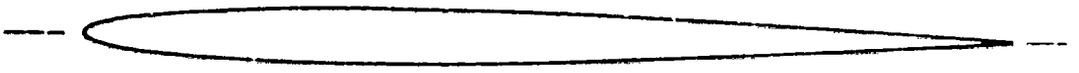

AIRFOIL COORDINATES

| x/c | y/c |
|---|---|
| 0.0 | 0.0 |
| 0.0125 | 0.00947 |
| 0.025 | 0.01307 |
| 0.05 | 0.01777 |
| 0.075 | 0.021 |
| 0.1 | 0.02341 |
| 0.15 | 0.02673 |
| 0.2 | 0.02869 |
| 0.25 | 0.02971 |
| 0.3 | 0.03001 |
| 0.4 | 0.02902 |
| 0.5 | 0.02647 |
| 0.6 | 0.02282 |
| 0.7 | 0.01832 |
| 0.8 | 0.01312 |
| 0.9 | 0.00724 |
| 0.95 | 0.00403 |
| 1.0 | 0.00063 |

CHARACTERISTICS

- Thickness, t/c = 0.06
- Leading Edge Radius, r/c = 0.004

TYPE OF DATA AND METHOD OF TEST

Two-dimensional tests in the Subsonic Insert of the Boeing Supersonic Wind Tunnel in Seattle, Wash.

Lift and pitching moments were determined by integration of surface static pressures.

Drag was determined by a traversing wake probe survey.

Model Chord = 7.0 in
Span = 12.0 in

SOURCES

1) Gabriel, E., Analysis of Two-Dimensional Wind Tunnel Tests of Rotor Blade Airfoils of Varying Camber and Leading Edge Radius, Boeing Doc. No. AERO INV. III-288, November 1965.

2) Gray, L., Liiva, J., Davenport, F., Wind Tunnel Tests of Thin Airfoils Oscillating Near Stall, USAAVLABS TR 68-89A, 1969.

NACA 0006

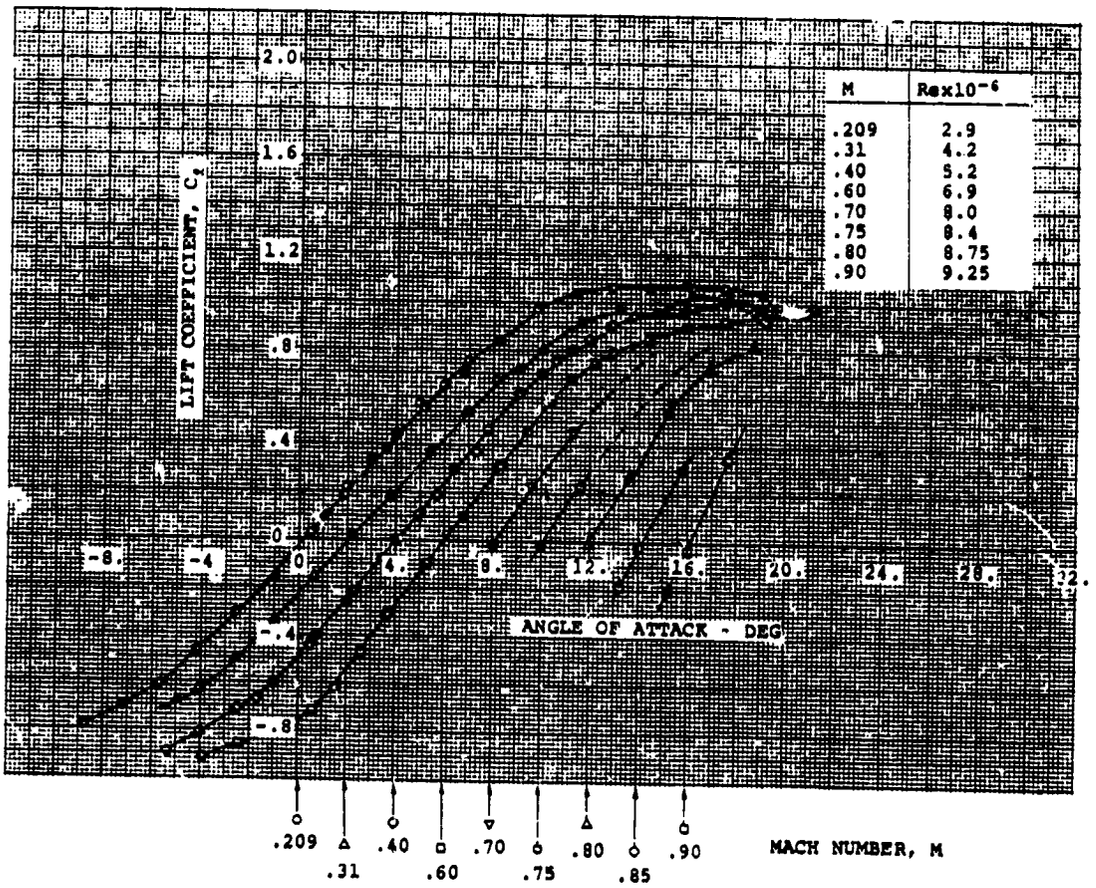
M | Rex10⁻⁶
.209 | 2.9
.31 | 4.2
.40 | 5.2
.60 | 6.9
.70 | 8.0
.75 | 8.4
.80 | 8.75
.90 | 9.25
LIFT COEFFICIENT, $C_l$
2.0
1.6
1.2
.8
.4
0
-.4
-.8
-8.
-4
0
4.
8.
12.
16.
20.
24.
28.
32.
ANGLE OF ATTACK - DEG
.209
.31
.40
.60
.70
.75
.80
.85
.90
MACH NUMBER, M

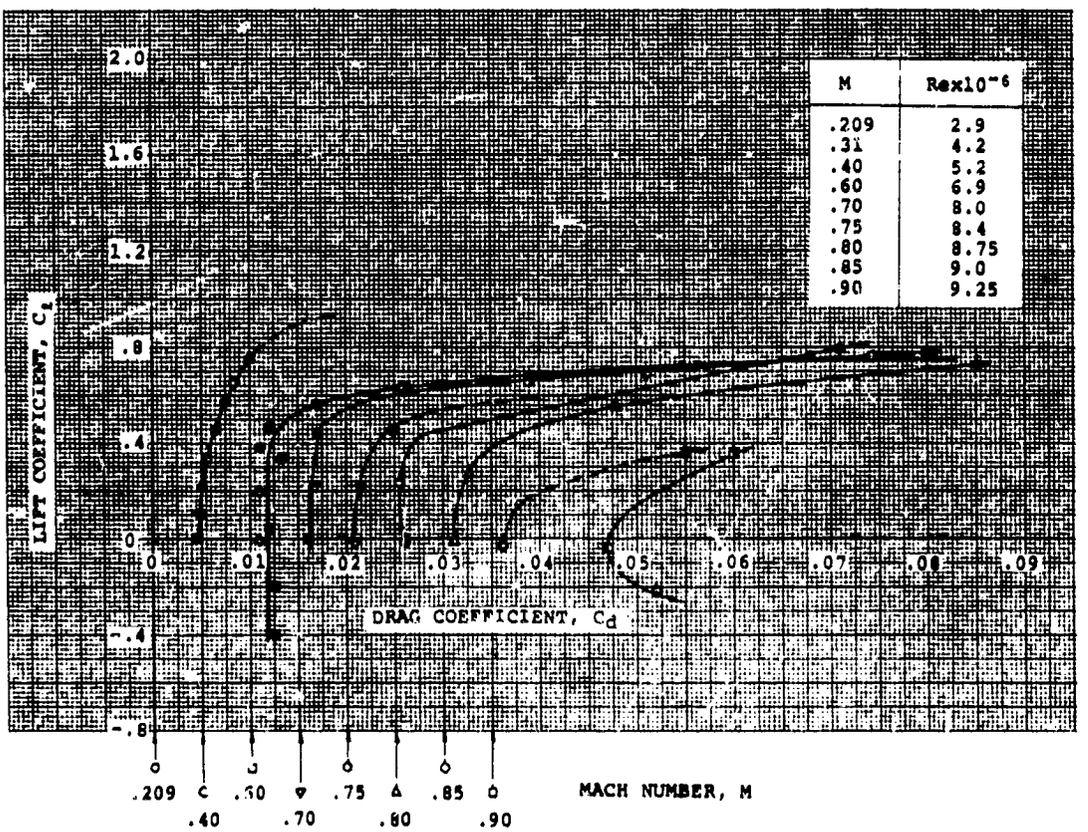
M | Rex10⁻⁶
.209 | 2.9
.31 | 4.2
.40 | 5.2
.60 | 6.9
.70 | 8.0
.75 | 8.4
.80 | 8.75
.85 | 9.0
.90 | 9.25
LIFT COEFFICIENT, $C_l$
2.0
1.6
1.2
.8
.4
0
-.4
-.8
0
.01
.02
.03
.04
.05
.06
.07
.08
.09
DRAG COEFFICIENT, $C_d$
.209
.40
.60
.70
.75
.80
.85
.90
MACH NUMBER, M

NACA 0006

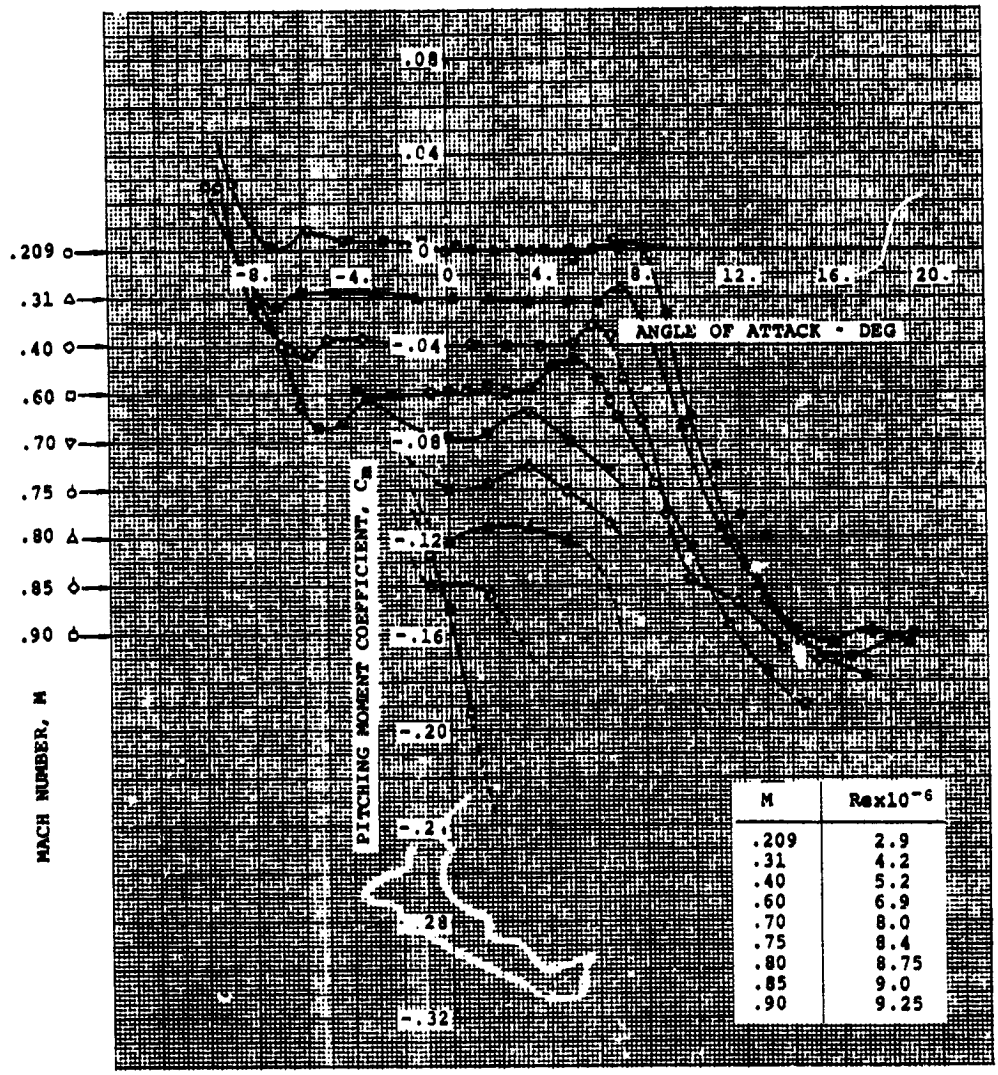
.08
.04
0
-.04
-.08
-.12
-.16
-.20
-.24
-.28
-.32
-8.
-4.
0
4.
8.
12.
16.
20.
ANGLE OF ATTACK - DEG
PITCHING MOMENT COEFFICIENT, $C_m$
MACH NUMBER, M
.209
.31
.40
.60
.70
.75
.80
.85
.90
M | Rex10⁻⁶
.209 | 2.9
.31 | 4.2
.40 | 5.2
.60 | 6.9
.70 | 8.0
.75 | 8.4
.80 | 8.75
.85 | 9.0
.90 | 9.25

AIRFOIL: NACA 0012 1.3.20

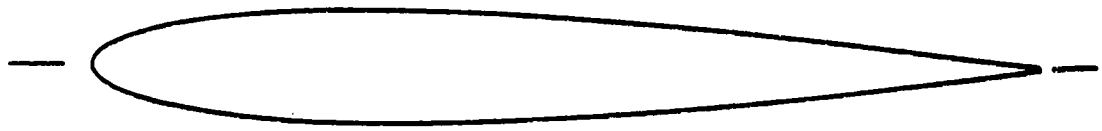

## AIRFOIL COORDINATES

| x/c | y/c |
|---|---|
| 0.0 | 0.0 |
| 0.0005 | 0.0040 |
| 0.0010 | 0.0056 |
| 0.0025 | 0.0087 |
| 0.0050 | 0.0122 |
| 0.0075 | 0.0149 |
| 0.0100 | 0.0170 |
| 0.0125 | 0.0189 |
| 0.015 | 0.0206 |
| 0.02 | 0.0236 |
| 0.03 | 0.0284 |
| 0.04 | 0.0323 |
| 0.05 | 0.0355 |
| 0.06 | 0.0383 |
| 0.08 | 0.0430 |
| 0.10 | 0.0469 |
| 0.12 | 0.0499 |
| 0.14 | 0.0524 |
| 0.16 | 0.0544 |
| 0.18 | 0.0560 |
| 0.20 | 0.0574 |
| 0.225 | 0.0586 |
| 0.25 | 0.0594 |
| 0.275 | 0.0599 |
| 0.3 | 0.0600 |
| 0.325 | 0.0599 |
| 0.35 | 0.0595 |
| 0.375 | 0.0588 |
| 0.4 | 0.0580 |
| 0.425 | 0.0569 |
| 0.45 | 0.0558 |
| 0.475 | 0.0544 |
| 0.5 | 0.0529 |
| 0.55 | 0.0495 |
| 0.6 | 0.0456 |
| 0.65 | 0.0413 |
| 0.7 | 0.0366 |
| 0.75 | 0.0315 |
| 0.8 | 0.0262 |
| 0.85 | 0.0205 |
| 0.9 | 0.0145 |
| 0.95 | 0.0080 |
| 1.00 | 0.0013 |

## CHARACTERISTICS

- Thickness, t/c = 0.12
- Leading Edge Radius, r/c = 0.0158

## TYPE OF DATA AND METHOD OF TESTS

The wind tunnel tests were carried out in the National Physical Laboratory, NPL, 36 in. x 14 in. (0.92 m x 0.36 m) transonic tunnel, at Teddington, Middlesex, England.

Lift and pitching moments were found by integration of surface static pressures. Profile drag was determined by wake measurements.

All measurements were obtained with a roughness band of 230-270 mesh carborundum between 0 and 2% chord on both surfaces. The floor and the ceiling of the test section were slotted. No corrections for wall constraints have been applied to the data.

Model Chord = 10 in (25.4 cm)
Span = 14 in (35.6 cm)

## SOURCE

Gregory, N., Wilby, P.G., NPL 9615 and NACA 0012. A Comparison of Aerodynamic Data, ARC C.P. No. 1261, 1973.

NACA 0012

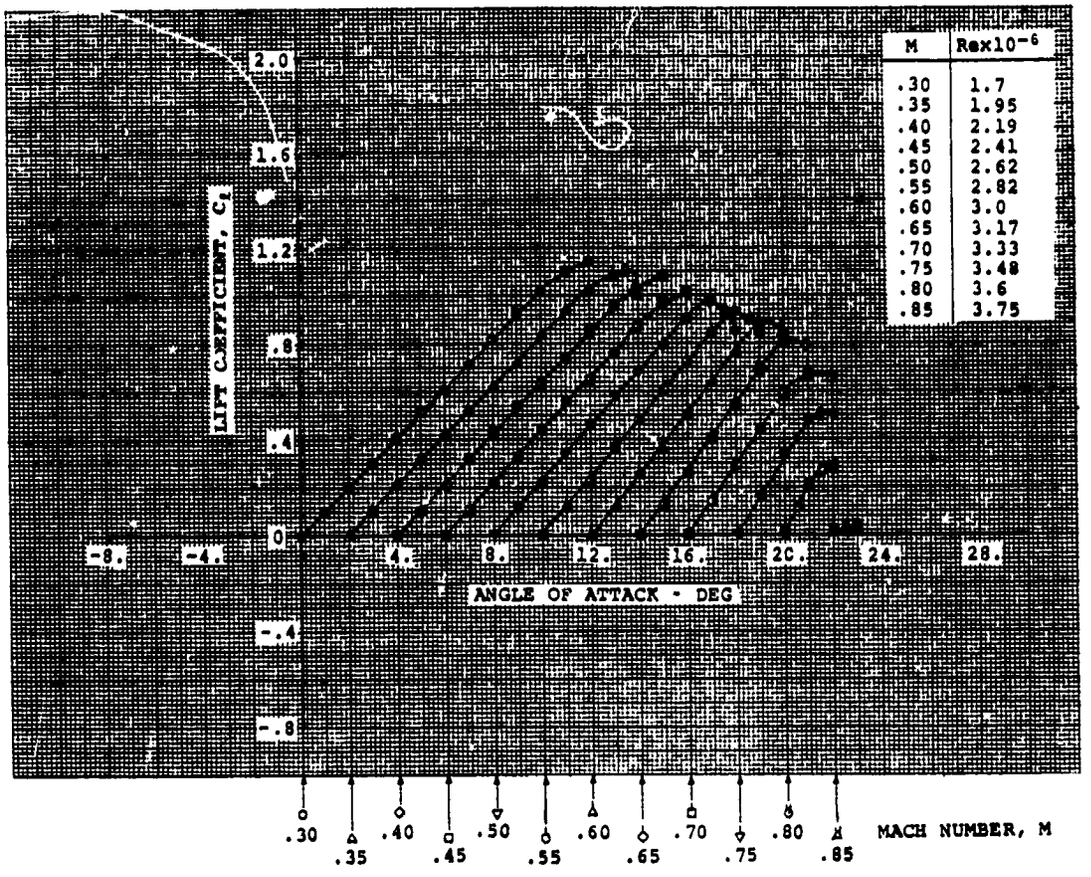
M
Rex10⁻⁶
.30 1.7
.35 1.95
.40 2.19
.45 2.41
.50 2.62
.55 2.82
.60 3.0
.65 3.17
.70 3.33
.75 3.48
.80 3.6
.85 3.75
LIFT COEFFICIENT, $C_l$
2.0
1.6
1.2
.8
.4
0
-.4
-.8
-8.
-4.
4.
8.
12.
16.
20.
24.
28.
ANGLE OF ATTACK - DEG
.30 .35 .40 .45 .50 .55 .60 .65 .70 .75 .80 .85
MACH NUMBER, M

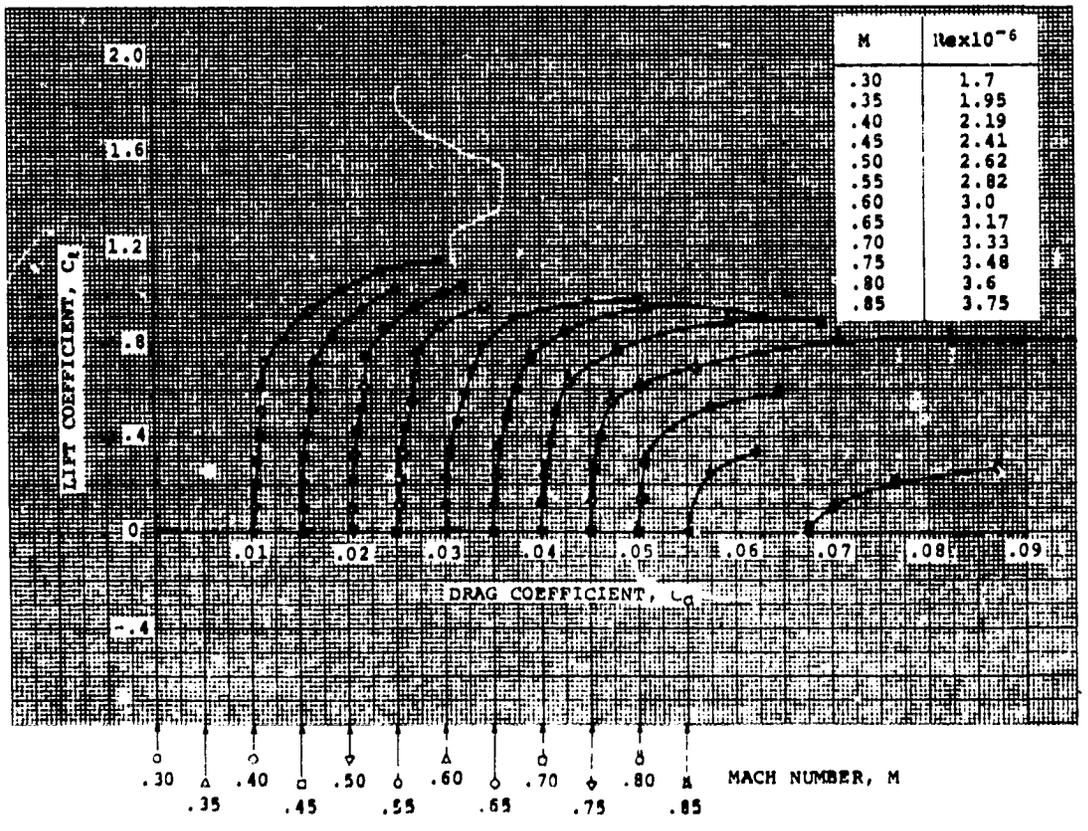
M
Rex10⁻⁶
.30 1.7
.35 1.95
.40 2.19
.45 2.41
.50 2.62
.55 2.82
.60 3.0
.65 3.17
.70 3.33
.75 3.48
.80 3.6
.85 3.75
LIFT COEFFICIENT, $C_l$
2.0
1.6
1.2
.8
.4
0
-.4
.01
.02
.03
.04
.05
.06
.07
.08
.09
DRAG COEFFICIENT, $C_d$
.30 .35 .40 .45 .50 .55 .60 .65 .70 .75 .80 .85
MACH NUMBER, M

NACA 0012

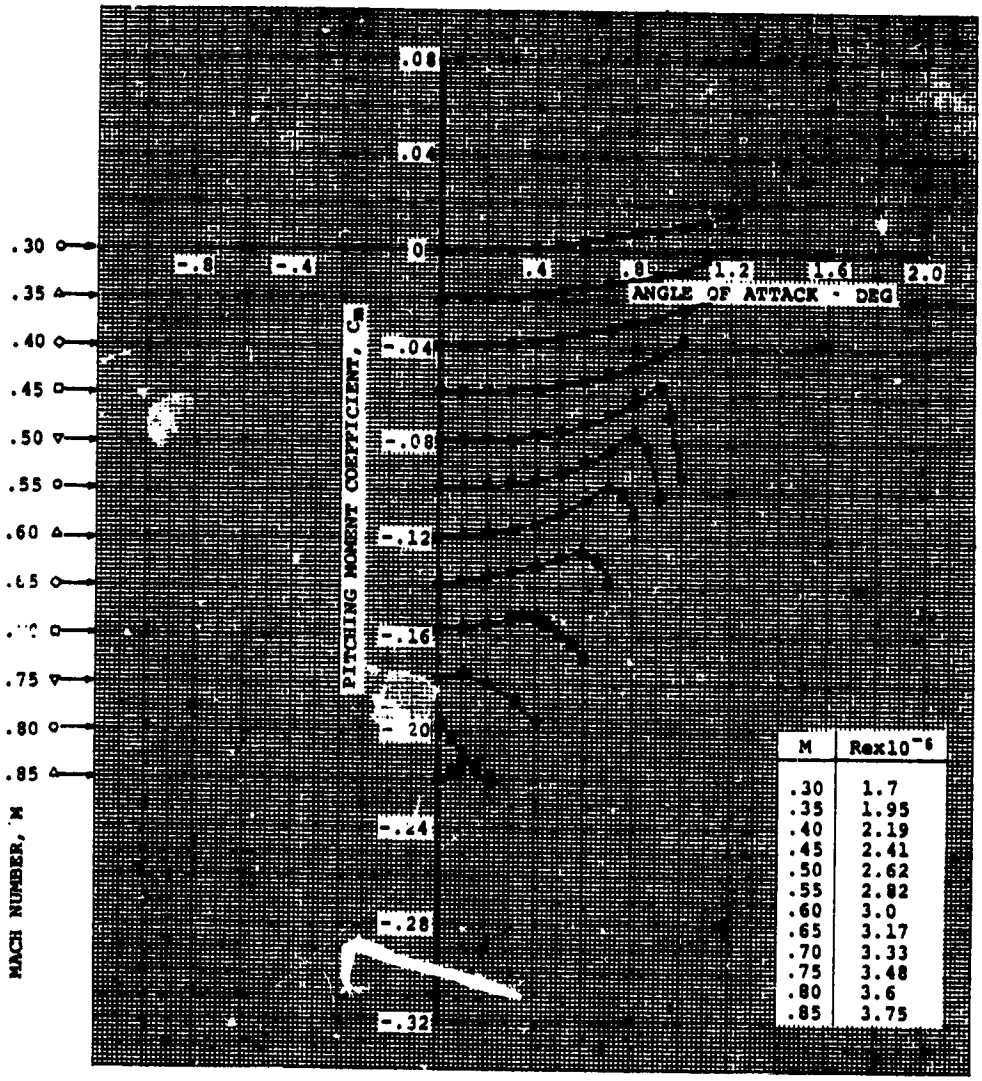
.08
.04
0
-.04
-.08
-.12
-.16
-.20
-.24
-.28
-.32
-.8
-.4
.4
.8
1.2
1.6
2.0
ANGLE OF ATTACK - DEG
PITCHING MOMENT COEFFICIENT, $C_m$
.30
.35
.40
.45
.50
.55
.60
.65
.70
.75
.80
.85
MACH NUMBER, M
M | Rex10$^{-6}$
.30 | 1.7
.35 | 1.95
.40 | 2.19
.45 | 2.41
.50 | 2.62
.55 | 2.82
.60 | 3.0
.65 | 3.17
.70 | 3.33
.75 | 3.48
.80 | 3.6
.85 | 3.75

AIRFOIL: NACA 0012 (Including Reverse Flow) 1.3.30

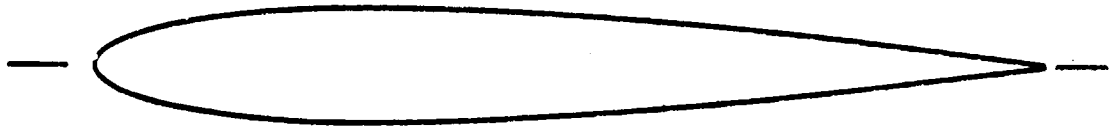

AIRFOIL COORDINATES

| x/c | y/c |
|---|---|
| 0.0 | 0.0 |
| 0.0125 | 0.01894 |
| 0.025 | 0.02615 |
| 0.05 | 0.03555 |
| 0.075 | 0.042 |
| 0.1 | 0.04683 |
| 0.15 | 0.05345 |
| 0.2 | 0.05737 |
| 0.25 | 0.05941 |
| 0.3 | 0.06002 |
| 0.4 | 0.05803 |
| 0.5 | 0.05294 |
| 0.6 | 0.04563 |
| 0.7 | 0.03664 |
| 0.8 | 0.02623 |
| 0.9 | 0.01448 |
| 0.95 | 0.00807 |
| 1.0 | 0.00126 |

CHARACTERISTICS

- Thickness, t/c = 0.12
- Leading Edge Radius, r/c = 0.0158

TYPE OF DATA AND METHOD OF TEST

The test was run in the Langley low-turbulence pressure tunnel. The tunnel, as used in the present test, has a closed, rectangular test section 7.5 ft high and 3 ft wide.

Lift, drag and pitching moments were measured with a multicomponent strain-gage balance.

Model Chord = 6.0 in
Span = 36.0 in

SOURCE

Critzos, Heyson, and Boswinkle, Aerodynamic Characteristics of NACA 0012 Airfoil Section at Angles of Attack from 0° to 180°, NACA TN 3361, January 1955.

NACA 0012 INCLUDING REVERSE FLOW

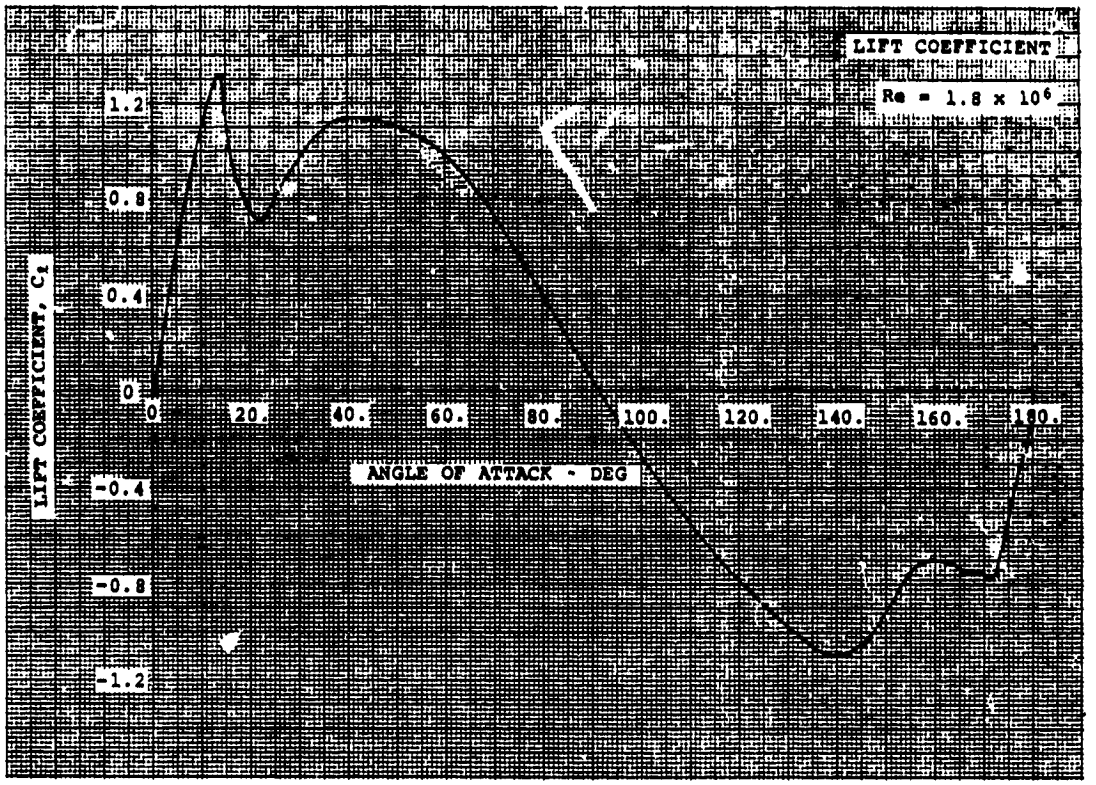


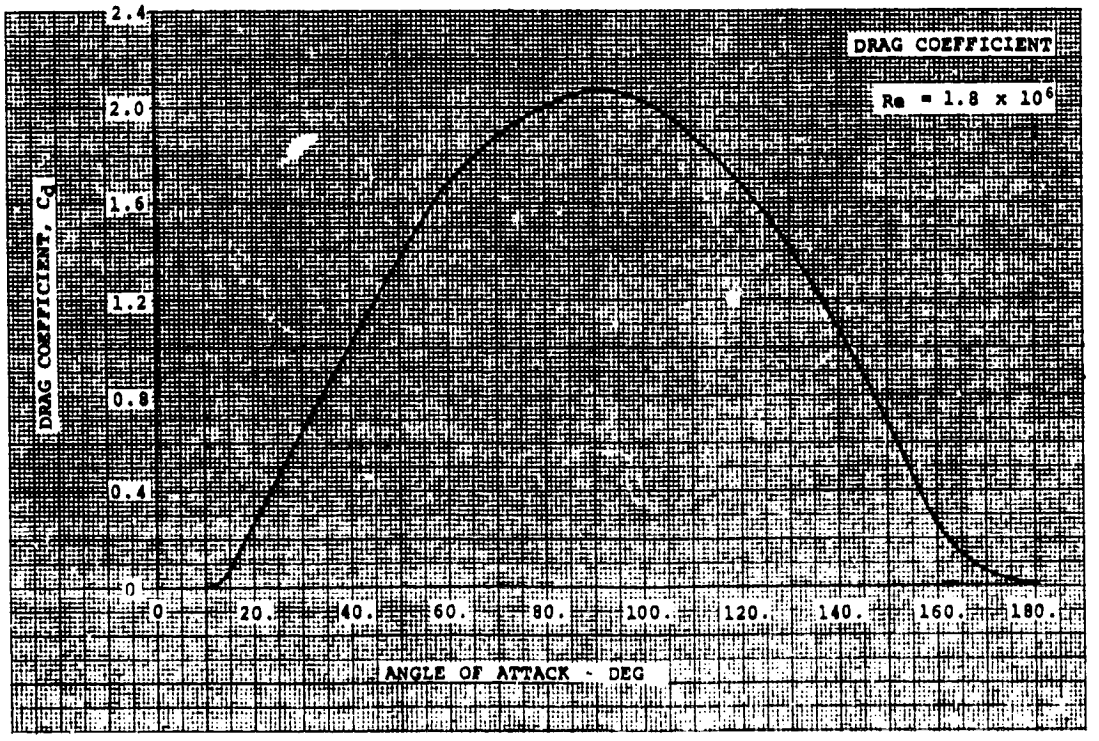

NACA 0012 INCLUDING REVERSE FLOW

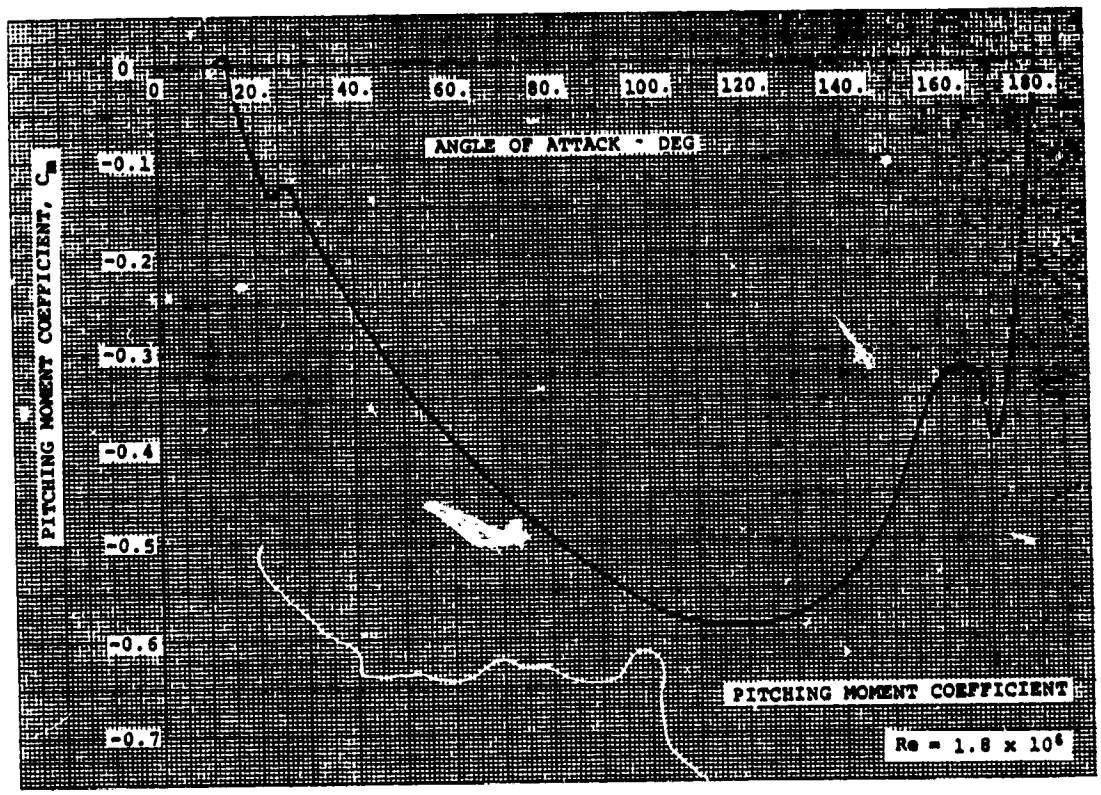

AIRFOIL: NACA 0012 with 0° T.E. Tab (H-34) 1.3.40

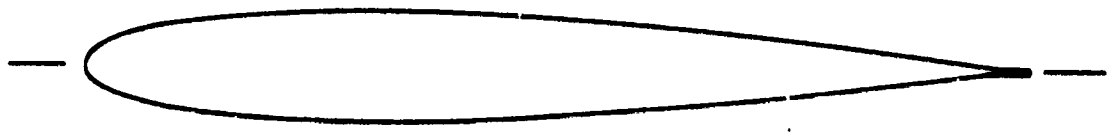

## AIRFOIL COORDINATES

| x/c | $y/c_u$ | $y/c_\ell$ |
|---|---|---|
| 0.0 | 0.0 | 0.0 |
| 0.0122 | 0.01854 | -0.01848 |
| 0.0244 | 0.02683 | -0.02551 |
| 0.04878 | 0.03561 | -0.03468 |
| 0.0732 | 0.04176 | -0.04097 |
| 0.09756 | 0.04595 | -0.04507 |
| 0.14634 | 0.05215 | -0.05171 |
| 0.19512 | 0.05597 | -0.05532 |
| 0.2439 | 0.05796 | -0.05737 |
| 0.29268 | 0.05855 | -0.05805 |
| 0.39024 | 0.05661 | -0.0561 |
| 0.4878 | 0.05165 | -0.05165 |
| 0.58536 | 0.04452 | -0.04452 |
| 0.68293 | 0.03575 | -0.03575 |
| 0.78049 | 0.02559 | -0.02559 |
| 0.87805 | 0.01413 | -0.01413 |
| 0.92683 | 0.00787 | -0.00787 |
| 0.963 | 0.00293 | -0.00293 |
| 1.0 | 0.00293 | -0.00293 |

## CHARACTERISTICS

- Thickness, t/c = 0.117
- Leading Edge Radius, r/c = 0.0154
- Trailing Edge Tab from x/c = 0.963 to x/c = 1.0
- Trailing Edge Tab Thickness, $t_{tab}/c$ = 0.00586
- Trailing Edge Tab Angle, $\delta_{tab}$ = 0°

### TYPE OF DATA AND METHOD OF TEST

Two-dimensional test conducted in a special insert in the United Aircraft Corporation (UAC) large subsonic wind tunnel.

A mechanical balance measured lift and drag directly.

A Baldwin-Lima-Hamilton bending beam equipped with strain gages was used to obtain pitching moment.

The airfoil model was equipped with 29 static pressure taps.

Drag was measured with a wake probe.

The model was made from an untwisted portion of a production Sikorsky H-34 main rotor blade.

The H-34 airfoil differs from the NACA 0012 by a slight increase in upper surface bluntness from the L.E. to 0.15.c, a reduction in lower surface maximum thickness (see coordinates at 0.3 .c), and the addition of a 0.037.c trailing edge tab.

Model Chord = 16.4 in
Span = 32.7 in

### SOURCE

Lizak, A.A., Two-Dimensional Wind Tunnel Tests of an H-34 Main Rotor Airfoil Section, TREC TR 60-53, September 1960.

NACA 0012 (MODIFIED) WITH 0° T.E. TAB

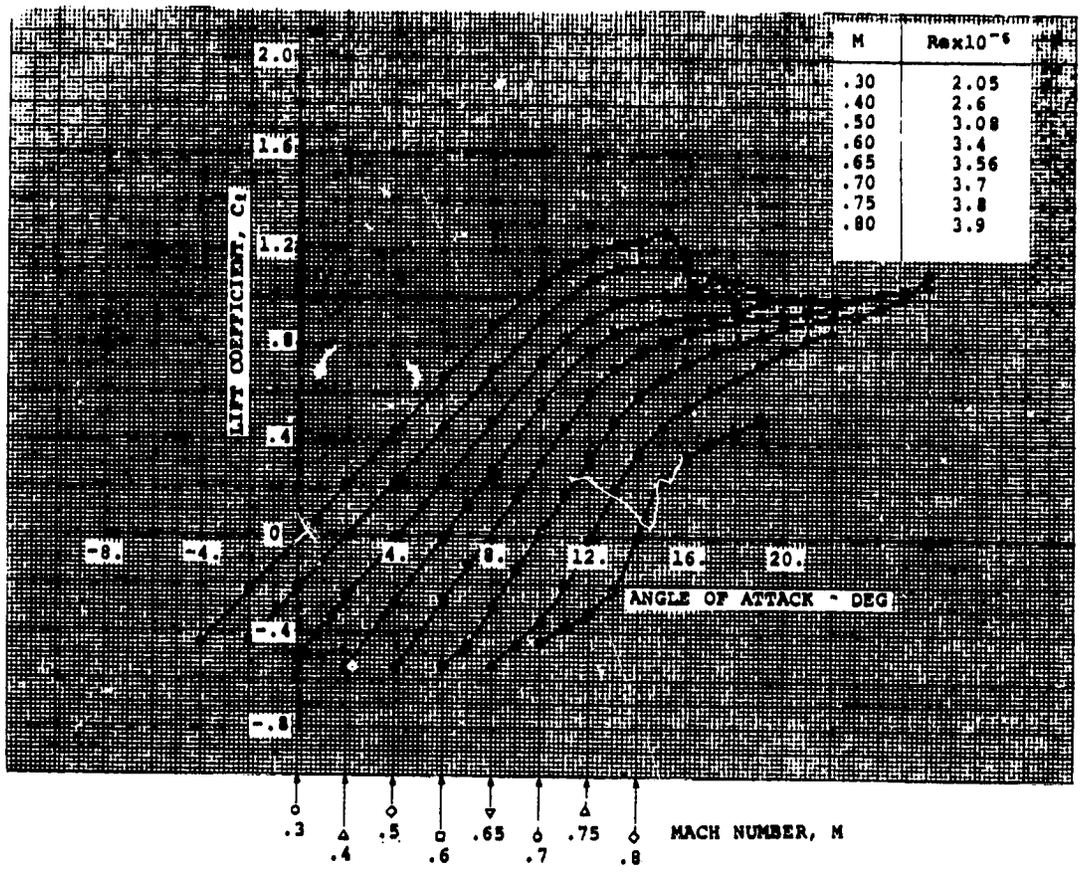


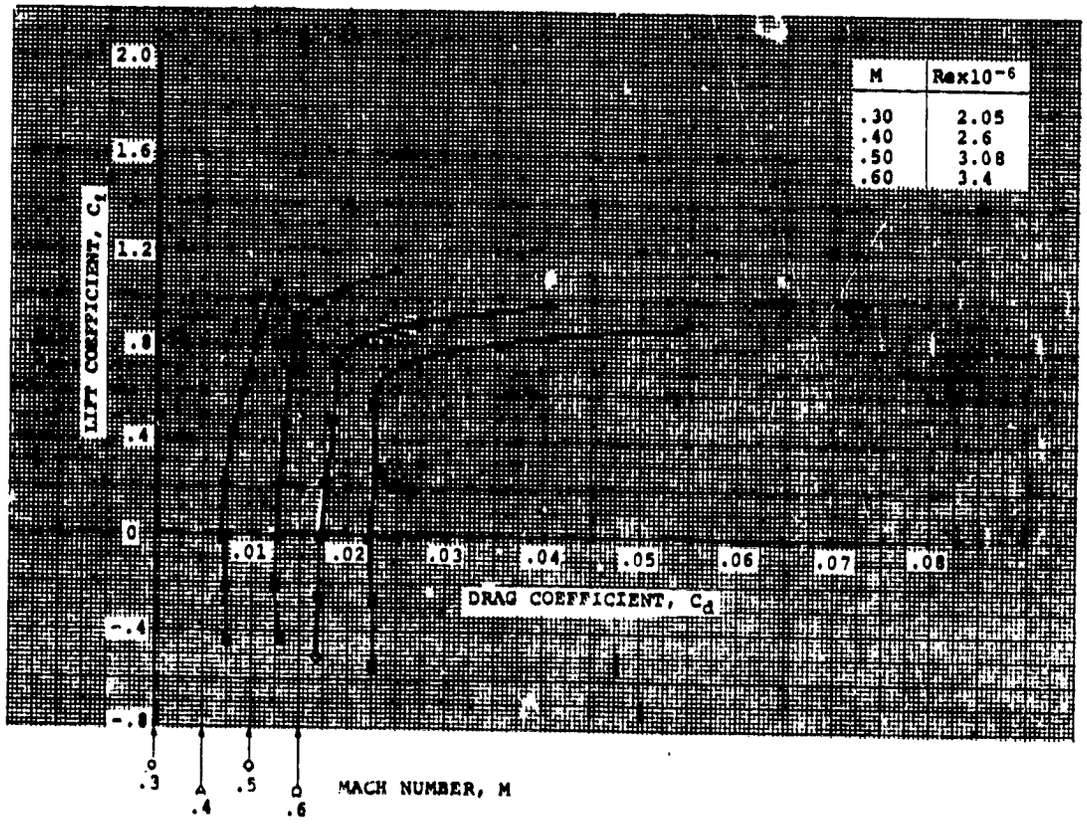

NACA 0012 (MODIFIED) WITH 0° T.E. TAB

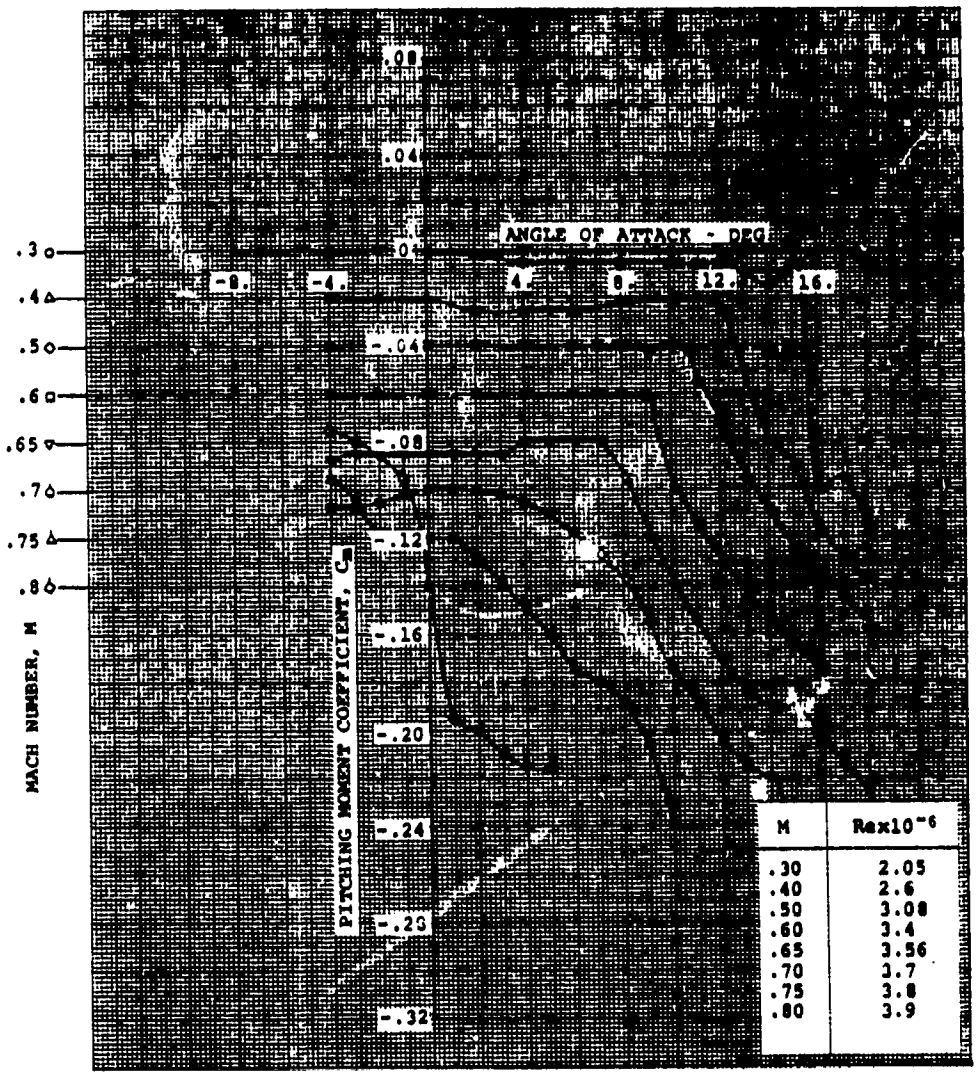

AIRFOIL: NACA 0012 with -3° T.E. Tab (H-34) 1.3.50

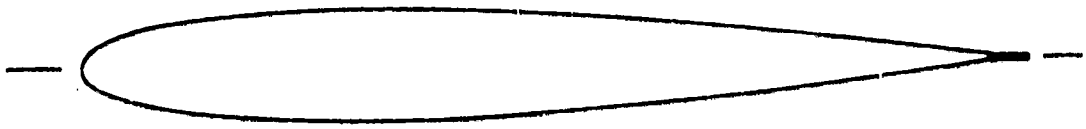

## AIRFOIL COORDINATES

| x/c | $y/c_u$ | $y/c_\ell$ |
|---|---|---|
| 0.0 | 0.0 | 0.0 |
| 0.0122 | 0.01854 | -0.01848 |
| 0.0244 | 0.02683 | -0.02551 |
| 0.04878 | 0.03561 | -0.03468 |
| 0.0732 | 0.04176 | -0.04097 |
| 0.09756 | 0.04595 | -0.04507 |
| 0.14634 | 0.05215 | -0.05171 |
| 0.19512 | 0.05597 | -0.05532 |
| 0.2439 | 0.05796 | -0.05737 |
| 0.29268 | 0.05855 | -0.05805 |
| 0.39024 | 0.05661 | -0.0561 |
| 0.4878 | 0.05165 | -0.05165 |
| 0.58536 | 0.04452 | -0.04452 |
| 0.68293 | 0.03575 | -0.03575 |
| 0.78049 | 0.02559 | -0.02559 |
| 0.87805 | 0.01413 | -0.01413 |
| 0.92683 | 0.00787 | -0.00787 |
| 0.963 | 0.00293 | -0.00293 |
| 1.0 | 0.00487 | -0.00099 |

## CHARACTERISTICS

- Thickness, t/c = 0.117
- Leading Edge Radius, r/c = 0.0154
- Trailing Edge Tab from x/c = 0.963 to x/c = 1.0
- Trailing Edge Tab Thickness, $t_{tab}/c$ = 0.00596
- Trailing Edge Tab Angle, $\delta_{tab}$ = -3°

### TYPE OF DATA AND METHOD OF TEST

Two-dimensional test conducted in a special insert in the United Aircraft Corporation (UAC) large subsonic wind tunnel.

A mechanical balance measured lift and drag directly.

A Baldwin-Lima-Hamilton bending beam equipped with strain gages was used to obtain pitching moment.

The airfoil model was equipped with 29 static pressure taps.

The model was made from an untwisted portion of a production Sikorsky H-34 main rotor blade.

The H-34 airfoil differs from the NACA 0012 by a slight increase in upper surface bluntness from the L.E. to 0.15.c, a reduction in lower surface maximum thickness (see coordinates at 0.3.c), and the addition of a 0.037.c trailing edge tab.

Model Chord = 16.4 in
Span = 32.7 in

### SOURCE

Lizak, A.A., Two-Dimensional Wind Tunnel Tests of an H-34 Main Rotor Airfoil Section, TREC TR 60-53, September 1960.

1.3.50-2

NACA 0012 (MODIFIED) WITH -3° T.E. TAB

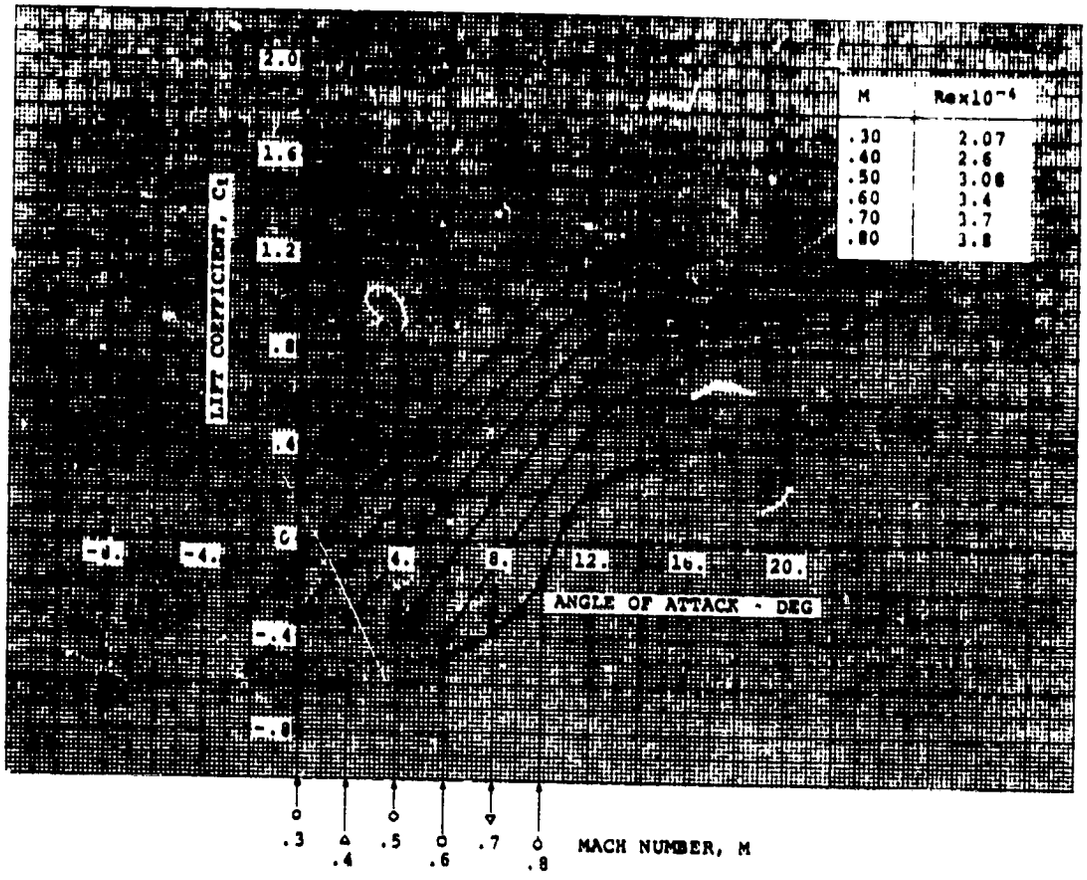

NACA 0012 (MODIFIED) WITH -3° T.E. TAB

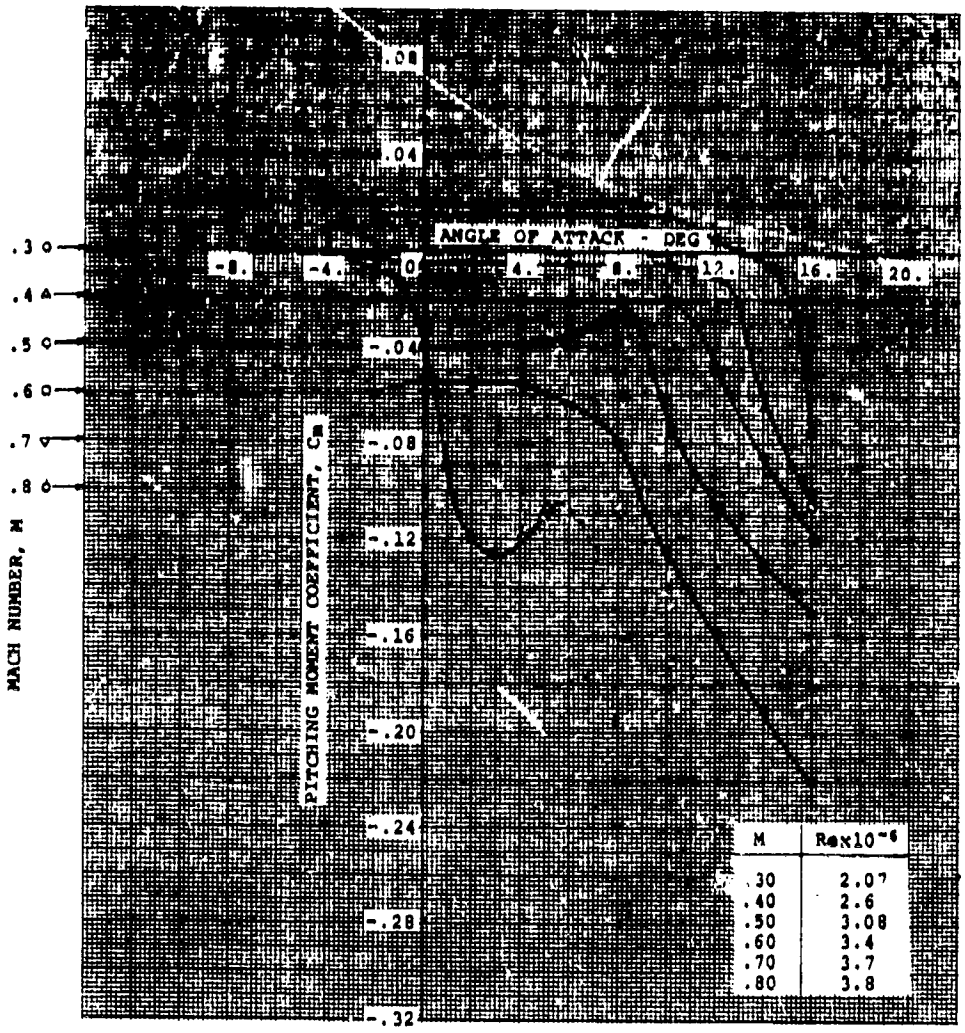

AIRFOIL: NACA 0015 1.3.60

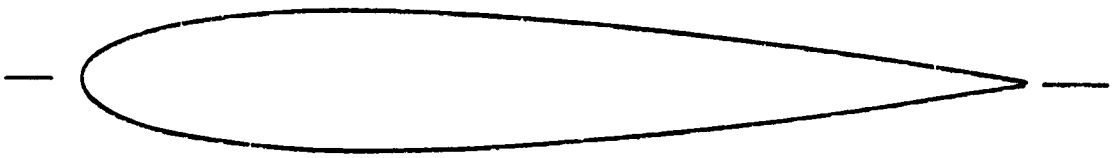

AIRFOIL COORDINATES

| x/c | y/c |
|---|---|
| 0.0 | 0.0 |
| 0.0125 | 0.02367 |
| 0.025 | 0.03268 |
| 0.05 | 0.04443 |
| 0.075 | 0.0525 |
| 0.1 | 0.05853 |
| 0.15 | 0.06682 |
| 0.2 | 0.07172 |
| 0.25 | 0.07427 |
| 0.3 | 0.07502 |
| 0.4 | 0.07254 |
| 0.5 | 0.06617 |
| 0.6 | 0.05704 |
| 0.7 | 0.0458 |
| 0.8 | 0.03279 |
| 0.9 | 0.0181 |
| 0.95 | 0.01008 |
| 1.0 | 0.00158 |

CHARACTERISTICS

- Thickness, t/c = 0.15
- Leading Edge Radius, r/c = 0.0248

TYPE OF DATA AND METHOD OF TEST

The tests were conducted in the Ames 1-by 3½-foot high speed wind tunnel, a low-turbulence, two-dimensional, continuous flow facility.

The airfoil models were equipped with 30 pressure orifices of 0.008 in. diameter, and were equipped with tightly fitting end plates flush with the tunnel walls.

Lift and quarter chord pitching moments were determined from measurements of the reactions on the tunnel walls of the forces experienced by the airfoil. Wake surveys were carried out with a movable rake of total-head tubes.

Broken lines in the data indicate that stream velocities were within 0.025M.

Model Chord = 6.0 in
Span = 12.0 in

SOURCE

Graham, D.J., Nitzberg, G.E., and Olson, R.N., A Systematic Investigation of Pressure Distributions at High Speeds Over Five Representative NACA Low-Drag and Conventional Airfoil Sections, NACA Report 832, 1945.

NACA 0015

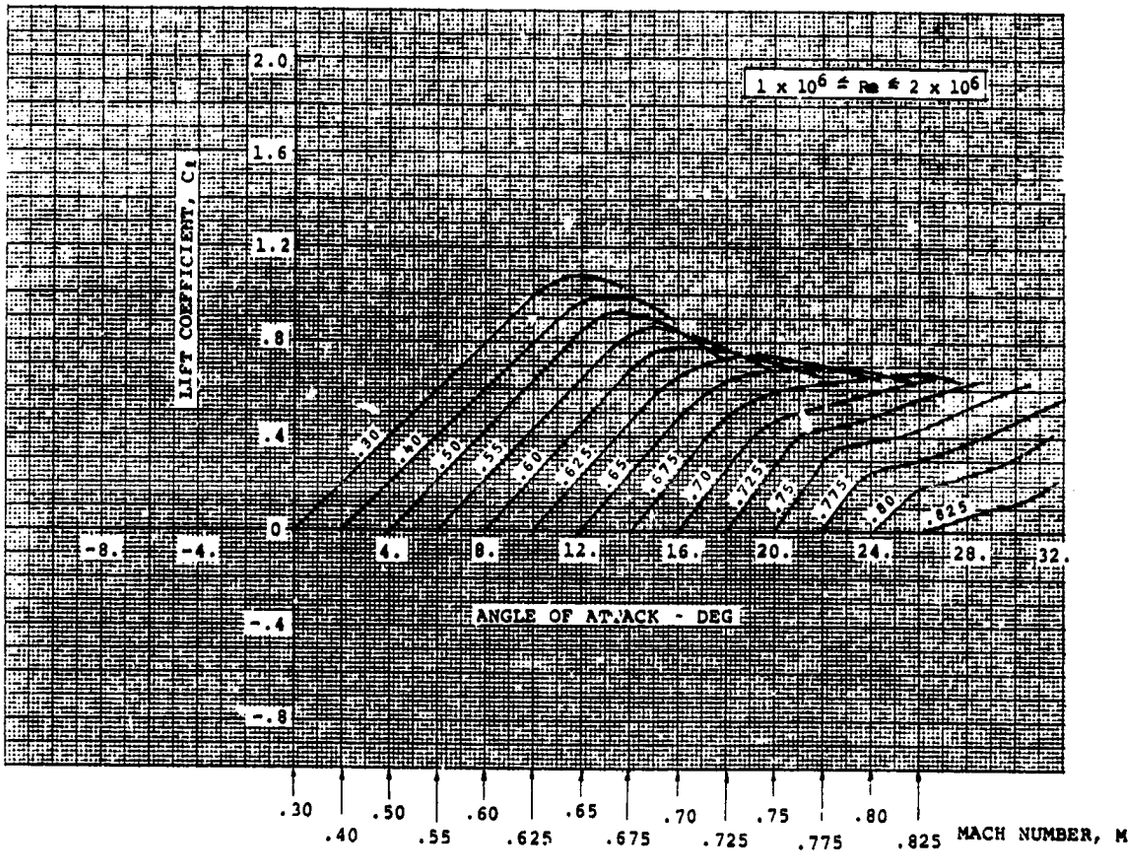
1 x 10^6 ≤ Re ≤ 2 x 10^6
LIFT COEFFICIENT, Cl
2.0
1.6
1.2
.8
.4
0
-.4
-.8
-8.
-4.
4.
8.
12.
16.
20.
24.
28.
32.
ANGLE OF ATTACK - DEG
.30
.40
.50
.55
.60
.625
.65
.675
.70
.725
.75
.775
.80
.825
MACH NUMBER, M

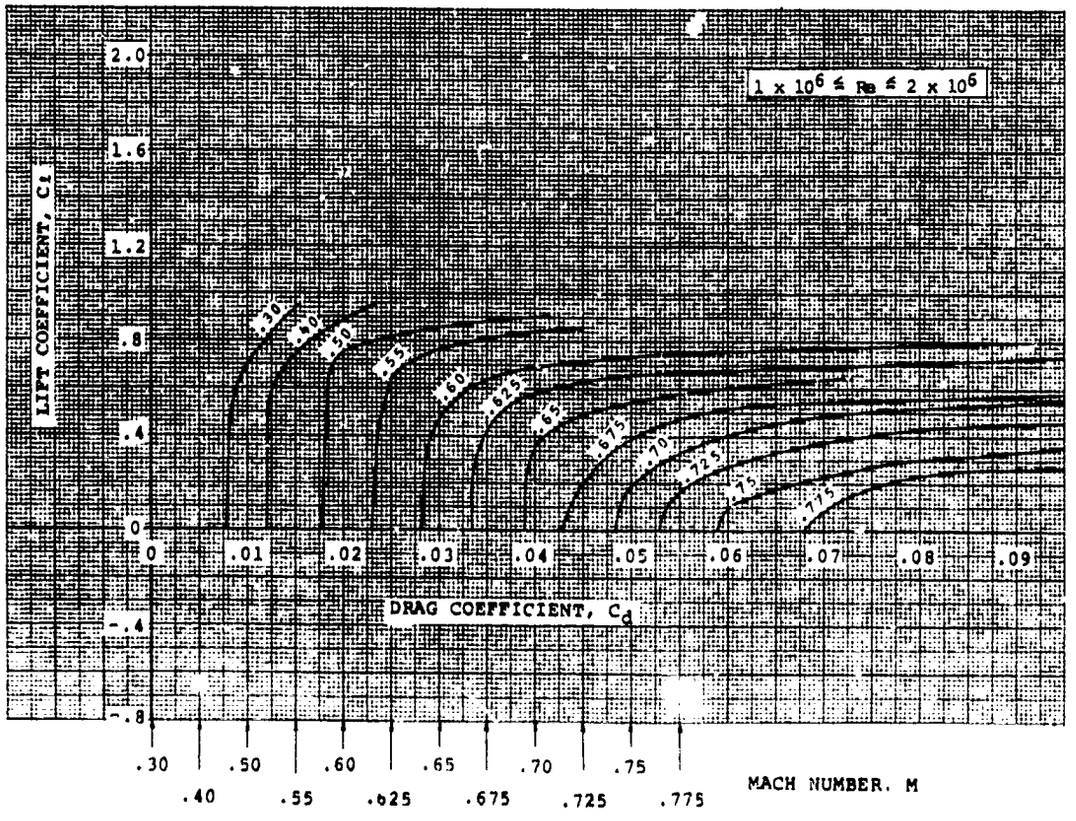
1 x 10^6 ≤ Re ≤ 2 x 10^6
LIFT COEFFICIENT, Cl
2.0
1.6
1.2
.8
.4
0
-.4
-.8
0
.01
.02
.03
.04
.05
.06
.07
.08
.09
DRAG COEFFICIENT, Cd
.30
.40
.50
.55
.60
.625
.65
.675
.70
.725
.75
.775
MACH NUMBER, M

NACA 0015

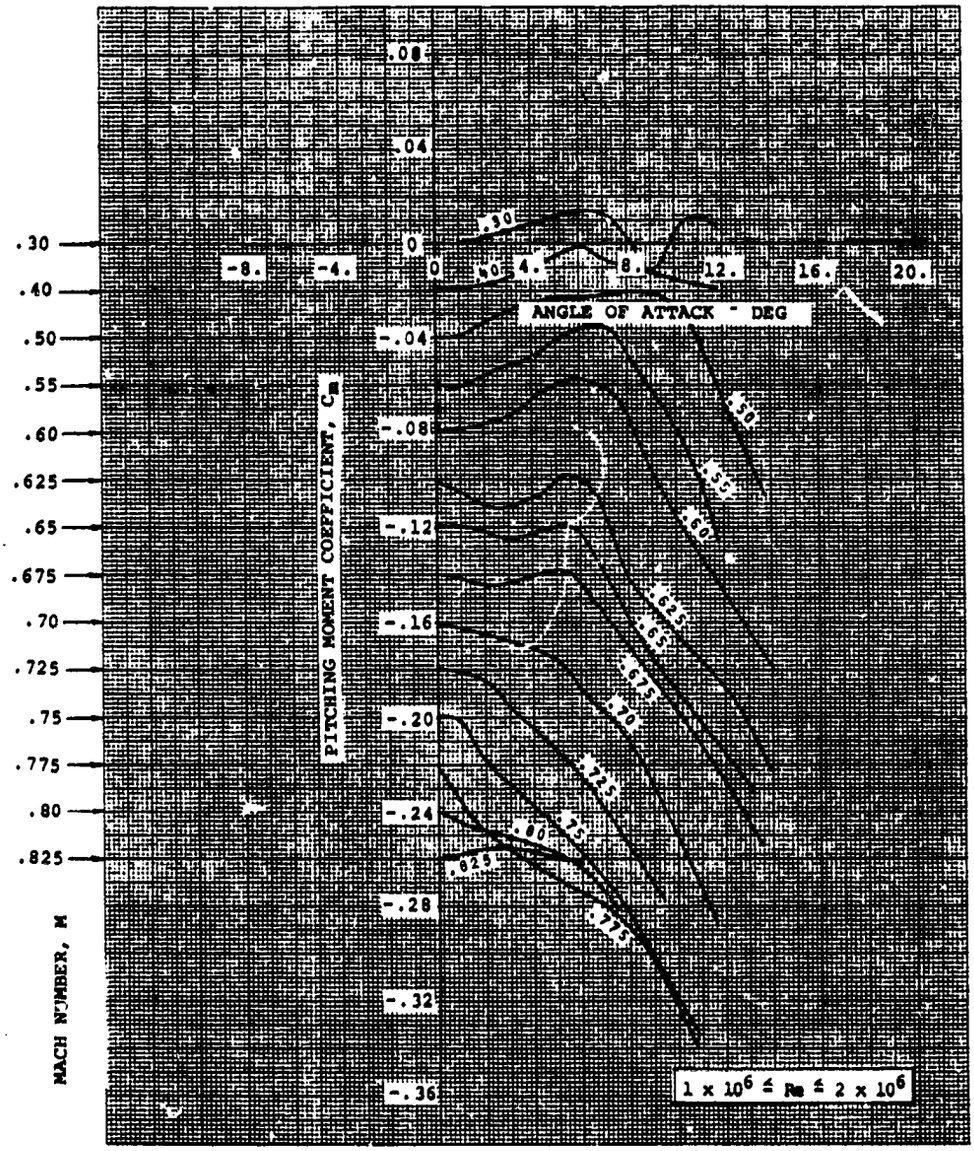
.08
.04
0
-.04
-.08
-.12
-.16
-.20
-.24
-.28
-.32
-.36
PITCHING MOMENT COEFFICIENT, $C_m$
-8.
-4.
0
4.
8.
12.
16.
20.
ANGLE OF ATTACK - DEG
.30
.40
.50
.55
.60
.625
.65
.675
.70
.725
.75
.775
.80
.825
MACH NUMBER, M
$1 \times 10^6 \leq Re \leq 2 \times 10^6$

AIRFOIL: NACA 23012

1.3.70

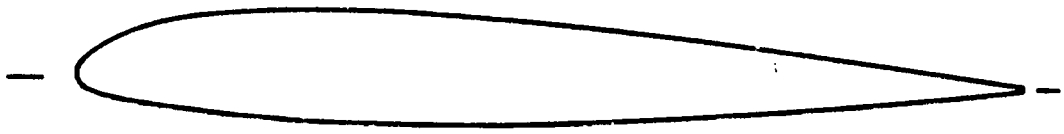

AIRFOIL COORDINATES

| x/c | $y/c_u$ | $y/c_\ell$ |
|---|---|---|
| 0.0 | 0.0 | 0.0 |
| .0125 | .0267 | -.0123 |
| .025 | .0361 | -.0171 |
| .050 | .0491 | -.0226 |
| .075 | .580 | -.0261 |
| .10 | .0643 | -.0292 |
| .15 | .0719 | -.0350 |
| .20 | .0750 | -.0397 |
| .25 | .0760 | -.0428 |
| .30 | .0755 | -.0446 |
| .40 | .0714 | -.0448 |
| .50 | .0641 | -.0417 |
| .60 | .0547 | -.0367 |
| .70 | .0436 | -.0300 |
| .80 | .0308 | -.0216 |
| .90 | .0168 | -.0123 |
| .95 | .0092 | -.0070 |
| 1.0 | .0013 | -.0013 |

CHARACTERISTICS

- Thickness, t/c = 0.12
- Leading edge radius, r/c = 0.0158
- Slope of radius through L.E. = 0.305

TYPE OF DATA AND METHOD OF TEST

Two-dimensional test in 8 in. by 18 in. blowdown tunnel at Aircraft Research Association (ARA) in Bedford, England.

Lift and pitching moments were calculated by integration of 43 surface static pressures distributed over the airfoil model. The drag was determined by wake rake measurements.

Model Chord = 12.7 cm (5.0 in )
Span = 20.3 cm (8.0 in )

SOURCE

Uhle, H., Windkanalmessungen am Profile NACA 23012 mit Original - und modifizierter Hinterkante, MBB TN D127-2/71, Nov. 3, 1971.

NACA 23012

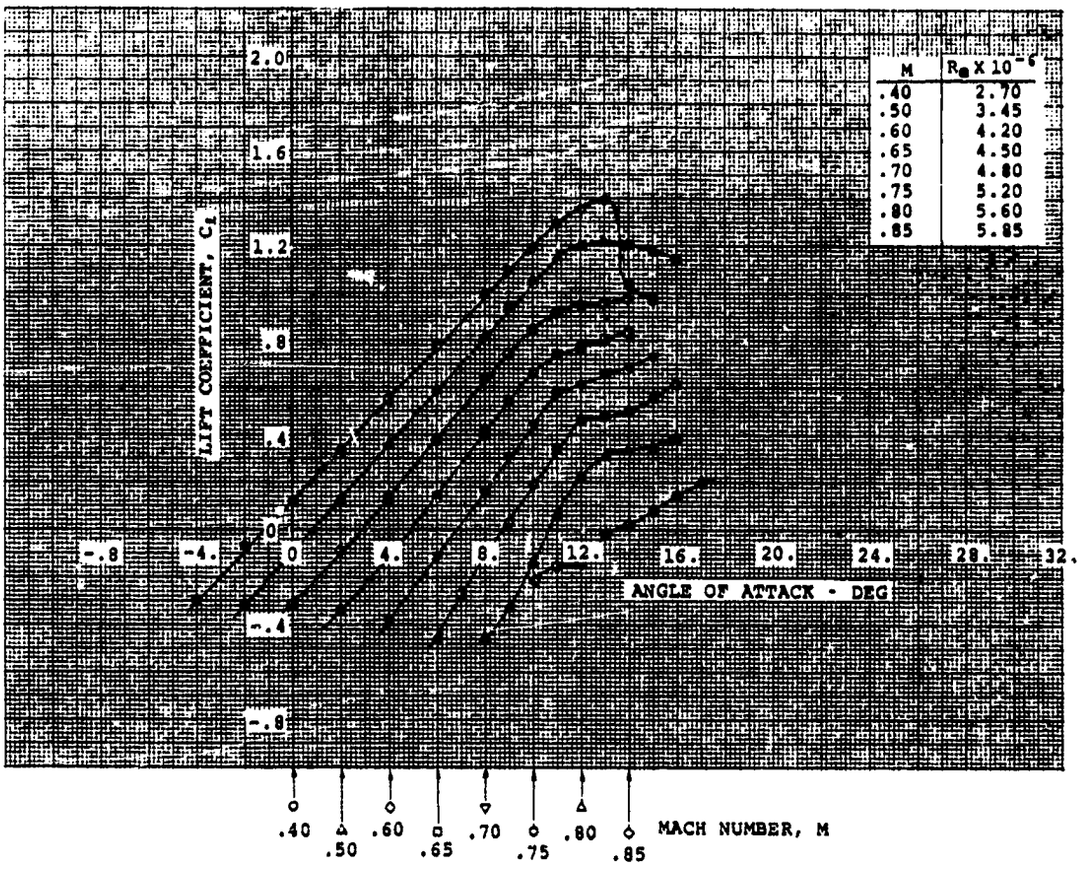
2.0
1.6
1.2
.8
.4
0
-.4
-.8
LIFT COEFFICIENT, $C_l$
-.8
-4.
0
4.
8.
12.
16.
20.
24.
28.
32.
ANGLE OF ATTACK - DEG
M | $R_e \times 10^{-6}$
.40 | 2.70
.50 | 3.45
.60 | 4.20
.65 | 4.50
.70 | 4.80
.75 | 5.20
.80 | 5.60
.85 | 5.85
.40
.50
.60
.65
.70
.75
.80
.85
MACH NUMBER, M

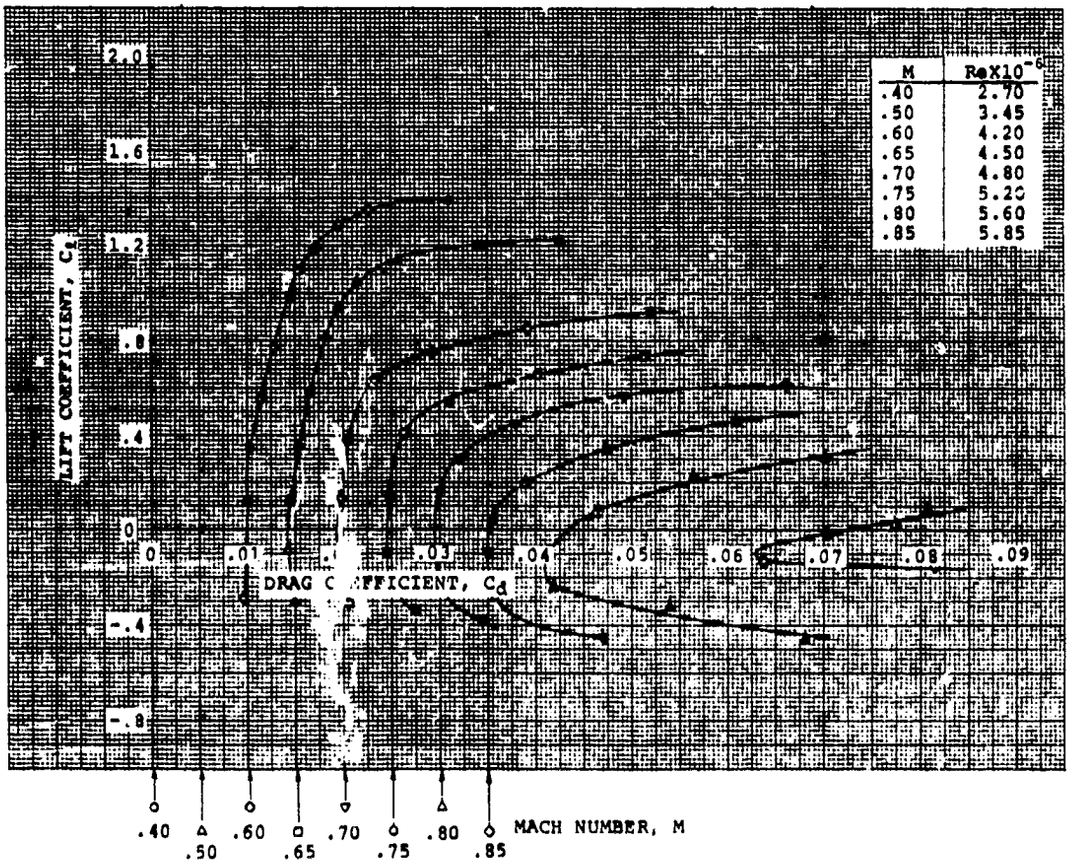
2.0
1.6
1.2
.8
.4
0
-.4
-.8
LIFT COEFFICIENT, $C_l$
0
.01
.02
.03
.04
.05
.06
.07
.08
.09
DRAG COEFFICIENT, $C_d$
M | $R_e \times 10^{-6}$
.40 | 2.70
.50 | 3.45
.60 | 4.20
.65 | 4.50
.70 | 4.80
.75 | 5.20
.80 | 5.60
.85 | 5.85
.40
.50
.60
.65
.70
.75
.80
.85
MACH NUMBER, M

NACA 23012

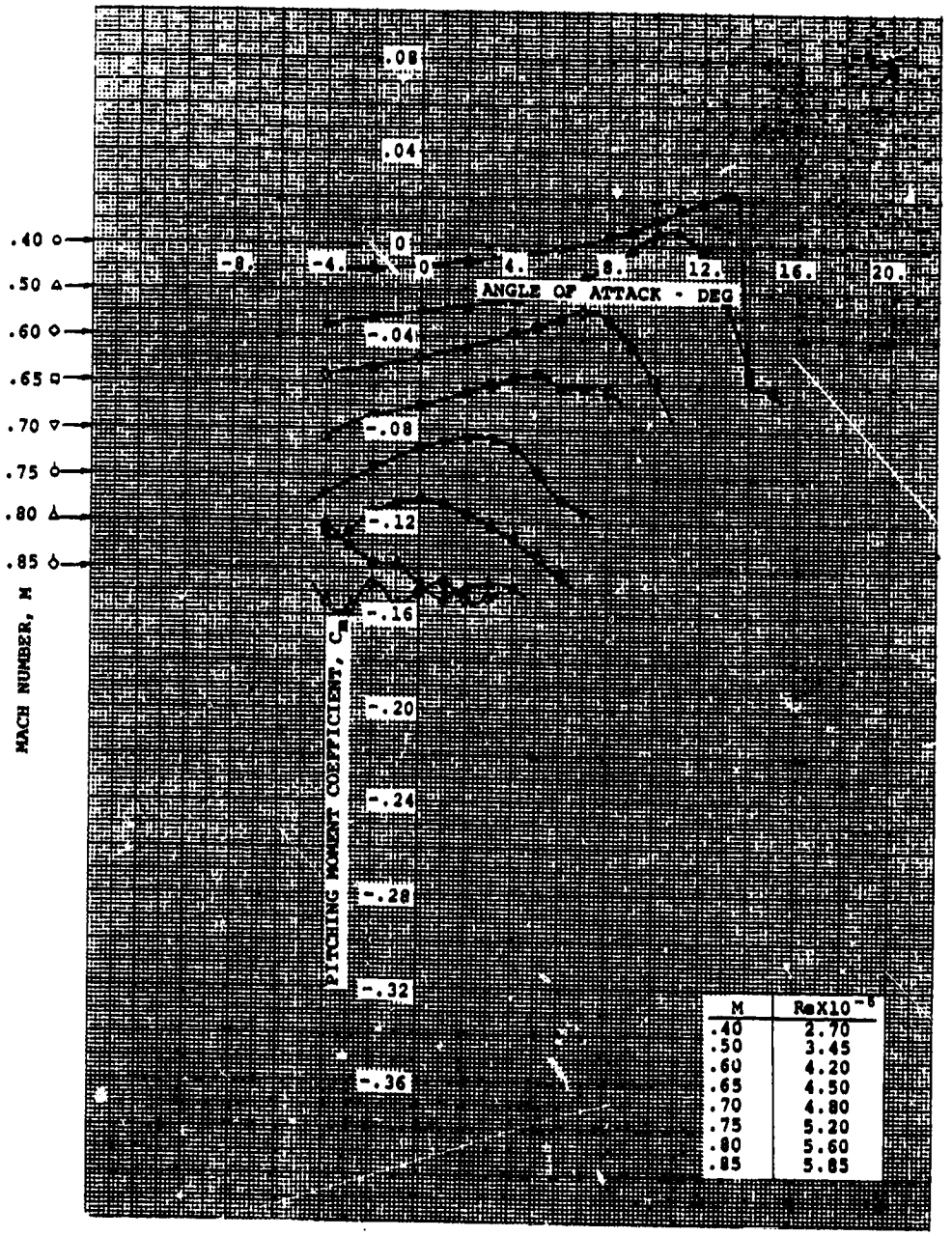
.08
.04
0
-.04
-.08
-.12
-.16
-.20
-.24
-.28
-.32
-.36
-8.
-4.
0
4.
8.
12.
16.
20.
ANGLE OF ATTACK - DEG
PITCHING MOMENT COEFFICIENT, $C_m$
MACH NUMBER, M
.40
.50
.60
.65
.70
.75
.80
.85
M | ReX10$^{-6}$
.40 | 2.70
.50 | 3.45
.60 | 4.20
.65 | 4.50
.70 | 4.80
.75 | 5.20
.80 | 5.60
.85 | 5.85

AIRFOIL: NACA 23012 with 0.043c T.E. Tab 1.3.80

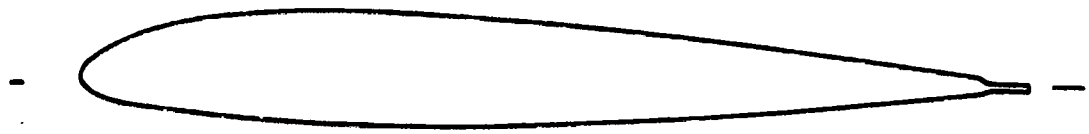

## AIRFOIL COORDINATES

| x/c | $y/c_u$ | $y/c_\ell$ |
|---|---|---|
| 0.0 | 0.0 | 0.0 |
| .0125 | .0267 | -.0123 |
| .025 | .0361 | -.0171 |
| .050 | .0491 | -.0226 |
| .075 | .0580 | -.0261 |
| .10 | .0643 | -.0292 |
| .15 | .0719 | -.0350 |
| .20 | .0750 | -.0397 |
| .25 | .0760 | -.0428 |
| .30 | .0755 | -.0446 |
| .40 | .0714 | -.0448 |
| .50 | .0641 | -.0417 |
| .60 | .0547 | -.0367 |
| .70 | .0436 | -.0300 |
| .80 | .0308 | -.0216 |
| .90 | .0168 | -.0123 |
| .95 | .0092 | -.0070 |
| 1.0 | .0043 | -.0043 |

## CHARACTERISTICS

- Thickness, t/c = 0.12
- Leading edge circle, r/c = 0.0158
- Slope of radius through L.E. = 0.305
- Trailing edge tab from x/c = 0.957 with abrupt to x/c = 1.00 transition from airfoil to tab

## TYPE OF DATA AND METHOD OF TEST

Two-dimensional test in 8 in. x 18 in. blowdown tunnel at Aircraft Research Association (ARA) in Bedford, England.

Lift and pitching moments were calculated by integration of 43 surface static pressures distributed over the airfoil model. The drag was determined by wake rake measurements.

Model Chord = 12.7 cm (5.0 in )
Span = 20.3 cm (8.0 in )

## SOURCE

Uhle, H., Windkanalmessungen am Profile NACA 23012 mit Original - und modifizierter Hinterkante, MBB TN D127-2/71, Nov. 3, 1971.

NACA 23012 WITH 0.043 C T.E. TAB AT 0°

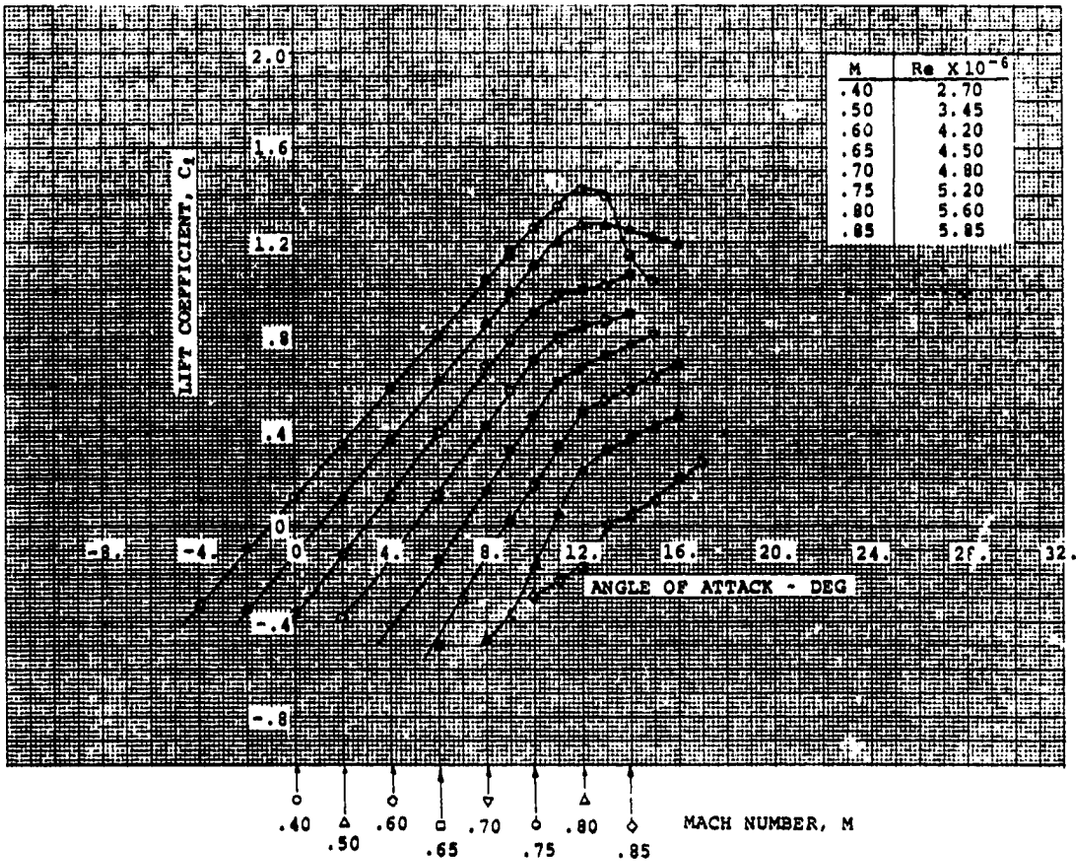


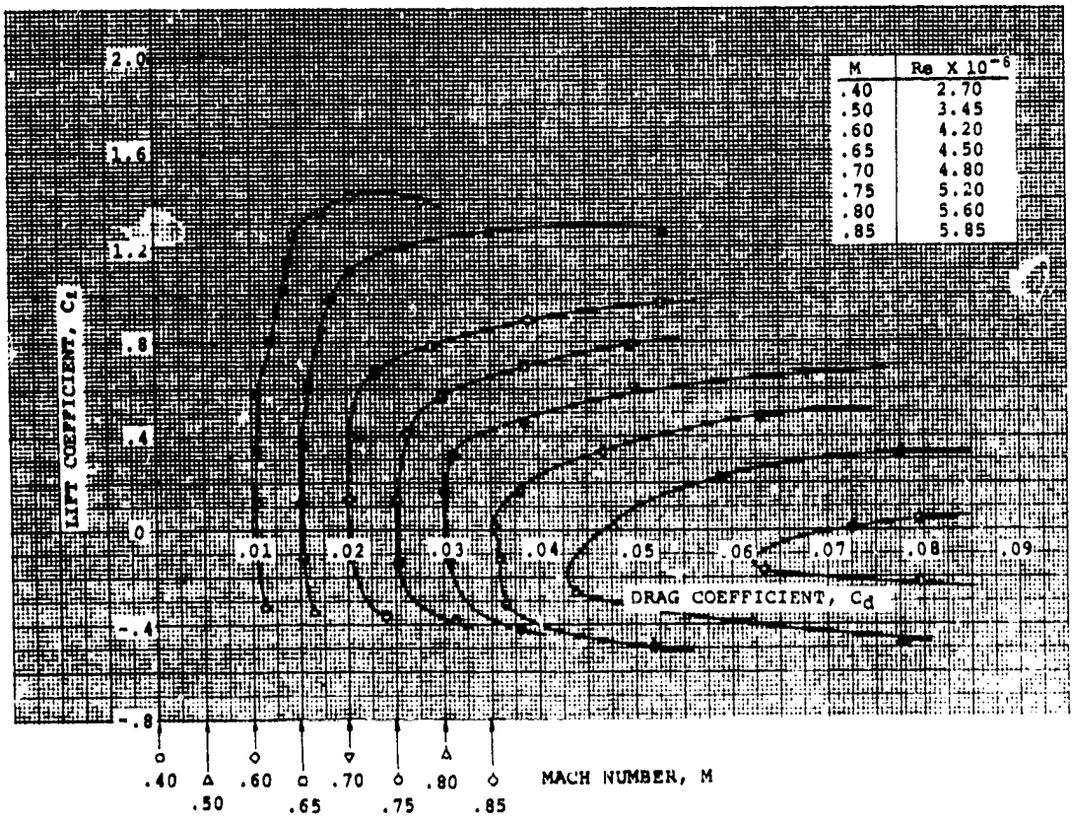

NACA 23012 WITH 0.043 C T.E. TAB AT 0°

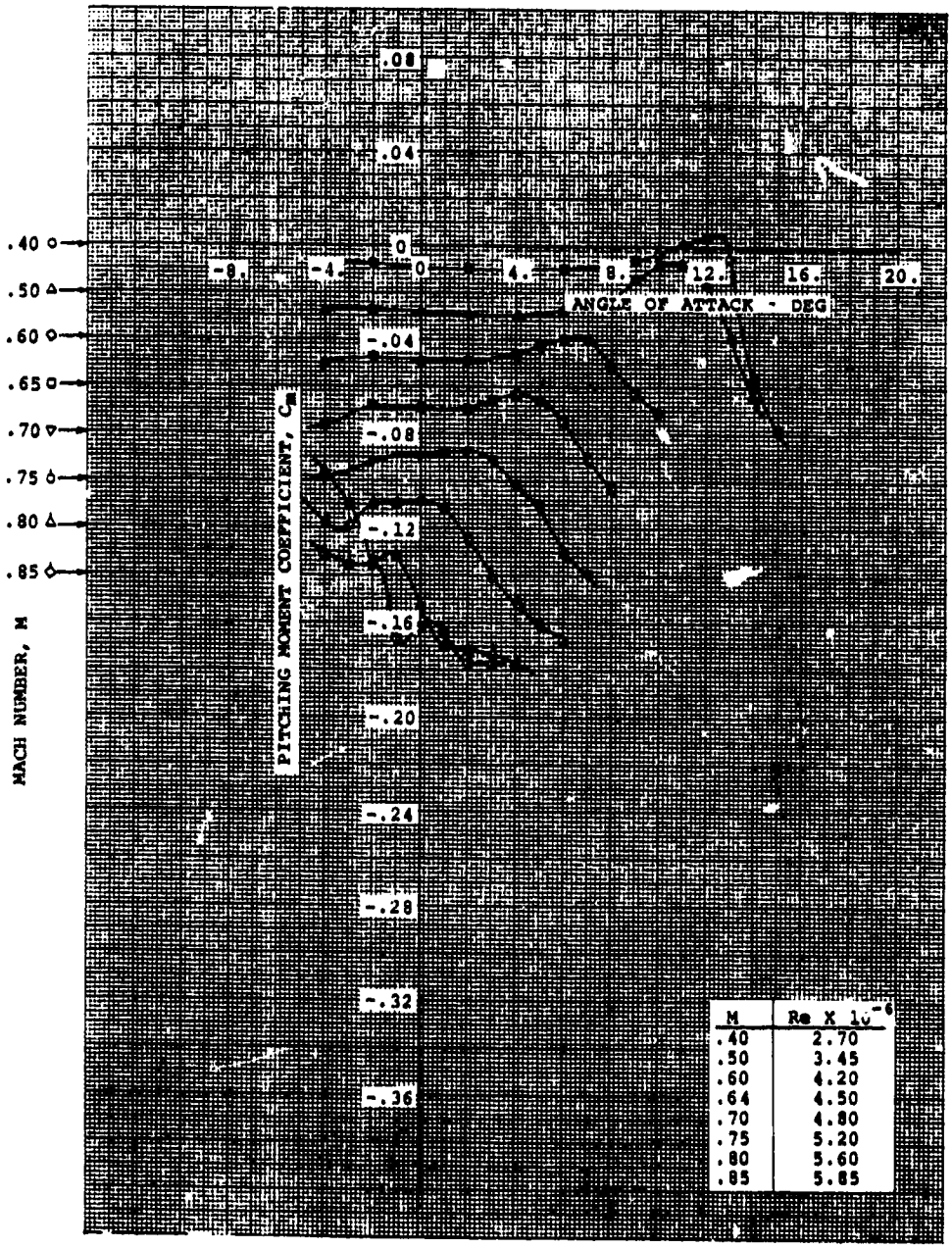

AIRFOIL: NACA 23012 with 0.087c T.E. Tab

1.3.90

## AIRFOIL COORDINATES

| x/c | $y/c_u$ | $y/c_\ell$ |
|---|---|---|
| 0.0 | 0.0 | 0.0 |
| .0125 | .0267 | -.0123 |
| .025 | .0361 | -.0171 |
| .050 | .0491 | -.0226 |
| .075 | .0580 | -.0261 |
| .10 | .0643 | -.0292 |
| .15 | .0719 | -.0350 |
| .20 | .0750 | -.0397 |
| .25 | .0760 | -.0428 |
| .30 | .0755 | -.0446 |
| .40 | .0714 | -.0448 |
| .50 | .0641 | -.0417 |
| .60 | .0547 | -.0367 |
| .70 | .0436 | -.0300 |
| .80 | .0308 | -.0216 |
| .90 | .0168 | -.0123 |
| .913 | .0043 | -.0043 |
| 1.0 | .0043 | -.0043 |

## CHARACTERISTICS

- Thickness, t/c = 0.12
- Leading edge circle, r/c = 0.0158
- Slope of radius through L.E. = 0.305
- Trailing edge tab from x/c = 0.913 with abrupt transition from airfoil to tab to x/c = 1.00
- 0° T.E. tab angle, measured from chord line

## TYPE OF DATA AND METHOD OF TEST

Two-dimensional test in 8 in. by 18 in. blowdown tunnel at Aircraft Research Association (ARA) in Bedford, England.

Lift and pitching moments were calculated by integration of 43 surface static pressures distributed over the airfoil model. The drag was determined by wake rake measurements.

Model Chord = 12.7 cm (5.0 in )
Span = 20.3 cm (8.0 in )

## SOURCE

Uhle, H., Windkanalmessungen am Profile NACA 23012 mit Original - und modifizierter Hinterkante, MBB TN D127-2/71, Nov. 3, 1971.

NACA 23012 WITH 0.087 C T.E. TAB AT 0°

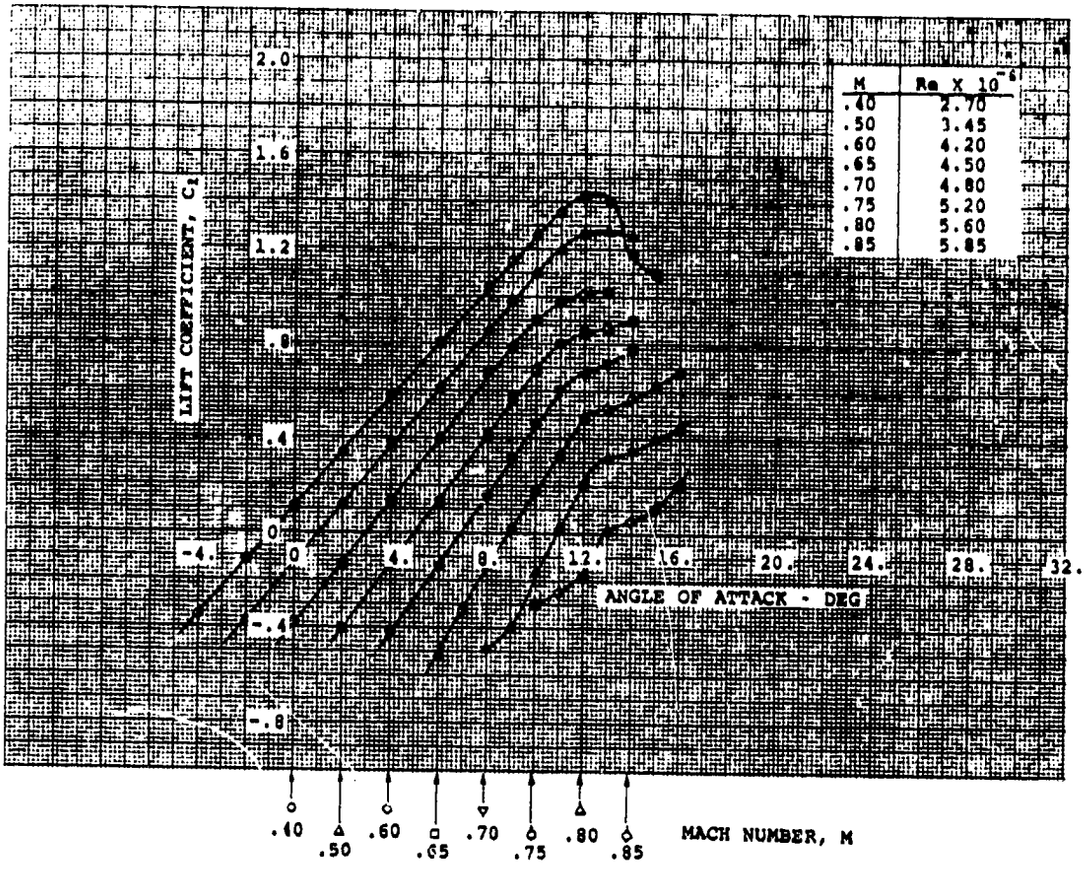


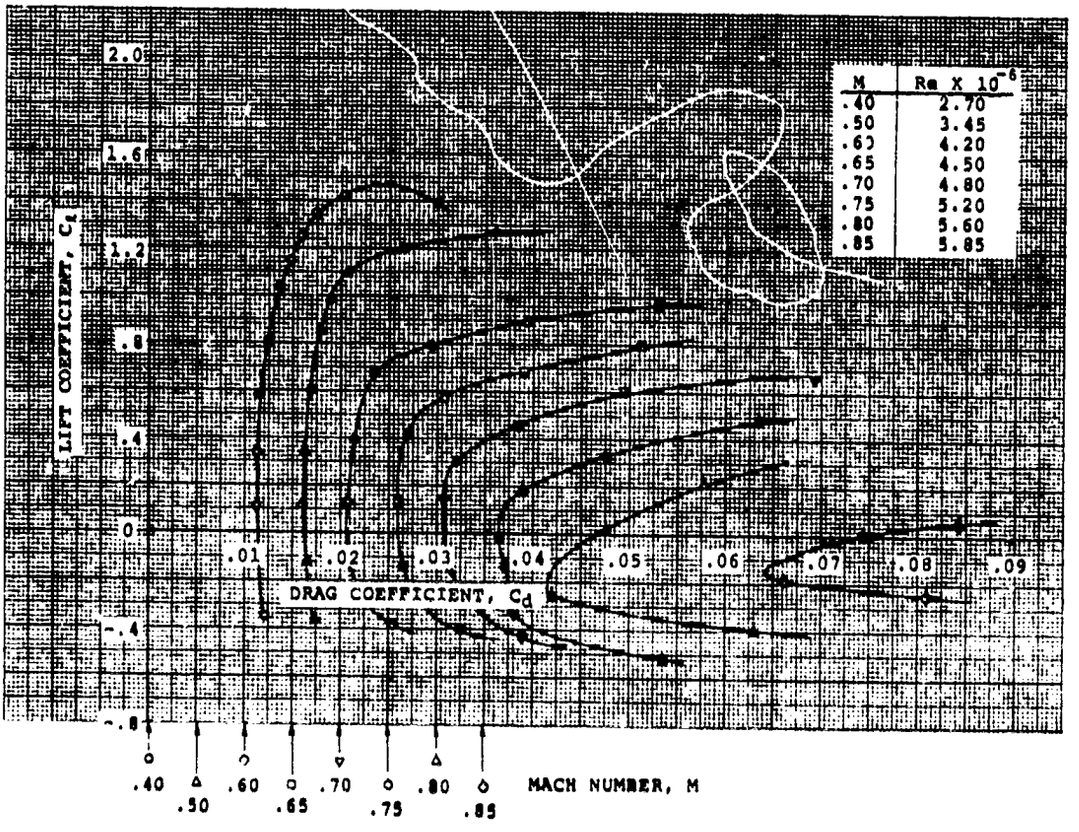

NACA 23012 WITH 0.087 C T.E. TAB AT 0°

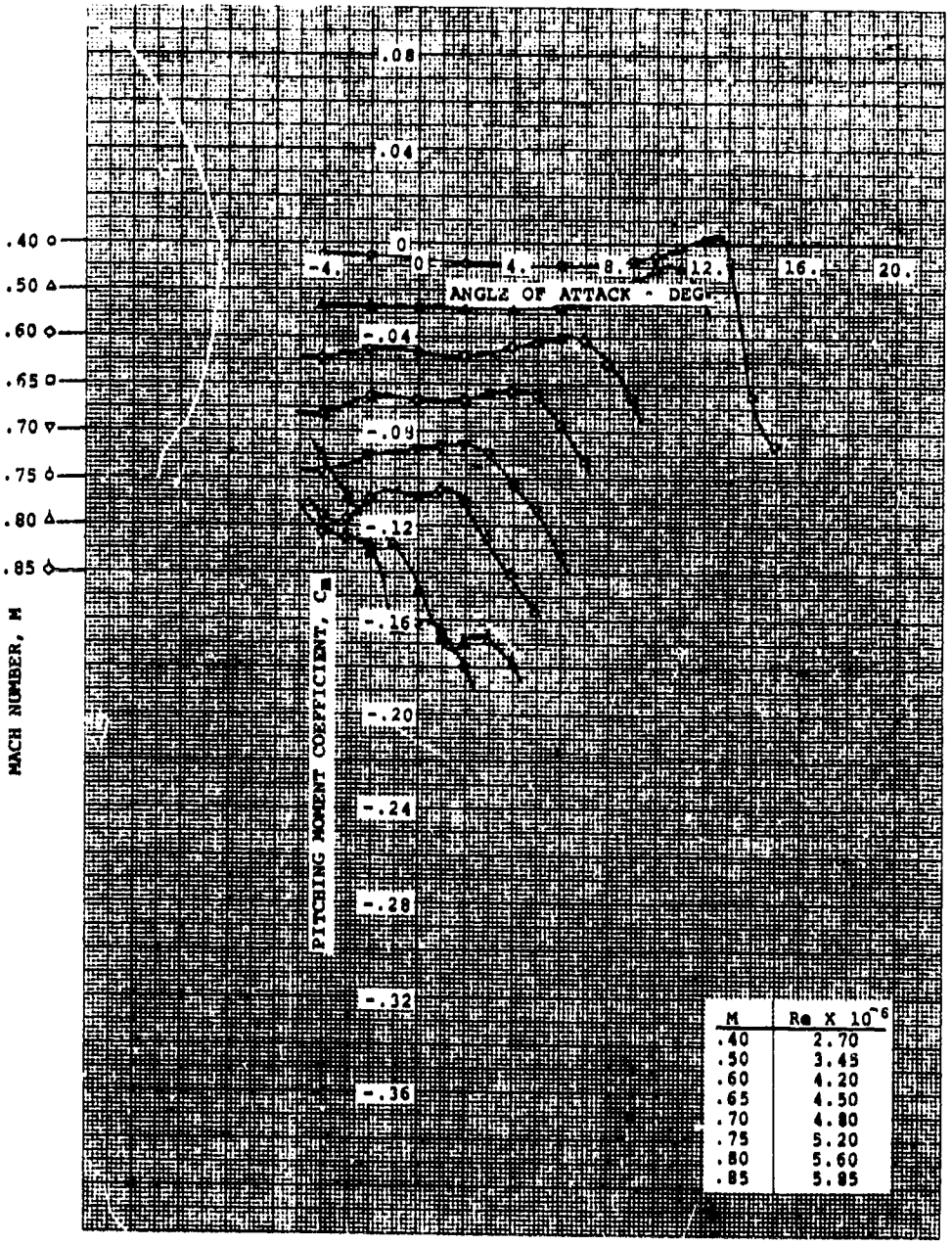

AIRFOIL: NACA 23015



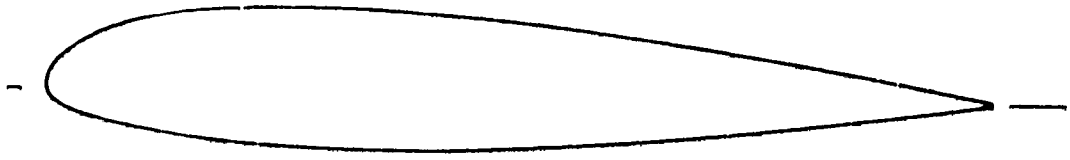

AIRFOIL COORDINATES

| x/c | $y/c_u$ | $y/c_\ell$ |
|---|---|---|
| 0.0 | 0.0 | 0.0 |
| 0.0125 | 0.0334 | -0.0154 |
| 0.025 | 0.0444 | -0.0225 |
| 0.05 | 0.0589 | -0.0304 |
| 0.075 | 0.069 | -0.0361 |
| 0.1 | 0.0764 | -0.0409 |
| 0.15 | 0.0852 | -0.0484 |
| 0.2 | 0.0892 | -0.0541 |
| 0.25 | 0.0908 | -0.0578 |
| 0.3 | 0.0905 | -0.0596 |
| 0.4 | 0.0859 | -0.0592 |
| 0.5 | 0.0774 | -0.0550 |
| 0.6 | 0.0661 | -0.0481 |
| 0.7 | 0.0525 | -0.0391 |
| 0.8 | 0.0373 | -0.0283 |
| 0.9 | 0.0204 | -0.0159 |
| 0.95 | 0.0112 | -0.0090 |
| 1.0 | 0.0016 | -0.0016 |

CHARACTERISTICS

- Thickness, t/c = 0.15
- Leading Edge Radius, r/c = 0.0248
- Slope of Radius Through Leading Edge = 0.305

TYPE OF DATA AND METHOD OF TEST

The tests were conducted in the Ames 1-by 3½-foot high-speed wind tunnel, a low-turbulence, two-dimensional, continuous flow facility.

The airfoil models were equipped with 30 pressure orifices of 0.008 in. diameter, and were equipped with tightly fitting end plates flush with the tunnel walls.

Lift and pitching moments were obtained by integration of the measured surface pressures. Wake surveys were carried out with a movable rake of total-head tubes.

Broken lines in the data indicate that stream velocities were within 0.025M.

Model Chord = 6.0 in
Span = 12.0 in

SOURCE

Graham, D.J., Nitzberg, G.E., and Olson, R.N., A Systematic Investigation of Pressure Distributions at High Speeds Over Five Representative NACA Low-Drag and Conventional Airfoil Sections, NACA Report 832, 1945.

NACA 23015

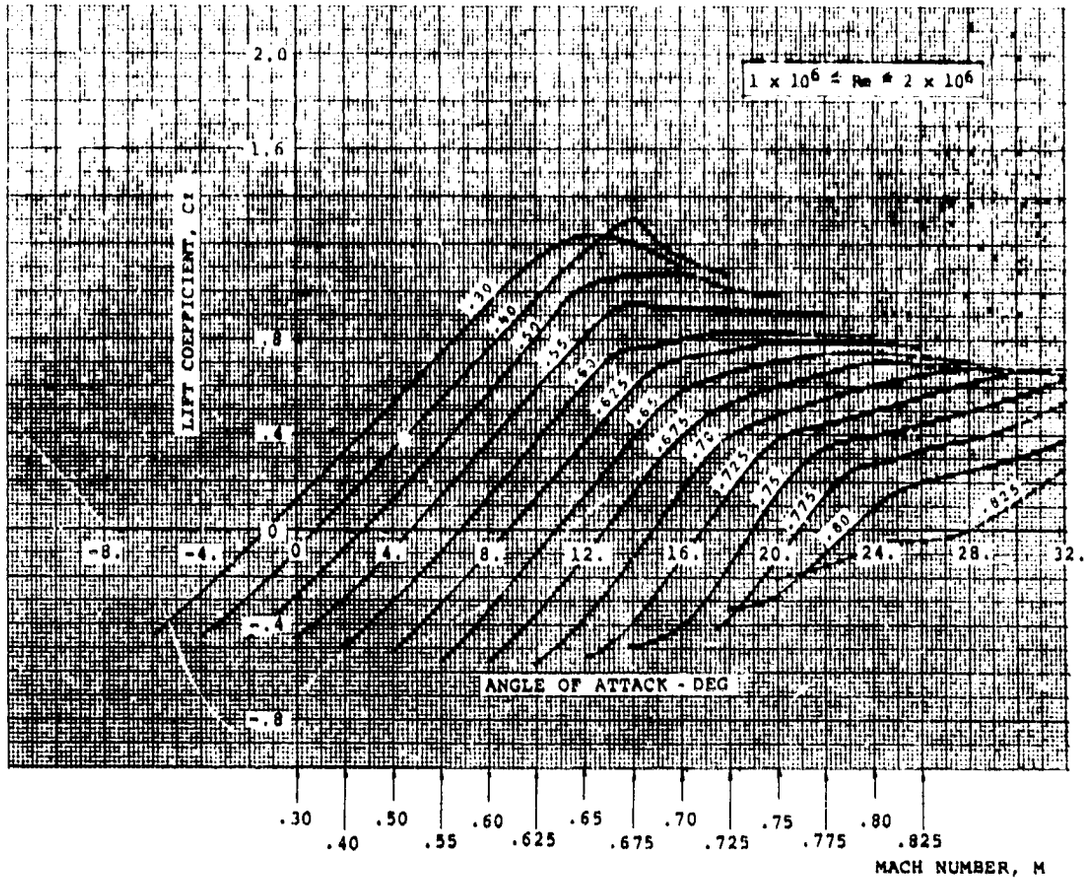
1 x 10^6 ≤ Re ≤ 2 x 10^6
LIFT COEFFICIENT, Cl
2.0
1.6
.8
.4
0
-.4
-.8
-8.
-4.
0
4.
8.
12.
16.
20.
24.
28.
32.
ANGLE OF ATTACK - DEG
.30
.40
.50
.55
.60
.625
.65
.675
.70
.725
.75
.775
.80
.825
MACH NUMBER, M

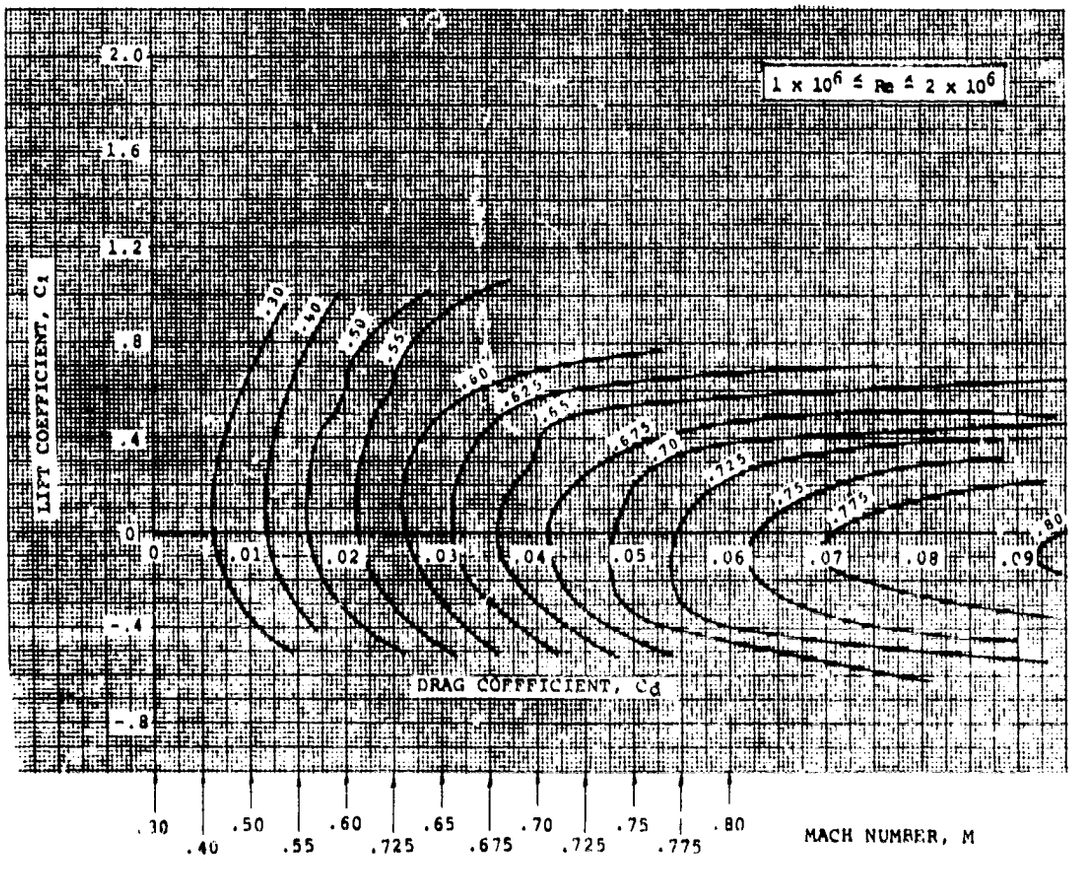
1 x 10^6 ≤ Re ≤ 2 x 10^6
LIFT COEFFICIENT, Cl
2.0
1.6
1.2
.8
.4
0
-.4
-.8
0
.01
.02
.03
.04
.05
.06
.07
.08
.09
DRAG COEFFICIENT, Cd
.30
.40
.50
.55
.60
.625
.65
.675
.70
.725
.75
.775
.80
MACH NUMBER, M

NACA 23015

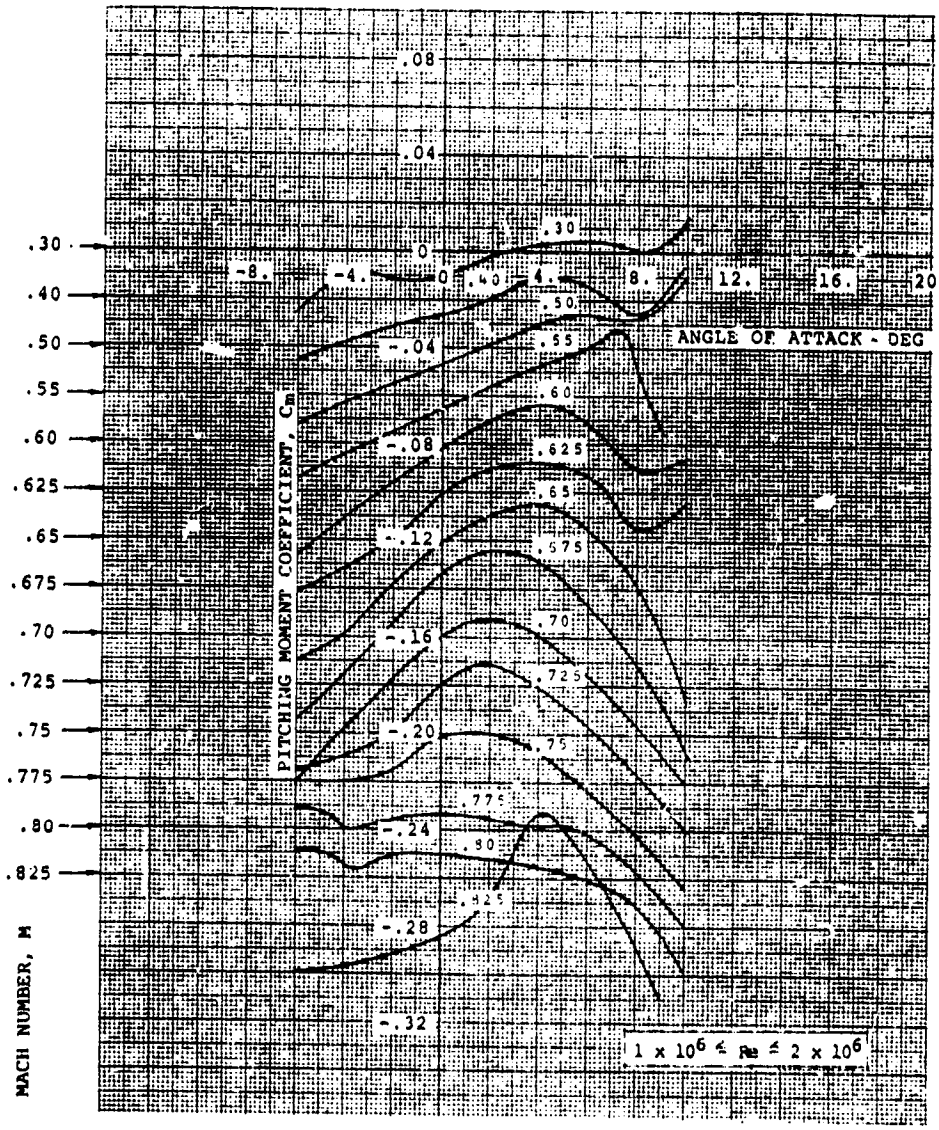
.08
.04
0
-.04
-.08
-.12
-.16
-.20
-.24
-.28
-.32
-8.
-4.
0
4.
8.
12.
16.
20.
ANGLE OF ATTACK - DEG
PITCHING MOMENT COEFFICIENT, $C_m$
MACH NUMBER, M
.30
.40
.50
.55
.60
.625
.65
.675
.70
.725
.75
.775
.80
.825
$1 \times 10^6 \leq Re \leq 2 \times 10^6$

AIRFOIL: NACA 63A009



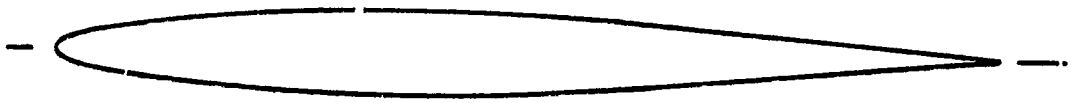

AIRFOIL COORDINATES

| x/c | y/c |
|---|---|
| 0.0 | 0.0 |
| 0.005 | 0.007375 |
| 0.0075 | 0.008875 |
| 0.0125 | 0.011262 |
| 0.025 | 0.015637 |
| 0.05 | 0.021712 |
| 0.075 | 0.02625 |
| 0.1 | 0.0299 |
| 0.15 | 0.035525 |
| 0.2 | 0.039575 |
| 0.25 | 0.0424 |
| 0.3 | 0.04419 |
| 0.35 | 0.04495 |
| 0.4 | 0.044725 |
| 0.45 | 0.043575 |
| 0.5 | 0.04153 |
| 0.55 | 0.0389 |
| 0.6 | 0.03559 |
| 0.65 | 0.031775 |
| 0.7 | 0.0275 |
| 0.75 | 0.023 |
| 0.8 | 0.01844 |
| 0.85 | 0.013875 |
| 0.9 | 0.009312 |
| 0.95 | 0.00475 |
| 1.0 | 0.0002 |

CHARACTERISTICS

- Thickness, t/c/ = 0.09
- Leading Edge Radius, r/c = 0.006075
- Trailing Edge Radius, r/c = 0.000225

TYPE OF DATA AND METHOD OF TEST

The tests were conducted in the Lockheed-California Company Fluid Dynamics Laboratory 4-by-4 foot supersonic wind tunnel, equipped with a two-dimensional subsonic test section. The tunnel is of the blow-down type. The floor and ceiling of the test section were perforated (porous).

Model forces were measured with two six-component strain gage balances. Drag was measured with a 40-tube pressure rake installed 14 inches downstream of the trailing edge of the model.

Model Chord = 8.0 in
Span = 48 .0 in

SOURCE

Sipe, O.E., Jr., and Gorenberg, N.B., Effect of Mach Number, Reynolds Number, and Thickness Ratio on the Aerodynamic Characteristics of NACA 63A-Series Airfoil Sections, U.S. Army A.M.L. TR 65-28, June 1965.

NACA 63A009

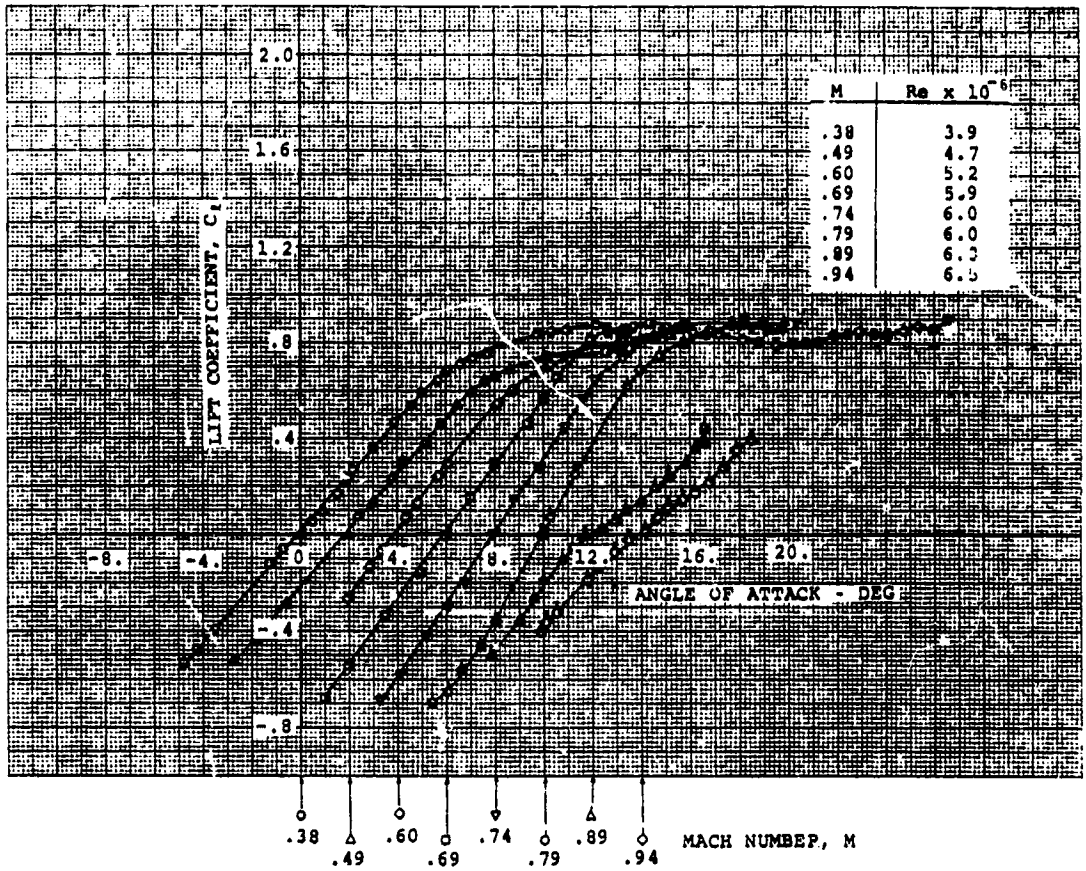
LIFT COEFFICIENT, $C_l$
2.0
1.6
1.2
.8
.4
0
-.4
-.8
-8.
-4.
0
4.
8.
12.
16.
20.
ANGLE OF ATTACK - DEG
M | Re x $10^{-6}$
.38 3.9
.49 4.7
.60 5.2
.69 5.9
.74 6.0
.79 6.0
.89 6.3
.94 6.5
.38 .49 .60 .69 .74 .79 .89 .94
MACH NUMBER, M

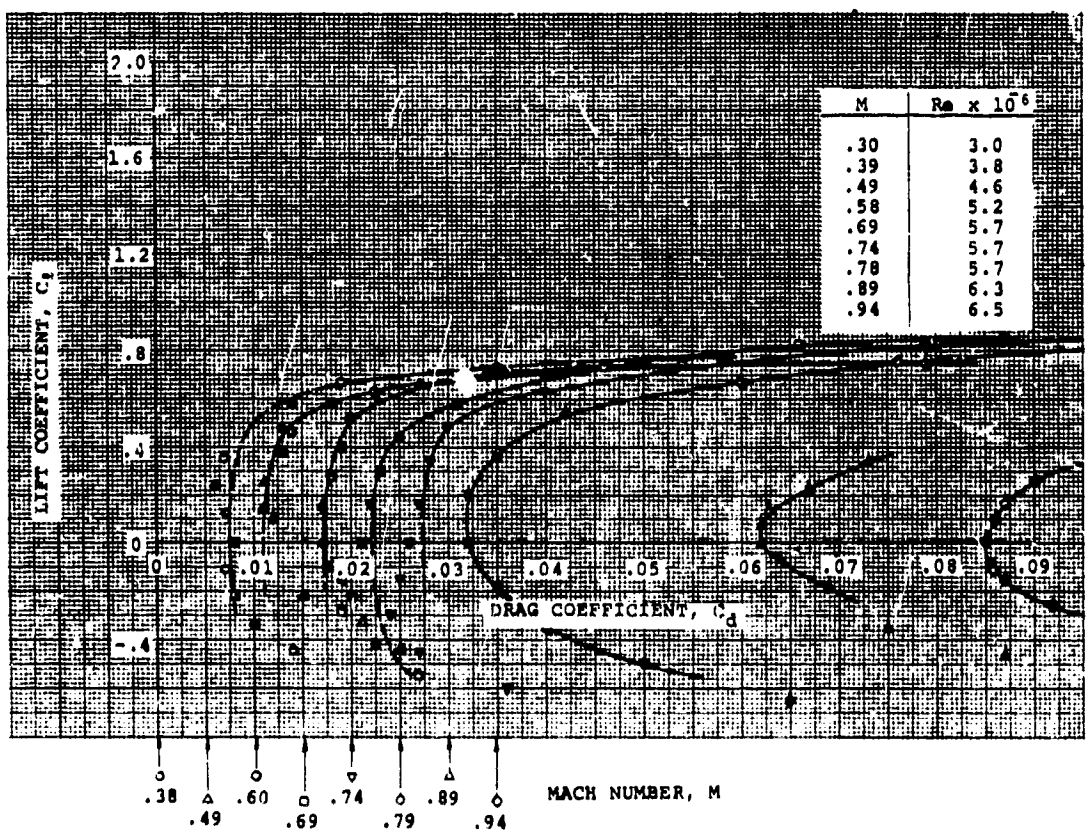
LIFT COEFFICIENT, $C_l$
2.0
1.6
1.2
.8
.4
0
-.4
0
.01
.02
.03
.04
.05
.06
.07
.08
.09
DRAG COEFFICIENT, $C_d$
M | Re x $10^{-6}$
.30 3.0
.39 3.8
.49 4.6
.58 5.2
.69 5.7
.74 5.7
.78 5.7
.89 6.3
.94 6.5
.38 .49 .60 .69 .74 .79 .89 .94
MACH NUMBER, M

NACA 63A009

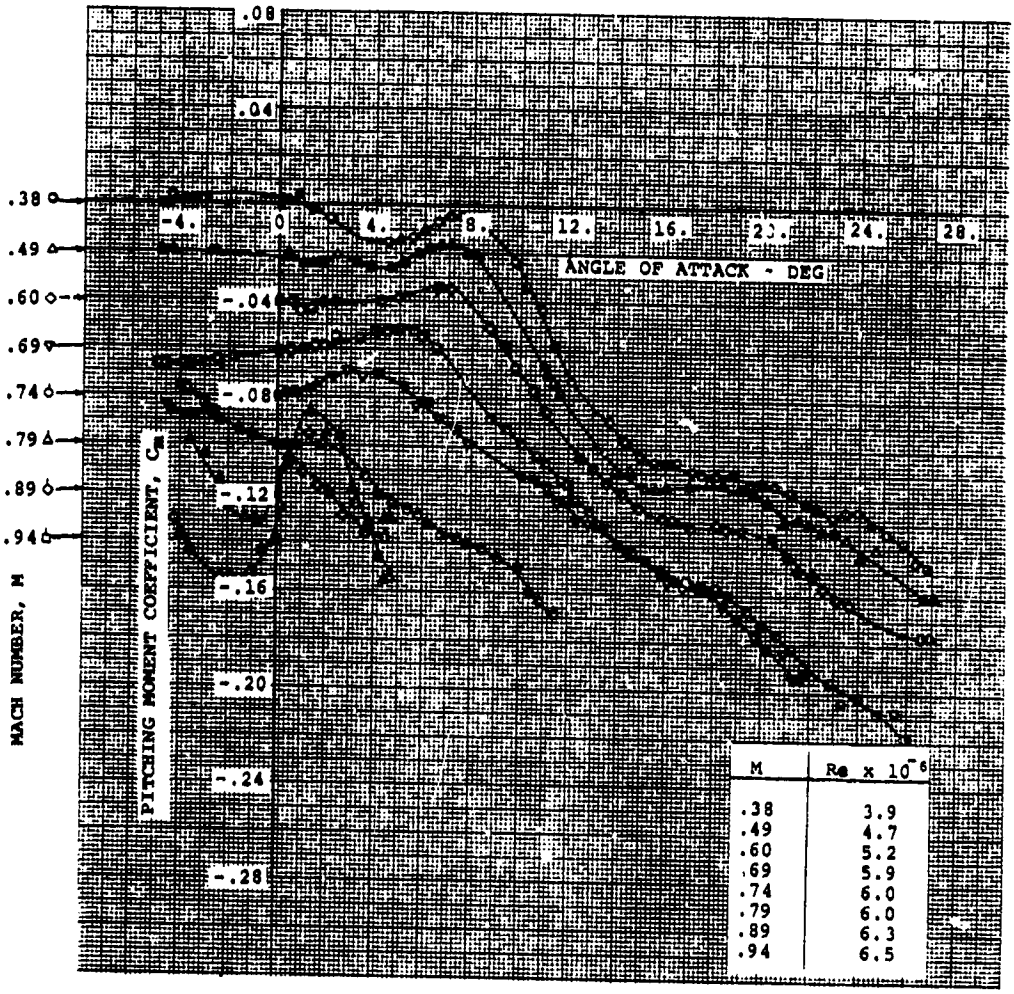
.08
.04
-.04
-.08
-.12
-.16
-.20
-.24
-.28
PITCHING MOMENT COEFFICIENT, $C_m$
-4.
0
4.
8.
12.
16.
20.
24.
28.
ANGLE OF ATTACK - DEG
.38
.49
.60
.69
.74
.79
.89
.94
MACH NUMBER, M
M | Re x $10^{-6}$
.38 | 3.9
.49 | 4.7
.60 | 5.2
.69 | 5.9
.74 | 6.0
.79 | 6.0
.89 | 6.3
.94 | 6.5

AIRFOIL: NACA 63A012 1.3.120

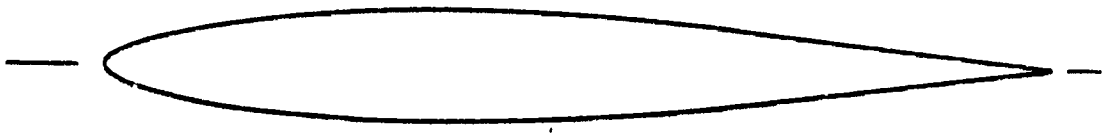

AIRFOIL COORDINATES

| x/c | y/c |
|---|---|
| 0.0 | 0.0 |
| 0.005 | 0.009725 |
| 0.0075 | 0.011725 |
| 0.0125 | 0.014925 |
| 0.025 | 0.020775 |
| 0.05 | 0.02895 |
| 0.075 | 0.03504 |
| 0.1 | 0.03994 |
| 0.15 | 0.047475 |
| 0.2 | 0.052875 |
| 0.25 | 0.05664 |
| 0.3 | 0.05901 |
| 0.35 | 0.05995 |
| 0.4 | 0.059575 |
| 0.45 | 0.057925 |
| 0.5 | 0.05517 |
| 0.55 | 0.051475 |
| 0.6 | 0.047 |
| 0.65 | 0.04186 |
| 0.7 | 0,03621 |
| 0.75 | 0.03026 |
| 0.8 | 0.02426 |
| 0.85 | 0.01826 |
| 0.9 | 0.01225 |
| 0.95 | 0.00625 |
| 1.0 | 0.00025 |

CHARACTERISTICS

- Thickness, t/c = 0.12
- Leading Edge Radius, r/c = 0.01075
- Trailing Edge Radius, r/c = 0.000275

TYPE OF DATA AND METHOD OF TEST

The tests were conducted in the Lockheed-California Company Fluid Dynamics Laboratory 4-by-4 foot supersonic wind tunnel, equipped with a two-dimensional subsonic test section. The tunnel is of the blow-down type. The floor and ceiling of the test section were perforated (porous).

Model forces were measured with two six-component strain gage balances. Drag was measured with a 40-tube pressure rake installed 14 inches downstream of the trailing edge of the model.

Model Chord = 8.0 in
Span = 48 in

SOURCE

Sipe, O.E., Jr., and Gorenberg, N.B., Effect of Mach Number, Reynolds Number, and Thickness Ratio on the Aerodynamic Characteristics of NACA 63A-Series Airfoil Sections, U.S. Army A.M.L. TR 65-28, June 1965.

NACA 63A012

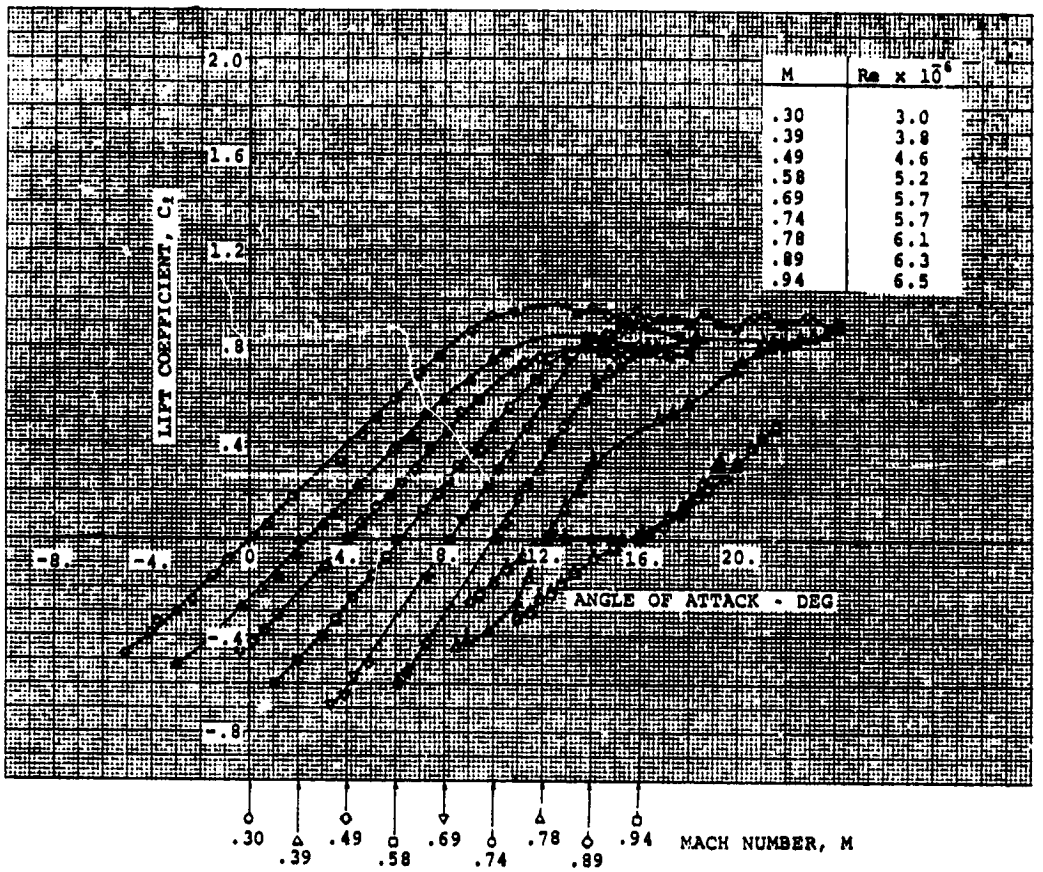
M | Re x 10^6
.30 | 3.0
.39 | 3.8
.49 | 4.6
.58 | 5.2
.69 | 5.7
.74 | 5.7
.78 | 6.1
.89 | 6.3
.94 | 6.5
LIFT COEFFICIENT, Cl
2.0
1.6
1.2
.8
.4
-.4
-.8
-8.
-4.
0
4.
8.
12.
16.
20.
ANGLE OF ATTACK - DEG
.30
.39
.49
.58
.69
.74
.78
.89
.94
MACH NUMBER, M

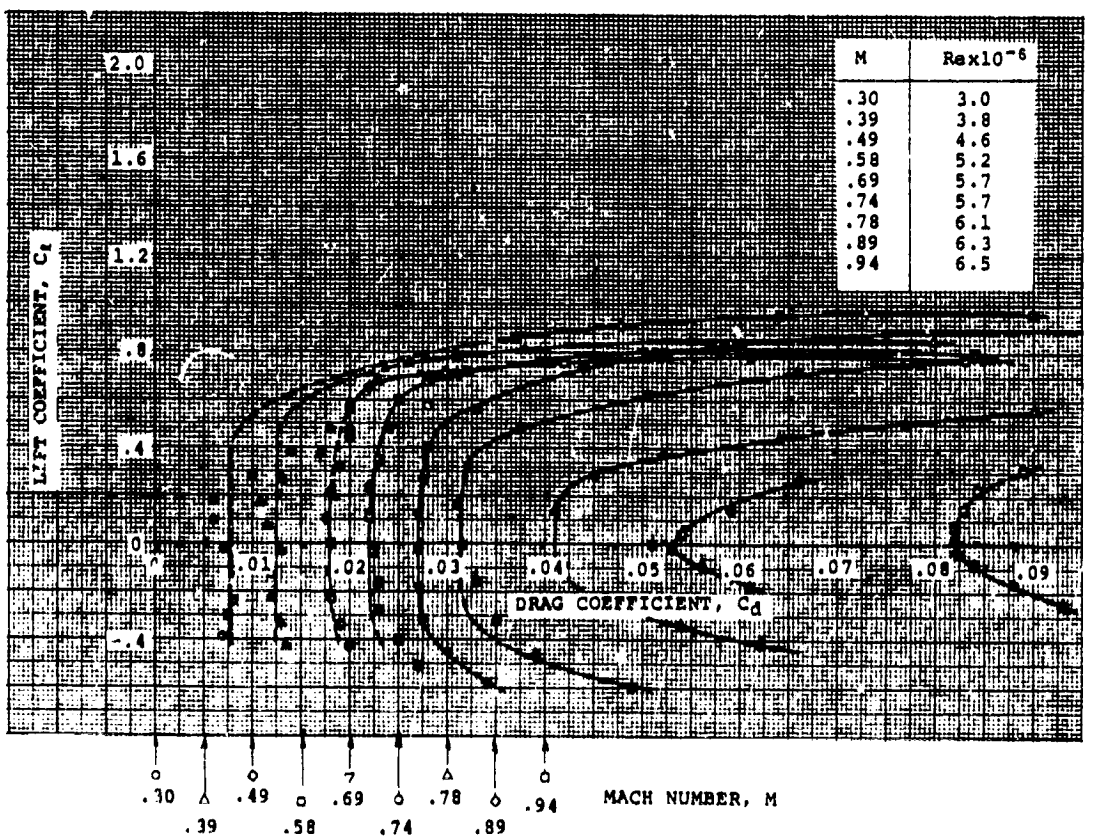
M | Rex10^-6
.30 | 3.0
.39 | 3.8
.49 | 4.6
.58 | 5.2
.69 | 5.7
.74 | 5.7
.78 | 6.1
.89 | 6.3
.94 | 6.5
LIFT COEFFICIENT, Cl
2.0
1.6
1.2
.8
.4
0
-.4
.01
.02
.03
.04
.05
.06
.07
.08
.09
DRAG COEFFICIENT, Cd
.30
.39
.49
.58
.69
.74
.78
.89
.94
MACH NUMBER, M

NACA 63A012

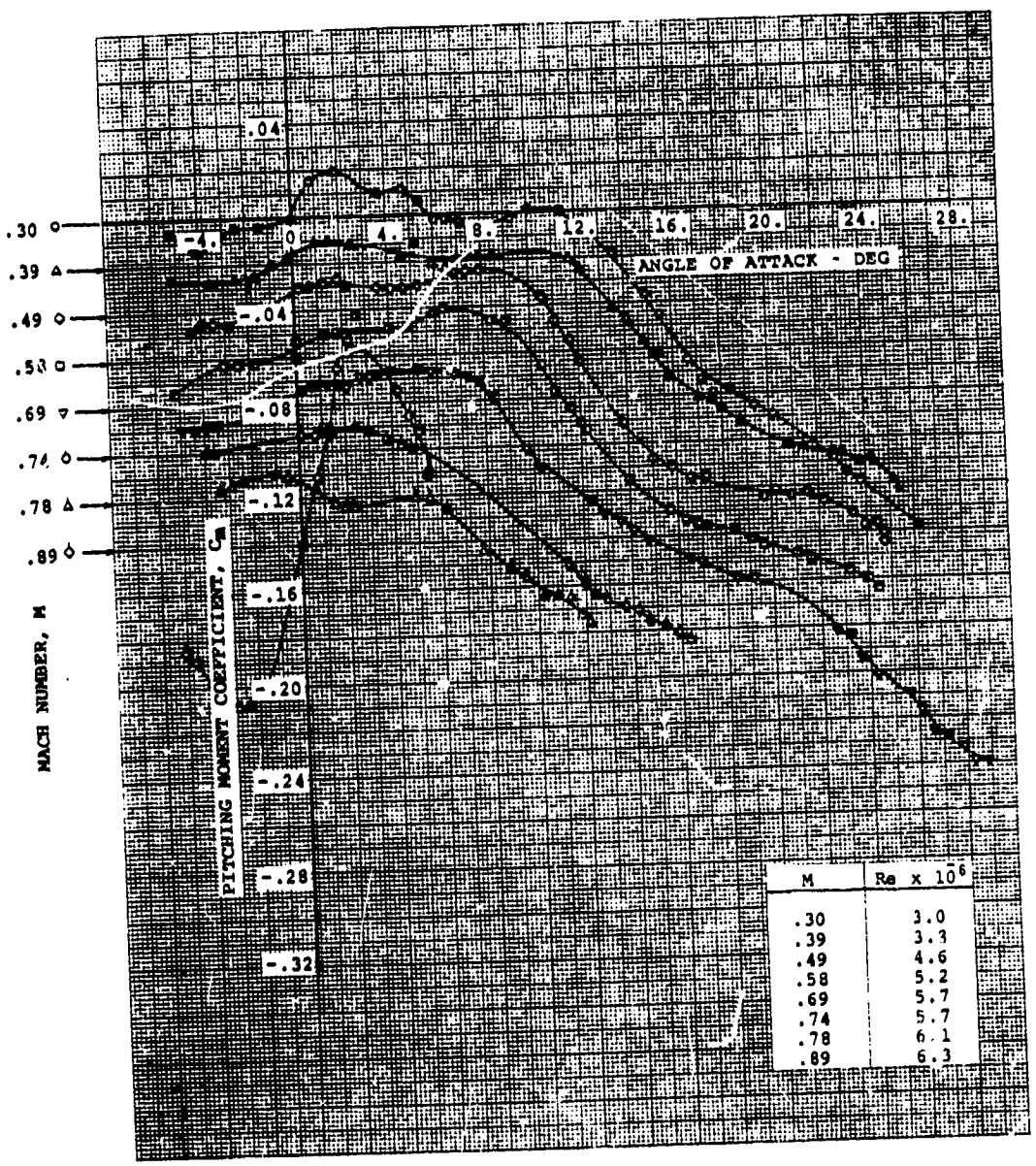
.04
-.04
-.08
-.12
-.16
-.20
-.24
-.28
-.32
-4.
0
4.
8.
12.
16.
20.
24.
28.
ANGLE OF ATTACK - DEG
PITCHING MOMENT COEFFICIENT, $C_m$
MACH NUMBER, M
.30
.39
.49
.58
.69
.74
.78
.89
M | Re x $10^6$
.30 | 3.0
.39 | 3.3
.49 | 4.6
.58 | 5.2
.69 | 5.7
.74 | 5.7
.78 | 6.1
.89 | 6.3

AIRFOIL: NACA 63A012 (Including Reverse Flow) 1.3.130

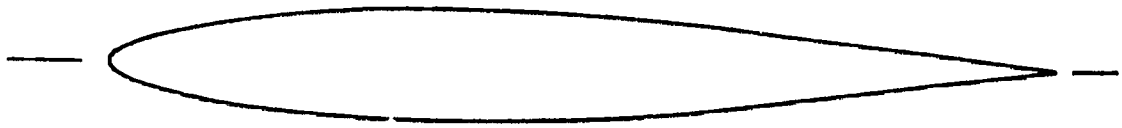

## AIRFOIL COORDINATES

| x/c | y/c |
|---|---|
| 0.0 | 0.0 |
| 0.005 | 0.009725 |
| 0.0075 | 0.011725 |
| 0.0125 | 0.014925 |
| 0.025 | 0.020775 |
| 0.05 | 0.02895 |
| 0.075 | 0.03504 |
| 0.1 | 0.03994 |
| 0.15 | 0.047475 |
| 0.2 | 0.052875 |
| 0.25 | 0.05664 |
| 0.3 | 0.05901 |
| 0.35 | 0.05995 |
| 0.4 | 0.059575 |
| 0.45 | 0.057925 |
| 0.5 | 0.05517 |
| 0.55 | 0.051475 |
| 0.6 | 0.047 |
| 0.65 | 0.04186 |
| 0.7 | 0.03621 |
| 0.75 | 0.03026 |
| 0.8 | 0.02426 |
| 0.85 | 0.01826 |
| 0.9 | 0.01225 |
| 0.95 | 0.00625 |
| 1.0 | 0.00025 |

## CHARACTERISTICS

- Thickness, t/c = 0.12
- Leading Edge Radius, r/c = 0.01075
- Trailing Edge Radius, r/c = 0.000275

## TYPE OF DATA AND METHOD OF TEST

The tests were conducted in the Lockheed-California Company Fluid Dynamics Laboratory 4-by-4 foot supersonic wind tunnel, equipped with a two-dimensional subsonic test section. The tunnel is of the blow-down type. The floor and ceiling of the test section were perforated (porous).

Model forces were measured with two six-component strain gage balances. Drag was measured with a 40-tube pressure rake installed 14 inches downstream of the trailing edge of the model.

Model Chord = 8.0 in
Span = 48 in

## SOURCE

Sipe, O.E., Jr., and Gorenberg, N.B., Effect of Mach Number, Reynolds Number, and Thickness Ratio on the Aerodynamic Characteristics of NACA 63A-Series Airfoil Sections, U.S. Army A.M.L. TR 65-28, June 1965.

# NACA 63A012 INCLUDING REVERSE FLOW

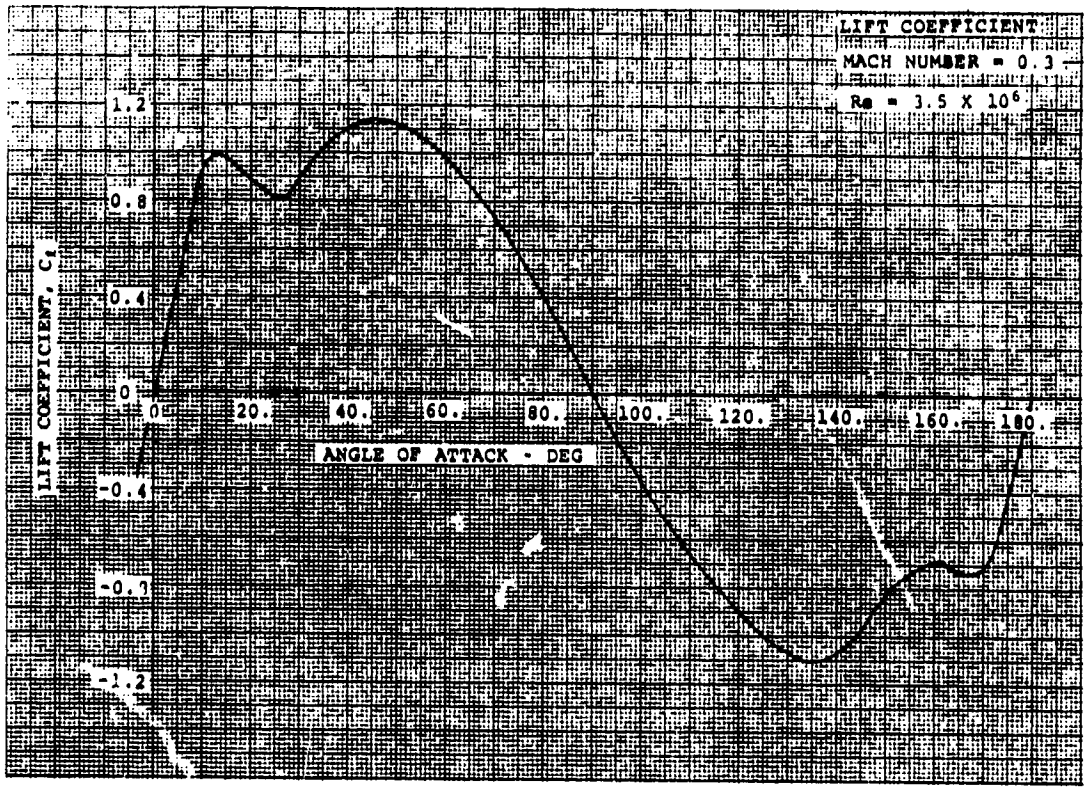


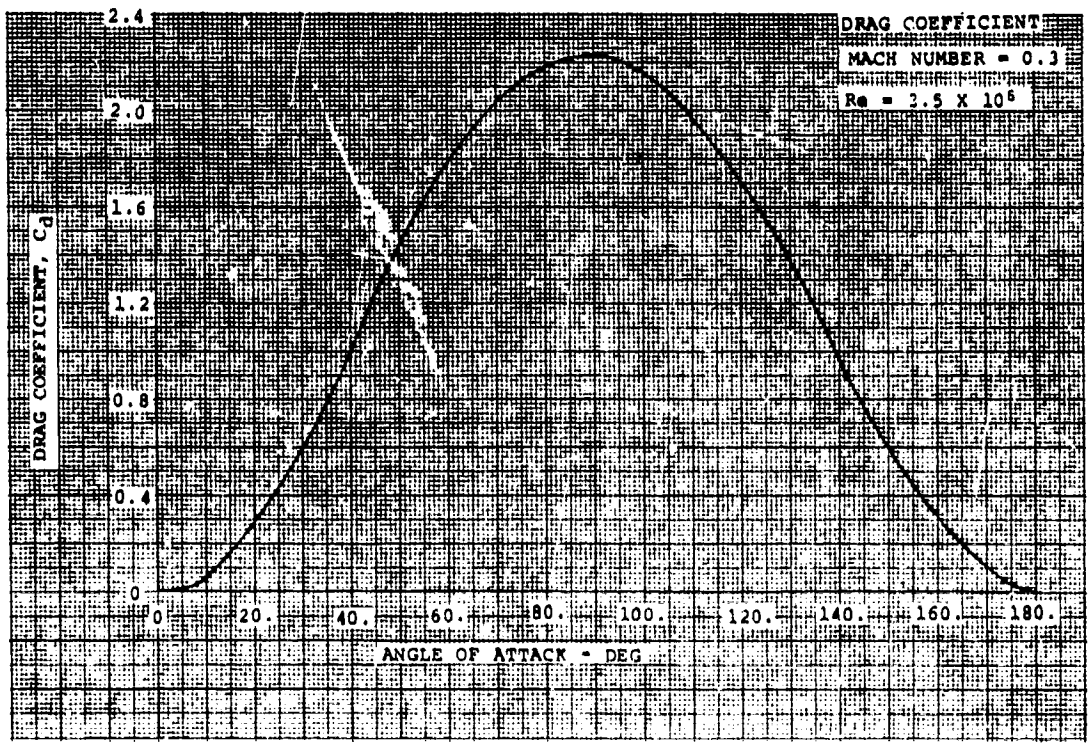

NACA 63A012 INCLUDING REVERSE FLOW

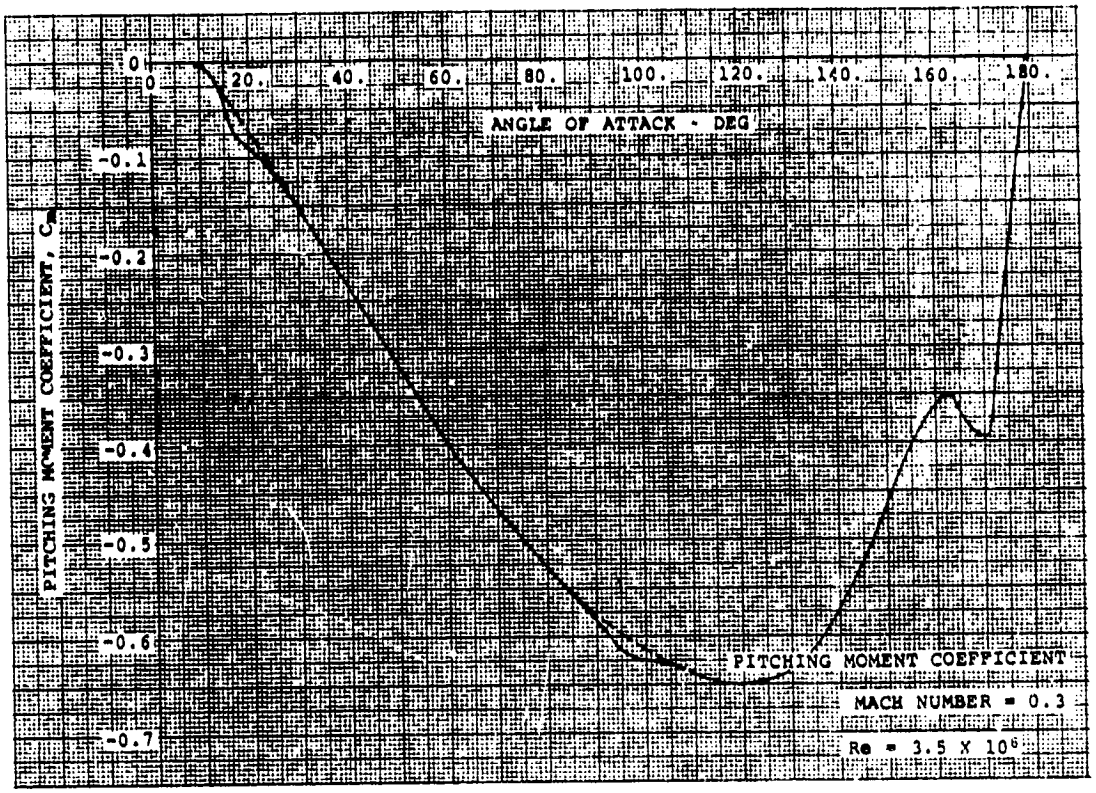

AIRFOIL: NACA 63A015

1.3.140

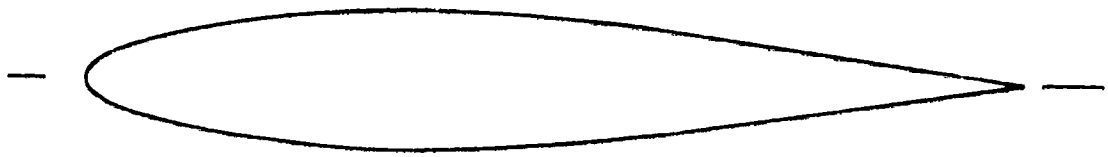

AIRFOIL COORDINATES

| x/c | y/c |
|---|---|
| 0.0 | 0.0 |
| 0.005 | 0.012025 |
| 0.0075 | 0.014475 |
| 0.0125 | 0.018437 |
| 0.025 | 0.02579 |
| 0.05 | 0.036175 |
| 0.075 | 0.04382 |
| 0.1 | 0.049975 |
| 0.15 | 0.059425 |
| 0.2 | 0.06619 |
| 0.25 | 0.07091 |
| 0.3 | 0.07384 |
| 0.35 | 0.07496 |
| 0.4 | 0.07435 |
| 0.45 | 0.07215 |
| 0.5 | 0.068575 |
| 0.55 | 0.063875 |
| 0.6 | 0.0582 |
| 0.65 | 0.051725 |
| 0.7 | 0.04467 |
| 0.75 | 0.03731 |
| 0.8 | 0.02991 |
| 0.85 | 0.02255 |
| 0.9 | 0.015125 |
| 0.95 | 0.0095 |
| 1.0 | 0.000325 |

CHARACTERISTICS

- Thickness, t/c = 0.15
- Leading Edge Radius, r/c = 0.0163
- Trailing Edge Radius, r/c = 0.000375

TYPE OF DATA AND METHOD OF TEST

The tests were conducted in the Lockheed-California Company Fluid Dynamics Laboratory 4-by-4 foot supersonic wind tunnel, equipped with a two-dimensional subsonic test section. The tunnel is of the blow-down type. The floor and ceiling of the test section were perforated (porous).

Model forces were measured with two six-component strain gage balances. Drag was measured with a 40-tube pressure rake installed 14 inches downstream of the trailing edge of the model.

Model Chord = 8.0 in
Span = 48 in

SOURCE

Sipe, O.E., Jr., and Gorenberg, N.B., Effect of Mach Number, Reynolds Number, and Thickness Ratio on the Aerodynamic Characteristics of NACA 63A-Series Airfoil Sections, U.S. Army A.M.L. TR 65-28, June 1965.

NACA 63A015

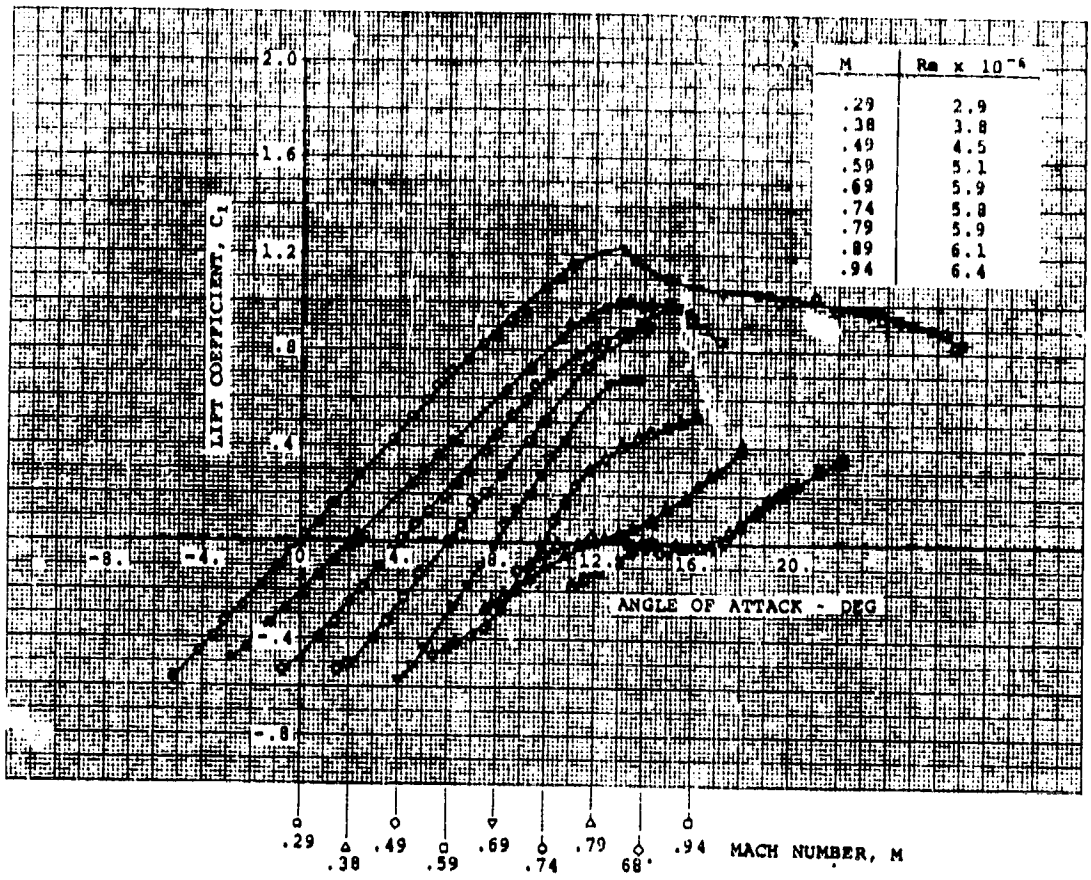
M | Re x 10⁻⁶
.29 2.9
.38 3.8
.49 4.5
.59 5.1
.69 5.9
.74 5.8
.79 5.9
.89 6.1
.94 6.4
LIFT COEFFICIENT, $C_l$
2.0
1.6
1.2
.8
.4
0
-.4
-.8
-8.
-4.
0
4.
8.
12.
16.
20.
ANGLE OF ATTACK - DEG
.29
.38
.49
.59
.69
.74
.79
.94
68
MACH NUMBER, M

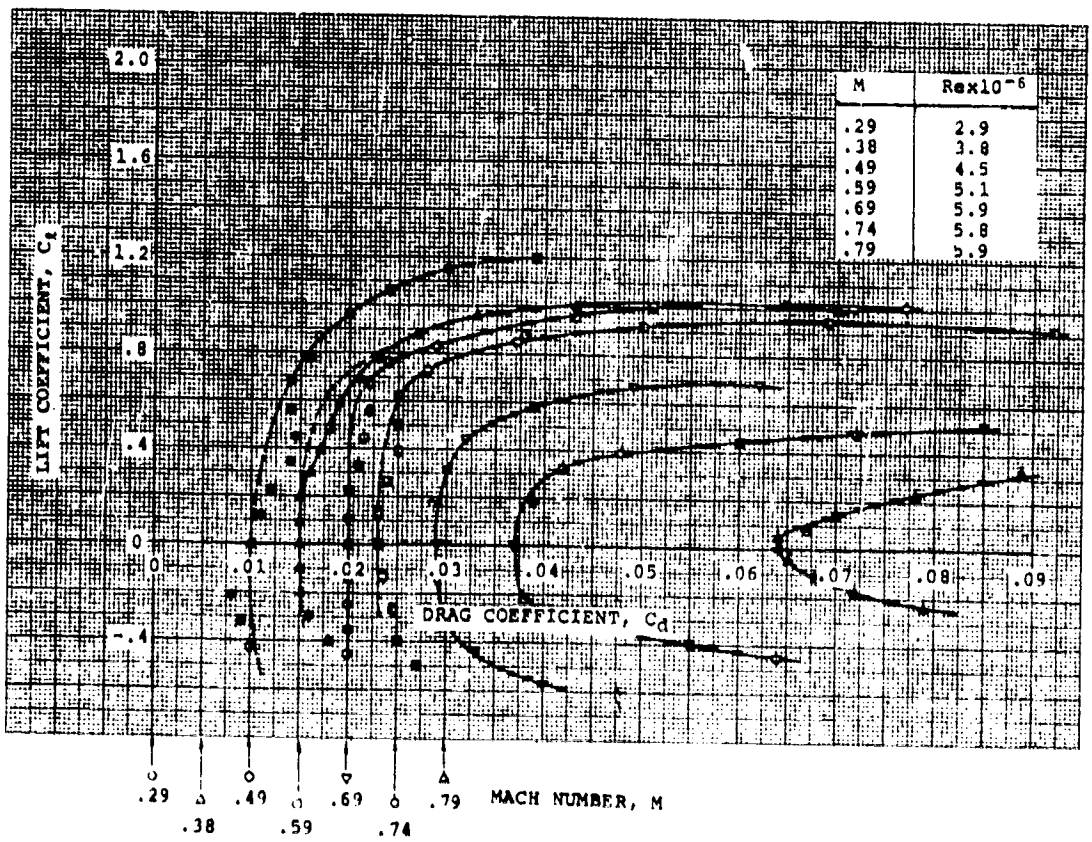
M | Rex10⁻⁶
.29 2.9
.38 3.8
.49 4.5
.59 5.1
.69 5.9
.74 5.8
.79 5.9
LIFT COEFFICIENT, $C_l$
2.0
1.6
1.2
.8
.4
0
-.4
0
.01
.02
.03
.04
.05
.06
.07
.08
.09
DRAG COEFFICIENT, $C_d$
.29
.38
.49
.59
.69
.74
.79
MACH NUMBER, M

NACA 63A015

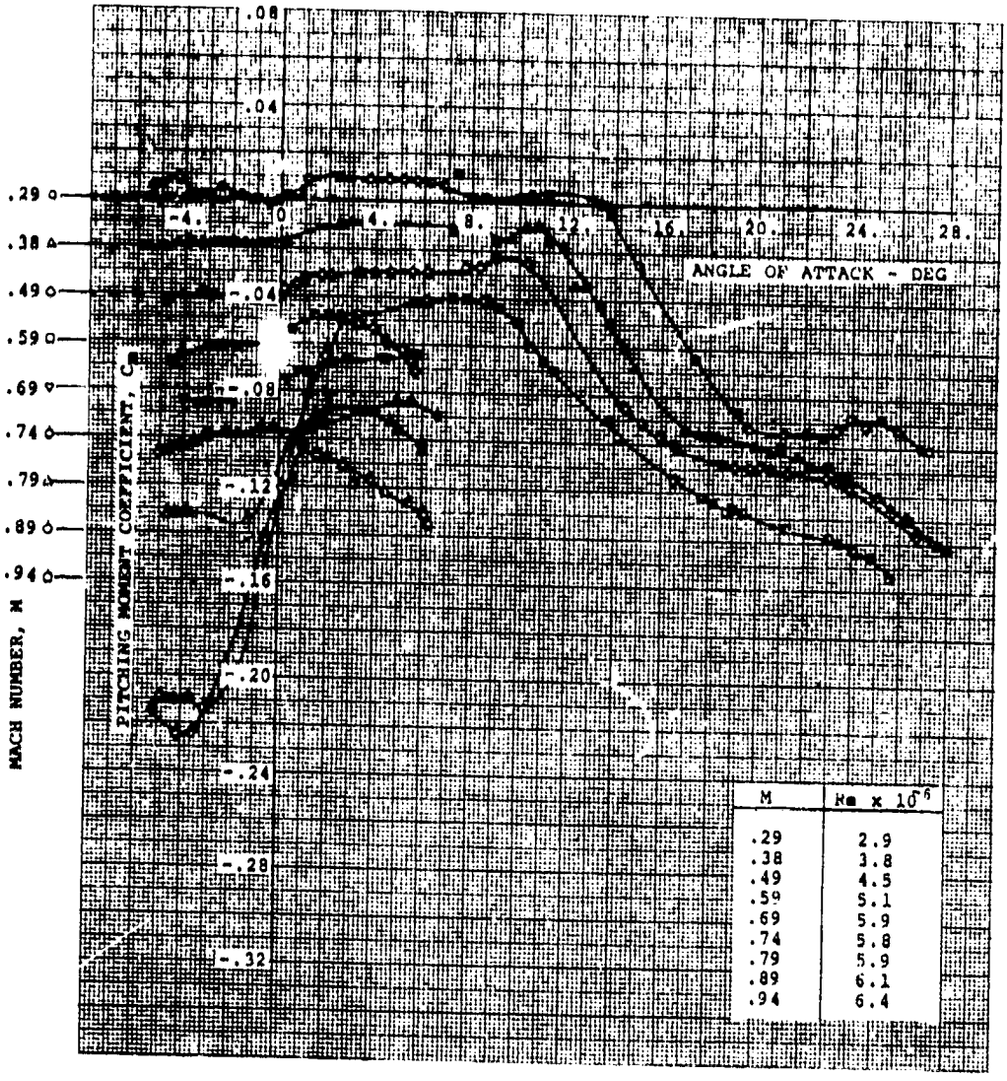
.08
.04
-.04
-.08
-.12
-.16
-.20
-.24
-.28
-.32
-4.
0
4.
8.
12.
16.
20.
24.
28.
ANGLE OF ATTACK - DEG
.29
.38
.49
.59
.69
.74
.79
.89
.94
MACH NUMBER, M
PITCHING MOMENT COEFFICIENT, Cm
M
Re x 10^6
.29 2.9
.38 3.8
.49 4.5
.59 5.1
.69 5.9
.74 5.8
.79 5.9
.89 6.1
.94 6.4

AIRFOIL: NACA 63A018



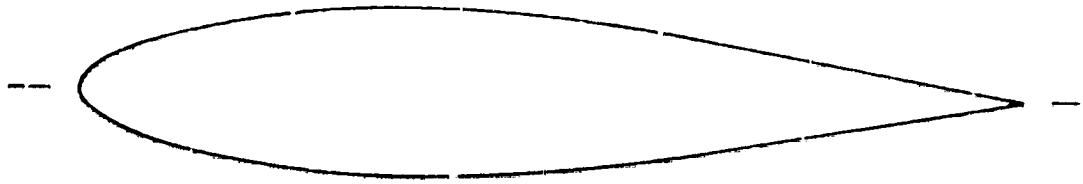

AIRFOIL COORDINATES

| x/c | y/c |
|---|---|
| 0.0 | 0.0 |
| 0.005 | 0.014225 |
| 0.0075 | 0.017112 |
| 0.0125 | 0.021737 |
| 0.025 | 0.030625 |
| 0.05 | 0.043412 |
| 0.075 | 0.0526 |
| 0.1 | 0.06 |
| 0.15 | 0.7139 |
| 0.2 | 0.079625 |
| 0.25 | 0.08522 |
| 0.3 | 0.08866 |
| 0.35 | 0.089975 |
| 0.4 | 0.08909 |
| 0.45 | 0.0863 |
| 0.5 | 0.081812 |
| 0.55 | 0.076262 |
| 0.6 | 0.06954 |
| 0.65 | 0.061375 |
| 0.7 | 0.05296 |
| 0.75 | 0.04422 |
| 0.8 | 0.03546 |
| 0.85 | 0.0267 |
| 0.9 | 0.017925 |
| 0.95 | 0.009175 |
| 1.0 | 0.0004 |

CHARACTERISTICS

- Thickness, t/c = 0.18
- Leading Edge Radius, r/c = 0.0228
- Trailing Edge Radius, r/c = 0.000475

TYPE OF DATA AND METHOD OF TEST

The tests were conducted in the Lockheed-California Company Fluid Dynamics Laboratory 4-by-4 foot supersonic wind tunnel, equipped with a two-dimensional subsonic test section. The tunnel is of the blow-down type. The floor and ceiling of the test section were perforated (porous).

Model forces were measured with two six-component strain gage balances. Drag was measured with a 40-tube pressure rake installed 14 inches downstream of the trailing edge of the model.

Model Chord = 8.0 in
Span = 48 in

SOURCE

Sipe, O.E., Jr., and Gorenberg, N.B., Effect of Mach Number, Reynolds Number, and Thickness Ratio on the Aerodynamic Characteristics of NACA 63A-Series Airfoil Sections, U.S. Army A.M.L. TR 65-28, June 1965.

1.7.150-2

NACA 63A018

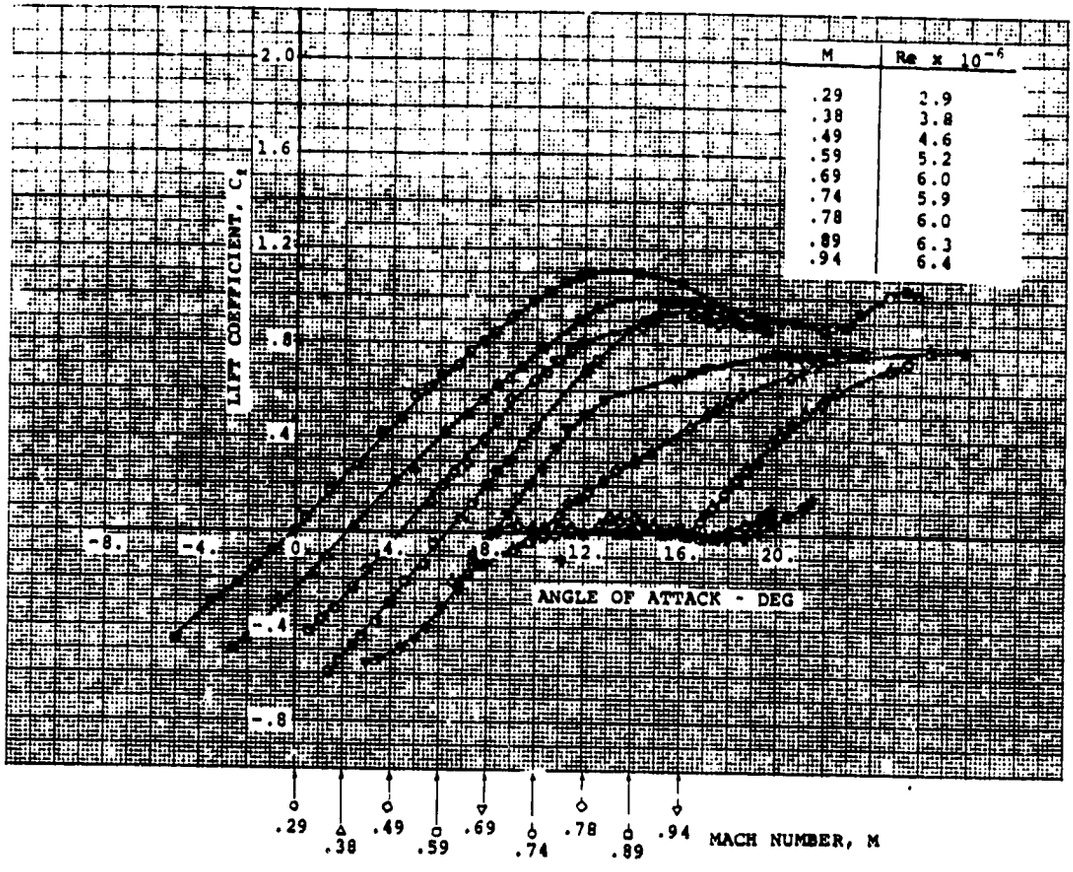


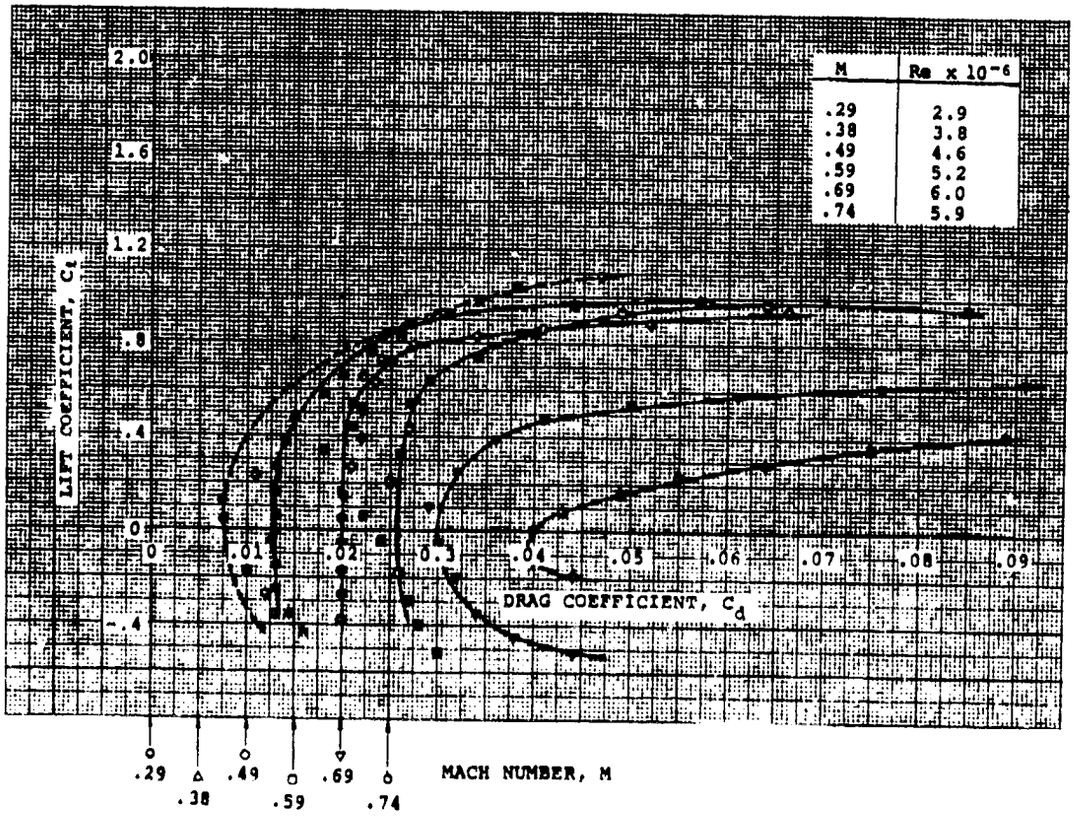

NACA 63A018

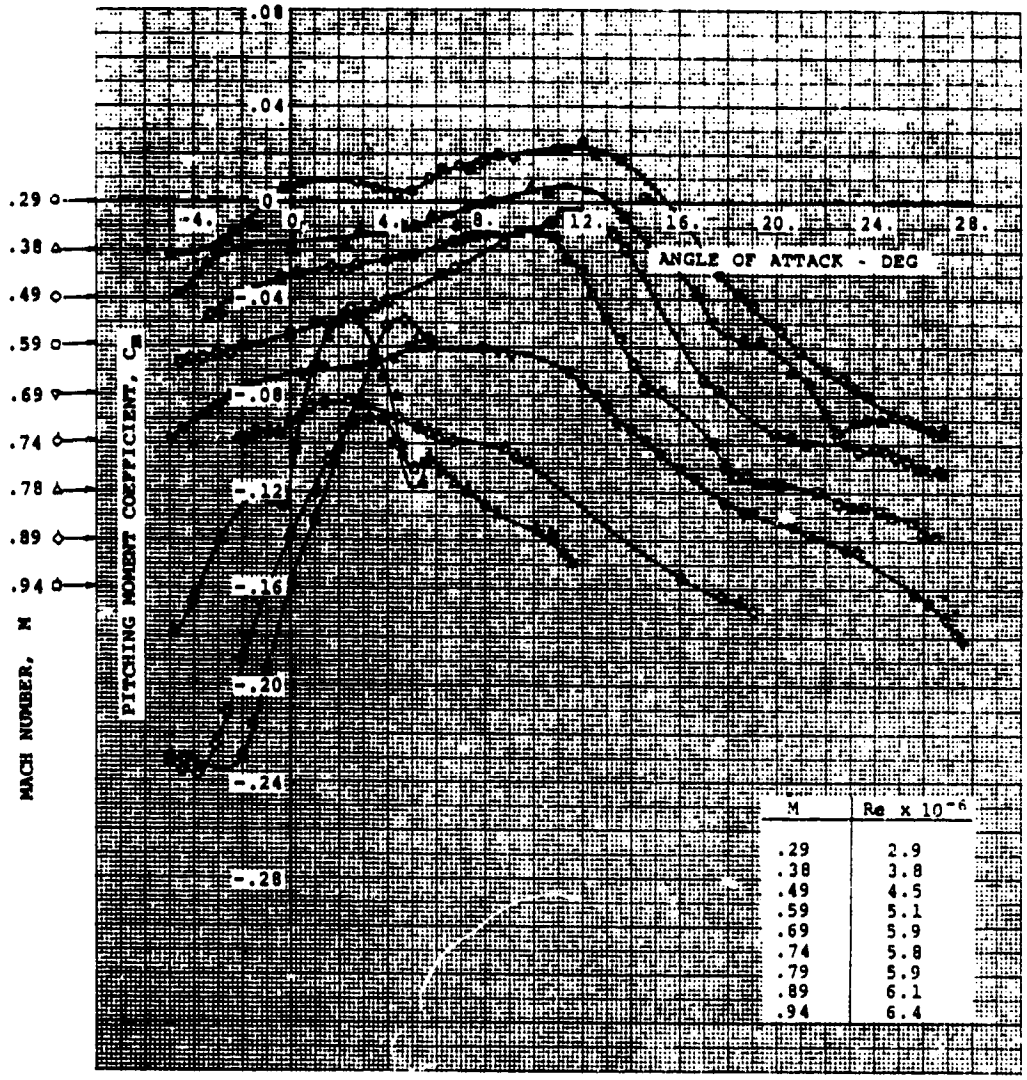
.08
.04
0
-.04
-.08
-.12
-.16
-.20
-.24
-.28
-4.
0
4.
8.
12.
16.
20.
24.
28.
ANGLE OF ATTACK - DEG
PITCHING MOMENT COEFFICIENT, $C_m$
MACH NUMBER, M
.29
.38
.49
.59
.69
.74
.78
.89
.94
M | Re x $10^{-6}$
.29 | 2.9
.38 | 3.8
.49 | 4.5
.59 | 5.1
.69 | 5.9
.74 | 5.8
.79 | 5.9
.89 | 6.1
.94 | 6.4

AIRFOIL: NACA 64A(4.5)08



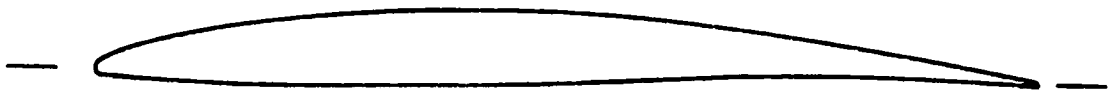

AIRFOIL COORDINATES

| $x/c_u$ | $y/c_u$ | $x/c_l$ | $y/c_l$ |
|---|---|---|---|
| 0.0 | 0.0 | 0.0 | 0.0 |
| 0.00362 | 0.00770 | 0.00638 | -0.00517 |
| 0.00596 | 0.00957 | 0.00904 | -0.00601 |
| 0.01074 | 0.01261 | 0.01426 | -0.00718 |
| 0.02297 | 0.01825 | 0.02703 | -0.00875 |
| 0.04773 | 0.02673 | 0.05227 | -0.01050 |
| 0.07264 | 0.03341 | 0.07736 | -0.01152 |
| 0.09762 | 0.03904 | 0.10238 | -0.01222 |
| 0.14772 | 0.04817 | 0.15228 | -0.01304 |
| 0.19792 | 0.05524 | 0.20208 | -0.01338 |
| 0.24819 | 0.06065 | 0.25181 | -0.01334 |
| 0.29850 | 0.06465 | 0.30150 | -0.01297 |
| 0.34884 | 0.06731 | 0.35116 | -0.01223 |
| 0.39919 | 0.06868 | 0.40081 | -0.01114 |
| 0.44955 | 0.06840 | 0.45045 | -0.00926 |
| 0.49950 | 0.06677 | 0.50010 | -0.00691 |
| 0.55022 | 0.06395 | 0.54978 | -0.00427 |
| 0.60049 | 0.06009 | 0.59951 | -0.00152 |
| 0.65072 | 0.05536 | 0.64928 | 0.00110 |
| 0.70091 | 0.05006 | 0.69909 | 0.00316 |
| 0.75107 | 0.04408 | 0.74893 | 0.00453 |
| 0.80130 | 0.03711 | 0.79870 | 0.00495 |
| 0.85131 | 0.02862 | 0.84869 | 0.00384 |
| 0.90096 | 0.01977 | 0.89904 | 0.00230 |
| 0.95056 | 0.01061 | 0.94944 | 0.00043 |
| 1.0 | 0.0 | 1.0 | 0.0 |

CHARACTERISTICS

- Thickness ratio, t/c = 0.080
- Leading edge radius, r/c = 0.00456
  Center of L.E. circle x/c = 0.00446, y/c = 0.00095
- Trailing edge radius, r/c = 0.001568

TYPE OF DATA AND METHOD OF TEST

Two-dimensional test in the subsonic insert of the Boeing Supersonic Wind Tunnel in Seattle, Wash.

Lift and pitching moments were measured on a balance.

Drag was determined with a wake rake survey.

End plate tares have been applied to the pitching moment measurements.

Model Chord = 6.38 in
Span = 12.0 in

SOURCE

Dadone, L., Experimental Investigation of the Properties of a Family of NACA 64AXXX Airfoils, Boeing Document D170-10021-1, October 1969.

NACA 64A(4.5)08

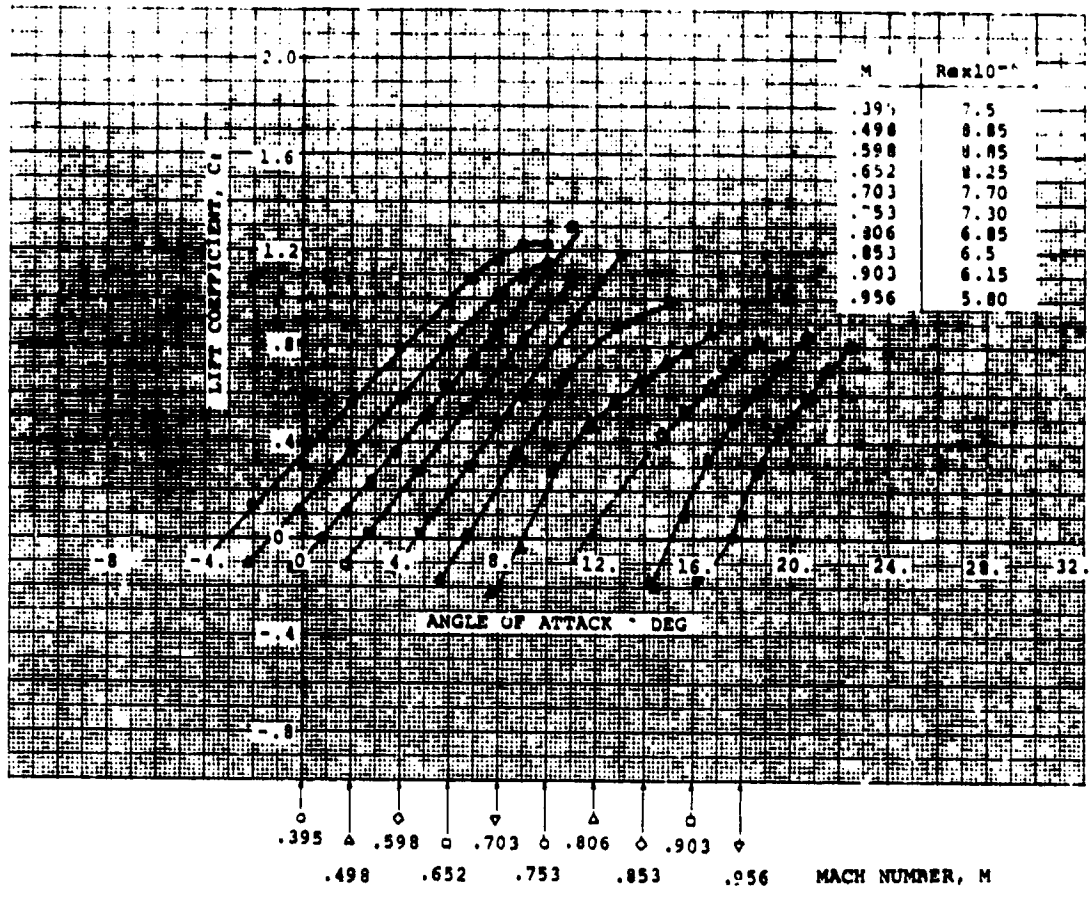


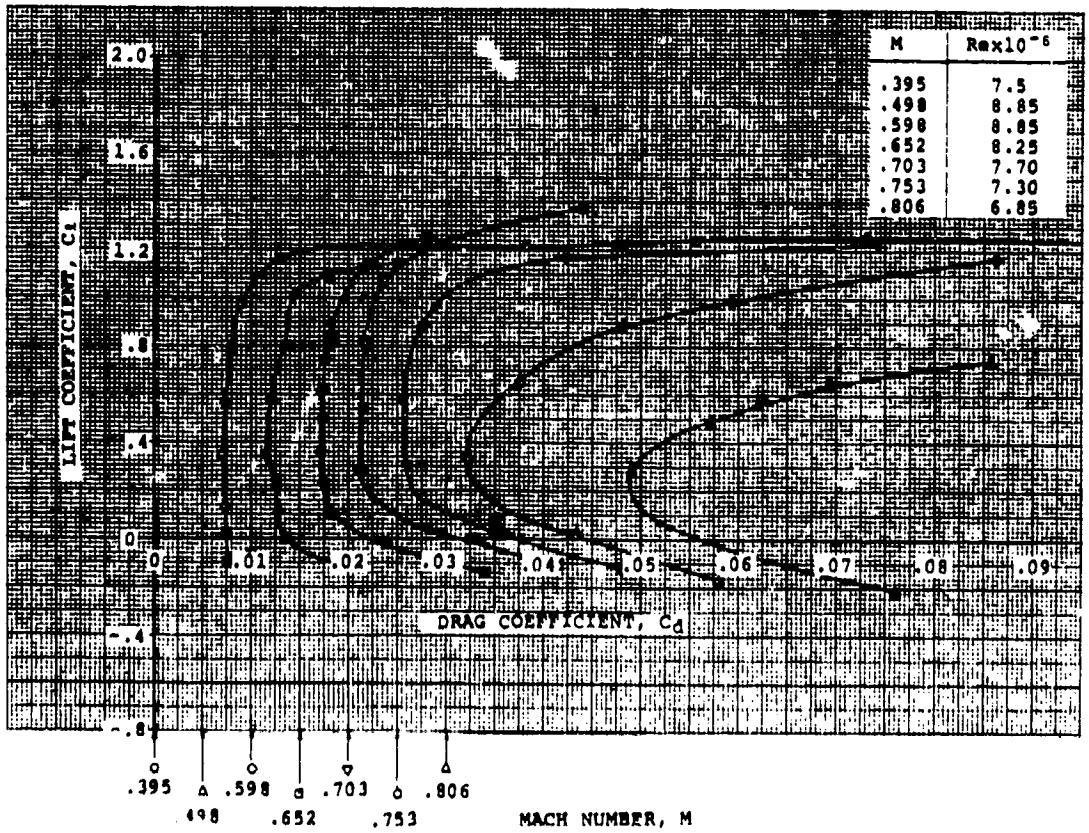

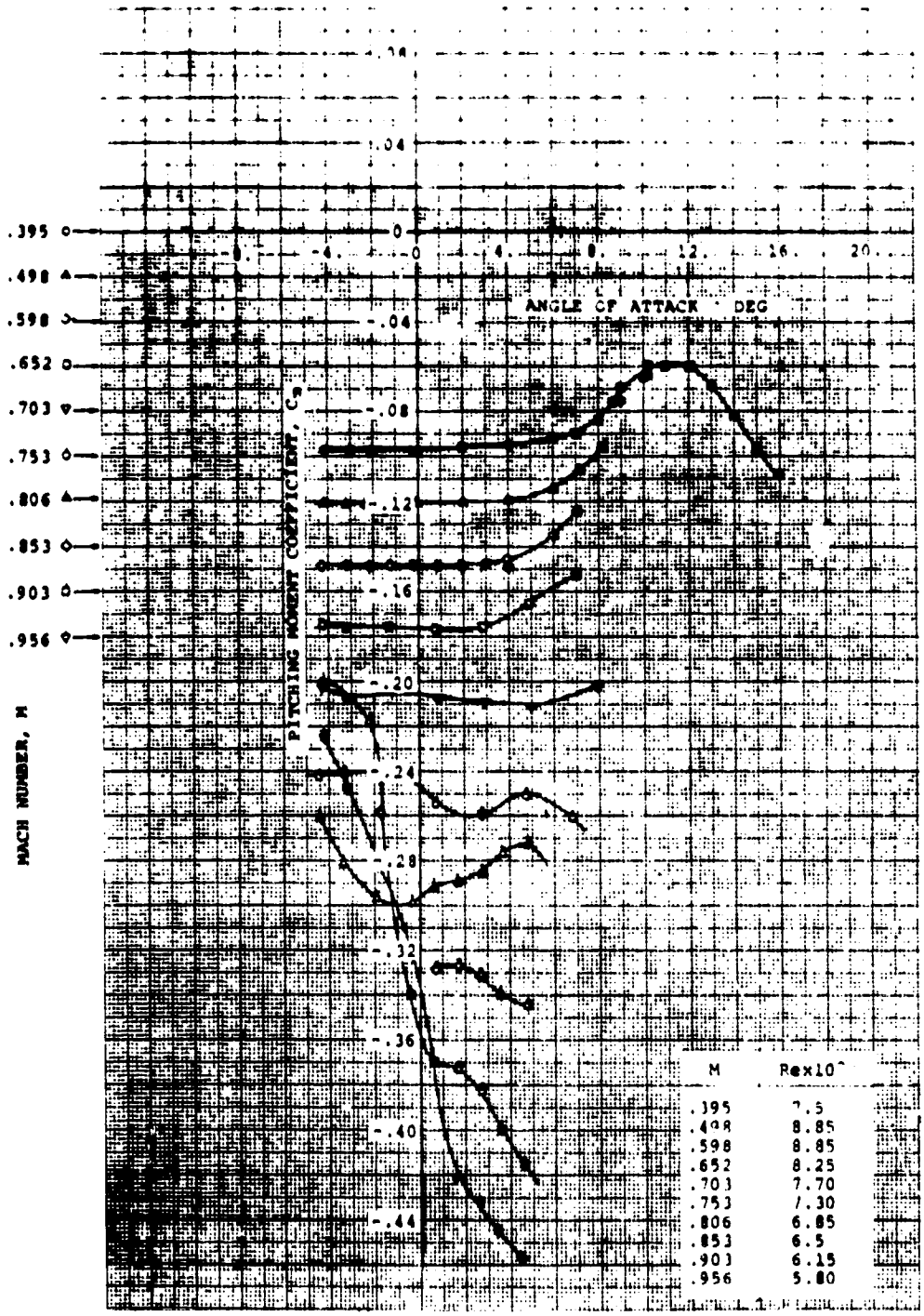
.04
0
-.04
-.08
-.12
-.16
-.20
-.24
-.28
-.32
-.36
-.40
-.44
-4.
0
4.
8.
12.
16.
20.
ANGLE OF ATTACK, DEG
PITCHING MOMENT COEFFICIENT, $C_m$
MACH NUMBER, M
.395
.498
.598
.652
.703
.753
.806
.853
.903
.956
M
Rex10^
.395
7.5
.498
8.85
.598
8.85
.652
8.25
.703
7.70
.753
7.30
.806
6.85
.853
6.5
.903
6.15
.956
5.80

AIRFOIL: NACA 64A608



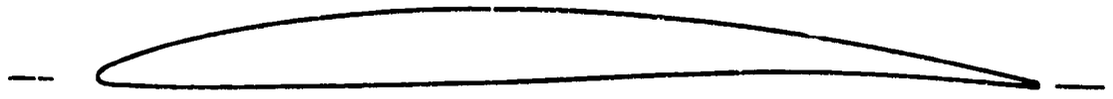

AIRFOIL COORDINATES

| $x/c_u$ | $y/c_u$ | $x/c_l$ | $y/c_l$ |
|---|---|---|---|
| 0.0 | 0.0 | 0.0 | 0.0 |
| 0.00320 | 0.00801 | 0.00680 | -0.00464 |
| 0.00547 | 0.01005 | 0.00953 | -0.00530 |
| 0.01018 | 0.01340 | 0.01482 | -0.00616 |
| 0.02232 | 0.01971 | 0.02768 | -0.00705 |
| 0.04699 | 0.02932 | 0.05301 | -0.00769 |
| 0.07186 | 0.03696 | 0.07814 | -0.00778 |
| 0.09684 | 0.04343 | 0.10316 | -0.00766 |
| 0.14697 | 0.05396 | 0.15303 | -0.00712 |
| 0.19723 | 0.062[illegible] | 0.20277 | -0.00635 |
| 0.24759 | 0.0685[illegible] | 0.25241 | -0.00542 |
| 0.29800 | 0.07324 | 0.30200 | -0.00434 |
| 0.34845 | 0.07648 | 0.35133 | -0.00304 |
| 0.39892 | 0.07827 | 0.40108 | -0.00154 |
| 0.44940 | 0.07825 | 0.45060 | 0.00060 |
| 0.49987 | 0.07675 | 0.50013 | 0.00307 |
| 0.55029 | 0.07389 | 0.54971 | 0.00568 |
| 0.60065 | 0.06985 | 0.59935 | 0.00824 |
| 0.65096 | 0.06477 | 0.64904 | 0.01052 |
| 0.70121 | 0.05892 | 0.69879 | 0.01204 |
| 0.75143 | 0.05215 | 0.74857 | 0.01266 |
| 0.80174 | 0.04407 | 0.79826 | 0.01200 |
| 0.85173 | 0.03398 | 0.84827 | 0.00930 |
| 0.90128 | 0.02341 | 0.89872 | 0.00602 |
| 0.95975 | 0.01242 | 0.94925 | 0.00229 |
| 1.0 | 0.0 | 1.0 | 0.0 |

## CHARACTERISTICS

- Thickness ratio, t/c = 0.080
- Leading edge radius, r/c = 0.00456
  Center of L.E. circle
  x/c = 0.00438, y/c = 0.00125
- Trailing edge radius, r/c = 0.001568

## TYPE OF DATA AND METHOD OF TEST

Two-dimensional test in the subsonic insert of the Boeing Supersonic Wind Tunnel in Seattle, Wash.

Lift and pitching moments were measured on a balance.

Drag was determined with a wake rake survey.

End plate tares have been applied to pitching moment measurements.

Model Chord = 6.38 in
Span = 12.0 in

## SOURCE

Dadone L., Experimental Investigation of the Properties of a Family of NACA 64AXXX Airfoils, Boeing Document D170-10021-1, October 1969.

NACA RM A6A08

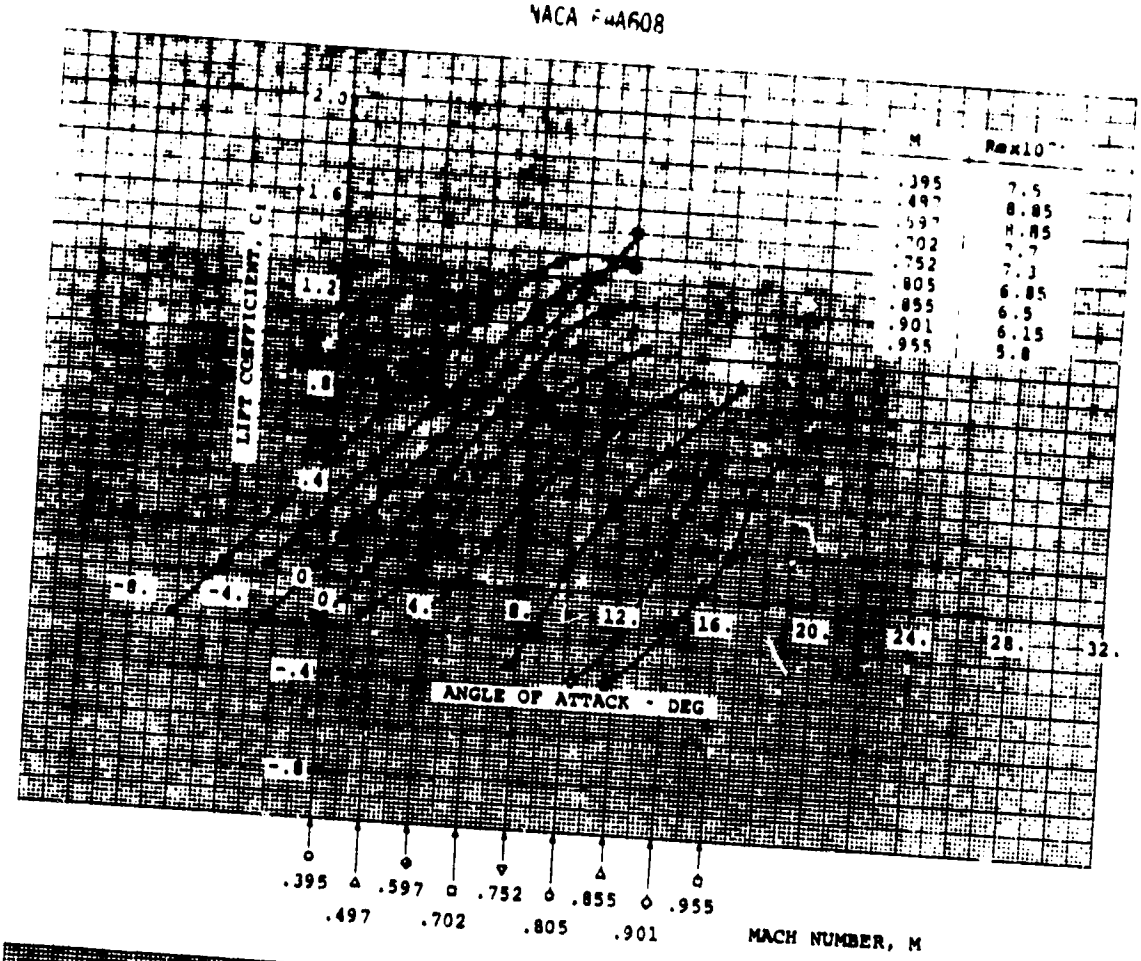


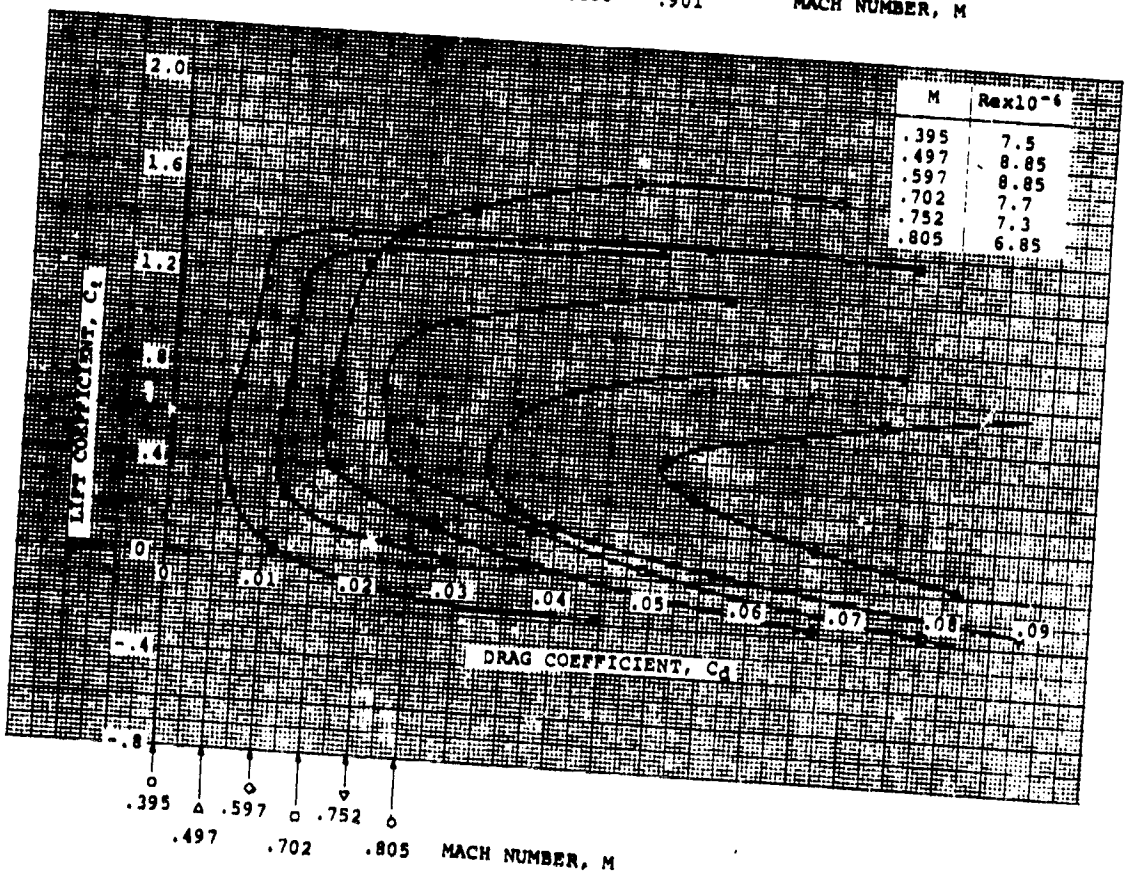

NACA 64A608

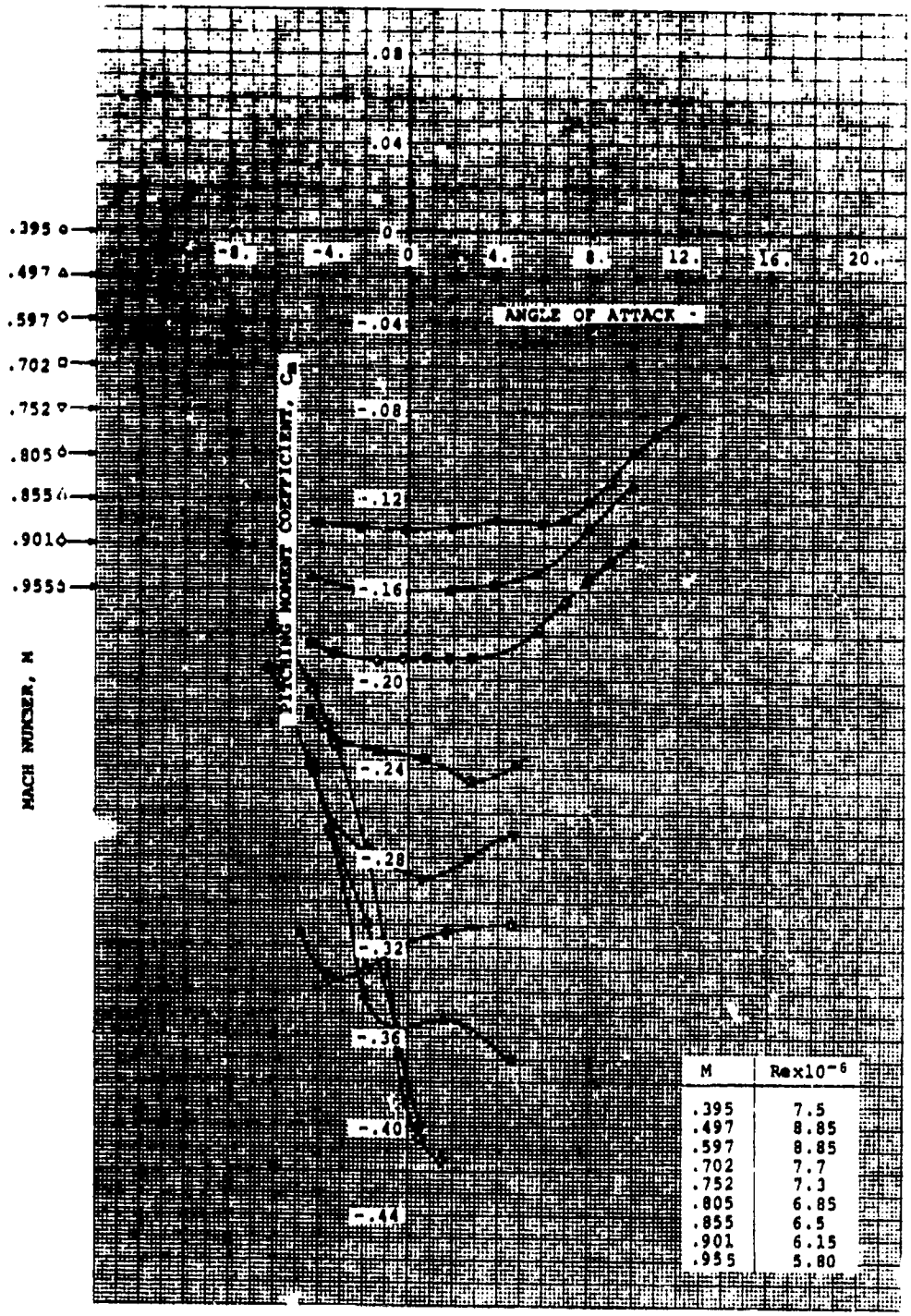
.08
.04
0
-.04
-.08
-.12
-.16
-.20
-.24
-.28
-.32
-.36
-.40
-.44
-8.
-4.
0
4.
8.
12.
16.
20.
ANGLE OF ATTACK - α
PITCHING MOMENT COEFFICIENT, Cm
MACH NUMBER, M
.395
.497
.597
.702
.752
.805
.855
.901
.955
M | Rex10⁻⁶
.395 | 7.5
.497 | 8.85
.597 | 8.85
.702 | 7.7
.752 | 7.3
.805 | 6.85
.855 | 6.5
.901 | 6.15
.955 | 5.80

AIRFOIL: NACA 64A312

1.3.180

AIRFOIL COORDINATES

| $x/c_u$ | $y/c_u$ | $x/c_l$ | $y/c_l$ |
|---|---|---|---|
| 0.0 | 0.0 | 0.0 | 0.0 |
| 0.00362 | 0.01053 | 0.00638 | -0.00884 |
| 0.00596 | 0.01288 | 0.00904 | -0.01050 |
| 0.01075 | 0.01661 | 0.01425 | -0.01299 |
| 0.02297 | 0.02341 | 0.02703 | -0.01708 |
| 0.04772 | 0.03342 | 0.05228 | -0.02260 |
| 0.07263 | 0.04115 | 0.07737 | -0.02656 |
| 0.09761 | 0.04758 | 0.10239 | -0.02969 |
| 0.14771 | 0.05785 | 0.15229 | -0.03443 |
| 0.19791 | 0.06564 | 0.20209 | -0.03773 |
| 0.24818 | 0.07150 | 0.25182 | -0.03996 |
| 0.29849 | 0.07565 | 0.30151 | -0.04119 |
| 0.34883 | 0.07813 | 0.35117 | -0.04141 |
| 0.39919 | 0.07899 | 0.40081 | -0.04062 |
| 0.44955 | 0.07769 | 0.45045 | -0.03827 |
| 0.49990 | 0.07475 | 0.50010 | -0.03485 |
| 0.55021 | 0.07045 | 0.54979 | -0.03067 |
| 0.60048 | 0.06500 | 0.59952 | -0.02595 |
| 0.65071 | 0.05879 | 0.64929 | -0.02114 |
| 0.70089 | 0.05219 | 0.69911 | -0.01671 |
| 0.75105 | 0.04513 | 0.74895 | -0.01273 |
| 0.80127 | 0.03742 | 0.79873 | -0.00939 |
| 0.85126 | 0.02871 | 0.84874 | -0.00706 |
| 0.90091 | 0.01974 | 0.89909 | -0.00503 |
| 0.95051 | 0.01057 | 0.94949 | -0.00321 |
| 1.0 | 0.0 | 1.0 | 0.0 |

CHARACTERISTICS

- Thickness ratio, t/c = 0.120
- Leading edge radius, r/c = 0.01044
  Center of L.E. circle
  x/c = 0.01034, y/c = 0.00147
- Trailing edge radius, r/c = 0.001568

TYPE OF DATA AND METHOD OF TEST

Two-dimensional test in the subsonic insert of the Boeing Supersonic Wind Tunnel in Seattle, Wash.

Lift and pitching moments were measured on a balance.

Drag was determined with a wake rake survey.

End plate tares have been applied to the pitching moment measurements.

Model Chord = 6.38 in
Span = 12.0 in

SOURCE

Dadone, L., Experimental Investigation of the Properties of a Family of NACA 64AXXX Airfoils, Boeing Document D170-10021-1, October 1969.

NACA RM A52I2

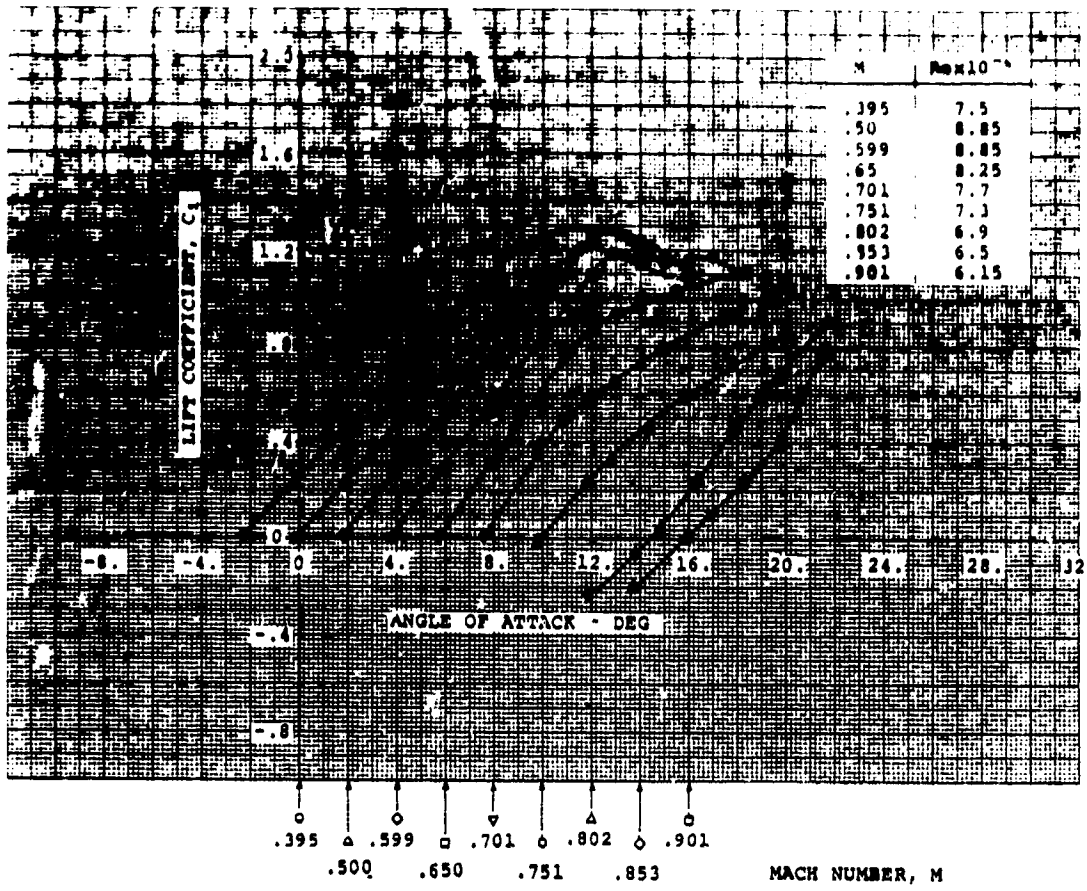


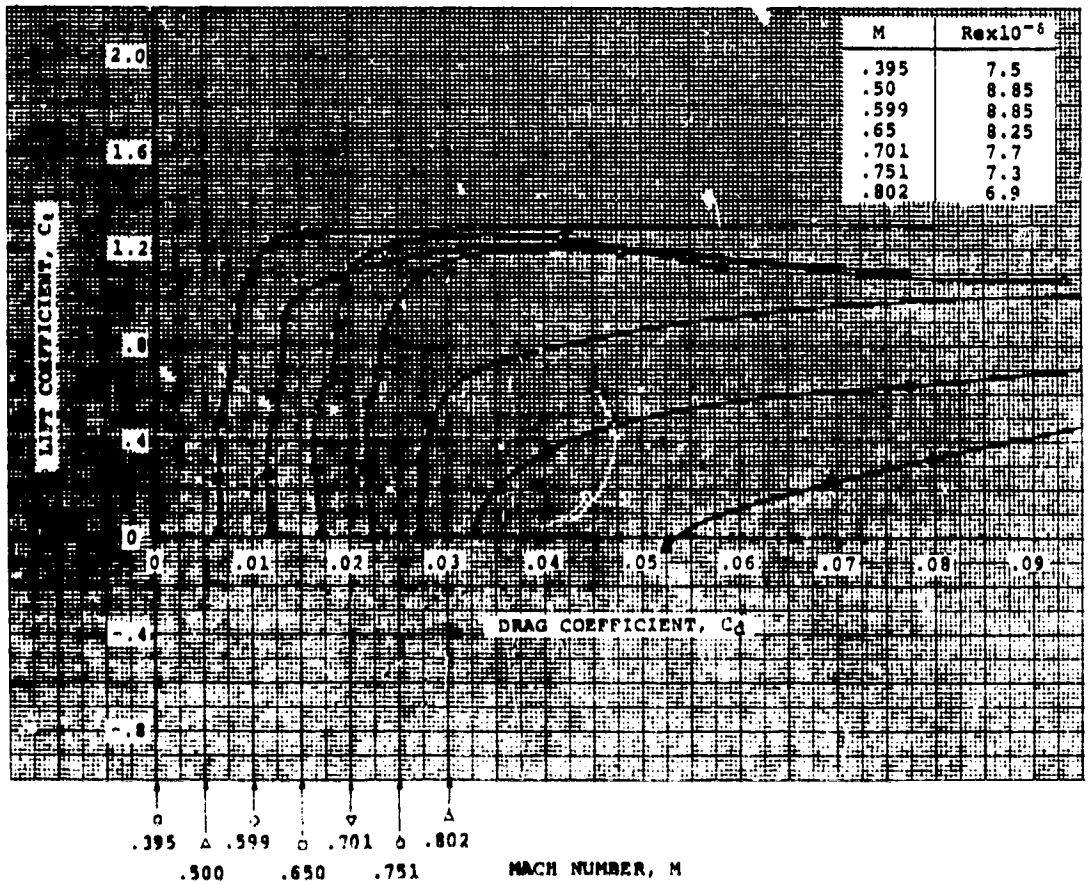

NACA 64A312

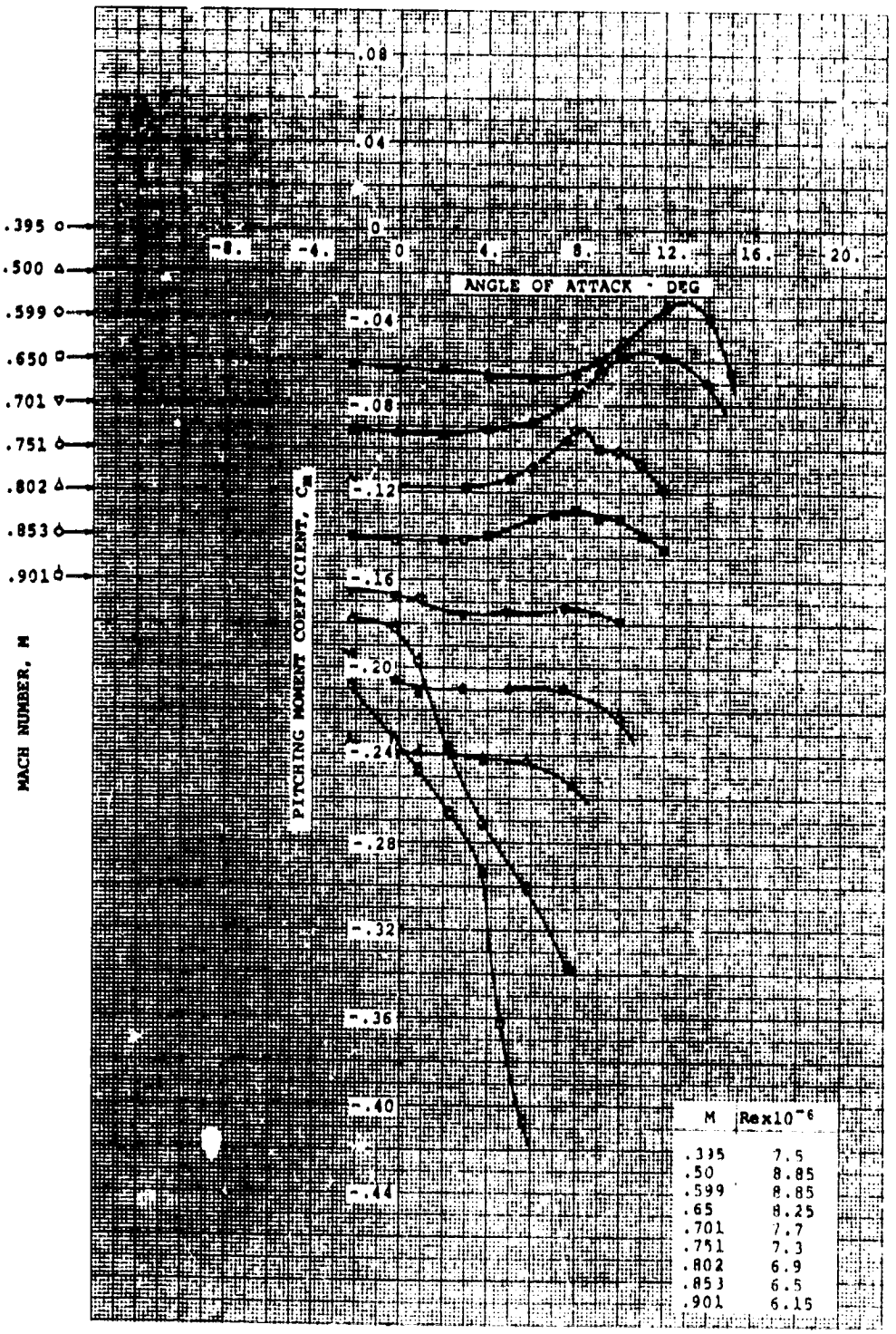
.08
.04
0
-.04
-.08
-.12
-.16
-.20
-.24
-.28
-.32
-.36
-.40
-.44
-8.
-4.
0
4.
8.
12.
16.
20.
ANGLE OF ATTACK - DEG
PITCHING MOMENT COEFFICIENT, $C_m$
MACH NUMBER, M
.395
.500
.599
.650
.701
.751
.802
.853
.901
M | Rex10⁻⁶
.395 | 7.5
.50 | 8.85
.599 | 8.85
.65 | 8.25
.701 | 7.7
.751 | 7.3
.802 | 6.9
.853 | 6.5
.901 | 6.15

AIRFOIL: NACA 64A(4.5)12

1.3.190

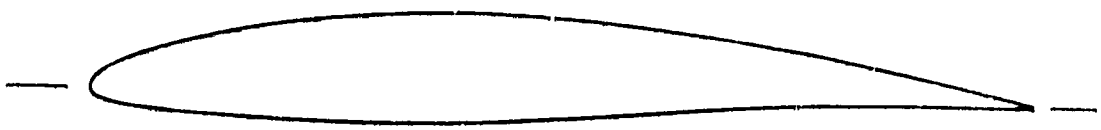

AIRFOIL COORDINATES

| $x/c_u$ | $y/c_u$ | $x/c_l$ | $y/c_l$ |
|---|---|---|---|
| 0.0 | 0.0 | 0.0 | 0.0 |
| 0.00295 | 0.01083 | 0.00705 | -0.00830 |
| 0.00521 | 0.01335 | 0.00979 | -0.00978 |
| 0.00989 | 0.01738 | 0.01511 | -0.01196 |
| 0.02198 | 0.02487 | 0.02802 | -0.01538 |
| 0.04659 | 0.03601 | 0.05341 | -0.01978 |
| 0.07145 | 0.04470 | 0.07855 | -0.02281 |
| 0.09642 | 0.05196 | 0.10358 | -0.02513 |
| 0.14657 | 0.06364 | 0.15343 | -0.02851 |
| 0.19687 | 0.07256 | 0.20313 | -0.03071 |
| 0.24727 | 0.07935 | 0.25272 | -0.03204 |
| 0.29774 | 0.08424 | 0.30226 | -0.03256 |
| 0.34825 | 0.08729 | 0.35175 | -0.03221 |
| 0.39879 | 0.08857 | 0.40121 | -0.03102 |
| 0.44933 | 0.08755 | 0.45067 | -0.02841 |
| 0.49985 | 0.08473 | 0.50015 | -0.02487 |
| 0.55032 | 0.08040 | 0.54968 | -0.02072 |
| 0.60072 | 0.07476 | 0.59928 | -0.01619 |
| 0.65106 | 0.06819 | 0.64894 | -0.01172 |
| 0.70133 | 0.06104 | 0.69867 | -0.00783 |
| 0.75157 | 0.05321 | 0.74843 | -0.00460 |
| 0.80190 | 0.04439 | 0.79810 | -0.00233 |
| 0.85188 | 0.03406 | 0.84812 | -0.00160 |
| 0.90136 | 0.02238 | 0.89864 | -0.00131 |
| 0.95076 | 0.01239 | 0.94924 | -0.00135 |
| 1.0 | 0.0 | 1.0 | 0.0 |

CHARACTERISTICS

- Thickness ratio, t/c = 0.120
- Leading edge radius,
  r/c = 0.01044
  Center of L.E. circle
  x/c = 0.01021, y/c = 0.00218
- Trailing edge radius,
  r/c = 0.001568

TYPE OF DATA AND METHOD OF TEST

Two-dimensional test in the subsonic insert of the Boeing Supersonic Wind Tunnel in Seattle, Wash.

Lift and pitching moments were measured on a balance.

Drag was determined with a wake rake survey.

End plate tares have been applied to the pitching moment measurements.

Model Chord = 6.38 in
Span = 12.0 in

SOURCE

Dadone, L., Experimental Investigation of the Properties of a Family of NACA 64AXXX Airfoils, Boeing Document D170-10021-1, October 1969.

NACA 64A(4.5)12

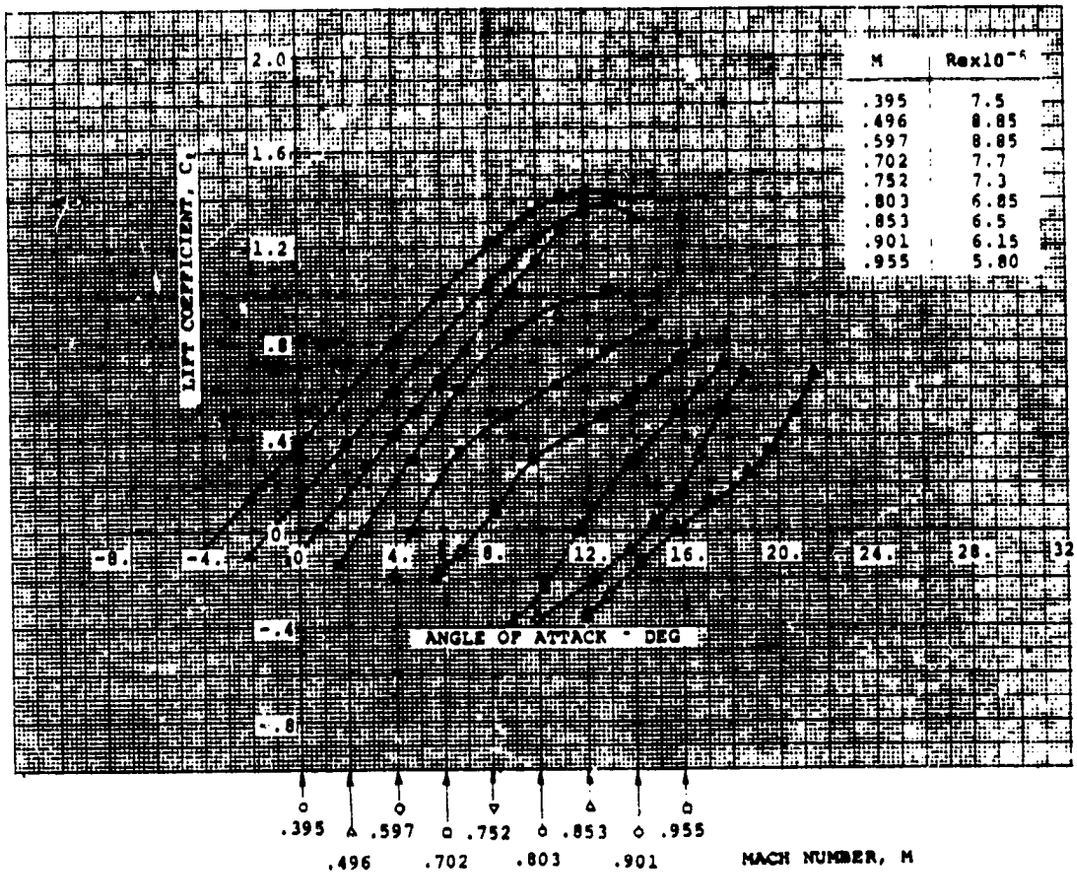


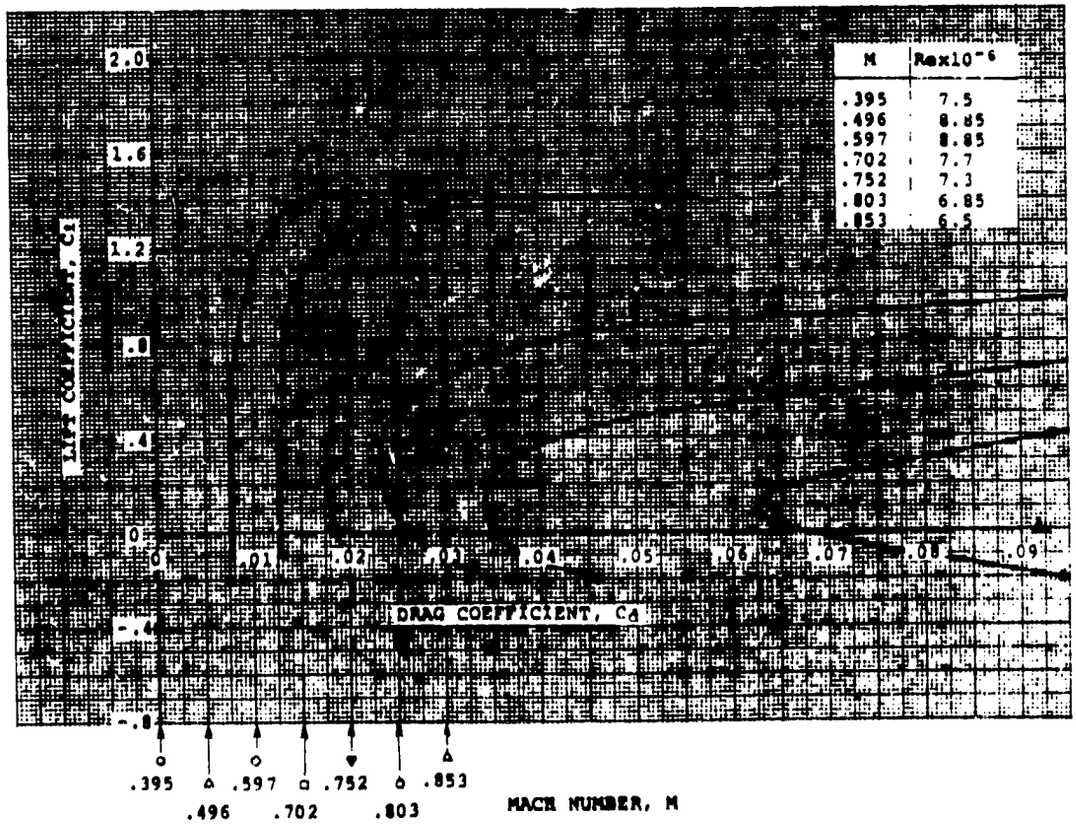

NACA 64A(4,5)12

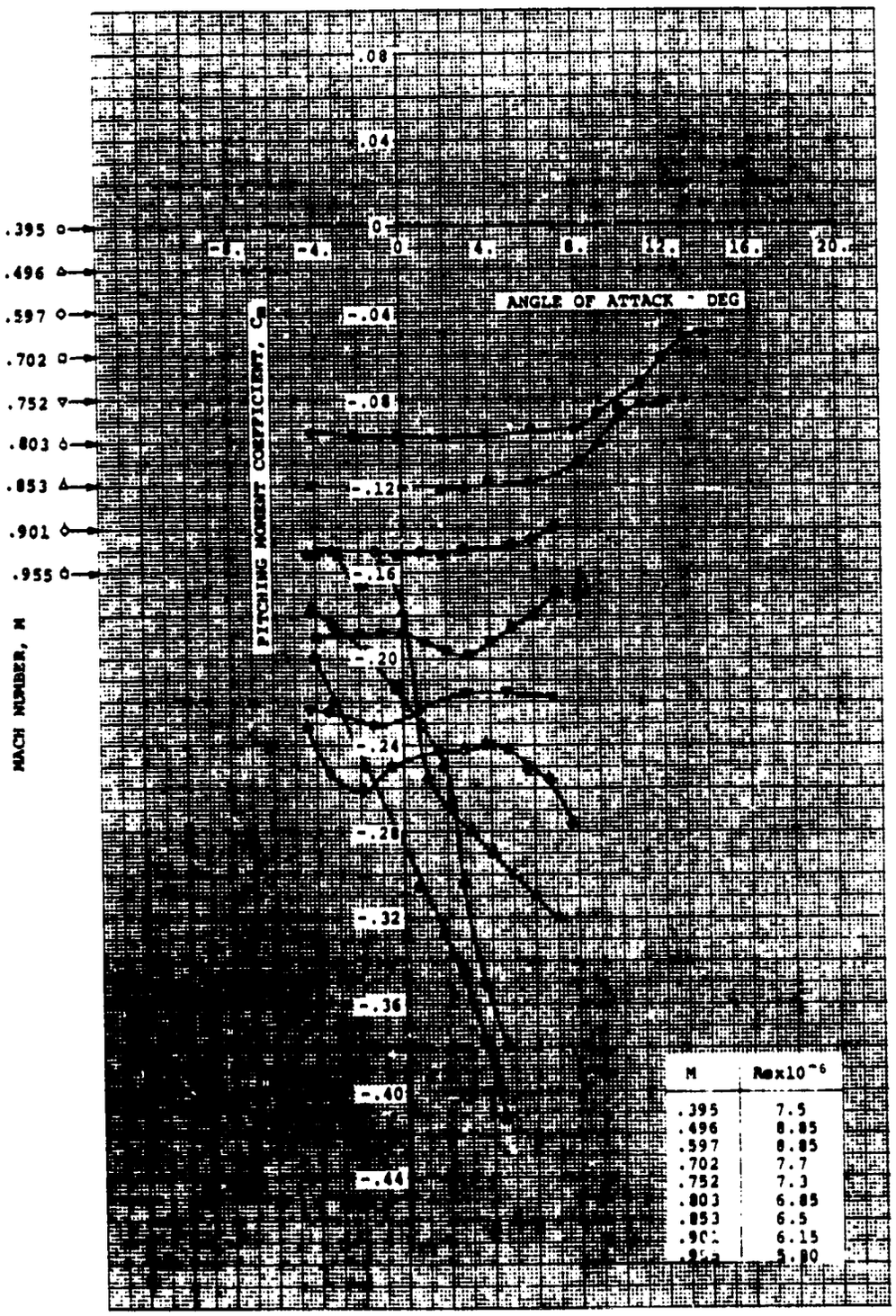

AIRFOIL: NACA 64A612

1.3.200

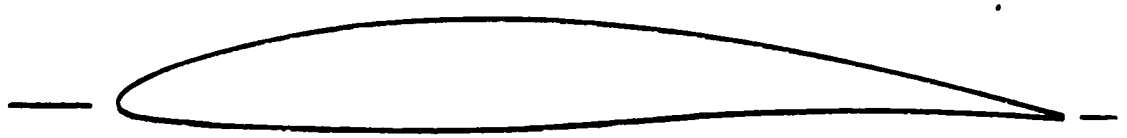

AIRFOIL COORDINATES

| $x/c_u$ | $y/c_u$ | $x/c_l$ | $y/c_l$ |
|---|---|---|---|
| 0.0 | 0.0 | 0.0 | 0.0 |
| 0.00232 | 0.01109 | 0.00768 | -0.00772 |
| 0.00449 | 0.01378 | 0.01051 | -0.00902 |
| 0.00906 | 0.01812 | 0.01594 | -0.01088 |
| 0.02100 | 0.02628 | 0.02900 | -0.01362 |
| 0.04548 | 0.03855 | 0.05452 | -0.01692 |
| 0.07029 | 0.04820 | 0.07971 | -0.01902 |
| 0.09525 | 0.05630 | 0.10475 | -0.02053 |
| 0.14544 | 0.06939 | 0.15456 | -0.02256 |
| 0.19584 | 0.07947 | 0.20416 | -0.02366 |
| 0.24637 | 0.08718 | 0.25363 | -0.02510 |
| 0.29699 | 0.09281 | 0.30301 | -0.02391 |
| 0.34767 | 0.09645 | 0.35233 | -0.02301 |
| 0.39838 | 0.09815 | 0.40162 | -0.02142 |
| 0.44911 | 0.09740 | 0.45089 | -0.01855 |
| 0.49980 | 0.09471 | 0.50020 | -0.01489 |
| 0.55043 | 0.09034 | 0.54957 | -0.01077 |
| 0.60096 | 0.08452 | 0.59904 | -0.00642 |
| 0.65141 | 0.07759 | 0.64859 | -0.00230 |
| 0.70178 | 0.06989 | 0.69822 | 0.00106 |
| 0.75209 | 0.06128 | 0.74791 | 0.00353 |
| 0.80252 | 0.05134 | 0.79748 | 0.00473 |
| 0.85250 | 0.03940 | 0.84750 | 0.00389 |
| 0.90181 | 0.02700 | 0.89819 | 0.00242 |
| 0.95101 | 0.01419 | 0.94899 | 0.00052 |
| 1.0 | 0.0 | 1.0 | 0.0 |

CHARACTERISTICS

- Thickness ratio, t/c = 0.120
- Leading edge radius,
  r/c = 0.01044
  Center of L.E. circle
  x/c = 0.01004, y/c = 0.00286
- Trailing edge radius,
  r/c = 0.001568

TYPE OF DATA AND METHOD OF TEST

Two-dimensional test in the subsonic insert of the Boeing Supersonic Wind Tunnel in Seattle, Wash.

Lift and pitching moments were measured on a balance.

Drag was determined with a wake rake survey.

End plate tares have been applied to the pitching moment measurements.

Model Chord = 6.38 in
Span = 12.0 in

SOURCE

Dadone, L., Experimental Investigation of the Properties of a Family of NACA 64AXXX Airfoils, Boeing Document D170-10021-1, October 1969.

NACA 64A612

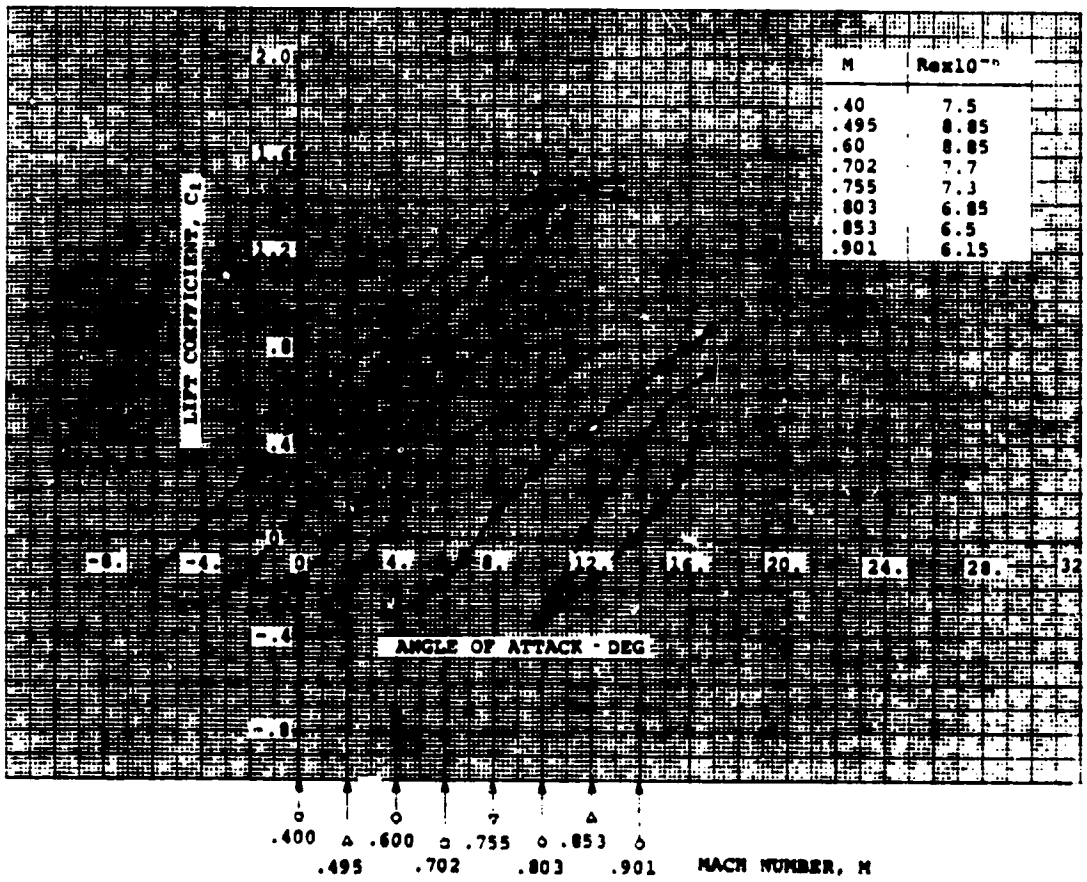
M
Rex10⁻⁶
.40 7.5
.495 8.85
.60 8.85
.702 7.7
.755 7.3
.803 6.85
.853 6.5
.901 6.15
LIFT COEFFICIENT, Cl
2.0
1.6
1.2
.8
.4
0
-.4
-.8
-8.
-4.
0
4.
8.
12.
16.
20.
24.
28.
32.
ANGLE OF ATTACK - DEG
.400
.495
.600
.702
.755
.803
.853
.901
MACH NUMBER, M

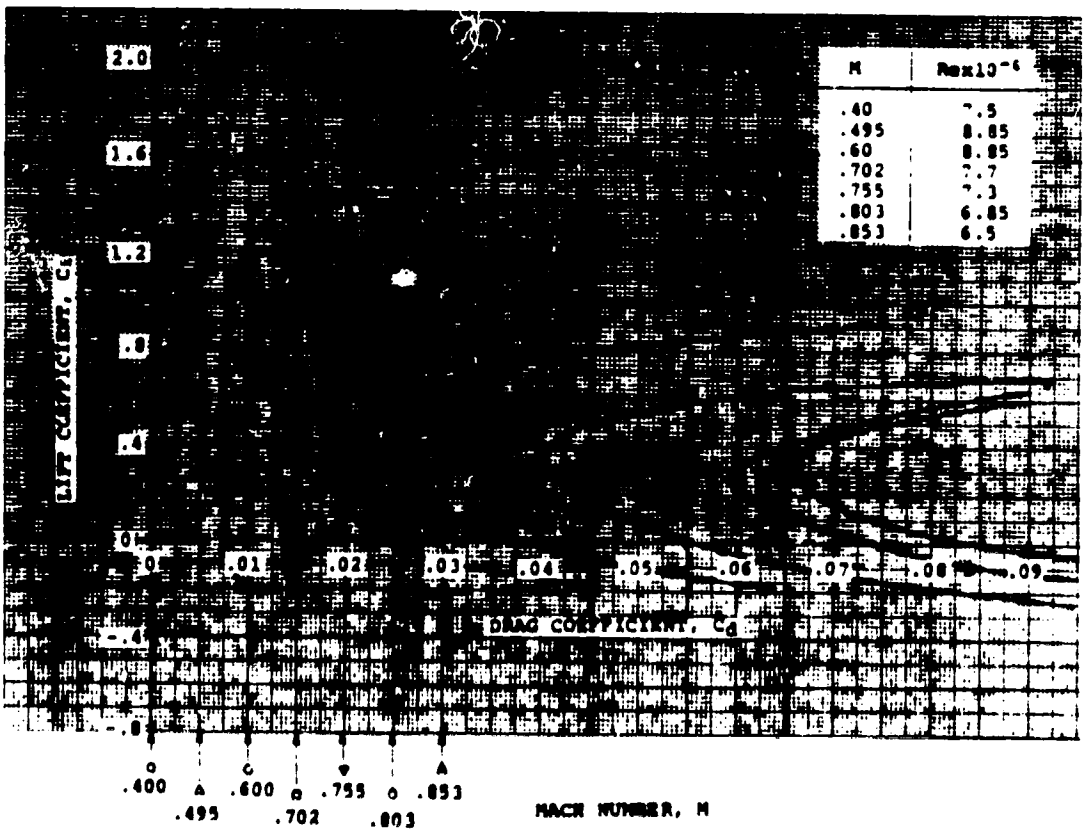
M
Rex10⁻⁶
.40 7.5
.495 8.85
.60 8.85
.702 7.7
.755 7.3
.803 6.85
.853 6.5
LIFT COEFFICIENT, Cl
2.0
1.6
1.2
.8
.4
0
-.4
-.8
0
.01
.02
.03
.04
.05
.06
.07
.08
.09
DRAG COEFFICIENT, Cd
.400
.495
.600
.702
.755
.803
.853
MACH NUMBER, M

NACA 64A612

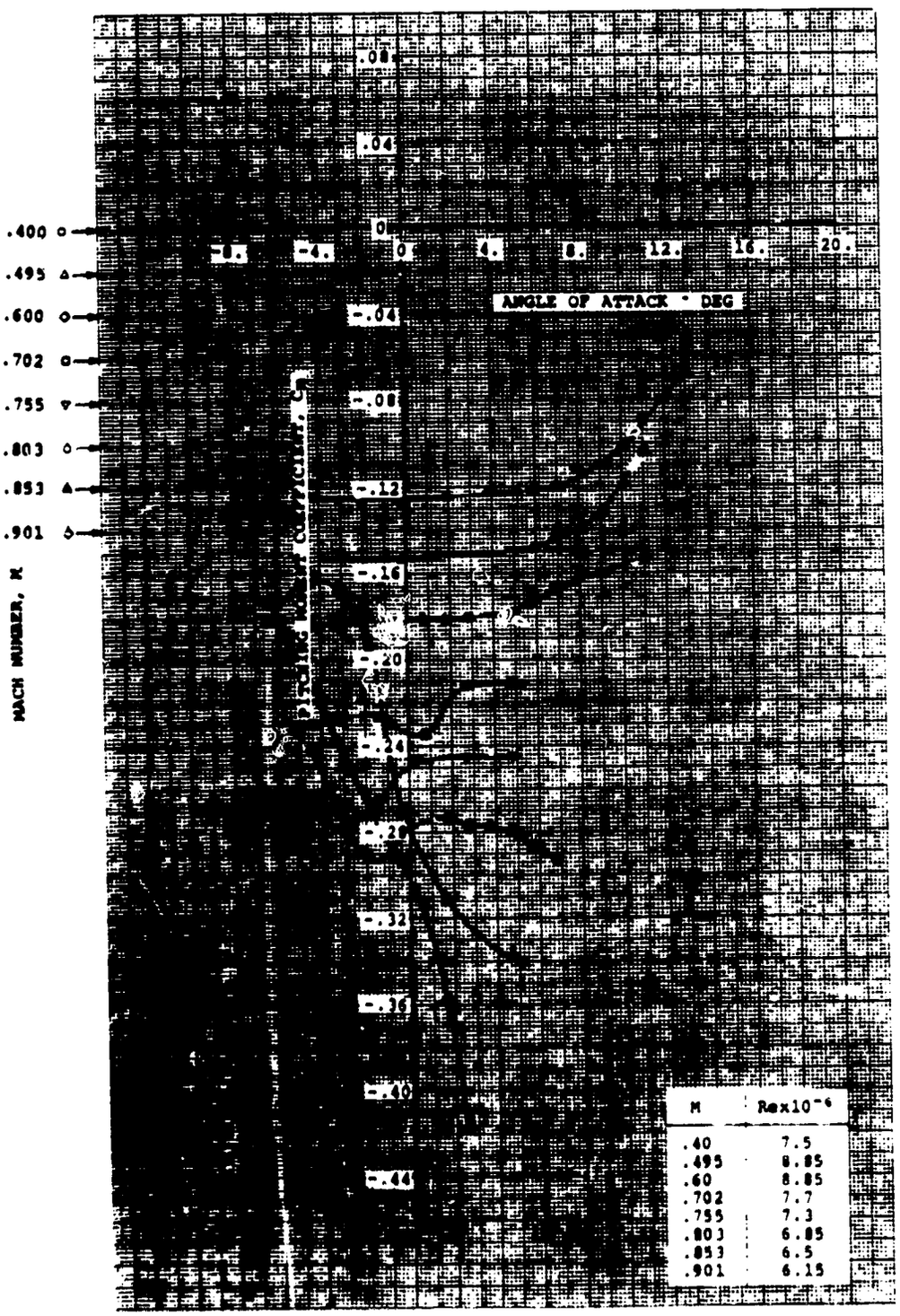
.08
.04
0
-.04
-.08
-.12
-.16
-.20
-.24
-.28
-.32
-.36
-.40
-.44
-8.
-4.
0
4.
8.
12.
16.
20.
ANGLE OF ATTACK ° DEG
PITCHING MOMENT COEFFICIENT, $C_m$
MACH NUMBER, M
.400
.495
.600
.702
.755
.803
.853
.901
M
Rex10⁻⁶
.40
7.5
.495
8.85
.60
8.85
.702
7.7
.755
7.3
.803
6.85
.853
6.5
.901
6.15

AIRFOIL: NACA 64A516



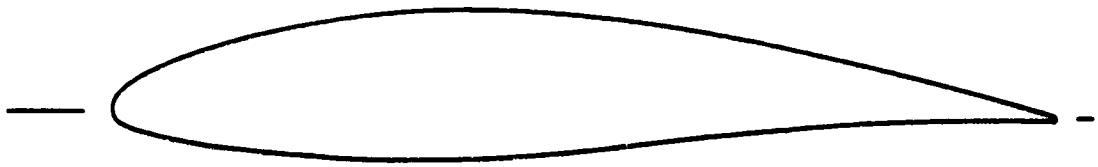

AIRFOIL COORDINATES

| $x/c_u$ | $y/c_u$ | $x/c_l$ | $y/c_l$ |
|---|---|---|---|
| 0.0 | 0.0 | 0.0 | 0.0 |
| 0.00204 | 0.01387 | 0.00796 | -0.01106 |
| 0.00418 | 0.01706 | 0.01082 | -0.01310 |
| 0.00871 | 0.02218 | 0.01629 | -0.01615 |
| 0.02057 | 0.03178 | 0.02943 | -0.02123 |
| 0.04498 | 0.04599 | 0.05502 | -0.02796 |
| 0.06975 | 0.05704 | 0.08025 | -0.03272 |
| 0.09471 | 0.06625 | 0.10529 | -0.03644 |
| 0.14491 | 0.08101 | 0.15509 | -0.04198 |
| 0.19536 | 0.09224 | 0.20464 | -0.04573 |
| 0.24595 | 0.10072 | 0.25405 | -0.04815 |
| 0.29665 | 0.10673 | 0.30335 | -0.04931 |
| 0.34741 | 0.11037 | 0.35259 | -0.04917 |
| 0.39821 | 0.11161 | 0.40179 | -0.04767 |
| 0.44902 | 0.10978 | 0.45098 | -0.04407 |
| 0.49978 | 0.10570 | 0.50022 | -0.03919 |
| 0.55047 | 0.09974 | 0.54953 | -0.03343 |
| 0.60105 | 0.09219 | 0.59895 | -0.02711 |
| 0.65154 | 0.08372 | 0.64846 | -0.02098 |
| 0.70194 | 0.07460 | 0.69806 | -0.01547 |
| 0.75227 | 0.06473 | 0.74773 | -0.01072 |
| 0.80274 | 0.05374 | 0.79726 | -0.00701 |
| 0.85270 | 0.04109 | 0.84730 | -0.00502 |
| 0.90194 | 0.02806 | 0.89806 | -0.00354 |
| 0.95105 | 0.01470 | 0.94895 | -0.00244 |
| 1.0 | 0.0 | 1.0 | 0.0 |

CHARACTERISTICS

- Thickness ratio, t/c = 0.160
- Leading edge radius, r/c = 0.01807
  Center of L.E. circle x/c = 0.01758, y/c = 0.00418
- Trailing edge radius, r/c = 0.001568

TYPE OF DATA AND METHOD OF TEST

Two-dimensional test in the subsonic insert of the Boeing Supersonic Wind Tunnel in Seattle, Wash.

Lift and pitching moments were measured on a balance.

Drag was determined with a wake rake survey.

End plate tares have been applied to the pitching moment measurements.

Model Chord = 6.38 in
Span = 12.0 in

SOURCE

Dadone, L., Experimental Investigation of the Properties of a Family of NACA 64AXXX Airfoils, Boeing Document D170-10021-1, October 1969.

NACA 64A516

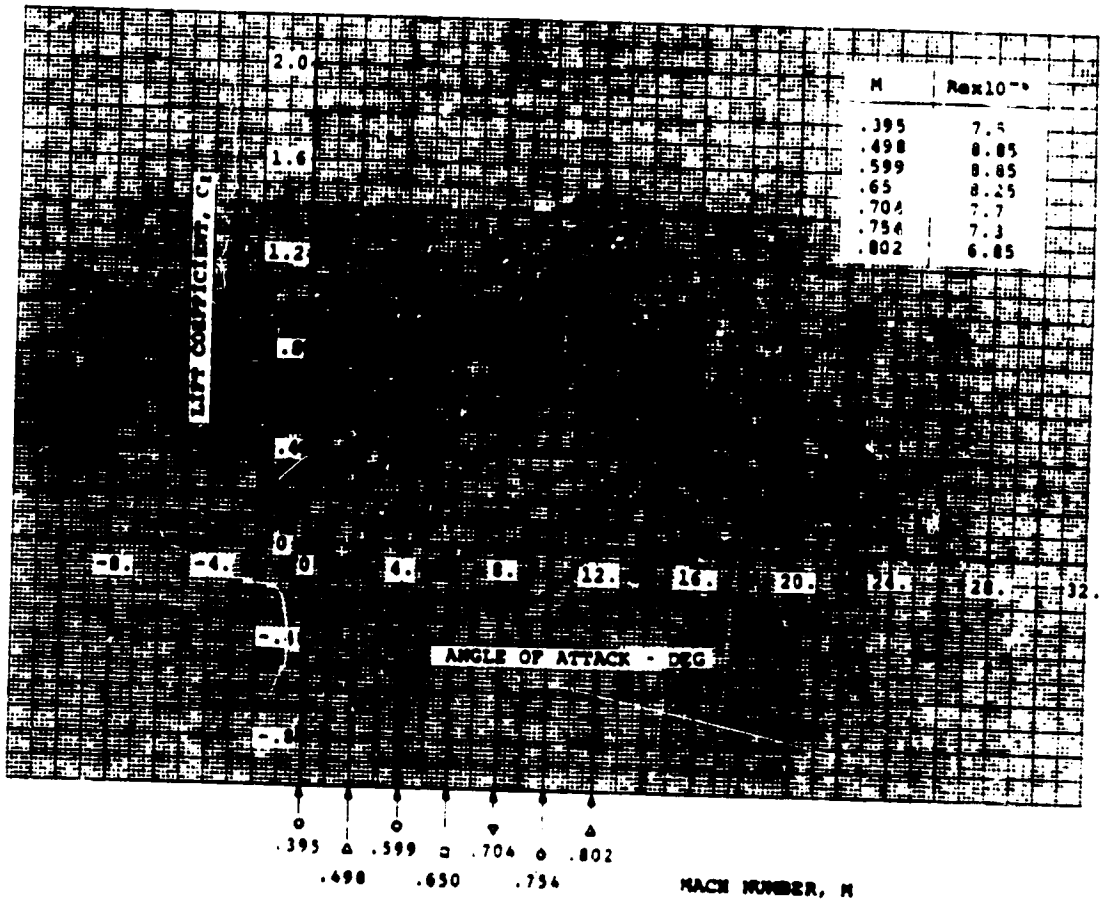
M
Rex10⁻⁶
.395 7.5
.498 8.85
.599 8.85
.65 8.25
.704 7.7
.754 7.3
.802 6.85
LIFT COEFFICIENT, $C_l$
2.0
1.6
1.2
.8
.4
0
-.4
-.8
-8.
-4.
0
4.
8.
12.
16.
20.
24.
28.
32.
ANGLE OF ATTACK - DEG
.395 .498 .599 .650 .704 .754 .802
MACH NUMBER, M

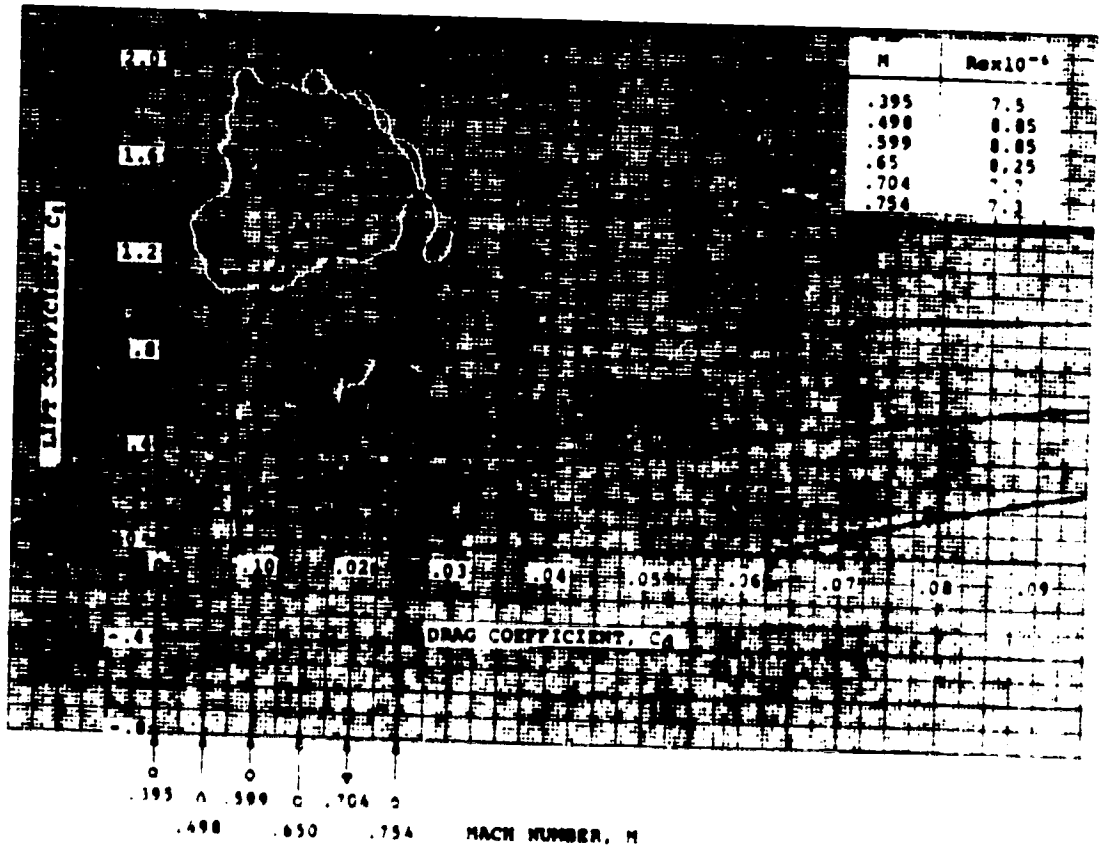
M
Rex10⁻⁶
.395 7.5
.498 8.85
.599 8.85
.65 8.25
.704
.754 7.3
LIFT COEFFICIENT, $C_l$
1.6
1.2
.8
.4
0
-.4
-.8
.01
.02
.03
.04
.05
.06
.07
.08
.09
DRAG COEFFICIENT, $C_d$
.395 .498 .599 .650 .704 .754
MACH NUMBER, M

NACA 64A516

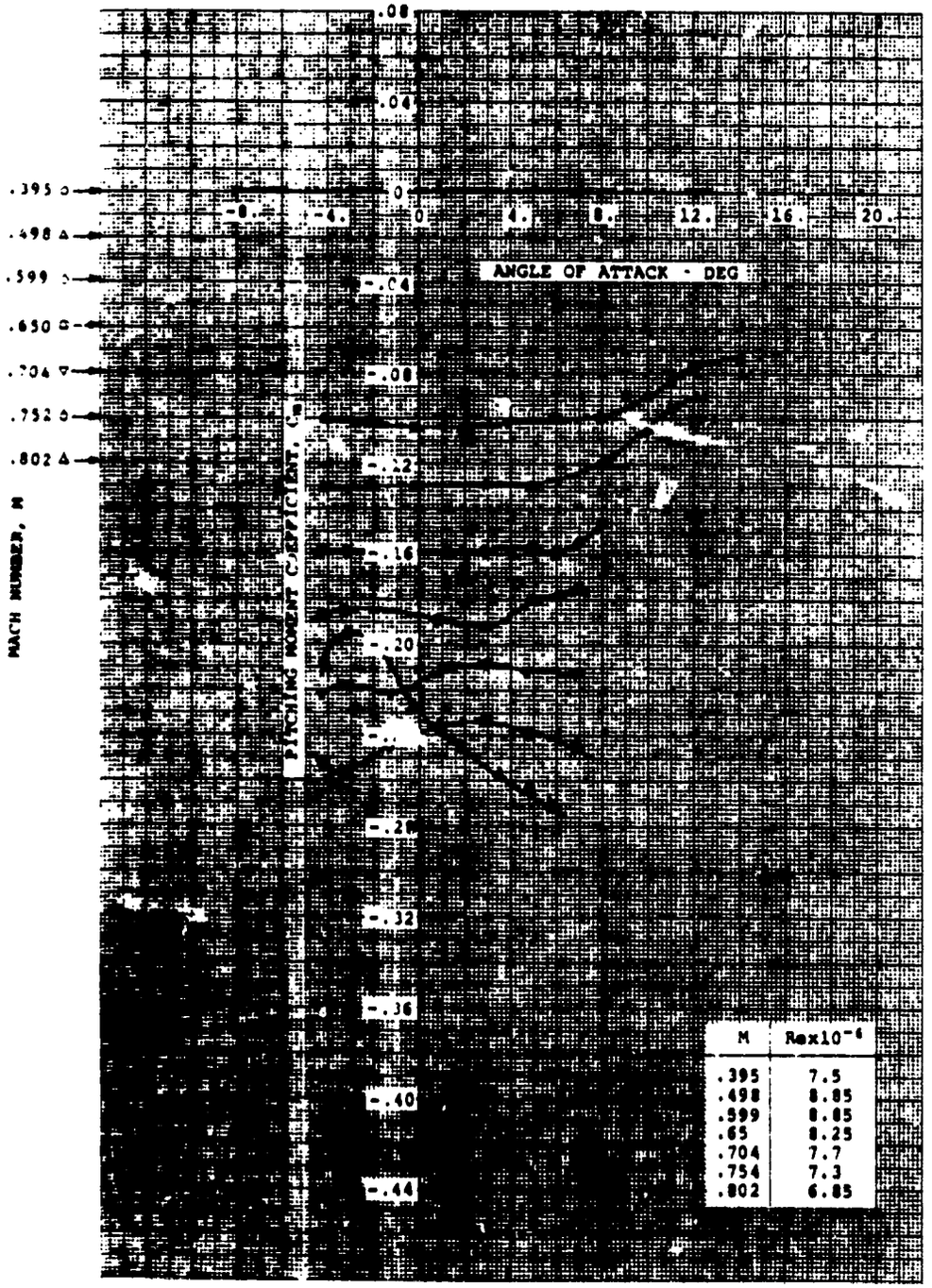
.08
.04
0
-.04
-.08
-.12
-.16
-.20
-.24
-.28
-.32
-.36
-.40
-.44
-8.
-4.
0
4.
8.
12.
16.
20.
ANGLE OF ATTACK - DEG
PITCHING MOMENT COEFFICIENT, Cm
MACH NUMBER, M
.395
.498
.599
.650
.704
.752
.802
M
Rex10⁻⁶
.395 7.5
.498 8.85
.599 8.85
.65 8.25
.704 7.7
.754 7.3
.802 6.85

AIRFOIL: NACA 8-H-12



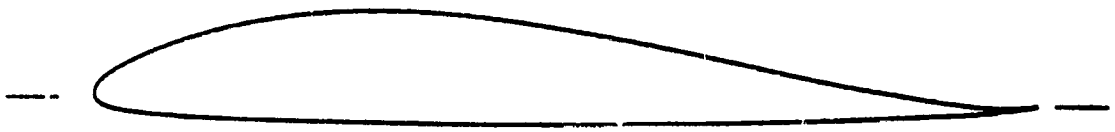

AIRFOIL COORDINATES

| $x/c_u$ | $y/c_u$ | $x/c_l$ | $y/c_l$ |
|---|---|---|---|
| 0.0 | 0.0 | 0.0 | 0.0 |
| 0.00147 | 0.01229 | 0.00853 | -0.00819 |
| 0.00358 | 0.0152 | 0.01142 | -0.00946 |
| 0.00804 | 0.02006 | 0.01696 | -0.01128 |
| 0.0198 | 0.02941 | 0.0302 | -0.01415 |
| 0.04424 | 0.04312 | 0.05576 | -0.01736 |
| 0.06914 | 0.0538 | 0.08086 | -0.0192 |
| 0.09427 | 0.06263 | 0.10573 | -0.02059 |
| 0.14497 | 0.07626 | 0.15503 | -0.02242 |
| 0.19607 | 0.08605 | 0.20393 | -0.02351 |
| 0.24754 | 0.09243 | 0.25246 | -0.02417 |
| 0.29969 | 0.09533 | 0.30031 | -0.02455 |
| 0.35174 | 0.09432 | 0.34826 | -0.0249 |
| 0.40292 | 0.0903 | 0.39708 | -0.02494 |
| 0.4536 | 0.0842 | 0.4464 | -0.02476 |
| 0.5039 | 0.07666 | 0.4961 | -0.02436 |
| 0.55387 | 0.06795 | 0.54613 | -0.02377 |
| 0.60358 | 0.05846 | 0.59642 | -0.02290 |
| 0.65311 | 0.0485 | 0.64689 | -0.02178 |
| 0.7025 | 0.03838 | 0.6975 | -0.02034 |
| 0.75184 | 0.02838 | 0.74816 | -0.0186 |
| 0.80118 | 0.01895 | 0.79882 | -0.01645 |
| 0.8506 | 0.01046 | 0.8494 | -0.01384 |
| 0.90016 | 0.00343 | 0.89984 | -0.01051 |
| 0.94995 | -0.00119 | 0.95005 | -0.00629 |
| 1.0 | 0.0 | 0.0 | 0.0 |

CHARACTERISTICS

- Thickness, t/c = 0.12
- Leading Edge Radius, r/c = 0.01325
- Slope of Radius Through Leading Edge = 0.344

TYPE OF DATA AND METHOD OF TEST

Two-dimensional test in the Langley low-turbulence wind tunnel. The dimensions of the test section were 3' x 7.5'. In preparation for the test, the model was sanded down in a chordwise direction with No. 400 carborundum paper.

Lift and pitching moments were obtained from balance readings, the drag was obtained from wake measurements. Some surface pressure measurements were also made.

All tests were run at low speeds.

The data presented was acquired at $R_c = 2.6 \times 10^6$.

Model Chord = 24.0 in
Span = 35.5 in

SOURCE

Stivers, L.S., Jr., Rice, F.J., Jr., Aerodynamic Characteristics of Four NACA Airfoil Sections Designed for Helicopter Rotor Blades, NACA WR L-29, 1946.

NACA 8-H-012

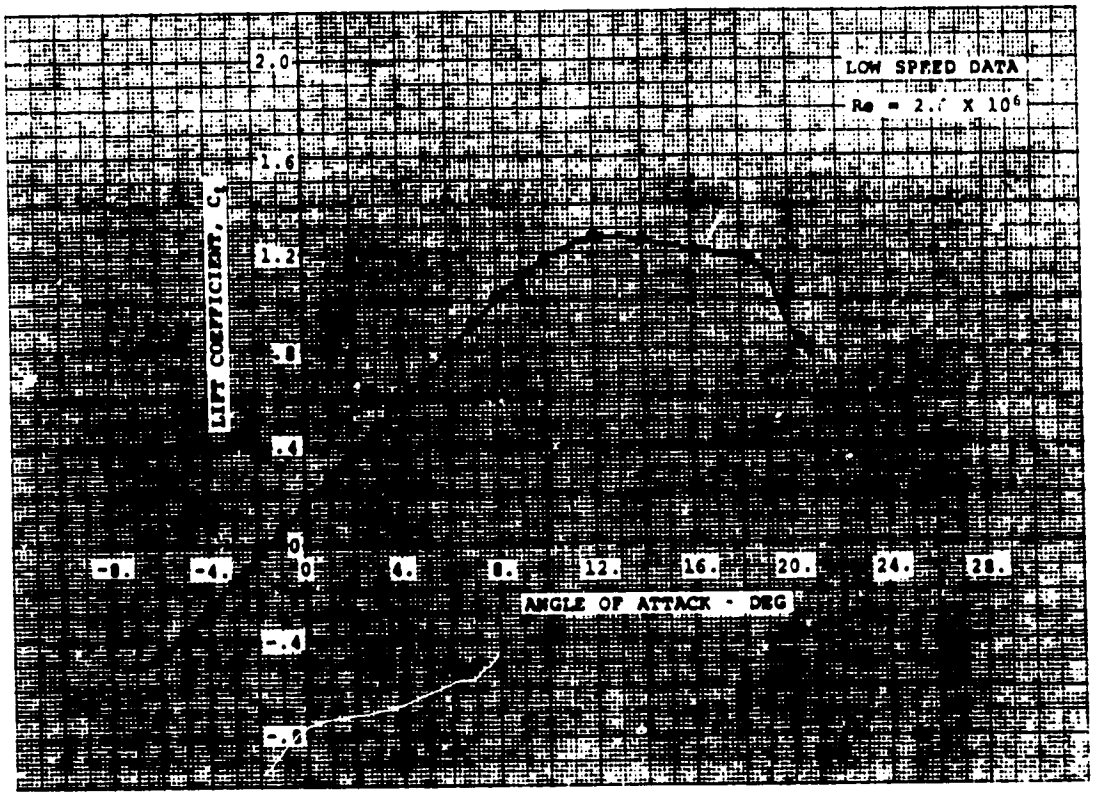
LOW SPEED DATA
Re = 2.7 X 10⁶
LIFT COEFFICIENT, $C_l$
2.0
1.6
1.2
.8
.4
0
-.4
-.8
-8.
-4.
0
4.
8.
12.
16.
20.
24.
28.
ANGLE OF ATTACK - DEG

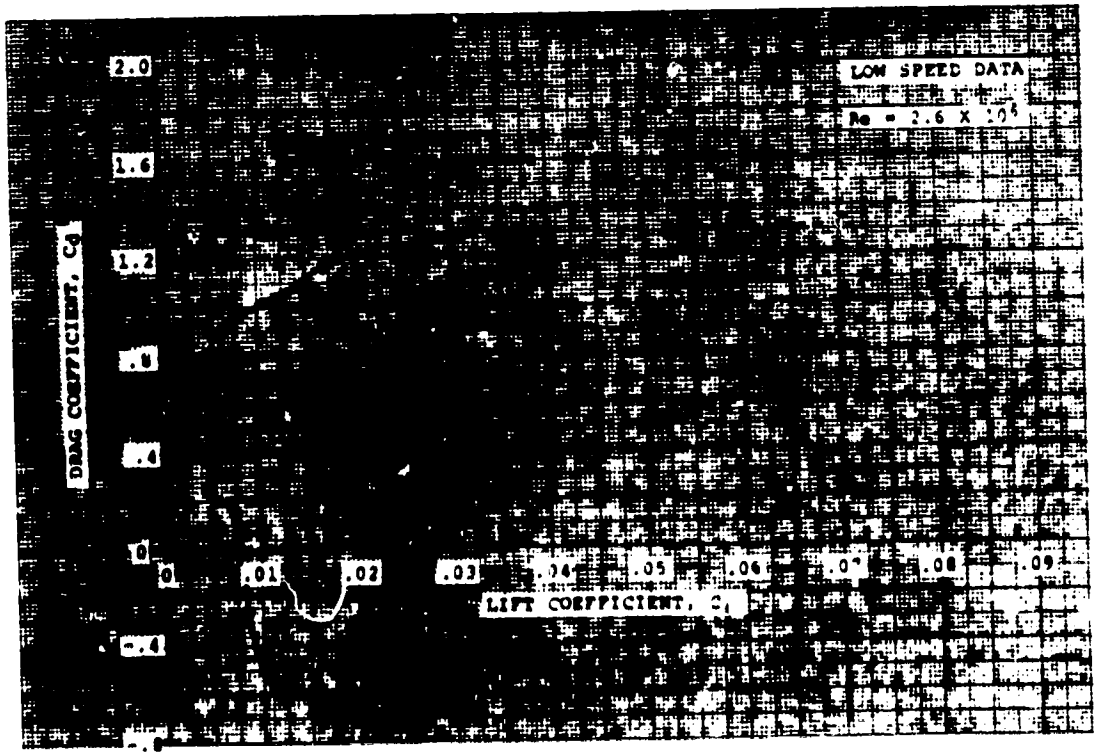
LOW SPEED DATA
Re = 2.6 X 10⁶
DRAG COEFFICIENT, $C_d$
2.0
1.6
1.2
.8
.4
0
-.4
0
.01
.02
.03
.04
.05
.06
.07
.08
.09
LIFT COEFFICIENT, $C_l$

NACA 8-H-012

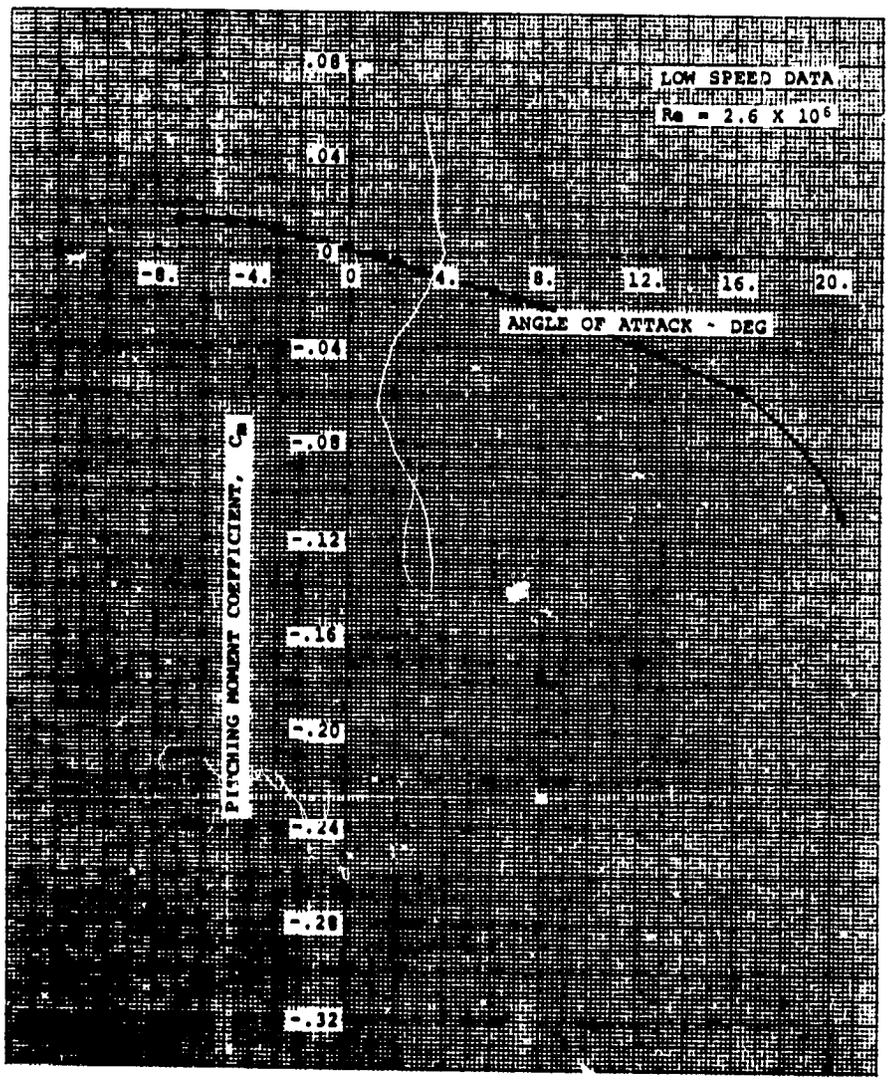
LOW SPEED DATA
Re = 2.6 X 10^6
.08
.04
0
-.04
-.08
-.12
-.16
-.20
-.24
-.28
-.32
-8.
-4.
0
4.
8.
12.
16.
20.
ANGLE OF ATTACK - DEG
PITCHING MOMENT COEFFICIENT, Cm

AIRFOIL: V13006-0.7 1.3.230

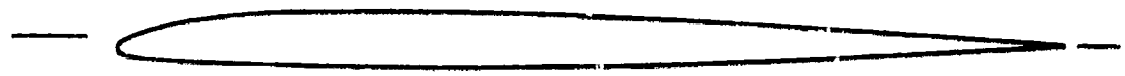

AIRFOIL COORDINATES (*)

| x/c | $y/c_u$ | $y/c_l$ |
|---|---|---|
| -0.002 | -0.0117 | -0.0117 |
| 0.0 | -0.0064 | -0.0171 |
| 0.0025 | -0.004 | -0.019 |
| 0.0075 | -0.0013 | -0.0208 |
| 0.0125 | 0.0012 | -0.0219 |
| 0.025 | 0.0057 | -0.0235 |
| 0.05 | 0.0127 | -0.0255 |
| 0.075 | 0.0177 | -0.0268 |
| 0.1 | 0.0216 | -0.0275 |
| 0.15 | 0.026 | -0.0286 |
| 0.2 | 0.0285 | -0.0294 |
| 0.25 | 0.0295 | -0.0299 |
| 0.3 | 0.0299 | -0.03 |
| 0.4 | 0.029 | -0.029 |
| 0.5 | 0.0265 | -0.0265 |
| 0.6 | 0.0228 | -0.0228 |
| 0.7 | 0.0185 | -0.0183 |
| 0.8 | 0.0131 | -0.0131 |
| 0.9 | 0.0072 | -0.0072 |
| 0.95 | 0.004 | -0.004 |
| 1.0 | 0.0006 | -0.0006 |

(*)Coordinates defined in the Vertol reference system, where the reference line approximately bisects the aft 50% of an airfoil.

CHARACTERISTICS

- Thickness, t/c = 0.06
- Leading Edge Radius:
  r/c = 0.007
- Center of Leading Edge
  Circle at x/c = 0.005
  y/c = -0.0117

TYPE OF DATA AND METHOD OF TEST

Two-dimensional tests in the subsonic insert of the Boeing supersonic wind tunnel in Seattle, Washington.

Lift and pitching moments were determined by integration of surface static pressures.

Drag was determined by a traversing wake probe survey.

Model Chord = 7.0 in
Span = 12.0 in

SOURCE

1) Gabriel, E.,"Analysis two-dimensional Wind Tunnel Tests of Rotor Blade Airfoils of Varying Camber and Leading Edge Radius", Boeing Document AERO INV.III-288, November,1965.
2) Gray, L., Liiva, J,Davenport, F., "Wind Tunnel Tests of Thin Airfoils Oscillating Near Stall, USAAVLABS TR 68-89A, 1969.

V13006-0.7

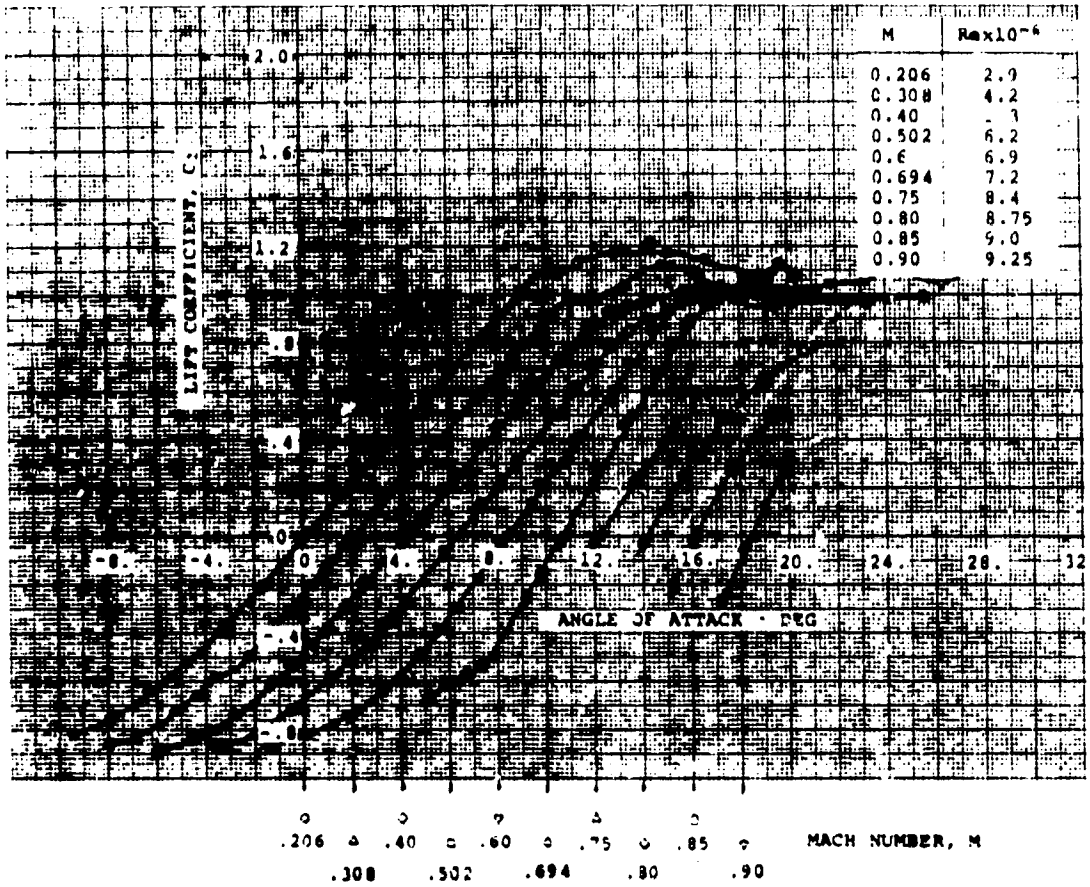
M
Rex10⁻⁶
0.206 2.9
0.308 4.2
0.40 5.3
0.502 6.2
0.6 6.9
0.694 7.2
0.75 8.4
0.80 8.75
0.85 9.0
0.90 9.25
LIFT COEFFICIENT, $C_L$
2.0
1.6
1.2
.8
.4
0
-.4
-.8
-0.
-4.
0
4.
8.
12.
16.
20.
24.
28.
32.
ANGLE OF ATTACK - DEG
.206 .308 .40 .502 .60 .694 .75 .80 .85 .90
MACH NUMBER, M

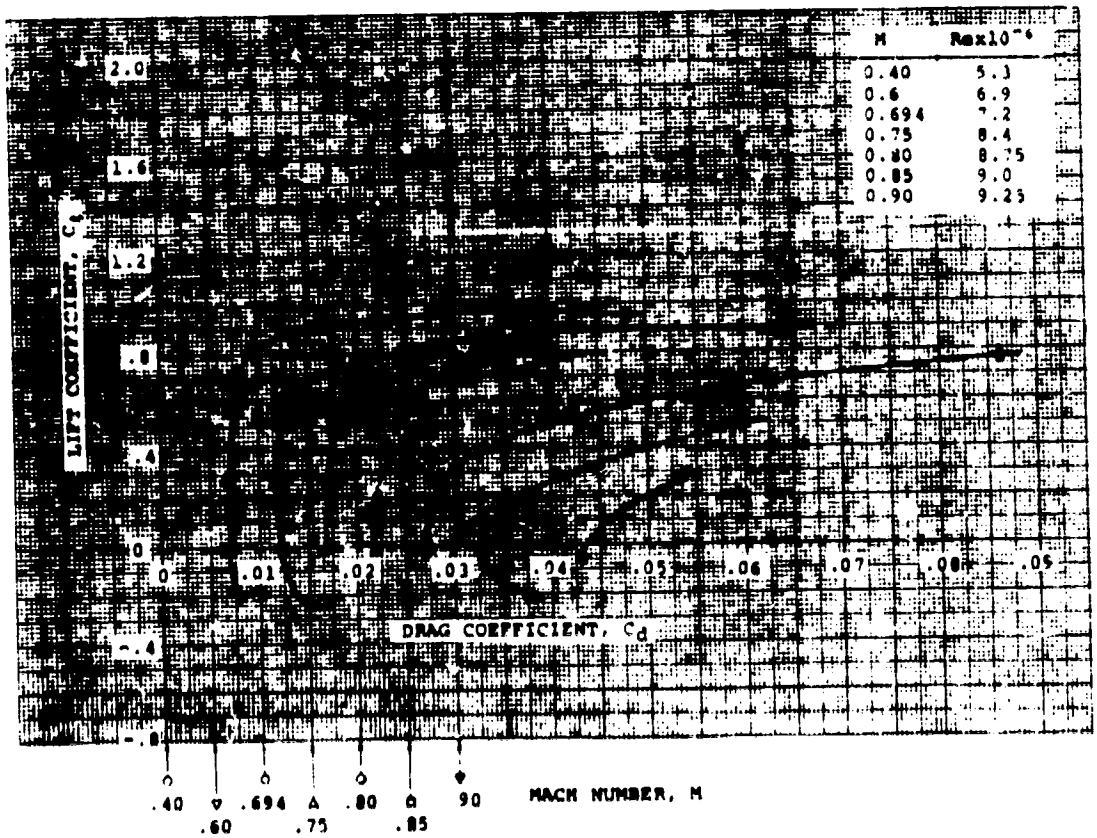
M
Rex10⁻⁶
0.40 5.3
0.6 6.9
0.694 7.2
0.75 8.4
0.80 8.75
0.85 9.0
0.90 9.25
LIFT COEFFICIENT, $C_L$
2.0
1.6
1.2
.8
.4
0
-.4
-.8
0
.01
.02
.03
.04
.05
.06
.07
.08
.09
DRAG COEFFICIENT, $C_d$
.40 .60 .694 .75 .80 .85 .90
MACH NUMBER, M

V13006-0.7

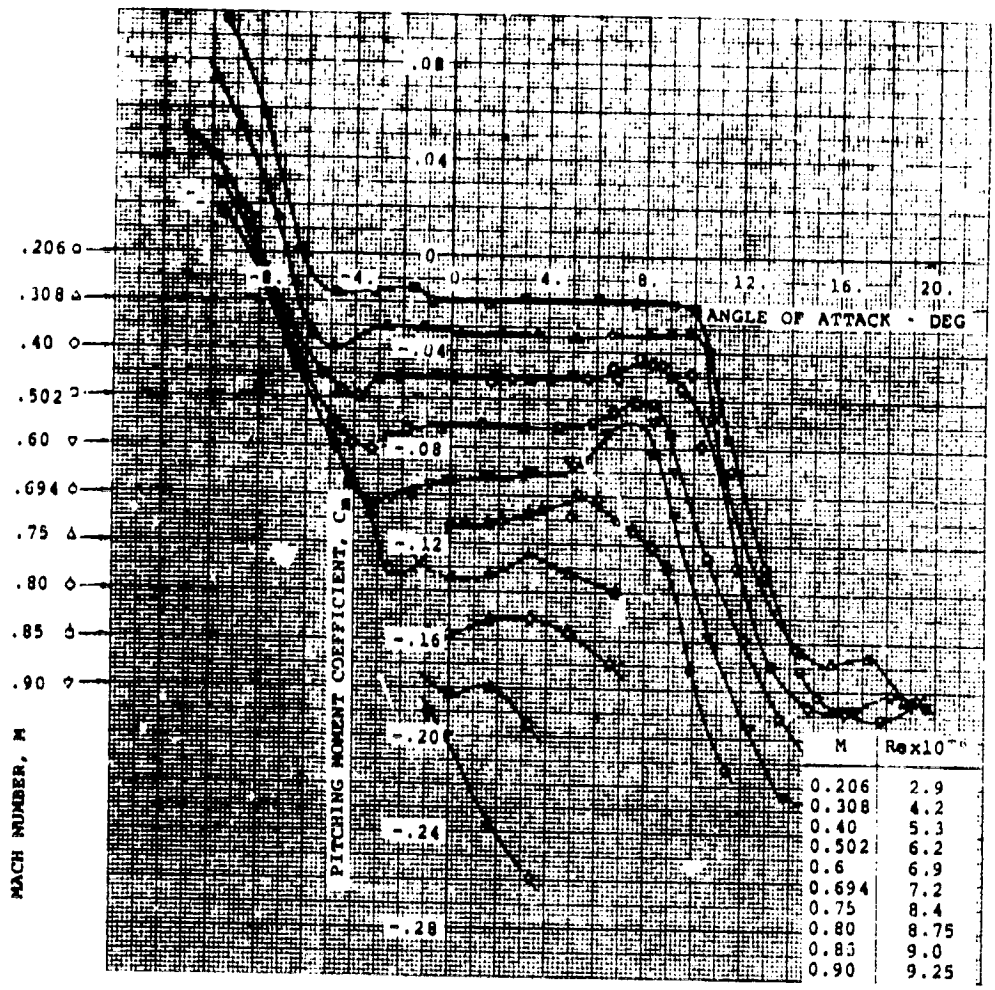
.08
.04
0
-.04
-.08
-.12
-.16
-.20
-.24
-.28
-8.
-4.
0
4.
8.
12.
16.
20.
ANGLE OF ATTACK - DEG
PITCHING MOMENT COEFFICIENT, Cm
MACH NUMBER, M
.206
.308
.40
.502
.60
.694
.75
.80
.85
.90
M
Rex10⁻⁶
0.206 2.9
0.308 4.2
0.40 5.3
0.502 6.2
0.6 6.9
0.694 7.2
0.75 8.4
0.80 8.75
0.85 9.0
0.90 9.25

AIRFOIL: V(1.9)3009-1.25



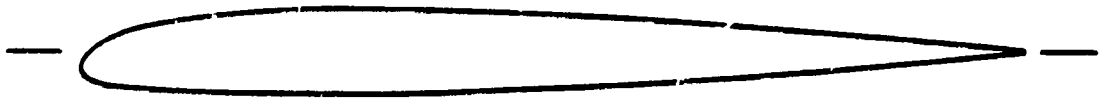

AIRFOIL COORDINATES (*)

| x/c | $x/c_{upp}$ | $y/c_{low}$ |
|---|---|---|
| 0.0 | -0.01763 | -0.01763 |
| 0.005 | -0.00585 | -0.02767 |
| 0.0125 | +0.00199 | -0.03211 |
| 0.025 | 0.01022 | -0.03608 |
| 0.05 | 0.02078 | -0.03979 |
| 0.075 | 0.02778 | -0.04149 |
| 0.1 | 0.03295 | -0.0427 |
| 0.15 | 0.0387 | -0.04395 |
| 0.2 | 0.0424 | -0.0446 |
| 0.25 | 0.04425 | -0.04505 |
| 0.3 | 0.04495 | -0.04505 |
| 0.35 | 0.04468 | -0.04468 |
| 0.4 | 0.04379 | -0.04379 |
| 0.5 | 0.03985 | -0.03985 |
| 0.6 | 0.03415 | -0.03415 |
| 0.7 | 0.02686 | -0.02686 |
| 0.8 | 0.01863 | -0.01863 |
| 0.9 | 0.01014 | -0.01014 |
| 0.95 | 0.0056 | -0.0056 |
| 1.0 | 0.00055 | -0.00055 |

(*)Coordinates defined in the Vertol reference system, where the reference line approximately bisects the aft 50% of an airfoil.

CHARACTERISTICS

- Thickness, t/c = 0.09
- Leading Edge Radius, r/c = 0.0125
- Center of Leading Edge Circle at x/c = 0.0125
  y/c = -0.01763

TYPE OF DATA AND METHOD OF TEST

Two-dimensional tests in the subsonic insert of the Boeing supersonic wind tunnel in Seattle, Washington.

Lift and pitching moment were determined by integration of surface static pressures.

Drag was determined by a traversing wake probe survey.

The tests were conducted at total pressures of about 50 psia to simulate full-scale Reynolds Numbers.

Model Chord = 6.0 in
Span = 12.0 in

SOURCE

Gabriel, E., "Analysis of two-dimensional Wind Tunnel Tests of Rotor Blade Airfoils of Varying Camber and Leading Edge Radius", Boeing Aero. Inv. III-288, 11 November, 1965.

V(1.9)3009-1.25

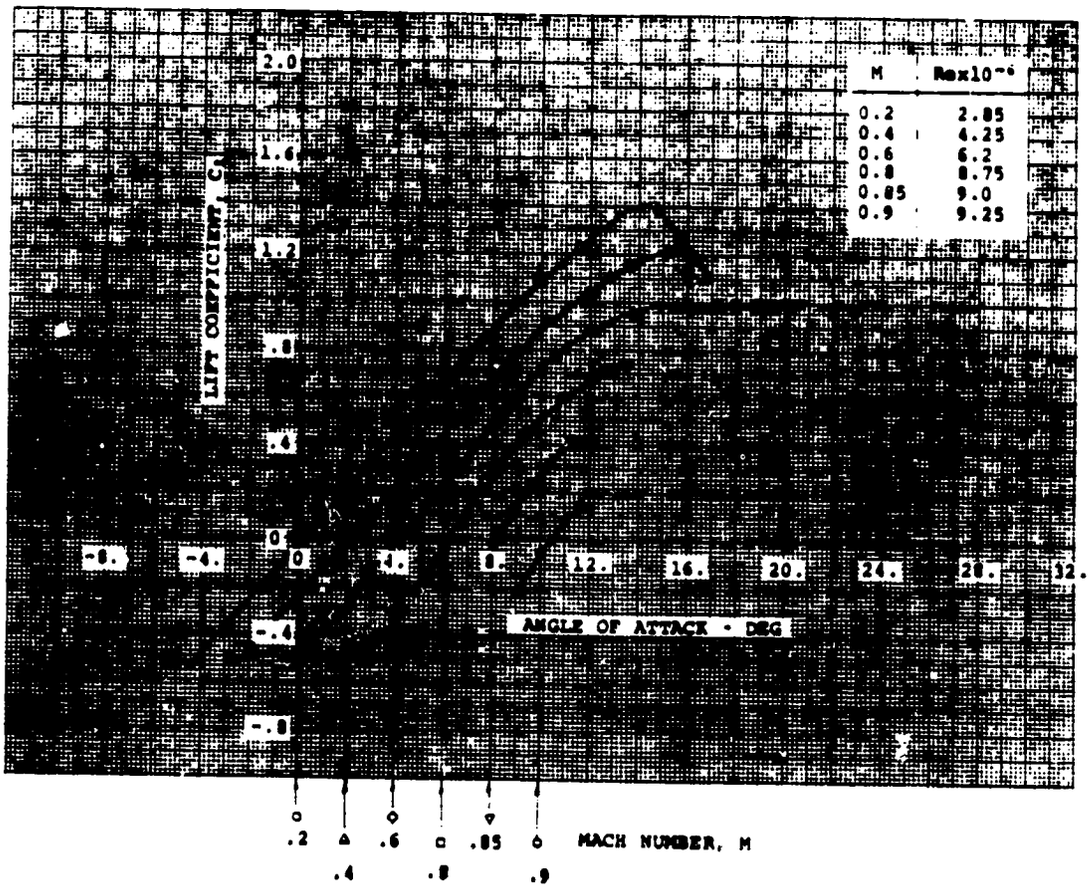
M | Rex10⁻⁶
0.2 | 2.85
0.4 | 4.25
0.6 | 6.2
0.8 | 8.75
0.85 | 9.0
0.9 | 9.25
LIFT COEFFICIENT, CL
2.0
1.6
1.2
.8
.4
0
-.4
-.8
-8.
-4.
0
4.
8.
12.
16.
20.
24.
28.
32.
ANGLE OF ATTACK - DEG
.2
.4
.6
.8
.85
.9
MACH NUMBER, M

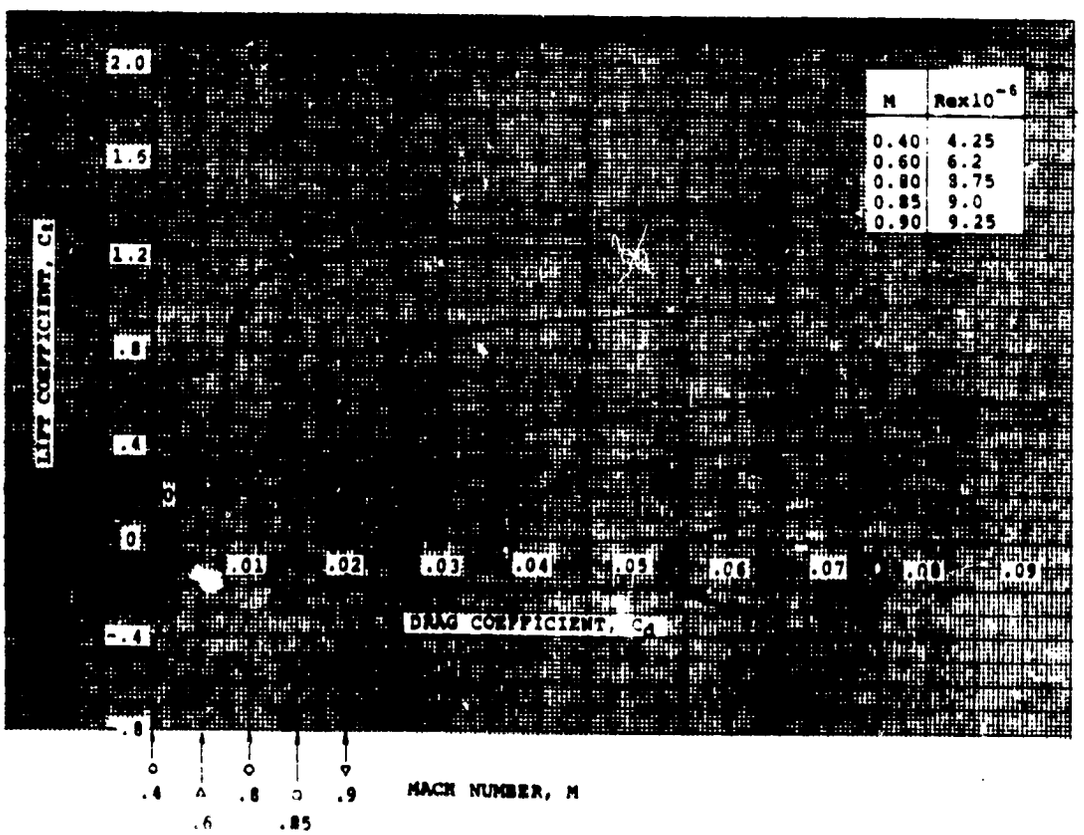
M | Rex10⁻⁶
0.40 | 4.25
0.60 | 6.2
0.80 | 8.75
0.85 | 9.0
0.90 | 9.25
LIFT COEFFICIENT, CL
2.0
1.6
1.2
.8
.4
0
-.4
-.8
.01
.02
.03
.04
.05
.06
.07
.08
.09
DRAG COEFFICIENT, CD
.4
.6
.8
.85
.9
MACH NUMBER, M

V(1.9)3009-1.25

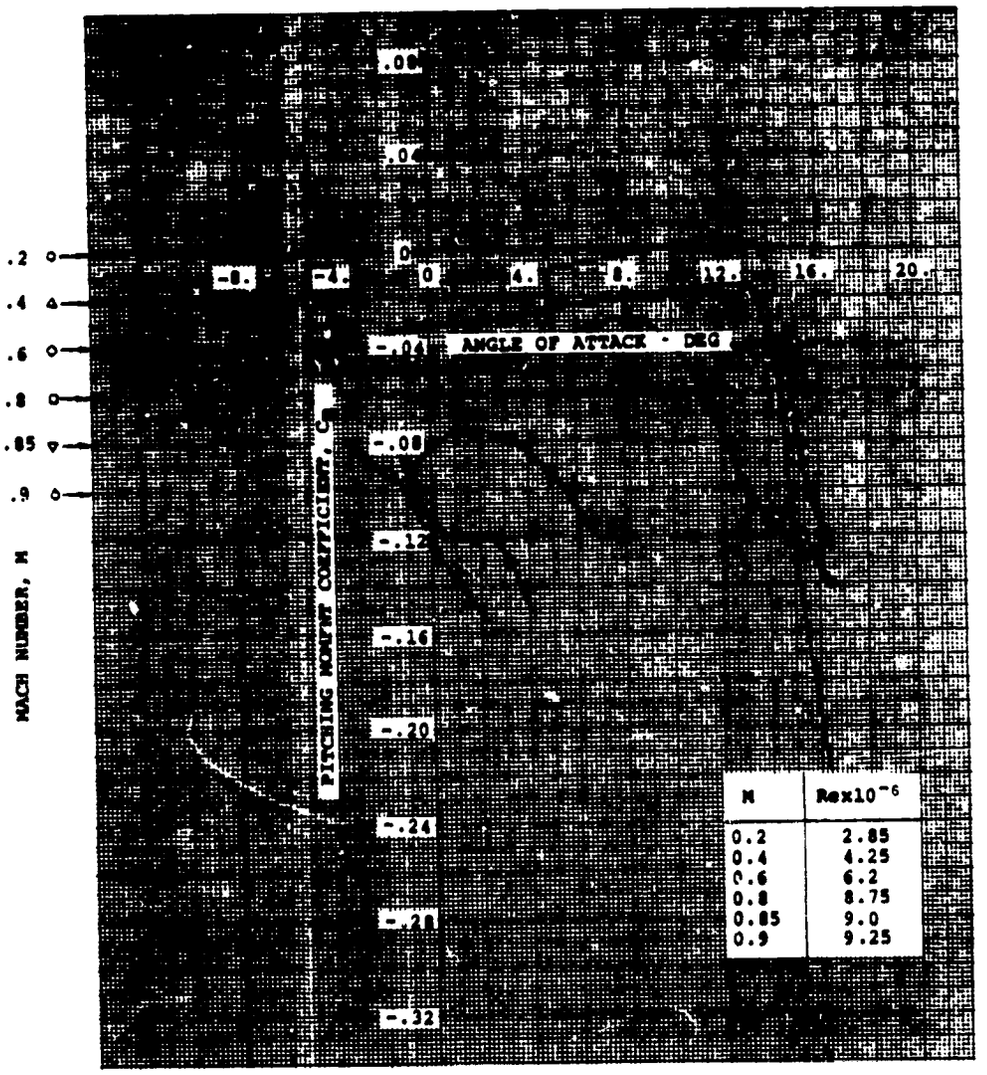
.04
.0
0
-8.
-4.
0
4.
8.
12.
16.
20.
ANGLE OF ATTACK - DEG
-.04
-.08
-.12
-.16
-.20
-.24
-.28
-.32
PITCHING MOMENT COEFFICIENT, $C_m$
MACH NUMBER, M
.2
.4
.6
.8
.85
.9
M
Rex10$^{-6}$
0.2 2.85
0.4 4.25
0.6 6.2
0.8 8.75
0.85 9.0
0.9 9.25

AIRFOIL: V23010-1.58 With 0° T.E. Tab 1.3.250

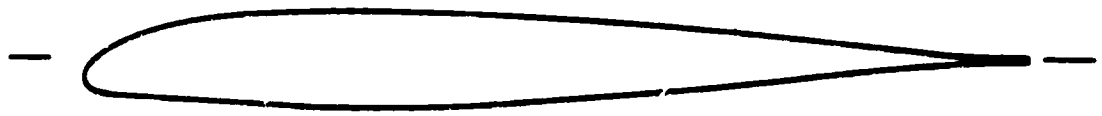

AIRFOIL COORDINATES (*)

| x/c | $y/c_u$ | $y/c_l$ |
|---|---|---|
| 0.0 | -0.0225 | -0.0225 |
| 0.005 | -0.0078 | -0.0329 |
| 0.01 | -0.0024 | -0.0362 |
| 0.015 | 0.0019 | -0.0378 |
| 0.025 | 0.0096 | -0.0394 |
| 0.035 | 0.0155 | -0.0404 |
| 0.047 | 0.0214 | -0.0412 |
| 0.06 | 0.0265 | -0.042 |
| 0.08 | 0.0327 | -0.0434 |
| 0.11 | 0.0396 | -0.0449 |
| 0.15 | 0.0455 | -0.0471 |
| 0.19 | 0.0489 | -0.0494 |
| 0.23 | 0.0499 | -0.0513 |
| 0.27 | 0.0499 | -0.0522 |
| 0.31 | 0.0497 | -0.05215 |
| 0.35 | 0.049 | -0.0517 |
| 0.39 | 0.048 | -0.0505 |
| 0.43 | 0.0465 | -0.0487 |
| 0.47 | 0.0446 | -0.0468 |
| 0.51 | 0.0424 | -0.044 |
| 0.55 | 0.0397 | -0.0412 |
| 0.59 | 0.0369 | -0.038 |
| 0.63 | 0.0336 | -0.0346 |
| 0.67 | 0.0301 | -0.0308 |
| 0.71 | 0.0263 | -0.0269 |
| 0.75 | 0.0223 | -0.0226 |
| 0.79 | 0.0181 | -0.0182 |
| 0.83 | 0.0137 | -0.0136 |
| 0.87 | 0.0093 | -0.0093 |
| 0.91 | 0.0056 | -0.0057 |
| 0.945 | 0.0028 | -0.0031 |
| 0.96 | 0.00235 | -0.00235 |
| 1.0 | 0.00235 | -0.00235 |

(*)Coordinates defined in the Vertol reference system, where the reference line approximately bisects the aft 50% of an airfoil.

## CHARACTERISTICS

- Thickness, t/c = 0.102
- Leading Edge Radius, r/c = 0.0158
- Center of Leading Edge Circle at x/c = 0.0158, y/c = -0.0225
- Trailing Edge Tab from x/c = 0.96 to x/c = 1.0

## TYPE OF DATA AND METHOD OF TEST

Two-dimensional tests in the Subsonic Insert of the Boeing Supersonic Wind Tunnel in Seattle, Wash.

Lift and pitching moments were determined with a balance.

Drag was determined by a traversing wake probe survey.

Model Chord = 6.38 in
Span = 12.0 in

## SOURCES


1) LaPrete, R., Storwick, E.M., Peterson, L.D., Boeing Wind Tunnel Test 927, Boeing Doc. No. D2-24066-1, 1966.

2) Eierman, R.L., Nyholm, J.R., Schreiber, R.E., Russell, J.H., Data Report BSWT 412, Boeing Doc. No. D6-20518, Dec. 1967.

3) Dadone, L.U., & McMullen, J., HLH/ATC Rotor System Two-Dimensional Airfoil Test, D301-10071-1, Dec. 1971.

V23010-1.58 WITH 0° T.E. TAB

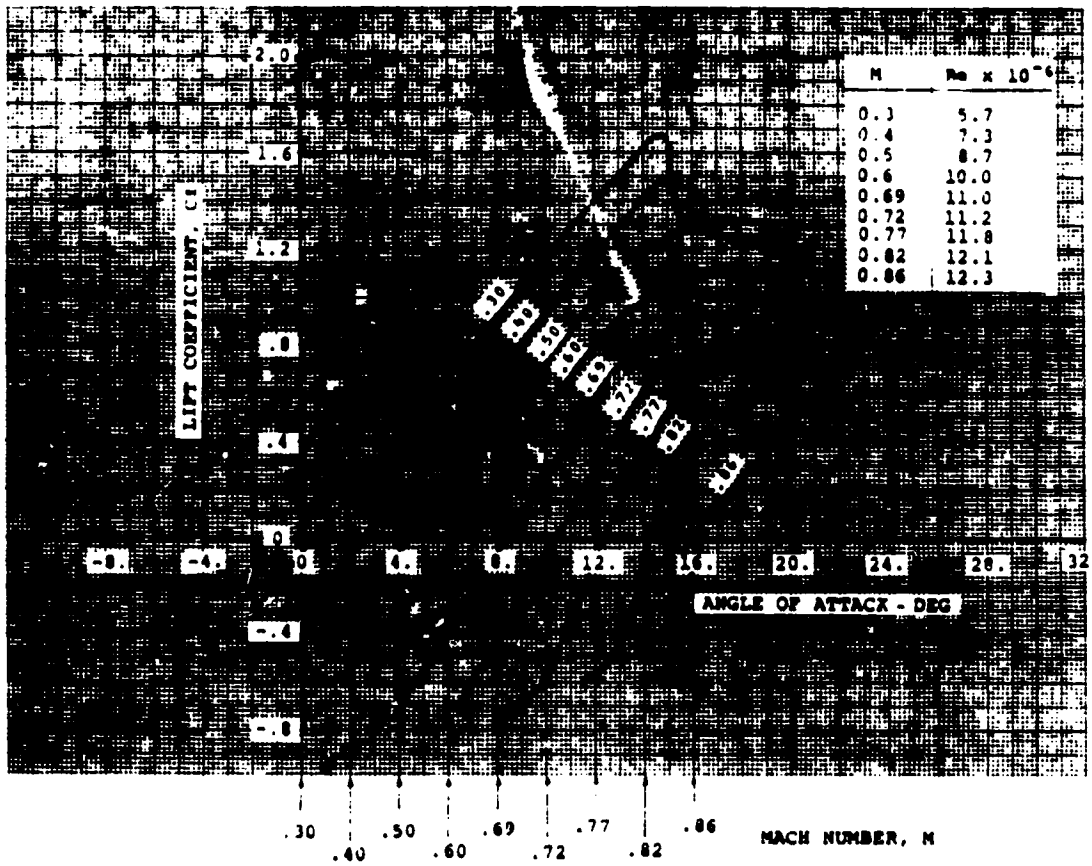


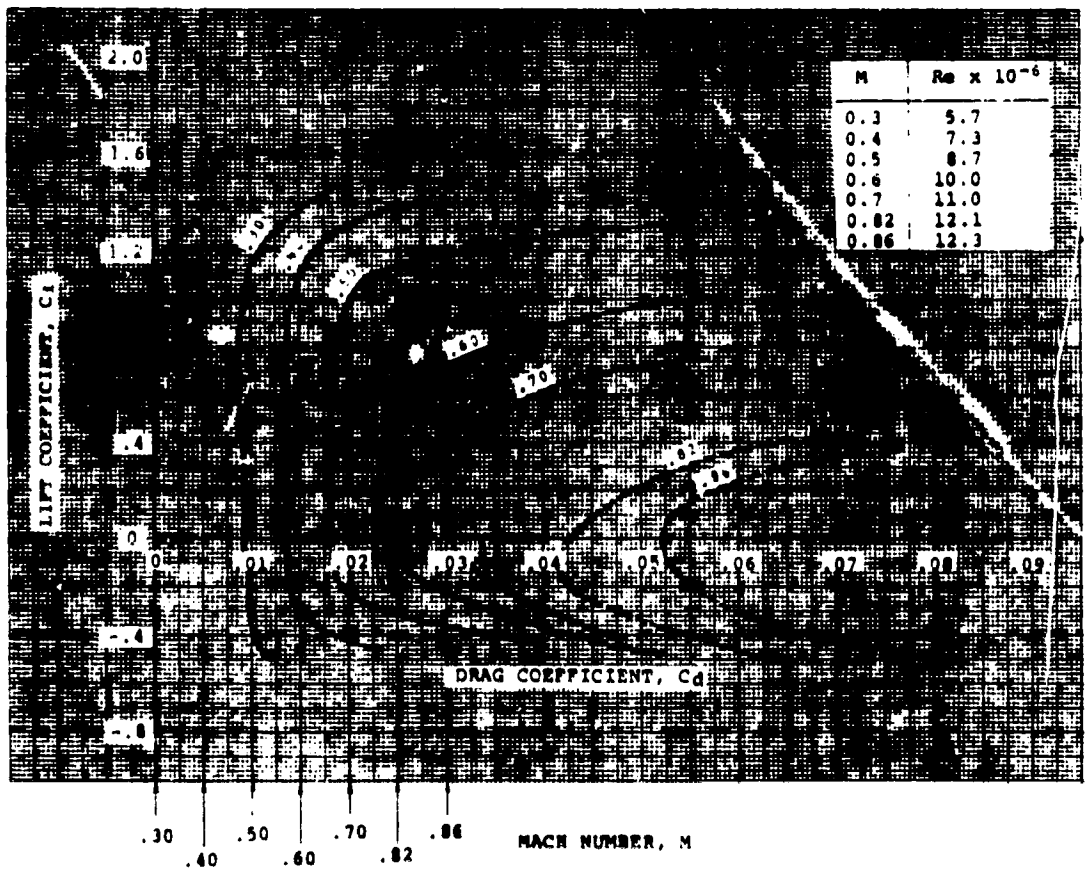

V23010-1.58 WITH 0° T.E. TAB

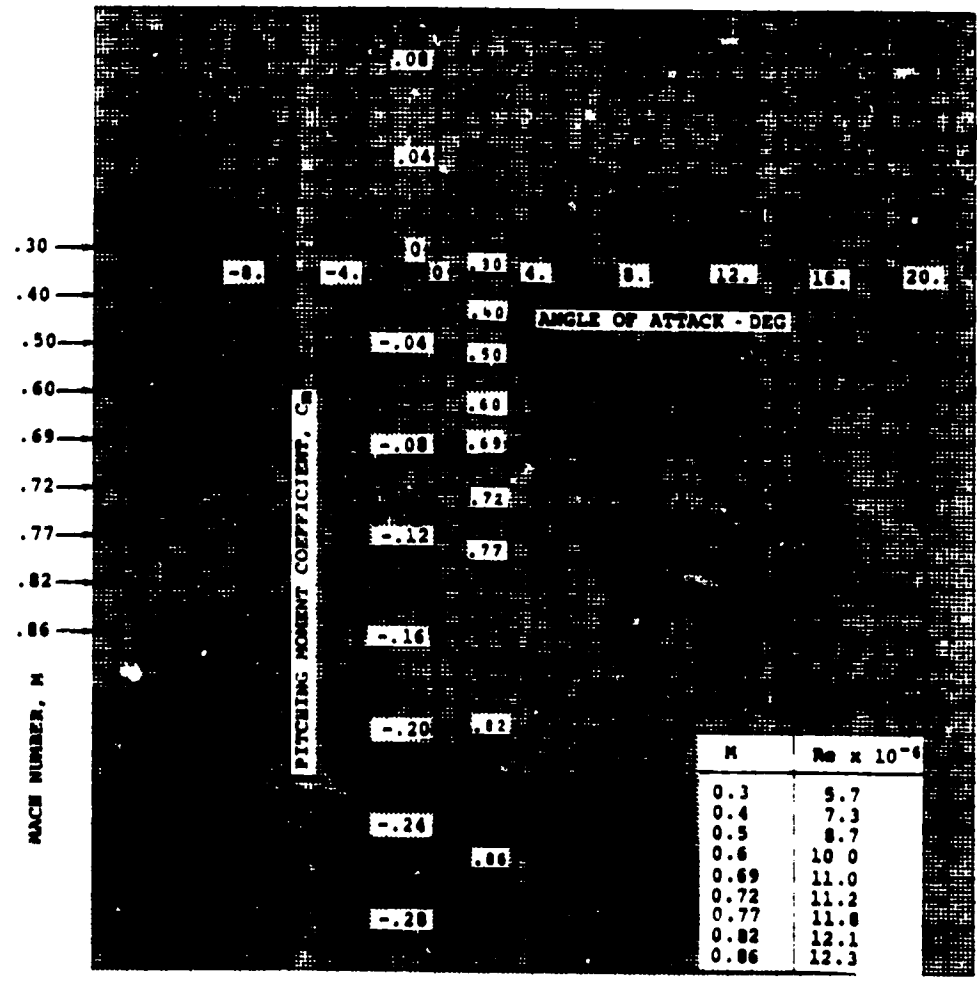

AIRFOIL: V23010-1.58 with -3° T.E. Tab 1.3.260

AIRFOIL COORDINATES (*)

| x/c | $y/c_u$ | $y/c_l$ |
|---|---|---|
| 0.0 | -0.0225 | -0.0225 |
| 0.005 | -0.0078 | -0.0329 |
| 0.01 | -0.0024 | -0.0362 |
| 0.015 | 0.0019 | -0.0378 |
| 0.025 | 0.0096 | -0.0394 |
| 0.035 | 0.0155 | -0.0404 |
| 0.047 | 0.0214 | -0.0412 |
| 0.06 | 0.0265 | -0.042 |
| 0.08 | 0.0327 | -0.0434 |
| 0.11 | 0.0396 | -0.0449 |
| 0.15 | 0.0455 | -0.0471 |
| 0.19 | 0.0489 | -0.0494 |
| 0.23 | 0.0499 | -0.0513 |
| 0.27 | 0.0499 | -0.0522 |
| 0.31 | 0.0497 | -0.05215 |
| 0.35 | 0.049 | -0.0517 |
| 0.39 | 0.048 | -0.0505 |
| 0.43 | 0.0465 | -0.0487 |
| 0.47 | 0.0446 | -0.0468 |
| 0.51 | 0.0424 | -0.044 |
| 0.55 | 0.0397 | -0.0412 |
| 0.59 | 0.0369 | -0.038 |
| 0.63 | 0.0336 | -0.0346 |
| 0.67 | 0.301 | -0.0308 |
| 0.71 | 0.0263 | -0.0269 |
| 0.75 | 0.0223 | -0.0226 |
| 0.79 | 0.0181 | -0.0182 |
| 0.83 | 0.0137 | -0.0136 |
| 0.87 | 0.0093 | -0.0093 |
| 0.91 | 0.0056 | -0.0057 |
| 0.945 | 0.0028 | -0.0031 |
| 0.96 | 0.00235 | -0.00235 |
| 1.0 | 0.00445 | -0.00025 |

(*)Coordinates defined in the Vertol reference system, where the reference line approximately bisects the aft 50% of an airfoil.

## CHARACTERISTICS

- Thickness, t/c = 0.102
- Leading Edge Radius, r/c = 0.0158
- Center of Leading Edge Circle at x/c = 0.0158, y/c = -0.0225
- Trailing Edge Tab from x/c = 0.96 to x/c = 1.0

## TYPE OF DATA AND METHOD OF TEST

Two-dimensional tests in the Subsonic Insert of the Boeing Supersonic Wind Tunnel in Seattle, Wash.

Lift and pitching moments were determined with a balance.

Drag was determined by a traversing wake probe survey.

Model Chord = 6.38 in
Span = 12.0 in

## SOURCES


1) LaPrete, R., Storwick, E.M., Peterson, L.D., Boeing Wind Tunnel Test 927, Boeing Doc. No. D2-24066-1, 1966.

2) Eierman, R.L., Nyholm, J.R., Schreiber, R.E., Russell, J.H., Data Report BSWT 412, Boeing Doc. No. D6-20518, Dec. 1967.

3) Dadone, L.U., & McMullen, J., HLH/ATC Rotor System Two-Dimensional Airfoil Test, Boeing Doc. No. D301-10071-1, Dec. 1971.

V23010-1.58 WITH 3° T.E. TAB

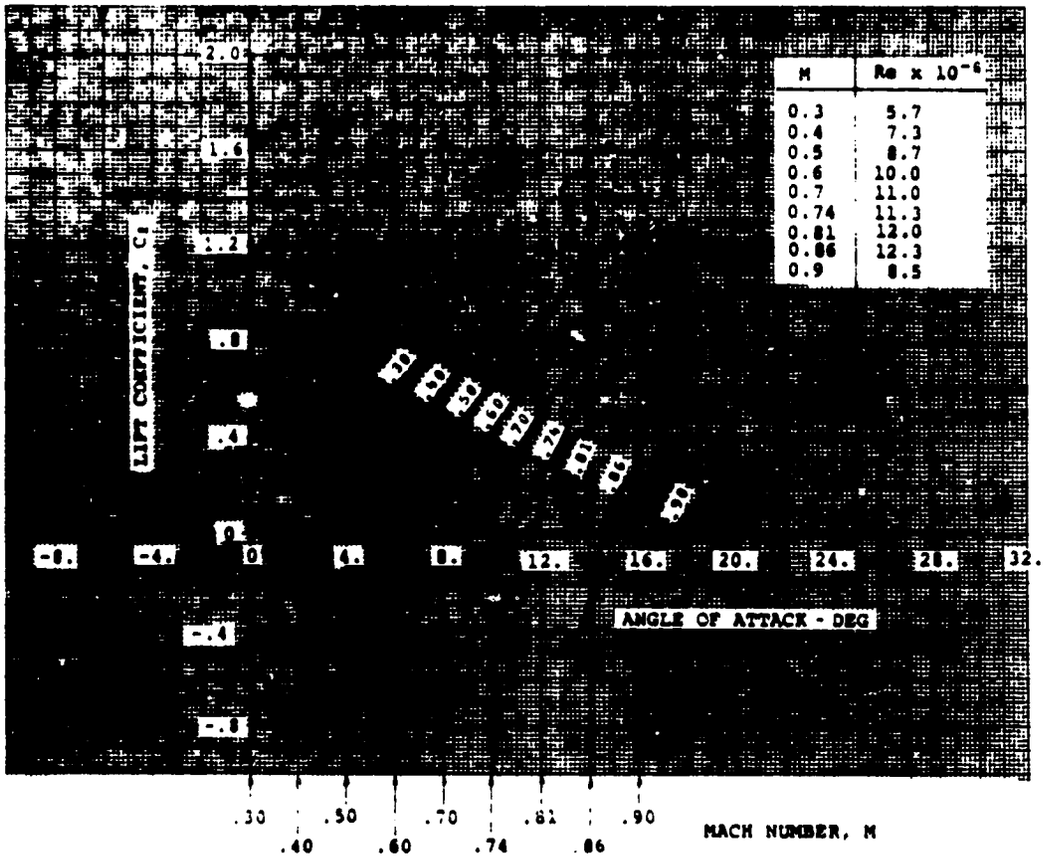


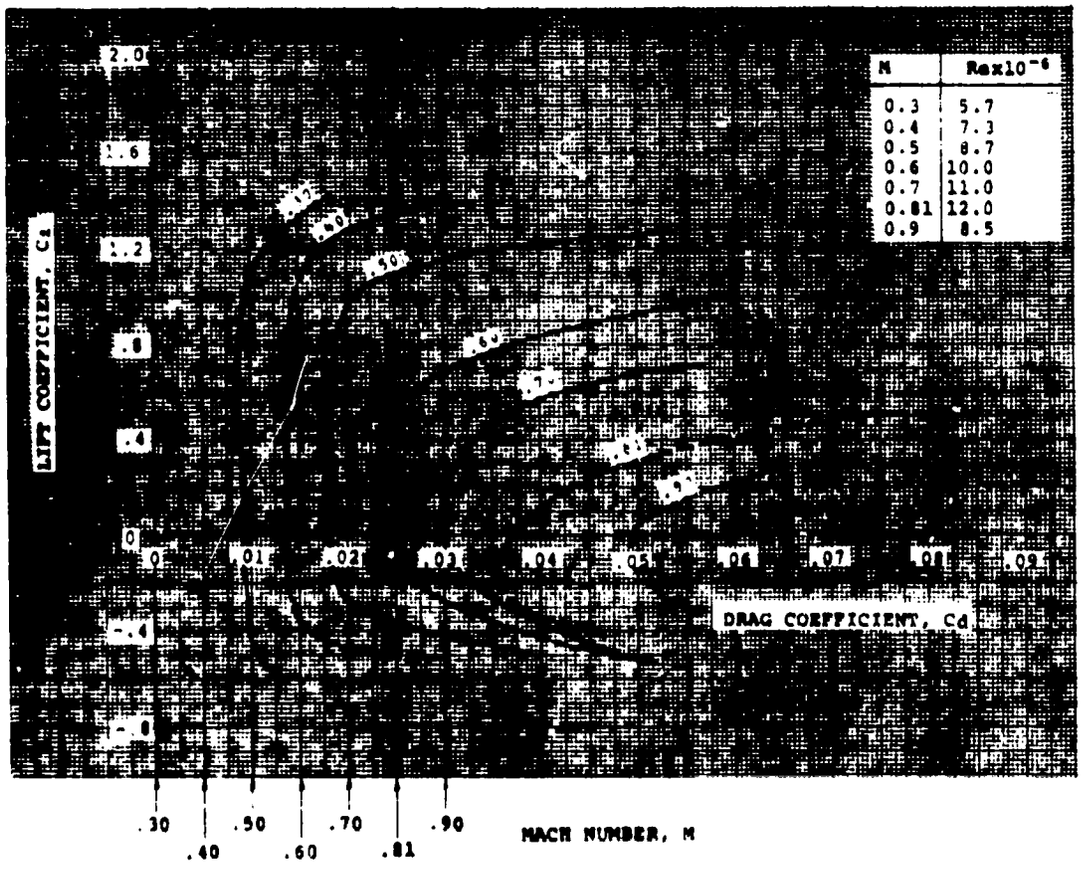

V23010-1.58 WITH 3° T.E. TAB

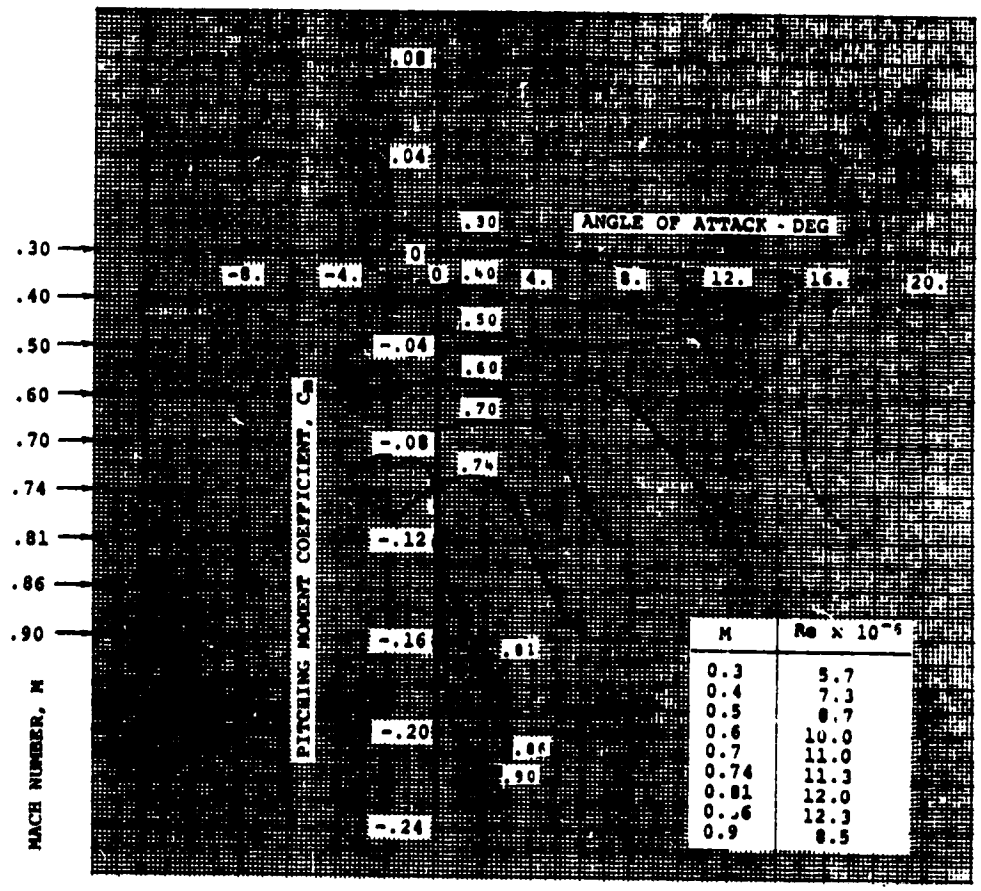

# AIRFOIL: V23010-1.58 With 0° T.E. Tab (Reverse Flow)

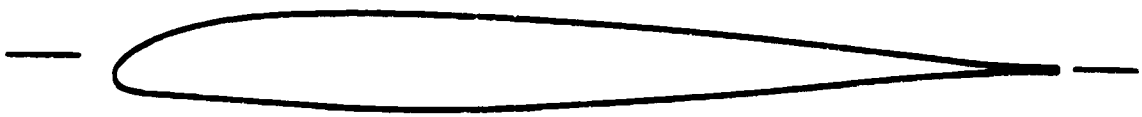

AIRFOIL COORDINATES (*)

| x/c | $y/c_u$ | $y/c_l$ |
|---|---|---|
| 0.0 | -0.0225 | -0.0225 |
| 0.005 | -0.0078 | -0.0329 |
| 0.01 | -0.0024 | -0.0362 |
| 0.015 | 0.0019 | -0.0378 |
| 0.025 | 0.0[illegible]6 | -0.0394 |
| 0.035 | 0.015. | -0.0404 |
| 0.047 | 0.0[illegible]4 | -0.0412 |
| 0.06 | 0.0[illegible] | -0.042 |
| 0.08 | 0.0[illegible] | -0.0434 |
| 0.11 | 0.0[illegible] | -0.0449 |
| 0.15 | 0.0485 | -0.0471 |
| 0.19 | 0.0482 | -0.0494 |
| 0.23 | 0.0499 | -0.0513 |
| 0.27 | 0.0499 | -0.0522 |
| 0.31 | 0.0497 | -0.05215 |
| 0.35 | 0.049 | -0.0517 |
| 0.39 | 0.048 | -0.0505 |
| 0.43 | 0.0465 | -0.0487 |
| 0.47 | 0.0446 | -0.0468 |
| 0.51 | 0.0424 | -0.044 |
| 0.55 | 0.0397 | -0.0412 |
| 0.59 | 0.0369 | -0.038 |
| 0.63 | 0.0336 | -0.0346 |
| 0.67 | 0.0301 | -0.0308 |
| 0.71 | 0.0263 | -0.0269 |
| 0.75 | 0.0223 | -0.0226 |
| 0.79 | 0.0181 | -0.0182 |
| 0.83 | 0.[illegible] | -0.0136 |
| 0.87 | 0.0093 | -0.0093 |
| 0.91 | 0.0056 | -0.0057 |
| 0.945 | 0.0028 | -0.0031 |
| 0.96 | 0.00235 | -0.00235 |
| 1.0 | 0.00235 | -0.00235 |

(*)Coordinates defined in the Vertol reference system, where the reference line approximately bisects the aft 50% of an airfoil.

## CHARACTERISTICS

- Thickness, t/c = 0.102
- Leading Edge Radius, r/c 0.0158
- Center of Leading Edge Circle at x/c = 0.0158, y/c = -0.0225
- Trailing Edge Tab from x/c = 0.96 to x/c = 1.0

**TYPE OF DATA AND METHOD OF TEST**

Two-dimensional test in the Subsonic Insert of the Boeing Supersonic Wind Tunnel in Seattle, Wash.

Lift and pitching moments were obtained by integration of surface differential static pressures.

A limited amount of drag data was acquired by a traversing wake probe survey.

The data was obtained over a range of angles of attack from 160° to 200°.

Model Chord = 6.38 in
Span = 12.0 in

**SOURCE**

Gray, L., Dadone, L.U., Gross, D.W., Child, R.F., Wind Tunnel Investigation of Airfoils Oscillating in Reverse Flow, USAAVLABS TR

1.3.270-2

V23010-1.58 WITH 0° T.E. TAB IN REVERSE FLOW

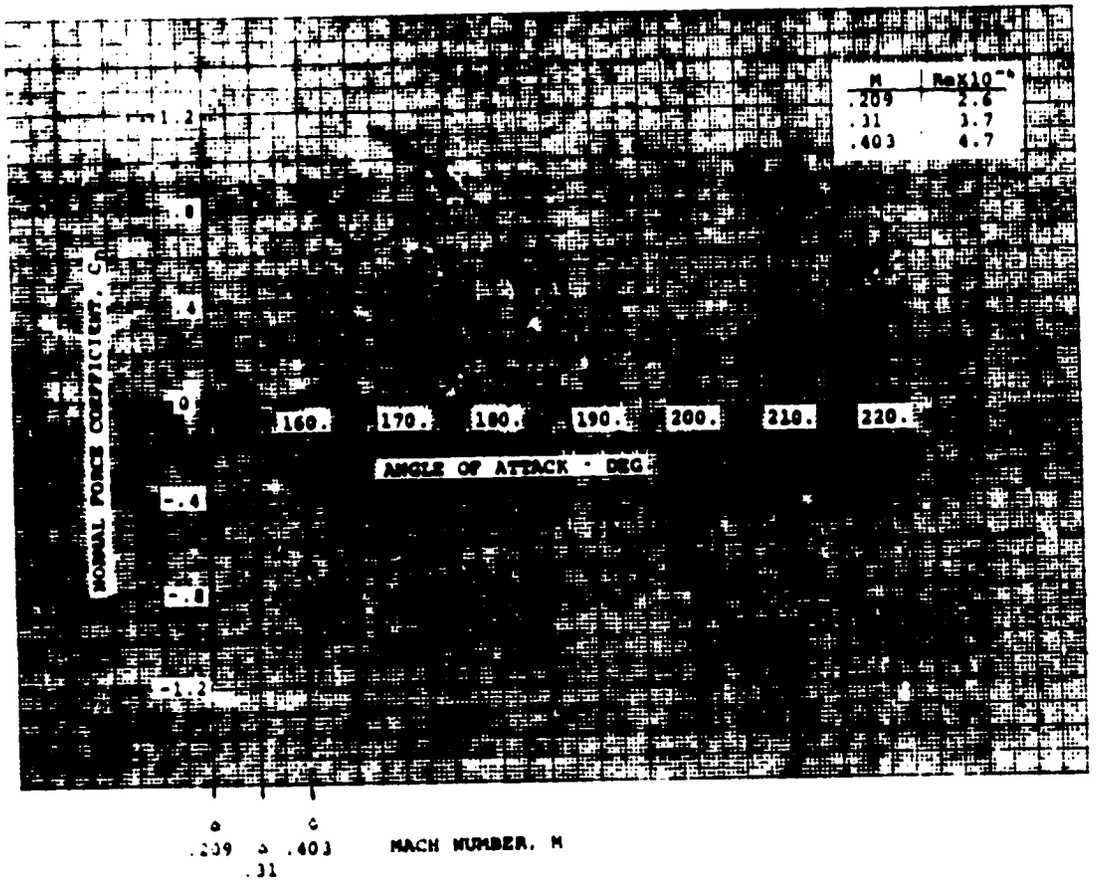


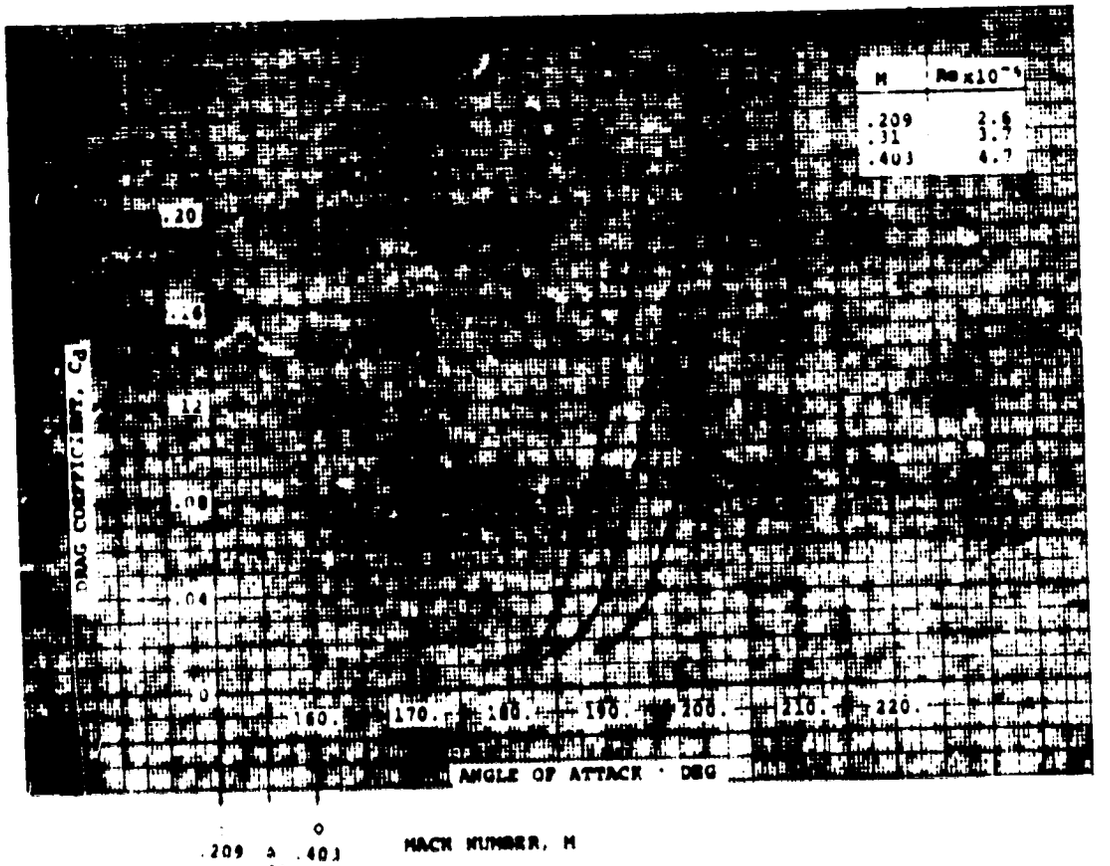

V23010-1.58 WITH 0° T.E. TAB IN REVERSE FLOW

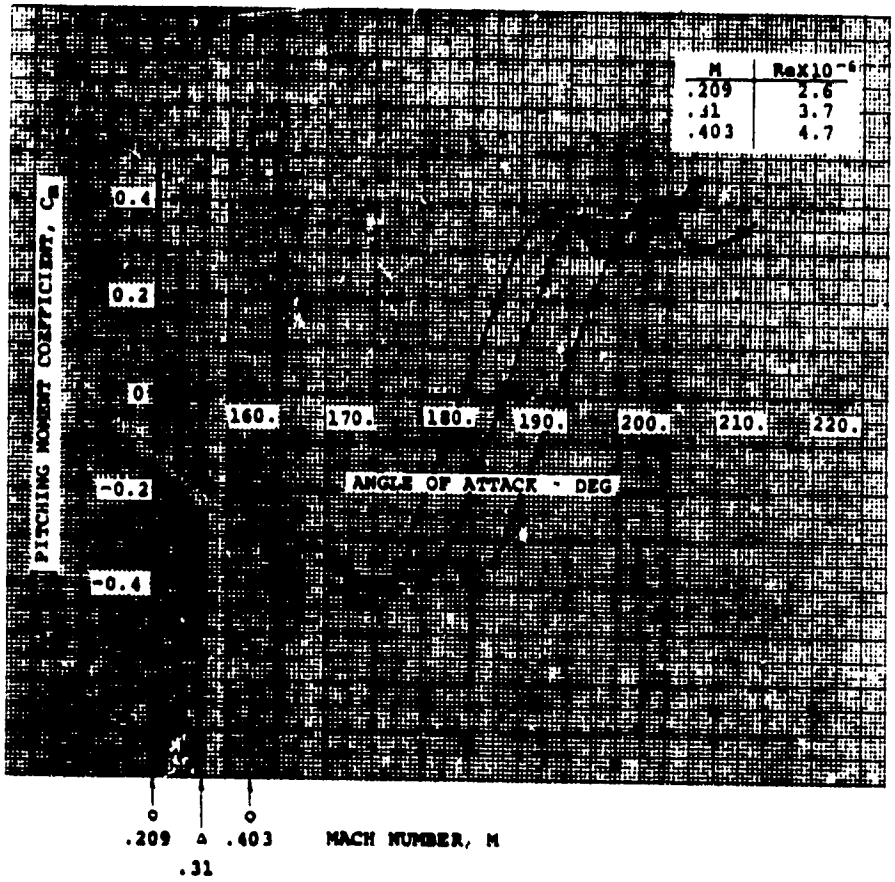

AIRFOIL: V23010-1.58 With -3° T.E. Tab (Reverse Flow)

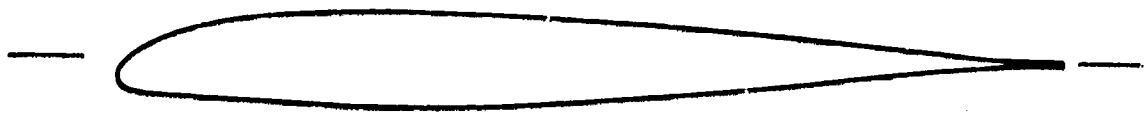

AIRFOIL COORDINATES (*)

| x/c | $y/c_u$ | $y/c_l$ |
|---|---|---|
| 0.0 | -0.0225 | -0.0225 |
| 0.005 | -0.0078 | -0.0329 |
| 0.01 | -0.0024 | -0.0362 |
| 0.015 | 0.0019 | -0.0378 |
| 0.025 | 0.0096 | -0.0394 |
| 0.035 | 0.0155 | -0.0404 |
| 0.047 | 0.0214 | -0.0412 |
| 0.06 | 0.0265 | -0.042 |
| 0.08 | 0.0327 | -0.0434 |
| 0.11 | 0.0396 | -0.0449 |
| 0.15 | 0.0455 | -0.0471 |
| 0.19 | 0.0489 | -0.0494 |
| 0.23 | 0.0499 | -0.0513 |
| 0.27 | 0.0499 | -0.0522 |
| 0.31 | 0.0497 | -0.05215 |
| 0.35 | 0.049 | -0.0517 |
| 0.39 | 0.048 | -0.0505 |
| 0.43 | 0.0465 | -0.0487 |
| 0.47 | 0.0446 | -0.0468 |
| 0.51 | 0.0424 | -0.044 |
| 0.55 | 0.0397 | -0.0412 |
| 0.59 | 0.0369 | -0.038 |
| 0.63 | 0.0336 | -0.0346 |
| 0.67 | 0.0301 | -0.0308 |
| 0.71 | 0.0263 | -0.0269 |
| 0.75 | 0.0223 | -0.0226 |
| 0.79 | 0.0181 | -0.0182 |
| 0.83 | 0.0137 | -0.0136 |
| 0.87 | 0.0093 | -0.0093 |
| 0.91 | 0.0056 | -0.0057 |
| 0.945 | 0.0028 | -0.0031 |
| 0.96 | 0.00235 | -0.00235 |
| 1.0 | 0.00445 | -0.00025 |

(*)Coordinates defined in the Vertol reference system, x are the reference line approximately bisects the aft 50% of an airfoil.

CHARACTERISTICS

- Thickness, t/c = 0.102
- Leading Edge Radius, r/c = 0.0158
- Center of Leading Edge Circle at x/c = 0.0138, y/c = -0.0225
- Trailing Edge Tab from x/c = 0.96 to x/c = 1.0

TYPE OF DATA AND METHOD OF TEST

Two-dimensional test in the Subsonic Insert of the Boeing Supersonic Wind Tunnel in Seattle, Wash.

Lift and pitching moments were obtained by integration of surface differential static pressures.

The data was obtained over a range of angles of attack from 160° to 200°.

Model Chord = 6.38 in
Span = 12.0 in

SOURCE

Gray, L., Dadone, L.U., Gross, D.W., Child, R.F., Wind Tunnel Investigation of Airfoils Oscillating in Reverse Flow, USAAVLABS TR

1.3.280-2

V23010-1.58 WITH -3° T.E. TAB IN REVERSE FLOW

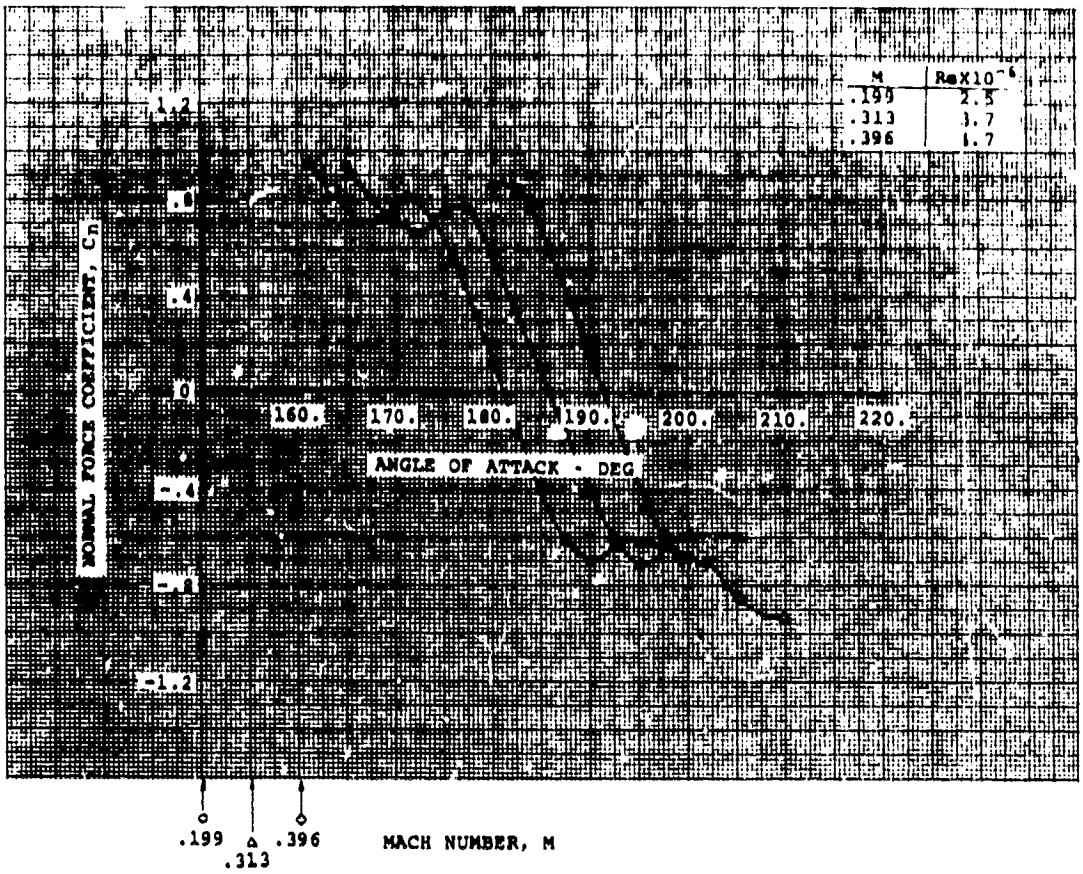

V23010-1.58 WITH -3° T.E. TAB IN REVERSE FLOW

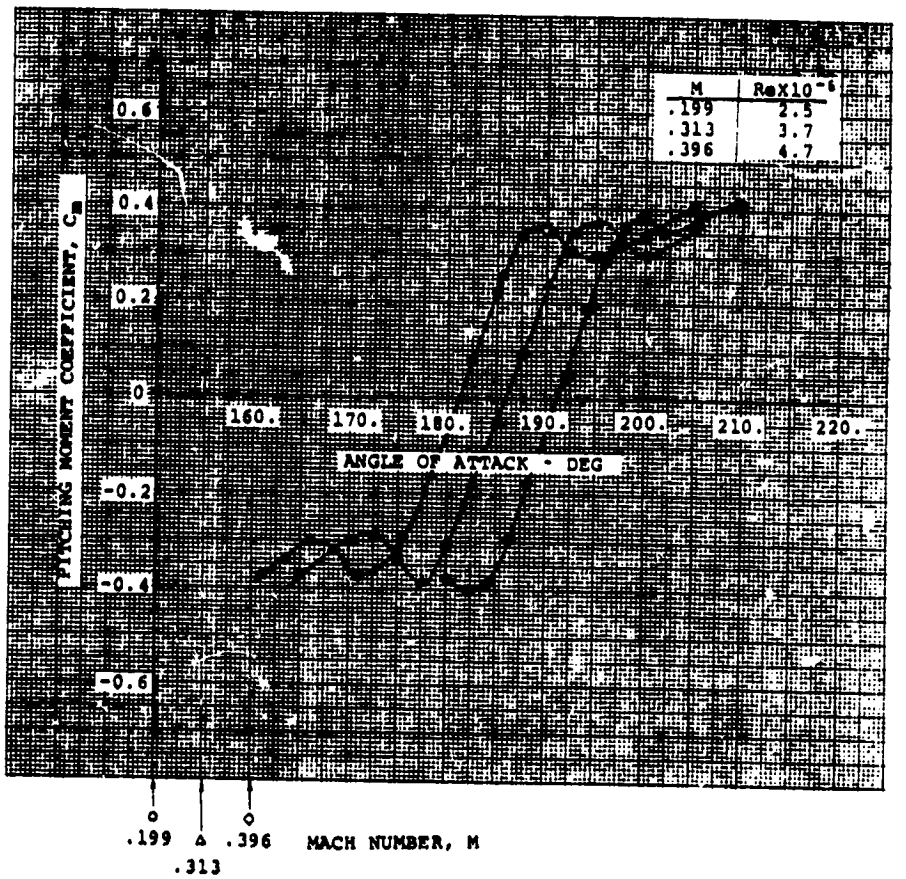

AIRFOIL: V23010-1.58 with +3° T.E. Tab (Reverse Flow)

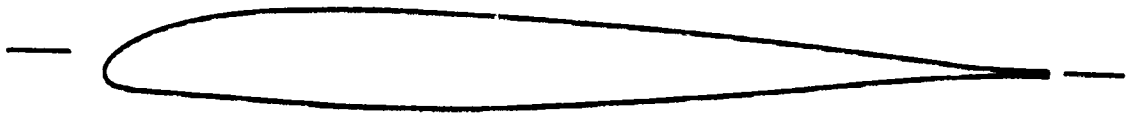

AIRFOIL COORDINATES (*)

| x/c | $y/c_u$ | $y/c_l$ |
|---|---|---|
| 0.0 | -0.0225 | -0.0225 |
| 0.005 | -0.0078 | -0.0329 |
| 0.01 | -0.0024 | -0.0362 |
| 0.015 | 0.0019 | -0.0378 |
| 0.025 | 0.0096 | -0.0394 |
| 0.035 | 0.0155 | -0.0404 |
| 0.047 | 0.0214 | -0.0412 |
| 0.06 | 0.0265 | -0.042 |
| 0.08 | 0.0327 | -0.0434 |
| 0.11 | 0.0396 | -0.0449 |
| 0.15 | 0.0455 | -0.0471 |
| 0.19 | 0.0489 | -0.0494 |
| 0.23 | 0.0499 | -0.0513 |
| 0.27 | 0.049 | -0.0517 |
| 0.39 | 0.048 | -0.0505 |
| 0.43 | 0.0465 | -0.0487 |
| 0.47 | 0.0446 | -0.0468 |
| 0.51 | 0.0424 | -0.044 |
| 0.55 | 0.0397 | -0.0412 |
| 0.59 | 0.0369 | -0.038 |
| 0.63 | 0.0336 | -0.0346 |
| 0.67 | 0.0301 | -0.0308 |
| 0.71 | 0.0263 | -0.0269 |
| 0.75 | 0.0223 | -0.0226 |
| 0.79 | 0.0181 | -0.0182 |
| 0.83 | 0.0137 | -0.0136 |
| 0.87 | 0.0093 | -0.0093 |
| 0.91 | 0.0056 | -0.0057 |
| 0.945 | 0.0028 | -0.0031 |
| 0.96 | 0.00235 | -0.00235 |
| 1.0 | 0.00025 | -0.00445 |

(*)Coordinates defined in the Vertol reference system, where the reference line approximately bisects the aft 50% of an airfoil.

CHARACTERISTICS

- Thickness, t/c = 0.102
- Leading Edge Radius, r/c = 0.0158
- Center of Leading Edge Circle at x/c = 0.0158, y/c = -0.0225
- Trailing Edge Tab from x/c = 0.96 to x/c = 1.0

TYPE OF DATA AND METHOD OF TEST

Two-dimensional test in the Subsonic Insert of the Boeing Supersonic Wind Tunnel in Seattle, Wash.

Lift and pitching moments were obtained by integration of surface differential static pressures.

The data was obtained over a range of angles of attack from 160° to 200°.

Model Chord = 6.38 in
Span = 12.0 in

SOURCE

Gray, L., Dadone, L.U., Gross, G.W., Child, R.F., Wind Tunnel Investigation of Airfoils Oscillating in Reverse Flow, USAAVLABS TR

1.3.290-2

V23010-1.58 WITH +3° T.E. TAB IN REVERSE FLOW

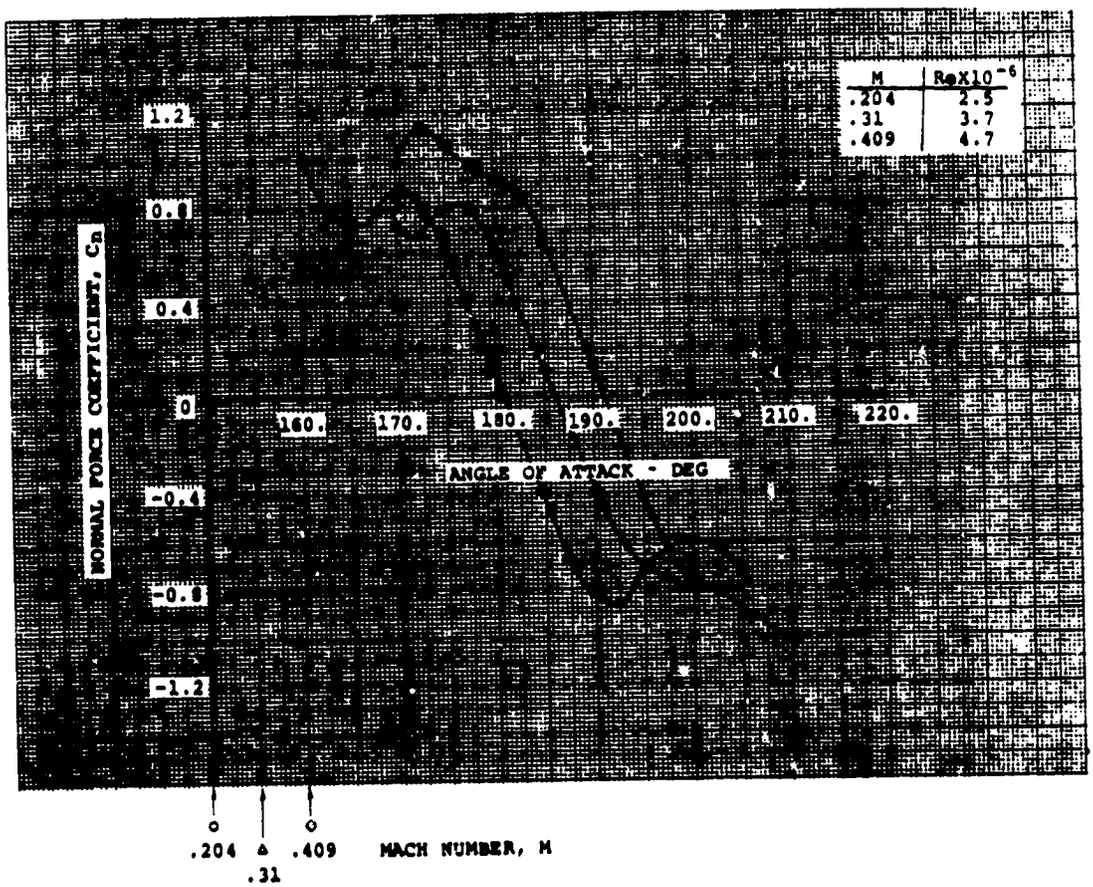

V23010-1.58 WITH +3° T.E. TAB IN REVERSE FLOW

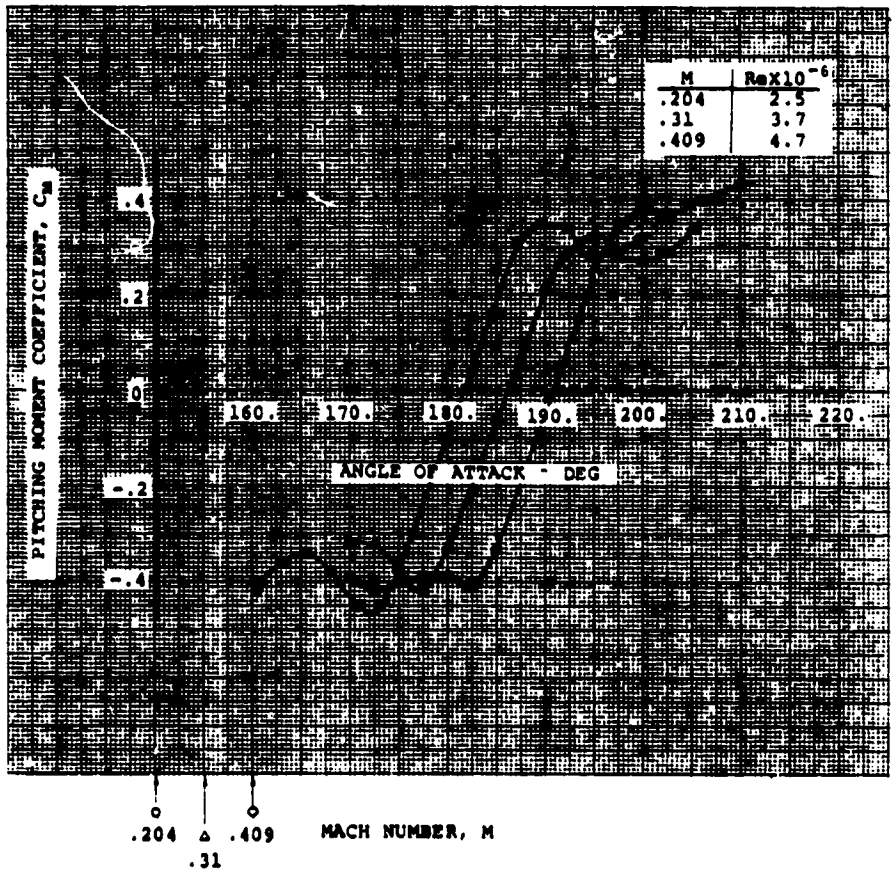

AIRFOIL: V43012-1.58 With 0° T.E. Tab 1.3.300

AIRFOIL COORDINATES

| x/c | $y/c_u$ | $y/c_l$ |
|---|---|---|
| 0.0 | 0.0 | 0.0 |
| .01 | .0321 | -.0077 |
| .02 | .0423 | -.0090 |
| .03 | .0503 | -.0100 |
| .04 | .0571 | -.0108 |
| .05 | .0631 | -.0108 |
| .075 | .0745 | -.0110 |
| .09 | .0791 | -.0115 |
| .11 | .0840 | -.0130 |
| .125 | .0869 | -.0142 |
| .15 | .0901 | -.0167 |
| .18 | .0920 | -.0200 |
| .21 | .0929 | -.0231 |
| .245 | .0926 | -.0260 |
| .28 | .0920 | -.0281 |
| .32 | .0905 | -.0299 |
| .36 | .0880 | -.0310 |
| .40 | .0850 | -.0315 |
| .44 | .0820 | -.0314 |
| .48 | .0780 | -.0310 |
| .52 | .0733 | -.0304 |
| .56 | .0685 | -.0293 |
| .60 | .0635 | -.0279 |
| .64 | .0582 | -.0263 |
| .68 | .0527 | -.0244 |
| .72 | ..0469 | -.0222 |
| .76 | .0410 | -.0198 |
| .80 | .0350 | -.0172 |
| .83 | .0301 | -.0149 |
| .86 | .0253 | -.0125 |
| .89 | .0203 | -.0100 |
| .91 | .0167 | -.0084 |
| .925 | .0140 | -.0070 |
| .94 | .0113 | -.0057 |
| .955 | .0084 | -.0043 |
| .98 | .0038 | -.0020 |
| 1.0 | .00235 | -.00235 |
| 1.10 | .00235 | -.00235 |

CHARACTERISTICS

- Thickness, t/c = 0.12
- Leading Edge Circle,
  r/c = 0.0158
  Center at x/c = 0.0138
  y/c = 0.0077
- Trailing Edge Tab
  from x/c = 1.00
  to x/c = 1.10

TYPE OF DATA AND METHOD OF TEST

Two-dimensional test in the Subsonic Insert of the Boeing Supersonic Wind Tunnel in Seattle, Wash.

Lift and pitching moments were measured with a balance

Pitching moments were reduced about 0.25.c of the nominal chord without the T.E. extension. Drag was determined by a traversing wake probe survey.

Model Chord = 7.018 in (including 10% T.E. extension)
Span = 12.0 in

SOURCE

Dadone, L., & McMullen, J., HLH/ATC Rotor System Two-Dimensional Airfoil Test, Boeing Document D301-10071-1, December 1971.

NOTE:

1) The V43012-1.58 non-dimensional coefficients were determined by using the total 7.018 in. chord.

V43012-1.58 WITH 0° T.E. TAB

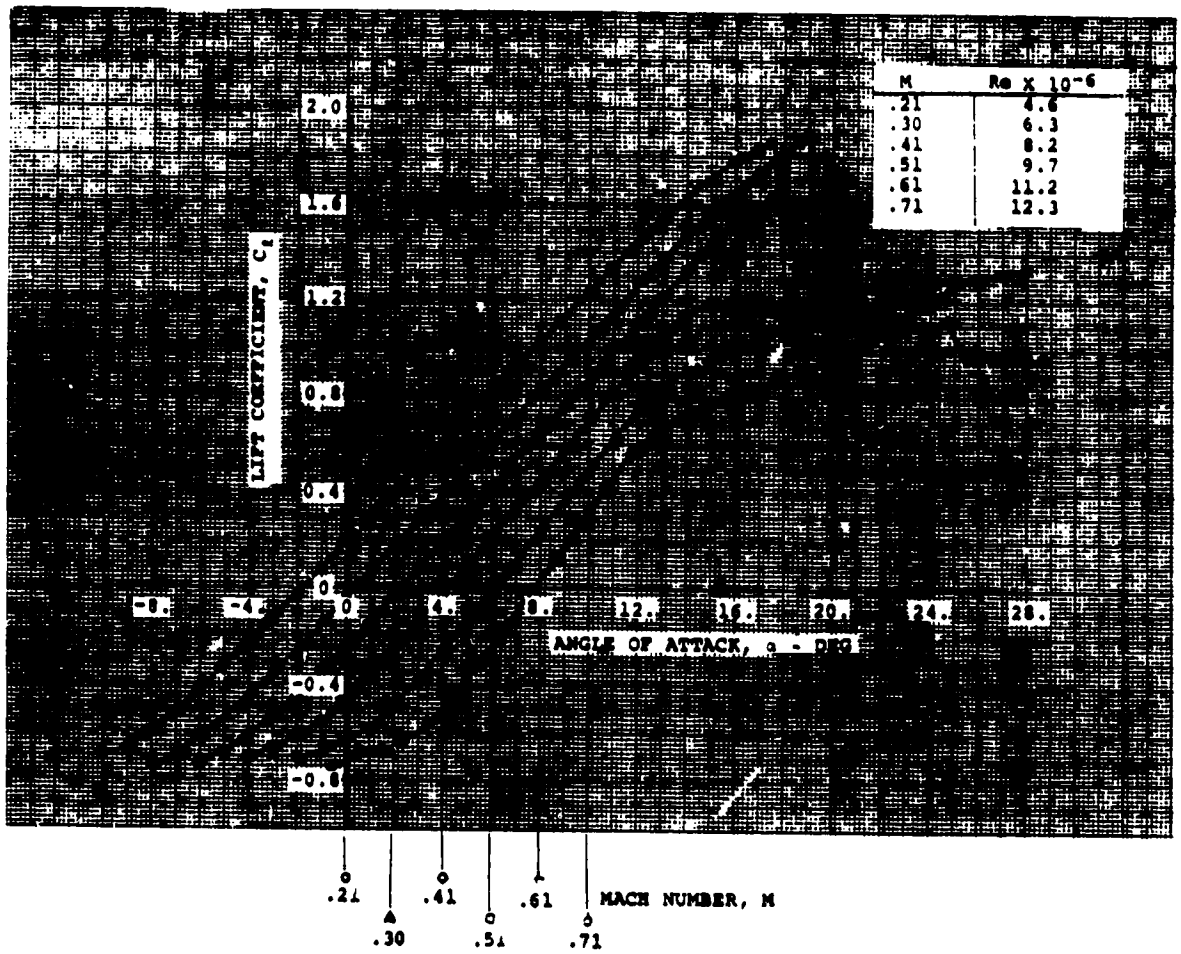


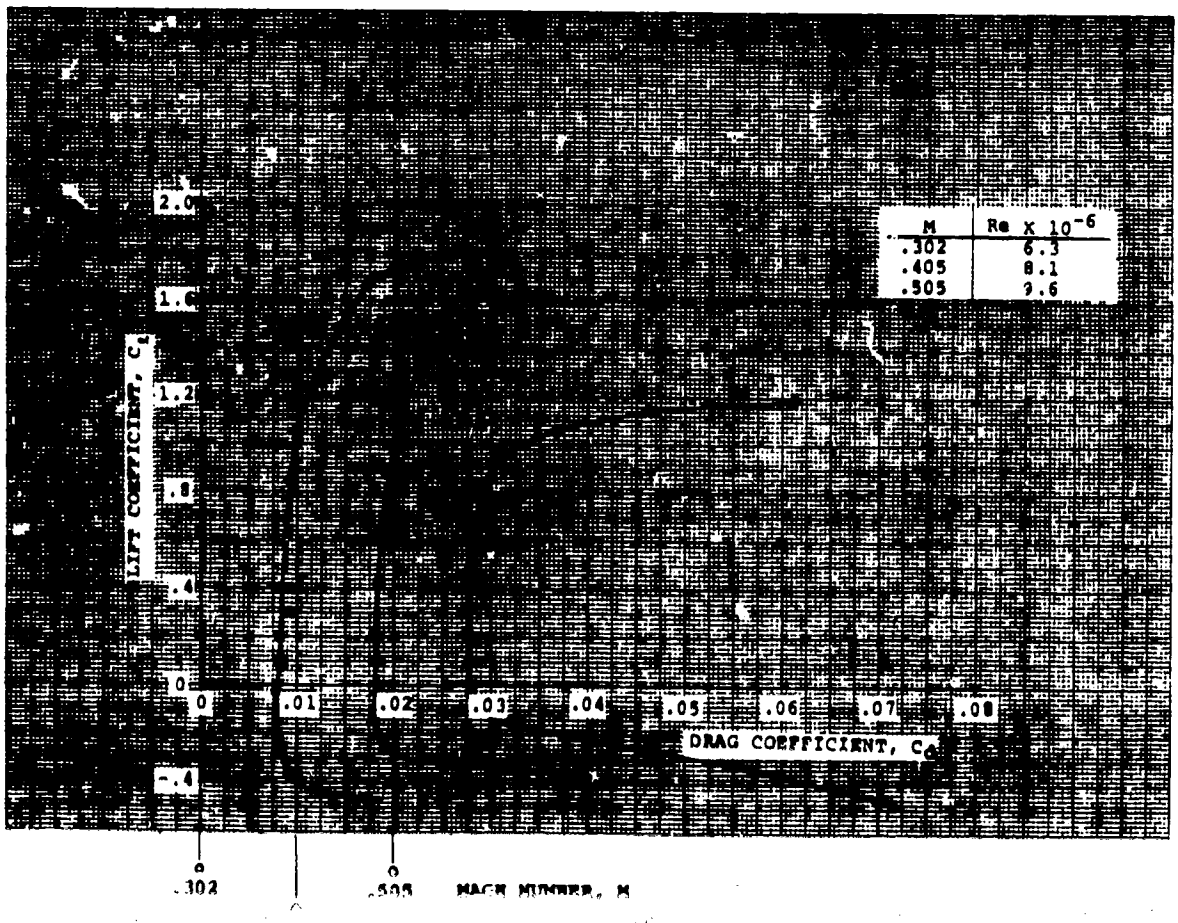

V43012-1.58 WITH 0° T.E. TAB

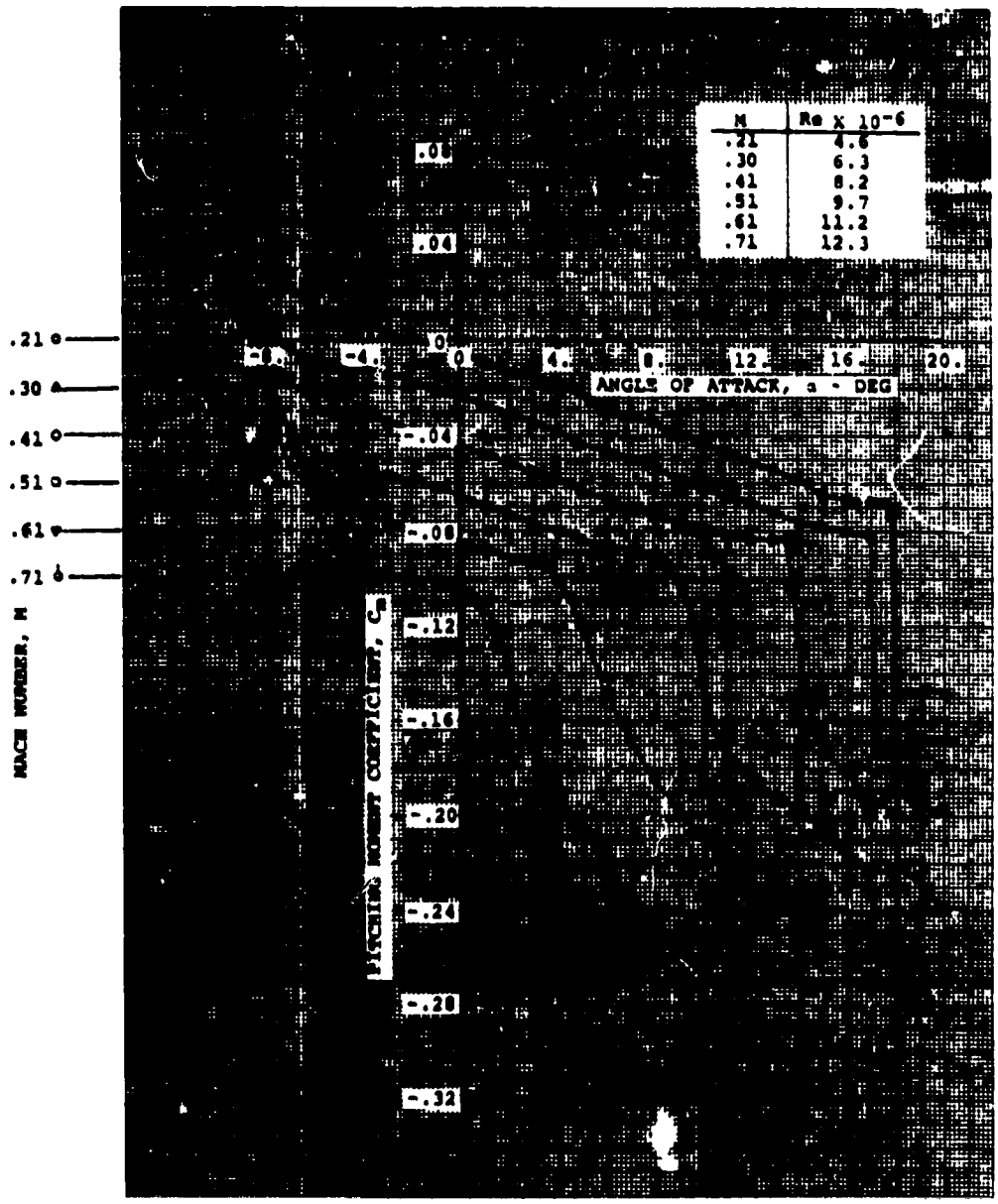

AIRFOIL: V43012-1.58 With -6° T.E. Tab 1.3.310

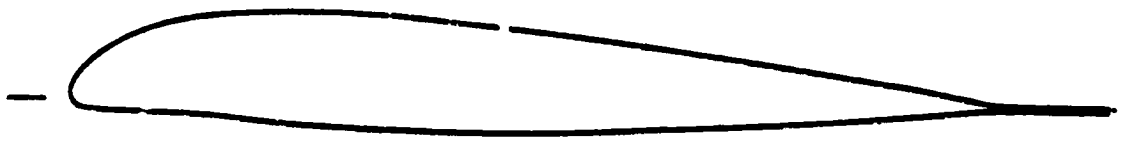

**AIRFOIL COORDINATES**

| x/c | $y/c_u$ | $y/c_l$ |
|---|---|---|
| 0.0 | 0.0 | 0.0 |
| .01 | .0321 | -.0077 |
| .02 | .0423 | -.0090 |
| .03 | .0503 | -.0100 |
| .04 | .0571 | -.0108 |
| .05 | .0631 | -.0108 |
| .075 | .0745 | -.0110 |
| .09 | .0791 | -.0115 |
| .11 | .0840 | -.0130 |
| .125 | .0869 | -.0142 |
| .15 | .0901 | -.0167 |
| .18 | .0920 | -.0200 |
| .21 | .0929 | -.0231 |
| .245 | .0926 | -.0260 |
| .28 | .0920 | -.0281 |
| .32 | .0905 | -.0299 |
| .36 | .0880 | -.0310 |
| .40 | .0850 | -.0315 |
| .44 | .0820 | -.0314 |
| .48 | .0780 | -.0310 |
| .52 | .0733 | -.0304 |
| .56 | .0685 | -.0293 |
| .60 | .0635 | -.0279 |
| .64 | .0582 | -.0263 |
| .68 | .0527 | -.0244 |
| .72 | .0469 | -.0222 |
| .76 | .0410 | -.0198 |
| .80 | .0350 | -.0172 |
| .83 | .0301 | -.0149 |
| .86 | .0253 | -.0125 |
| .89 | .0203 | -.0100 |
| .91 | .0167 | -.0084 |
| .925 | .0140 | -.0070 |
| .94 | .0113 | -.0057 |
| .955 | .0084 | -.0043 |
| .98 | .0038 | -.0020 |
| 1.0 | .00235 | -.00235 |
| 1.05 | .00235 | -.00235 |
| 1.10 | .00760 | +.00290 |

**CHARACTERISTICS**

- Thickness, t/c = 0.12
- Leading Edge Circle,
  r/c = 0.0158
  Center at x/c = 0.0138
  y/c = 0.0077
- Trailing Edge Tab Extension
  from x/c = 1.00
  to x/c = 1.10
  Tab Deflected at x/c = 1.05

TYPE OF DATA AND METHOD OF TEST

Two-dimensional test in the Subsonic Insert of the Boeing Supersonic Wind Tunnel in Seattle, Wash.

Lift and pitching moments were measured with a balance.

Pitching moments were resolved about 0.25.c of the nominal chord without the T.E. extension.

Model Chord = 7.018 in
(including 10% T.E. extension)
Span = 12.0 in

SOURCE

Dadone, L., & McMullen, J., HLH/ATC Rotor System Two-Dimensional Airfoil Test, Boeing Document D301-10071-1, December 1971.

NOTE:

1) The V43012-1.58 non-dimensional coefficients were determined by using the total 7.018 in. chord.

1.3.310-2

V43012-1.58 WITH -6° T.E. TAB

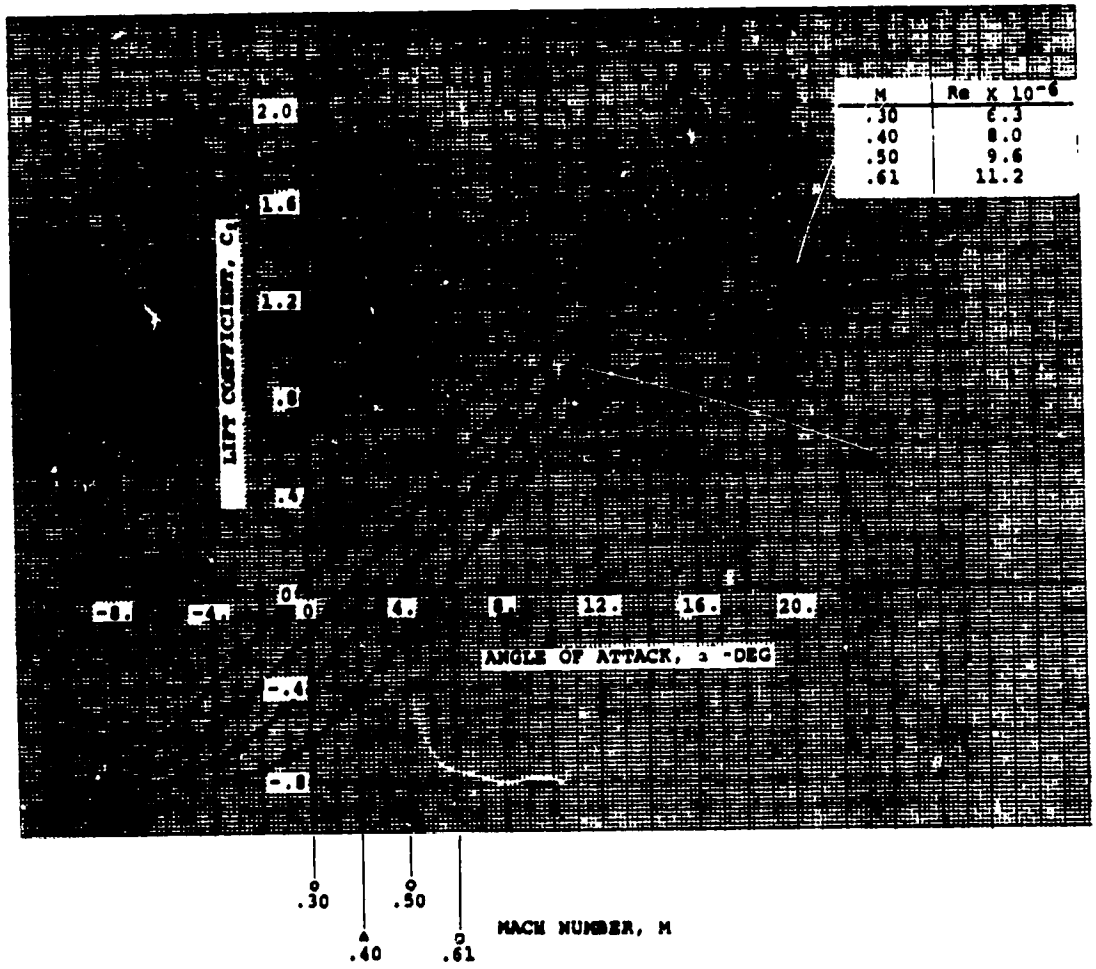

V43012-1.58 WITH -6° T.E. TAB

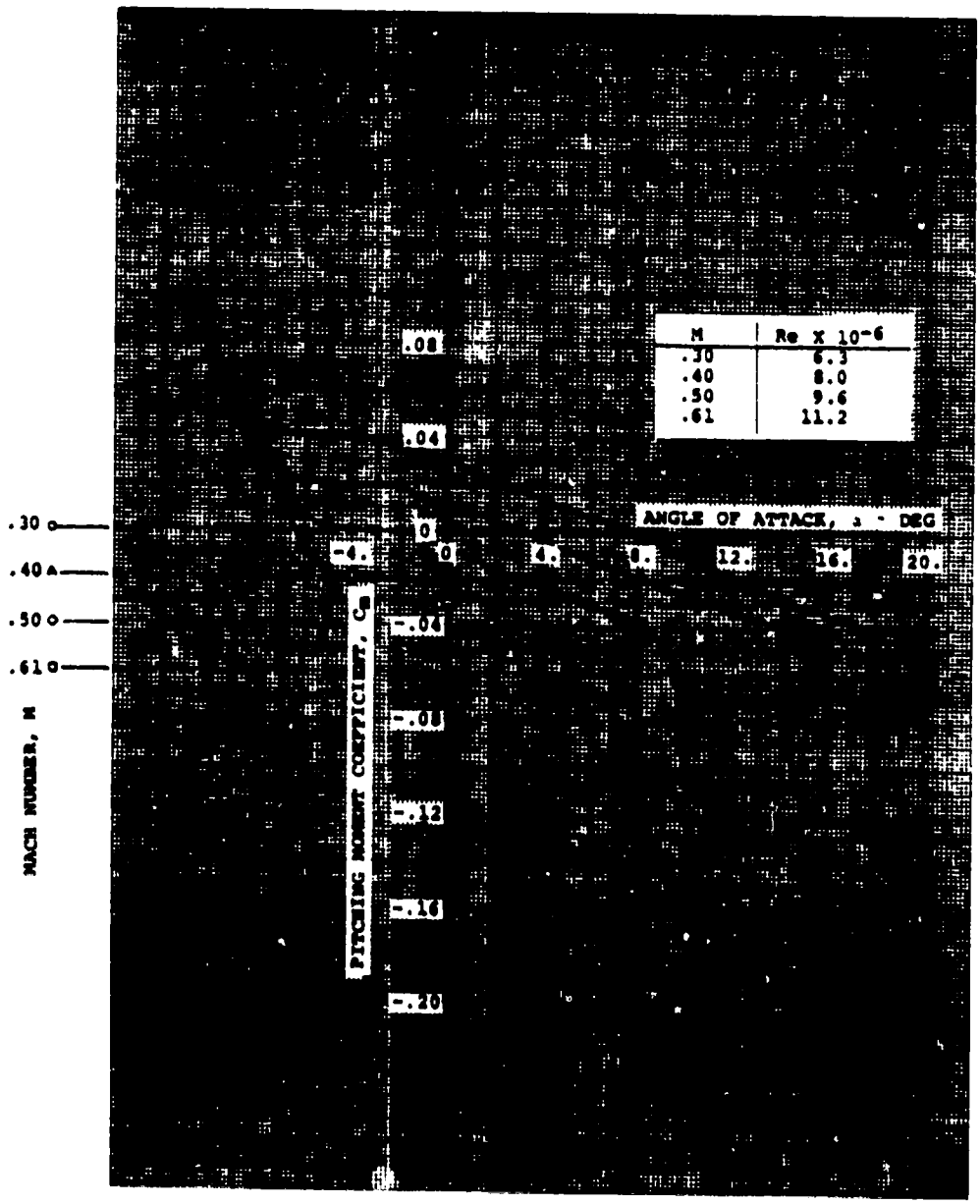

AIRFOIL: SA 13109-1.58 1.3.320

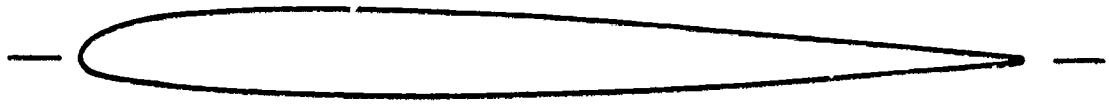

AIRFOIL COORDINATES

| $x/c_u$ | $y/c_u$ | $x/c_l$ | $y/c_l$ |
|---|---|---|---|
| 0.0 | 0. | 0. | 0. |
| .0100 | .0192 | .0150 | -.0153 |
| .0221 | .0268 | .0280 | -.0194 |
| .0472 | .0365 | .0528 | -.0237 |
| .0729 | .0429 | .0771 | -.0262 |
| .0986 | .0472 | .1014 | -.0280 |
| .1500 | .0519 | .1500 | -.0311 |
| .2007 | .0535 | .1993 | -.0337 |
| .2508 | .0537 | .2492 | -.0357 |
| .3008 | .0531 | .2992 | -.0369 |
| .4007 | .0503 | .3993 | -.0374 |
| .5006 | .0454 | .4994 | -.0358 |
| .6005 | .0387 | .5995 | -.0321 |
| .7003 | .0306 | .6997 | -.0265 |
| .8002 | .0214 | .7998 | -.0194 |
| .9001 | .0114 | .8999 | -.0108 |
| .9500 | .0062 | .9500 | -.0060 |
| 1. | .0009 | 1. | -.0009 |

CHARACTERISTICS

- NACA 13109 Modified
- Leading Edge Radius, 0.0158c

TYPE OF DATA AND METHOD OF TEST

Two-dimensional test in the S3 MA Subsonic-Transonic Onera Wind Tunnel in Modane.

Lift, drag and pitching moments were calculated by pressure distribution integration.

Uncorrected results.

Model Chord = 0.21 m
Span = 0.56 m

SOURCE

PV d'Essais Onera No. 1 - 604 GY fascicule 1/4
Essais En Courant De Profils De Pale D'Helicoptere Pour Sud-Avaiation - Profil SA 131 09 1.58

SA13109-1.58

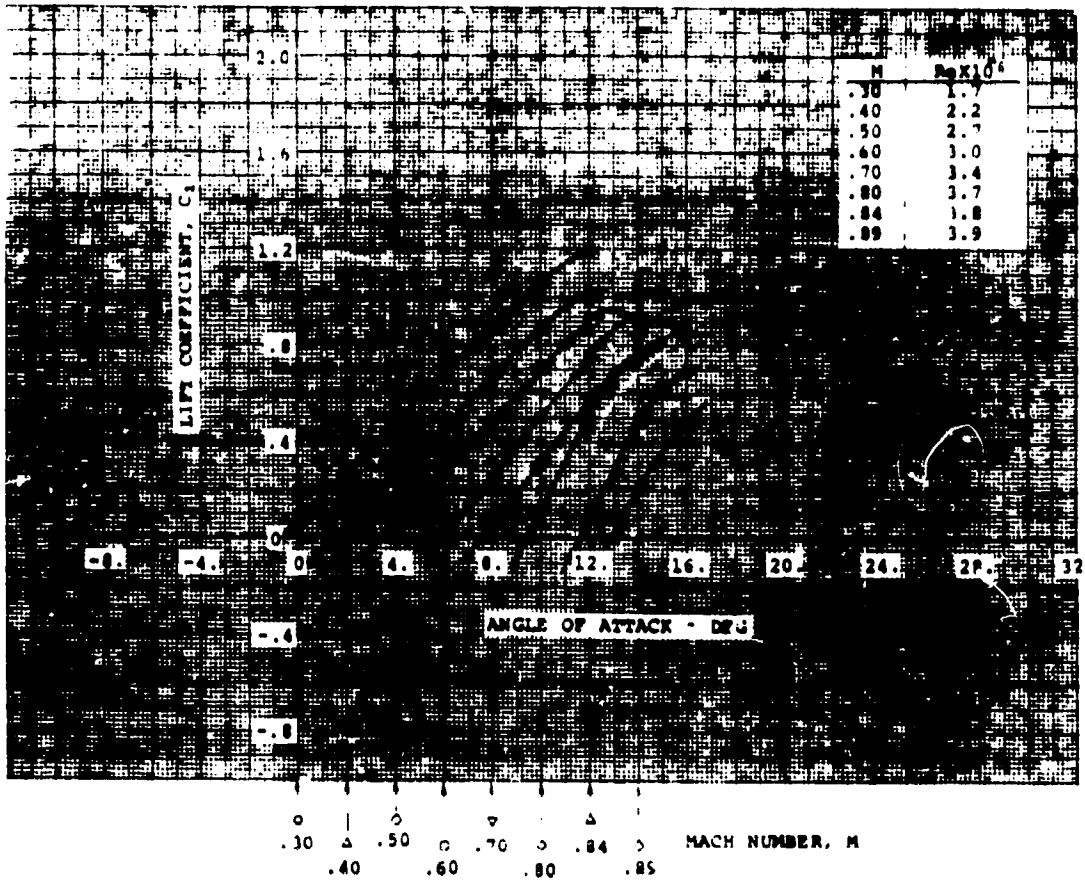
LIFT COEFFICIENT, $C_L$
2.0
1.6
1.2
.8
.4
0
-.4
-.8
-8.
-4.
0
4.
8.
12.
16.
20
24.
28.
32.
ANGLE OF ATTACK - DEG
M
Re X10⁶
.30
1.7
.40
2.2
.50
2.7
.60
3.0
.70
3.4
.80
3.7
.84
3.8
.89
3.9
.30
.40
.50
.60
.70
.80
.84
.85
MACH NUMBER, M

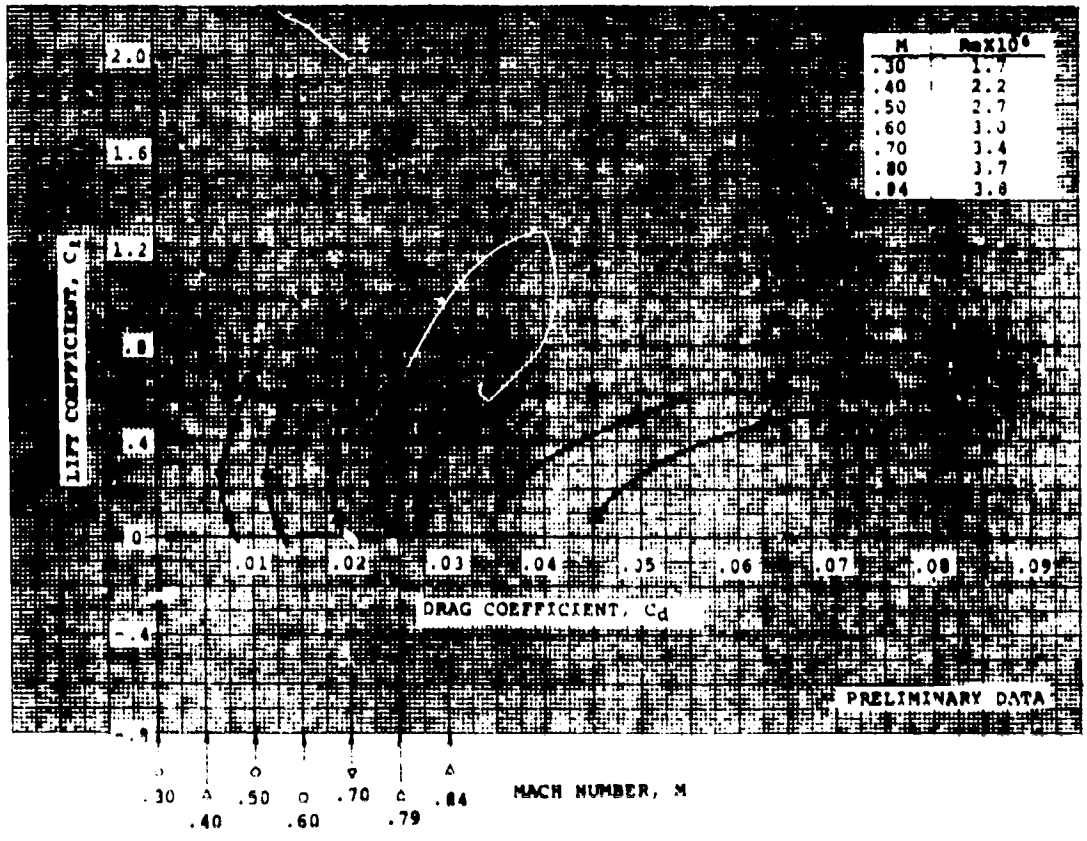
LIFT COEFFICIENT, $C_L$
2.0
1.6
1.2
.8
.4
0
-.4
-.8
.01
.02
.03
.04
.05
.06
.07
.08
.09
DRAG COEFFICIENT, Cd
M
Re X10⁶
.30
1.7
.40
2.2
.50
2.7
.60
3.0
.70
3.4
.80
3.7
.84
3.8
* PRELIMINARY DATA
.30
.40
.50
.60
.70
.79
.84
MACH NUMBER, M

SA13109-1.5R

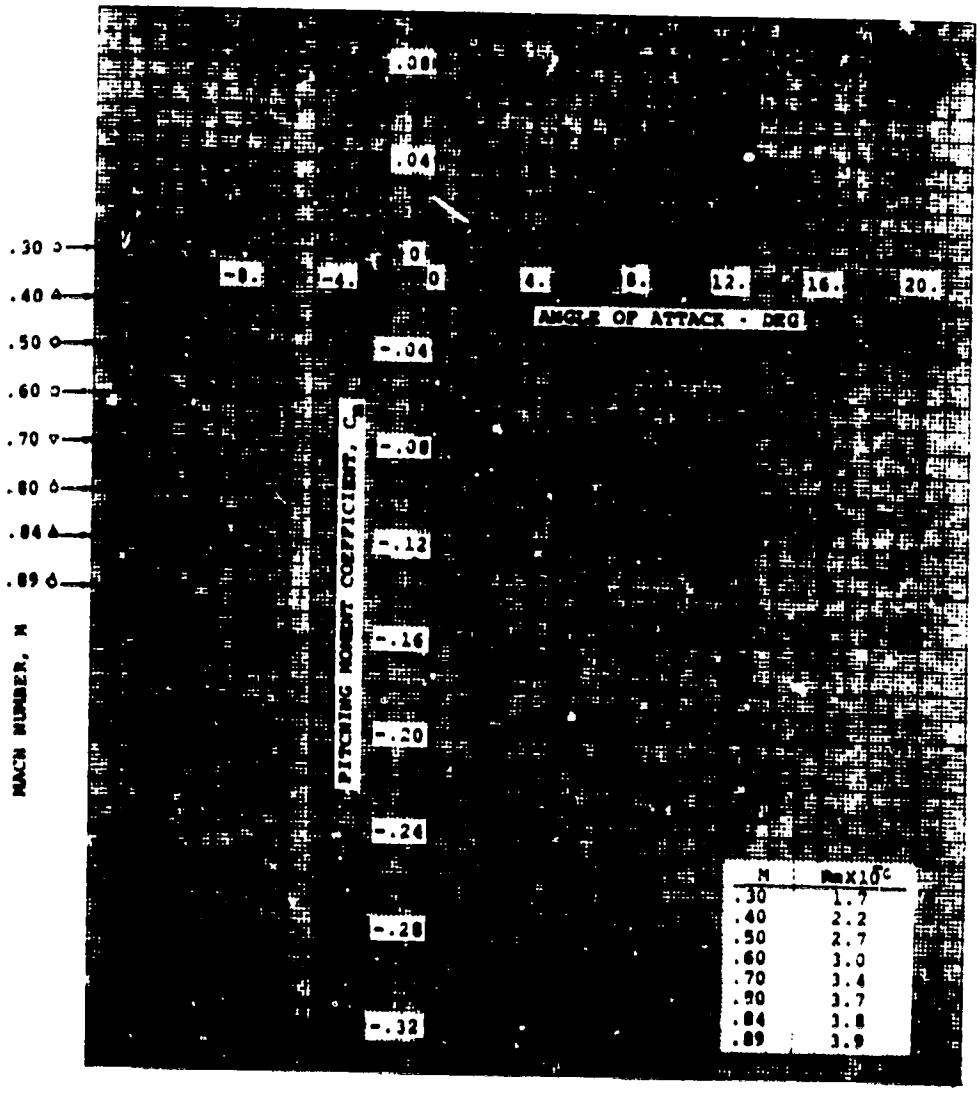
.08
.04
0
-.04
-.08
-.12
-.16
-.20
-.24
-.28
-.32
PITCHING MOMENT COEFFICIENT, $C_m$
-8.
-4.
0
4.
8.
12.
16.
20.
ANGLE OF ATTACK - DEG
.30
.40
.50
.60
.70
.80
.84
.89
MACH NUMBER, M
M | $R_m \times 10^6$
.30 | 1.7
.40 | 2.2
.50 | 2.7
.60 | 3.0
.70 | 3.4
.80 | 3.7
.84 | 3.8
.89 | 3.9

## AIRFOIL COORDINATES

| x/c | $y/c_u$ |
|---|---|
| 0.0 | -0.01366 |
| 0.00443 | -0.00155 |
| 0.00586 | +0.00001 |
| 0.00857 | 0.00268 |
| 0.01359 | 0.00649 |
| 0.01726 | 0.00893 |
| 0.02172 | 0.01163 |
| 0.02589 | 0.01392 |
| 0.03065 | 0.01633 |
| 0.03602 | 0.01883 |
| 0.04209 | 0.02140 |
| 0.04905 | 0.02407 |
| 0.05297 | 0.02545 |
| 0.05723 | 0.02687 |
| 0.06183 | 0.02832 |
| 0.06682 | 0.02980 |
| 0.07227 | 0.03131 |
| 0.07828 | 0.03306 |
| 0.08152 | 0.03365 |
| 0.08495 | 0.03476 |
| 0.08858 | 0.03528 |
| 0.09244 | 0.03612 |
| 0.09656 | 0.03698 |
| 0.10098 | 0.03786 |
| 0.10574 | 0.03876 |
| 0.11076 | 0.03969 |
| 0.11622 | 0.04065 |
| 0.12239 | 0.04165 |
| 0.12928 | 0.04271 |
| 0.13688 | 0.04381 |

Coordinates continued on page 1.3.330-4

## CHARACTERISTICS

- Thickness, t/c = 0.113
- Leading edge radius: r/c = 0.01883, with center at x/c = 0.01883, y/c = -0.0137
- Profile is circular for 40° of arc on upper surface
- Profile joins smoothly with NACA 0012 shape at x/c = 0.28333 on the upper surface and at x/c = 0.3409 on the lower surface

### TYPE OF DATA AND METHOD OF TESTS

The wind tunnel tests were carried out in the National Physical Laboratory, NPL, 36 in. x 14 in. (0.92 m x 0.36 m) transonic tunnel, at Teddington, Middlesex, England.

Lift and pitching moments were found by integration of surface static pressures. Profile drag was determined by wake measurements.

All measurements were obtained with a roughness band of 230-270 mesh carborundum between 0 and 2% chord on both surfaces. The floor and the ceiling of the test section were slotted. No corrections for wall constraints have been applied to the data.

Model Chord = 10 in (25.4 cm)
Span = 14 in (35.6 cm)

### SOURCE

Gregory, N., Wilby, P.G., NPL 9615 and NACA 0012. A Comparison of Aerodynamic Data, ARC C.P. No. 1261, 1973.

NPL 9615

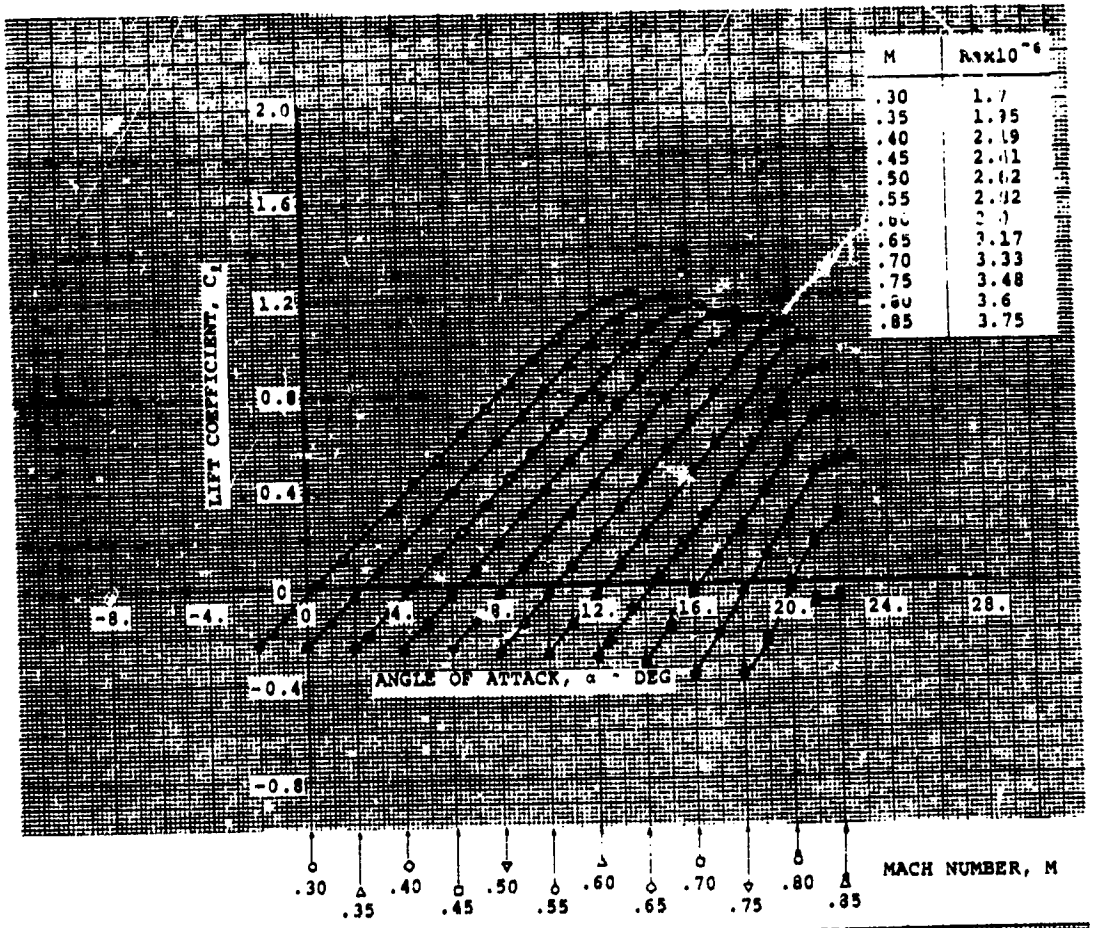
M
Rex10⁻⁶
.30 1.7
.35 1.95
.40 2.19
.45 2.41
.50 2.62
.55 2.82
.60
.65 3.17
.70 3.33
.75 3.48
.80 3.6
.85 3.75
LIFT COEFFICIENT, $C_L$
2.0
1.6
1.2
0.8
0.4
0
-0.4
-0.8
-8.
-4.
0
4.
8.
12.
16.
20.
24.
28.
ANGLE OF ATTACK, α - DEG
.30 .35 .40 .45 .50 .55 .60 .65 .70 .75 .80 .85
MACH NUMBER, M

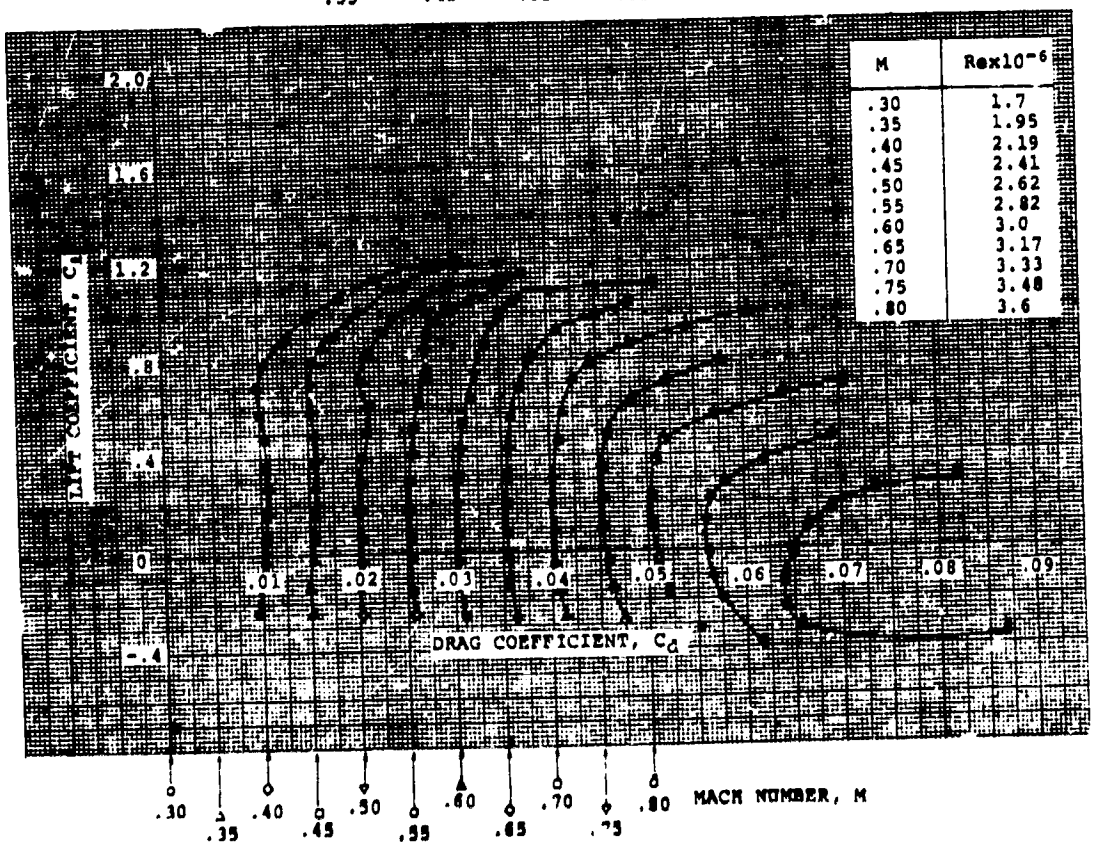
M
Rex10⁻⁶
.30 1.7
.35 1.95
.40 2.19
.45 2.41
.50 2.62
.55 2.82
.60 3.0
.65 3.17
.70 3.33
.75 3.48
.80 3.6
LIFT COEFFICIENT, $C_L$
2.0
1.6
1.2
.8
.4
0
-.4
.01
.02
.03
.04
.05
.06
.07
.08
.09
DRAG COEFFICIENT, $C_d$
.30 .35 .40 .45 .50 .55 .60 .65 .70 .75 .80
MACH NUMBER, M

NPL 9615

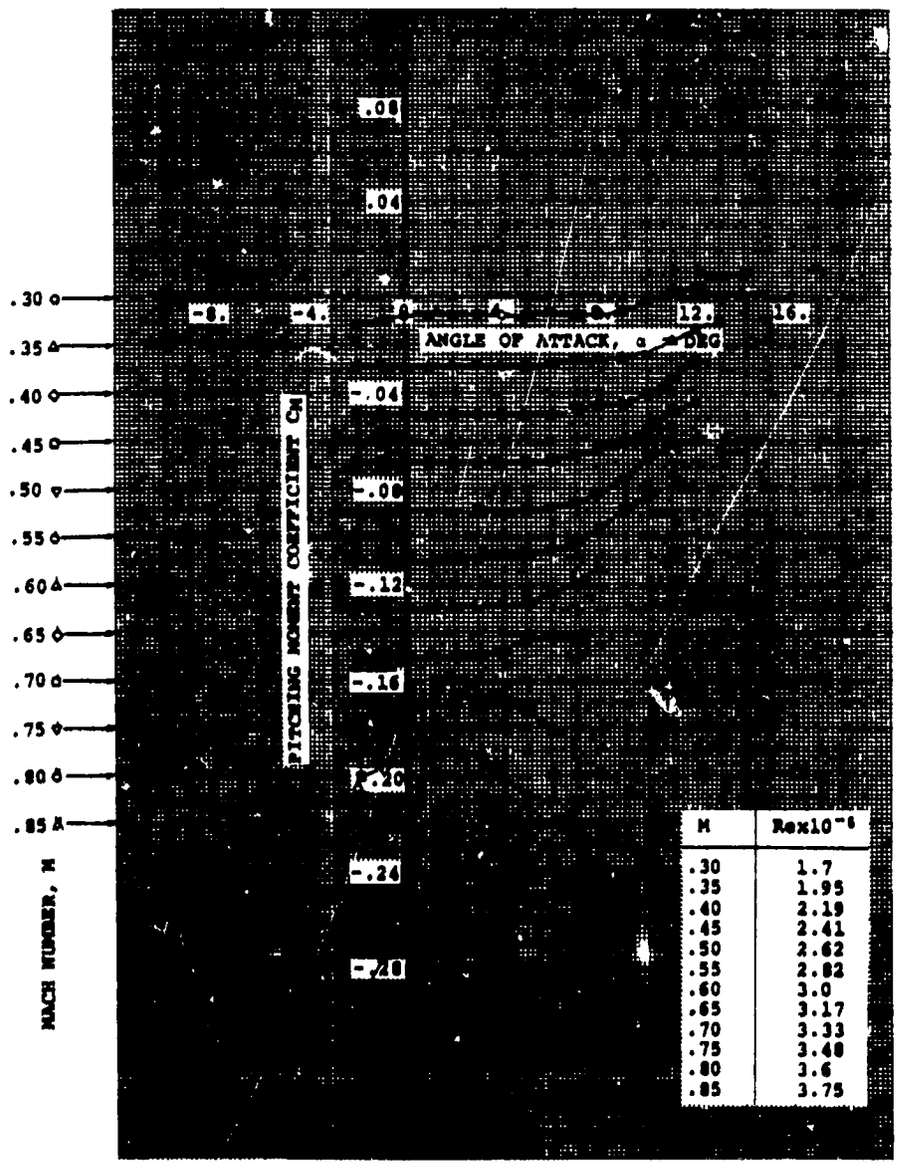
.00
.04
-.04
-.08
-.12
-.16
-.20
-.24
-.28
-8.
-4.
0
4.
8.
12.
16.
ANGLE OF ATTACK, α DEG
PITCHING MOMENT COEFFICIENT Cm
.30
.35
.40
.45
.50
.55
.60
.65
.70
.75
.80
.85
MACH NUMBER, M
M
Rex10⁻⁶
.30 1.7
.35 1.95
.40 2.19
.45 2.41
.50 2.62
.55 2.82
.60 3.0
.65 3.17
.70 3.33
.75 3.48
.80 3.6
.85 3.75

| $x/c_u$ | $y/c_u$ |
|---|---|
| 0.14520 | 0.04494 |
| 0.15403 | 0.04609 |
| 0.16378 | 0.04724 |
| 0.17425 | 0.04838 |
| 0.18544 | 0.04950 |
| 0.19734 | 0.05059 |
| 0.20995 | 0.05164 |
| 0.22358 | 0.05264 |
| 0.23700 | 0.05339 |
| 0.25094 | 0.05424 |
| 0.26450 | 0.05499 |
| 0.28333 | 0.05565 |
| 0.3175 | 0.0564 |
| 0.3409 | 0.0565 |
| 0.3642 | 0.0564 |
| 0.4115 | 0.0554 |
| 0.4351 | 0.0546 |
| 0.4821 | 0.0525 |
| 0.5292 | 0.0498 |
| 0.5763 | 0.0466 |
| 0.6234 | 0.0430 |
| 0.6704 | 0.0389 |
| 0.7176 | 0.0345 |
| 0.7646 | 0.0297 |
| 0.8177 | 0.0247 |
| 0.8588 | 0.0193 |
| 0.9059 | 0.0136 |
| 0.9529 | 0.0076 |
| 0.9765 | 0.0045 |
| 1.0000 | 0.0013 |

| $x/c_\ell$ | $y/c_\ell$ |
|---|---|
| 0.0 | -0.01366 |
| 0.0002 | -0.01600 |
| 0.0008 | -0.01810 |
| 0.0019 | -0.02080 |
| 0.0033 | -0.02300 |
| 0.0056 | -0.02540 |
| 0.0089 | -0.02730 |
| 0.0130 | -0.03010 |
| 0.0184 | -0.03245 |
| 0.0236 | -0.03415 |
| 0.0290 | -0.03540 |
| 0.03535 | -0.03652 |
| 0.04330 | -0.03781 |
| 0.04985 | -0.03870 |
| 0.05900 | -0.03986 |
| 0.07232 | -0.04143 |
| 0.09030 | -0.04340 |
| 0.10055 | -0.04446 |
| 0.11098 | -0.04547 |
| 0.13182 | -0.04736 |
| 0.15269 | -0.04911 |
| 0.17355 | -0.05065 |
| 0.19444 | -0.05202 |
| 0.21532 | -0.05321 |
| 0.23624 | -0.05422 |
| 0.25715 | -0.05504 |
| 0.27806 | -0.05568 |
| 0.29899 | -0.05615 |
| 0.31990 | -0.05640 |
| 0.34090 | -0.05650 |
| 0.3642 | -0.0564 |
| 0.4115 | -0.0554 |
| 0.4351 | -0.0546 |
| 0.4821 | -0.0525 |
| 0.5292 | -0.0498 |
| 0.5763 | -0.0466 |
| 0.6234 | -0.0430 |
| 0.6704 | -0.0389 |
| 0.7176 | -0.0345 |
| 0.7646 | -0.0297 |
| 0.8117 | -0.0247 |
| 0.8588 | -0.0193 |
| 0.9059 | -0.0136 |
| 0.9529 | -0.0076 |
| 0.9765 | -0.0045 |
| 1.0000 | -0.0013 |

AIRFOIL: NPL 9626



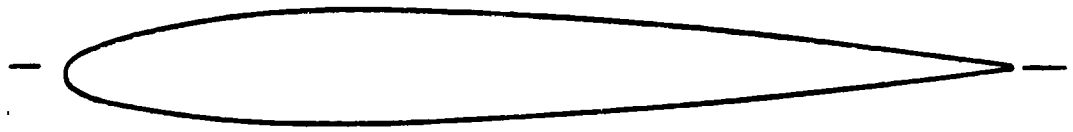

## AIRFOIL COORDINATES

| x/c | $y/c_u$ | $y/c_l$ |
|---|---|---|
| 0.0 | -0.01100 | -0.01100 |
| 0.00020 | -0.00791 | -0.01342 |
| 0.00050 | -0.00613 | -0.01482 |
| 0.00100 | -0.00415 | -0.01637 |
| 0.00160 | -0.00238 | -0.01772 |
| 0.00241 | -0.00054 | -0.01912 |
| 0.00350 | +0.00159 | -0.02047 |
| 0.00500 | 0.00356 | -0.02192 |
| 0.00650 | 0.00522 | -0.02337 |
| 0.00800 | 0.00667 | -0.02457 |
| 0.00961 | 0.00816 | -0.02557 |
| 0.01500 | 0.01202 | -0.02878 |
| 0.02153 | 0.01574 | -0.03155 |
| 0.03806 | 0.02237 | -0.03703 |
| 0.05904 | 0.02919 | -0.04199 |
| 0.08427 | 0.03572 | -0.04670 |
| 0.11349 | 0.04202 | -0.05106 |
| 0.14645 | 0.04775 | -0.05494 |
| 0.18280 | 0.05267 | -0.05787 |
| 0.22221 | 0.05644 | -0.05979 |
| 0.26430 | 0.05891 | -0.06074 |
| 0.30866 | 0.05999 | -0.06067 |
| 0.35486 | 0.05938 | -0.05971 |
| 0.40245 | 0.05794 | -0.05794 |
| 0.45099 | 0.05576 | -0.05576 |
| 0.5 | 0.05294 | -0.05294 |
| 0.54901 | 0.04960 | -0.04960 |
| 0.59755 | 0.04583 | -0.04583 |
| 0.64514 | 0.04176 | -0.04176 |
| 0.69134 | 0.03747 | -0.03747 |
| 0.73570 | 0.03308 | -0.03308 |
| 0.77779 | 0.02866 | -0.02866 |
| 0.81720 | 0.02430 | -0.02430 |
| 0.85355 | 0.02011 | -0.02011 |
| 0.88651 | 0.01614 | -0.01614 |
| 0.91573 | 0.01250 | -0.01250 |
| 0.94096 | 0.00925 | -0.00925 |
| 0.96194 | 0.00648 | -0.00648 |
| 0.97847 | 0.00424 | -0.00424 |
| 0.99039 | 0.00260 | -0.00260 |
| 0.99759 | 0.00160 | -0.00160 |
| 1.0 | 0.00126 | -0.00126 |

## CHARACTERISTICS

- Thickness, t/c = 0.12066
- Designed for optimum peaky pressure distributions at $0.6 < M < 0.7$
- Rear half is symmetrical and identical to NACA 0012

**TYPE OF DATA AND METHOD OF TEST**

The wind tunnel tests were carried out in the National Physical Laboratory, NPL, 36 in. x 14 in. (0.92 m x 0.36 m) transonic tunnel, at Teddington, Middlesex, England.

Lift and pitching moments were found by integration of surface static pressures. Profile drag was determined by wake measurements.

All measurements were obtained with a roughness band of 230-270 mesh carborundum between 0 and 2% chord on both surfaces.

Model Chord = 10 in (25.4 cm)
Span = 14 in (35.6 cm)

**SOURCE**

Wilby, P.G., Gregory, N., and Quincey, V.G., Aerodynamic Characteristics of NPL 9629 and NPL 9627, Further Aerofoils Designed for Helicopter Rotor Use, A.R.C. C.P. No. 1262, November 1969.

NPL 9626

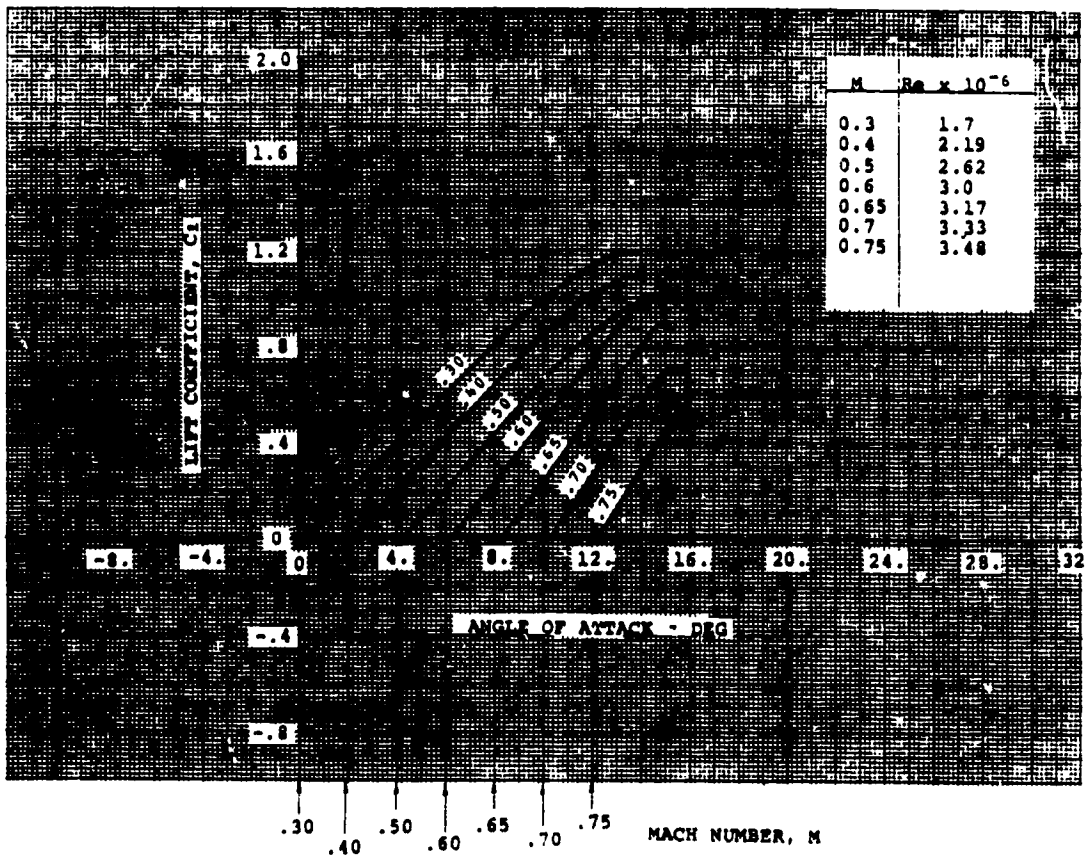
M
Re x 10⁻⁶
0.3 1.7
0.4 2.19
0.5 2.62
0.6 3.0
0.65 3.17
0.7 3.33
0.75 3.48
LIFT COEFFICIENT, Cl
2.0
1.6
1.2
.8
.4
0
-.4
-.8
-8.
-4.
0
4.
8.
12.
16.
20.
24.
28.
32.
ANGLE OF ATTACK - DEG
.30
.40
.50
.60
.65
.70
.75
MACH NUMBER, M

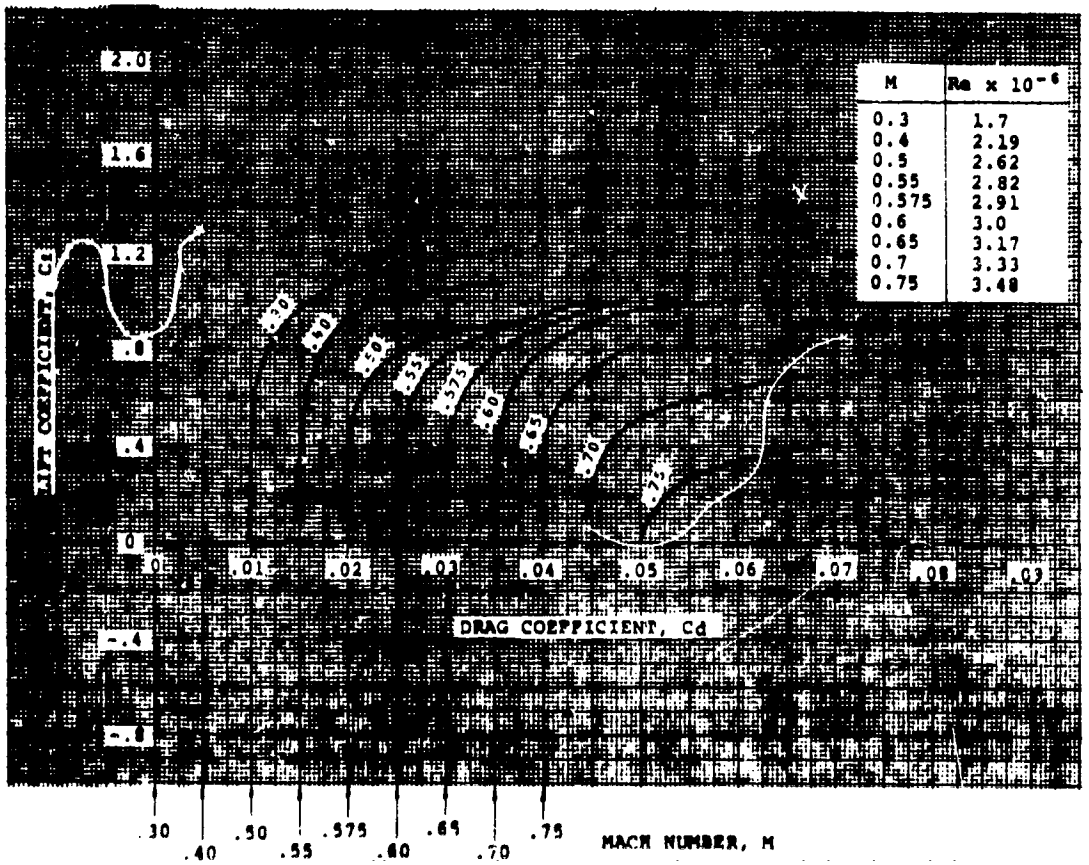
M
Re x 10⁻⁶
0.3 1.7
0.4 2.19
0.5 2.62
0.55 2.82
0.575 2.91
0.6 3.0
0.65 3.17
0.7 3.33
0.75 3.48
LIFT COEFFICIENT, Cl
2.0
1.6
1.2
.8
.4
0
-.4
-.8
0
.01
.02
.03
.04
.05
.06
.07
.08
.09
DRAG COEFFICIENT, Cd
.30
.40
.50
.55
.575
.60
.65
.70
.75
MACH NUMBER, M

NPL 9626

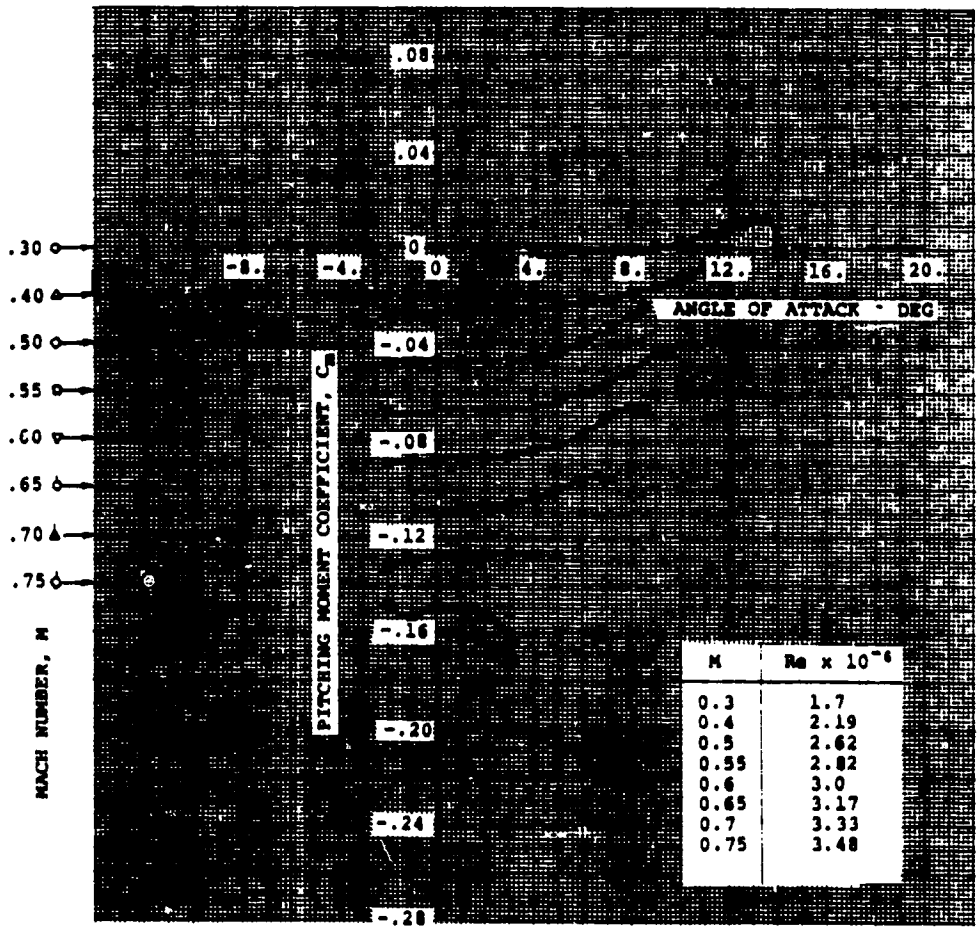
.08
.04
0
-.04
-.08
-.12
-.16
-.20
-.24
-.28
-8.
-4.
0
4.
8.
12.
16.
20.
ANGLE OF ATTACK - DEG
PITCHING MOMENT COEFFICIENT, $C_m$
MACH NUMBER, M
.30
.40
.50
.55
.60
.65
.70
.75
M
Re x $10^{-6}$
0.3 1.7
0.4 2.19
0.5 2.62
0.55 2.82
0.6 3.0
0.65 3.17
0.7 3.33
0.75 3.48

AIRFOIL: NPL 9627

1.3.350

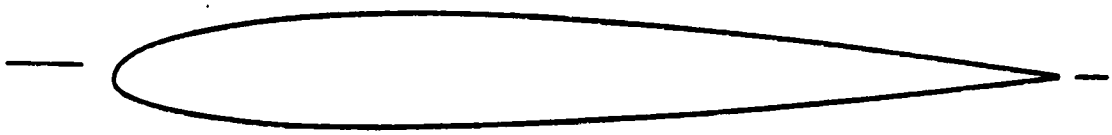

AIRFOIL COORDINATES

| x/c | $y/c_u$ | $y/c_l$ |
|---|---|---|
| 0.0 | -0.01600 | -0.01600 |
| 0.00020 | -0.01301 | -0.01842 |
| 0.00050 | -0.01127 | -0.01982 |
| 0.00100 | -0.00935 | -0.02137 |
| 0.00160 | -0.00764 | -0.02272 |
| 0.00241 | -0.00583 | -0.02412 |
| 0.00350 | -0.00389 | -0.02547 |
| 0.00500 | -0.00132 | -0.02692 |
| 0.00650 | +0.00060 | -0.02837 |
| 0.00800 | 0.00243 | -0.02957 |
| 0.00961 | 0.00415 | -0.03057 |
| 0.01500 | 0.00896 | -0.03378 |
| 0.02153 | 0.01336 | -0.03655 |
| 0.03806 | 0.02183 | -0.04203 |
| 0.05904 | 0.02872 | -0.04762 |
| 0.08427 | 0.03548 | -0.05279 |
| 0.11349 | 0.04182 | -0.05707 |
| 0.14645 | 0.04725 | -0.06035 |
| 0.18280 | 0.05173 | -0.06261 |
| 0.22221 | 0.05502 | -0.06382 |
| 0.26430 | 0.05730 | -0.06399 |
| 0.30866 | 0.05849 | -0.06313 |
| 0.35486 | 0.05866 | -0.06134 |
| 0.40245 | 0.05764 | -0.05875 |
| 0.45099 | 0.05574 | -0.05600 |
| 0.5 | 0.05294 | -0.05294 |
| 0.54901 | 0.04960 | -0.04960 |
| 0.59755 | 0.04583 | -0.04583 |
| 0.64514 | 0.04176 | -0.04176 |
| 0.69134 | 0.03747 | -0.03747 |
| 0.73570 | 0.03308 | -0.03308 |
| 0.77779 | 0.02866 | -0.02866 |
| 0.81720 | 0.02430 | -0.02430 |
| 0.85355 | 0.02011 | -0.02011 |
| 0.88651 | 0.01614 | -0.01614 |
| 0.91573 | 0.01250 | -0.01250 |
| 0.94096 | 0.00925 | -0.00925 |
| 0.96194 | 0.00648 | -0.00648 |
| 0.97847 | 0.00424 | -0.00424 |
| 0.99039 | 0.00260 | -0.00260 |
| 0.99759 | 0.00160 | -0.00160 |
| 1.0 | 0.00126 | -0.00126 |

CHARACTERISTICS

- Thickness, t/c = 0.12265
- Designed to improve the performance of the NPL 9629 at M = 0.5
- Rear half is symmetrical and identical to NACA 0012

TYPE OF DATA AND METHOD OF TEST

The wind tunnel tests were carried out in the National Physical Laboratory, NPL, 36 in x 14 in (0.92 m x 0.36 m) transonic tunnel, at Teddington, Middlesex, England.

Lift and pitching moments were found by integration of surface static pressures. Profile drag was determined by wake measurements.

All measurements were obtained with a roughness band of 230-270 mesh carborundum between 0 and 2% chord on both surfaces.

Model Chord = 10 in (25.4 cm)
Span = 14 in (36.0 cm)

SOURCE

Wilby, P.G., Gregory, N., and Quincey, V.G., Aerodynamic Characteristics of NPL 9629 and NPL 9627, Further Aerofoils Designed for Helicopter Rotor Use, A.R.C. C.P. No. 1262, November 1969.

NPL 9627

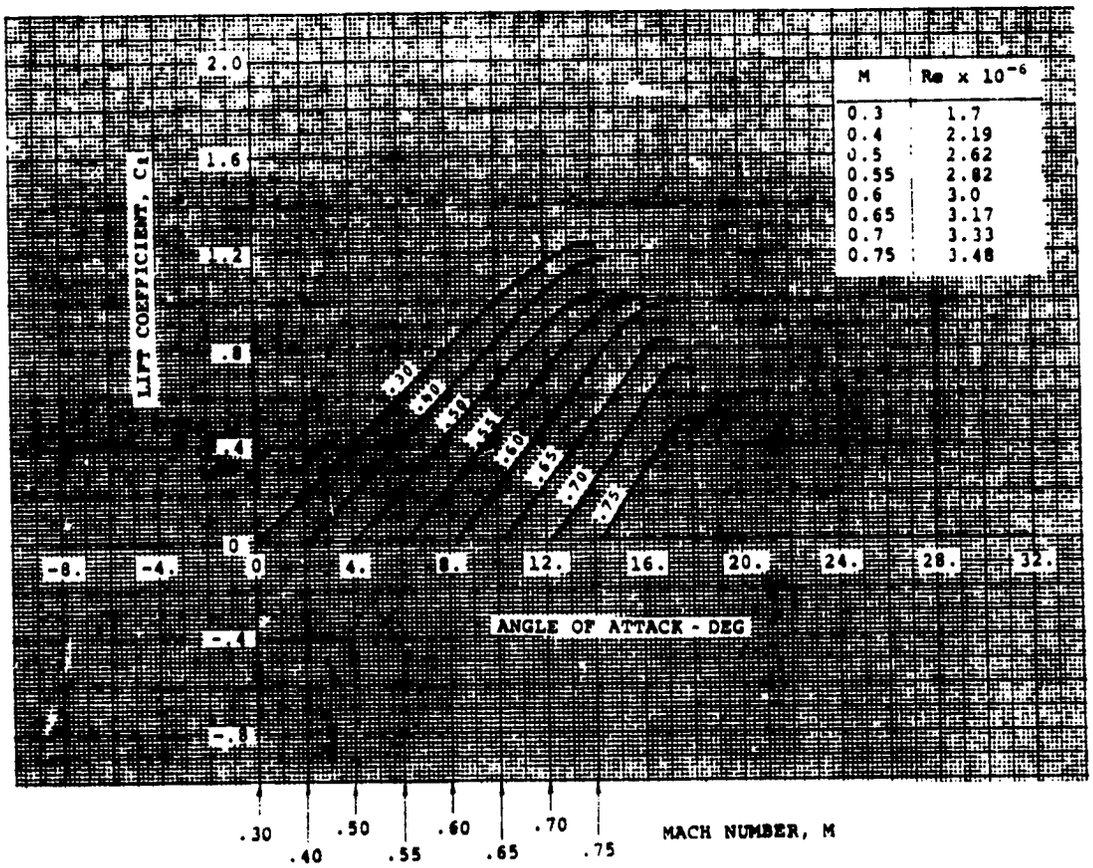
LIFT COEFFICIENT, $C_L$
2.0
1.6
1.2
.8
.4
0
-.4
-.8
-8.
-4.
0
4.
8.
12.
16.
20.
24.
28.
32.
ANGLE OF ATTACK - DEG
.30
.40
.50
.55
.60
.65
.70
.75
MACH NUMBER, M
M | Re x $10^{-6}$
0.3 | 1.7
0.4 | 2.19
0.5 | 2.62
0.55 | 2.82
0.6 | 3.0
0.65 | 3.17
0.7 | 3.33
0.75 | 3.48

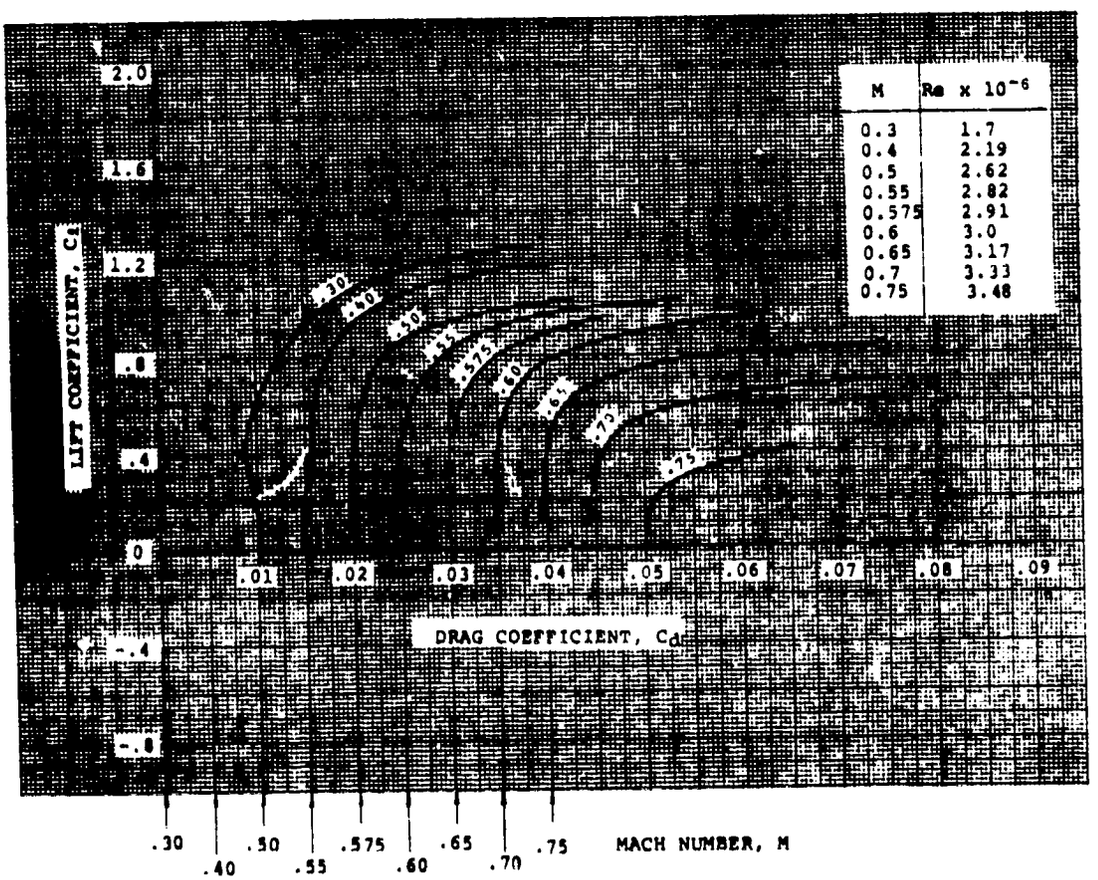
LIFT COEFFICIENT, $C_L$
2.0
1.6
1.2
.8
.4
0
-.4
-.8
.01
.02
.03
.04
.05
.06
.07
.08
.09
DRAG COEFFICIENT, $C_d$
.30
.40
.50
.55
.575
.60
.65
.70
.75
MACH NUMBER, M
M | Re x $10^{-6}$
0.3 | 1.7
0.4 | 2.19
0.5 | 2.62
0.55 | 2.82
0.575 | 2.91
0.6 | 3.0
0.65 | 3.17
0.7 | 3.33
0.75 | 3.48

NPL 9627

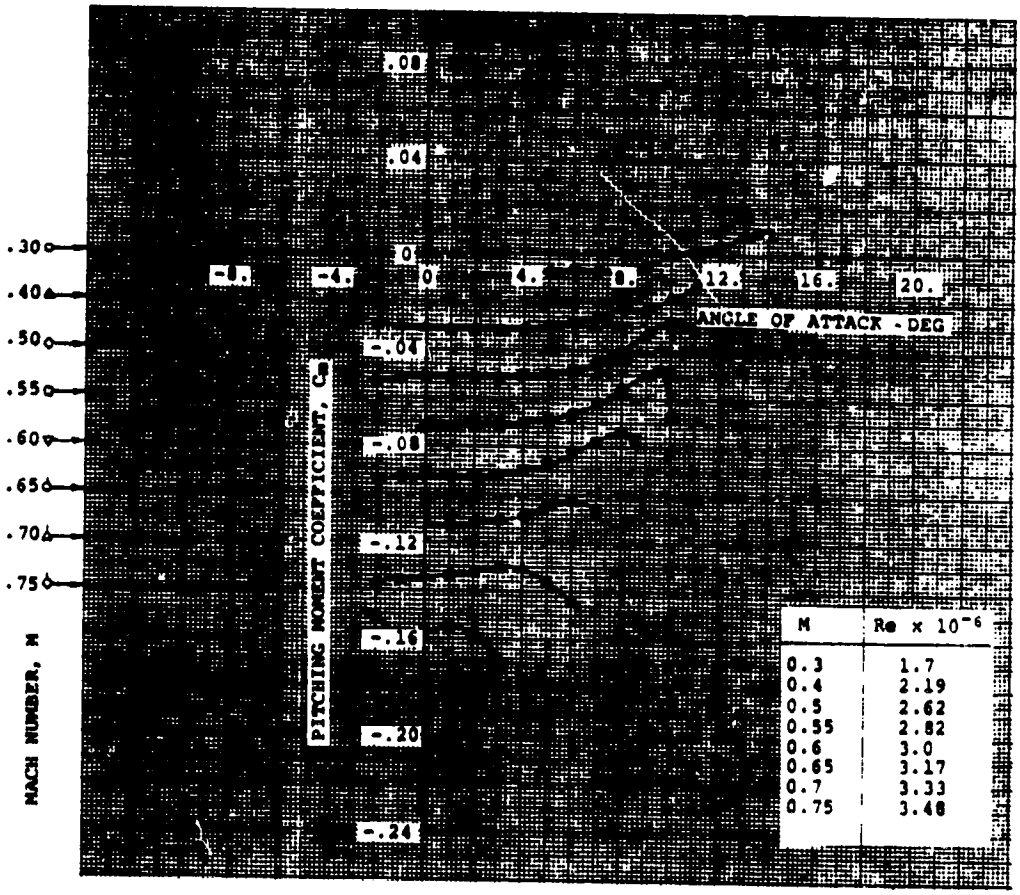
.08
.04
0
-.04
-.08
-.12
-.16
-.20
-.24
PITCHING MOMENT COEFFICIENT, $C_m$
-8.
-4.
0
4.
8.
12.
16.
20.
ANGLE OF ATTACK - DEG
.30
.40
.50
.55
.60
.65
.70
.75
MACH NUMBER, M
M
Re x $10^{-6}$
0.3 1.7
0.4 2.19
0.5 2.62
0.55 2.82
0.6 3.0
0.65 3.17
0.7 3.33
0.75 3.48

AIRFOIL: NPL 9660



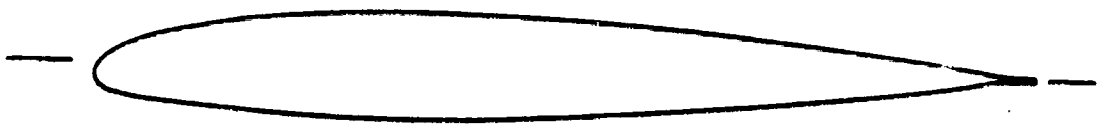

## AIRFOIL COORDINATES

| x/c | $y/c_u$ |
|---|---|
| 0.0 | -0.01366 |
| 0.00443 | -0.00155 |
| 0.00586 | +0.00001 |
| 0.00857 | 0.00268 |
| 0.01359 | 0.00649 |
| 0.01726 | 0.00893 |
| 0.02172 | 0.01163 |
| 0.02589 | 0.01392 |
| 0.03065 | 0.01633 |
| 0.03602 | 0.01883 |
| 0.04209 | 0.02140 |
| 0.04905 | 0.02407 |
| 0.05297 | 0.02545 |
| 0.05723 | 0.02687 |
| 0.06183 | 0.02832 |
| 0.06682 | 0.02980 |
| 0.07227 | 0.03131 |
| 0.07828 | 0.03306 |
| 0.08152 | 0.03365 |
| 0.08495 | 0.03476 |
| 0.08858 | 0.03528 |
| 0.09244 | 0.03612 |
| 0.09656 | 0.03698 |
| 0.10098 | 0.03786 |
| 0.10574 | 0.03876 |
| 0.11076 | 0.03969 |
| 0.11622 | 0.04065 |
| 0.12239 | 0.04165 |
| 0.12928 | 0.04271 |
| 0.13688 | 0.04381 |

Coordinates continued on page 1.3.360-4

## CHARACTERISTICS

- Thickness, t/c = 0.113
- Leading edge radius: r/c = 0.01883, with center at x/c = 0.01883, y/c = -0.0137
- Profile is circular for 40° of arc on upper surface
- NPL 9615 contour modified to include a 0.035c trailing edge tab in the neutral position.

### TYPE OF DATA AND METHOD OF TESTS

The wind tunnel tests were carried out in the National Physical Laboratory, NPL, 36 in. x 14 in. (0.92 m x 0.36 m) transonic tunnel, at Teddington, Middlesex, England.

Lift and pitching moments were found by integration of surface static pressures. Profile drag was determined by wake measurements.

All measurements were obtained with a roughness band of 230-270 mesh carborundum between 0 and 2% chord on both surfaces. The floor and the ceiling of the test section were slotted. No corrections for wall constraints have been applied to the data.

Model Chord = 10 in (25.4 cm)
Span = 14 in (35.6 cm)

### SOURCE

Wilby, P.G., Effect of Production Modifications to the Rear of Westland Lynx Rotor Blade on Sectional Aerodynamic Characteristics, RAE TR 73043, February 1973.

NPL 9660

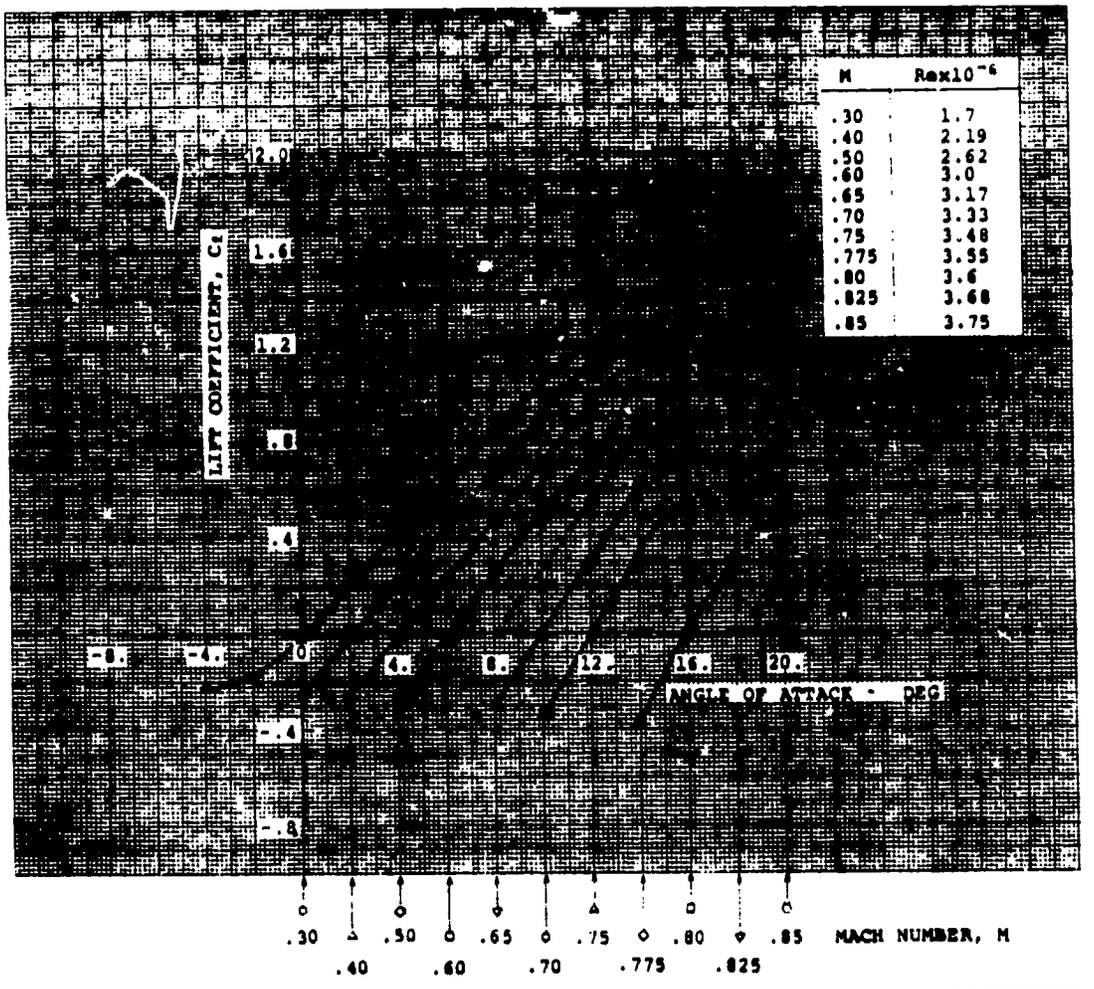
M Rex10⁻⁶
.30 1.7
.40 2.19
.50 2.62
.60 3.0
.65 3.17
.70 3.33
.75 3.48
.775 3.55
.80 3.6
.825 3.68
.85 3.75
LIFT COEFFICIENT, Ci
2.0
1.6
1.2
.8
.4
0
-.4
-.8
-8.
-4.
0
4.
8.
12.
16.
20.
ANGLE OF ATTACK - DEG
.30 .40 .50 .60 .65 .70 .75 .775 .80 .825 .85
MACH NUMBER, M

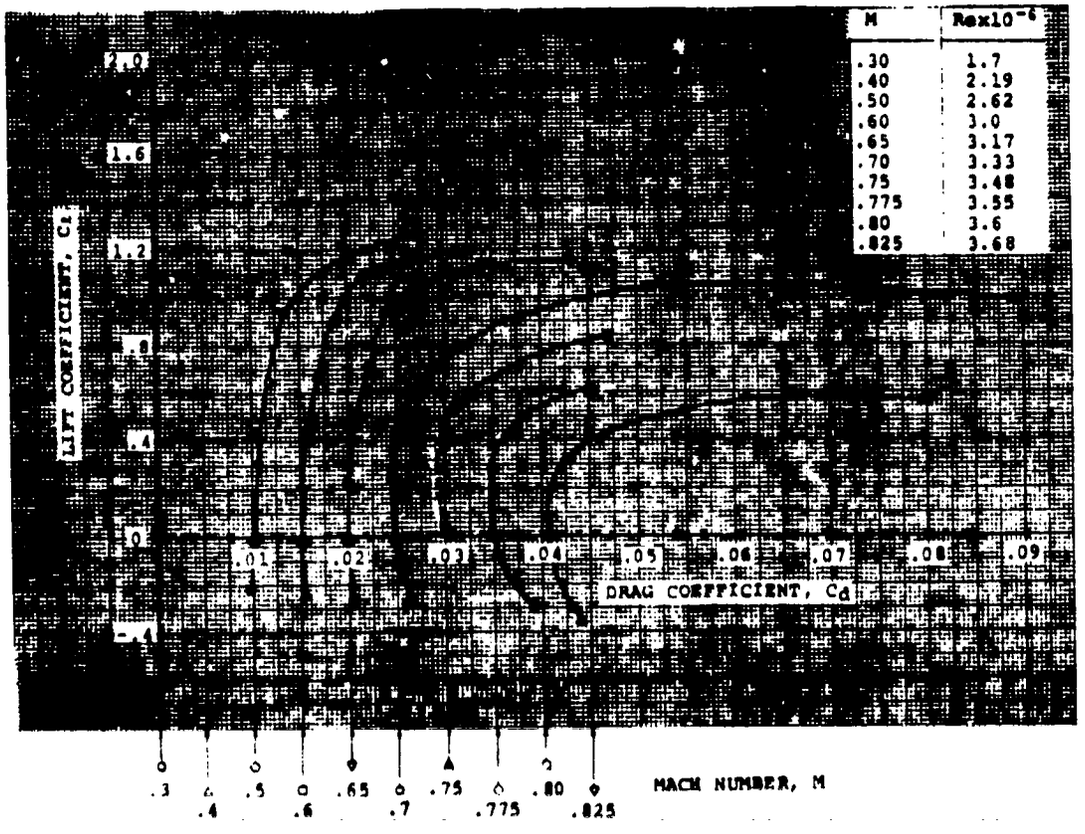
M Rex10⁻⁶
.30 1.7
.40 2.19
.50 2.62
.60 3.0
.65 3.17
.70 3.33
.75 3.48
.775 3.55
.80 3.6
.825 3.68
LIFT COEFFICIENT, Ci
2.0
1.6
1.2
.8
.4
0
-.4
.01 .02 .03 .04 .05 .06 .07 .08 .09
DRAG COEFFICIENT, Cd
.3 .4 .5 .6 .65 .7 .75 .775 .80 .825
MACH NUMBER, M

NPL 9660

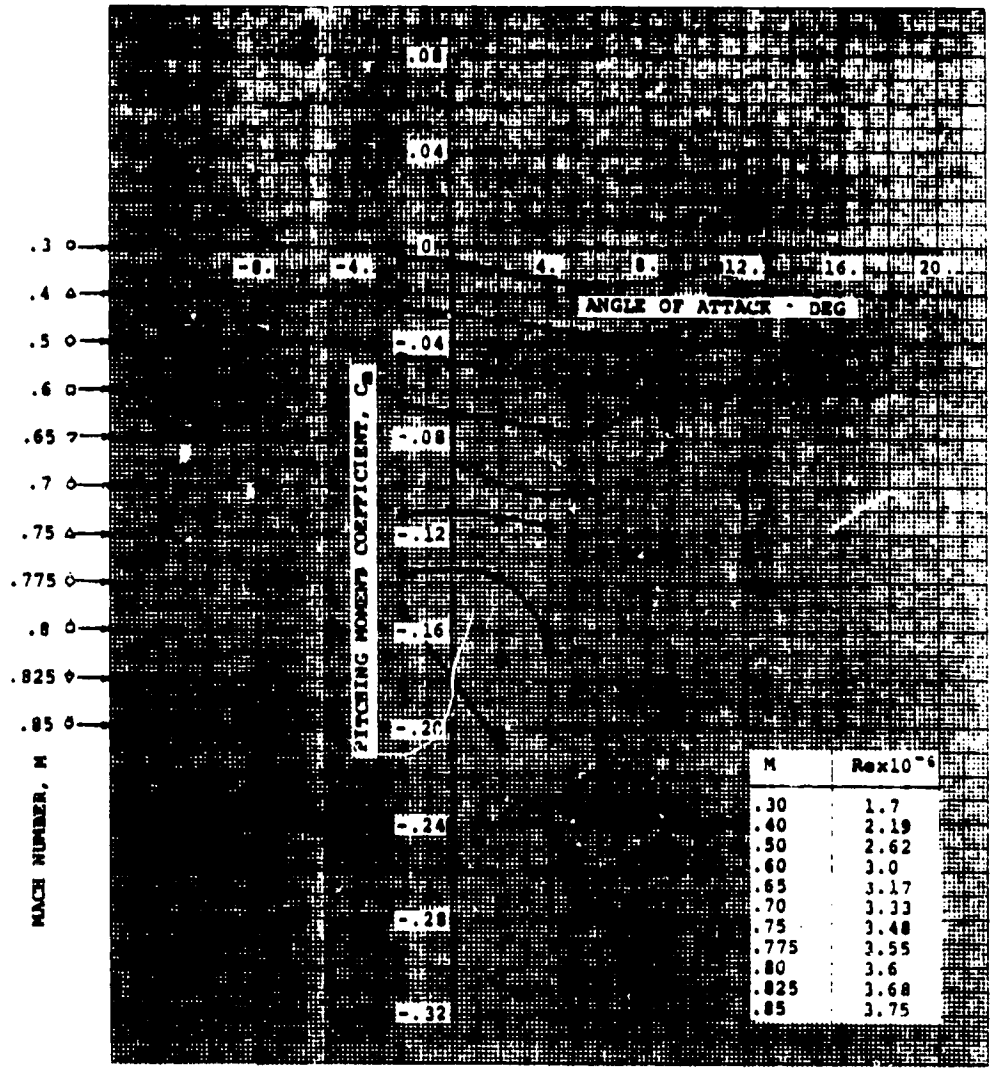
.01
.04
0
-.04
-.08
-.12
-.16
-.20
-.24
-.28
-.32
PITCHING MOMENT COEFFICIENT, $C_m$
-8.
-4.
4.
8.
12.
16.
20.
ANGLE OF ATTACK - DEG
.3
.4
.5
.6
.65
.7
.75
.775
.8
.825
.85
MACH NUMBER, M
M | Rex10⁻⁶
.30 | 1.7
.40 | 2.19
.50 | 2.62
.60 | 3.0
.65 | 3.17
.70 | 3.33
.75 | 3.48
.775 | 3.55
.80 | 3.6
.825 | 3.68
.85 | 3.75

| $x/c_u$ | $y/c_u$ |
|---|---|
| 0.14520 | 0.04494 |
| 0.15403 | 0.04609 |
| 0.16378 | 0.04724 |
| 0.17425 | 0.04838 |
| 0.18544 | 0.04950 |
| 0.19734 | 0.05059 |
| 0.20995 | 0.05164 |
| 0.22358 | 0.05264 |
| 0.23700 | 0.05339 |
| 0.25094 | 0.05424 |
| 0.26450 | 0.05499 |
| 0.28333 | 0.05565 |
| 0.3175 | 0.0564 |
| 0.3409 | 0.0565 |
| 0.3642 | 0.0564 |
| 0.4115 | 0.0554 |
| 0.4351 | 0.0546 |
| 0.4821 | 0.0525 |
| 0.5292 | 0.0498 |
| 0.5763 | 0.0466 |
| 0.6234 | 0.0430 |
| 0.6704 | 0.0389 |
| 0.7176 | 0.0345 |
| 0.77779 | 0.02838 |
| 0.8152 | 0.02395 |
| 0.85355 | 0.01915 |
| 0.88651 | 0.01450 |
| 0.91573 | 0.01020 |
| 0.94096 | 0.00625 |
| 0.96194 | 0.00280 |
| 0.97847 | 0.00190 |
| 0.99039 | 0.00190 |
| 0.99759 | 0.00173 |
| 1.0 | 0.00130 |

| $x/c_\ell$ | $y/c_\ell$ |
|---|---|
| 0.0 | -0.01366 |
| 0.0002 | -0.01600 |
| 0.0008 | -0.01810 |
| 0.0019 | -0.02080 |
| 0.0033 | -0.02300 |
| 0.0056 | -0.02540 |
| 0.0089 | -0.02730 |
| 0.0130 | -0.03010 |
| 0.0184 | -0.03245 |
| 0.0236 | -0.03415 |
| 0.0290 | -0.03540 |
| 0.03535 | -0.03652 |
| 0.04330 | -0.03781 |
| 0.04985 | -0.03870 |
| 0.05900 | -0.03986 |
| 0.07232 | -0.04143 |
| 0.09030 | -0.04340 |
| 0.10055 | -0.04446 |
| 0.11098 | -0.04547 |
| 0.13182 | -0.04736 |
| 0.15269 | -0.04911 |
| 0.17355 | -0.05065 |
| 0.19444 | -0.05202 |
| 0.21532 | -0.05321 |
| 0.23624 | -0.05422 |
| 0.25715 | -0.05504 |
| 0.27806 | -0.05568 |
| 0.29899 | -0.05615 |
| 0.31990 | -0.05640 |
| 0.34090 | -0.05650 |
| 0.3642 | -0.0564 |
| 0.4115 | -0.0554 |
| 0.4351 | -0.0546 |
| 0.4821 | -0.0525 |
| 0.5292 | -0.0498 |
| 0.5763 | -0.0466 |
| 0.6234 | -0.0430 |
| 0.6704 | -0.0389 |
| 0.7176 | -0.0345 |
| 0.77779 | -0.02838 |
| 0.8152 | -0.02395 |
| 0.85355 | -0.01915 |
| 0.88651 | -0.01450 |
| 0.91573 | -0.01020 |
| 0.94096 | -0.00625 |
| 0.96194 | -0.00280 |
| 0.97847 | -0.00190 |
| 0.99039 | -0.00190 |
| 0.99759 | -0.00173 |
| 1.0 | -0.00130 |

AIRFOIL: NACA - CAMBRÉ

1.3.370

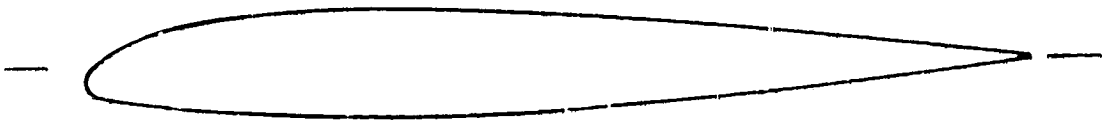

## AIRFOIL COORDINATES

| x/c | $y/c_u$ | $y/c_l$ |
|---|---|---|
| 0. | -.0169 | -.0169 |
| .0055 | -.0028 | -.0276 |
| .0104 | .00235 | -.0307 |
| .0195 | .00975 | -.0338 |
| .0293 | .0161 | -.0360 |
| .0402 | .0220 | -.0379 |
| .050 | .0263 | -.0395 |
| .0597 | .0299 | -.0408 |
| .0707 | .0334 | -.0425 |
| .854 | .0374 | -.0440 |
| .10 | .0408 | -.0456 |
| .1195 | .0445 | -.0475 |
| .140 | .0477 | -.0493 |
| .158 | .050 | -.0507 |
| .177 | .0519 | -.0521 |
| .195 | .0534 | -.0535 |
| .226 | .0554 | -.0554 |
| .256 | .0566 | -.0566 |
| .287 | .05735 | -.05735 |
| .311 | .0576 | -.0576 |
| .330 | .0575 | -.0575 |
| .366 | .0571 | -.0571 |
| .415 | .0557 | -.0557 |
| .450 | .0541 | -.0541 |
| .50 | .0515 | -.0515 |
| .537 | .0492 | -.0492 |
| .573 | .0466 | -.0466 |
| .610 | .0438 | -.0438 |
| .646 | .0407 | -.0407 |
| .683 | .0374 | -.0374 |
| .732 | .0328 | -.0328 |
| .768 | .0291 | -.0291 |
| .817 | .0238 | -.0238 |
| .854 | .0197 | -.0197 |
| .878 | .0168 | -.0168 |
| .915 | .0124 | -.0124 |
| .939 | .0093 | -.0093 |
| .963 | .0061 | -.0061 |
| .975 | .0045 | -.0045 |
| 1.0 | .0012 | -.0012 |

## CHARACTERISTICS

NACA 0011,8 profile with a cambered leading edge extension.

## TYPE OF DATA AND METHOD OF TEST

Two-dimensional test in the S3MA subsonic-transonic onera wind tunnel in Modane. Lift and pitching moments were calculated by pressure distribution integration. Drag was determined by a transvering wake probe survey.

Model Chord = 0.215 m
Span = 0.560 m

## SOURCE

Onera Note Technique D'Information No. 3 - 0805 GY fascicule 1/2 "Essais en courant plan a S3MA du profil NACA 0012 a extension cambree de bord d'attaque (resultats couriges des effets de parois)."

# NACA-CAMBRÉ

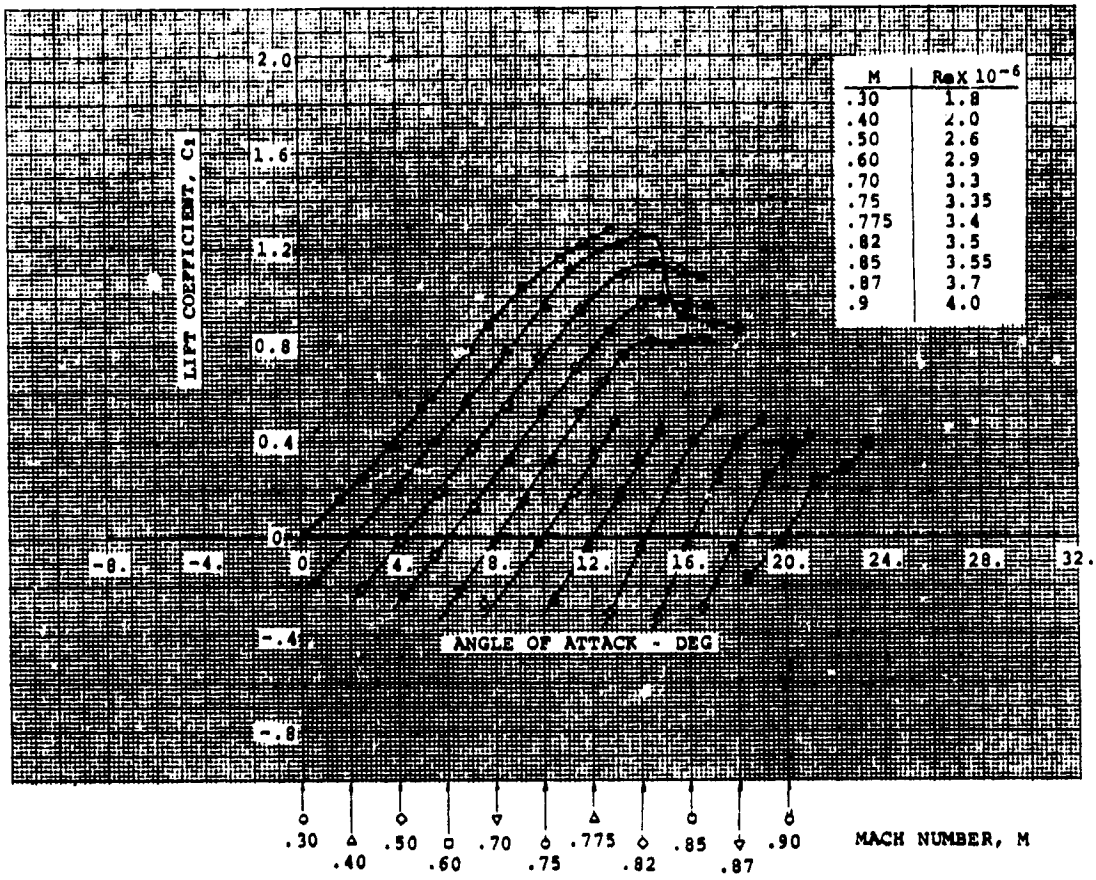


| M | Rex $10^{-6}$ |
|---|---|
| .30 | 1.8 |
| .40 | 2.0 |
| .50 | 2.6 |
| .60 | 2.9 |
| .70 | 3.3 |
| .75 | 3.35 |
| .775 | 3.4 |
| .82 | 3.5 |
| .85 | 3.55 |
| .87 | 3.7 |
| .9 | 4.0 |

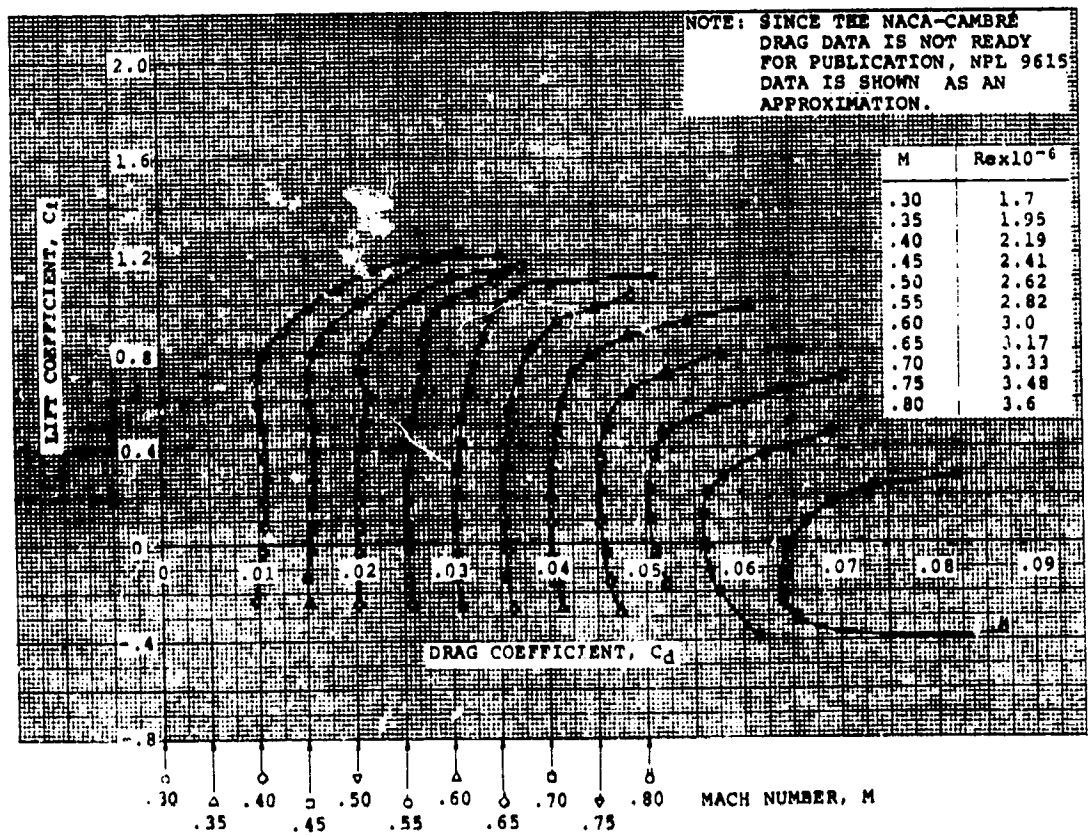


| M | Rex$10^{-6}$ |
|---|---|
| .30 | 1.7 |
| .35 | 1.95 |
| .40 | 2.19 |
| .45 | 2.41 |
| .50 | 2.62 |
| .55 | 2.82 |
| .60 | 3.0 |
| .65 | 3.17 |
| .70 | 3.33 |
| .75 | 3.48 |
| .80 | 3.6 |

NACA-CAMBRE

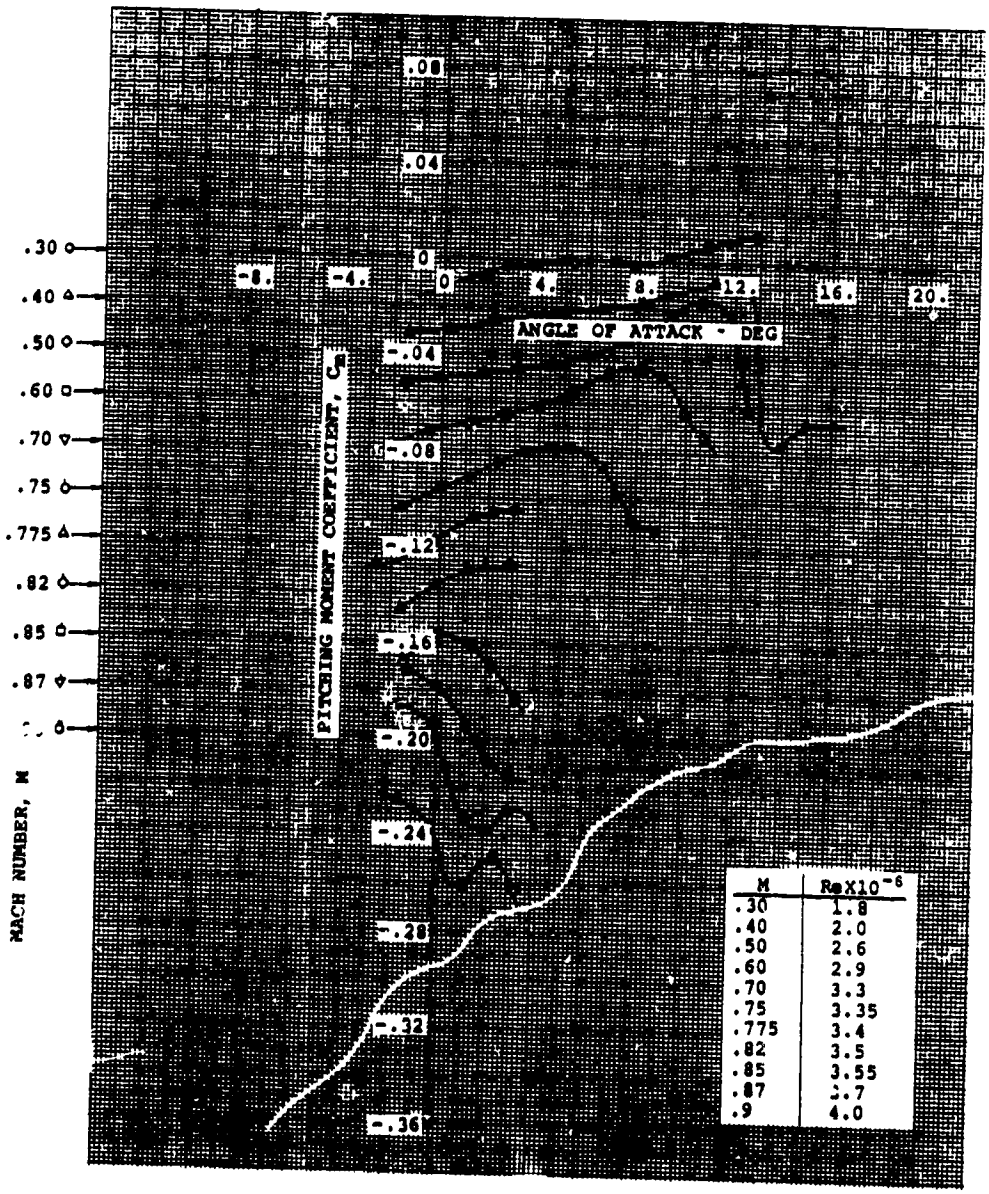
.08
.04
0
-.04
-.08
-.12
-.16
-.20
-.24
-.28
-.32
-.36
-8.
-4.
0
4.
8.
12.
16.
20.
ANGLE OF ATTACK - DEG
PITCHING MOMENT COEFFICIENT, $C_m$
MACH NUMBER, M
.30
.40
.50
.60
.70
.75
.775
.82
.85
.87
.9
M | $Re \times 10^{-6}$
.30 | 1.8
.40 | 2.0
.50 | 2.6
.60 | 2.9
.70 | 3.3
.75 | 3.35
.775 | 3.4
.82 | 3.5
.85 | 3.55
.87 | 3.7
.9 | 4.0

AIRFOIL: VR-7 WITH 0° T.E. TAB

1.3.380

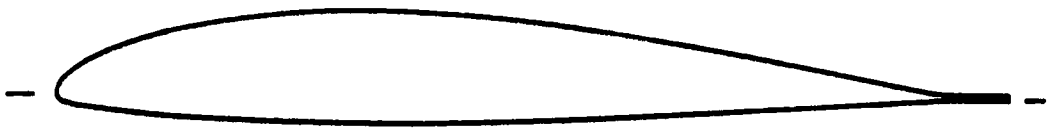

## AIRFOIL COORDINATES

| x/c | $y/c_u$ | $y/c_l$ |
|---|---|---|
| 0. | 0. | 0. |
| .005 | .0165 | -.00575 |
| .01 | .0218 | -.0081 |
| .02 | .0298 | -.0109 |
| .03 | .03615 | -.0129 |
| .04 | .0415 | -.01445 |
| .05 | .04605 | -.01585 |
| .06 | .05025 | -.01710 |
| .07 | .0541 | -.01805 |
| .085 | .0593 | -.01985 |
| .102 | .0645 | -.02145 |
| .12 | .0691 | -.02285 |
| .14 | .0737 | -.0241 |
| .16 | .0775 | -.0251 |
| .18 | .0808 | -.0260 |
| .20 | .0838 | -.0266 |
| .225 | .0867 | -.0273 |
| .255 | .0892 | -.0280 |
| .29 | .0909 | -.0285 |
| .33 | .0914 | -.0289 |
| .37 | .0905 | -.0290 |
| .41 | .0887 | -.0285 |
| .45 | .0856 | -.0275 |
| .49 | .0816 | -.0260 |
| .53 | .0767 | -.0240 |
| .57 | .0710 | -.0220 |
| .61 | .0646 | -.0199 |
| .65 | .0580 | -.0179 |
| .69 | .0514 | -.0159 |
| .73 | .0447 | -.0138 |
| .77 | .0374 | -.01075 |
| .81 | .0301 | -.00845 |
| .845 | .0235 | -.0064 |
| .88 | .0167 | -.00425 |
| .91 | .0105 | -.00235 |
| .935 | .0062 | -.0006 |
| .96 | .0050 | 0.0 |
| 1.01 | .0050 | 0.0 |

## CHARACTERISTICS

- Thickness, t/c = 0.12
- Leading Edge Circle
  r/c = .0113

  Center at x/c = .01055
  y/c = .004

- Trailing Edge Tab
  from x/c = .96
  to x/c = 1.01
  T.E. Tab Thickness,
  t/c = 0.005

TYPE OF DATA AND METHOD OF TEST

Two-dimensional test in the subsonic insert of the Boeing Supersonic Wind Tunnel in Seattle, Wash.

Lift and pitching moments were measured with a balance.

Drag was determined by a traversing wake probe survey.

Model Chord = 6.38 in
Span = 12 in

SOURCE

Dadone, L., and McMullen, J., "HLH/ATC Rotor System Two-Dimensional Airfoil Test", Boeing Document D301-10071-1, December 1971.

VR-7 WITH 0° T.E. TAB

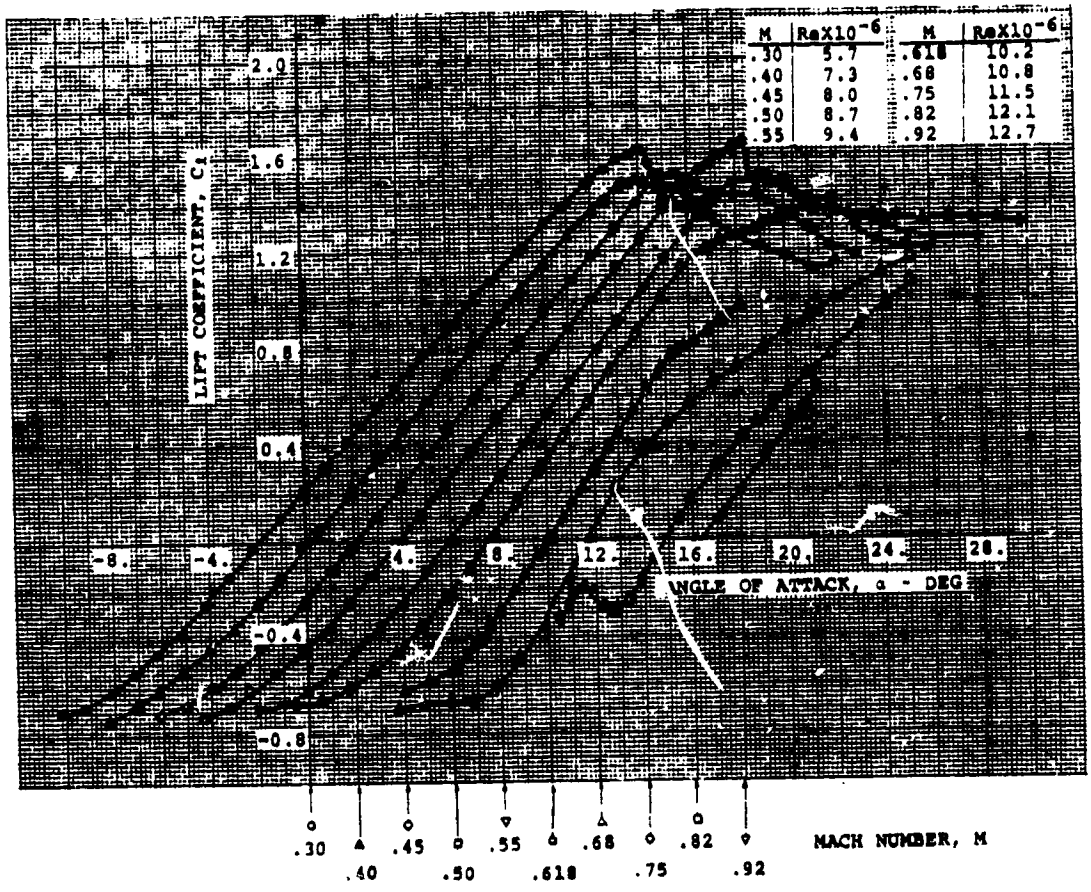


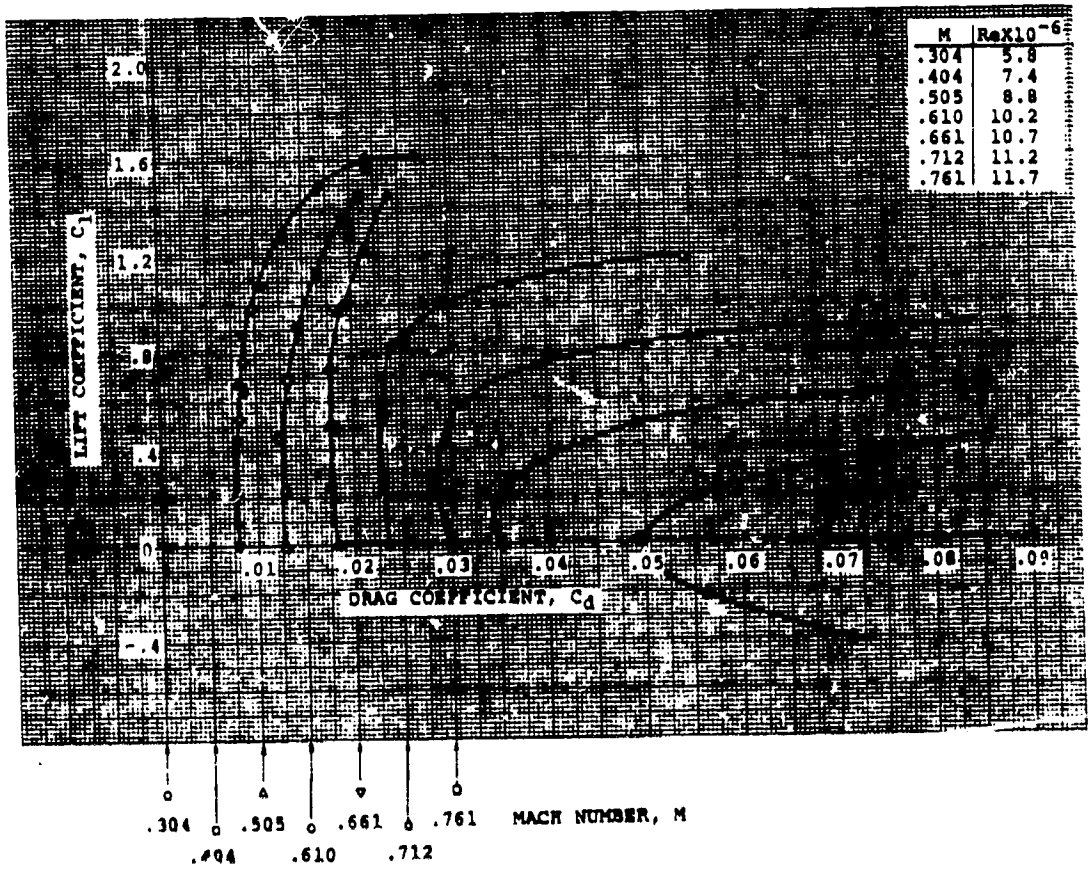

VR-7 WITH 0° T.E. TAB

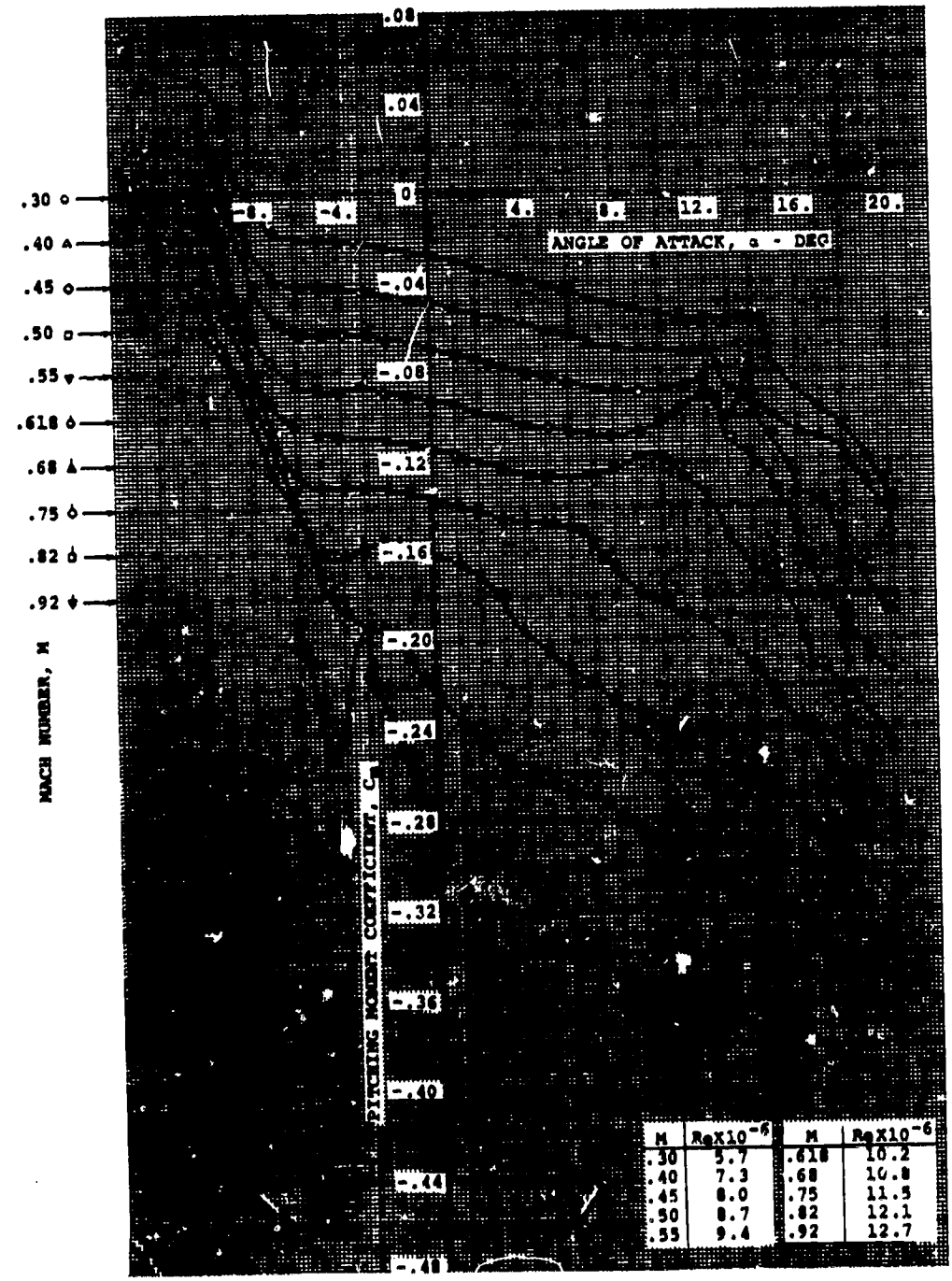

AIRFOIL: VR-7 WITH -3.1° T.E. TAB

1.3.390

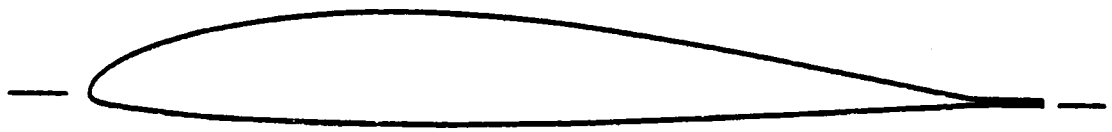

AIRFOIL COORDINATES

| x/c | $y/c_u$ | $y/c_\ell$ |
|---|---|---|
| 0. | 0. | 0. |
| .005 | .0165 | -.00575 |
| .01 | .0218 | -.0081 |
| .02 | .0298 | -.0109 |
| .03 | .03615 | -.0129 |
| .04 | .0415 | -.01445 |
| .05 | .04605 | -.01585 |
| .06 | .05025 | -.01710 |
| .07 | .0541 | -.01805 |
| .085 | .0593 | -.01985 |
| .102 | .0645 | -.02145 |
| .12 | .0691 | -.02285 |
| .14 | .0737 | -.0241 |
| .16 | .0775 | -.0251 |
| .18 | .0808 | -.0260 |
| .20 | .0858 | -.0266 |
| .225 | .0867 | -.0273 |
| .255 | .0892 | -.0280 |
| .29 | .0909 | -.0285 |
| .33 | .0914 | -.0289 |
| .37 | .0905 | -.0290 |
| .41 | .0887 | -.0285 |
| .45 | .0856 | -.0275 |
| .53 | .0767 | -.0240 |
| .57 | .0710 | -.0220 |
| .61 | .0646 | -.0199 |
| .65 | .0580 | -.0179 |
| .69 | .0514 | -.0158 |
| .73 | .0447 | -.0138 |
| .77 | .0374 | -.01075 |
| .81 | .0301 | -.00845 |
| .845 | .0235 | -.0064 |
| .88 | .0167 | -.00425 |
| .91 | .0105 | -.00235 |
| .935 | .0062 | -.0006 |
| .96 | .0050 | 0.0 |
| 1.01 | .00771 | .00271 |

CHARACTERISTICS

- Thickness, t/c = 0.12
- Leading Edge Circle:

  r/c = .0113

  Center at x/c = .01055
  y/c = .004
- Trailing edge tab

  from x/c = .96
  to x/c = 1.01

  Tab thickness, t/c = 0.005

TYPE OF DATA AND METHOD OF TEST

Two-dimensional test in the subsonic insert of the Boeing supersonic wind tunnel in Seattle, Washington.

Lift and pitching moments were measured with a balance.

Model Chord = 6.38 in
Span = 12 in

SOURCE

Dadone, L., & McMullen J., "HLH/ATC Rotor System Two-Dimensional Airfoil Test", Boeing Document D301-10071-1, Dec. 1971

VR-7 WITH -3.1° T.E. TAB

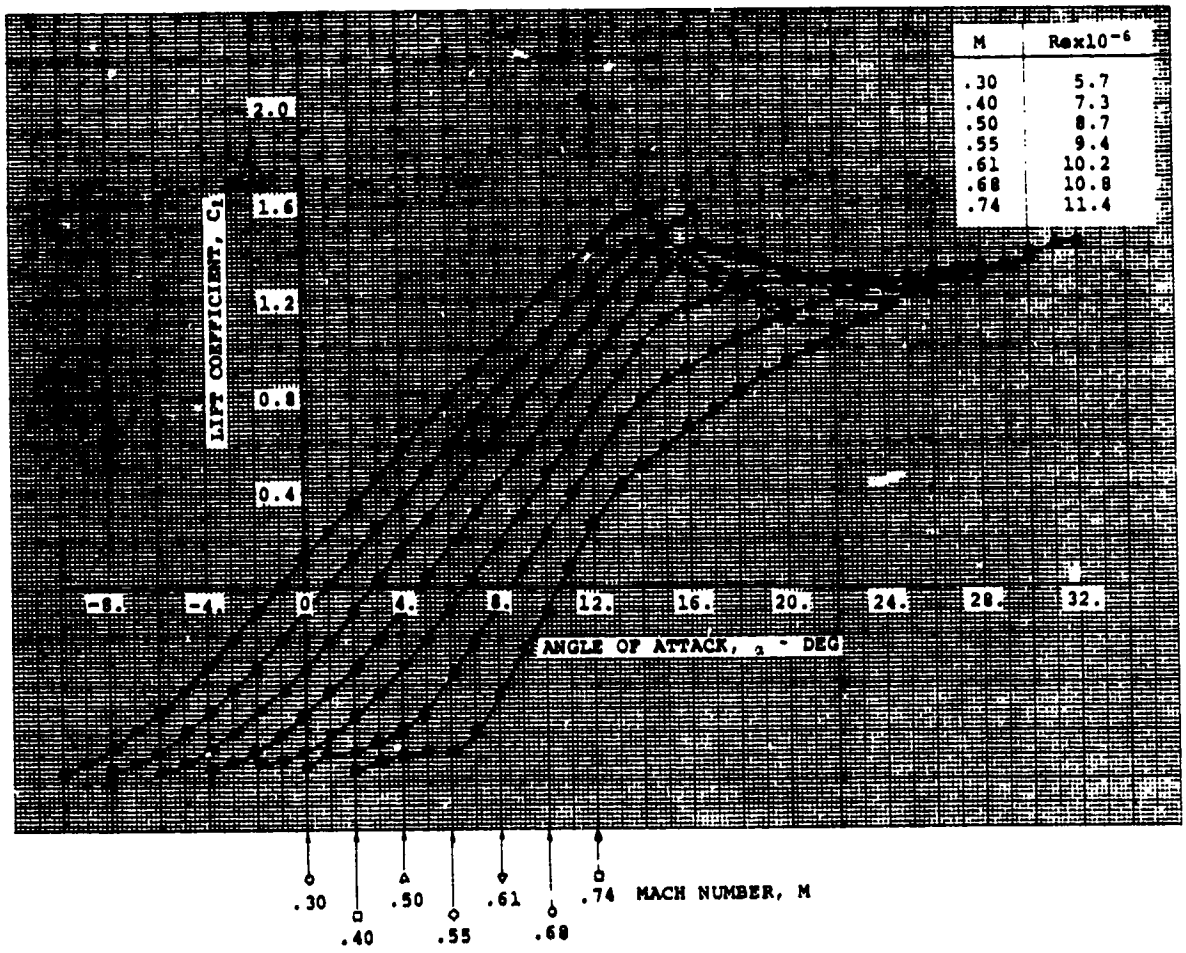

VR-7 WITH -3.1° T.E. TAB

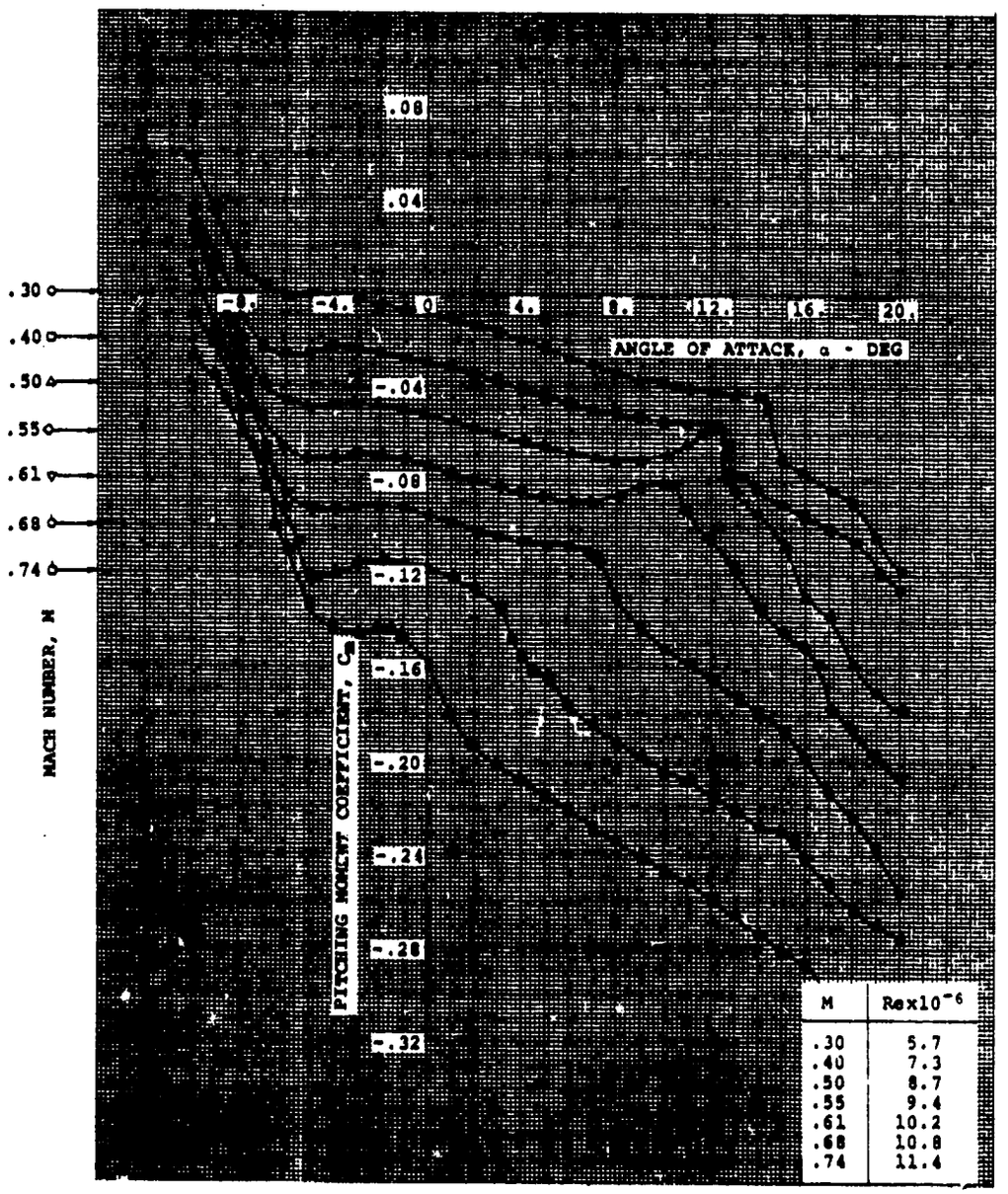

AIRFOIL: VR-7 With -5.9° T.E.TAB 1.3.400

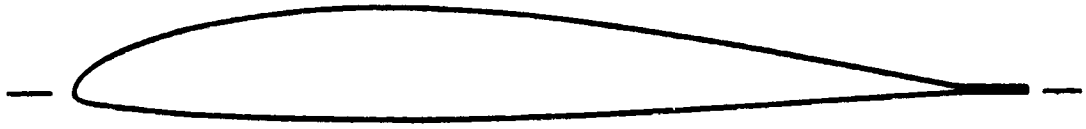

AIRFOIL COORDINATES

| x/c | $y/c_u$ | $y/c_\ell$ |
|---|---|---|
| 0. | 0. | 0. |
| .005 | .0165 | -.00575 |
| .01 | .0218 | -.0081 |
| .02 | .0298 | -.0109 |
| .03 | .03615 | -.0129 |
| .04 | .0415 | -.01445 |
| .05 | .04605 | -.01585 |
| .06 | .05025 | -.01710 |
| .07 | .0541 | -.01805 |
| .085 | .0593 | -.01985 |
| .102 | .0645 | -.02145 |
| .12 | .0691 | -.02285 |
| .14 | .0737 | -.0241 |
| .16 | .0775 | -.0251 |
| .18 | .0808 | -.0260 |
| .20 | .0838 | -.0266 |
| .225 | .0867 | -.0273 |
| .255 | .0892 | -.0280 |
| .29 | .0909 | -.0285 |
| .33 | .0914 | -.0289 |
| .37 | .0905 | -.0290 |
| .41 | .0887 | -.0285 |
| .45 | .0856 | -.0275 |
| .49 | .0816 | -.0260 |
| .53 | .0767 | -.0240 |
| .57 | .0710 | -.0220 |
| .61 | .0646 | -.0199 |
| .65 | .0580 | -.0179 |
| .69 | .0514 | -.0158 |
| .73 | .0447 | -.0138 |
| .77 | .0374 | -.01075 |
| .81 | .0301 | -.00845 |
| .845 | .0235 | -.0064 |
| .88 | .0167 | -.00425 |
| .91 | .0105 | -.00235 |
| .935 | .0062 | -.0006 |
| .96 | .0050 | 0.0 |
| 1.01 | .01017 | .00517 |

CHARACTERISTICS

- Thickness, t/x = 0.12
- Leading Edge Circle:

  r/c = .0113
  Center at x/c = .01055
  y/c = .004

- Trailing edge tab:

  From x/c = .96
  to x/c = 1.01

T.E. Tab Thickness, t/c = 0.005

TYPE OF DATA AND METHOD OF TEST

Two-dimensional test in the subsonic insert of the Boeing supersonic wind tunnel in Seattle, Washington.

Lift and pitching moments were measured with a balance.

Model Chord = 6.38 in
Span = 12. in

SOURCE

Dadone, L., & McMullen, J., "HLH/ATC Rotor System Two-dimensional Airfoil Test", Boeing Document D301-10071-1, December, 1971

VR-7 WITH -5.9° T.E. TAB

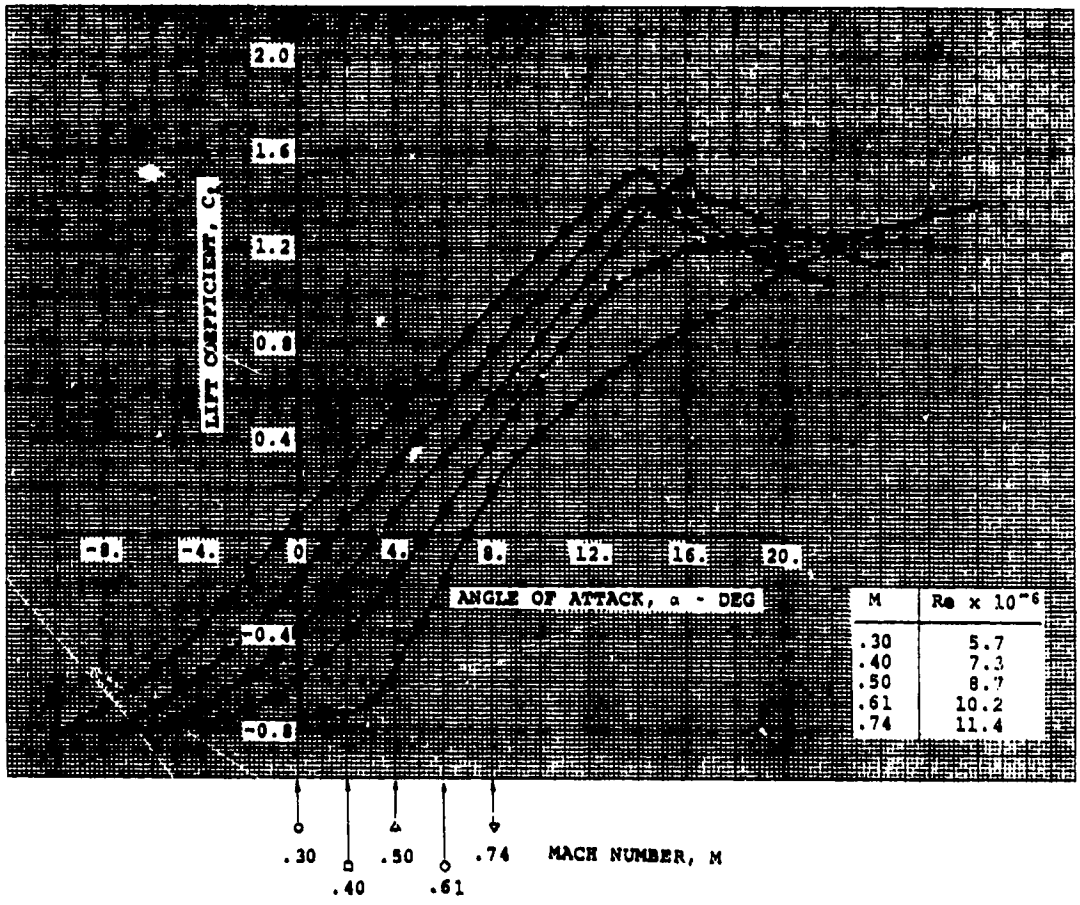

VR-7 WITH -5.9° T.E. TAB

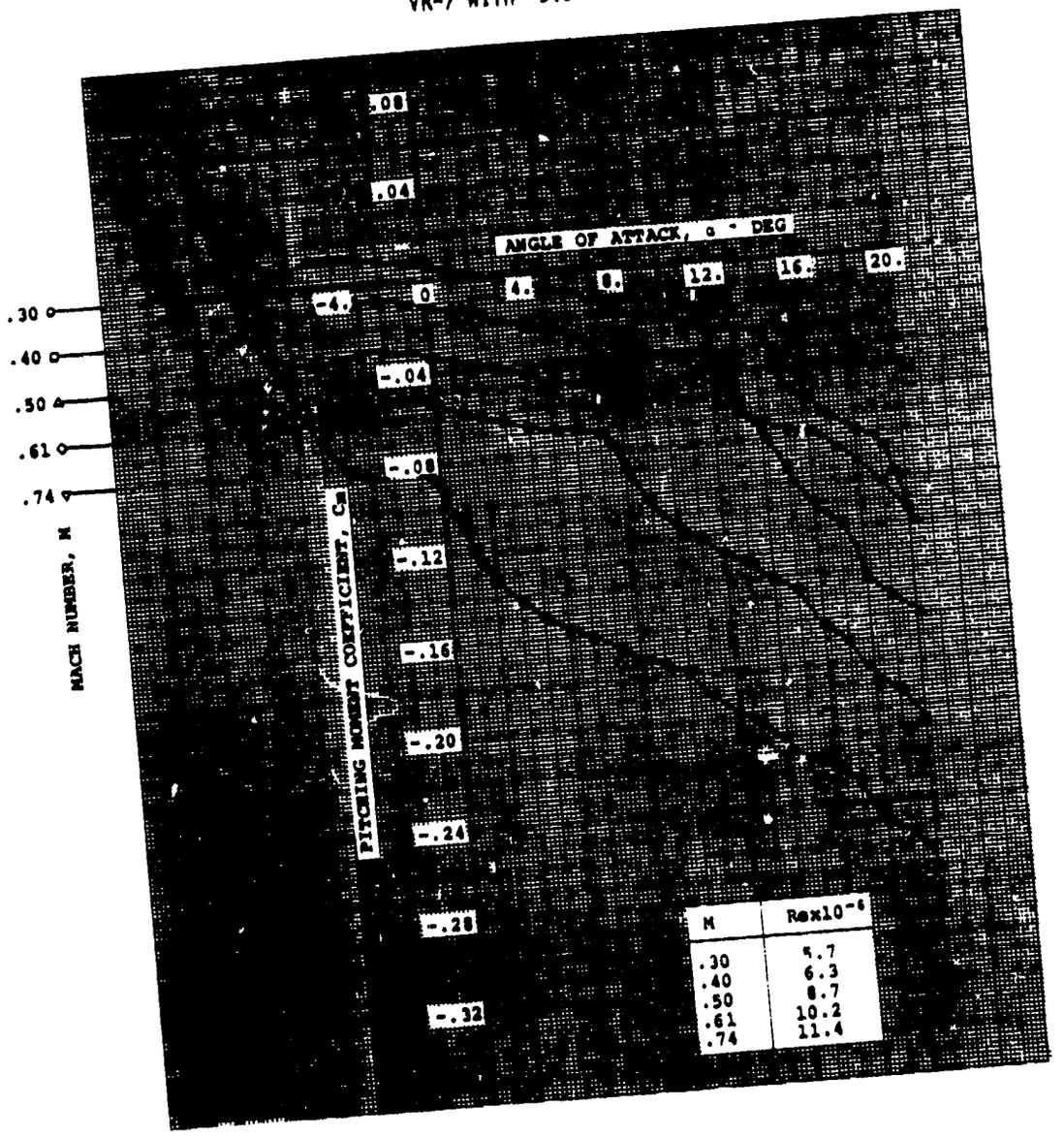

AIRFOIL: VR-8 With 0° T.E. TAB



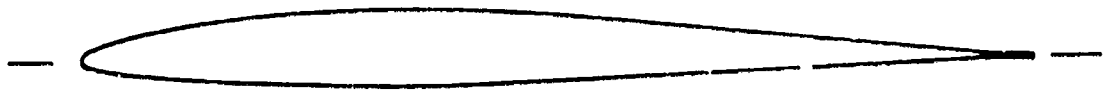

AIRFOIL COORDINATES

| x/c | $y/c_{upp}$ | $y/c_{low}$ |
|---|---|---|
| 0. | 0. | 0. |
| .005 | .00850 | -.00535 |
| .01 | .01175 | -.0737 |
| .015 | .01425 | -.00880 |
| .025 | .0183 | -.01090 |
| .035 | .0217 | -.01255 |
| .05 | .0261 | -.01465 |
| .07 | .0309 | -.01685 |
| .095 | .0357 | -.0190 |
| .125 | .0402 | -.0212 |
| .16 | .0444 | -.0232 |
| .20 | .0480 | -.0250 |
| .25 | .0510 | -.0266 |
| .30 | .0530 | -.0277 |
| .35 | .0535 | -.0280 |
| .40 | .0525 | -.0276 |
| .45 | .0502 | -.0265 |
| .50 | .0467 | -.0247 |
| .55 | .0426 | -.0225 |
| .60 | .0380 | -.0200 |
| .65 | .0333 | -.0175 |
| .70 | .0285 | -.0150 |
| .75 | .0237 | -.0125 |
| .80 | .0190 | -.0100 |
| .85 | .01428 | -.0075 |
| .89 | .01048 | -.0055 |
| .92 | .00761 | -.0040 |
| .945 | .00524 | -.00275 |
| .96 | .003404 | -.001596 |
| 1.01 | .003404 | -.001596 |

CHARACTERISTICS

- Thickness, t/x = 0.08
- Leading Edge Circle:

  r/c = 0.00585

  Center at x/c = 0.0058
  y/c = 0.00088
- Trailing Edge Tab:

  from x/c = 0.96
  to x/c = 1.01

  T.E. Tab Thickness, t/c = 0.005

TYPE OF DATA AND METHOD OF TEST

Two-dimensional test in the subsonic insert of the Boeing supersonic wind tunnel in Seattle, Washington.

Lift and Pitching moments were measured with a balance.

Drag was determined by a traversing wake probe survey.

Model Chord = 6.38 in
Span = 12. in

SOURCE

Dadone, L., & McMullen, J., "HLH/ATC Rotor System Two-dimensional Airfoil Test", Boeing Document, D301-10071-1, December, 1971

VR-8 WITH 0° T.E. TAB

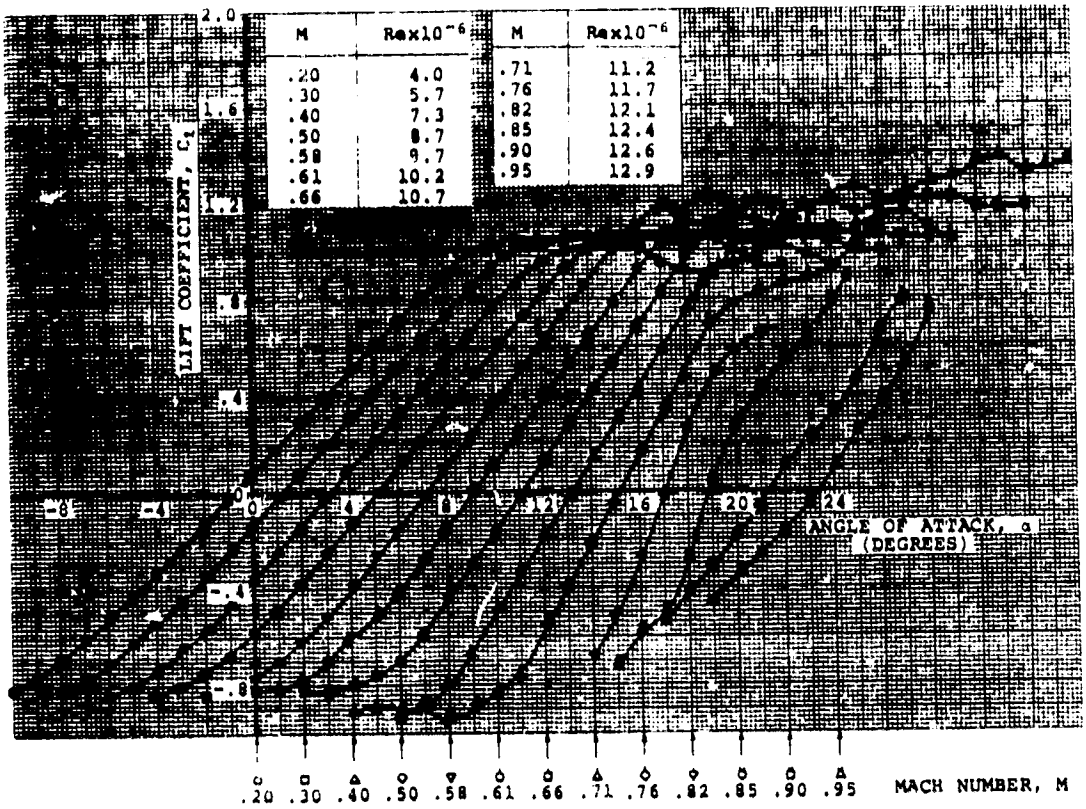


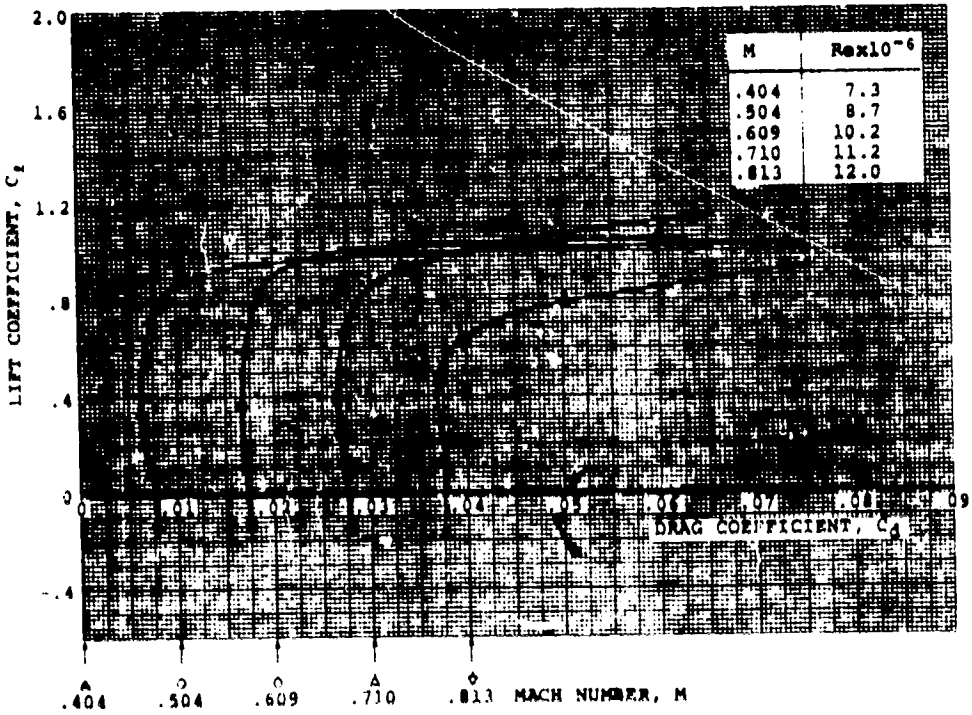

VR-8 WITH 0° T.E. TAB

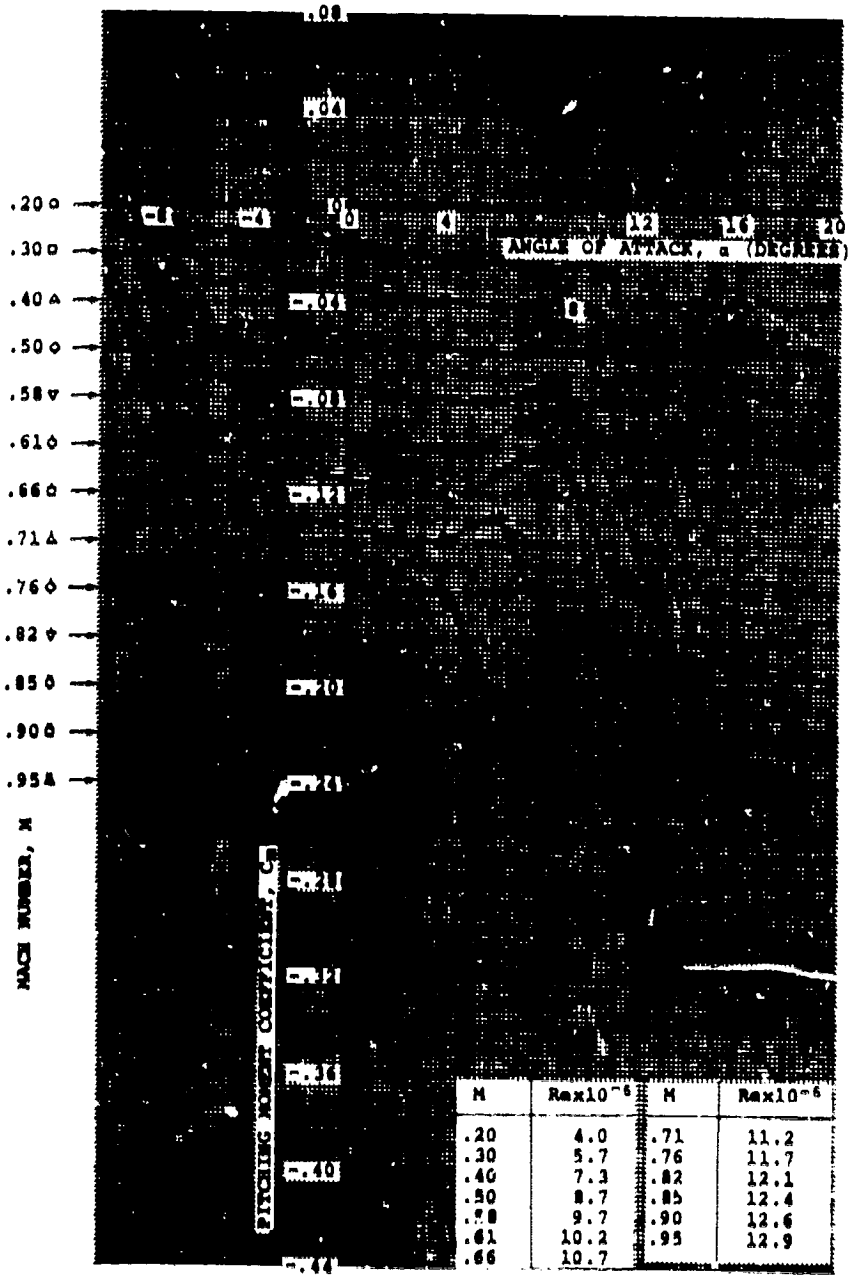


| M | Rax10⁻⁶ | M | Rax10⁻⁶ |
|---|---|---|---|
| .20 | 4.0 | .71 | 11.2 |
| .30 | 5.7 | .76 | 11.7 |
| .40 | 7.3 | .82 | 12.1 |
| .50 | 8.7 | .85 | 12.4 |
| .58 | 9.7 | .90 | 12.6 |
| .61 | 10.2 | .95 | 12.9 |
| .66 | 10.7 | | |

AIRFOIL: VR-7.1 With -1° T.E. TAB 1.3.420

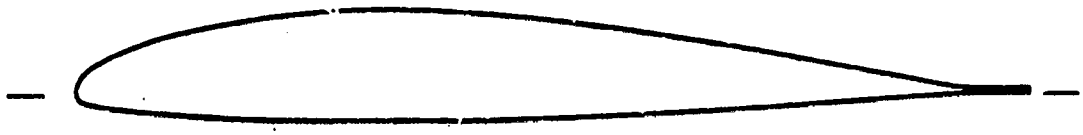

AIRFOIL COORDINATES

| x/c | $y/c_u$ | $y/c_\ell$ |
|---|---|---|
| 0. | 0. | 0. |
| .005 | | -.00575 |
| .01 | | -.0081 |
| .02 | | -.0109 |
| .03 | | -.0129 |
| .04 | | -.01445 |
| .05 | See Note | -.01585 |
| .06 | | -.01710 |
| .07 | | -.01805 |
| .085 | | -.01985 |
| .102 | .0645 | -.02145 |
| .12 | .0691 | -.02285 |
| .14 | .0737 | -.0241 |
| .16 | .0775 | -.0251 |
| .18 | .0808 | -.0260 |
| .20 | .0838 | -.0266 |
| .225 | .0867 | -.0273 |
| .255 | .0892 | -.0280 |
| .29 | .0909 | -.0285 |
| .33 | .0914 | -.0289 |
| .37 | .0905 | -.0290 |
| .41 | .0887 | -.0285 |
| .45 | .0856 | -.0275 |
| .49 | .0816 | -.0260 |
| .53 | .0767 | -.0240 |
| .57 | .0710 | -.0220 |
| .61 | .0646 | -.0199 |
| .65 | .0580 | -.0179 |
| .69 | .0514 | -.0158 |
| .73 | .0447 | -.0138 |
| .77 | .0374 | -.01075 |
| .81 | .0301 | -.00845 |
| .845 | .0235 | -.0064 |
| .88 | .0167 | -.00425 |
| .91 | .0105 | -.00235 |
| .935 | .0062 | -.0006 |
| .96 | .0050 | 0.0 |
| 1.01 | .00587 | .00087 |

CHARACTERISTICS

- Thickness, t/c = 0.12
- Leading Edge Circle:
  r/c =.0113
  Center at x/c = .01055
  y/c = .004
- Trailing Edge Tab
  from x/c = .96
  to x/c = 1.01

T.E. Tab Thickness, t/c = 0.005

TYPE OF DATA AND METHOD OF TEST

Two-dimensional test in the subsonic insert of the Boeing supersonic wind tunnel in Seattle, Wash.

Lift and Pitching moments were measured with a balance.

Model Chord = 6.38 in
Span = 12. in

SOURCE

Dadone, L., & McMullen, J.,"HLH/ATC Rotor System Two-dimensional Airfoil Test", Boeing Document D301-10071-1, December, 1971

NOTE: Same contour as the VR-7 airfoil except for the following coordinates:

| x/c | $y/c_u$ |
|---|---|
| .00050 | .00970 |
| .00180 | .01275 |
| .00390 | .01615 |
| .00670 | .02000 |
| .01050 | .02430 |
| .01550 | .02890 |
| .02120 | .03310 |
| .02800 | .03730 |

| x/c | $y/c_u$ |
|---|---|
| .03560 | .04120 |
| .04430 | .04510 |
| .05370 | .04890 |
| .06400 | .05260 |
| .07550 | .05640 |
| .08800 | .06030 |
| .10200 | .06450 |

# VR-7.1 WITH -1° T.E. TAB

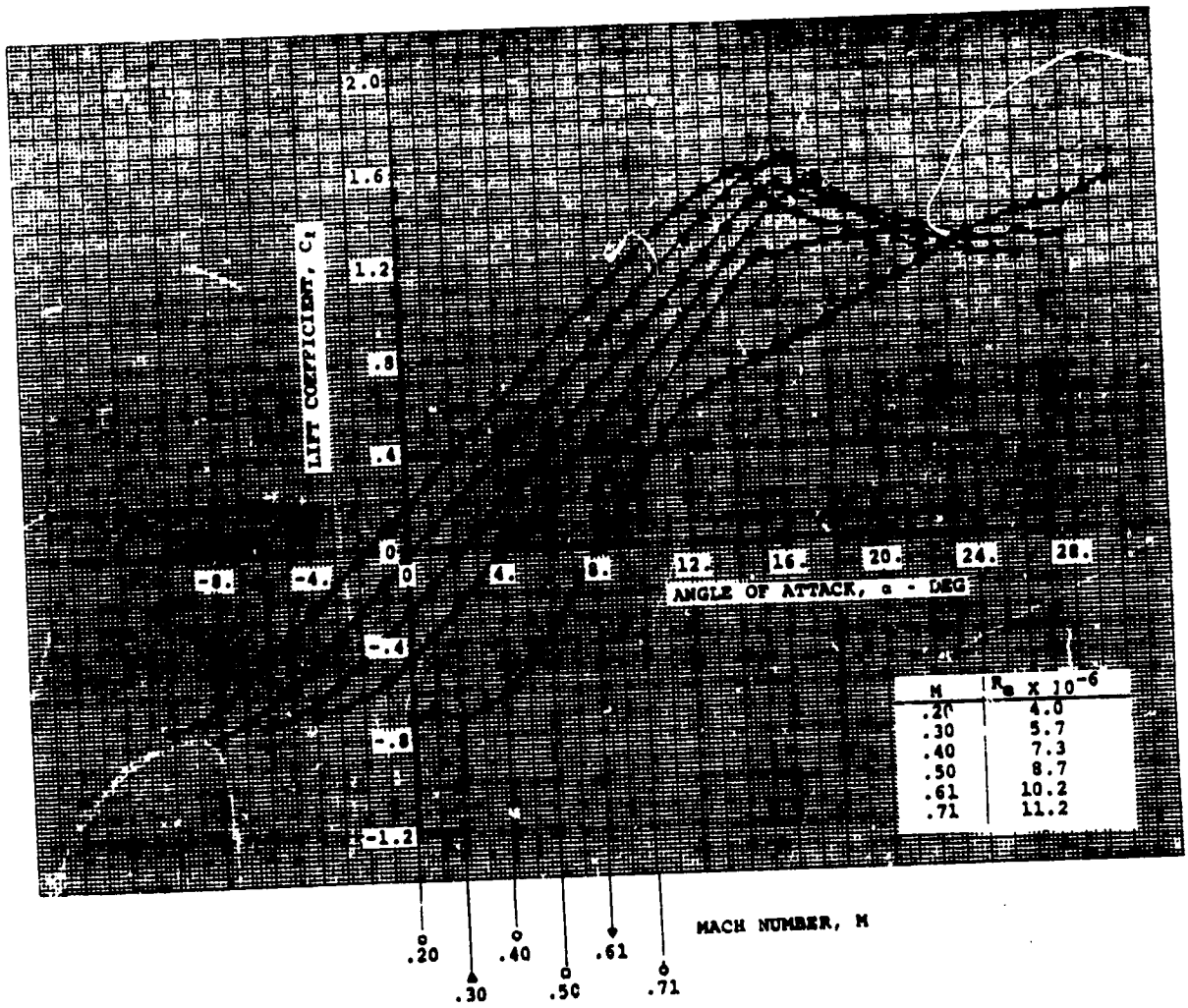

VR-7.1 WITH -1° T.E. TAB

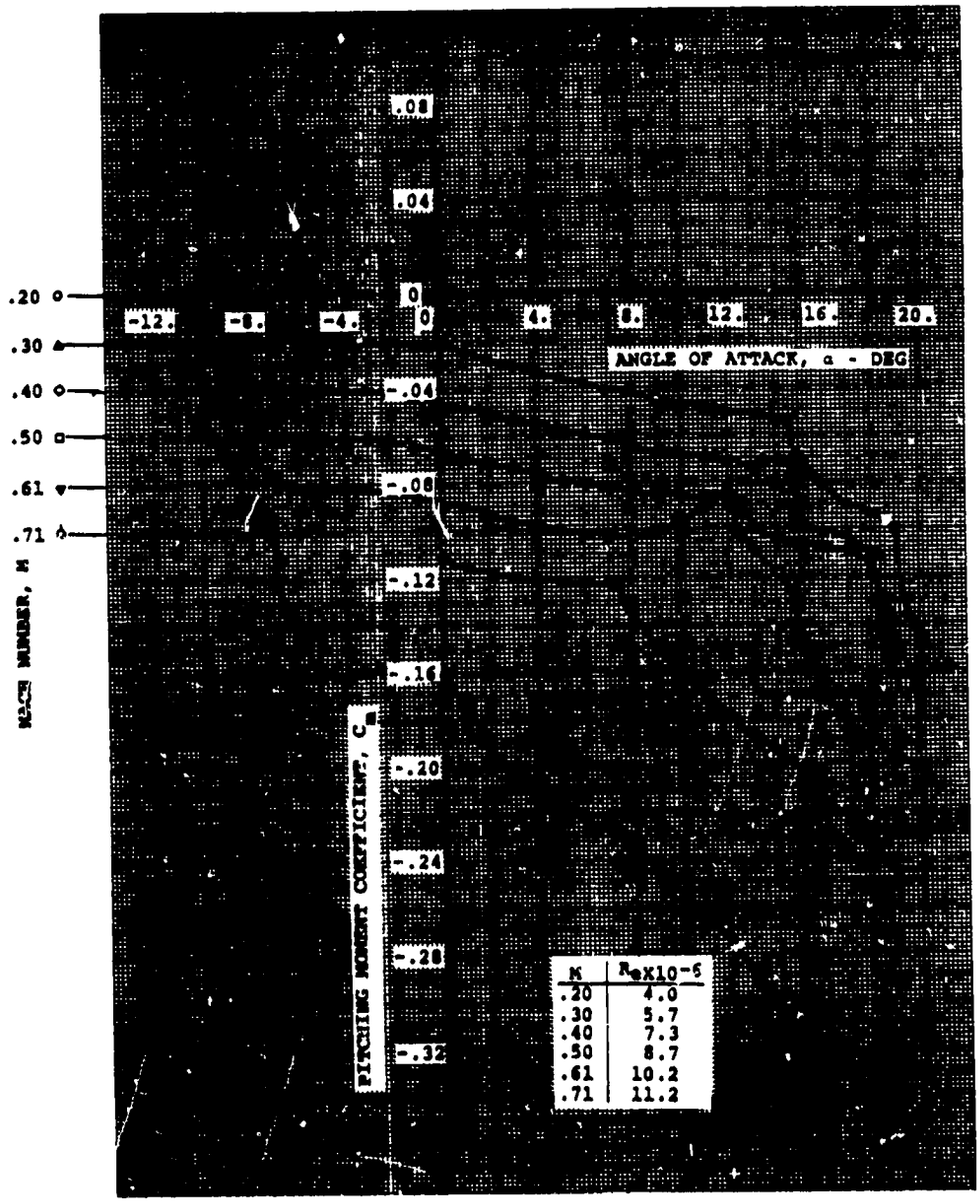

AIRFOIL: FX 69-H-098 (Wortmann) 1.3.430

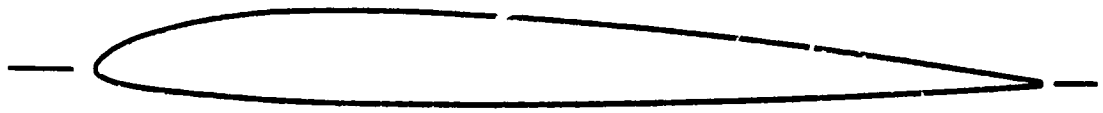

AIRFOIL COORDINATES:

| x/c | y/cu | y/cℓ |
|---|---|---|
| 0. | 0. | 0. |
| .0043 | .0096 | -.0069 |
| .0096 | .0148 | -.0096 |
| .0172 | .0204 | -.0122 |
| .0384 | .0320 | -.0171 |
| .0520 | .0377 | -.0192 |
| .0851 | .0486 | -.0231 |
| .1253 | .0573 | -.0264 |
| .1721 | .0630 | -.0292 |
| .2245 | .0661 | -.0313 |
| .2818 | .0666 | -.0323 |
| .3429 | .0654 | -.0324 |
| .4070 | .0631 | -.0317 |
| .4710 | .0598 | -.0305 |
| .5380 | .0553 | -.0288 |
| .6035 | .0501 | -.0267 |
| .6673 | .0442 | -.0242 |
| .7283 | .0377 | -.0215 |
| .7856 | .0312 | -.0186 |
| .8379 | .0248 | -.0156 |
| .8847 | .0185 | -.0126 |
| .9579 | .0072 | -.0064 |
| 1.0000 | .0009 | -.0013 |

CHARACTERISTICS

- Thickness, t/x = 0.098
- Leading Edge Radius, r/c = 0.006

TYPE OF DATA AND METHOD OF TEST

Wind tunnel tests conducted at the United Aircraft Research laboratories.

SOURCE

Kemp, L.K., "An Analytical Study for the Design of Advanced Rotor Airfoils", NASA CR-112297, March 23, 1973

FX 69-H-098

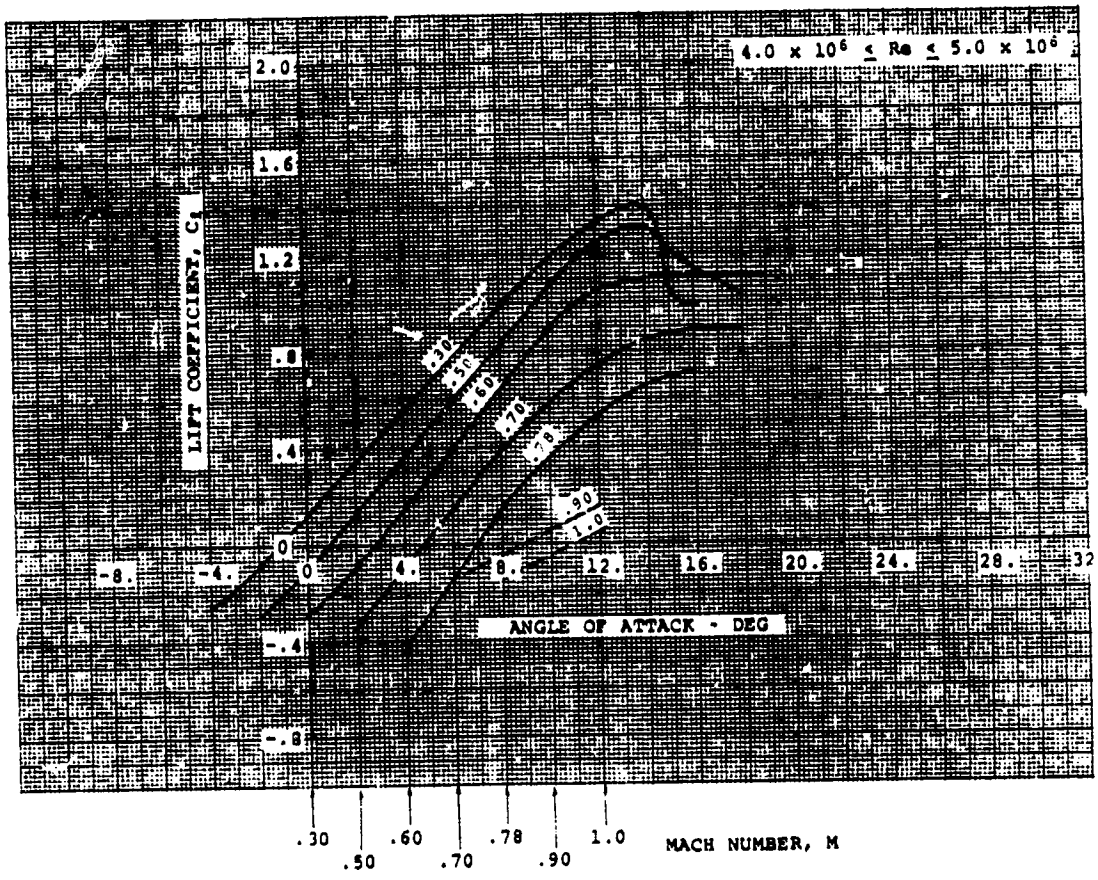


FX69-H-098 AIRFOIL

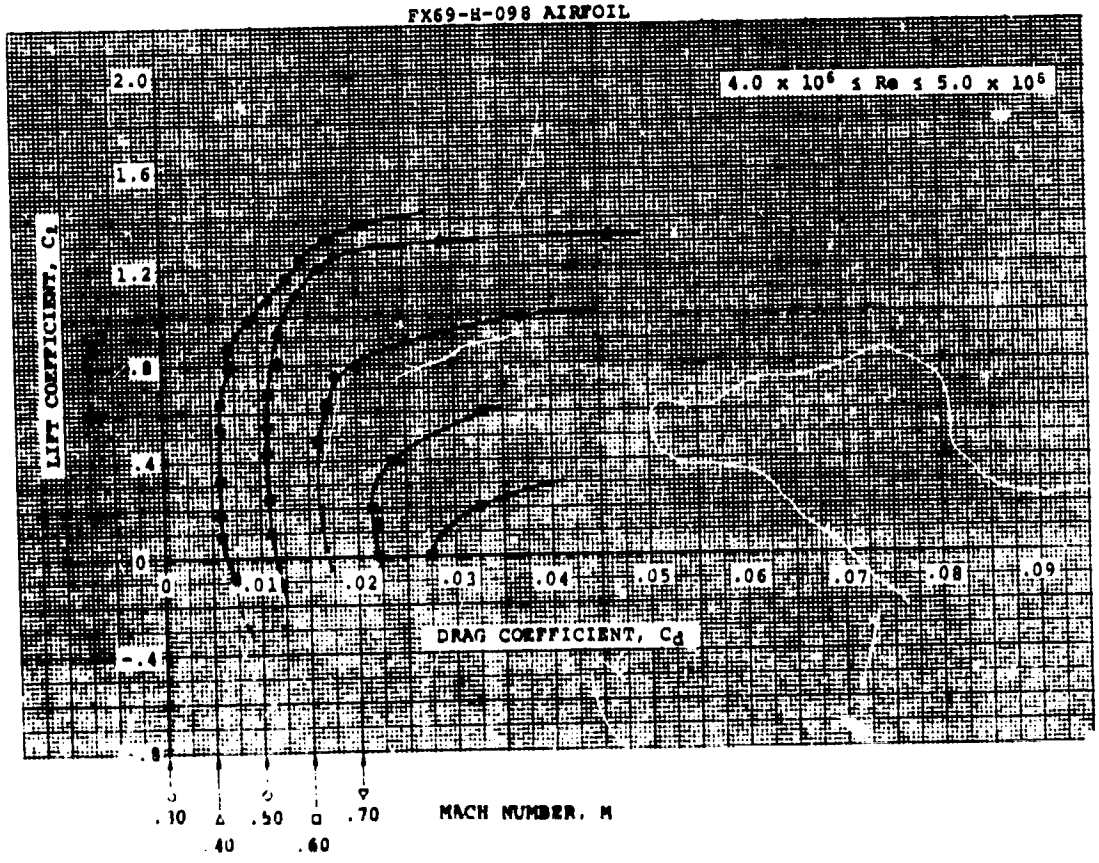

FX 69-H-098

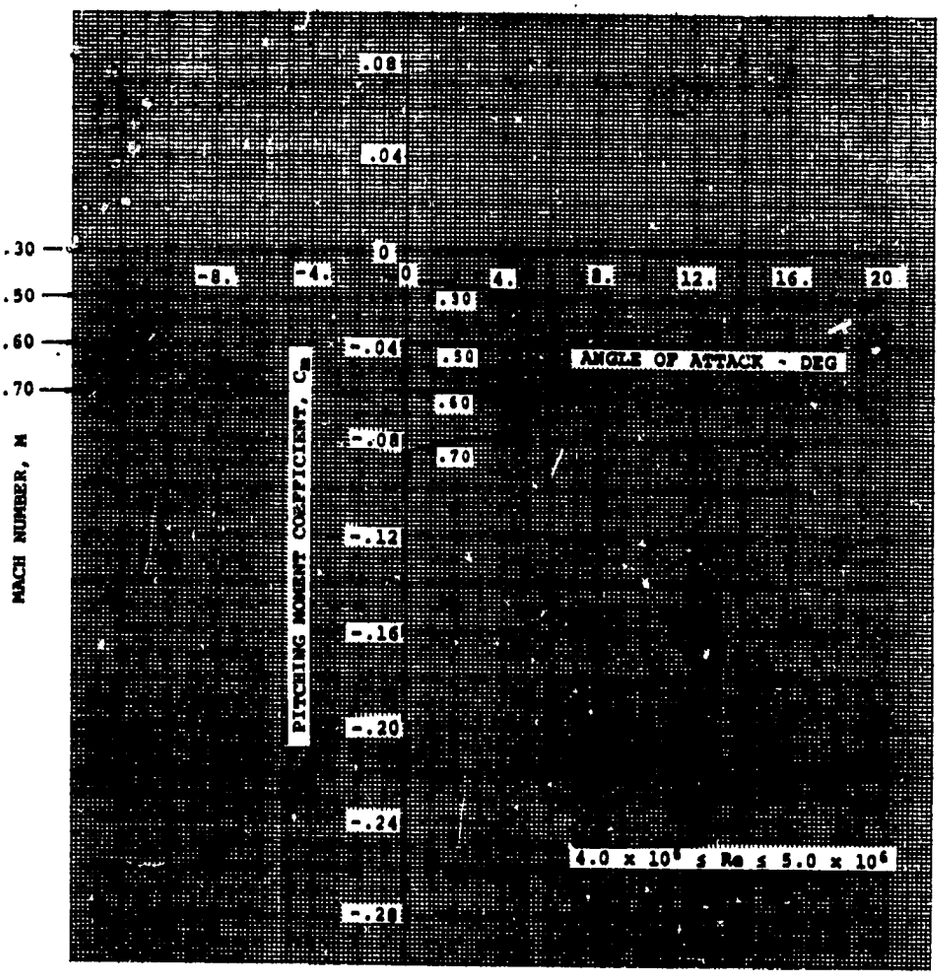
.08
.04
0
-.04
-.08
-.12
-.16
-.20
-.24
-.28
PITCHING MOMENT COEFFICIENT, $C_m$
-8.
-4.
0
4.
8.
12.
16.
20
ANGLE OF ATTACK - DEG
.30
.50
.60
.70
MACH NUMBER, M
$4.0 \times 10^6 \leq Re \leq 5.0 \times 10^6$

## 1.4.10 EVALUATION OF APPROXIMATE LIFT/DRAG POLARS

As long as the character of the stall does not change drastically with varying airfoil geometry or flow conditions, the lift/drag polars of a known section can be altered to reflect changes in:

- Overall camber
- Trailing edge reflex angle
- Mach Number
- Reynolds Number

The evaluation of the new drag polars is a function of the accuracy in specifying the effect of the variations being considered on:

- The maximum lift coefficient
- The design lift coefficient, or the lift for minimum drag
- The minimum drag level

Table I illustrates, step by step, the evaluation of the drag polar for the NACA 64A312 airfoil (data sheet 1.3.180) utilizing the polar of the NACA 64A(4.5)12 of data sheet 1.3.190. Columns (1) and (2) show a tabulation of lift and drag coefficients, respectively, for the NACA 64A(4.5)12. The design lift, maximum lift and minimum drag coefficients of this section are

$C_{\ell_i} = 0.45$

$C_{\ell_{MAX}} = 1.43$

$C_{d_{min}} = .0078$

Columns (3) and (4) of Table I list the values for the lift/drag polar normalized by use of the expressions:

$$\text{Normalized Lift} = \frac{C_\ell - C_{\ell_i}}{C_{\ell_{MAX}} - C_{\ell_i}} \qquad \text{(a)}$$

$$\text{Normalized Drag} = C_d - C_{d_{min}} \qquad \text{(b)}$$

The NACA 64A312 has the following characteristics:

$C_{\ell_i} = 0.3$

$C_{\ell_{MAX}} = 1.29$

$C_{d_{min}} = 0.0065$

The maximum lift and minimum drag values at M = 0.4 were obtained from data sheet 1.3.180 in order to illustrate the accuracy of this method. Columns (5) and (6) of Table I show the lift and drag coefficient values obtained by utilizing in expressions (a) and (b) the normalized values of columns (3) and (4) together with the $C_{\ell_i}$, $C_{\ell_{MAX}}$, and $C_{d_{min}}$ values for the new section.

Figure 1 compares the approximate lift drag polar with values from data sheet 1.3.180. The original NACA 64A(4.5)12 is also shown.

| KNOWN SECTION | | NORMALIZED VALUES | | ESTIMATED VALUES FOR RELATED SECTION | |
|---|---|---|---|---|---|
| ① | ② | ③ | ④ | ⑤ | ⑥ |
| NACA 64A(4.5)12 | | $\frac{C_\ell - C_{\ell_i}}{C_{\ell_{MAX}} - C_{\ell_i}}$ | $(C_d - C_{min})$ | NACA 64A312 | |
| $C_\ell$ | $C_d$ | | | $C_\ell$ | $C_d$ |
| 0. | 0.008 | -.4592 | 0.0002 | -.1546 | .0067 |
| .2 | 0.008 | -.2551 | 0.0002 | .0474 | .0067 |
| .4 | 0.0079 | -.0510 | 0.0001 | .2495 | .0066 |
| .6 | 0.0079 | .1531 | 0.0001 | .4516 | .0066 |
| .8 | 0.0084 | .3571 | 0.0006 | .6535 | .0071 |
| 1.0 | 0.0094 | .5612 | 0.0016 | .8556 | .0081 |
| 1.1 | 0.01 | .6633 | 0.0022 | .9557 | .0087 |
| 1.2 | 0.0109 | .7653 | 0.0031 | 1.0576 | .0096 |
| 1.3 | 0.0123 | .8673 | 0.0045 | 1.1586 | .0110 |
| 1.4 | 0.0152 | .9694 | 0.0074 | 1.2597 | .0139 |
| 1.42 | 0.0185 | .9900 | 0.0107 | 1.2810 | .0172 |
| 1.43 | 0.028 | 1.0 | 0.0202 | 1.29 | .0267 |

<u>NACA 64A(4.5)12</u>

$C_{\ell_i} = 0.45$

$C_{\ell_{MAX}} = 1.43$

$C_{d_{min}} = 0.0078$

<u>NACA 64A312</u>

$C_{\ell_i} = 0.30$

$C_{\ell_{MAX}} = 1.29$

$C_{d_{min}} = 0.0065$

TABLE I. Evaluation of the lift drag polar of the NACA 64A312 airfoil at M = 0.4 from data on a related airfoil.

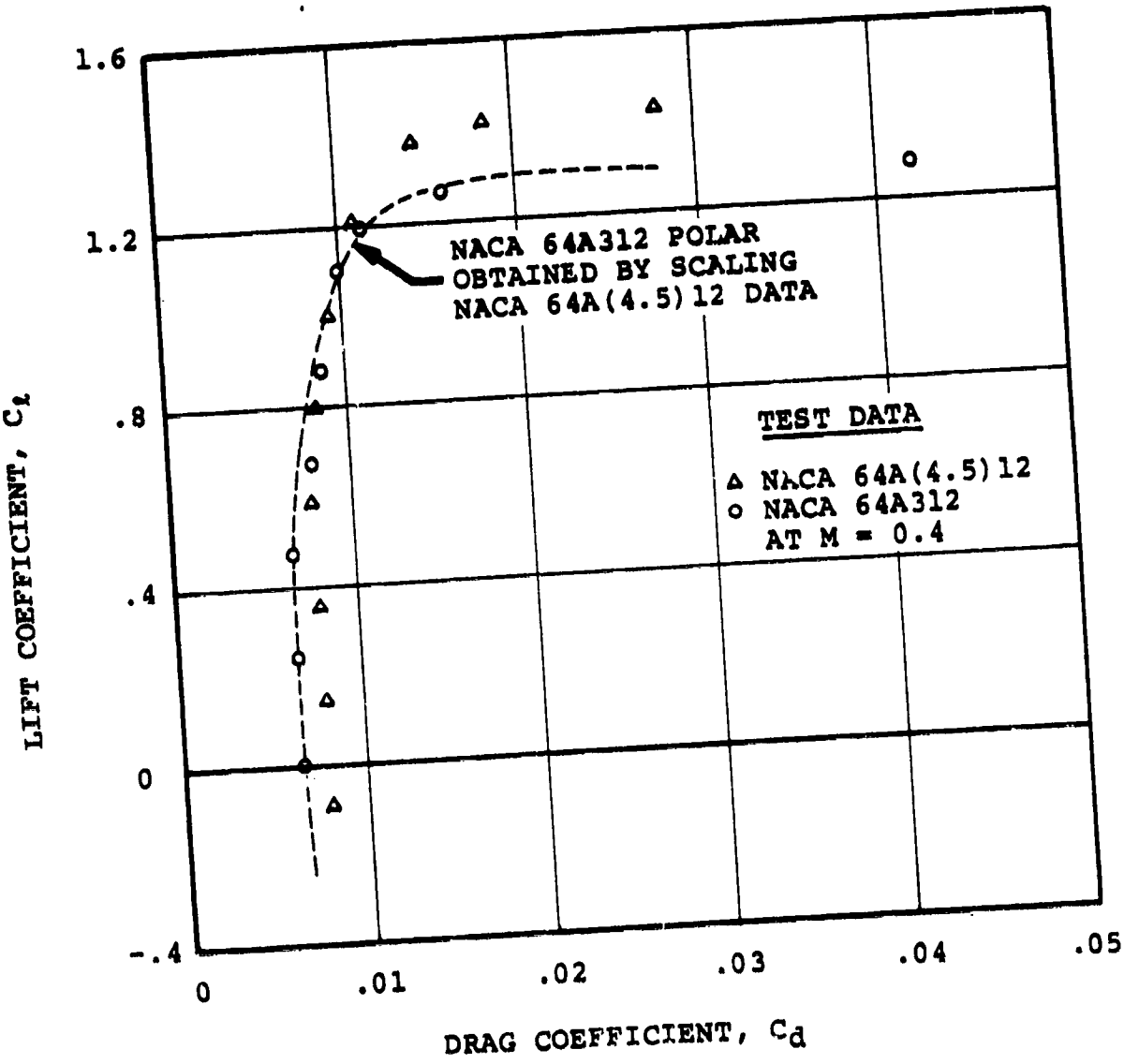


*Figure 1 Comparison between Estimated and Measured Drag Polars for the NACA 64A312 Airfoil.*

## 1.4.20 LIFT, DRAG AND PITCHING MOMENT COEFFICIENTS AT LARGE ANGLES OF ATTACK

Data Sheets 1.3.30 and 1.3.130 show data for the NACA 0012 and NACA 63A012 airfoils at angles of attack from $\alpha = 0°$ to $\alpha = 180°$. The main difference between the two sets of data, besides the airfoil section, is the fact that the NACA 0012 was obtained at low speed, $M = 0.1$, while the NACA 63A012 was tested at $M = 0.3$. However, except for small differences in the maximum values of the lift, drag, and pitching moment coefficients, the curves for the two airfoils are quite similar at angles above 20°. At angles from 0° to $\pm 20°$, i.e., within the normal operating range of the airfoils, the sectional characteristics are quite sensitive to flow and contour variations.

Portions of a helicopter rotor blade encounter very large angles of attack within the reverse flow region as a result of rotor operation in forward flight. Even though the velocities near and inside the reverse flow circle are small, an estimate is often required of the airloads the blade has to sustain within such a region.

Recent data is limited to the NACA 0012 and NACA 63A012, presented in data sheets 1.3.30 and 1.3.130. Additional data from Riegels(*) on the Gö420 and Gö623 airfoils (both cambered) is shown in Figures 1(a) and 1(b).

Figures 2, 3, and 4 show how the NACA 0012 data and the trends from Figures 1(a) and 1(b) can be utilized to estimate the sectional characteristics of the VR-7 airfoil for the complete range in angles of attack from 0° to 360°.

The approximate characteristics of Figures 2, 3, and 4 are subject to the following assumptions and limitations:

1. At angles of attack near 90° and 270°, it has been assumed that the lift is zero independently of airfoil shape, as at such conditions any section will behave nearly as a flat plate. Similarly, it has been assumed that the airfoil shape has a negligible effect on the drag at $\alpha = 90°$ and 270°.

2. The pitching moment about the quarter chord reaches its maximum value at $\alpha = 120°$ (and therefore at $\alpha = 240°$) for both the NACA 0012 and the NACA 63A012. As shown in Figure 1(a) this holds true for cambered airfoils as well.

---

(*) Riegels, F.W., Aerofoil Sections, BUTTERWORTHS SCIENTIFIC PUBLICATIONS, London, 1961.

3. Camber will influence the angles for zero lift and zero pitching moment in the vicinity of $\alpha = 180°$. Data sheets 1.3.270, 1.3.280 and 1.3.290 show data for the V23010-1.58 airfoil with various trailing edge configurations, at angles of attack from 160° to 200°. Unless test data is available, the determination of the sectional characteristics at low lift levels in reverse flow is extremely difficult, since the reversed airfoil has a sharp "leading edge" and a blunt "trailing edge", the first of which will cause laminar separation (with some reattachment bubble) and the second will prevent the establishment of the "Kutta-Joukowski" condition. Since the flow environment in the reverse flow region can be approximated only very roughly with present rotor performance prediction methods, under normal circumstances there is little to be gained from an accurate definition of the sectional characteristics at $160° < \alpha < 200°$, and unless directly applicable test data is available (e.g., the V23010-1.58) it should be sufficient to ignore camber and use the data for the NACA 0012 on NACA 63A012.

4. The only condition for which it is normally necessary to define the sectional characteristics at high angles of attack is for $10° < \alpha <$ at Mach Numbers up to $M = 0.5$, as the quasi-steady force and moment coefficients for such flow conditions are the basis for the approximate evaluation of dynamic stall delay effects.

5. The lift coefficient of a symmetrical section attains secondary maximum values at $\alpha = 40° \rightarrow 45°$ and again at $\alpha = 135° \rightarrow 140°$. It can be assumed that camber has negligible influence on the angle of attack for such secondary maximum lift values; however, some level adjustment should be made, since there is evidence that cambered sections, such as the ones shown in Figures 1(a) and 1(b), have different secondary peaks in maximum lift for angle of attack regions $20° \leq \alpha \leq 180°$ and $180° \leq \alpha \leq 340°$.

6. Some level adjustments in the characteristics at high angles of attack will generally be necessary to extend post stall data at different Mach Numbers.

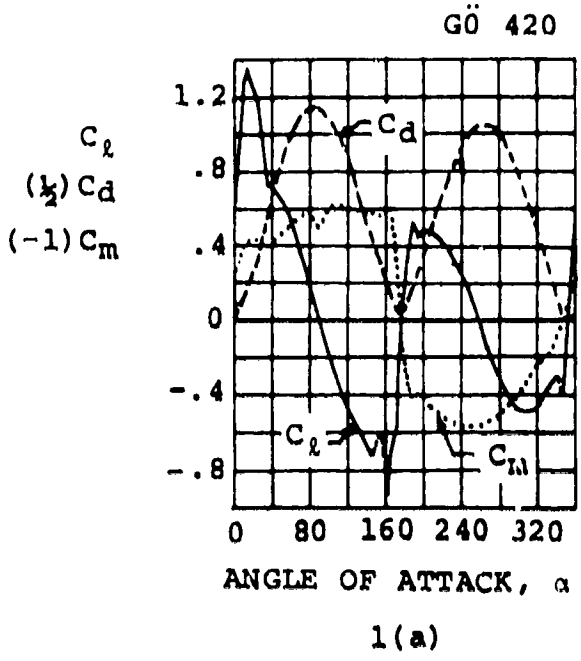


1(a)

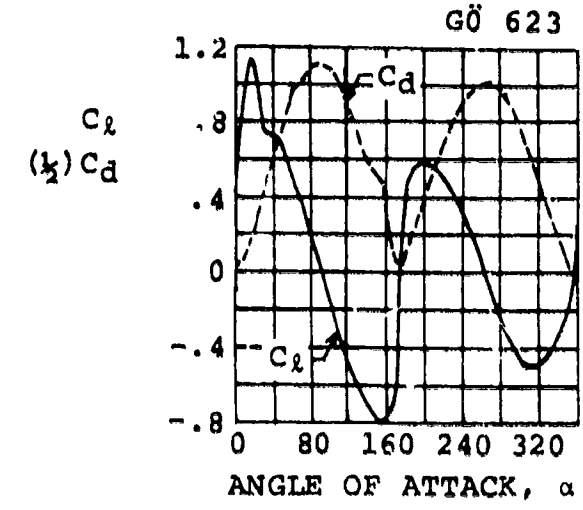


1(b)

*Figure 1 Sectional Characteristics of the Gö 420 and Gö 623 Airfoils at $0° \leq \alpha \leq 360°$ for $Re = 4.2 \times 10^6$*

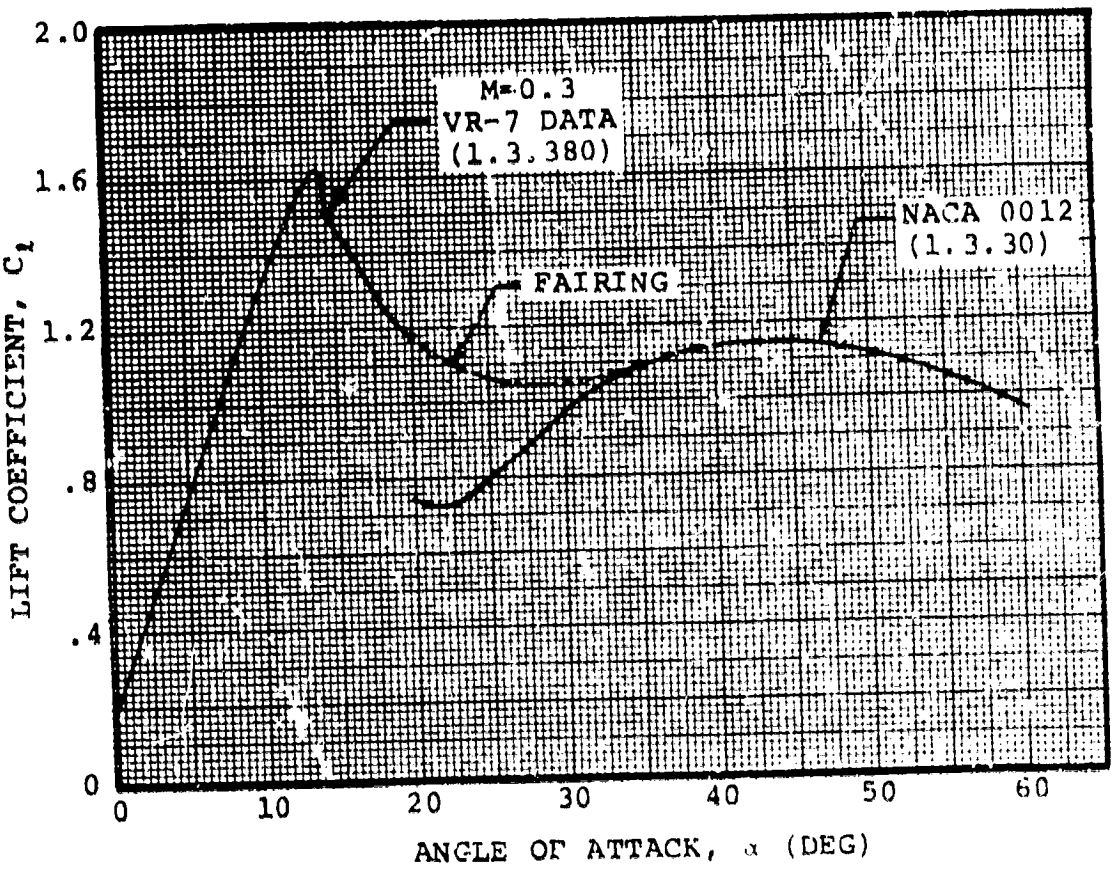


*Figure 2(a) Extension of VR-7 Airfoil Lift Data to High Positive Angles of Attack*

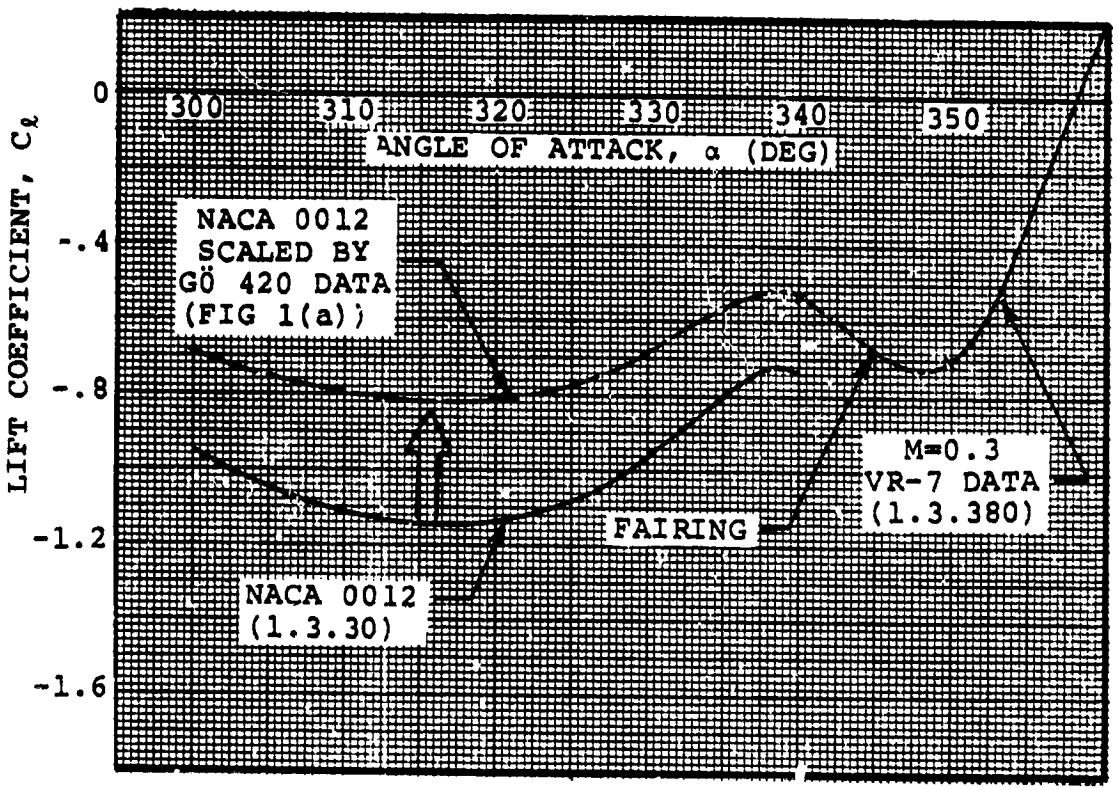


*Figure 2(b) Extension of VR-7 Airfoil Lift Data to High Angles of Attack*

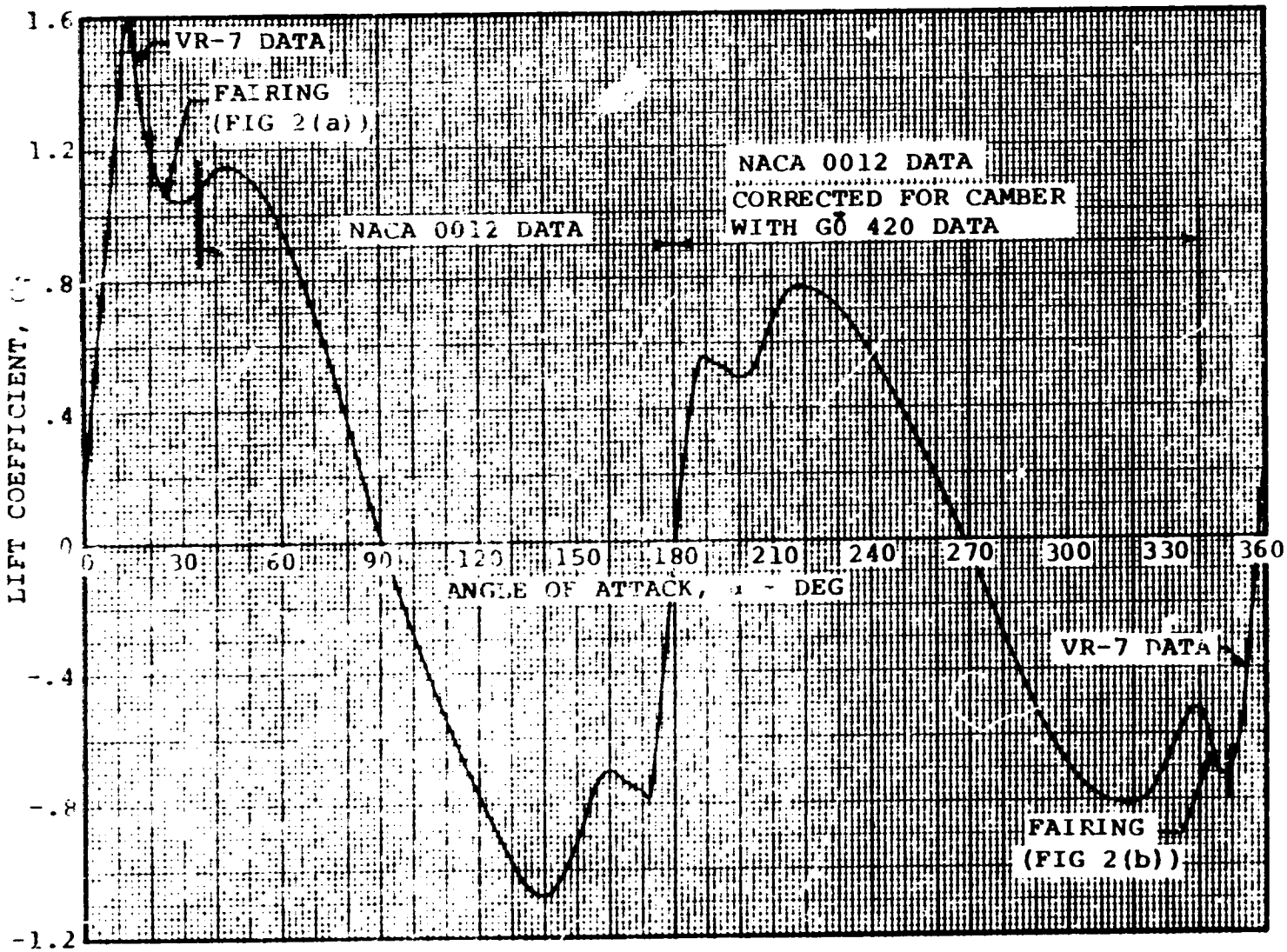


*Figure 2(c) Estimated Lift Coefficient Variation for the VR-7 Airfoil at $0° \leq \alpha \leq 360°$, $M = 0.3$*

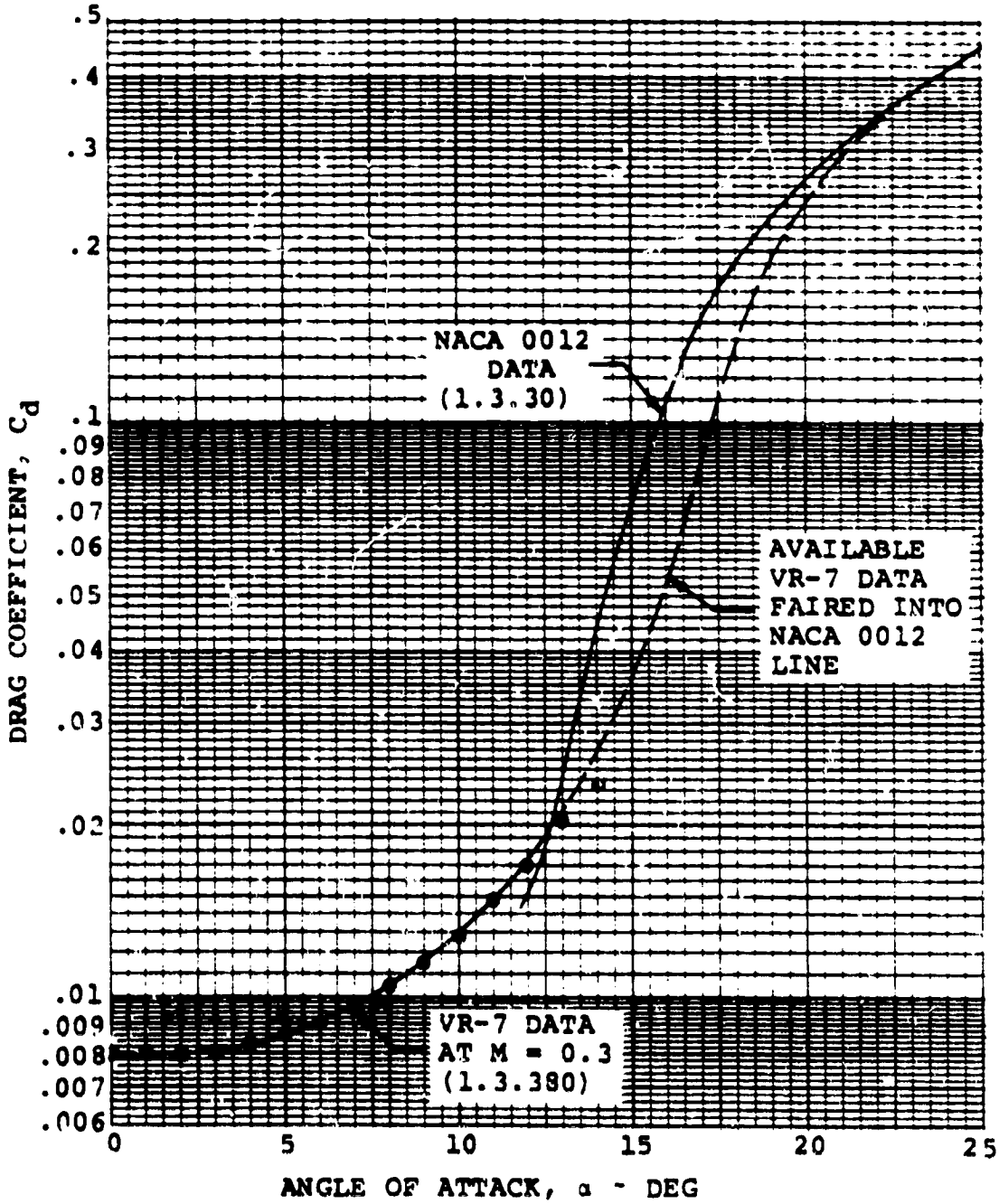


*Figure 3(a) Extension of VR-7 Airfoil Drag Data to High Positive Angles of Attack*

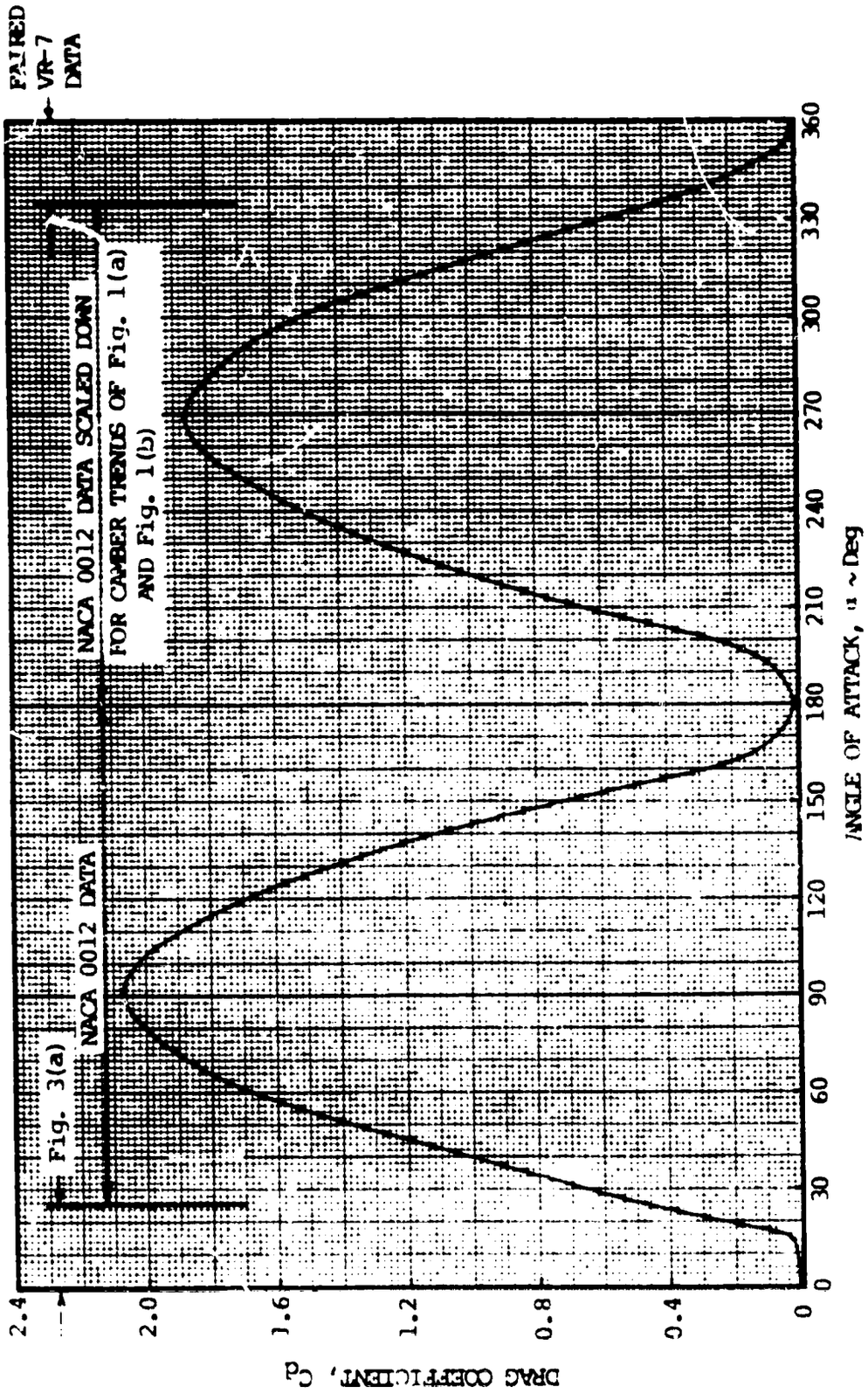


*Figure 3(b) Estimated Drag Coefficient Variation for the VR-7 Airfoil at $0° \leq \alpha \leq 360°$, $M = 0.3$.*

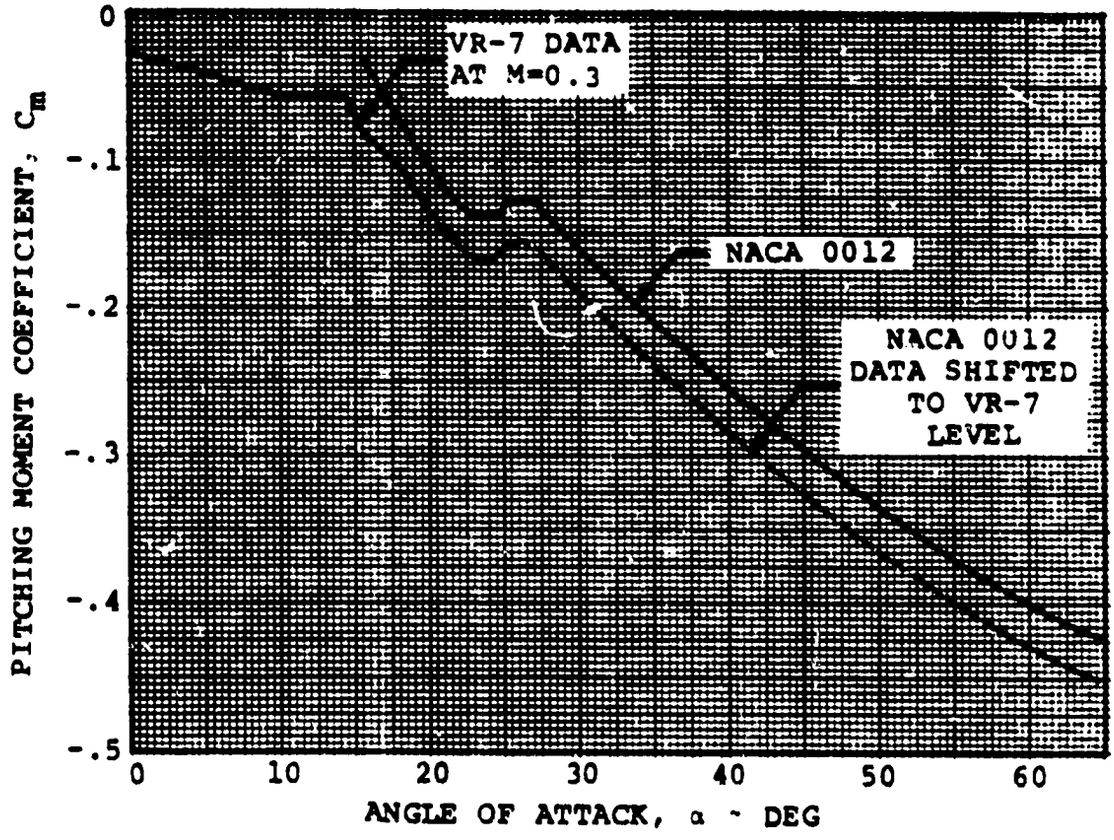


*Figure 4(a) Extension of VR-7 Airfoil Pitching Moment Data to High Positive Angles of Attack*

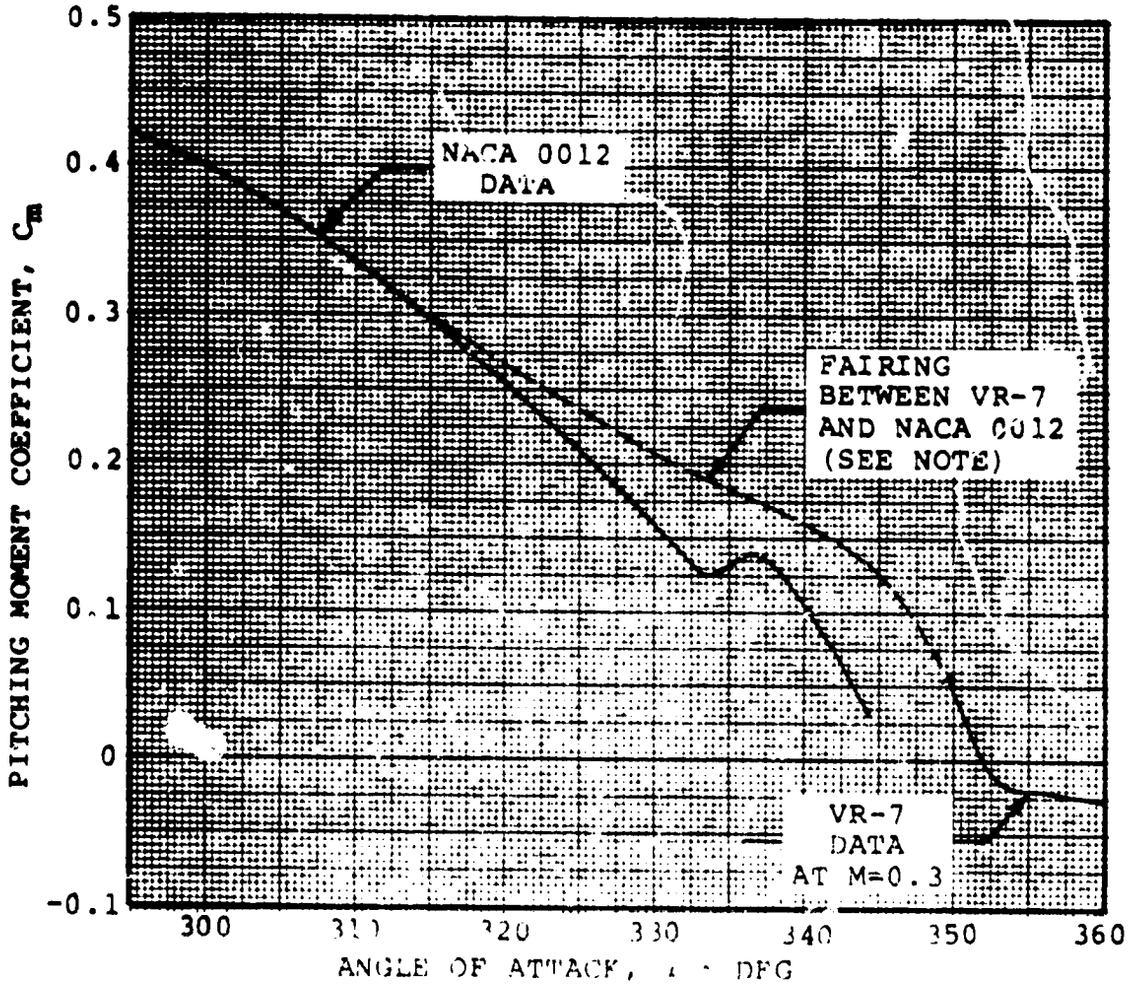


**NOTE:** THE DATA FOR THE GO 420 SECTION SUGGESTS THAT CAMBERED SECTIONS ATTAIN LOWER $|C_{m_{MAX}}|$ LEVELS FOR $180° < \alpha < 360°$ THAN FOR $0° < \alpha < 180°$. THEREFORE SHIFTING THE NACA 0012 LINE TO MATCH THE VR-7 AFTER-STALL LEVEL WOULD BE, AT LEAST QUALITATIVELY, INCORRECT BY COMPARISON WITH DATA IN FIGURE 1(a).

*Figure 4(b) Extension of VR-7 Airfoil Pitching Moment Data to High Negative Angles of Attack*

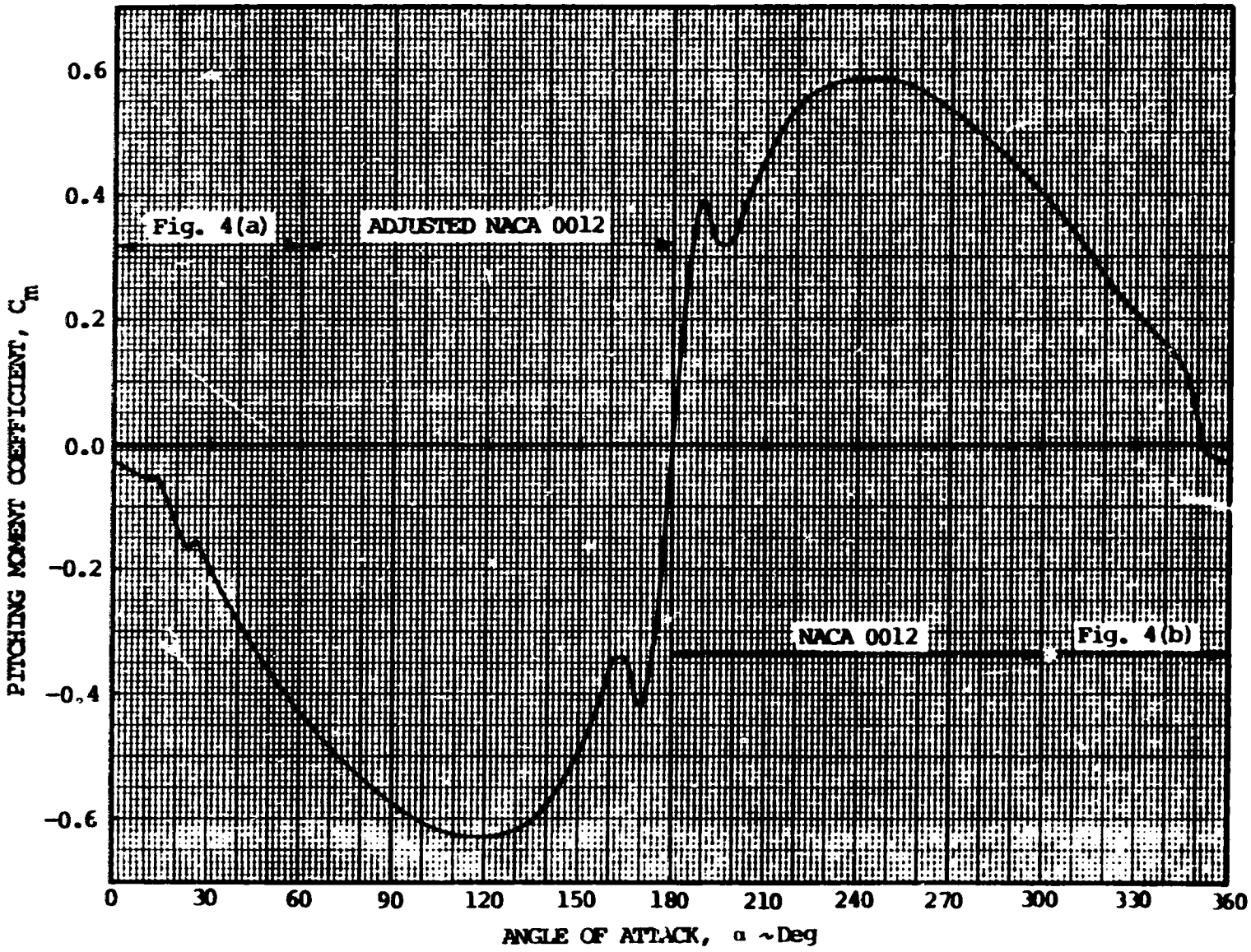


*Figure 4(c) Estimated Pitching Moment Coefficient Variation for the VR-7 Airfoil at $0° \leq \alpha \leq 360°$, $M = 0.3$.*